Journal of Applied Mechanics

(Contributions of the ASME Applied Mechanics Division)

Linear Theory of Gas Through a Semi-Infinite Porous Medium . . . . . R. E. Kidder 329
A Study of Plane-Polarized Oscillation in a Tube . . . . . J. J. Bailey 333
Photoelastic Study of Strain Waves Caused by Cavitation . . . . . G. W. Sutton 340
Turbulence in Small Air Jets . . . . . L. W. Lassiter 349
Thermoviscoelasticity: An Exploratory Study . . . . . George Gurevich and I. C. Gilbert 355
Distribution of Stresses and Strains Near End of a Crack . . . . . G. R. Irwin 361
Bending of a Prestressed Strip . . . . . Chih-Bing Ling 365
Axisymmetric Thermal Stresses in Spherical Shell . . . . . H. L. McDowell and E. Sternberg 376
Buckling Pressure of a Spheroid: A Biharmonic Eigenvalue Problem . . . . . G. Horvay 381
Method Developed for Determining Airy Stress Functions . . . . . Ching-Yuan Nuan 387
Plane Stress and Bending of Thin Plates . . . . . Eric Reissner 391
Deformation of Elastic Paraboloidal Shells of Revolution . . . . . C. N. De Silva 397
Buckling of Thin-Cylindrical Shell Under Hoop Stresses . . . . . N. J. Hoff 405
Thermal Response of Beams and Plates to Rapid Heating . . . . . B. A. Boley and A. D. Barber 413
Dynamic Stresses of an Elastic Cable Due to Impact . . . . . P. O. Ringleb 417
Strain-Hardening Energy of Fixed-Fixed Beam Specimens . . . . . W. C. Hagel and J. W. Clark 426
Theory of Propagation of Flexural Waves . . . . . E. A. Ripperger and H. N. Abramson 431
Forced Vibrations of Systems With Nonlinear Characteristics . . . . . S. Mahalingam 435
Plastic Flow During Transverse Impact . . . . . K. E. Bernhart, Jr., and W. Goldsmith 440
Vibrations in a Wide Curved Bar . . . . . B. W. Shaffer and R. N. Hetza, Jr. 447
Interaction Curves for Shear and Bending of Plastic Beams . . . . . P. G. Hodge, Jr. 453
Stress in the Block of an Inset Block . . . . . E. W. Rau, Jr. 457
Relationship of Hencky and von Karman in Plasticity Problems . . . . . Lee Lazzi 461
Collapse of Circular Tubes Under Internal Pressure . . . . . C. D. Weir 464

Discussion of Recent Methods

Problem of Incremental Deformation . . . . . J. N. Goodier 467

Book Reviews

Buckling of Levers Having Uniformly Distributed Mass . . . . . M. D. Gerard 475
Deflections of Circular Shafts of Variable Diameter . . . . . P. P. Chatterjee 477
Approximate Stress Distributions by Superposition . . . . . G. A. Zickert 478
Brief Notes on previously published papers by William Prager; H. H. Kurzweg; R. P. Steidel, Jr., Walter Prager; Bruce Sharma; D. S. Johnson; and M. M. Abbasi 481
Errata 490

SEPTEMBER, 1957

VOL. 24, NO. 3

Transactions of The American Society of Mechanical Engineers

f Applied Mechanics

Published Quarterly by

n Society of Mechanical Engineers

Unsteady Flow of Gas Through a Semi-Infinite Porous Medium

By R. E. KIDDER,[1] LA HABRA, CALIF.

This paper presents an analytic solution to a problem of the transient flow of gas within a one-dimensional semi-infinite porous medium. A perturbation method, carried out to include terms of the second order, is employed to obtain a solution of the nonlinear partial differential equation describing the flow of gas. The zero-order term of the solution represents the solution of the linearized partial differential equation of gas flow in porous media given by Green and Wilts (1).[2]

Nomenclature

The following nomenclature is used in the paper:

- k = permeability, darcys
- μ = viscosity, centipoises
- φ = porosity, fraction
- p = P/P_0
- p_1 = P_1/P_0
- P = pressure within porous medium, atm
- P_0 = initial pressure within porous medium, atm
- P_1 = pressure at outflow face of porous medium, atm
- A = cross-sectional area of porous medium, sq cm
- T = temperature of porous medium, deg F
- Q = rate of outflow of gases from porous medium, standard cc per sec (measured at 60 F and 1 atm)
- x = distance from outflow face of porous medium, cm
- t = time, sec
- τ = dimensionless time parameter
- ξ = dimensionless distance parameter
- w = $(1 - p^2)/\alpha$
- α = $1 - p_1^2$
- z = $\xi/2\sqrt{\tau}$
- $\mathrm{erf}(z)$ = error function of z

Introduction

The unsteady flow of gas through porous media is closely analogous to the unsteady conduction of heat in solids. There is an important difference, however, in that the unsteady conduction of heat in a solid is described by a linear partial differential equation (2), whereas the unsteady flow of gas in a porous medium is described by a nonlinear partial differential equation (3). This difference has caused the problem of unsteady gas flow in porous media to be attacked by different mathematical methods than those commonly employed in problems of the conduction of heat in solids.

Unsteady heat-conduction problems are commonly solved by such analytic methods as the Laplace or Fourier transform, the use of Green's functions, and so on (2). On the other hand, existing solutions of problems of unsteady gas flow in porous media have been obtained by nonanalytic methods (4, 5, 6). These nonanalytic methods consist of approximating the nonlinear partial differential equation of gas flow by an appropriate finite-difference equation, and of solving the difference equation by numerical methods, usually with the aid of digital computing equipment. An exception to this procedure is the approximate method employed by Roberts (7) in which a stepwise forward integration in time is accomplished by joining together the solutions of a sequence of appropriate linearizations of the nonlinear partial differential equation.

In the present paper the solution to a problem of the flow of gas in a porous medium is obtained by analytic rather than numerical methods. The solution is obtained by a perturbation procedure that is carried out to include terms of the second order. It is shown that the zero-order solution obtained by the perturbation method is a solution of the linearized partial differential equation of gas flow in porous media given by Green and Wilts (1). Comparison of the zero-order solution with the solution that includes terms through the second order suggests that results of moderate accuracy can be obtained by solving the linearized equation instead of the rigorous nonlinear equation.

Equations of Gas Flow

The unsteady isothermal flow of gas in a porous medium has been described in the literature (3) by the following nonlinear partial differential equation

$$\nabla^2(P^2) = (2\varphi\mu/k)\frac{\partial P}{\partial t} \quad \ldots\ldots\ldots\ldots\ldots\ldots [1]$$

For the special case of unsteady gas flow in a one-dimensional semi-infinite porous medium extending from x equals zero to x equals infinity, Equation [1] reduces to

$$\frac{\partial}{\partial x}\left(P\frac{\partial P}{\partial x}\right) = (\varphi\mu/k)\frac{\partial P}{\partial t} \quad \ldots\ldots\ldots\ldots\ldots\ldots [2]$$

In the derivation of Equation [1] it is assumed that:

1 The flow of gas follows Darcy's law; i.e., is in the viscous range.

2 The only phase flowing is a gas of constant composition and viscosity.

3 The density of the gas is directly proportional to the pressure (Boyle's law).

4 The permeability of the porous medium is constant and uniform.

5 Gravitational forces are neglected.

The problem to be solved is that of finding a solution $P(x, t)$ of Equation [2], subject to the initial condition

$$P(x, 0) = P_0, \quad 0 < x < \infty \quad \ldots\ldots\ldots\ldots\ldots\ldots [3]$$

and the boundary condition

$$P(0, t) = P_1 < P_0, \quad 0 \leqslant t < \infty \quad \ldots\ldots\ldots\ldots\ldots\ldots [4]$$

---

[1] Senior Research Physicist, California Research Corporation.

[2] Numbers in parentheses refer to the Bibliography at the end of the paper.

Presented at the Applied Mechanics Division Summer Conference, Berkeley, Calif., June 13–15, 1957, of The American Society of Mechanical Engineers.

Discussion of this paper should be addressed to the Secretary, ASME, 29 West 39th Street, New York, N. Y., and will be accepted until October 10, 1957, for publication at a later date. Discussion received after the closing date will be returned.

Note: Statements and opinions advanced in papers are to be understood as individual expressions of their authors and not those of the Society. Manuscript received by ASME Applied Mechanics Division, June 7, 1956. Paper No. 57—APM-13.

That is, it is assumed that the semi-infinite porous medium is initially filled with gas at a uniform pressure P_0; then (at time $t = 0$) the pressure at the outflow face of the porous medium (located at $x = 0$) is suddenly reduced from the value P_0 to a lower value P_1, and thereafter maintained at this reduced pressure P_1.

Having found the solution $P(x, t)$ to Equation [2], subject to the initial and Boundary Conditions [3] and [4], the rate Q at which gas leaves the outflow face of the porous solid can be determined from the relation

$$Q = \frac{AkP_1}{\mu}\left(\frac{540}{460 + T}\right)\left(\frac{\partial P}{\partial x}\right)_{x=0} \quad [5]$$

in which the ideal gas law has been assumed in order to reduce the volumetric rate of efflux to standard conditions of temperature and pressure (60 F and 1 atm).

It will be convenient before proceeding further to introduce the dimensionless pressure $p = P/P_0$, the dimensionless time $\tau = Pgt/\mu\varphi$, and the dimensionless distance $\xi = x/\sqrt{k}$. In terms of these dimensionless variables, Equation [2] and the initial and Boundary Conditions [3] and [4] become, respectively

$$\frac{\partial}{\partial \xi}\left(p\,\frac{\partial p}{\partial \xi}\right) = \frac{\partial p}{\partial \tau} \quad [6]$$

$$p(\xi, 0) = 1, \quad 0 < \xi < \infty \quad [7]$$

$$p(0, \tau) = p_1 = P_1/P_0, \quad 0 \leqslant \tau < \infty \quad [8]$$

Equation [5] giving the volumetric rate of efflux of gas Q becomes

$$Q = qp_1\left(\frac{\partial p}{\partial \xi}\right)_{\xi=0} \quad [9]$$

where

$$q = \frac{\sqrt{k}}{\mu} AP_0^2\left(\frac{540}{460 + T}\right) \quad [10]$$

The solution of Equation [6], subject to Conditions [7] and [8], is obtained by perturbation methods in the following section.

Solution of Equations of Gas Flow

The solution of Equation [6] is facilitated by the introduction of a new dimensionless dependent variable $w(\xi, \tau)$ that is related to the dimensionless pressure p according to

$$p^2 = 1 - \alpha w, \quad 0 < \alpha < 1 \quad [11]$$

in which $\alpha = 1 - p_1^2$. (The parameter α will lie between zero and unity because $p_1 = P_1/P_0$ lies between zero and unity.) Making use of Equation [11], it follows from Equations [6], [7], and [8] that w satisfies the partial differential equation

$$\frac{\partial^2 w}{\partial \xi^2} = (1 - \alpha w)^{-1/2}\,\frac{\partial w}{\partial \tau} \quad [12]$$

subject to the initial and boundary conditions, respectively

$$w(\xi, 0) = 0, \quad 0 < \xi < \infty \quad [13]$$

$$w(0, \tau) = 1, \quad 0 \leqslant \tau < \infty \quad [14]$$

The partial differential Equation [12] can be reduced to an ordinary (nonlinear) differential equation by the introduction of a new independent variable $z = \xi/2\sqrt{\tau}$. Written in terms of z, Equation [12] becomes

$$\frac{d^2 w}{dz^2} + \frac{2z}{\sqrt{(1 - \alpha w)}}\,\frac{dw}{dz} = 0, \quad 0 < \alpha < 1 \quad [15]$$

where w satisfies the terminal conditions

$$w(z = 0) = 1, \quad w(z = \infty) = 0 \quad [16]$$

In order to obtain a solution to Equation [15], subject to the Terminal Conditions [16], a perturbation procedure is employed in which w is expanded as a power series in the parameter α, the coefficients of the various powers of α being unknown functions of the independent variable z to be determined; i.e.

$$w = w^{(0)} + \alpha w^{(1)} + \alpha^2 w^{(2)} + \cdots \quad [17]$$

The radical appearing in Equation [15] is likewise expanded in the absolutely convergent power series

$$(1 - \alpha w)^{-1/2} = 1 + \frac{1}{2}\,\alpha w + \frac{3}{8}\,\alpha^2 w^2 + \cdots \quad [18]$$

The convergence of Power Series [18] is assured because αw $(= 1 - p^2)$ will certainly lie between the values zero and unity.

Substitution of Equations [18] and [17] into Equation [15], and collecting coefficients of like powers of the parameter α, leads to a sequence of linear differential equations to be solved recursively for the functions $w^{(0)}$, $w^{(1)}$, $w^{(2)}$, and so on. The first three equations of the sequence are

$$\frac{d^2 w^{(0)}}{dz^2} + 2z\,\frac{dw^{(0)}}{dz} = 0 \quad [19]$$

$$\frac{d^2 w^{(1)}}{dz^2} + 2z\,\frac{dw^{(1)}}{dz} = -\frac{z}{2}\,\frac{d}{dz}\,[w^{(0)}]^2 \quad [20]$$

$$\frac{d^2 w^{(2)}}{dz^2} + 2z\,\frac{dw^{(2)}}{dz} = -z\,\frac{d}{dz}\left\{w^{(0)}w^{(1)} + \frac{1}{4}\,[w^{(0)}]^2\right\} \quad [21]$$

The terminal conditions to be satisfied by the functions $w^{(i)}$ are

$$w^{(0)}(z = 0) = 1, \quad w^{(0)}(z = \infty) = 0 \quad [22]$$

$$w^{(i)}(z = 0) = w^{(i)}(z = \infty) = 0, \quad i = 1, 2, 3, \ldots \quad [23]$$

The solution of the zero-order Equation [19] is readily found to be

$$w^{(0)} = 1 - \operatorname{erf}(z) \quad [24]$$

in which the notation $\operatorname{erf}(z)$ denotes the error function of the argument z, the error function being defined as (6)

$$\operatorname{erf}(z) = (2/\pi^{1/2}) \int_0^z \exp(-x^2)\,dx \quad [25]$$

Making use of the result, Equation [24], the solution of the first-order Equation [20] is found to be

$$w^{(1)} = -(1/2\pi)\{w^{(0)}[1 + \pi^{1/2} z \exp(-z^2)] - \exp(-2z^2)\} \quad [26]$$

Similarly, employing the results, Equations [24] and [25], the solution to the second-order Equation [21] can be obtained. The solution to the second-order equation is rather lengthy and is given in the Appendix.

It is, in principle, possible to continue the calculations to obtain still higher-order terms in the Series Solution [17]. However, the complexity of the calculations increases rapidly with increasing order of the terms and it is not worth while to continue this method of calculation beyond the second-order term. Fortunately, as the tabulated values, Table 1, of the first three terms indicate, very little error is likely to be introduced by the neglect of terms of higher order than the second. For this reason, a close approximation to the exact solution of Equation [15] is given by the truncated series

$$w = w^{(0)} + \alpha w^{(1)} + \alpha^2 w^{(2)} \quad [27]$$

TABLE 1 NUMERICAL VALUES OF COEFFICIENTS APPEARING IN EQUATION [28]

Argument z	Zero-order coefficient $w^{(0)}$	First-order coefficient $w^{(1)}$	Second-order coefficient $w^{(2)}$
0.0	1.00000	0.00000	0.00000
0.1	0.88754	−0.01004	−0.00343
0.2	0.77730	−0.01893	−0.00611
0.3	0.67137	−0.02584	−0.00766
0.4	0.57161	−0.03037	−0.00809
0.5	0.47950	−0.03245	−0.00763
0.6	0.39614	−0.03236	−0.00661
0.7	0.32220	−0.03052	−0.00534
0.8	0.25790	−0.02748	−0.00410
0.9	0.20309	−0.02376	−0.00299
1.0	0.15730	−0.01982	−0.00210
1.2	0.08969	−0.01253	−0.00094
1.5	0.03389	−0.00514	−0.00025
2.0	0.00468	−0.00074	−0.00003

Substitution of this result into Equation [11] gives the final result

$$p^2 = 1 - \alpha w^{(0)} - \alpha^2 w^{(1)} - \alpha^3 w^{(2)} \ldots\ldots\ldots [28]$$

in which

$$z = \xi/2\sqrt{\tau} = \left(\frac{\varphi\mu}{kP_0}\right)^{1/2} (x/2t^{1/2}) \ldots\ldots\ldots [29]$$

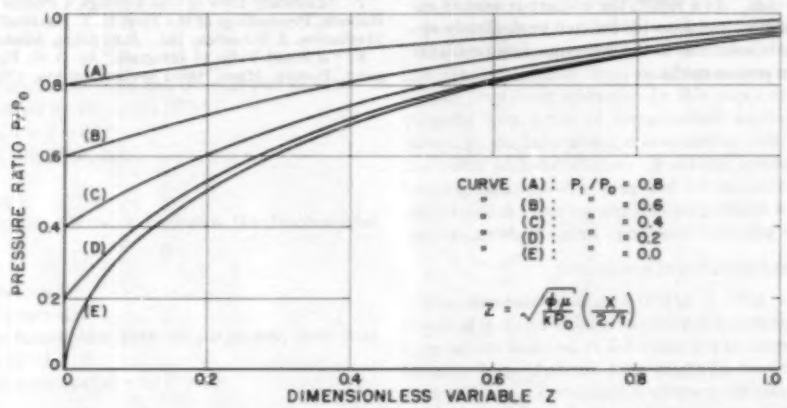

FIG. 1 PRESSURE RATIO P/P_0 AS A FUNCTION OF DIMENSIONLESS VARIABLE z

$$\alpha = 1 - p_1^2 = (P_0^2 - P_1^2)/P_0^2 \ldots\ldots\ldots [30]$$

$$p = P/P_0 \ldots\ldots\ldots [31]$$

Equations [28] through [31], together with the table of values of $w^{(0)}$, $w^{(1)}$, and $w^{(2)}$, Table 1, permit the pressure P of the gas within the porous medium to be determined readily for any point x and time t. Graphs of P/P_0 versus the dimensionless variable z, prepared from Equation [28] together with the tabulated values of $w^{(0)}$, $w^{(1)}$, and $w^{(2)}$, are given in Fig. 1 for several values of the parameter P_1/P_0.

LINEARIZATION OF PARTIAL DIFFERENTIAL EQUATION OF GAS FLOW IN POROUS MEDIA

If the first and second-order terms are neglected in the Expression [28], the zero-order solution

$$p^2 = 1 - \alpha w \ldots\ldots\ldots [32]$$

is obtained. This zero-order solution may be written in the alternative form

$$(P^2 - P_1^2)/(P_0^2 - P_1^2) = \text{erf}\left[(x/2t^{1/2})\left(\frac{\varphi\mu}{kP_0}\right)^{1/2}\right] \ldots [33]$$

To the same degree of approximation employed in obtaining Equation [33], the rate Q at which gas leaves the outflow face of the porous medium is given by

$$Q = \frac{1}{2} A(P_0^2 - P_1^2)\left(\frac{540}{460 + T}\right)\left(\frac{k\varphi}{\pi\mu P_a t}\right)^{1/2} \ldots\ldots [34]$$

A comparison of the values of P/P_0 obtained from the zero-order Solution [32] with the more accurate values obtained from Equation [28] shows that the values obtained from the two solutions differ by approximately 5 per cent at most. The largest discrepancy occurs in the extreme case in which P_1/P_0 approaches zero. Consequently, it appears that the accuracy of the zero-order solution will be sufficient for many engineering purposes.

Equation [33] is the exact solution of the linear partial differential equation

$$\frac{\partial^2}{\partial x^2}(P^2) = \frac{\varphi\mu}{kP_0}\frac{\partial}{\partial t}(P^2) \ldots\ldots\ldots [35]$$

subject to the initial and Boundary Conditions [3] and [4], respectively. (Equation [35] is a linear differential equation of the dependent variable P^2). Equation [35] is identical in form with the linearization of the nonlinear equation of gas flow given by Green and Wilts (1). The constant factor multiplying the time derivative on the right of Equation [35] is numerically different, however, in that Green and Wilts employ a constant value of P intermediate between P_0 and P_1 rather than the initial value P_0 itself.

The accuracy of the solution of the linear Equation [35], as applied to the particular problem of gas flow in a semi-infinite porous medium, suggests that the equation

$$\nabla^2(P^2) = \frac{\varphi\mu}{kP_0}\frac{\partial}{\partial t}(P^2) \ldots\ldots\ldots [36]$$

can be employed to obtain approximate solutions to other problems of gas flow in porous media as well. In using Equation [36], it is of course assumed that the initial state of the system is one in which the gas is not flowing and is at the uniform pressure P_0. It is evident that, in general, the approximate solutions obtained by use of the linearized Equation [36] will be most accurate in those cases in which the pressure P within the porous medium never differs greatly from the initial pressure P_0; i.e., cases in which P/P_0 is always of the order of unity.

It will be noted that Equation [1] can be written in the form

$$\nabla^2(P^2) = \frac{\varphi\mu}{kP}\frac{\partial}{\partial t}(P^2) \ldots\ldots\ldots [37]$$

so that Equation [36] is a particular linearization of Equation [37] in which the factor P in the denominator of Equation [37] is replaced by its initial value P_0. Since the left-hand members of Equations [36] and [37] are identical, it follows that the linearized Equation [36] becomes exact in the steady state.

Examples of typical boundary conditions to be imposed on the dependent variable P^2 of Equation [36] are the following:
Surfaces of constant pressure

$$P^2 = \text{const} \quad [38]$$

Impermeable surfaces

$$\frac{\partial(P^2)}{\partial n} = 0 \quad [39]$$

Surfaces of constant mass flow

$$\frac{\partial(P^2)}{\partial n} = \text{const} \quad [40]$$

in which the partial derivative with respect to n denotes the normal derivative at the surface.

Equation [36] is identical in form to the classical equation of heat conduction in solids. As a result, the numerous worked examples of heat-conduction problems (2) become immediately applicable as approximate solutions to the corresponding problems in the flow of gases in porous media.

Appendix

The solution $w^{(2)}$ of the second-order equation is the following

$$w^{(2)} = -(1/\pi)w^{(1)} + (1/8\pi^{5/2})z \exp(-3z^2) - (1/2\pi)w^{(0)} - (1/16\pi^{1/2})z(5 - 2z^2)\exp(-z^2)[w^{(0)}]^2 + (1/4\pi)(2 - z^2) \exp(-2z^2)w^{(0)} + (3^{5/2}/16\pi)[\text{erf}[3^{1/2}z] - \text{erf}(z)] \quad [41]$$

BIBLIOGRAPHY

1 "Nonsteady Flow of Gas Through a Porous Wall," by L. Green, Jr., and C. H. Wilts, Proceedings of the First U. S. National Congress of Applied Mechanics, J. Edwards, Inc., Ann Arbor, Mich., 1952, pp. 777–781.

2 "Conduction of Heat in Solids," by H. Carslaw and J. Jaeger, Clarendon Press, Oxford, England, 1947.

3 "Flow of Homogeneous Fluids," by M. Muskat, second printing, J. Edwards, Inc., Ann Arbor, Mich., 1946.

4 "Unsteady Flow of Gas Through Porous Media: One-Dimensional Case," by J. S. Aronofsky and R. Jenkins, Proceedings of the First U. S. National Congress of Applied Mechanics, J. Edwards, Inc., Ann Arbor, Mich., 1952, pp. 763–771.

5 "Unsteady Radial Flow of Gas Through Porous Media," by R. Jenkins and J. S. Aronofsky, JOURNAL OF APPLIED MECHANICS, Trans. ASME, vol. 75, 1953, pp. 210–214.

6 "Calculation of Unsteady-State Gas Flow Through Porous Media," by G. Bruce, D. Peaceman, H. Rachford, and J. Rice, *Journal of Petroleum Technology*, Trans. AIME, vol. 198, 1953, pp. 79–92.

7 "Unsteady Flow of Gas Through a Porous Medium," by R. C. Roberts, Proceedings of the First U. S. National Congress of Applied Mechanics, J. Edwards, Inc., Ann Arbor, Mich., 1952, pp. 773–776.

8 "A Short Table of Integrals," by B. O. Pierce, Ginn and Company, Boston, Mass., third revised edition, 1929, pp. 115–120.

A Type of Flame-Excited Oscillation in a Tube

By J. J. BAILEY,[1] HOUSTON, TEXAS

Propane-air mixtures were burned in an effectively open-ended tube containing a screen flameholder. Two types of instability were observed. Of these, one is described in some detail. A driving mechanism is proposed and examined in the light of Rayleigh's criterion. Finally, a linear, one-dimensional theory is presented, taking into account both the driving and damping effects in the system. The predictions of this theory are shown to be in good agreement with the experimental results.

Nomenclature

The following nomenclature is used in the paper:
(Unless otherwise stated, all units may be assumed to be in foot pound second degrees F units.)

- a = velocity amplitude of initial periodic disturbance in cold region of tube
- C = acoustic radiation coefficient
- c = sonic velocity
- d = distance of flameholder from downstream end of tube
- F = a function defined by Equation [17]
- i = by definition, $i = (-1)^{1/2}$
- k = ratio of sonic velocities, $\bar{c}_2/c_1$
- L = tube length
- $\mathbf{M}$ = Mach number
- N = harmonic number ($N = 1$ indicates the fundamental mode)
- p = pressure
- q = rate of heat release
- R = tube radius (internal)
- r = dimensionless flameholder position parameter, such that $r = (L_0 - d_0)/L_0$
- s = a flame speed, such that $s = v_1(\xi) - \dot{\xi}$
- T = temperature
- v = velocity
- x = a co-ordinate of length, positive downstream from flameholder
- α = by definition, $\alpha = \sigma/\omega$, a dimensionless parameter
- Λ = by definition, $\Lambda = \bar{\rho}_1/\bar{\rho}_2$
- λ = wave length
- ξ = x-co-ordinate of flame front
- ρ = density
- σ = by definition, $\sigma = \left.\dfrac{ds}{d\xi}\right|_{\bar{\xi}}$
- ω = angular frequency (radians/sec)
- ω_0 = natural frequency (without driving or damping effects)
- ω_D = frequency corrected for effects of flame only
- ω_L = frequency corrected for effects of acoustic radiation only
- $\tilde{\omega}$ = a dimensionless frequency parameter, such that $\tilde{\omega} = \omega L_0/c_1$

Subscripts

- 0 implies end corrections included in a length
- 1 implies a quantity in the cold region of the tube
- 2 implies a quantity in the hot region of the tube

Superscripts

- $\bar{}$ implies a time-averaged quantity (also sometimes a space-averaged quantity)
- $'$ implies a fluctuating quantity, whose time average is zero
- $\dot{}$ implies differentiation with respect to time

Introduction

Recently there has been considerable research on questions of flame stability and thermoacoustic oscillation. This emphasis has resulted largely from recent developments in aircraft and missile propulsion systems. In this paper are described two apparently new types of flame-excited oscillation in a tube observed in the laboratory, one occurring with cellular flames and the other with flat flames. A driving mechanism depending on varying flame speed is proposed for the latter case and a simple analysis of the driving and damping effects is made. The resulting theory shows good agreement with the experimental facts.

Apparatus and Experiment

The apparatus is shown in Fig. 1. The working section consisted of a Vycor tube containing a flameholder. The tube was open at one end and at the other it was connected to a tank sufficiently large that the tube might be considered open-ended at that end also. Combustible propane-air mixtures were supplied to the tube (through the tank) at known rates of flow and mixture strengths. Fig. 2 shows a typical flameholder. The flame-holding part is effectively a plane of brass gauze (30 mesh, 0.012-in-diam wire) lying perpendicular to the axis of the tube across the whole section. Other holders, differing in detail only, were used with little effect on the results obtained.

In practice, a combustible mixture was supplied to the tube with a mean flow velocity v_1, somewhat greater than the flame speed s, so that on ignition a flame was stabilized at the downstream end of the tube. On decreasing the flow velocity v_1, the flame descended into the tube, eventually taking up a plane configuration just above the gauze flameholder.

In the case of some rich mixtures the configuration might be cellular rather than flat and a type of self-excited oscillation apparently associated with the cellular configuration was observed. This instability, which occurred only over a very narrow range of mixtures, manifested itself by the build-up of a musical note produced by the apparatus. It was not investigated in detail and has not been explained. The regions in which these cellular phenomena occurred will be seen in Fig. 3.

In all cases (rich or lean) the flame would eventually take up a flat configuration above the holder, and as v_1 was still further reduced, this plane flame would approach the gauze more and more closely until it also became unstable. A musical note would then

[1] Engineer, Shell Development Company; formerly, Research Assistant, Harvard University, Cambridge, Mass.

Presented at the Applied Mechanics Division Summer Conference, Berkeley, Calif., June 13–15, 1957, of The American Society of Mechanical Engineers.

Discussion of this paper should be addressed to the Secretary, ASME, 29 West 39th Street, New York, N. Y., and will be accepted until October 10, 1957, for publication at a later date. Discussion received after the closing date will be returned.

Note: Statements and opinions advanced in papers are to be understood as individual expressions of their authors and not those of the Society. Manuscript received by ASME Applied Mechanics Division, July 31, 1956. Paper No. 57—APM-26.

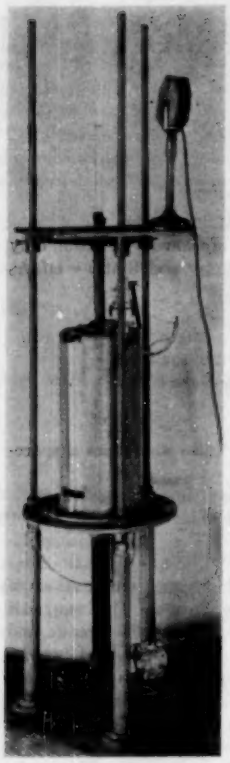

FIG. 1 THE APPARATUS

FIG. 2 A TYPICAL FLAMEHOLDER (The flame is held on brass screen which covers cross section of tube.)

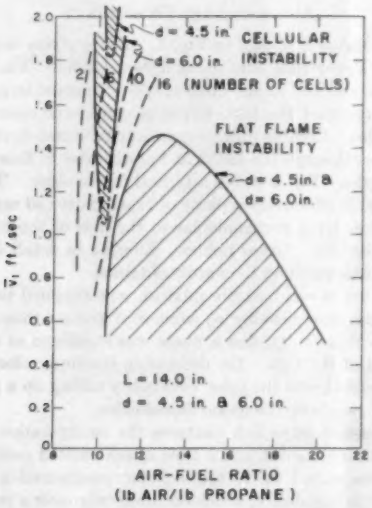
d = 4.5 in.
d = 6.0 in.
CELLULAR INSTABILITY
/16 (NUMBER OF CELLS)
FLAT FLAME INSTABILITY
d = 4.5 in. & d = 6.0 in.
L = 14.0 in.
d = 4.5 in. & 6.0 in.
$\bar{v}_1$ ft/sec
AIR-FUEL RATIO
(lb AIR/lb PROPANE)

FIG. 3 REGIONS OF INSTABILITY AND APPROXIMATE NUMBER OF CELLS, ON AXES OF MEAN FUEL-MIXTURE VELOCITY AND AIR-FUEL RATIO

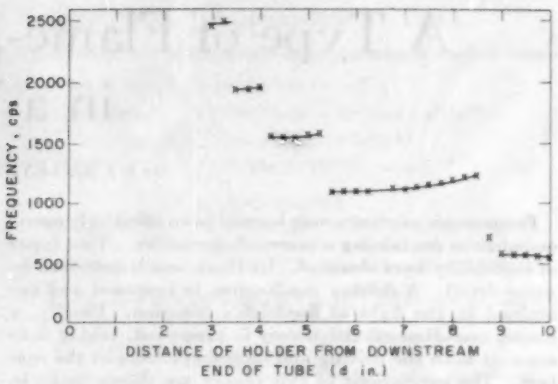

FIG. 4 FREQUENCIES OBSERVED VERSUS DISTANCE OF HOLDER FROM DOWNSTREAM END OF TUBE (Tube length L = 14.0 in.)

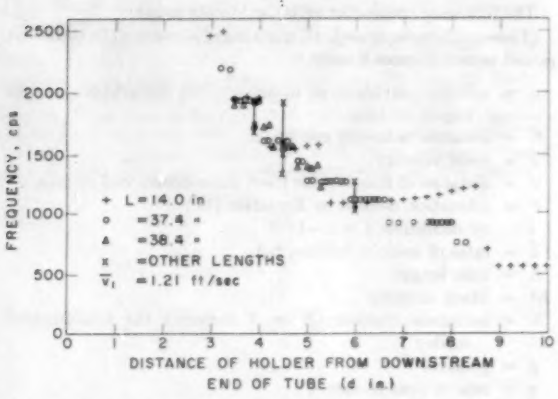

FIG. 5 FREQUENCIES OBSERVED VERSUS DISTANCE OF HOLDER FROM DOWNSTREAM END OF TUBE, PLOTTED FOR VARIOUS TUBE LENGTHS

be emitted, at first very quiet and very pure, but increasing in intensity until harmonics and later subharmonics also would be heard, these latter being associated with quite violent flame movement over a region perhaps $^1/_8$ in. long. Fig. 3 shows the region of instability for the flat flames as a function of upstream velocity v_1, and mixture strength, using a tube of length L = 14 in. with the flameholder a distance d = 4.5 in. from its downstream end. The region in fact was found to have little dependence on L and d over a wide range of values. It will be noted that it is bounded by a curve similar to the flame-speed curve for propane-air mixtures.

Changes in L and d, however, affect considerably the frequency of the note initially heard. Fig. 4 shows the frequencies observed for L = 14 in. and varying d. It will be shown that these frequencies are (very closely) natural frequencies of the tube. Fig. 5 shows the frequencies heard for a number of different values of both L and d. A criterion deciding which particular natural frequency is heard will be developed and the reason for the distinctive arrangement of the points in Figs. 4 and 5 will become apparent.

A Driving Mechanism and Rayleigh's Criterion

The first essential of an explanatory theory for the phenomena described is a driving mechanism. A possible driving mechanism attributable to the flame will first be analyzed. Then by consideration of the system as a whole and the losses involved, a more complete theory will be advanced. The treatment will be linear and one-dimensional and the driving and damping effects will be treated as (complex) perturbations to the natural frequencies.

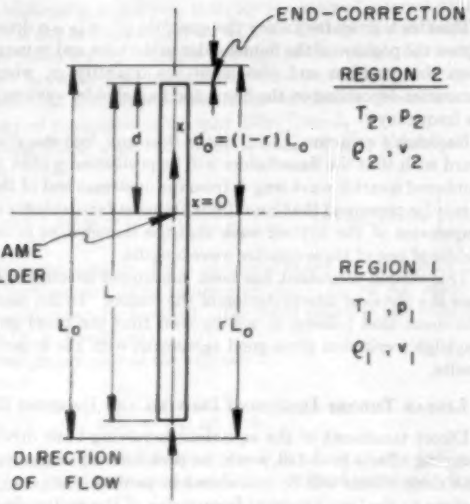

FIG. 6 NOMENCLATURE

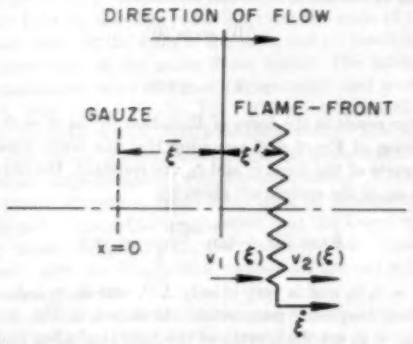

FIG. 7 QUANTITIES NEAR THE FLAME-FRONT. NOTE: $\bar{\xi} << \lambda$

The nomenclature used is shown in Figs. 6 and 7. It will be noted that the subscripts 1 and 2 refer to the regions upstream and downstream from the flame, respectively, and that the subscript 0 implies that end corrections have been included in lengths. The properties of particular interest are velocity v, temperature T, pressure p, and density ρ, and all these will be represented as consisting of time-average and fluctuating parts denoted $^-$ and $'$, respectively; thus the upstream velocity $v_1 = \bar{v}_1 + v_1'$, etc. All properties are considered as varying in space only with x, a coordinate of length with origin in the plane of the flameholder.

Then if the flame is considered as a discontinuity in the fluid properties at $x = \xi$, a flame speed s can be defined

$$s = v_1(\xi) - \dot{\xi}$$

or

$$s \simeq v_1(0) - \dot{\xi} \quad \ldots\ldots [1]$$

since experimentally $\xi \ll \lambda$, the wave length of the disturbances.

Now it was observed in the description of the foregoing experiment that once the flame had taken up a flat configuration just above the flameholder, further decreases in v_1 caused it to move still closer to the holder. It will be postulated then that $s = s(\xi)$, or

$$s \simeq s(\bar{\xi}) + \sigma\xi' \quad \ldots\ldots [2]$$

for small ξ', where

$$\sigma = \left.\frac{ds}{d\xi}\right|_{\bar{\xi}}$$

a positive constant with dimensions sec^{-1}. The physical reason for such a form for $s(\xi)$ is not clear, though it is likely to be due to a heat transfer, chemical, or aerodynamic effect of the holder. It must be observed also that this form of s [$s = s(\xi)$ and σ positive] was observed for steady flows—it will be assumed for unsteady flows also, a reasonable enough procedure, perhaps, for want of other information.

Now, since $\bar{v}_1(0) = s(\bar{\xi})$ and $\dot{\bar{\xi}} = \dot{\xi}'$

$$\sigma\xi' = v_1'(0) - \dot{\xi}'$$

Consider an initial small periodic disturbance such that $v_1'(0) = ae^{i\omega t}$

giving

$$\dot{\xi}' + \sigma\xi' - ae^{i\omega t} = 0$$

The solution of this equation is

$$\xi' = \frac{\sigma - i\omega}{\sigma^2 + \omega^2} ae^{i\omega t}$$

or, putting $\sigma/\omega = \alpha$, a dimensionless parameter

$$\xi' = \frac{\alpha - i}{\alpha^2 + 1} \frac{a}{\omega} e^{i\omega t} \quad \ldots\ldots [3]$$

and

$$\dot{\xi} = \frac{1 + \alpha i}{\alpha^2 + 1} ae^{i\omega t} \quad \ldots\ldots [4]$$

From the continuity of mass across the flame front

$$\rho_1(v_1 - \dot{\xi}) = \rho_2(v_2 - \dot{\xi}) \quad \ldots\ldots [5]$$

It can be shown that $(\rho'\bar{v})/(\bar{\rho}v') = 0(\mathbf{M})$, the Mach number (about 10^{-3} in this case) at all points not near velocity nodes and it will be seen later that in these cases of instability the flame front is not near a velocity node. So, subtracting the time-average part from Equation [5] and neglecting small quantities of the second order and of the order of the Mach number

$$\frac{\bar{\rho}_1}{\bar{\rho}_2}(v_1' - \dot{\xi}) = (v_2' - \dot{\xi})$$

Now

$$\frac{\bar{\rho}_1}{\bar{\rho}_2} = \frac{\bar{T}_2}{\bar{T}_1} + 0(\mathbf{M}_1^2) = \Lambda, \text{ say}$$

Then

$$v_2' = \Lambda v_1' - (\Lambda - 1)\dot{\xi}'$$

or from (4)

$$v_2'(0) = \frac{(\Lambda\alpha^2 + 1) - i\alpha(\Lambda - 1)}{\alpha^2 + 1} v_1'(0) \quad \ldots\ldots [6]$$

It will be noted that $v_2' \cong v_1'$ for α small, and $v_2' \simeq \Lambda v_1'$ for α large. The phase difference between v_1' and v_2' cannot exceed about 49 deg for $\Lambda = 7$, and tends to zero for α large or small.

Applying the momentum equation at the flame front

$$p_1 - p_2 = \rho_2 v_2^2 - \rho_1 v_1^2$$

Subtracting the time-average part of this equation and making the same approximations as before gives

$$p_1' - p_2' = \bar{\rho}_1\bar{v}_1(v_2' - v_1')$$

which may be rearranged as

$$1 - \frac{p_2'}{p_1'} = \frac{\rho_1'\bar{v}_1^2}{p_1'}\frac{\bar{\rho}_1 v_1'}{\rho_1'\bar{v}_1}\left[\frac{v_2'}{v_1'} - 1\right]$$

So, noting that $p_1'/\rho_1' = c_1^2$ and $(\rho_1'\bar{v}_1)/(\bar{\rho}_1 v_1') = 0(\mathsf{M}_1)$

$$1 - \frac{p_2'}{p_1'} = 0(\mathsf{M}_1)$$

Or, to the accuracy of this treatment

$$p_2'(0) = p_1'(0) \quad \ldots\ldots\ldots\ldots\ldots\ldots [7]$$

Before proceeding with the more exact analysis, in order to make clearer the significance of the parameters involved, it is convenient to examine the nature of the driving according to "Rayleigh's criterion." This famous statement[1] points out that (lossless) thermoacoustic systems are unstable to small periodic disturbances, if the fluctuating heat input is at a position such that it has a component in phase with the pressure fluctuations, i.e., $p' \cdot q' > 0$, where q is the rate of heat input.

In the present case it will be assumed that the combustion is always complete, so that $q = Cs$, where C is some real constant; i.e.

$$q' = Cs'$$
$$= C\sigma\xi'$$

or, from Equation [3]

$$q' = C\frac{\alpha^2 - i\alpha}{\alpha^2 + 1}v_1'(0)$$

Hence

$$[p' \cdot q']_{x=0} = C\frac{\alpha}{\alpha^2 + 1}[|p'||v'|]_{x=0} \quad \ldots\ldots\ldots [8]$$

$\alpha/(\alpha^2 + 1)$ is very small for α small or large, but rises to a maximum value of $^1/_2$ at $\alpha = 1$. It is of interest to note the physical reasons for this form. For α small the available fluctuating heat input, $|q'|$, is very small (i.e., nearly all the heat input is in the steady component $\bar{q}$), and vice versa for α large. On the other hand, for α small the phasing between p' and q' is very favorable

i.e. $$\frac{p' \cdot q'}{|p'||q'|} \simeq 1$$

for α small, while for α large p' and q' are almost exactly out of phase.

The method of running the apparatus previously described (i.e., decreasing $\bar{\xi}$ until the unstable region is reached) amounts in practice to starting with α very small and then, by increasing

$$\left.\frac{ds}{d\xi}\right|_{\bar{\xi}}$$

increasing α and $\alpha/(\alpha^2 + 1)$ also to the stage where a sound is heard—provided this occurs for some $\alpha < 1$. It must be noted that there is no physical certainty that values of α as great as 1 can in fact be attained for any given flame and flameholder system.

The value of $|p'||v'|$ varies (in the lossless case) sinusoidally in the tube, being zero at each velocity and pressure node. An open-ended tube contains effectively an even number of quarter-wave length and the quantity $|p'||v'|$ is positive in odd-numbered quarter wave lengths, counting from the upstream end of the tube.

[1] "The Explanation of Certain Acoustical Phenomena," by Lord Rayleigh, *Nature*, vol. 18, July 18, 1878, p. 319.

Thus for a given frequency the quantity $p' \cdot q'|_{x=0}$ depends in sign on the position of the flameholder in the tube and in magnitude upon this position and also upon the quantity α, which is a parameter depending on the flame and flameholder system and on the frequency.

Rayleigh's criterion, then, states that any frequency may be heard such that the flameholder will be positioned within an odd-numbered quarter wave length from the upstream end of the tube. It may be presumed that conditions are most favorable for natural frequencies of the system such that the flameholder is near the middle of one of these quarter wave lengths.

This simple treatment has been considered because it emphasizes the physical interpretation of the results. In the more basic treatment that follows, it will be seen that the blind appeal to Rayleigh's criterion gives good agreement with the experimental results.

A Linear Theory Including Driving and Damping Effects

Direct treatment of the equations involving both driving and damping effects in detail would be prohibitively complicated, so that these effects will be considered in turn as (complex) perturbations to the (real) natural frequencies of the system in the absence of driving and damping.

In the absence of driving and damping effects the boundary conditions at the flame front can be written

$$p_1'(0) = p_2'(0) \quad \ldots\ldots\ldots\ldots\ldots\ldots [7]$$

and

$$v_1'(0) = v_2'(0) \quad \ldots\ldots\ldots\ldots\ldots\ldots [9]$$

This latter result is the form of Equation [6] as $\alpha \to 0$. Using the notation of Fig. 6 and assuming that the sonic velocities in the two parts of the tube c_1 and $\bar{c}_2$, are constant, the natural frequencies ω_0, of the system are given by

$$\bar{k}\tan\bar{\omega}_0 r + \tan\frac{\bar{\omega}_0(1-r)}{\bar{k}} = 0 \quad \ldots\ldots\ldots [10]$$

where $\bar{k} = \bar{c}_2/c_1$ and is very closely $\Lambda^{1/2}$, and $\bar{\omega}_0 = \omega_0 L_0/c_1$, a dimensionless frequency parameter. As shown in Fig. 6, rL_0 and $(1-r)L_0 = d_0$ are the lengths of the tube (including end corrections) upstream and downstream, respectively, from the flameholder.

In the actual experiment T_2 (and so c_2 also) varied considerably over the volume concerned. The assumption of $c_2 = \bar{c}_2$ constant is made for mathematical convenience and it apparently gives good results. The natural frequencies of the system have been calculated assuming c_2 decreasing exponentially with x (a much closer approximation to the physical situation), but the differences are not significant, though the additional mathematical complication is very considerable.

It was shown earlier that the boundary conditions at the flame front taking into account the driving (or damping) effect of the flame are

$$p_1'(0) = p_2'(0) \quad \ldots\ldots\ldots\ldots\ldots\ldots [7]$$

and

$$v_2'(0) = \frac{(\bar{k}^2\alpha^2 + 1) - i\alpha(\bar{k}^2 - 1)}{\alpha^2 + 1}v_1'(0) \quad \ldots\ldots [6]$$

Application of these boundary conditions leads to the equation for the (complex) frequencies of the system, $\tilde{\omega}_D$

$$\bar{k}\tan\tilde{\omega}_D r + \frac{(\bar{k}^2\alpha^2 + 1) - i\alpha(\bar{k}^2 - 1)}{\alpha^2 + 1}\tan\tilde{\omega}_D\frac{(1-r)}{\bar{k}} = 0 \quad \ldots\ldots [11]$$

It is reasonable to suppose that, for the cases of interest at any rate, $\tilde{\omega}_D$ is not far removed from $\tilde{\omega}_0$. As the model that leads to the expression for $\tilde{\omega}_D$ includes driving (or damping), $\tilde{\omega}_D$ will be expected to contain an imaginary component (corresponding to an exponential time-dependence of the amplitude of oscillation). Also the real component of $\tilde{\omega}_D$ may differ from $\tilde{\omega}_0$.

Treating $\tilde{\omega}_D$ as a perturbed value of $\tilde{\omega}_0$, it may be shown to have the value

$$\tilde{\omega}_D = \tilde{\omega}_0 \left\{ 1 + (\alpha - i) \frac{\bar{k}^2 - 1}{\pi(N + 1/2)} \frac{\alpha}{\alpha^2 + 1} \cos \tilde{\omega}_0 r \sin \tilde{\omega}_0 r \right\} \quad [12]$$

where N is the number of the harmonic heard ($N = 1$ being the fundamental mode). The assumption $|\tilde{\omega}_D - \tilde{\omega}_0| \ll |\tilde{\omega}_0|$ made in the derivation can be justified. The form above is not valid for N small ($N = 1$ or 2, say).

The imaginary part of the expression

$$-i\tilde{\omega}_0 \frac{\bar{k}^2 - 1}{\pi(N + 1/2)} \frac{\alpha}{\alpha^2 + 1} \cos \tilde{\omega}_0 r \sin \tilde{\omega}_0 r$$

is of particular interest. Since at $x = 0$, $\cos \tilde{\omega}_0 r \sin \tilde{\omega}_0 r \propto |p_1'||v_1'|$, the form of this result agrees with that derived previously from Rayleigh's criterion.

The effects of damping will be considered next, using an essentially similar approach.

There are three principal causes of energy loss from the oscillation: (*a*) Loss by acoustic radiation from the ends of the tube, (*b*) viscous losses at the walls of the tube, and (*c*) losses caused by the pressure drop at the gauze flame holder. The tubes used in these experiments were effectively open-ended and were from 8 to 56 in. long and of 1/4 in. ID. The gauze flameholders were made of 30-mesh screen (0.012-in-diam wire). For apparatus of these dimensions it can be shown that the losses due to acoustic radiation are large compared with the other losses. In the following treatment, therefore, losses other than by acoustic radiation are neglected. It must be emphasized that the losses of interest are only those associated with the unsteady flow. Losses associated only with the steady flow component are not relevant to the present argument.

The wave form in a tube with an open end has been shown by Levine and Schwinger[2] to be effectively the same as it would be if the outgoing wave is considered as reflected a short distance (the end correction) from the end of the tube as an incoming wave with $(1 - C)$ of the amplitude of the outgoing wave. The quantity C is called the radiation coefficient.

If C_1 and C_2 are the radiation coefficients at the upstream and downstream ends of the tube, respectively, it can be shown (again for $N > 2$) that the complex frequencies $\tilde{\omega}_L$, due to these losses are

$$\tilde{\omega}_L = \tilde{\omega}_0 \left\{ 1 + \frac{i}{2(N + 1/2)\pi} \left[C_1 + \bar{k} C_2 \left(1 - \frac{\bar{k}^2 - 1}{\bar{k}^2} \cos^2 \tilde{\omega}_0 r \right) \right] \right\} \quad [13]$$

The imaginary part of this expression gives the rate of exponential decay of the amplitude of the initial periodic disturbance considered.

These two results, Equations [12] and [13], are obtained by considering the two cases (with driving effects and with losses) as perturbations on the lossless case with no driving (the usual assumptions in calculations of "natural frequencies"). These perturbations may be considered together to arrive at the (complex) frequency in the face of both driving effects and losses, giving the result

$$\tilde{\omega} = \tilde{\omega}_0 \left\{ 1 + \frac{1}{(N + 1/2)\pi} \left[(\bar{k}^2 - 1) \frac{\alpha^2}{\alpha^2 + 1} \cos \tilde{\omega}_0 r \sin \tilde{\omega}_0 r \right] + \frac{i}{(N + 1/2)\pi} \left[\frac{C_1}{2} + \bar{k} \frac{C_2}{2} \left(1 - \frac{\bar{k}^2 - 1}{\bar{k}^2} \cos^2 \tilde{\omega}_0 r \right) - (\bar{k}^2 - 1) \frac{\alpha}{\alpha^2 + 1} \cos \tilde{\omega}_0 r \sin \tilde{\omega}_0 r \right] \right\} \quad [14]$$

The stability of the system depends on the sign of the imaginary coefficient of $\tilde{\omega}_0$.

According to the results of Levine and Schwinger a good approximation for C is $1/3[\omega R/c]^3$, where R is the radius of the tube; so that for a given experimental arrangement C_1 and C_2 are closely proportional to $\tilde{\omega}_0^3$ and $C_1 \simeq \bar{k}^3 C_2$. $\bar{k}^3$ is substantially constant ($\bar{k} > 1$) for d constant and $\tilde{\omega}_0 r = rL\omega_0/c_1$ and so depends on ω_0 (r being fixed). That is, the expression from which the stability is determined depends for given physical conditions on the frequency considered.

At this stage it is of interest to compare the foregoing theoretical results with the experimental results and to make estimates of some of the important parameters. It will be recalled that the method of performing the experiment was to light the flame under conditions such that no noise was heard (stable) and then in effect to increase α until the instability occurred. The initial frequency heard was noted and, in so far as possible, the conditions of neutral stability.

It will be shown later that under the conditions of the experiment

$$\mathrm{Re}\left[\frac{\omega}{\omega_0} - 1 \right] = O(10^{-3})$$

so that the observed frequencies ω may be compared with the calculated natural frequencies ω_0. To make this comparison the value of $\bar{k}$ is required. To this end a series of temperature traverses was made in the hot region of the tube. A value $\bar{k} = 1.80$ has been used for comparison of the theoretical with the experimental results. This value seems perhaps unreasonably low, since the temperature ratio at the flame front is approximately 7.

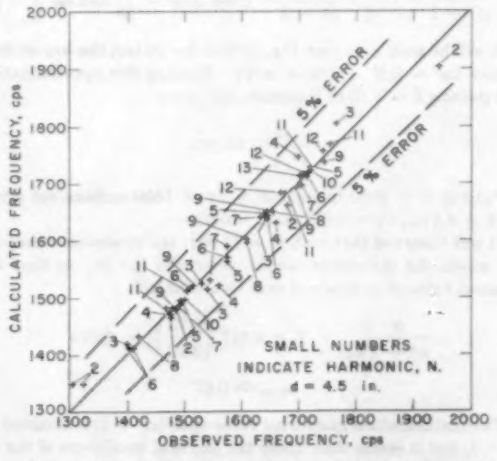

FIG. 8 COMPARISON OF OBSERVED FREQUENCIES WITH THOSE CALCULATED USING $\bar{k} = 1.80$

[2] "On the Radiation of Sound From an Unflanged Circular Pipe," by H. Levine and J. Schwinger, *Physical Review*, vol. 73, February, 1948, p. 383.

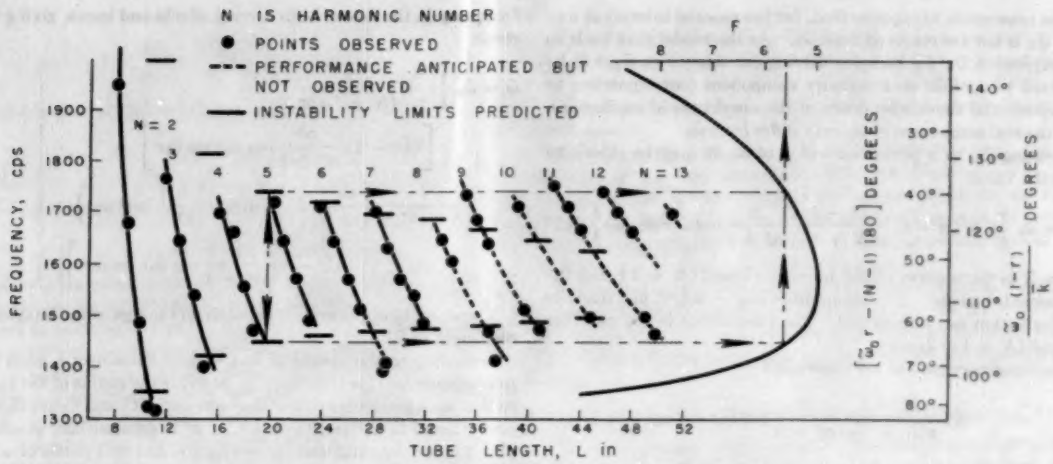

FIG. 9 FREQUENCY VERSUS TUBE LENGTH, SHOWING ALSO $\tilde{\omega}_0 r$, $\frac{\tilde{\omega}_0(1-r)}{\bar{k}}$, AND F, FOR $\bar{k} = 1.80$

However, there are very great heat losses for the hot part of the tube and the value quoted is in reasonable agreement with the temperature measurements made. In fact the heat losses are of the order of those predicted by the usual calculations. It would perhaps have been desirable to cut these losses to a minimum, but this was not experimentally convenient. Fig. 8 compares the observed frequencies ω, with the values of the natural frequencies ω_0, calculated from Equation [10], using $k = 1.80$. The agreement is very satisfactory.

In order to estimate the values of α occurring, the imaginary part of Equation [14] is equated to zero and hence, rearranging, for neutral stability

$$\frac{\alpha}{\alpha^2+1} = \frac{C_1 + \frac{C_2}{\bar{k}}[1 + (\bar{k}^2-1)\sin^2\tilde{\omega}_0 r]}{2(\bar{k}^2-1)\cos\tilde{\omega}_0 r \sin\tilde{\omega}_0 r} \quad \ldots\ldots [15]$$

Or, putting $C_1 = \bar{k}^2 C_2$

$$\frac{\alpha}{\alpha^2+1} = C_2\left[\frac{\bar{k}^2-\bar{k}+1}{\bar{k}^2-\bar{k}}\operatorname{cosec} 2\tilde{\omega}_0 r + \frac{1}{2\bar{k}}\tan\tilde{\omega}_0 r\right] \ldots [16]$$

It will be seen later (see Fig. 9) that for all but the lowest harmonics $\tilde{\omega}_0 r \simeq [(N-1)\pi + \pi/4]$. Making this approximation and putting $\bar{k} = 1.80$ in Equation [16] gives

$$\frac{\alpha}{\alpha^2+1} \simeq 2C_2$$

Putting $c_2 = 1980$ fps and $\tilde{\omega} \simeq 2\pi \times 1550$ radians/sec gives, for $d = 4.5$ in., $C_2 \simeq 0.017$, or $\alpha \simeq 0.03$.

It was observed that with $L = 14.0$ in. the minimum value of d for which the instability would occur was 3.0 in., so that the greatest value of α obtained may be estimated

$$\text{i.e.} \qquad \left.\frac{\alpha}{\alpha^2+1}\right|_{\max} \simeq 2 \times 0.017\left(\frac{4.73}{3.23}\right)^2 = 0.073$$

$$\text{i.e.} \qquad \alpha_{\max} \simeq 0.07$$

The mathematical maximum value of $\alpha/(\alpha^2+1)$ is attained for $\alpha = 1$, but it seems that under the physical conditions of the experiment this maximum cannot be attained. It is eminently reasonable that as $\frac{ds}{d\xi}\Big|_{\bar{\xi}}$ becomes small

should not increase without limit, and this apparently is the case here.

As $\cos\tilde{\omega}_0 r \sin\tilde{\omega}_0 r$ is of order unity and α^2 of order 10^{-3} the magnitude of the real perturbation to the natural frequency of the system, i.e.

$$\frac{1}{(N+\frac{1}{2})\pi}\left[(\bar{k}^2-1)\frac{\alpha}{\alpha^2+1}\cos\tilde{\omega}_0 r \sin\tilde{\omega}_0 r\right]$$

from Equation [14], can be estimated. As mentioned previously, it is very small (of order 10^{-3}) and not detectable by the experimental techniques used.

It has thus been shown that (in agreement with Rayleigh's criterion) only frequencies for which $\cos\tilde{\omega}_0 r \sin\tilde{\omega}_0 r > 0$ will be heard, i.e., that the flame must be within an odd-numbered quarter wave length counting from the upstream end of the tube. In general, there will be a number of natural frequencies that satisfy this condition, but it is possible also to predict which will first be heard (the "most unstable").

For the case of neutral stability

$$\frac{\alpha}{\alpha^2+1} = C_2\left[\frac{\bar{k}^2-\bar{k}+1}{\bar{k}^2-\bar{k}}\operatorname{cosec} 2\tilde{\omega}_0 r + \frac{1}{2\bar{k}}\tan\tilde{\omega}_0 r\right] \ldots [16]$$

The most unstable frequency for given physical conditions is that giving the smallest value of $\alpha/(\alpha^2+1)$ (it is assumed that $\alpha < 1$ for all attainable α). C_2 is proportional to ω^3 and so also, from Equation [10], to $[\tan^{-1}(-\bar{k}\tan\tilde{\omega}_0 r)]^3$.

In the present case put $\bar{k} = 1.80$. Then the theory predicts that the frequency heard will be that one that gives $\cos\tilde{\omega}_0 r \sin\tilde{\omega}_0 r > 0$ and gives the smallest possible value for a function F, defined by

$$F = [\tan^{-1}(-1.80\tan\tilde{\omega}_0 r)]^3\left(\operatorname{cosec} 2\tilde{\omega}_0 r + \frac{1}{6.05}\tan\tilde{\omega}_0 r\right) \ldots [17]$$

F may also be considered a function of $\tilde{\omega}_0(1-r)/\bar{k}$, or of ω_0 only for given d and $\bar{k}$.

Fig. 9 shows the observed frequencies for a constant value of $d = 4.5$ in. and lengths $L = 8$ to 51 in. The corresponding values of the function F are shown, as well as values of $[\tilde{\omega}_0 r - (N-1)\pi]$

and $\bar{\omega}_0(1 - r)/k$. When at a certain value of L a certain harmonic is first heard, the theory predicts that as L is increased the harmonic will still be heard, the corresponding value of the function F changing as L changes. When L is increased to such an extent that the value of F becomes less for another harmonic, that other harmonic will be heard instead.

The experimental results show good general agreement with this prediction. Differences in detail occur, but these can reasonably be ascribed to uncertainties in the conditions of the experiment and approximations in the theory.

It must be noted that the nature of the function F depends on a number of factors that in turn depend on the experimental arrangement, i.e., the value of $\bar{k}$ and the distribution and the nature of the losses. Thus, for example, while radiation losses are proportional to ω^3, and independent of L, viscous losses are approximately proportional to $\omega^{1/2}$ L and it is possible to conceive systems of significantly different behaviors from the present one.

It will be seen in Fig. 9 that actually the occurrence of the harmonics corresponds to a function F having a double minimum with a slightly greater maximum value between. Thus as L is increased (d being constant) the higher harmonics are heard in the order 9, 8, 10, 9, 11, 10, 12, 11, 13, etc., instead of 9, 10, 11, 12, 13, etc. This latter state of affairs was attained by modifying the apparatus in such a way as to alter substantially the distribution of losses. The occurrence of the conjectured maximum in F, however, has not been satisfactorily explained.

Conclusions

Two apparently new types of flame-excited oscillation have been reported and, in the case of that involving a flat flame configuration, some experimental data have been presented as well as a one-dimensional, linear theory.

The driving mechanism proposed depends on a flame speed that is a function of position (as well as mixture strength). The resultant instability is found to be in accordance with Rayleigh's criterion, and a procedure is demonstrated by which it is possible to select (from all the modes of oscillation which are driven by the action of the flame) that mode to which the system is least stable. The experimental results are found to be in good agreement with those predicted by the theory.

The "least stable" frequency is always one such that the flame is positioned within the second quarter wave length from the downstream end of the tube.

Acknowledgments

This work was performed at the Combustion Aerodynamics Laboratory of Harvard University, under the sponsorship of the Office of Ordnance Research, U. S. Army, under Contract No. DA-19-020-ORD-1092.

The author wishes especially to express his gratitude to Profs. H. W. Emmons and G. F. Carrier of Harvard University for their sustained interest and advice throughout the work.

A Photoelastic Study of Strain Waves Caused by Cavitation[1]

By G. W. SUTTON,[2] PHILADELPHIA, PA.

Ultra-high-speed photoelastic techniques have been applied to a study of the transient stresses and strains in a photoelastic plastic when subject to cavitation. A photocell, used to detect the transient strains, indicated that the time duration of the strains was about 2 microsec. Using an ultra-high-speed motion-picture camera, ultrasonic cavitation bubbles have been photographed collapsing on the surface of a photoelastic specimen, and the resulting strain wave in the solid has been photographed. The dynamic properties of a photoelastic material have been obtained in order to permit quantitative interpretation of the transients. This has indicated that the stresses due to cavitation may be as high as 2×10^8 psi. The photoelastic plastic, CR-39, was found to exhibit strain birefringence, and its strain-optic constant was found to be independent of the rate of loading.

Nomenclature

The following nomenclature is used in the paper:

c = wave speed of stress wave
d = diameter of stressed area
E = absolute value of elastic modulus
E^* = complex elastic modulus
E' = constant in Equation [3]
E'' = constant in Equation [3]
E_1 = real part of elastic modulus
E_2 = imaginary part of elastic modulus
f = frequency of harmonic oscillations
F = stress-fringe constant
G = strain-fringe constant
$i = \sqrt{-1}$
I = intensity of transmitted light
I_0 = maximum intensity of transmitted light
L = length of specimen bar
N = fringe order
t = time
u = longitudinal displacement
W = specimen thickness
x = longitudinal co-ordinate of bar
α = attenuation factor
δ = logarithmic decrement of damping
ϵ = strain
ϵ_1 = longitudinal strain
ϵ_2 = transverse strain
Λ = wave length
τ = period of harmonic oscillation
ϕ = argument of complex elastic modulus
ν = Poisson's ratio
ρ = mass density
σ = stress
σ_1 = longitudinal stress
$\bar{\sigma}_1$ = average stress caused by cavitation
σ_2 = transverse stress
ω = circular frequency of harmonic oscillations

Introduction

Although the laws governing the gross behavior of cavitation are well established, the study of the microscopic details of the vapor-bubble history and surface damage has been retarded by a lack of experimental techniques with adequate time resolution. Recently, acoustical methods of concentrating the vapor-bubble cloud on a small area of surface and an ultra-high-speed motion-picture camera have been developed by Dr. Albert T. Ellis (1, 2)[3] at the Hydrodynamics Laboratory of the California Institute of Technology. The shutter of this camera is a Kerr cell with crossed polaroids on each side. This suggested immediately that the transient stresses and strains due to cavitation could be investigated with photoelastic techniques. However, the laws concerning dynamic photoelasticity had not yet been established accurately; consequently, as a first step, a common photoelastic plastic, CR-39, was selected to make a comprehensive quantitative study of its static and dynamic photoelastic behavior.

Static Properties of CR-39

It appeared advisable to determine the static properties of CR-39, for two reasons: (*a*) To verify our experimental techniques by comparing the results of a static study with other similar studies; and (*b*) to compare the static properties with the dynamic properties.

CR-39 was selected as the photoelastic plastic because of its availability and because a considerable amount of experience on its fabrication has been obtained at the Guggenheim Aeronautical Laboratory at the California Institute of Technology. CR-39 is a thermosetting polymer of allyl-diglycol carbonate manufactured by the Cast Optic Corporation of Riverside, Conn., and, according to Coolidge (3):

"Essentially, its manufacture consists of reacting phosgene with diethylene glycol to obtain a chloroformate which is then esterified with allyl alcohol to produce the diglycol carbonate monomer. This monomer is polymerized by heating in the presence of a catalyst such as benzoyl peroxide to form the hard, strong, infusible, insoluble, clear, substantially colorless substance known as CR-39. The commercially obtainable sheets of CR-39 are cast-

[1] The results presented in this paper are based partly on a thesis submitted to the California Institute of Technology in June, 1955, in partial fulfillment of the Degree of Doctor of Philosophy. The investigation was sponsored by the Office of Naval Research under Contract N6onr-24420 (NR 062-059).

[2] Research Engineer, Missile and Ordnance Systems Department, General Electric Company; formerly, Research Fellow, California Institute of Technology, Pasadena, Calif. Assoc. Mem. ASME.

Presented at the Applied Mechanics Division Summer Conference, Berkeley, Calif., June 13–15, 1957, of The American Society of Mechanical Engineers.

Discussion of this paper should be addressed to the Secretary, ASME, 29 West 39th Street, New York, N. Y., and will be accepted until October 10, 1957, for publication at a later date. Discussion received after the closing date will be returned.

Note: Statements and opinions advanced in papers are to be understood as individual expressions of their authors and not those of the Society. Manuscript received by ASME Applied Mechanics Division, July 24, 1956. Paper No. 57—APM-15.

[3] Numbers in parentheses refer to the Bibliography at the end of the paper.

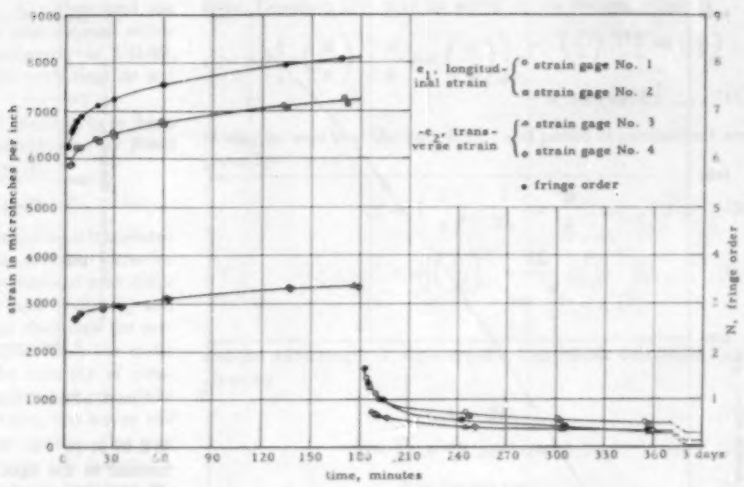

FIG. 1 TYPICAL CREEP TEST OF CR-39, SHOWING STRAIN AND BIREFRINGENCE FOR 2100 PSI TENSION, SPECIMEN 0.252 IN. THICK

polymerized between glass plates producing optically beautiful surfaces."

Experimental Procedure. The static tests were made on a simple tensile specimen with a working section 0.252 in. thick, 0.500 in. wide, and 3 in. long. Baldwin A-8 wire strain gages, which are limited to strains up to 1 per cent, were cemented to the front and back of the specimen in both the longitudinal and transverse directions. The strain was indicated directly by a Baldwin-Foxboro portable strain indicator which could be read to within 10 microin. The strain-gage constant was checked by comparing the wire strain gages against two calibrated Huggenberger mechanical extensometers.

The specimen was placed in the spherical mirror polariscope designed by Goetz (4), for which the light source is a low-pressure mercury-vapor lamp, used with a Wratten 77A filter to produce monochromatic light of 5461Å wave length. The fringe order in the specimen was determined by a calibrated Babinet-Soleil compensator that could be read easily to within $^1/_{100}$ of a fringe line with only visual observation.

Creep tests were made by applying constant loads to the specimen for 180 min during which time the strain and fringe order were determined; the load was then removed and readings were made for another 180 min.

TABLE 1 STATIC PROPERTIES OF CR-39

Property	Manufacturer's data	Coolidge's data	Author's data
Tensile strength, psi.	5000–6000	7000[a]	.....
Elastic modulus, psi.....	2.5–3.3 × 10^5	2.7 × 10^5	3.76 × 10^{5a}
Poisson's ratio.	.....	.....	0.443
Strain creep...	.....	Yes	Yes (see text)
Specific gravity	1.31	.....	1.326
Stress-fringe constant, psi-in/fringe, 5461Å.....	86.6	78.5[b]	90.8[a]
Optical creep..	None	20%/180 min	Yes (see text)
Strain-fringe constant, in/fringe....	.....	.....	3.48 × 10^{-4}
Refractive index, N_D...	1.50398	.....	.....

[a] Immediately after application of load.
[b] Stress was increased by increments to 4300 psi during 14 min; time between increments varied from 1 to 2 min.

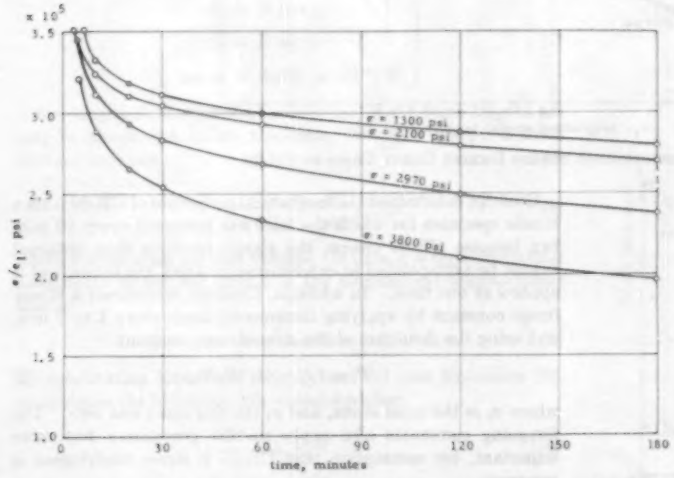

FIG. 2 RATIO OF STRESS TO STRAIN DURING CREEP TESTS OF CR-39 TENSION SPECIMEN

Results. Fig. 1 shows the indicated strain for a typical creep test, where it is evident that CR-39 is viscoelastic. Fig. 2 shows the ratio of stress, based on original area, to strain plotted as a function of time, where it is evident that the secant modulus decreases with both time and stress. Fig. 3 shows stress versus strain 10 min after the application of load, at which time the Young's modulus is 3.36 × 10^5 psi.

Fig. 4 shows the axial strain versus the transverse strain. For uniaxial stress, Poisson's ratio is given by the slope of the line, which is 0.443.

Fig. 5 shows the fringe order N as a function of the difference in principal strains, from which it is evident that the birefringence of CR-39 is proportioned to strain rather than to stress. The strain-fringe constant for plane stress, defined as

$$G = (\epsilon_1 - \epsilon_2)W/N \quad \ldots\ldots\ldots [1]$$

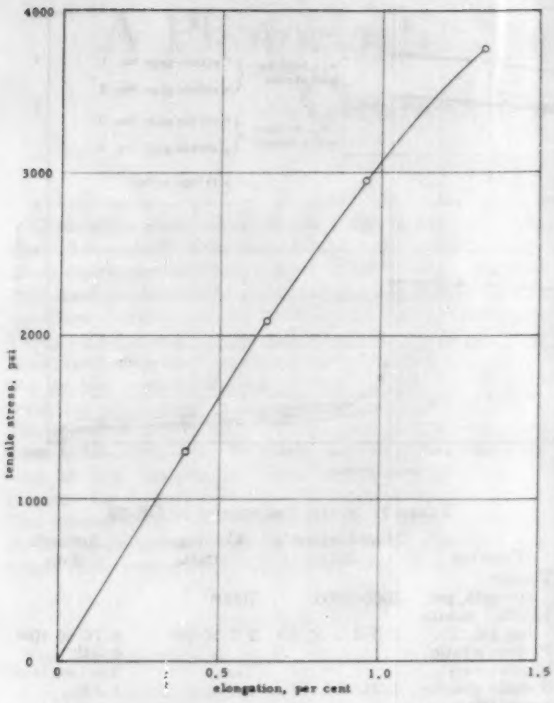

FIG. 3 TENSILE STRESS VERSUS LONGITUDINAL STRAIN AFTER 10 MIN OF CREEP FOR CR-39 TENSILE SPECIMEN

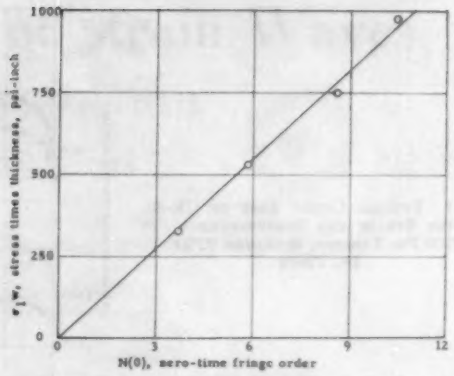

FIG. 6 ZERO-TIME FRINGE ORDER VERSUS STRESS FOR CR-39

is 3.48×10^{-4} in./fringe, where ϵ_1 and ϵ_2 are the principal strains normal to the light path, W is the width of the specimen, and N is the fringe order.

Finally, in Fig. 6, the fringe order at the time of loading, as determined by extrapolation, is plotted against the product of stress and specimen width. The slope of this curve is the so-called stress-optic constant F, and is 90.8 psi-in./fringe. This value decreases with time as the plastic creeps.

Discussion. Table 1 is a summary of the author's data in comparison with the data by Coolidge (3), and the manufacturer's data. The procedure by which the manufacturer obtained the data is not known, but the reasons for the discrepancy with Coolidge's data are evident from an examination of his experimental techniques.

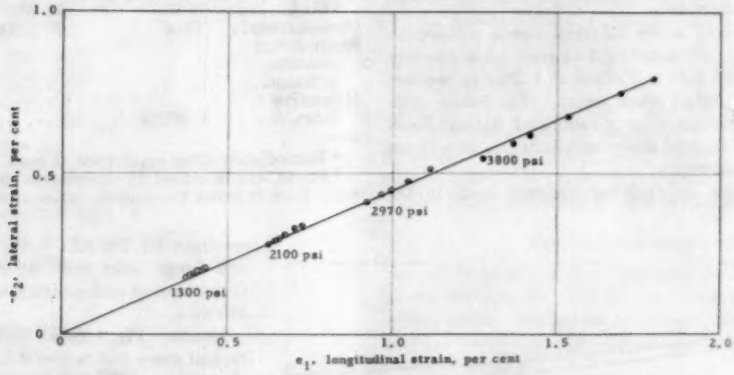

FIG. 4 LATERAL VERSUS LONGITUDINAL STRAIN DURING CREEP TESTS OF CR-39

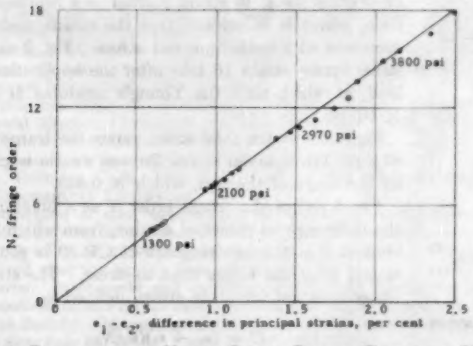

FIG. 5 BIREFRINGENCE VERSUS STRAIN DURING CREEP FOR CR-39

Coolidge determined the mechanical properties of CR-39 from a tensile specimen for which the load was increased every 10 min, but because CR-39 creeps, the elastic modulus thus obtained cannot be extrapolated to experiments in which the entire load is applied at one time. In addition, Coolidge determined a stress-fringe constant by applying incremental loads every 1 to 2 min, and using the definition of the stress-fringe constant

$$F = (\sigma_1 - \sigma_2)W/N \quad \ldots\ldots\ldots\ldots\ldots\ldots [2]$$

where σ_1 is the axial stress, and σ_2 (in this case) was zero. The foregoing comments also apply to this procedure; but more important, his assumption that CR-39 is stress birefringent is incorrect.

In passing, it also should be noted that Coolidge did observe a change in the fringe pattern with time in a beam subject to pure

bending. In reducing these data, however, Coolidge used the Bernoulli beam equations and did not take into account either the strain-creep characteristics or the nonlinearity of CR-39; hence his data on the change of fringe order with time do not correspond to those of Fig. 1.

It also should be noted that two other plastics have been reported as strain birefringent; namely, polyethylene by Fried and Shoup (5), and a special nylon by Hetényi (6).

Dynamic Properties of CR-39

The foregoing static properties of CR-39 cannot be extrapolated to make quantitative photoelastic observations of stress waves for two reasons: (*a*) The dynamic strain-fringe constant may differ from the static value; for instance, Senior and Wells (7) and Flynn (8) measured the dynamic stress-fringe constants for several other plastics and found them to be higher than the static value. (*b*) Since CR-39 is viscoelastic, the velocity of compressional and shear waves will depend on the wave lengths of the Fourier components of the wave, and in addition, the waves will become attenuated as they travel through the plastic. One way of describing these phenomena is to ascribe to the material a complex modulus which is a function of the wave length or the frequency of the Fourier components of the wave (9) as follows:

Dynamic Mechanical Properties of CR-39. If it is assumed that CR-39 is a Voigt solid at any one frequency of harmonic oscillations, the stress-strain relationship may be expressed as follows

$$\sigma = E'\epsilon + E''d\epsilon/dt \quad [3]$$

where σ and ϵ are the stress and strain, respectively, t is time, and E' and E'' are functions of the frequency ω of the applied strain; that is

$$\epsilon = \epsilon_0 e^{i\omega t} \quad [4]$$

Equation [3] then becomes

$$\sigma = (E' + i\omega E'')\epsilon \quad [5]$$

Therefore $E' + i\omega E''$ may be considered to be a complex modulus; that is

$$E^* = E' + i\omega E'' = E_1 + iE_2 = Ee^{i\varphi} \quad [6]$$

where

$$\left.\begin{aligned} E_1 &= E\cos\varphi \\ E_2 &= E\sin\varphi \\ \tan\varphi &= E_2/E_1 = \omega E''/E' \end{aligned}\right\} \quad [7]$$

For longitudinal stress waves in a bar, if the wave lengths are long in comparison to the thickness, Newton's law for a small element becomes

$$\rho\frac{\partial^2 u}{\partial t^2} = \frac{\partial\sigma}{\partial x} \quad [8]$$

where ρ is the mass per unit volume, t is time, x is the longitudinal co-ordinate of the bar, and u is the longitudinal displacement; that is

$$\epsilon = \partial u/\partial x \quad [9]$$

By substituting Equations [5], [6], and [9] into Equations [8], one obtains the following differential equation

$$\rho\frac{\partial^2 u}{\partial t^2} = Ee^{i\varphi}\frac{\partial^2 u}{\partial x^2} \quad [10]$$

When a bar of length L is executing free-free longitudinal vibrations, Equation [10] may be solved for its motion, which is

$$u = \cos\left[t\left(\frac{E}{\rho}\right)^{1/2}\frac{\pi}{L}\cos\left(\frac{\varphi}{2}\right)\right]e^{-t\left(\frac{E}{\rho}\right)^{1/2}\frac{\pi}{L}\sin\left(\frac{\varphi}{2}\right)} \times \sin(\pi x/L) \quad [11]$$

It may be seen that the frequency f and period of oscillation τ are given by

$$f = \left(\frac{E}{\rho}\right)^{1/2}\frac{1}{2L}\cos\frac{\varphi}{2} \quad [12]$$

$$\tau = \left(\frac{\rho}{E}\right)^{1/2}\frac{2L}{\cos\frac{\varphi}{2}} \quad [13]$$

and the wave length Λ, wave speed c, logarithmic decrement δ are given by

$$\Lambda = 2L \quad [14]$$

$$c = f\Lambda = (E/\rho)^{1/2}\cos(\varphi/2) \quad [15]$$

$$\delta = 2\pi\tan(\varphi/2) \quad [16]$$

As a given wave travels along the bar, it is attenuated as $e^{-\alpha x}$; it may similarly be shown that the attenuation factor α is given by

$$\alpha = (\delta/\Lambda)\cos^2\frac{\varphi}{2} \quad [17]$$

The foregoing constants were determined from free-free vibrations of various length bars of CR-39, in which the strain was measured by Baldwin C-19 wire strain gages. For the shorter bars, a correction was made for the thickness, using data from experiments made by Morse (10), and from a theoretical analysis by Bancroft (11). The results of the experments on CR-39 are shown in Figs. 7, 8, and 9. From these, it is evident that with increasing frequency, the wave speed, logarithmic decrement, attenuation factor, and E all increase. All dynamic values of E are greater than any reported static values.

Dynamic Strain-Fringe Constant. Based on the correlation of the photoelastic fringe order to the strain, it appeared desirable to make similar measurements during transient stresses; that is,

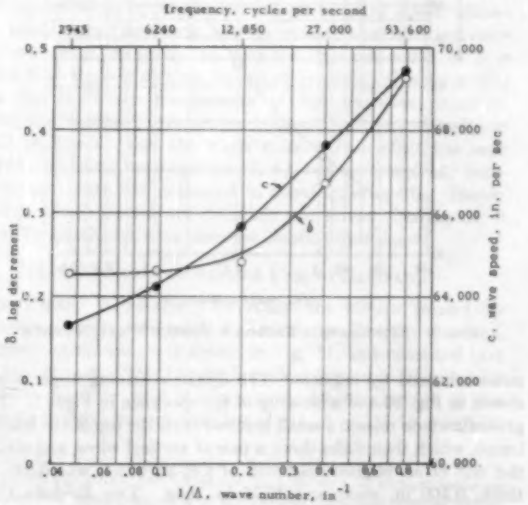

Fig. 7 Wave Speed and Logarithmic Decrement Versus Frequency and Wave Number for CR-39

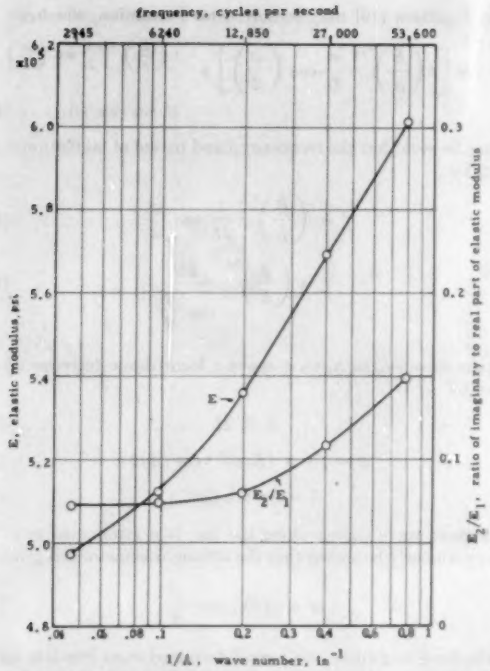

FIG. 8 ELASTIC MODULUS AND RATIO OF IMAGINARY TO REAL PARTS OF ELASTIC MODULUS VERSUS FREQUENCY AND WAVE NUMBER FOR CR-39

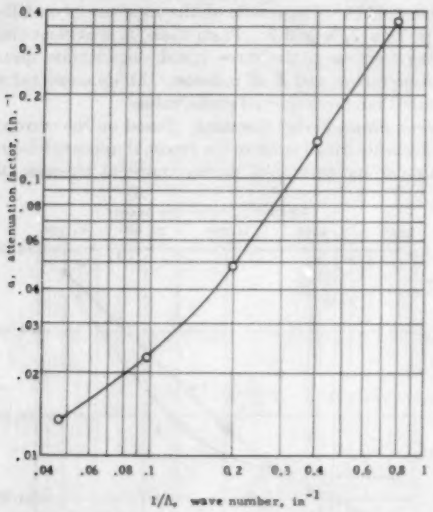

FIG. 9 ATTENUATION FACTOR α VERSUS WAVE NUMBER

stresses caused by impacts. The dynamic loading apparatus is shown in Fig. 10 and a close-up of the specimen in Fig. 11. The procedure is to release a small hammer from the top of the loading frame, which then slides down a pair of vertical wires, and strikes the end of an aligned specimen of CR-39 which was 0.248 in. thick, 0.500 in. wide, and 10.75 in. long. Two Baldwin C-19 strain gages, the gage constant of which as given by the manufacturer was guaranteed to be within 3 per cent, were cemented

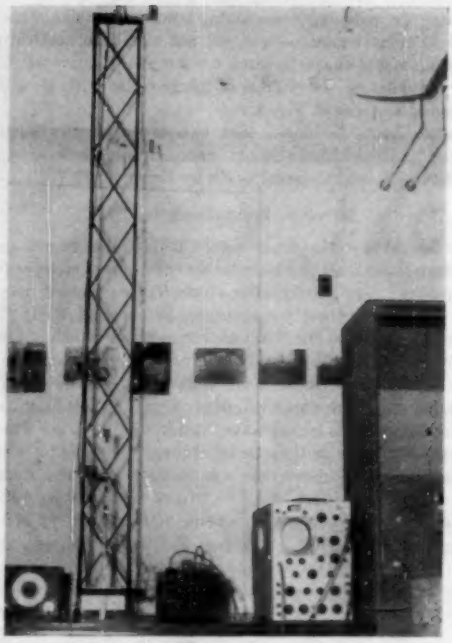

FIG. 10 DYNAMIC LOADING APPARATUS
(*Left*, Photomultiplier; *center*, loading frame with wire strain gages cemented to specimen; *right*, strain gage bridge and oscilloscope.)

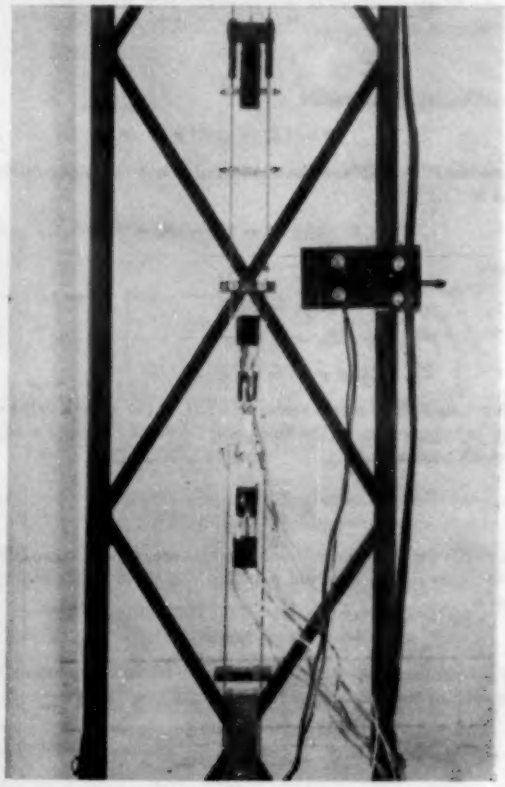

FIG. 11 CLOSE-UP OF DYNAMIC LOADING APPARATUS

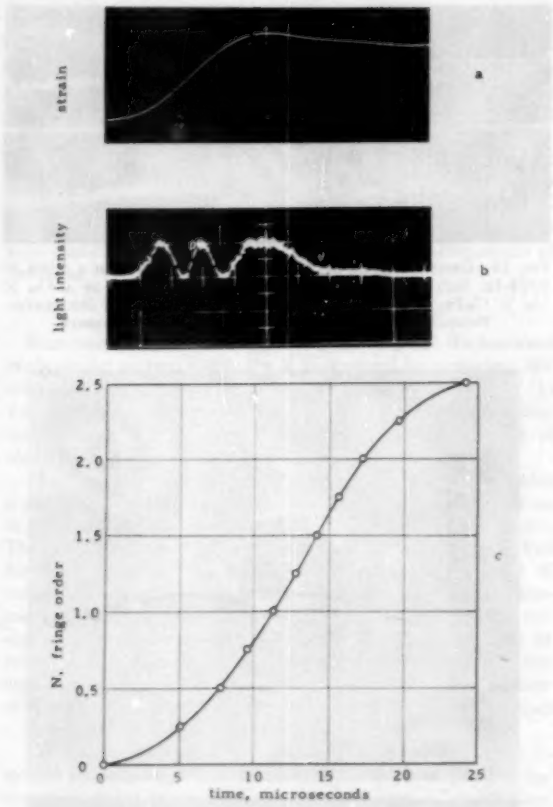

FIG. 12 (a) OSCILLOGRAPH RECORD OF LONGITUDINAL STRAIN ON LEADING EDGE OF STRESS WAVE. (b) OSCILLOGRAPH RECORD OF TRANSMITTED LIGHT. (c) FRINGE ORDER VERSUS TIME, FROM (b)

on the specimen in the longitudinal direction, and two in the transverse direction.

By comparing the strain in the two directions during the passage of a stress wave, Poisson's ratio was found to be 0.44, which is the static value within experimental error.

To determine the strain-fringe constant, the loading frame was placed in a polariscope and a monochromatic circularly polarized light beam of 5461Å was directed through the space between the strain gages. The light intensity was detected by an IP21 multiplier phototube whose output was amplified and displayed on one of the Tektronix oscilloscopes; the strain in the longitudinal direction was simultaneously detected by a bridge circuit similar to one used by Ripperger (12), and displayed on another Tektronix oscilloscope. Oscillograms were made with Dumont-Land oscillograph cameras. Fig. 12 shows two such oscillograms, together with the fringe order, which is given by

$$N(t) = \frac{1}{\pi} \sin^{-1} \sqrt{[I(t)/I_0]} \quad \ldots\ldots\ldots\ldots [18]$$

where I_0 is the peak light intensity, and $I(t)$ and $N(t)$ are the instantaneous light intensity and fringe order, respectively. The oscillograms are for the leading edge of the strain wave, the rise time of which was about 25 microsec. The fringe order versus strain for the leading edge is shown in Fig. 13 and the slope, which is the strain fringe constant, is $3.42 \times 10^{-4} \pm 3$ per cent in./fringe. This value is the same as the static value within experimental error.

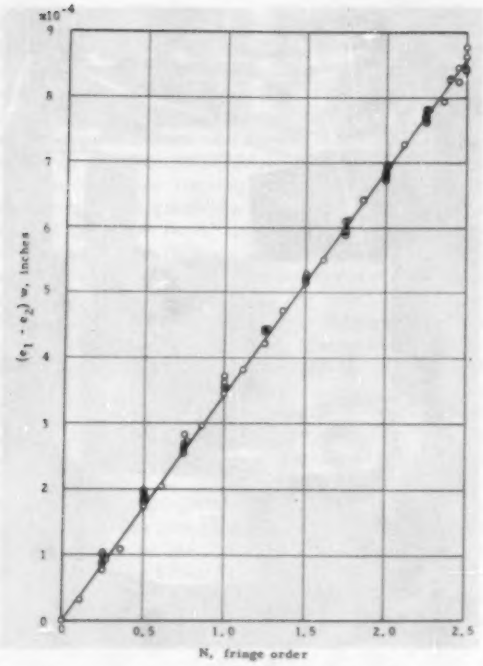

FIG. 13 NUMBER OF FRINGES VERSUS STRAIN FOR LEADING EDGE OF STRESS WAVE FOR CR-39. EIGHT RUNS. LIGHT WAVE LENGTH, 5461Å

These tests also indicate that CR-39 is strain birefringent rather than stress birefringent, which is the usual relation used in photoelasticity.[4] Note that both Equations [1] and [2] are valid for an elastic material, the birefringent constants being related by

$$F = GE/(1 + \nu)$$

and stress birefringence cannot be distinguished from strain birefringence in an isotropic solid subject to plane stress. However, plastics are viscoelastic to some extent; that is, E increases with increasing frequency, so that the dynamic value of E is greater than the static value, the exact dynamic value depending upon the frequency components of the transient situation. Therefore, if a plastic is strain birefringent, the dynamic value of F will be greater than the static value. This effect has been observed by other investigators (7, 8), but unfortunately transient strains were not measured in those experiments. Hence, although those plastics are definitely not stress birefringent, it cannot be concluded that they are strain birefringent.

TIME DURATION OF STRAINS DUE TO CAVITATION

Experimental Apparatus. To study the strains caused by cavitation, the acoustic method devised by Ellis (2) was used. The essential apparatus is shown in Fig. 14, and consisted of a glass beaker, a barium-titanate ferroelectric ring surrounded by closed-cell sponge rubber, and a specimen holder, which in this case is a 1-in-thick base of stainless steel. A $^1/_{16} \times ^1/_{16} \times ^1/_8$-in.

[4] After this paper was submitted for publication, A. B. J. Clark reported on the strain per fringe for both creep and impact tests on CR-39, at the annual meeting of the Society for Experimental Stress Analysis, Pittsburgh, Pa., May 16–18, 1956. Although the results were not conclusive, it was suggested that CR-39 may be strain-birefringent.

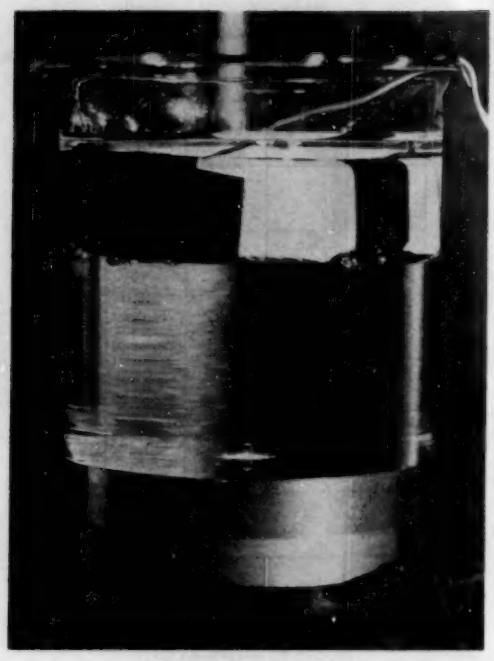

FIG. 14 ACOUSTIC CAVITATION IN WATER
(Small bubble cloud can be seen on top of photoelastic specimen.)

specimen of CR-39 was held in the center of the base, and the beaker was filled with distilled and deaerated water.

The electrode surfaces of the barium-titanate ring were connected to an audio-oscillator amplifier circuit, which excited the first mode of the oscillations of the water-base system when tuned to 22,000 cycles per sec. The maximum pressure amplitude of the water is on the center line of the beaker at the base. As the power to the barium titanate is increased, the minimum pressure during the negative part of the cycle drops below vapor pressure and cavitation forms on the upper surface of the specimen. The cavitation is visible in Fig. 14 in the form of a small bubble cloud.

The beaker was placed in a polariscope with a modified optical system so that a magnified image of the specimen was projected onto a screen in which a square hole was cut. In this way, only the light from an area 0.004 in. square on the specimen passed through the slit, the intensity of which was detected by an IP21 multiplier phototube, which was immersed in liquid nitrogen to reduce the noise level. The phototube output was amplified by a Tektronix Type 121 amplifier, and displayed on a Tektronix Type 513D oscilloscope. The frequency response of the amplifier is 12 megacycles and of the oscilloscope 18 megacycles. The frequency response of the phototube, as determined by light pulses through a Kerr cell of 0.08-microsec duration, was at least as high as that of the oscilloscope.

Experimental Results. The light slit was centered 0.006 in. below the upper surface of the CR-39 specimen. As the oscillator amplitude was increased, a distinct sine wave became visible on the oscilloscope, the frequency of which corresponded to that of the oscillator. As the oscillator was tuned to the lowest resonant frequency, 22,000 cps, the wave form of the light intensity became distorted from sinusoidal toward a saw-tooth form. When the bubble cloud formed, a spike appeared on the oscilloscope screen, at the part of the cycle where the pressure becomes positive. Typical oscillograms are shown in Fig. 15. The spikes were present only when the bubble cloud was present. The lower oscillogram, a double exposure, shows that the time between spikes is not constant. The time duration of the spike was about 2 microsec. When the slit was moved down away from the upper end of the specimen, or toward either side of the specimen, the spikes gradually decreased in amplitude, but the time duration of the spike remained constant. The amplitude of the spike corresponds to about one quarter of a fringe line, and was apparently insensitive to the bubble-cloud size or amplitude of the exciting pressure cycle. It should be mentioned that the

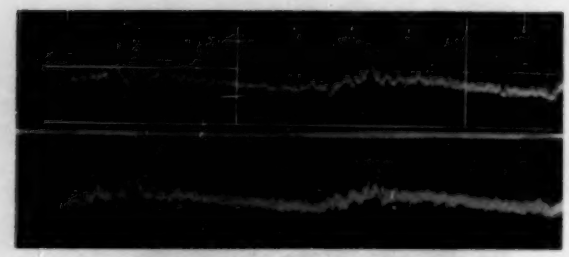

FIG. 15 OSCILLOGRAPHS OF LIGHT INTENSITY THROUGH A 0.004 × 0.004-IN. SLIT CENTERED 0.006 IN. BELOW SURFACE OF A 1/16 × 1/16 × 1/8-IN. CR-39 SPECIMEN WHEN CAVITATION IS OCCURRING. HORIZONTAL SWEEP-TIME 10 MICROSEC PER DIVISION

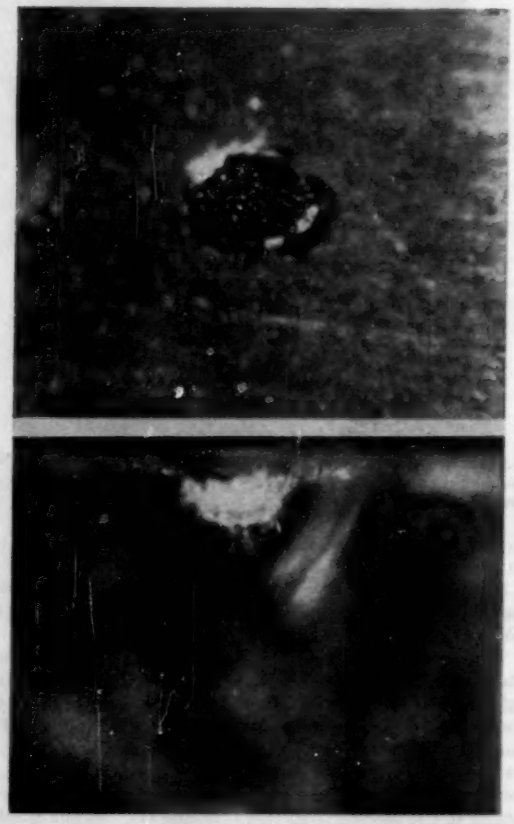

FIG. 16 PHOTOMICROGRAPHS OF A 1/16 × 1/16-IN. SPECIMEN OF CR-39 AFTER 5 MIN OF CAVITATION DAMAGE

concentration of vapor bubbles seemed to be greatest at the center of the bubble cloud, just above the surface of the specimen.

Fig. 16 shows photomicrographs of the top and sides of a specimen that had been subject to about 5 min of cavitation. There is a large irregular hole in the center, surrounded by individual holes which are about 0.001 in. diam.

The strain wave resulting from the cavitation did not exhibit the viscoelastic dispersion or dissipation that is typical of CR-39 at lower frequencies; this indicates the internal damping is negligible and the wave speed, and hence the elastic modulus, is approximately constant for the higher frequency components of the spike.

Ultra-High-Speed Motion Pictures

Experimental Apparatus. In order to photograph the transient isochromatic pattern due to the strains caused by cavitation, the ultra-high-speed motion-picture camera developed by Ellis (1) was utilized. This camera has a repetition rate up to one million frames per sec for about a millisec with a frame exposure of about 0.08 microsec.

The camera is a revolving-mirror type; the mirror distributes a series of images onto the inner periphery of a stationary drum in which a $7^1/_2$ ft length of 35 mm Tri-X film has been placed. The exposure for each frame is achieved by a Kerr cell. The Kerr cell consists of a glass container, on the front and back of which are crossed polaroids so that normally no light is transmitted through the cell. On either side of the cell are two flat electrodes spaced 0.25 in. apart; when a voltage difference of 13,000 volts exists across the electrodes, the nitrobenzene in the container becomes sufficiently optically active to rotate the plane of the light that had been polarized by the front polaroid so that it passes through the rear polaroid.

The Kerr cell is electrically pulsed for about 0.08 microsec to achieve each frame, and is pulsed continuously only during one revolution of the mirror. During this revolution, a General Electric FT524 flash tube is illuminated by discharging through it the energy stored in a bank of capacitors. Suitable inductances cause the light intensity to be almost constant for about a millisec.

To photograph the strains due to cavitation, a slightly different cavitation beaker was used. A circularized light polariscope with a light background was used so that the entire field, including the cavitation bubbles, would be visible; specimens with thicknesses of 0.25, 0.0625, and 0.020 in. were used. The resonant frequency for this beaker was 10 kilocycles per sec.

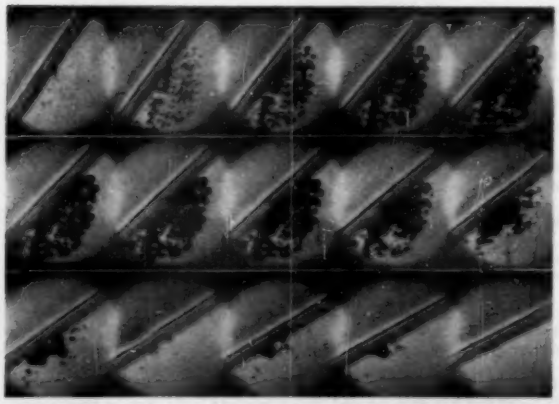

Fig. 17 10-Kc Bubble-Cloud Cycle, Taken With Ultra-High-Speed Camera; ×5

Results. Fig. 17 shows a series of consecutive frames taken at 150,000 frames per sec of a 0.25-in-thick specimen. The lower right-hand line represents the edge of the specimen; it is blurred because of the small depth of field of the lens. The other two dark lines are time-edge isochromatics, caused by leaving the specimen immersed in water for too long a period of time. However, they provided a sensitive means to detect fractional changes in the isochromatics resulting from transient strains. The twelfth frame shows a shift of about $^1/_4$ of a fringe just after the collapse of the bubble cloud. In addition, the entire specimen is also darkened. Only one frame is affected; this is caused by the short time duration of the transient and the large speed of propagation of the stress wave.

In subsequent runs, half a dozen cases of fringe shift just after bubble collapse were observed; this also was observed in the 0.0625-in. specimen, but not in the 0.020-in. specimen. When the fringe shift was observed, it always occurred in the immediate vicinity of the bubble collapse. These bubbles did not exhibit spherical symmetry; on the other hand, the affected area in the specimen was always spherical, centered below the last bubbles to collapse.

Because of the blurring of the edge of the specimen, it was not possible to determine photographically the initially strained area. However, it may be postulated that initially the cavitation pressure acts only on the area corresponding to a small pit; that is, a diameter of 0.001 in. It may be assumed that, during the initial pulse, the lateral elongations are zero; then the observed fringe order is

$$N = \frac{1}{G}\int \epsilon_1 dx \qquad [19]$$

where ϵ_1 is the strain normal to the surface. Now, for plane strain, the stress σ_1 normal to the surface is given by

$$\sigma_1 = \frac{(1-\nu)E\epsilon_1}{(1+\nu)(1-2\nu)} \qquad [20]$$

where ν is Poisson's ratio. When ϵ_1 is eliminated from Equations [19] and [20], the following expression is obtained for the average stress $\overline{\sigma_1}$

$$\overline{\sigma_1} = \frac{1}{d}\int_{-d/2}^{+d/2} \sigma_1 dx = \frac{EGN(1-\nu)}{d(1+\nu)(1-2\nu)} \qquad [21]$$

where d is the diameter over which the stress acts initially. The elastic modulus is not known accurately for ultra-high-frequency components, but to obtain an order-of-magnitude estimate of the average stress, it may be estimated as 7×10^5 psi. With $G = 3.42 \times 10^{-4}$ in/fringe, $N = {}^1/_4$, and $d = 0.001$ in., the average stress $\overline{\sigma_1}$ is about 2×10^5 psi.

Conclusion

The ultra-high-speed photoelastic techniques have yielded quantitative information on the time duration of stresses due to cavitation and the magnitude of the stresses. Additional study of the behavior of photoelastic materials at higher frequencies and stresses is required, as well as a method of direct calibration of axially symmetric impacts. It also appears desirable to obtain better depth of field and magnification of the photographic image.

Acknowledgments

The author wishes to express his appreciation to Prof. M. S. Plesset and Dr. A. T. Ellis for their aid and guidance during this study.

BIBLIOGRAPHY

1 "Observations on Cavitation Bubble Collapse," by A. T. Ellis.

California Institute of Technology, Hydrodynamics Laboratory Report No. 21-12, December, 1952.

2 "Production of Accelerated Cavitation Damage by an Acoustic Field in a Cylindrical Cavity," by A. T. Ellis, California Institute of Technology, Hydrodynamics Laboratory Report No. 21-14, September, 1955.

3 "An Investigation of the Mechanical and Stress-Optic Properties of Columbia Resin, CR-39," by D. J. Coolidge, Jr., Proceedings of the Society for Experimental Stress Analysis, vol. 6, no. 1, 1948, pp. 74–82.

4 "A Modified Optical Arrangement for Photoelastic Measurements," by A. Goetz, *Review of Scientific Instruments*, vol. 5, no. 2, 1934, p. 84.

5 "A Study in Photoplasticity," by B. Fried and N. H. Shoup, TR No. 3, ONR Contract N7onr-330-III NR 064-121, State College of Washington, May, 1953.

6 "A Study in Photoplasticity," by M. Hetényi, Proceedings of the First U. S. National Congress of Applied Mechanics, Ann Arbor, Michigan, 1952, pp. 499–502.

7 "A Photoelastic Study of Stress Waves," by D. A. Senior and A. A. Wells, *Philosophical Magazine*, vol. 7, 1946, pp. 463–469.

8 "Studies in Dynamic Photoelasticity," by P. D. Flynn, PhD thesis, Illinois Institute of Technology, Chicago, Ill., 1954.

9 "Stress Waves in Solids," by H. Kolsky, Oxford University Press, Oxford, England, 1953, p. 110.

10 "Dispersion of Compressional Waves in Isotropic Rods of Rectangular Cross Section," by R. W. Morse, *Journal of the Acoustical Society of America*, vol. 20, 1948, pp. 833–838.

11 "The Velocity of Longitudinal Waves in Cylindrical Bars," by D. Bancroft, *Physical Review*, vol. 59, 1941, pp. 588–593.

12 "Longitudinal Impact of Cylindrical Bars," by E. A. Ripperger, Proceedings of the Society for Experimental Stress Analysis, vol. 10, no. 1, 1952, pp. 209–226.

Turbulence in Small Air Jets at Exit Velocities Up to 705 Feet per Second

By L. W. LASSITER,[1] MARIETTA, GA.

Turbulence intensity, scale, and spectrum measurements were made on model jets of 1 in. and 2-in. diam at various mean velocities. The indications are that only in the fully developed flow is turbulence intensity invariant with mean velocity; intensity in the core, in the turbulent annulus, and in the transition region decreases in varying degrees with mean velocity increase. Longitudinal and radial scales of turbulence were found to increase in the annulus in proportion to about the square root of axial distance, and longitudinal scale is about 65 per cent greater than radial scale. Both radial and longitudinal scales seem to be essentially constant with mean velocity. Turbulence spectra were found to consist of a sharply peaked band of frequencies in the core, degenerating to a slightly peaked broad band at points in the mixing regions.

Nomenclature

The following nomenclature is used in the paper:

- D = nozzle-exit diameter
- f_p = peak frequency of turbulence spectrum
- L = scale of velocity fluctuations
- L_x = longitudinal scale
- L_y = radial scale
- R = correlation coefficient
- R' = correlation coefficient corrected for hot-wire length
- R_x = axial correlation
- R_y = radial correlation
- U = mean velocity
- U_0 = mean velocity on center line at jet exit
- u' = root-mean square-fluctuation velocity
- x, y = flow field co-ordinates; x is axial distance from jet exit, y radial distance from jet center line

Introduction

In the theoretical work of Lighthill (1)[2] it has been shown that the intensity and scale of turbulence of the jet are significant with regard to the generation of jet noise. Hot-wire measurements thus have been made in connection with some of the basic NACA jet-noise studies (2, 3). Emphasis was placed on surveying the high-velocity region of the jet near the nozzle exit since it was apparent that a large part of the noise was generated in that region.

Corrsin (5) presents some turbulence measurements for 1-in-diam and 3-in-diam circular air jets at mean velocities of 30 and 67 fps, respectively. The axial component of turbulence was measured for the 3-in-diam jet at various radial distances from the center line and at axial distances of from 1 to 12 diam from the nozzle. Similar measurements for a 1-in-diam jet were made at axial distances of 5 to 40 diam from the nozzle.

The present studies are partly an extension of the turbulence-intensity measurements of Corrsin in the jet-mixing region to velocities of 705 fps. In addition, spectra of these axial-velocity fluctuations are presented for a range of jet velocities. Scale data obtained at various axial distances for 1 and 2-in-diam jets also are presented.

Apparatus

Nozzles. Four convergent circular nozzles were employed in the tests. Two of these were of 1-in. throat diameter; the other two were of 2-in. throat diameter. The duplication of sizes arose from the use of two test configurations requiring different outside-nozzle sizes. One set of nozzles was of 6 in. OD and 4 in. length, made of polished steel and wood for the 1-in. and 2-in. throat diameters, respectively. The other set, of throat diameters 1 in. and 2 in. also, had outside diameters of 21 in., lengths of 15 in., and was made of wood. The inlet fairings for all nozzles were formed by circular arcs and a cylindrical tailpipe of about 1 diam length was used with each nozzle.

Test Configurations. The two test setups used are shown schematically in Fig. 1. Configuration B was constructed for the more-or-less exploratory measurements and yielded the larger part of the intensity measurements with a 1-in. nozzle. It consisted simply of a settling chamber of about 5 ft length and 6 in. diam, to which was fitted either the 1-in. steel nozzle or a 2-in. wood nozzle. Roughly half the length of the chamber was taken

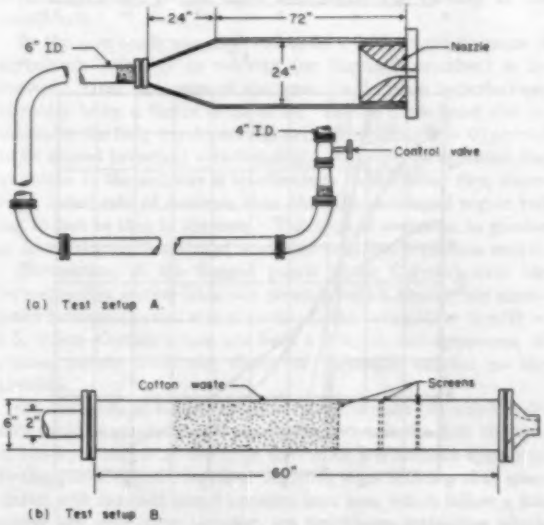

Fig. 1 Schematic Drawings of Test Configurations Used

---

[1] Aircraft Design Engineer Specialist, Lockheed Aircraft Corporation; formerly, Physicist, Langley Laboratory, National Advisory Committee for Aeronautics, Langley Field, Va.

[2] Numbers in parentheses refer to the Bibliography at the end of the paper.

Presented at the Applied Mechanics Division Summer Conference, Berkeley, Calif., June 13–15, 1957, of The American Society of Mechanical Engineers.

Discussion of this paper should be addressed to the Secretary, ASME, 29 West 39th Street, New York, N. Y., and will be accepted until October 10, 1957, for publication at a later date. Discussion received after the closing date will be returned.

Note: Statements and opinions advanced in papers are to be understood as individual expressions of their authors and not those of the Society. Manuscript received by ASME Applied Mechanics Division, November 15, 1956. Paper No. 57—APM-34.

up by a packing of cotton waste used to isolate the nozzle from valve and feeder-line disturbance, both acoustic and aerodynamic. Two double layers of screen were placed between this packing and the nozzle to assist in establishing a uniform and low turbulence level at the nozzle inlet. Some of the data to be presented later will verify that this scheme was successful.

Configuration A was not completed until about midway of the tests and was used mainly for scale measurements, where longer times of uninterrupted running were desirable. It consisted of a more carefully designed settling chamber of 8 ft over-all length and 24 in. ID. In this setup, it was found simpler to isolate the entire settling chamber from the line and control valve than to divide the chamber as was done with configuration B. To do this, small amounts of a rubberized-horsehair material were placed just upstream of the settling chamber and just downstream of the control valve. Although this arrangement permitted flow separation in the diffuser, the center-line turbulence levels at the jet exit were only slightly higher than those of the 1-in. nozzle in setup B; thus it was felt that the arrangement was satisfactory.

Figs. 2(*a*) and (*b*) give sample mean-velocity profiles from the 1-in. and 2-in. nozzles used in the test stands B and A, respectively. These indicate fairly uniform exit velocities and show that the decreases in the streamwise direction are about the same in each case.

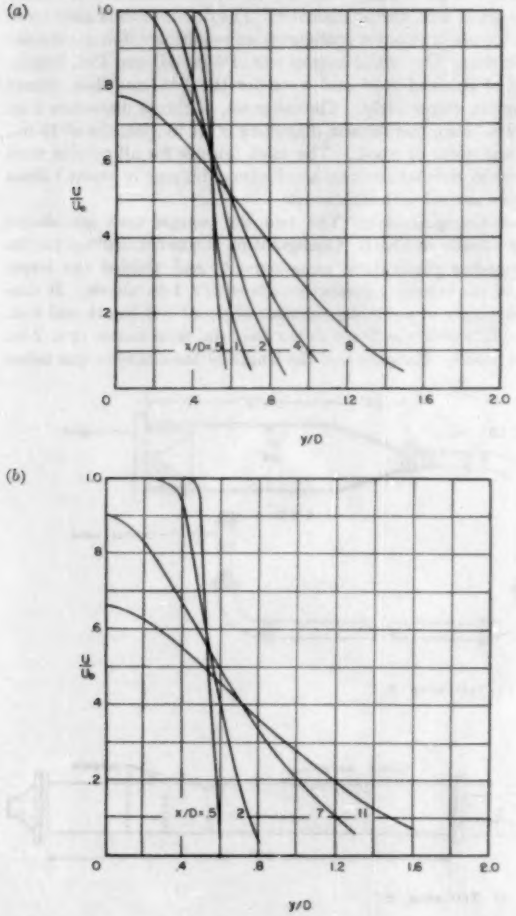

FIG. 2 MEAN VELOCITY PROFILES OF TEST JETS, U_0 = 705 FPS

Instrumentation. The hot-wire system used in the tests was constructed by the Instrument Research Division of the Langley Laboratory. The wires were of 80–20 per cent platinum-iridium, $^1/_{16}$ in. long and 0.0003 in. diam. Output signals from the wire (which employed constant-current operation) were put into a compensating amplifier which resulted in an over-all system response that is flat within ±5 per cent from 20 to 10,000 cycles per sec (cps), with cutoff at 10 cps and 15,000 cps. It was felt that this response was satisfactory for studies of the turbulence in the regions considered herein. From the amplifier output, intensity levels were obtained by means of a thermocouple root-mean-square voltmeter; frequency spectra were obtained with the aid of a panoramic analyzer, and in some cases magnetic-tape recordings were made to afford a permanent record.

TEST PROCEDURES

Types of Data Obtained. Three types of turbulence data were obtained. These are (*a*) intensity, (*b*) space correlations, and (*c*) frequency spectra. In all cases these were limited to the axial component u' of the turbulence. In addition to these data there were the usual aerodynamic measurements necessary to detemine flow velocities, density, temperature, and so on.

Flow Regions Considered. Fig. 3 which summarizes some results of jet-flow studies (6, 7) will serve to indicate the flow regions investigated in the present tests. Flow from a jet can be divided into the three general regions denoted in the figure by A, B, and C. Region A extends 4 to 5 diam downstream of the nozzle and contains the potential core, or unmixed fluid, and a surrounding turbulent annulus which is characterized by high turbulence levels and large shear forces.

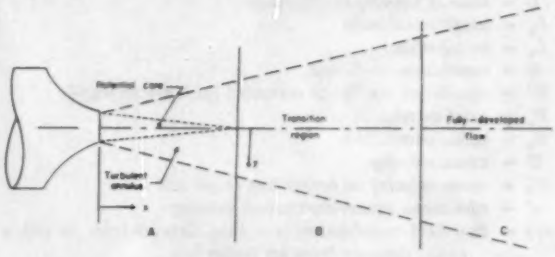

FIG. 3 SCHEMATIC DIAGRAM OF FLOW FIELD OF AIR JETS

In region B, which extends from the potential core to about 10 or 15 diam from the nozzle, the entire cross section is characterized by intense turbulence. However, the flow is not yet fully developed, this occurring only at points downstream of this transition region, i.e., in region C.

The tests discussed herein were limited to regions A and B, since these regions are believed to be of greatest significance in noise generation. The scale measurements were further limited to region B and only the turbulent annulus of region A.

Correlation Coefficients. By definition, the correlation coefficient R is defined as

$$R = \frac{\overline{u_1 u_2}}{\overline{u^2}}$$

From spatial correlation between points separated a distance ds in the flow, the scale of turbulence is defined as

$$L = \int_0^\infty R\, ds$$

where ds may be measured radially or axially and results in, respectively, radial and longitudinal turbulence scales.

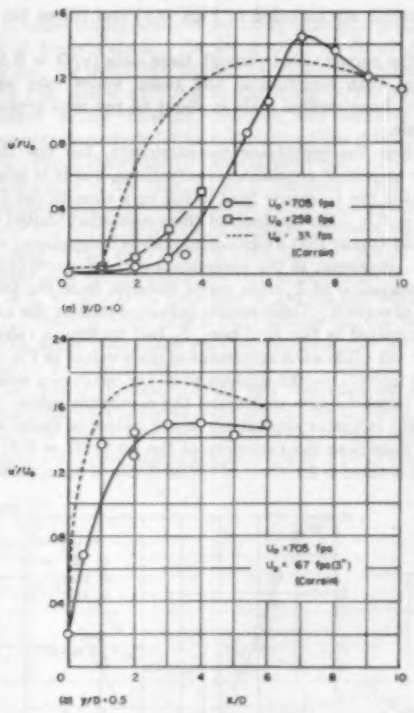

FIG. 4 LONGITUDINAL PROFILES OF AXIAL TURBULENCE COMPONENT; $D = 1$ IN., $U_0 = 705$ FPS

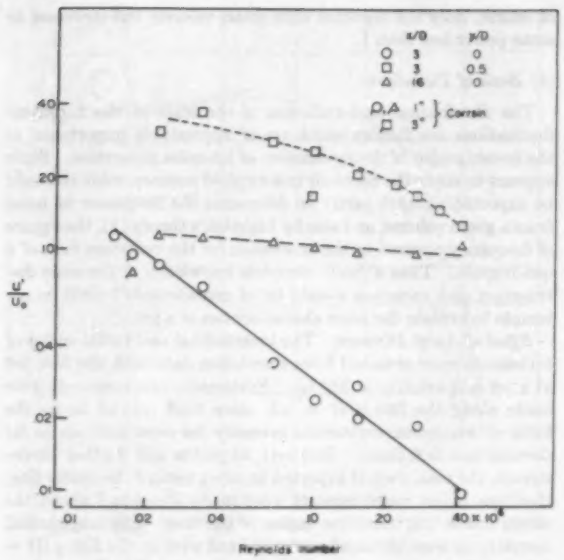

FIG. 5 TURBULENCE INTENSITY AS A FUNCTION OF REYNOLDS NUMBER FOR THREE LOCATIONS IN JET; $D = 1$

RESULTS AND DISCUSSION

(a) *Intensity of Turbulence*

Effect of Axial Distance. Fig. 4 illustrates the variations of turbulence intensity u'/U_0 along the streamwise direction for the 1-in. jet of the present tests and allows comparisons with Corrsin's data (5) for lower mean velocities. Mean exit velocity in the present tests was 705 fps. Fig. 4(*a*) compares the intensity variations at this exit velocity along the center line of the 1-in. jet with those measured by Corrsin for a 1-in. jet at 33 fps exit velocity. In addition, a segment of the curve for an intermediate velocity (258 fps) from the present tests is included. From the two complete curves it appears that the maximum turbulence intensity is practically the same at 705 fps and 33 fps, but there are large differences in intensity at points upstream of the maximum. Corrsin obtained a sharp increase of intensity as early as 1 diam downstream of the nozzle; whereas the present data indicate a more gradual increase with distance at 705 fps. This leads to a more clearly defined maximum at the higher velocity. If the curve segment for 258 fps may be included as being further indicative of a trend, then it appears that development of turbulence intensity along the center line is delayed by an increase in exit velocity. It was observed that the initial turbulence on the center line at 705 fps was less than 0.1 per cent, indicating that the attempt to minimize initial turbulence level was successful.

Fig. 4(*b*) compares 1-in. jet data along the line $y/D = 0.5$ from the present tests at 705 fps with Corrsin's data for a 3-in. jet at 67 fps. Although this is probably not as valid a comparison as the preceding one because of the diameter difference involved, the indications are much the same, with exception of the fact that the maximum of the two curves of Fig. 4(*b*) shows a decided difference in intensity.

Effect of Mean Velocity or Reynolds Number. In order to make a more detailed study of the variation in turbulence intensity u'/U_0 with mean exit velocity U_0, three points in the flow of the 1-in. jet were chosen for further observation. These were: (i) $x/D = 3$, $y/D = 0$, in the potential core; (ii) $x/D = 3$, $y/D = 0.5$, in the turbulent annulus surrounding the core; and (iii) $x/D = 16$, $y/D = 0$, a point in the region where fully developed turbulence is expected. Fig. 5 illustrates the variation in u'/U_0 for these three points as U_0 was varied from 40 to 705 fps. Although only velocity was variable in the present tests, Reynolds number was chosen as the abscissa because of its more inclusive nature and because it probably allows a better comparison of data with Corrsin's 3-in. jet data. The Reynolds numbers calculated were arbitrarily based on jet diam and center-line velocity at the nozzle exit.

In the core there was observed to be a fairly rapid decrease of turbulence intensity as velocity (or Reynolds number) is increased. Over the range of the tests the decrease in turbulence intensity is by a factor of 10 or so. On the other hand, the intensity in the fully developed region ($x/D = 16$, $y/D = 0$) proved to be almost invariant with velocity. As might be expected, the variation in the annulus is intermediate to the other two, showing a faster rate of decrease than the fully developed region but not so fast as that in the core. This type of variation, in greater or lesser degree, was found to characterize the transition region.

Comparison of the flagged points (from Corrsin) with the corresponding curves from the present tests indicates fair agreement between the two sets of data. In the case $x/D = 3$, $y/D = 0.5$, where Corrsin's data are from a 3-in. jet, this agreement, of course, results from the choice of Reynolds number as the abscissa.

On the basis of near field sound-pressure data (3) which indicate that the greatest noise generation occurs in the first 10 diam of the flow, curves of the type shown for the annulus appear to be the ones of concern to noise. As such, these indicate that associated with far-field sound pressure increases, which follow a 4th power law with mean velocity, are turbulence intensities which follow a low negative-power law. The fluctuation velocity (u'),

of course, does not decrease with mean velocity but increases as some power less than 1.

(b) *Scale of Turbulence*

The distribution and variation of the scale of the turbulent fluctuations are factors which are of appreciable importance in the investigation of the mechanism of jet-noise generation. Scale appears to enter the problem in a twofold manner, since it would be expected at least partly to determine the frequency of noise from a given volume, and also by Lighthill's theory (1), the square of frequency appears in the expression for the radiation field of a quadrupole. Thus a fairly complete knowledge of the scale distribution and variation should be of considerable benefit in attempts to explain the noise characteristics of a jet.

Effect of Axial Distance. The longitudinal and radial scales of turbulence were obtained from correlation data with the 2-in. jet at a jet exit velocity of 348 fps. Systematic measurements were made along the line $y/D = 0.5$, since that proved to be the locus of maximum turbulence intensity for cross sections as far downstream as 6 diam. However, at points still farther downstream, the maximum is expected to move toward the center line; therefore a few measurements were made along and about the center line in the transition region of the flow. The longitudinal correlations were obtained with the fixed wire on the line $y/D = 0.5$ and the movable wire along a line inclined just enough to clear the wake of the fixed wire. Radial correlations were obtained with the fixed wire on the line $y/D = 0.5$ and the movable wire at points $y/D > 0.5$. The resulting scale values are arbitrarily assigned to the co-ordinates of the fixed wire in every case. Fig. 6 illustrates the results obtained in the form of dimensionless scale as a function of dimensionless axial distance: Fig. 6(*a*) gives the longitudinal scale results and Fig. 6(*b*) gives the radial scale results. In addition to the measurements along $y/D = 0.5$ a few measurements were made on or about the jet center line downstream of the potential core. The data from these measurements are included in Figs. 6(*a*) and (*b*) as the square points.

From the curves faired through these data ($y/D = 0.5$) it appears that both longitudinal and radial scales vary about as $\sqrt{(x/D)}$. Longitudinal scale is about 65 per cent greater than radial scale.

Regarding the center-line measurements, too few data are available to permit conclusive observations, but it is interesting to note that the L_x points tend to fall very close to the L_x-curve for $y/D = 0.5$. On the basis of these somewhat limited data, it thus would appear that longitudinal scale is independent of radial position. However, in the investigation of reference (4), a systematic variation of L_x with radial distance from the jet center line was observed. Those results indicated that at the axial stations considered in Fig. 6(*a*) here, L_x had maximum values for $0 < y/D < 0.5$. Thus the agreement of scale values in Fig. 6(*a*) for $y/D = 0$ and $y/D = 0.5$ appears to be the result of a selection of stations which happen to bracket the maximum value.

Fig. 6(*b*) indicates appreciably lower values of radial scale on the axis than near the periphery of the jet ($y/D = 0.5$). Thus apparently there is an effect of radial distance upon radial scale,

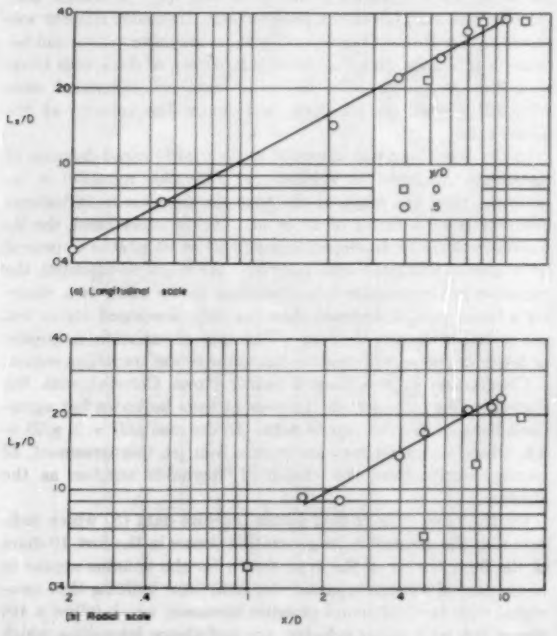

FIG. 6 SCALE VARIATIONS IN 2-IN. AIR JET; $U_0 = 348$ FPS

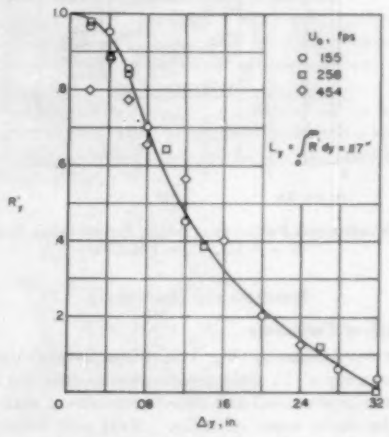

FIG. 7 RADIAL CORRELATION CURVE FOR 1-IN. JET AT VARIOUS EXIT VELOCITIES; $x/D = 6$, $y/D = 0$

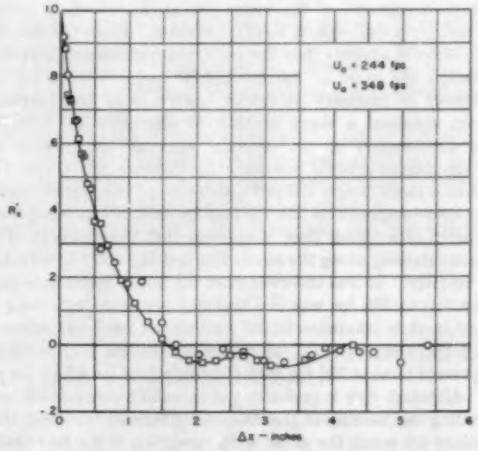

FIG. 8 LONGITUDINAL CORRELATION DATA FOR 2-IN. JET AT DIFFERENT MEAN EXIT VELOCITIES; $x/D = 5$, $y/D = 0$

leading to larger eddies near the periphery than on the center line.

Effect of Mean Velocity. In an attempt to determine what effect, if any, the mean flow has on the scale of the axial fluctuations, the 1-in. nozzle with test configuration B was operated at three rather widely different velocities and radial-correlation measurements were made for each velocity at the point $x/D = 6$, $y/D = 0$. Fig. 7 shows that if there is any variation, it is within the scatter limits of the data, for all of the data of Fig. 7 can be approximated satisfactorily by a single curve. Integration of the area under this curve (without the negative portions, which were omitted only in this test) yields a scale $L_y/D = 0.117$.

Fig. 8 compares longitudinal correlation data from the 2-in. jet at $x/D = 5$, $y/D = 0$ for velocities of 244 fps and 348 fps. Although the velocity range here is considerably more limited than that of Fig. 8, the indications are that longitudinal scale does not vary with jet velocity either.

Effect of Nozzle Diameter. With test configuration B, radial correlation data were obtained from jets of 1 in. and 2-in. diam at the point $x/D = 6$, $y/D = 0$ for the purpose of investigating the variation of scale with nozzle diameter. Fig. 9 plots the correla-

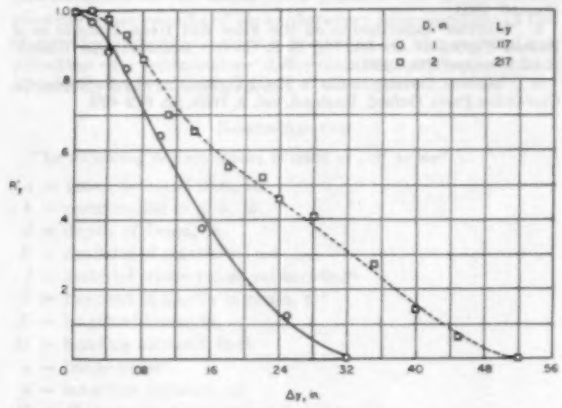

FIG. 9 RADIAL CORRELATION CURVES FOR JETS OF 1 IN. AND 2 IN. DIAM; $U_0 = 258$ FPS, $x/D = 6$, $y/D = 0$

tion curves obtained at a mean velocity of 258 fps. Integrations of the areas under these curves indicate a value of $L_y = 0.117$ in. for the 1-in. jet and 0.217 in. for the 2-in. jet. Although these numbers represent a ratio of only 1.85, that is probably close enough to justify the usual assumption that scale varies directly with nozzle diameter, or conversely that L_y/D is constant for a given point of geometrical similarity in jets of various diameters.

(c) *Spectra of Turbulence*

Since for each turbulence-intensity point obtained, it was possible by means of a panoramic analyzer to obtain a simultaneous frequency analysis, a considerable number of such analyses was made with the 1-in. nozzle. To a lesser extent, the same procedure was followed with the 2-in. nozzle.

Effect of Axial Distance. Fig. 10 presents a series of spectra based on an idealized rectangular filter of bandwidth 1 cps to illustrate the variation of turbulence spectrum with distance from the nozzle along the jet center line. These spectra, of course, relate to measurements with a hot wire and are, therefore, referred to a stationary frame of reference. Several observations regarding the spectra can be made:

1 In the core the fluctuations are of very limited frequency content. This characteristic has been observed previously (5, 8, 9) and was referred to in one case (8) as "extremely regular velocity fluctuations."

2 On the other hand, the spectra outside the potential core are of considerably wider frequency limits, although there is still a tendency for a single, rather flat maximum to occur.

3 This maximum occurs at lower frequencies as axial distance from the nozzle is increased. For the 1-in. nozzle at 705 fps mean velocity, the maximum varied from over 5000 cps at $x/D = 0.5$ to about 500 cps at $x/D = 10$. Presumably still greater distances eventually will result in a spectrum which peaks at subaudible frequencies.

Effect of Mean Velocity. From spectra similar to those of Fig. 10 over a range of velocities, a systematic variation of the peak frequency of the spectra was observed. By defining the

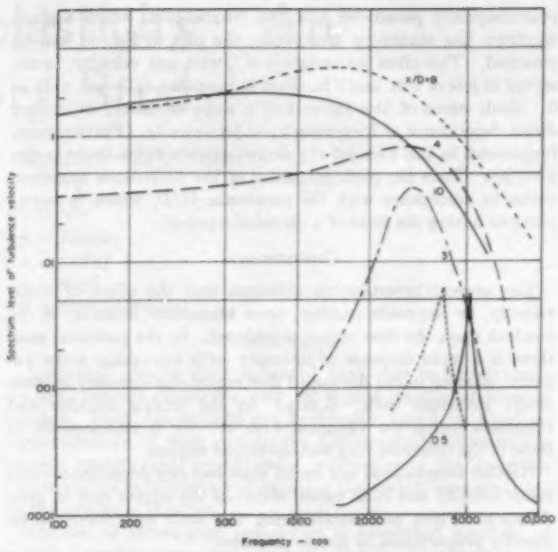

FIG. 10 SPECTRA OF AXIAL VELOCITY FLUCTUATIONS ALONG CENTER LINE OF 1-IN. AIR JET; $U_0 = 706$ FPS

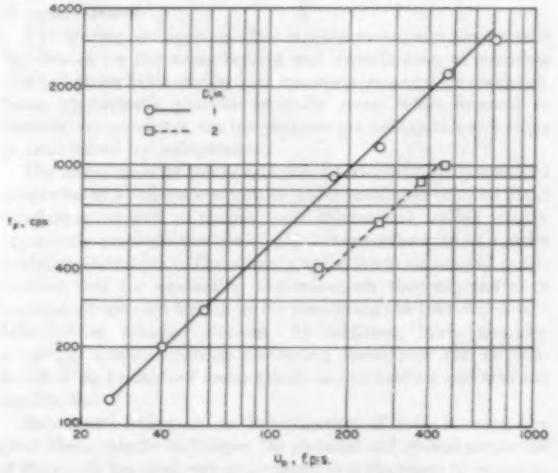

FIG. 11 EFFECT OF JET VELOCITY ON PEAK FREQUENCY OF TURBULENCE SPECTRUM; $x/D = 3$, $y/D = 0$

peak-frequency parameter f_p as the frequency at which a given spectrum has maximum magnitude, the plot of Fig. 11 can be obtained. This gives the variation of f_p with exit velocity, as observed in jets of 1 in. and 2 in. diam at the point $x/D = 3$, $y/D = 0$. Each curve of this figure has a slope of unity, indicating direct dependence of frequency upon jet velocity. Furthermore, frequencies in the 1-in. jet are almost exactly twice those in the 2-in. jet. Thus the peak frequency of the turbulence spectrum varies in accordance with the parameter U/D, which is recognized as having the form of a Strouhal number.

Conclusions

The present investigation indicates that the effect of mean velocity, or Reynolds number, upon turbulence intensity is dependent upon the flow region considered. In the potential cone there is a rapid decrease of intensity with increasing mean velocity, whereas in the developed flow region the intensity is practically invariant with velocity. In the mixing annulus and transition region the variation with velocity is intermediate to those of the potential cone and developed regions.

Neither longitudinal nor radial scale had any dependence upon mean velocity and both varied about as the square root of axial distance. From radial-scale tests, the scale was found to be directly proportional to nozzle diameter.

The spectra of the fluctuations were characterized by a band of random components, the center frequency of which varies in accordance with a form of the Strouhal number. In the potential cone this band had very narrow frequency limits, and in the annulus and transition regions the band was of rather broad limits.

BIBLIOGRAPHY

1 "On Sound Generated Aerodynamically," by M. J. Lighthill, Proceedings of the Royal Society of London, vol. 222, February 23, 1954, pp. 1–32.

2 "Experimental Studies of Noise From Subsonic Jets in Still Air," by L. W. Lassiter and H. H. Hubbard, NACA TN 2757, August, 1952.

3 "The Near Noise Field of Static Jets and Some Model Studies of Devices for Noise Reduction," by L. W. Lassiter and H. H. Hubbard, NACA TN 3187, July, 1954.

4 "Intensity, Scale, and Spectra of Turbulence in Mixing Region of Free Subsonic Jet," by J. C. Laurence, NACA TN 3561, September, 1955.

5 "Investigations of Flow in an Axially Symmetrical Heated Jet of Air," by S. S. Corrsin, NACA Wartime Report No. W-94, 1943.

6 "Investigations of the Turbulent Mixing Regions Formed by Jets," by A. M. Kuethe, Trans. ASME, vol. 57, 1935, pp. A-87–A-95.

7 "Transport of Momentum, Mass, and Heat in Turbulent Jets," by L. G. Alexander, Thomas Baron, and E. W. Cominga, University of Illinois Engineering Experimental Station, Technical Report 8, May 10, 1951.

8 "Further Experiments on the Flow and Heat Transfer in a Heated Turbulent Air Jet," by S. S. Corrsin and Mahinder Uberoi, NACA Report 998, 1950.

9 "Modern Developments in Fluid Dynamics," by S. Goldstein, Clarendon Press, Oxford, England, vol. 2, 1938, pp. 672–673.

Photothermoelasticity: An Exploratory Study[1]

By GEORGE GERARD[2] AND A. C. GILBERT,[3] NEW YORK, N. Y.

This paper summarizes the optical and physical properties of the photoelastic model material Paraplex P-43 over the temperature range from room temperature to −40 F. Descriptions are presented of techniques and equipment developed to obtain the modulus of elasticity, the material fringe value, and the thermal-expansion coefficient as a function of temperature. Experimental investigations were conducted into the plane-stress problems of a disk contracting upon an elastic inclusion and the transient thermal-stress field produced by a temperature differential suddenly applied to the upper edge of a long beam. The data are correlated with theory using the material properties obtained in the calibration phase. Also included are photographic results of an exploratory investigation of the thermal-shock phenomenon produced by the sudden application of a temperature differential upon plastic beams of various length-depth ratios.

Nomenclature

The following nomenclature is used in the paper:

a = inner radius of disk, in.
b = outer radius of disk, in.
d = depth of beam, in.
E = modulus of elasticity, psi
f = material fringe value, psi-in/fringe
I = moment of inertia of beam, in^4
L = length of beam, in.
M = bending moment, in-lb
n = fringe order
p = interface preasure, psi
Q = photoelastic figure of merit, fringes/in.
Q_α = photothermoelastic figure of merit, fringes/in-deg F
r = radial co-ordinate in disk, in.
t = thickness of model, in.
T = temperature, deg F
y = distance from neutral axis in beam, in.
α = coefficient of thermal expansion, micro-in/in-deg F
ϵ = strain
$\epsilon_T = (\Delta L/L)_{T_0} - (\Delta L/L)_T$
σ = stress, psi
ν = Poisson's ratio

Subscripts

p = plastic
r = radial
s = steel
θ = circumferential

Introduction

Analytical results have indicated that, due to aerodynamic heating, aircraft structures may experience significant thermal stresses. Such calculations are necessarily based on idealized representations of wing structures. Consequently, considerable interest centers upon experimental verification of the transient-temperature distributions and resulting thermal stresses predicted by the available theories.

The use of strain-gage techniques is somewhat involved at elevated temperatures and generally entails large-scale metal models and extensive heating facilities for thermal-stress measurements. Therefore, it is of considerable importance to establish the value of other techniques for quantitative measurements of thermal stresses.

A promising new approach to this problem employs photoelastic techniques for the measurement and visualization of complete thermal-stress fields arising from transient-temperature gradients. Since photoelastic plastics generally creep when exposed to elevated temperatures, the temperature gradient in this technique is established by refrigeration.

The importance of joints and the deterioration of mechanical properties of a full-scale structure under simulated thermal flight conditions, as well as thermal and geometrical scaling effects, apparently preclude the use of photothermoelasticity as a strict modeling technique. The primary value lies in its use as a quantitative tool for evaluating thermal-stress theories, and as a particularly graphic technique for visualizing the time-dependent behavior of thermal stresses. In addition, fairly complex structural models utilizing cementing techniques can be constructed[4] and analyzed under simultaneous loading and thermal conditions.

Before embarking on an investigation of models using the photothermoelastic technique, the physical and optical properties of the model material were determined over the range of temperatures covered in the subsequent investigations. The test procedures and equipment developed to treat this phase of the investigation are discussed.

In order to assess the accuracy of the photothermoelastic technique, disk and long beam models were selected for investigation. By inserting a steel plug in a plastic disk and cooling the combination, a stress field is induced owing to the different thermal coefficients of expansion of the two materials. The experimental results were correlated with theory and good agreement was obtained.

Experimental results for beams suddenly cooled by dry ice on one edge are presented. By utilizing the experimentally determined temperature distribution, fringe orders were computed and compared with the experimentally observed values for a

[1] Sponsored by United States Air Force through the Office of Scientific Research, Air Research and Development Command.

[2] Assistant Director, Research Division, College of Engineering, New York University. Mem. ASME.

[3] Formerly, Associate Engineering Scientist, Research Division, College of Engineering, New York University. Now, Supervisor of Dynamics, North American Aviation Inc., Downey, Calif. Mem. ASME.

Presented at the Applied Mechanics Division Summer Conference, Berkeley, Calif., June 13–15, 1957, of The American Society of Mechanical Engineers.

Discussion of this paper should be addressed to the Secretary, 29 West 39th Street, New York, N. Y., and will be accepted until October 10, 1957, for publication at a later date. Discussion received after the closing date will be returned.

Note: Statements and opinions advanced in papers are to be understood as individual expressions of their authors and not those of the Society. Manuscript received by ASME Applied Mechanics Division, August 3, 1956. Paper No. 57—APM-25.

[4] "Note on Photoelastic Study of a Swept-Wing Model," by G. Gerard and R. Papirno, *Journal of the Aeronautical Sciences*, vol. 21, December, 1954, pp. 846–847.

long beam. Again good agreement was obtained, tending to substantiate the photothermoelastic procedure.

Because of considerable interest in the thermal-shock phenomenon, a study of thermal shock on short beams of various length-depth ratios is presented. Since the study was of an exploratory nature, the results are presented mainly in the form of a series of photographs showing the history of the thermal-stress build-up and decay.

Properties of Photoelastic Plastic

Introduction. This section is concerned with the basic optical and physical properties of the photoelastic plastic, Paraplex P-43. This material is a castable polyester resin supplied by Rohm and Haas Company in liquid form. It is cast into plates with the addition of a suitable catalyst. This material was selected for use in this investigation because of its freedom from time-edge effect and the relative ease with which it can be cemented.

The test procedures and equipment used to determine the material fringe value, modulus of elasticity, and coefficient of thermal expansion as functions of temperature are discussed. The results are presented graphically for the individual properties and also in the form of a photothermoelastic figure of merit pertinent to thermal-stress problems. Figure-of-merit data on some other commonly used photoelastic materials are presented also.

In Table 1, some room-temperature physical properties of cured Paraplex P-43 are given as supplied by the Rohm and Haas Company.

Table 1 Physical Properties of Cured Paraplex P-43

Shrinkage during cure, per cent by vol	7.00
Specific gravity	1.235
Refractive index	1.5564
Thermal conductivity, Btu/(sq ft-hr-deg F/in.)	1.25
Specific heat, Btu/lb-deg F	0.32

Experimental Equipment. To evaluate the properties of Paraplex P-43 at low temperatures, a styrofoam cold chamber was constructed as shown in Fig. 1. The cold chamber was divided internally by a partition into refrigerant and test sections. Dry-ice pellets and a small variable-speed fan located in the refrigerant section insured a uniform temperature distribution in the test section.

The model was visible in the test section through a pair of double-pane-glass viewing windows. The presence of four glass sheets in the optical path did not cause any disturbance in the polariscope. Fogging or clouding of the windows was avoided by use of silica gel between each of the glass sheets and in the test section.

In all tests, the temperature of the model was determined utilizing 0.020-in. wire copper-constantan thermocouples cemented into the specimen. The method of installation of the thermocouples yielded temperature data which were average values across the model thickness. A Leeds and Northrup potentiometer was used in conjunction with standard thermocouple compensation methods. The over-all accuracy of the instrumentation and installation techniques resulted in an estimated maximum error of ±1 deg F in the average temperature reading.

The loading machine used in this investigation was of 1000-lb capacity and employed a pneumatic loading system. Calibration of the loading system indicated a maximum error of ±½ per cent in the range of loads used in this program.

The determination of the modulus of elasticity and the thermal-expansion coefficient involve accurate resolution of strain data.

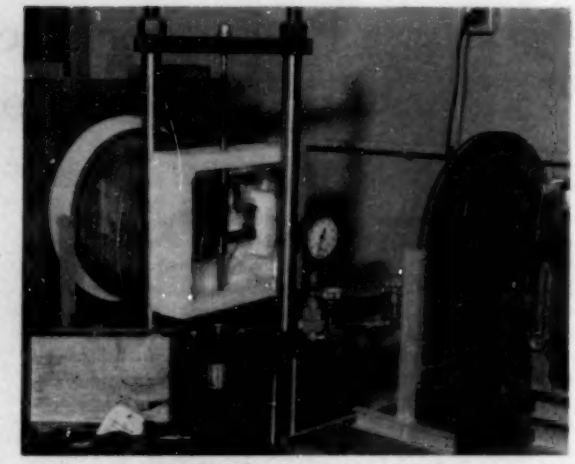

Fig. 1 Cold Chamber With Front Cover Removed Showing Beam-Bending Setup Positioned in Polariscope

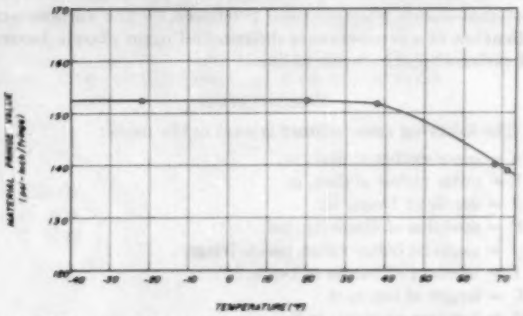

Fig. 2 Material Fringe Value for Paraplex P-43 Cured Resin

To obtain accurate strain data, an optical strain reader consisting of a matched pair of objective lenses, two rhomboidal prisms, and a filar micrometer eyepiece was constructed. Gage scratch marks inscribed on the specimen appear superimposed in the field of the filar eyepiece, permitting a single measurement of the relative movement of the gage marks. The strain reader has a least count of 42 micro-in/in. in the 2.640-in. gage length and is described fully elsewhere.[4]

Material Fringe Value. The material fringe values of Paraplex P-43 over the temperature range from +70 to −40F were obtained by use of beam tests employing the test equipment illustrated in Fig. 1.

At each temperature level, data on fringe order n versus distance from the neutral axis y were reduced from photographs for each bending test. The slope n/y was then plotted as a function of $M/I = \sigma/y$ and the material fringe value was computed from the relation

$$f = \frac{(\sigma/y)}{(n/y)}\, t \qquad [1]$$

The material fringe value as a function of temperature is presented in Fig. 2.

Modulus of Elasticity. The apparatus for determining the modulus of elasticity was similar to that used in obtaining the

[4] "Dual Objective Optical Micrometer for Strain Measurements," by R. Papirno, A. C. Gilbert, and H. Becker, *Review of Scientific Instruments*, vol. 27, October, 1956, pp. 854–855.

material fringe value with the exception that a tensile load was used instead of an applied bending moment. The cold chamber was used in conjunction with the strain reader. Thermocouples were inserted in the model at both ends and the model temperature was stabilized before loading commenced.

The modulus of elasticity was determined from conventional stress-strain plots for each temperature. In all cases, the maximum applied stress was kept well below the proportional limit of the material. The time under applied load was kept to a minimum to reduce any possible creep effects in the specimen. This procedure was repeated at the various temperatures over the range of interest. Fig. 3 presents the modulus of elasticity as a function of temperature from +70 to −40 F.

Thermal-Expansion Coefficient. The tensile-test model was placed in the cold chamber free of the loading jigs and the displacement between the gage marks was recorded for the various temperatures. By using 32 F as the reference temperature, the incremental change in length was determined and plotted versus temperature as shown in Fig. 4. The test data indicate essentially a linear relationship in the temperature range of the test. Therefore, the thermal-expansion coefficient has the following value

$$\alpha = 35 \text{ micro-in/in-deg F} \quad [2]$$

Photothermoelastic Figure of Merit. In conventional photoelastic work, materials are rated according to a figure of merit defined as

$$Q = E/f \quad [3]$$

The higher the value of Q, the more sensitive is the material fringewise (f) for a given value of E.

For photothermoelastic work, the sensitivity of a material to stresses induced by thermal conditions can be defined by a photothermoelastic figure of merit

$$Q_\alpha = \alpha E/f \quad [4]$$

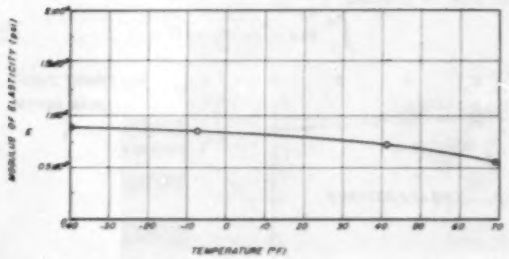

FIG. 3 MODULUS OF ELASTICITY FOR PARAPLEX P-43 CURED RESIN

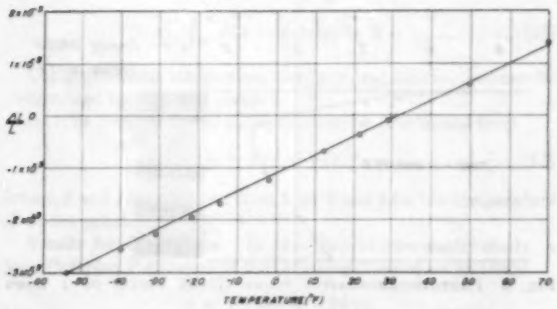

FIG. 4 $\Delta L/L$ FOR PARAPLEX P-43 CURED RESIN

TABLE 2 FIGURES OF MERIT AT ROOM TEMPERATURE

Material	Q (fringes/in.)	Q_α (fringes/in-deg F)
Araldite 6060	7930	0.21
Bakelite BT-61 893	6980	0.23
Columbia resin CR-39	2700	0.13
Paraplex P-43	3900	0.13

Again, the higher the value of Q_α, the more sensitive is the material fringewise (f) for a given value of αE. In Table 2, the room-temperature figures of merit of commonly used photoelastic materials are listed.

THERMAL STRESSES IN A DISK

Introduction. In structural components, thermal stresses arise in two distinct ways. For a uniform temperature field, interference between two mating elements as a result of different thermal-expansion coefficients can produce thermal stresses. Also, in a nonuniform temperature field, thermal stresses are induced as a result of nonuniform expansion of adjacent fibers under the temperature gradient.

To investigate the quantitative value of the photothermoelastic technique, a plastic disk with a steel plug in the center in a uniform temperature field, and a plastic beam with a suddenly applied differential on one edge were selected for investigation. These simple models are representative of the interference and thermal-gradient cases, respectively, and moreover are amenable to straightforward theoretical analysis. Thus they are ideal models for evaluation of photothermoelasticity.

The experimental results and analysis of the disk are presented in this section and that of the beam in the next section.

Experimental Procedure. A plastic disk was machined from the same lot of Paraplex P-43 sheet as used to obtain the optical and physical properties given herein. The center of the disk was fitted carefully with a steel plug and the unit was placed in the cold chamber and polariscope shown in Fig. 1. To insure a uniform temperature field in the model, thermocouples were inserted in both the plastic disk and steel plug.

In Fig. 5, one half of the model with thermocouples installed is shown for temperature differentials of 27 and 72 deg F. The fringe pattern is the Lamé distribution commonly associated with a disk under internal pressure as a result of the differential contractions of the plastic disk and steel plug.

Analysis of Model. The interface pressure between the disk and plug is a function of the temperature differential ΔT and is given by the following[6]

$$p = \frac{(\delta/a)E_p E_s(b^2 - a^2)}{(1 - \nu_s)E_p(b^2 - a^2) + E_s[(1 + \nu_p)b^2 + (1 - \nu_p)a^2]} \quad [5]$$

where

$$\delta/a = (\epsilon_T)_p - \alpha_s \Delta T$$

The quantity $(\epsilon_T)_p$ can be obtained from Fig. 4 by subtracting the $\Delta L/L$-value at the test temperature from that at room temperature, T_0.

The difference in principal stresses at any radial location r is given by

$$\sigma_r - \sigma_\theta = 2p/[1 - (a/b)^2](r/a)^2 \quad [6]$$

The fringe order at a radial co-ordinate observed in the model as a result of this principal-stress difference is

$$n = (\sigma_r - \sigma_\theta)t/f \quad [7]$$

[6] "An Introduction to the Theory of Elasticity for Engineers and Physicists," by R. V. Southwell, Oxford University Press, London, England, second edition, 1941, pp. 406–407.

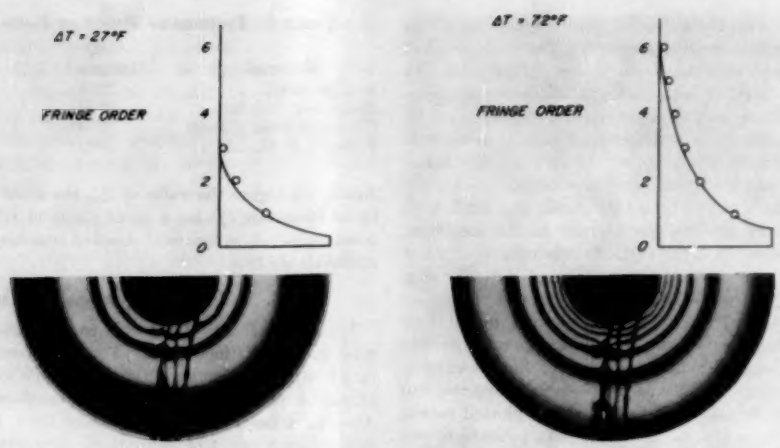

FIG. 5 PHOTOTHERMOELASTIC STUDY (LIGHT FIELD) OF A DISK CONTRACTING UPON AN ELASTIC INCLUSION
(Test points are observed fringe orders and solid line was computed from measured temperature.)

By combining Equations [6] and [7]

$$n = 2pt/[1 - (a/b)^2]f(r/a)^2 \quad [8]$$

where p is given by Equation [5].

Results. The following values were used in Equations [5], [8]:

(*a*) Model dimensions

$a = 0.375$ in., $b = 1.25$ in., $t = 0.250$ in.

(*b*) Steel plug

$E_s = 30 \times 10^6$ psi, $\nu_s = 0.3$, $\alpha_s = 7$ micro-in/in-deg F

(*c*) Paraplex P-43 disk

The pertinent properties are given in Figs. 2 to 4. The room temperature was 77 F and $\nu_s = 0.36$.

In Fig. 5, the theoretical and experimentally obtained fringe orders are shown as a function of the radial co-ordinate for $\Delta T = 27$ F and 72 F. A correction to the theoretical fringe order was necessary to account for a $^1/_2$ fringe order at $r/a = 1.36$ at room temperature due to the slight shrink fit of the model assembly. The correction consisted of adding the fringe-order correction computed by use of Equation [8] to the theoretical value.

It is to be noted that Equation [5] is an approximate solution of the model investigated because of the three-dimensional character of the stress field in the region of the interface. The relatively good agreement obtained in Fig. 5, however, suggests that the theoretical analysis is of an accuracy within the experimental errors of the tests.

THERMAL STRESSES IN BEAMS

To evaluate the photothermoelastic technique under conditions where thermal gradients exist, a long beam was selected for investigation. The temperature gradient was introduced by suddenly applying dry ice to the entire upper edge of the beam. In addition to the long beam, a photographic study was made of the end effects in shorter beams.

Experimental Procedure. To separate the heat-transfer analysis from the thermal-stress analysis the transient-temperature distribution was determined directly from thermocouples cemented into the center of the beam. By assuming that the upper surface of the beam was at the surface temperature of the dry ice and the lower surface of the beam at room temperature (during the first few minutes of the test), five temperature points were known for constructing the temperature distribution for each time interval.

The thermocouple readings were taken simultaneously with photographs of the fringe pattern in all cases. Typical fringe patterns of the center portion of the beam at selected times after application of the dry ice are shown in Fig. 6.

Analysis of a Long Beam. The analysis of the beam at a selected time, for the purpose of predicting theoretically the fringe-order distribution from the temperature distribution, requires a trial-and-error procedure. The following steps were used in the analysis starting from the known temperature distribution:

(*a*) At each point in the cross-section plot $E\epsilon_T$ using the data of Figs. 3 and 4.

(*b*) From equilibr .n considerations the following two conditions must be satisfied

$$\int_0^d E(\epsilon - \epsilon_T)dy = 0 \quad [9]$$

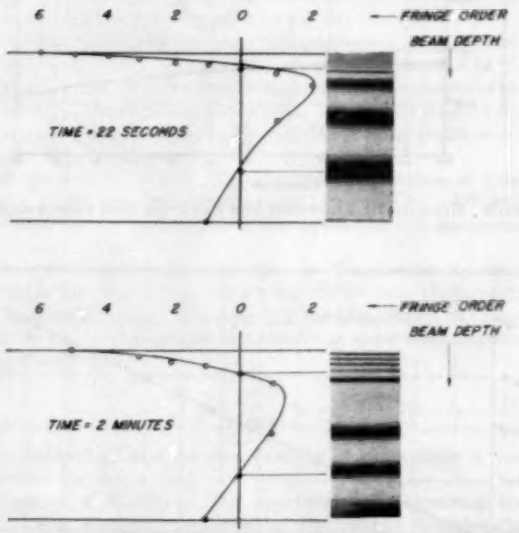

FIG. 6 PHOTOTHERMOELASTIC STUDY (DARK FIELD) OF A LONG BEAM
(Test points are observed fringe orders and solid line was computed from measured temperature distribution.)

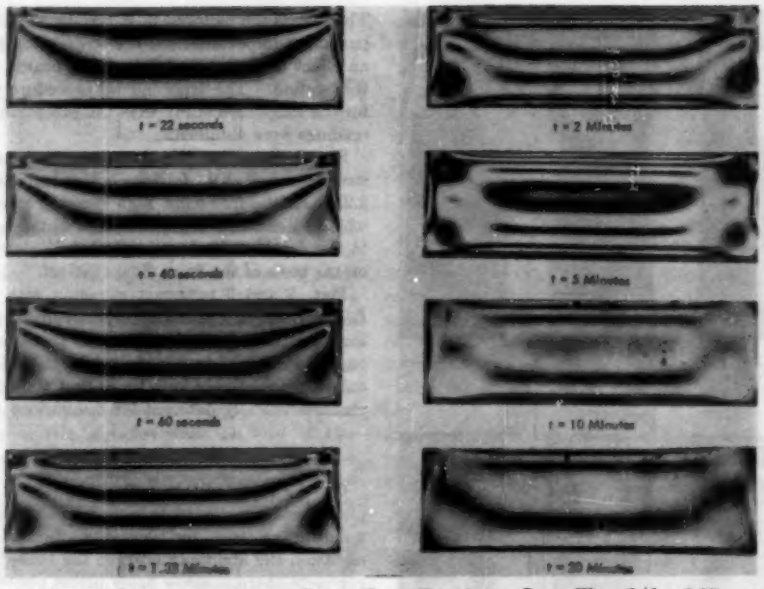

FIG. 7 PHOTOTHERMOELASTIC STUDY (DARK FIELD) OF A BEAM WITH $L/d = 3.25$
(Dark specks are due to dry ice.)

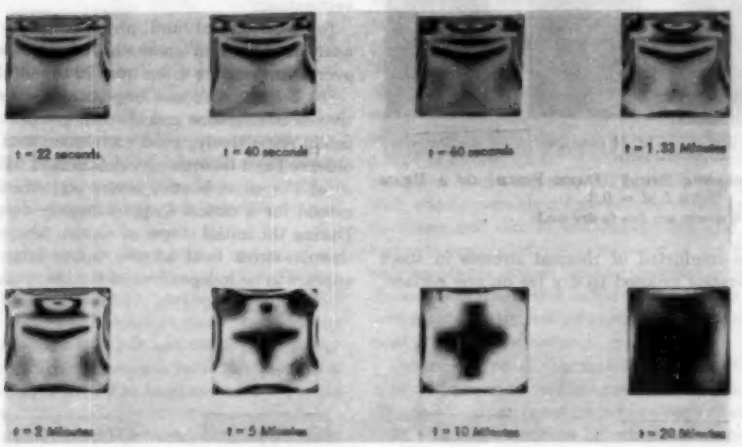

FIG. 8 PHOTOTHERMOELASTIC STUDY (DARK FIELD) OF A BEAM WITH $L/d = 1$
(Dark specks are due to dry ice.)

$$\int_0^d E(\epsilon - \epsilon_T)y \, dy = 0 \quad \ldots\ldots\ldots\ldots [10]$$

Using graphical integration, the $(\epsilon - \epsilon_T)$ distribution can be determined by trial and error.

(*c*) The fringe order at each point can be determined from

$$n = E(\epsilon - \epsilon_T)t/f \quad \ldots\ldots\ldots\ldots\ldots [11]$$

where E and f are obtained from Figs. 2 and 3 for the temperature T at the point.

Results for Long Beam. In the photothermoelastic study, a long Paraplex P-43 beam of the following dimensions was used

$$d = 1 \text{ in.}, t = 0.50 \text{ in.}$$

In Fig. 6, the experimentally observed fringe order at 22 sec and 2 min after the application of dry ice is shown together with the theoretical fringe orders calculated from the experimental temperature distribution.

It can be observed that good agreement is obtained again tending to substantiate the photothermoelastic technique. Any creep effects which may have existed in the plastic model apparently are sufficiently small so as to have a negligible influence upon the degree of correlation obtained between test and theory. In usual applications of this technique the thermal stresses rather than fringe orders would be of interest. However, in this exploratory study, a direct companion of theory and test data is desirable and therefore the fringe orders rather than thermal stresses were correlated.

Short-Beam Study. In order to demonstrate the versatility and graphic nature of the photothermoelastic technique, an

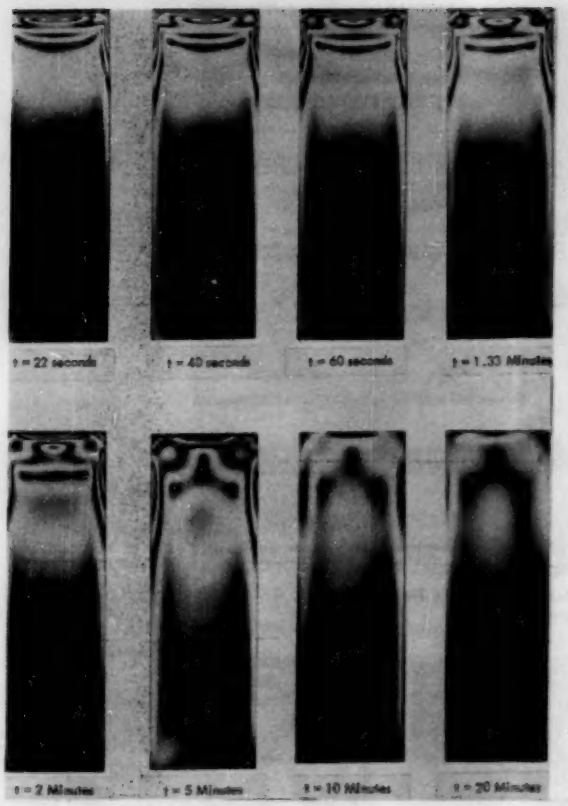

FIG. 9 PHOTOTHERMOELASTIC STUDY (DARK FIELD) OF A BEAM WITH $L/d = 0.3$
(Dark specks are due to dry ice.)

exploratory study was conducted of thermal stresses in short beams of various L/d-ratios exposed to dry ice on one surface. The results are pictorial in nature as shown in Figs. 7 to 9. Of particular importance are the stresses at the ends of the beam, an effect unimportant for the long beams treated previously in this section. The experimental procedure was the same as used for the long-beam study with the exception that no temperature readings were obtained.

Fig. 7 illustrates the time-dependent nature of the thermal stresses as well as the fairly severe end effects for a beam of $L/d = 3.25$. At the free ends, high shearing stresses can be observed which extend into the beam for a distance approximately equal to the depth of the beam. Such behavior would be anticipated on the basis of the Saint Venant effect.

Figs. 8 and 9 represent elements with beam dimensions of $L/d = 1$ and $L/d = 0.308$, respectively. It is interesting to note that the thermal-shock pattern at the upper edge and free end regions in Figs. 7 to 9 is almost identical for short times. It is only after relatively long times that the fringe pattern becomes characteristically different for the various L/d-ratio elements.

CONCLUSIONS

On the basis of this exploratory study, it appears that the photothermoelastic technique has considerable promise as a quantitative tool for verifying thermal-stress analyses. In addition, the ability to observe the time-dependent behavior of complete thermal-stress fields places photothermoelasticity in a unique position in the experimental thermal-stress-analysis field.

More specifically, the following are the conclusions of this investigation:

(*a*) The optical and physical properties pertinent to the analysis of thermal stresses have been obtained for Paraplex P-43 over a temperature range from 70 to −40 F.

(*b*) For the disk and long-beam models which are representative of interference and thermal-gradient type of thermal-stress fields, respectively, good correlation was obtained between the observed and theoretically determined fringe distributions.

(*c*) For short beams, severe end effects were observed which extend for a distance approximately equal to the beam depth. During the initial stages of sudden temperature application, the thermal-stress field at the upper edge and free-end regions appears to be independent of the beam dimensions.

Analysis of Stresses and Strains Near the End of a Crack Traversing a Plate

By G. R. IRWIN,[1] WASHINGTON, D. C.

A substantial fraction of the mysteries associated with crack extension might be eliminated if the description of fracture experiments could include some reasonable estimate of the stress conditions near the leading edge of a crack particularly at points of onset of rapid fracture and at points of fracture arrest. It is pointed out that for somewhat brittle tensile fractures in situations such that a generalized plane-stress or a plane-strain analysis is appropriate, the influence of the test configuration, loads, and crack length upon the stresses near an end of the crack may be expressed in terms of two parameters. One of these is an adjustable uniform stress parallel to the direction of a crack extension. It is shown that the other parameter, called the stress-intensity factor, is proportional to the square root of the force tending to cause crack extension. Both factors have a clear interpretation and field of usefulness in investigations of brittle-fracture mechanics.

Introduction

DURING and subsequent to the recent World War, investigations of fracturing have shared in the general growth of applied-mechanics research. Among the fracture failures responsible for interest in this field were those of welded ships, gas-transmission lines, large oil-storage tanks, and pressurized cabin planes. The propagation of a brittle crack across one or more plates in which the average tensile stress was thought to be safely below the yield strength is a prominent feature of these examples.

As a result of these investigations there was a revival of interest in the Griffith theory of fracture strength (1).[2] It was pointed out independently by Orowan (2) and by the author (3) that a modified Griffith theory is helpful in understanding the development of a rapid fracture which is sustained with energy from the surrounding stress field. Expositions of this idea have been given (3, 4, 5) using such terms as fracture work rate and strain-energy release rate.

The basic idea of the modified Griffith theory is that, at onset of unstable fast fracturing, one can equate the fracture work per unit crack extension to the rate of disappearance of strain energy from the surrounding elastically strained material. The term, disappearance of strain energy, refers to the loss of strain energy which would occur if the system were isolated from receiving energy, for example, from movement of the forces applying tension to the material. For convenience this is referred to here as the fixed-grip strain-energy release rate. Since the strain-energy disappearance rate at any moment depends on the load magnitudes rather than on movement of the points of load application, use of the fixed-grip strain-energy release-rate concept is not limited to fixed-grip experiments.

It is the purpose of this paper to describe the relation of these terms to the elastic stresses and strains near the leading edge of a somewhat brittle crack. For purposes of this paper "somewhat brittle" means that a region of large plastic deformations may exist close to the crack but does not extend away from the crack by more than a small fraction of the crack length.

Previous investigations (3–7) have established a viewpoint with respect to the mechanics of fracturing which may be summarized in part as follows:

The fixed-grip strain-energy release rate has the same role as an influence controlling time rate of crack extension as the longitudinal load has in controlling time rate of plastic extension of a tensile bar. In the latter case the force per unit area tending to cause plastic extension is the longitudinal stress. In the former case a motivating force per unit thickness can be defined quite generally in terms of the rate of conversion of strain energy to thermal energy during crack extension. This generalized force is the rate of decrease of the fixed-grip strain energy with crack extension on a unit-thickness basis. Also this energy rate can be regarded as composed of two terms: (*a*) The strain-energy loss rate associated with nonrecoverable displacements of the points of load application (assumed zero in this discussion); and (*b*) the strain-energy loss rate associated with extension of the fracture accompanied only by plastic strains local to the crack surfaces. The second of these two terms, herein called $\mathcal{G}$, appears to be the force component most directly related to crack extension and the one with the most practical usefulness.

Determination of characteristic values of $\mathcal{G}$ for onset or arrest of rapid fracturing and the applications of such measurements to "fail-safe" design procedures have been discussed elsewhere (4, 5, 8, 9). It will be shown here that the tensile stresses near the crack tip and normal to the plane of the crack are determined by the force tendency $\mathcal{G}$. The discussion is arranged so as to develop relationships useful in the analysis of fracture experiments whether the purpose of the work is to determine characteristic $\mathcal{G}$-values or simply to determine the stress field near the leading edge of the crack.

The material of this paper is, at one point, related to Sneddon's analysis of stresses near an embedded crack having the shape of a flat circular disk (10). Otherwise, for simplicity and bearing in mind the service fracture failures referred to in the foregoing, discussion is restricted to a straight crack in a plate. It is assumed the plate thickness is small enough compared to the crack length so that generalized plane stress constitutes a useful two-dimensional viewpoint. In addition it is assumed the crack is moving, as brittle cracks generally do move, along a path normal to the direction of greatest tension, so that the component of shear stress resolved on the line of expected extension of the crack is zero.

---

[1] Superintendent, Mechanics Division, U. S. Naval Research Laboratory.

[2] Numbers in parentheses refer to the Bibliography at the end of the paper.

Presented at the Applied Mechanics Division Summer Conference, Berkeley, Calif., June 13–15, 1957, of The American Society of Mechanical Engineers.

Discussion of this paper should be addressed to the Secretary, ASME, 29 West 39th Street, New York, N. Y., and will be accepted until October 10, 1957, for publication at a later date. Discussion received after the closing date will be returned.

Note: Statements and opinions advanced in papers are to be understood as individual expressions of their authors and not those of the Society. Manuscript received by ASME Applied Mechanics Division, February 19, 1956. Paper No. 57—APM-22.

Representative Stress Fields Associated With Cracks

A paper by Westergaard (11) gave a convenient semi-inverse method for solving a certain class of plane-strain or plane-stress problems. Let $\overline{Z}$, Z, and Z' represent successive derivatives with respect to z of a function $\overline{Z}(z)$, where z is $(x + iy)$. Assume that the Airy stress function may be represented by

$$F = \mathrm{Re}\overline{Z} + y\, Im\overline{Z} \quad [1]$$

then

$$\sigma_x = \frac{\partial^2 F}{\partial y^2} = \mathrm{Re}Z - y\, ImZ' \quad [2]$$

$$\sigma_y = \frac{\partial^2 F}{\partial x^2} = \mathrm{Re}\, Z + y\, ImZ' \quad [3]$$

$$\tau_{xy} = -\frac{\partial^2 F}{\partial x \partial y} = -y\, \mathrm{Re}\, Z' \quad [4]$$

By choices of the function $Z(z)$, Westergaard showed solutions for stress distribution as influenced by bearing pressures or cracks in a variety of situations. The class of problems which can be solved in this way is limited to those such that τ_{xy} is zero along the x-axis.

In particular, if a large plate contains a single crack on the x-axis whose length is small compared to the plate dimensions or a colinear series of such cracks, and if the applied loads are such that τ_{xy} is zero along the x-axis, then the stress distribution is readily constructed with the aid of Westergaard's semi-inverse procedures.

Two examples of such problems were given by Westergaard (11) as follows:

1 A central straight crack of length $2a$ along the x-axis in an infinite plate with a biaxial field of tension σ at large distances from the crack

$$Z(z) = \frac{\sigma}{[1 - (a/z)^2]^{1/2}} \quad [5]$$

2 A series of equally spaced straight cracks of length $2a$, on the x-axis in an infinite plate with biaxial stress σ, as before, and with the distance between the crack centers, l

$$Z(z) = \frac{\sigma}{\left[1 - \left(\frac{\sin \pi a/l}{\sin \pi z/l}\right)^2\right]^{1/2}} \quad [6]$$

Three additional examples obtainable with the semi-inverse procedure suggested by Westergaard are as follows:

3 Single crack along the x-axis extending from $-a$ to a with a wedge action applied to produce a pair of "splitting forces" of magnitude P located at $x = b$ (see Fig. 1)

$$Z(z) = \frac{Pa}{\pi(z - b)z}\left[\frac{1 - (b/a)^2}{1 - (a/z)^2}\right]^{1/2} \quad [7]$$

4 The situation of example 3 with an additional pair of forces of magnitude P at $x = -b$

$$Z(z) = \frac{2Pa}{\pi(z^2 - b^2)}\left[\frac{1 - (b/a)^2}{1 - (a/z)^2}\right]^{1/2} \quad [8]$$

5 Example 3 repeated along the x-axis at intervals l, and with the wedge action centered so that b is zero

$$Z(z) = \frac{P \sin \frac{\pi a}{l}}{l\left(\sin \frac{\pi z}{l}\right)^2}\left[1 - \left(\frac{\sin \frac{\pi a}{l}}{\sin \frac{\pi z}{l}}\right)^2\right]^{-1/2} \quad [9]$$

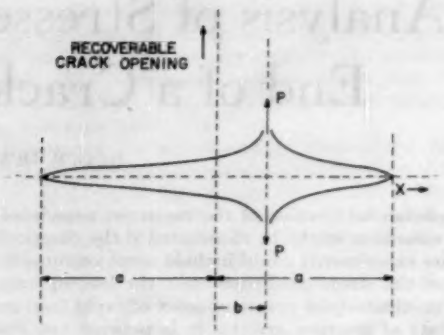

Fig. 1 Opening of a Crack by Wedge Forces

In all of these problems a uniform compression, $-\sigma_{xx}$, may be added to the value of σ_x given by Equation [2]. Since linearized elasticity relations are assumed to apply, one may obtain the Z-function for combined tension and wedge action by adding the appropriate Z-function for tension to the appropriate Z-function for a pair of wedge forces.

As an extending crack moves across a plate of finite width the crack may attain sufficient length so that the tensile forces acting to cause crack extension are not sufficiently accurate when obtained using infinite plate relations such as those of Equations [5] and [7]. The major adjustment required is that of the total load across the x-axis from the end of the crack to the side of the plate. A convenient way to make this adjustment, if the crack is centered, is to use expressions for Z such as in examples 2 and 5. The side boundaries of the plate would then be taken to occur at $x = -l/2$ and $x = +l/2$. In the stress distributions resulting from examples 2 and 5 the shearing stress τ_{xy} is zero along the side boundaries. However, the side boundaries are represented as possessing a distribution of x-direction loads which should be absent. Depending upon the objectives of the stress analysis this defect may be outweighed in importance by the convenience of having an approximate solution of the problem in compact form.

Suppose, next, that the situation to be studied is a crack extending across a finite-width plate from one of the plate side boundaries. Let the intersection of the crack with the side boundary be the origin of co-ordinates and let the line of crack extension be the positive portion of the x-axis, the end of the crack being at $x = a$. It will be assumed that weights or blocks have been set against the side boundaries so as to prevent or greatly reduce the tendency of these boundaries to move in the negative x-direction as the crack extends. In this event Z-functions similar to those of examples 2 and 5 may again be employed as a convenient means for obtaining a compact approximation to the stress distribution. In this situation the side boundaries of the plate would be assumed to be at $x = 0$ and at $x = l/2$.

In any of the foregoing examples the only stress acting at the edges of the crack is the optional added stress in the x-direction $-\sigma_{xx}$. An uncertainty as to proper choice of σ_{xx} exists for the example discussed previously of a crack extending from one side of a finite-width plate. In addition, if the crack moves rapidly, determination of the stress distribution away from the crack will require a dynamic-stress analysis.

Stress Environment of the End of the Crack

However, the stress distribution near the end of the crack can be expressed (a) independently of uncertainties of both magnitude of applied loads and of the dynamic unloading influences, and (b) in such a way that records from several strain gages placed near the

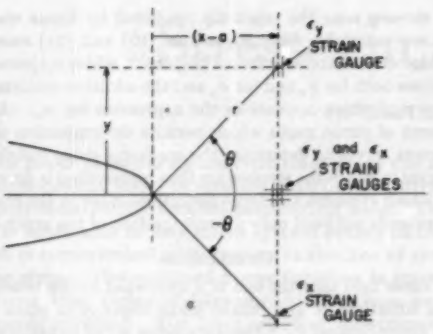

FIG. 2 RELATION OF r AND θ TO y AND $(x - a)$ AND EXAMPLES OF LOCATIONS FOR STRAIN GAGES

end of the crack serve to determine the "crack-tip stress distribution."

Consider for all of the five examples the substitution of variables

$$z = a + re^{i\theta}$$

where

$$r^2 = (x - a)^2 + y^2 \text{ and } \tan\theta = y/(x - a)$$

as shown in Fig. 2.

If one assumes quantities such as r/a and $r/(a - b)$ may be neglected in comparison to unity, one finds in each case

$$\sigma_y = \left(\frac{E\mathcal{G}}{\pi}\right)^{1/2} \frac{\cos\theta/2}{\sqrt{(2r)}}\left(1 + \sin\frac{\theta}{2}\sin\frac{3\theta}{2}\right) \quad [10]$$

and

$$\sigma_x = \left(\frac{E\mathcal{G}}{\pi}\right)^{1/2} \frac{\cos\dfrac{\theta}{2}}{\sqrt{(2r)}}\left(1 - \sin\frac{\theta}{2}\sin\frac{3\theta}{2}\right) - \sigma_{ox} \quad [11]$$

where E is Young's modulus. $\mathcal{G}$ is independent of r and of θ and will be discussed in following sections of this paper.

For a crack traversing a plate, the thickness of which is considerably smaller than the crack length, a generalized plane-stress viewpoint is appropriate and σ_z is zero. However, for comparison with results obtained by Sneddon (10) one may consider for the moment the set of three extensional stresses which would pertain to a plane-strain analysis. Sneddon studied the stress distribution predicted by linear elastic theory in the vicinity of a "penny-shaped" crack embedded in a much larger solid material and subjected to tension perpendicular to the plane of the crack. For the extensional stresses in the close neighborhood of the crack outer boundary, Sneddon gave expressions identical to Equations [10] and [11] with regard to the functional relationship of σ_x and σ_y to r and θ. A third extensional stress directed parallel to the outer boundary of the penny-shaped crack was given by Sneddon with the remark that no counterpart to this third extensional stress existed in a two-dimensional analysis of stresses near a crack. However, the remark applies only to the two-dimensional analysis assuming generalized plane stress. For the two-dimensional analysis assuming plane strain the third extensional stress, which is Poisson's ratio times the sum of σ_x and σ_y, as in Equations [10] and [11], is the counterpart to Sneddon's third extensional stress component. Thus for any small region around the outer boundary of Sneddon's penny-shaped crack, the stresses, strains, and displacements correspond to a situation which is locally one of plane strain. The preceding comment becomes intuitively obvious when one considers that, in Sneddon's example, all particle displacements lie in planes which contain the axis of symmetry. These planes would approximate to a set of parallel planes within any region whose dimensions are very small compared to distance from the region to the axis of symmetry.

FORCE TENDING TO CAUSE CRACK EXTENSION

As the crack extends, an energy transfer from mechanical or strain energy into other forms occurs in the vicinity of the crack. The process is such that transfer of strain energy to heat dominates.

$\mathcal{G}$ is the magnitude of this energy exchange associated with unit extension of the crack and may be regarded as the force tending to cause crack extension. This may be seen as follows:

The linear elasticity relations resulting from Equations [5] through [11] correspond to a parabolic shape for the crack opening near the crack tip. In Fig. 3 the origin of x, y-co-ordinates has been shifted so that the crack opening, shown by the dashed line,

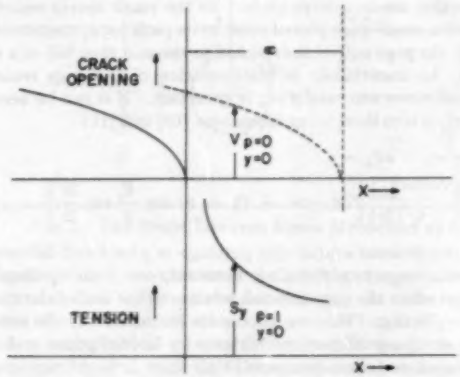

FIG. 3 LINEAR-ELASTIC-THEORY CRACK OPENINGS AND STRESSES NEAR END OF A CRACK

extends to $x = \alpha$. It is assumed α is very small compared to the length of the crack. If y-direction tensions given by

$$S_y(p) = p\left(\frac{E\mathcal{G}}{\pi}\right)^{1/2} \frac{1}{\sqrt{(2x)}} \quad [12]$$

are exerted on the edges of the crack from $x = 0$ to $x = \alpha$, and p is increased from zero to 1, the crack is closed up so that the crack opening appears to end at the origin as shown by the full line. The factor p may be regarded as a proportional loading parameter. To the same approximation as Equation [10], the crack opening from $x = 0$ to $x = \alpha$ at any time during the closure operation is given by

$$v(p) = (1 - p)\frac{2}{E}\left(\frac{E\mathcal{G}}{\pi}\right)^{1/2}\sqrt{[2(\alpha - x)]} \quad [13]$$

Since the degree of closure is a linear function of S_y the work done by the closing forces as p is varied from zero to 1 is given by

$$\int_0^\alpha S_y(1)v(0)dx = \frac{2\mathcal{G}}{\pi}\int_0^\alpha\left(\frac{\alpha - x}{x}\right)^{1/2} dx = \alpha\mathcal{G} \quad [14]$$

Thus $\alpha\mathcal{G}$ is the "fixed grip" loss of energy from the strain-energy field as the crack extends by the amount α and the generalized force interpretation of $\mathcal{G}$ is apparent.

For mathematical simplicity the foregoing calculation was

based upon the linear elasticity stresses and crack-opening displacements in the immediate vicinity of the crack tip. One should not assume, however, that local stress relaxation and crack-opening distortion by plastic flow necessarily change the rate of loss of strain energy with crack extension from that indicated in the foregoing by an appreciable amount. The procedure leading to Equation [14] is equivalent to finding the derivative with respect to crack length of the total strain energy under fixed-grip conditions. The contribution to this calculation from a small circular region enclosing the crack tip is relatively small. In situations such as those of Equations [5] through [9], the fraction of $\mathcal{G}$ contributed from this region is, in fact, only about a third of the ratio of the outer radius of the region to the half length a of the crack. Thus if plastic strains near a crack affect the stress field only within distances from the crack, small in relation to the crack length, then the influence of these plastic strains on the calculation of $\mathcal{G}$ is correspondingly small.

Remarks on Measurement Methods

Consider the situation suggested earlier of a crack moving in the x-direction across a large plate. As the crack moves under and beyond a strain gage placed close to its path for ϵ_y measurement, Fig. 2, the gage output is expected to rise and then fall to a small value. An uncertainty in interpretation of the gage record in terms of stress will exist if σ_{zz} is uncertain. If it can be assumed that σ_{zz} is zero then, using Equations [10] and [11]

$$E\epsilon_y = \sigma_y - \nu\sigma_x = \left(\frac{E\mathcal{G}}{\pi}\right)^{1/2} \frac{\cos\theta/2}{\sqrt{(2r)}}\left[(1-\nu) + (1+\nu)\sin\frac{\theta}{2}\sin\frac{3\theta}{2}\right] \quad \ldots\ldots [15]$$

where ν is Poisson's ratio. By putting $r = y \csc\theta$ and differentiating with respect to θ with y constant, one finds ϵ_y should be greatest when the gage position relative to the end of the crack is at $\theta = 70$ deg. This result is quite insensitive to the assumed value of ν (unpublished calculations by L. McFadden and J. H. Hancock based upon Equation [9]).

A better situation for analysis purposes exists if both ϵ_y and ϵ_x are measured. In this event one has

$$\sigma_y = \frac{E}{1-\nu^2}(\epsilon_y + \nu\epsilon_x) \quad \ldots\ldots [16]$$

Differentiating Expression [10] for σ_y with respect to θ holding y constant, one finds the maximum will occur when the measurement position is at 73.4 deg. As a crack moves under and beyond the position of measurement of ϵ_y and ϵ_x the quantity $(\epsilon_y + \nu\epsilon_x)$ plotted against time should have a maximum at that angle. Thus with θ, r, and $(\epsilon_y + \nu\epsilon_x)$ known for a particular location of the crack, the stress-intensity factor $(E\mathcal{G}/\pi)^{1/2}$, and the crack extension force $\mathcal{G}$ existing at the moment of that crack location can be calculated.

The stresses near the crack tip predicted by linear elasticity theory are calculable from Equations [10] and [11] except for knowledge of the intensity factor $(E\mathcal{G}/\pi)^{1/2}$, which appears in the expressions both for σ_x and for σ_y and the additive uniform stress factor $-\sigma_{zz}$, which appears in the expression for σ_x. Any arrangement of strain gages which permits determination of these two factors serves to determine the crack-tip stress distribution. The region in which the stresses are thus represented is an annular region which excludes any large distortions close to the crack but which extends outward only a small fraction of the crack length.

Conclusions

The stress field near the end of a somewhat brittle tensile fracture, in situations of generalized plane stress or of plane strain, can be approximated by a two-parameter set of equations. The most significant of these parameters, the intensity factor, is $(E\mathcal{G}/\pi)^{1/2}$ for plane stress where $\mathcal{G}$ is the force tending to cause crack extension.[8] When the experimental situation permits use of strain gages at distances from the crack tip, small compared to the crack length, values of $\mathcal{G}$ and σ_{zz} may be evaluated conveniently by measuring local strain at selected positions.

BIBLIOGRAPHY

1 "The Phenomenon of Rupture and Flow in Solids," by A. A. Griffith, Philosophical Transactions of the Royal Society of London, series A, vol. 221, 1920, pp. 163–198.

2 "Fundamentals of Brittle Behavior in Metals," by E. Orowan, Fatigue and Fracture of Metals (MIT Symposium, June, 1950), John Wiley & Sons, Inc., New York, N. Y., 1952, p. 154.

3 "Fracture Dynamics," by G. R. Irwin, Fracturing of Metals, ASM, 1948, p. 152.

4 "Fracturing and Fracture Dynamics," by G. R. Irwin and J. A. Kies, *Welding Journal*, vol. 31, Research Supplement, February, 1952, pp. 95s–100s.

5 "Critical Energy Rate Analysis of Fracture Strength of Large Welded Structures," by G. R. Irwin and J. A. Kies, *Welding Journal*, vol. 33, Research Supplement, April, 1954, pp. 193s–198s.

6 "Strain Energy Release Rates for Fractures Caused by Wedge Action," by A. A. Wells, NRL Report No. 4705, March, 1956.

7 "Onset of Fast Crack Propagation in High Strength Steel and Aluminum Alloys," by G. R. Irwin, Proceedings of 1955 Sagamore Conference on Strength Limitations of Metals, Syracuse University, N. Y., March, 1956, pp. 289–305.

8 "The Relation of Crack Extension Force to Onset of Fast Fracturing," by T. W. George, G. R. Irwin, and J. A. Kies, I.A.S. Meeting, January 23–26, 1956.

9 "Energy Release Rates During Fracturing of Perforated Plates," by M. W. Brossman and J. A. Kies, NRL Memorandum Report No. 370, November, 1954.

10 "The Distribution of Stress in the Neighborhood of a Crack in an Elastic Solid," by I. N. Sneddon, Proceedings of the Physical Society of London, vol. 187, 1946, p. 229.

11 "Bearing Pressures and Cracks," by H. M. Westergaard, Trans. ASME, vol. 61, 1939, pp. A-49–A-53.

[8] For plane strain, one substitutes $E/(1-\nu^2)$ for E in the expression for the stress-intensity factor. No change in the magnitude of the stress-intensity factor occurs because $\mathcal{G}$, for plane strain, is $(1-\nu^2)$ times $\mathcal{G}$ for plane stress.

Stresses in a Perforated Strip

By CHIH-BING LING,[1] TAIWAN, CHINA

This paper presents an analytic solution of the classical problem dealing with the stresses in an infinite strip having an unsymmetrically located perforating hole. The solution is applicable to any stress system acting in the strip, which is symmetrical with respect to the line of symmetry of the strip. The required stress function is constructed by using four series of biharmonic functions and a biharmonic integral. The four series of biharmonic functions are formed from a class of periodic harmonic functions specially constructed for the purpose. The solution can be regarded as a complete solution of the problem in the sense that, unlike the previous solutions by Howland, Stevenson, and Knight for a symmetrically perforated strip, it is valid in the entire strip. Numerical examples are given for the fundamental cases of longitudinal tension and transverse bending.

Introduction

THE stresses in an infinite strip having a symmetrically located perforating hole when the strip is under a longitudinal tension were investigated by Howland (1)[2] in 1930. The method used in his solution is essentially one of successive approximations such that the required solution is the sum of a series of biharmonic functions any one of which cancels the normal and tangential stresses on one of the boundaries due to the previous solution. Later, Howland in 1934 with the collaboration of Stevenson (2) extended the method to unsymmetrical stress systems acting in the same symmetrically perforated strip, and worked out in detail the cases of transverse bending with or without shear. The longitudinal tension case as just mentioned also was solved by Knight (3) in 1934 in a way which is more direct than that used by Howland. Nevertheless, all the solutions are valid in the neighborhood of the hole only.

In this paper an analytic solution for the stresses in an infinite strip having an unsymmetrically located perforating hole will be presented. The solution is applicable to any stress system acting in the strip, which is symmetrical with respect to the line of symmetry of the strip. The required stress function is constructed by using four series of biharmonic functions and a biharmonic integral. The four series of biharmonic functions are formed from a class of periodic harmonic functions as defined in Appendix 1. The present solution can be regarded as a complete solution of the problem in the sense that, unlike the previous solutions, it is valid in the entire strip. In what follows, the method of solution is first described and then numerical examples are given for the fundamental cases of longitudinal tension and transverse bending.

[1] Director, Aeronautical Research Laboratory, Taichung; also, Acting Director, Institute of Mathematics, Academia Sinica, Taipei.

[2] Numbers in parentheses refer to the Bibliography at the end of the paper.

Presented at the Applied Mechanics Division Summer Conference, Berkeley, Calif., June 13–15, 1957, of The American Society of Mechanical Engineers.

Discussion of this paper should be addressed to the Secretary, ASME, 29 West 39th Street, New York, N. Y., and will be accepted until October 10, 1957, for publication at a later date. Discussion received after the closing date will be returned.

Note: Statements and opinions advanced in papers are to be understood as individual expressions of their authors and not those of the Society. Manuscript received by ASME Applied Mechanics Division, May 14, 1956. Paper No. 57—APM-8.

Method of Solution

Consider an infinite strip of uniform width $2b$, perforated unsymmetrically by a circular hole of radius λb. Let the origin of the co-ordinates be at the center of the hole and the x-axis parallel to the edges of the strip. For convenience, the rectangular co-ordinates (x, y) henceforth will be regarded as dimensionless quantities referring to a typical length b or one half of the width of the strip. The edges of the strip will be represented by the lines $y = 1 - c$ and $(-1 - c)$, respectively, as shown in Fig. 1; c being a quantity numerically less than unity.

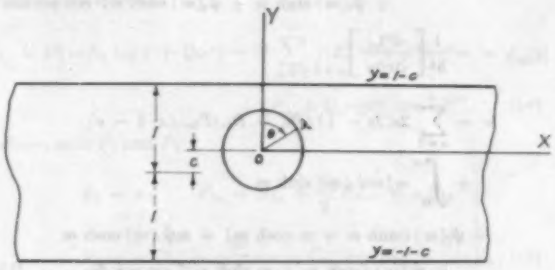

Fig. 1 The Strip, Lengths Being Measured by b

Suppose that in the absence of the hole the stresses in the strip are derived from a basic stress function χ_0. In order to allow for the effect of the hole, an auxiliary stress function χ_1 is constructed, using series of suitable biharmonic functions and a biharmonic integral, such that the corresponding stresses vanish at x infinity or the ends of the strip as well as along the edges. This is added to χ_0 so that the required stress function is given by

$$\chi = \chi_0 + \chi_1 \quad \ldots\ldots [1]$$

The boundary conditions at the rim of the hole are then satisfied by adjusting the coefficients of superposition attached to the series of biharmonic functions. The biharmonic functions have singularities at the origin. Such singularities eventually will be excluded from the material of the strip by the perforating hole.

Suppose further that the basic stress function is even in x; that is, it is symmetrical with respect to the y-axis or the line of symmetry of the strip. Consequently, the auxiliary stress function is also even in x. It will be constructed as follows

$$\chi_1 = b^2 \sum_{s=0}^{\infty} A_{2s} S_{2s}(x, y) + b^2 \sum_{s=1}^{\infty} D_{2s} S_{2s-1}(x, y)$$

$$+ b^2 \sum_{s=1}^{\infty} (y + c) B_{2s} S_{2s-1}(x, y) + b^2 \sum_{s=1}^{\infty} C_{2s} \left[(y + c) S_{2s}(x, y) \right.$$

$$\left. + S_{2s-1}(x, y)/(2s - 1) \right] + b^2 \int_0^{\infty} \left[\psi_1(m) \cosh m(y + c) \right.$$

$$+ \psi_2(m) (y + c) \sinh m(y + c) + \psi_3(m) \sinh m(y + c)$$

$$\left. + \psi_4(m) (y + c) \cosh m(y + c) \right] \cos mx \, dm \quad \ldots\ldots [2]$$

where S_s are periodic harmonic functions defined in Appendix 1; $A_{2s}, B_{2s}, \ldots$ being coefficients of superposition and ψ_n arbitrary functions. The auxiliary stress function thus constructed satis-

fies the biharmonic equation $\nabla^4\chi_1 = 0$ as required, where $\nabla^4 = \nabla^2\nabla^2$ and ∇^2 stands for the Laplace operator $\partial^2/\partial x^2 + \partial^2/\partial y^2$. Besides, it satisfies the conditions of single-valuedness of stresses and displacements throughout the strip.

The stresses derived from χ_1 vanish at x infinity while for $y = 1 - c$ the normal and tangential stresses are found as follows

$$
\begin{aligned}
[\sigma_y]_1 &= \frac{1}{b^2}\left[\frac{\partial^2\chi_1}{\partial x^2}\right]_{y=1-c} \\
&= -A_0 S_2(x, 1-c) \\
&\quad - \sum_{s=1}^{\infty} 2s(2s+1)(A_{2s} + C_{2s}) S_{2s+2}(x, 1-c) \\
&\quad - \int_0^{\infty} m^2\{\psi_1(m)\cosh m + \psi_2(m)\sinh m \\
&\qquad + \psi_3(m)\sinh m + \psi_4(m)\cosh m\}\cos mx\, dm \\
[\tau_{xy}]_1 &= -\frac{1}{b^2}\left[\frac{\partial^2\chi_1}{\partial x \partial y}\right]_{y=1-c} \\
&= -\sum_{s=1}^{\infty} 2s(2s-1)(B_{2s} + D_{2s}) T_{2s+1}(x, 1-c) \\
&\quad + \int_0^{\infty} m\{m\psi_1(m)\sinh m \\
&\quad + \psi_2(m)(\sinh m + m\cosh m) + m\psi_3(m)\cosh m \\
&\qquad + \psi_4(m)(\cosh m + m\sinh m)\}\sin mx\, dm \quad \ldots\ldots [3]
\end{aligned}
$$

Also for $y = -1 - c$,

$$
\begin{aligned}
[\sigma_y]_2 &= -A_0 S_2(x, -1-c) \\
&\quad - \sum_{s=1}^{\infty} 2s(2s+1)(A_{2s} - C_{2s}) S_{2s+2}(x, -1-c) \\
&\quad - \int_0^{\infty} m^2\{\psi_1(m)\cosh m + \psi_2(m)\sinh m \\
&\qquad - \psi_3(m)\sinh m - \psi_4(m)\cosh m\}\cos mx\, dm \\
[\tau_{xy}]_2 &= \sum_{s=1}^{\infty} 2s(2s-1)(B_{2s} - D_{2s}) T_{2s+1}(x, -1-c) \\
&\quad - \int_0^{\infty} m\{m\psi_1(m)\sinh m + \psi_2(m)(\sinh m + m\cosh m) \\
&\qquad - m\psi_3(m)\cosh m - \psi_4(m)(\cosh m + m\sinh m)\}\sin mx\, dm \quad [4]
\end{aligned}
$$

These edge stresses vanish identically provided that by Fourier transforms

$$
\begin{aligned}
&m^2\{\psi_1(m)\cosh m + \psi_2(m)\sinh m + \psi_3(m)\sinh m \\
&\qquad + \psi_4(m)\cosh m\} = -A_0 U_2(1-c) \\
&\qquad\quad - \sum_{s=1}^{\infty} 2s(2s+1)(A_{2s} + C_{2s}) U_{2s+2}(1-c) \\
&m\{m\psi_1(m)\sinh m + \psi_2(m)(\sinh m + m\cosh m) \\
&\qquad + m\psi_3(m)\cosh m + \psi_4(m)(\cosh m + m\sinh m)\} \\
&\qquad\quad = \sum_{s=1}^{\infty} 2s(2s-1)(B_{2s} + D_{2s}) U_{2s+1}(1-c) \\
&m^2\{\psi_1(m)\cosh m + \psi_2(m)\sinh m - \psi_3(m)\sinh m \\
&\qquad - \psi_4(m)\cosh m\} = -A_0 U_2(-1-c) \\
&\qquad\quad - \sum_{s=1}^{\infty} 2s(2s+1)(A_{2s} - C_{2s}) U_{2s+2}(-1-c) \\
&m\{m\psi_1(m)\sinh m + \psi_2(m)(\sinh m + m\cosh m) \\
&\qquad - m\psi_3(m)\cosh m - \psi_4(m)(\cosh m + m\sinh m)\} \\
&\qquad\quad = \sum_{s=1}^{\infty} 2s(2s-1)(B_{2s} - D_{2s}) U_{2s+1}(-1-c) \quad \ldots\ldots [5]
\end{aligned}
$$

where

$$
\left.
\begin{aligned}
U_{2s+1}(\pm 1 - c) &= \frac{2}{\pi}\int_0^{\infty} T_{2s+1}(x, \pm 1 - c)\sin mx\, dx \\
U_{2s+2}(\pm 1 - c) &= \frac{2}{\pi}\int_0^{\infty} S_{2s+2}(x, \pm 1 - c)\cos mx\, dx
\end{aligned}
\right\} \quad \ldots [6]
$$

Integrating by parts, the integrals become

$$
\left.
\begin{aligned}
U_{2s+1}(\pm 1 - c) &= \frac{2m^{2s-1}}{\pi(2s)!}\int_0^{\infty} S_2(x, \pm 1 - c)\cos mx\, dx \\
U_{2s+2}(\pm 1 - c) &= \frac{2m^{2s}}{\pi(2s+1)!} \\
&\quad \times \int_0^{\infty} S_2(x, \pm 1 - c)\cos mx\, dx
\end{aligned}
\right\} \quad \ldots [7]
$$

From Appendix 1

$$
\left.
\begin{aligned}
S_2(x, \pm 1 - c) = -\frac{\pi^2}{4}\Bigg\{ &\frac{\cos\frac{\pi}{2}(1 \mp c)}{\cos\frac{\pi}{2}x - \cos\frac{\pi}{2}(1 \mp c)} \\
&- \frac{\sin^2\frac{\pi}{2}(1 \mp c)}{\left[\cos\frac{\pi}{2}x - \cos\frac{\pi}{2}(1 \mp c)\right]^2}\Bigg\}
\end{aligned}
\right\} \quad \ldots\ldots [8]
$$

we find by Cauchy's theorem of residues

$$
\int_0^{\infty} S_2(x, \pm 1 - c)\cos mx\, dx = \frac{m\pi\cosh m(1 \pm c)}{\sinh 2m} \quad \ldots\ldots [9]
$$

The foregoing results lead to

$$
\left.
\begin{aligned}
-\frac{1}{2}\psi_1(m) &= \frac{A_0(1 + m\coth m)\cosh mc}{m(\sinh 2m + 2m)} \\
&\quad + \sum_{s=1}^{\infty}\frac{m^{2s-1}}{(2s-1)!}\,\frac{\begin{matrix}A_{2s}(1 + m\coth m)\cosh mc \\ + C_{2s}(m + \tanh m)\sinh mc\end{matrix}}{\sinh 2m + 2m} \\
&\quad + \sum_{s=1}^{\infty}\frac{m^{2s-1}}{(2s-2)!}\,\frac{B_{2s}\cosh mc + D_{2s}\tanh m\sinh mc}{\sinh 2m + 2m} \\
\frac{1}{2}\psi_2(m) &= \frac{A_0\cosh mc}{\sinh 2m + 2m} \\
&\quad + \sum_{s=1}^{\infty}\frac{m^{2s}}{(2s-1)!}\,\frac{A_{2s}\cosh mc + C_{2s}\tanh m\sinh mc}{\sinh 2m + 2m} \\
&\quad + \sum_{s=1}^{\infty}\frac{m^{2s-1}}{(2s-2)!}\,\frac{B_{2s}\coth m\cosh mc + D_{2s}\sinh mc}{\sinh 2m + 2m} \\
-\frac{1}{2}\psi_3(m) &= \frac{A_0(1 + m\tanh m)\sinh mc}{m(\sinh 2m - 2m)}
\end{aligned}
\right\} \quad \ldots [10]
$$

$$+\sum_{s=1}^{\infty}\frac{m^{2s-1}}{(2s-1)!}\frac{A_{2s}(1+m\tanh m)\sinh mc+C_{2s}(m+\coth m)\cosh mc}{\sinh 2m-2m}$$

$$+\sum_{s=1}^{\infty}\frac{m^{2s-1}}{(2s-2)!}\frac{B_{2s}\sinh mc+D_{2s}\coth m\cosh mc}{\sinh 2m-2m}$$

$$\frac{1}{2}\psi_4(m)=\frac{A_0\sinh mc}{\sinh 2m-2m}$$

$$+\sum_{s=1}^{\infty}\frac{m^{2s}}{(2s-1)!}\frac{A_{2s}\sinh mc+C_{2s}\coth m\cosh mc}{\sinh 2m-2m}$$

$$+\sum_{s=1}^{\infty}\frac{m^{2s-1}}{(2s-2)!}\frac{B_{2s}\tanh m\sinh mc+D_{2s}\cosh mc}{\sinh 2m-2m}\quad\ldots[10]\ (cont.)$$

It is noted that on substituting these values into the function χ_1 in Equation [2] the integral becomes divergent at the lower limit because the integrand becomes

$$-\{2A_0+3(y-1+c)(cA_0+C_2+D_2)\}/(2m^2)$$

as m tends to zero. However, if this term is subtracted from the integrand such that the resulting integrand becomes constant as m tends to zero, the new integral is now convergent. Such a modification is permissible for it does not affect the convergence at the upper limit as well as the stresses derived from the integral.

Define a pair of polar co-ordinates (r, θ) by

$$z=x+iy=ire^{-i\theta}$$

that is

$$x=r\sin\theta\qquad y=r\cos\theta\quad\ldots\ldots[11]$$

Also, suppose that the normal and tangential stresses derived from the basic stress function χ_0 take the following values at $r=\lambda$ or the rim of the hole

$$[\sigma_r]_0=\sum_{n=0}^{\infty}a_n\cos n\theta,\qquad [\tau_{r\theta}]_0=\sum_{n=1}^{\infty}c_n\sin n\theta\ldots.[12]$$

Note that the equality $a_1=c_1$ implies the condition of zero force resultant at the rim of the hole. In order to satisfy the boundary conditions of zero traction at the rim of the hole, these stresses must be annulled by those derived from the auxiliary stress function χ_1.

To proceed further, it is necessary to express χ_1 in polar co-ordinates (r, θ). Such an expression for S_s is given in Appendix 1. The corresponding expression for the biharmonic integral can be obtained with the aid of the following expansions

$$\cosh m(y+c)\cos mx=\sum_{n=0}^{\infty}\left\{\frac{\cosh mc}{(2n)!}(mr)^{2n}\cos 2n\theta+\frac{\sinh mc}{(2n+1)!}(mr)^{2n+1}\cos(2n+1)\theta\right\}$$

$$\sinh m(y+c)\cos mx=\sum_{n=0}^{\infty}\left\{\frac{\sinh mc}{(2n)!}(mr)^{2n}\cos 2n\theta+\frac{\cosh mc}{(2n+1)!}(mr)^{2n+1}\cos(2n+1)\theta\right\}\quad\ldots[13]$$

Consequently we may write in the following condensed form, except for a constant

$$\chi_1=b^2(-E_0\log r+Q_0r^2)+b^2\sum_{n=1}^{\infty}\{(E_n+F_nr^2)r^{-n}+(P_n+Q_nr^2)r^n\}\cos n\theta\ldots\ldots[14]$$

where, save F_1 and P_1

$$E_0=A_0,\qquad E_{2n}=A_{2n}+\frac{1}{2}B_{2n+2}+cC_{2n}$$

$$E_{2n-1}=D_{2n}+\frac{2n+1}{2(2n-1)}C_{2n}+cB_{2n}\quad\ldots[15]$$

$$F_{2n}=\frac{1}{2}B_{2n},\qquad F_{2n+1}=\frac{1}{2}C_{2n}$$

and

$$P_n=-{}^nA_0A_0-\sum_{s=1}^{\infty}({}^n\alpha_{2s}A_{2s}+{}^n\beta_{2s}B_{2s}+{}^n\gamma_{2s}C_{2s}+{}^n\delta_{2s}D_{2s})$$

$$Q_n={}^n\alpha_0{}^*A_0+\sum_{s=1}^{\infty}({}^n\alpha_{2s}{}^*A_{2s}+{}^n\beta_{2s}{}^*B_{2s}+{}^n\gamma_{2s}{}^*C_{2s}+{}^n\delta_{2s}{}^*D_{2s})\quad\ldots[16]$$

in which

$${}^n\alpha_0=-{}^n\Omega_0+\frac{2(K_n{}^*-cK_n)}{(2-2c)^{n+1}}-\frac{(n-2)K_{n-1}}{n(2-2c)^n}$$

$${}^n\alpha_{2s}=-{}^n\Omega_{2s}+\binom{n+2s-1}{n}\frac{2(n+2s)(K_{n+2s}{}^*-cK_{n+2s})}{(2-2c)^{n+2s+1}}-\frac{n-2}{n}\binom{n+2s-2}{n-1}\frac{(n+2s-1)K_{n+2s-1}}{(2-2c)^{n+2s}}$$

$${}^n\beta_{2s}=\frac{1}{2}({}^{n-1}\Omega_{2s-1}+2c\,{}^n\Omega_{2s-1})+\binom{n+2s-2}{n}\frac{2(n+2s-1)(K_{n+2s-1}-cK_{n+2s-1}{}^*)}{(2-2c)^{n+2s}}$$

$$-\binom{n+2s-3}{n-1}\frac{(n+2s-2)K_{n+2s-2}{}^*}{(2-2c)^{n+2s-1}}\quad\ldots[17]$$

$${}^n\gamma_{2s}=-\frac{1}{2}\left(\frac{n-2}{n}{}^{n-1}\Omega_{2s}+2c\,{}^n\Omega_{2s}\right)+\binom{n+2s-1}{n}\frac{2(n+2s)(J_{n+2s}{}^*-cJ_{n+2s})}{(2-2c)^{n+2s+1}}$$

$$-\frac{n-2}{n}\binom{n+2s-2}{n-1}\frac{(n+2s-1)J_{n+2s-1}}{(2-2c)^{n+2s}}$$

$${}^n\delta_{2s}={}^n\Omega_{2s-1}+\binom{n+2s-2}{n}\frac{2(n+2s-1)(J_{n+2s-1}-cJ_{n+2s-1}{}^*)}{(2-2c)^{n+2s}}-\binom{n+2s-3}{n-1}\frac{(n+2s-2)J_{n+2s-2}{}^*}{(2-2c)^{n+2s-1}}$$

and

$$
\left.
\begin{aligned}
{}^{n}\alpha_0^* &= \frac{K_{n+1}}{(2-2c)^{n+2}} \\
{}^{n}\alpha_{2s}^* &= \binom{n+2s}{n+1}\frac{(n+2s+1)K_{n+2s+1}}{(2-2c)^{n+2s+2}} \\
{}^{n}\beta_{2s}^* &= -\frac{1}{2}{}^{n+1}\Omega_{2s-1} + \binom{n+2s-1}{n+1}\frac{(n+2s)K_{n+2s}^*}{(2-2c)^{n+2s+1}} \\
{}^{n}\gamma_{2s}^* &= \frac{1}{2}{}^{n+1}\Omega_{2s} + \binom{n+2s}{n+1}\frac{(n+2s+1)J_{n+2s+1}}{(2-2c)^{n+2s+2}} \\
{}^{n}\delta_{2s}^* &= \binom{n+2s-1}{n+1}\frac{(n+2s)J_{n+2s}^*}{(2-2c)^{n+2s+1}}
\end{aligned}
\right\} \quad \ldots [18]
$$

Here the coefficients ${}^{n}\Omega_s$ are defined in Appendix 1 while the integrals K_k, K_k^*, J_k, and J_k^* are defined as follows

$$
\left.
\begin{aligned}
K_{2k} = J_{2k}^* &= \frac{(2-2c)^{2k+1}}{2(2k)!}\int_0^\infty m^{2k}\left(\frac{\sinh 2mc}{\sinh 2m+2m} + \frac{\sinh 2mc}{\sinh 2m-2m}\right)dm \\
K_{2k+1} &= \frac{(2-2c)^{2k+2}}{(2k+1)!}\int_0^\infty m^{2k+1}\left(\frac{\cosh^2 mc}{\sinh 2m+2m} + \frac{\sinh^2 mc}{\sinh 2m-2m}\right)dm \\
J_{2k+1}^* &= \frac{(2-2c)^{2k+2}}{(2k+1)!}\int_0^\infty m^{2k+1}\left(\frac{\sinh^2 mc}{\sinh 2m+2m} + \frac{\cosh^2 mc}{\sinh 2m-2m}\right)dm \\
K_{2k}^* &= \frac{(2-2c)^{2k+1}}{(2k)!}\int_0^\infty m^{2k}\left(\coth m\cosh^2 mc}{\sinh 2m+2m} + \frac{\tanh m\sinh^2 mc}{\sinh 2m-2m}\right)dm \\
J_{2k} &= \frac{(2-2c)^{2k+1}}{(2k)!}\int_0^\infty m^{2k}\left(\frac{\tanh m\sinh^2 mc}{\sinh 2m+2m} + \frac{\coth m\cosh^2 mc}{\sinh 2m-2m}\right)dm \\
K_{2k+1}^* &= \frac{(2-2c)^{2k+2}}{2(2k+1)!}\int_0^\infty m^{2k+1}\left(\frac{\coth m\sinh 2mc}{\sinh 2m+2m} + \frac{\tanh m\sinh 2mc}{\sinh 2m-2m}\right)dm \\
J_{2k+1} &= \frac{(2-2c)^{2k+2}}{2(2k+1)!}\int_0^\infty m^{2k+1}\left(\frac{\tanh m\sinh 2mc}{\sinh 2m+2m} + \frac{\coth m\sinh 2mc}{\sinh 2m-2m}\right)dm
\end{aligned}
\right\} \quad \ldots [19]
$$

each of which tends to unity as the positive integer k tends to infinity. The evaluation of the integrals will be discussed later in Appendix 2. Here F_1 and P_1 are not defined. Since they are the coefficients of the trivial term $r\cos\theta$, they will eventually disappear from the expressions for the stresses.

The normal and tangential stresses derived from χ_1 are as follows

$$
\left.
\begin{aligned}
\sigma_r &= \frac{1}{b^2}\left(\frac{1}{r}\frac{\partial\chi_1}{\partial r} + \frac{1}{r^2}\frac{\partial^2\chi_1}{\partial\theta^2}\right) \\
&= -E_0 r^{-2} + 2Q_0 - \sum_{n=1}^{\infty}\left[\{n(n+1)E_n + (n-1)(n+2)F_n r^2\}r^{-n-2} + \{n(n-1)P_n + (n-2)(n+1)Q_n r^2\}r^{n-2}\right]\cos n\theta \\
\tau_{r\theta} &= -\frac{1}{b^2}\frac{\partial}{\partial r}\left(\frac{1}{r}\frac{\partial\chi_1}{\partial\theta}\right) \\
&= -\sum_{n=1}^{\infty}\left[\{n(n+1)E_n + n(n-1)F_n r^2\}r^{-n-2} - \{n(n-1)P_n + n(n+1)Q_n r^2\}r^{n-2}\right]\sin n\theta
\end{aligned}
\right\} \quad \ldots [20]
$$

Hence the boundary conditions of zero traction at the rim of the hole, $r = \lambda$, are satisfied provided that

$$a_0 - E_0\lambda^{-2} + 2Q_0 = 0$$

and for $n \geq 1$

$$
\left.
\begin{aligned}
a_n - \{n(n+1)E_n + (n-1)(n+2)F_n\lambda^2\}\lambda^{-n-2} - \{n(n-1)P_n + (n-2)(n+1)Q_n\lambda^2\}\lambda^{n-2} &= 0 \\
c_n - \{n(n+1)E_n + n(n-1)F_n\lambda^2\}\lambda^{-n-2} + \{n(n-1)P_n + n(n+1)Q_n\lambda^2\}\lambda^{n-2} &= 0
\end{aligned}
\right\} \quad \ldots [21]
$$

When $n = 1$, the equations give $a_1 = c_1$ so that the condition of zero force resultant at the rim of the hole is satisfied. The set of equations may be replaced by

$$
\left.
\begin{aligned}
E_0 &= a_0\lambda^2 + 2Q_0\lambda^2 \\
E_n &= \frac{(n+2)c_n - na_n}{2n(n+1)}\lambda^{n+2} + (n-1)P_n\lambda^{2n} + nQ_n\lambda^{2n+2} \qquad (n \geq 1) \\
F_n &= \frac{a_n - c_n}{2(n-1)}\lambda^n - nP_n\lambda^{2n-2} - (n+1)Q_n\lambda^{2n} \qquad (n \geq 2)
\end{aligned}
\right\} \quad \ldots [22]
$$

A formal solution of the set of equations by the method of successive approximations is as follows. Write

$$E_n = \sum_{p=0}^{\infty} E_n^{(p)}, \qquad F_n = \sum_{p=0}^{\infty} F_n^{(p)} \quad \ldots [23]$$

where

$$
\left.
\begin{aligned}
E_0^{(0)} &= a_0\lambda^2, \qquad E_n^{(0)} = \frac{(n+2)c_n - na_n}{2n(n+1)}\lambda^{n+2} \\
F_n^{(0)} &= \frac{a_n - c_n}{2(n-1)}\lambda^n
\end{aligned}
\right\} \quad \ldots [24]
$$

and by iteration

$$
\left.
\begin{aligned}
E_0^{(p)} &= 2\lambda^2 Q_0^{(p-1)} \\
E_n^{(p)} &= (n-1)\lambda^{2n}P_n^{(p-1)} + n\lambda^{2n+2}Q_n^{(p-1)} \\
F_n^{(p)} &= -n\lambda^{2n-2}P_n^{(p-1)} - (n+1)\lambda^{2n}Q_n^{(p-1)}
\end{aligned}
\right\} \quad \ldots [25]
$$

in which $P_n^{(p-1)}$ and $Q_n^{(p-1)}$ are found from $E_n^{(p-1)}$ and $F_n^{(p-1)}$ by means of Equations [16] and [15].

The validity of the preceding method of solution of the set of equations depends upon the convergence of the series in Equations [23]. An analytic proof of convergence may be established by the method used by Howland (4) and Knight (3). However, for the sake of brevity no further detail will be given here. From physical consideration alone, it seems likely that there will be convergence as long as the perforating hole does not touch the edge of the strip; i.e., when

$$\lambda < 1 - |c| \qquad [26]$$

It is now a straightforward matter to calculate the stress at any point in the strip. In particular, the stress along the rim of the hole is given by

$$[\sigma_\theta]_\lambda = \frac{1}{b^2}\left[\frac{\partial^2\chi}{\partial r^2}\right]_{r=\lambda} = \frac{1}{b^2}[\nabla^2\chi]_{r=\lambda}$$

$$= \frac{1}{b^2}[\nabla^2\chi_0]_{r=\lambda} + 4Q_0 - 4\sum_{n=1}^{\infty}\{(n-1)F_n\lambda^{-n} - (n+1)Q_n\lambda^n\}\cos n\theta \qquad [27]$$

Again, the stress along the edges at $(x, y) = (0, \pm 1 \mp c)$ across the narrowest section is given by

$$[\sigma_x]_{0,\,\pm 1-c} = \frac{1}{b^2}\left[\frac{\partial^2\chi}{\partial y^2}\right]_{0,\,\pm 1-c} = \frac{1}{b^2}[\nabla^2\chi]_{0,\,\pm 1-c}$$

$$= \frac{1}{b^2}[\nabla^2\chi_0]_{0,\,\pm 1-c} - 2\sum_{s=1}^{\infty}(2s-1)B_{2s}S_{2s}(0, \pm 1 - c) + \frac{4}{(1 \mp c)^2}A_0\begin{matrix}H_1\\ H_1^*\end{matrix}$$

$$+ 4\sum_{s=1}^{\infty}\frac{2s(2s+1)}{(1 \mp c)^{2s+2}}\left(A_{2s}\begin{matrix}H_{2s+1}\\ H_{2s+1}^*\end{matrix} \pm C_{2s}\begin{matrix}L_{2s+1}\\ L_{2s+1}^*\end{matrix}\right)$$

$$+ 4\sum_{s=1}^{\infty}\frac{2s(2s-1)}{(1 \mp c)^{2s+1}}\left(B_{2s}\begin{matrix}H_{2s}\\ H_{2s}^*\end{matrix} \pm D_{2s}\begin{matrix}L_{2s}\\ L_{2s}^*\end{matrix}\right) \qquad [28]$$

where H_s, H_s^*, L_s, and L_s^* are integrals depending upon c only, the notation of which will be given later in Appendix 2.

Longitudinal-Tension and Transverse-Bending Cases

The preceding solution is applicable to any stress system acting in the strip, which is even in x. Two fundamental cases of this nature deserve special attention. One is the case of longitudinal tension, in which the basic stress function is given by

$$\chi_0 = \frac{1}{2}Tb^2y^2 \qquad [29]$$

where T is the longitudinal tension per unit width of the strip. By comparing the stresses at $r = \lambda$ derived from this function with Equations [12], it gives

$$a_0 = -a_2 = c_2 = \frac{1}{2}T \qquad [30]$$

the rest of the coefficients a_n and c_n being all zero.

The other is the case of transverse bending, in which the basic stress function is given by

$$\chi_0 = \frac{1}{4}Mb^2(y+c)^2 \qquad [31]$$

where $-Mb^2$ is the total bending moment across the strip. This gives

$$\left.\begin{aligned} -a_0 = -a_2 = c_2 &= \frac{3}{4}Mc \\ a_1 = -a_3 = c_1 = c_3 &= \frac{3}{8}M\lambda \end{aligned}\right\} \qquad [32]$$

the rest of a_n and c_n being all zero.

The Limiting Case

In the limiting case $c = 0$, the perforating hole becomes symmetrically located in the strip and consequently the problem reduces to the one considered by Howland, Stevenson, and Knight. When $c = 0$, the following values vanish identically

$$\left.\begin{aligned} &\omega_{2n+1} = 0, \quad K_{2n} = J_{2n}^* = 0, \quad K_{2n+1}^* = J_{2n+1} = 0 \\ &\text{and} \\ &{}^{2n+1}\alpha_{2s} = {}^{2n+1}\alpha_{2s}^* = {}^{2n+1}\beta_{2s} = {}^{2n+1}\beta_{2s}^* = 0 \\ &{}^{2n}\gamma_{2s} = {}^{2n}\gamma_{2s}^* = {}^{2n}\delta_{2s} = {}^{2n}\delta_{2s}^* = 0 \end{aligned}\right\} \qquad [33]$$

where ω_k is defined in Appendix 1.

If the given stress system acting in the strip has the further property of being even in y as in the case of longitudinal tension, then we also have

$$\left.\begin{aligned} &\psi_2 = \psi_4 = 0, \quad C_{2n} = D_{2n} = 0, \quad a_{2n+1} = c_{2n+1} = 0 \\ &P_{2n+1} = Q_{2n+1} = 0, \quad E_{2n+1} = F_{2n+1} = 0 \end{aligned}\right\} \qquad [34]$$

On the other hand, if the given stress system acting in the strip has the further property of being odd in y as in the case of transverse bending, then we also have

$$\left.\begin{aligned} &\psi_1 = \psi_3 = 0, \quad A_{2n} = B_{2n} = 0, \quad a_{2n} = c_{2n} = 0 \\ &P_{2n} = Q_{2n} = 0, \quad E_{2n} = F_{2n} = 0 \end{aligned}\right\} \qquad [35]$$

Consequently the solutions in such cases become considerably simplified.

Numerical Examples

The foregoing solution will be illustrated by the following numerical examples:

1 In the longitudinal-tension case: for $c = 1/2$, $\lambda = 1/4$ and $c = 1/4$, $\lambda = 1/4$.

2 In the transverse-bending case: for $c = 1/2$, $\lambda = 1/4$ and $c = 1/4$, $\lambda = 1/4$.

First, compute the coefficients in Equations [17] and [18], for $c = 1/2$ and $1/4$, respectively, with the aid of Tables 5, 7 in the Appendix. Next, compute the coefficients E_n, F_n, P_n, and Q_n by the method of successive approximations. For the sake of brevity, the results in the case $c = 1/2$ only are shown in Tables 1 and 2. Values of A_n, B_n, C_n, and D_n are then readily obtained from Equations [15].

The expressions of the stress σ_θ around the rim of the hole and the stress σ_x along the edges have been given previously in Equations [27] and [28], respectively. The most important are the stresses across the narrowest section of the strip. Using also Tables 6, 8 in the Appendix the values are found as in Tables 3 and 4.

It may be mentioned that the values of the stresses in the limiting case $c = 0$ and $\lambda = 1/4$ are obtained by interpolation from Howland and Stevenson's results (1, 2). The stress-concentration factor in the longitudinal-tension case is defined as the ratio of maximum stress in the strip to the average stress across the same section of the strip. The results also are shown graphically in Figs. 2 and 3, respectively.

TABLE 1 THE COEFFICIENTS FOR $c = 1/2$

Coeff.	2s	n=0	n=1	n=2	n=3	n=4	n=5	n=6	n=7	n=8
${}^{n}\alpha_{2s}$	0	-	-	3.1792×10^{-1}	3.0753×10^{-1}	2.4367×10^{-1}	1.9820×10^{-1}	1.6657×10^{-1}	1.4277×10^{-1}	1.2502×10^{-1}
	2	-	-	8.9568	1.1997x10	1.5000x10	1.7997x10	2.1002x10	2.3999x10	2.7018x10
	4	-	-	5.0005x10	9.9991x10	1.7501×10^{2}	2.7999×10^{2}	4.2017×10^{2}	6.0001×10^{2}	8.2500×10^{2}
	6	-	-	1.4701×10^{2}	3.9199×10^{2}	8.8226×10^{2}	1.7640×10^{3}	3.2340×10^{3}	5.5440×10^{3}	9.0090×10^{3}
	8	-	-	3.2408×10^{2}	1.0800×10^{3}	2.9700×10^{3}	7.1280×10^{3}	1.5444×10^{4}	3.0888×10^{4}	5.7915×10^{4}
${}^{n}\beta_{2s}$	2	-	-	2.0364	1.9932	1.9990	1.9977	2.0001	1.9997	2.0002
	4	-	-	2.2498x10	3.7987x10	5.7502x10	8.0995x10	1.0851×10^{2}	1.3996×10^{2}	1.7546×10^{2}
	6	-	-	8.5004x10	1.9999x10	4.0251×10^{2}	7.2786×10^{2}	1.2179×10^{3}	1.9200×10^{3}	2.8875×10^{3}
	8	-	-	2.1351×10^{2}	6.4390×10^{2}	1.6169×10^{3}	3.5700×10^{3}	7.1610×10^{3}	1.3332×10^{4}	2.3381×10^{4}
${}^{n}\gamma_{2s}$	2	-	-	9.9067	1.3542x10	1.6407x10	1.9497x10	2.2487x10	2.5500x10	2.8481x10
	4	-	-	5.4840x10	1.0843×10^{2}	1.8743×10^{2}	2.9752×10^{2}	4.4315×10^{2}	6.2988×10^{2}	8.6250×10^{2}
	6	-	-	1.5746×10^{2}	4.1655×10^{2}	9.3073×10^{2}	1.8521×10^{3}	3.3810×10^{3}	5.7750×10^{3}	9.3550×10^{3}
	8	-	-	3.4192×10^{2}	1.1340×10^{3}	3.1050×10^{3}	7.4250×10^{3}	1.6038×10^{4}	3.1991×10^{4}	5.9846×10^{4}
${}^{n}\delta_{2s}$	2	-	-	1.6076	1.9753	1.9591	1.9952	1.9958	1.9996	1.9995
	4	-	-	2.3805x10	4.0102x10	5.9938x10	8.4014x10	1.1198×10^{2}	1.4414×10^{2}	1.8000×10^{2}
	6	-	-	8.9939x10	2.1006×10^{2}	4.1996×10^{2}	7.5648×10^{2}	1.2600×10^{3}	1.9800×10^{3}	2.9700×10^{3}
	8	-	-	2.2398×10^{2}	6.7233×10^{2}	1.6800×10^{3}	3.6960×10^{3}	7.3920×10^{3}	1.3728×10^{4}	2.4024×10^{4}

TABLE 1 (*Continued*)

Coeff.	2s	n=0	n=1	n=2	n=3	n=4	n=5	n=6	n=7	n=8
${}^{n}\alpha_{2s}^{*}$	0	1.1646	1.1393	1.0055	1.0042	1.0003	1.0000	1.0000	1.0000	1.0000
	2	6.0328	1.2050x10	2.0005x10	3.0001x10	4.0001x10	5.0000x10	7.0001x10	8.9999x10	1.1000×10^{2}
	4	2.0005x10	6.0002x10	1.4000×10^{2}	2.7999×10^{2}	5.0401×10^{2}	8.3999×10^{2}	1.3200×10^{3}	1.9800×10^{3}	2.8600×10^{3}
	6	4.2001x10	1.6800×10^{2}	5.0401×10^{2}	1.2600×10^{3}	2.7720×10^{3}	5.5440×10^{3}	1.0296×10^{4}	1.8018×10^{4}	3.0030×10^{4}
	8	7.2001x10	3.6000×10^{2}	1.3200×10^{3}	3.9600×10^{3}	1.0296×10^{4}	2.4024×10^{4}	5.1480×10^{4}	1.0296×10^{5}	1.9448×10^{5}
${}^{n}\beta_{2s}^{*}$	2	1.4572	2.5391	3.5012	4.5024	5.5004	6.4999	7.5001	8.4999	9.5010
	4	1.0504x10	2.7015x10	5.5004x10	9.7498x10	1.5750×10^{2}	2.3800×10^{2}	3.4204×10^{2}	4.7250×10^{2}	6.3250×10^{2}
	6	2.7502x10	9.7498x10	2.6250×10^{2}	5.9500×10^{2}	1.1971×10^{3}	2.2050×10^{3}	3.7950×10^{3}	6.1875×10^{3}	9.6525×10^{3}
	8	5.2500x10	2.3800×10^{2}	7.9808×10^{2}	2.2050×10^{3}	5.3130×10^{3}	1.1550×10^{4}	2.3166×10^{4}	4.3544×10^{4}	7.7578×10^{4}
${}^{n}\gamma_{2s}^{*}$	2	7.3570	1.4194x10	2.2027x10	3.2582x10	4.5000x10	5.9511x10	7.5999x10	9.4518x10	1.1500×10^{2}
	4	2.2027x10	6.5165x10	1.5000x10	2.9756×10^{2}	5.3199×10^{2}	8.8217×10^{2}	1.3800×10^{3}	2.0625×10^{3}	2.9700×10^{3}
	6	4.5000x10	1.7853×10^{2}	5.3199×10^{2}	1.3233×10^{3}	2.8980×10^{3}	5.7750×10^{3}	1.0692×10^{4}	1.8662×10^{4}	3.1031×10^{4}
	8	7.5999x10	3.7807×10^{2}	1.3800×10^{3}	4.1250×10^{3}	1.0692×10^{4}	2.4882×10^{4}	5.3196×10^{4}	1.0618×10^{5}	2.0020×10^{5}
${}^{n}\delta_{2s}^{*}$	2	2.2786	3.4705	4.0167	5.0375	6.0002	7.0038	7.9998	9.0005	9.9999
	4	1.2050x10	3.0225x10	6.0002x10	1.0506×10^{2}	1.6800×10^{2}	2.5201×10^{2}	3.6000×10^{2}	4.9500×10^{2}	6.6000×10^{2}
	6	3.0001x10	1.0506×10^{2}	2.7999×10^{2}	6.3003×10^{2}	1.2600×10^{3}	2.3100×10^{3}	3.9600×10^{3}	6.4350×10^{3}	1.0010×10^{4}
	8	5.5999x10	2.5201×10^{2}	8.3999×10^{2}	2.3100×10^{3}	5.5440×10^{3}	1.2012×10^{4}	2.4024×10^{4}	4.5045×10^{4}	8.0080×10^{4}

TABLE 2 THE COEFFICIENTS FOR THE CASE $c = 1/2$ AND $\lambda = 1/4$

n	Longitudinal tension case (T = 1)				Transverse bending case (K = 1)			
	E_n	F_n	P_n	Q_n	E_n	F_n	P_n	Q_n
0	3.3742×10^{-2}	-	-	$+1.9935\times10^{-2}$	-2.9785×10^{-2}	-	-	-5.0778×10^{-2}
1	-6.0405×10^{-5}	-	-	-1.5464×10^{-2}	4.1611×10^{-4}	-	-	-8.0976×10^{-2}
2	1.2633×10^{-3}	-4.0698×10^{-2}	8.2142×10^{-2}	-6.9989×10^{-2}	1.0222×10^{-3}	-3.3190×10^{-2}	8.9497×10^{-2}	-1.2245×10^{-1}
3	2.5734×10^{-5}	-6.3015×10^{-4}	6.2344×10^{-2}	-1.0284×10^{-1}	6.0098×10^{-5}	-1.4613×10^{-3}	7.5122×10^{-2}	-1.5512×10^{-1}
4	2.4041×10^{-6}	-5.1985×10^{-5}	6.3925×10^{-2}	-1.3687×10^{-1}	2.7041×10^{-6}	-5.8653×10^{-5}	7.4903×10^{-2}	-1.8998×10^{-1}
5	1.8811×10^{-7}	-3.8024×10^{-6}	6.2471×10^{-2}	-1.6846×10^{-1}	2.1319×10^{-7}	-4.3173×10^{-6}	7.3425×10^{-2}	-2.2451×10^{-1}
6	1.4123×10^{-8}	-2.7356×10^{-7}	6.2366×10^{-2}	-1.9966×10^{-1}	1.6148×10^{-8}	-3.1314×10^{-7}	7.3686×10^{-2}	-2.6006×10^{-1}
7	1.0067×10^{-9}	-1.8934×10^{-8}	6.1815×10^{-2}	-2.3009×10^{-1}	1.1707×10^{-9}	-2.2037×10^{-8}	7.3984×10^{-2}	-2.9630×10^{-1}
8	6.9771×10^{-11}	-1.2845×10^{-9}	6.1389×10^{-2}	-2.6014×10^{-1}	8.2790×10^{-11}	-1.5250×10^{-9}	7.4609×10^{-2}	-3.3341×10^{-1}

TABLE 3 LONGITUDINAL-TENSION CASE, FOR $T = 1$

Case	$c = 1/2, \lambda = 1/4$	$c = 1/4, \lambda = 1/4$	$c = 0, \lambda = 1/4$
Stress $[\sigma_\theta]_\lambda$ at $\theta = 0$	4.136	3.430	3.22
Stress-concentration factor	3.102	2.573	2.415
Stress $[\sigma_\theta]_\lambda$ at $\theta = \pi$	3.472	3.258	3.22
Stress-concentration factor	2.604	2.444	2.415
Stress $[\sigma_x]_{0,\ 1-c}$	0.671	0.922	0.94
Stress-concentration factor	0.503	0.692	0.705
Stress $[\sigma_x]_{0,\ -1-c}$	0.830	0.879	0.94
Stress-concentration factor	0.623	0.659	0.705

TABLE 4 TRANSVERSE-BENDING CASE, FOR $M = 1$

Case	$c = 1/2, \lambda = 1/4$	$c = 1/4, \lambda = 1/4$	$c = 0, \lambda = 1/4$
Stress $[\sigma_\theta]_\lambda$ at $\theta = 0$	3.768	2.028	0.77
Stress at the same point, strip unperforated	1.125	0.750	0.375
Stress $[\sigma_\theta]_\lambda$ at $\theta = \pi$	1.775	0.458	−0.77
Stress at the same point, strip unperforated	0.375	0	−0.375
Stress $[\sigma_x]_{0,\ 1-c}$	0.227	1.240	1.495
Stress at the same point, strip unperforated	1.500	1.500	1.500
Stress $[\sigma_x]_{0,\ -1-c}$	−1.651	−1.575	−1.495
Stress at the same point, strip unperforated	−1.500	−1.500	−1.500

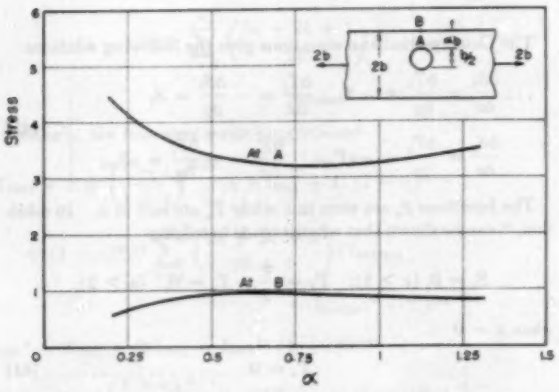

FIG. 2 LONGITUDINAL-TENSION CASE

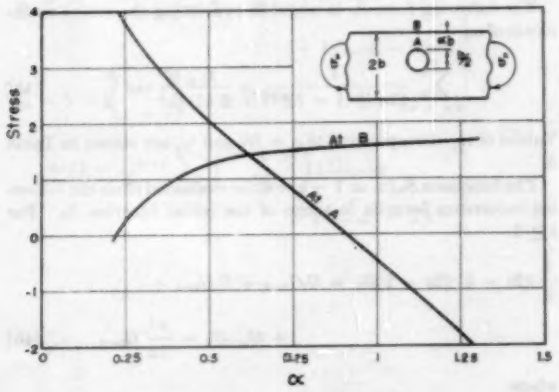

FIG. 3 TRANSVERSE-BENDING CASE

BIBLIOGRAPHY

1 "On the Stresses in the Neighborhood of a Circular Hole in a Strip Under Tension," by R. C. J. Howland, Philosophical Transactions of the Royal Society of London, series A, vol. 229, 1930, pp. 49–86.

2 "Biharmonic Analysis in a Perforated Strip," by R. C. J. Howland and A. C. Stevenson, Philosophical Transactions of the Royal Society of London, series A, vol. 232, 1934, pp. 155–222.

3 "On the Stresses in a Perforated Strip," by R. C. Knight, *Quarterly Journal of Mathematics*, Oxford series, vol. 5, 1934, pp. 255–268.

4 "Stresses in a Plate Containing an Infinite Row of Holes," by R. C. J. Howland, Proceedings of the Royal Society of London, series A, vol. 148, 1935, pp. 471–491.

5 "Infinite Series," by K. Knopp, Hafner, 1947, p. 247.

6 "On Evaluation of Howland's Integrals," by C. B. Ling and C. W. Nelson, *Annals of Academia Sinica*, no. 2, part 2, 1955, pp. 45–50 (Taiwan, China).

7 "Tables of Values of 16 Integrals of Algebraic-Hyperbolic Type," by C-B. Ling, to appear elsewhere.

Appendix 1

A CLASS OF PERIODIC HARMONIC FUNCTIONS

Define a function W_0 of a complex variable z by

$$W_0(z) = -\log\left\{\sinh\frac{\pi z}{4}\sinh\frac{\pi(z-2i+2ic)}{4}\right\} \quad \ldots\ldots [36]$$

which possesses logarithmic singularities at the points $z = 4ni$ and $2(2n+1-c)i$, where n takes all integral and zero values; c being a constant numerically less than unity. Again, define a class of functions with poles of integral orders at the same points by

$$W_s(z) = \frac{(-i)^s}{(s-1)!}\frac{d^s}{dz^s}W_0(z) \quad \ldots\ldots [37]$$

The functions have the following expansions valid near the origin

$$\left.\begin{aligned} W_0(z) &= -\log(-iz) + \sum_{n=0}^{\infty} {}^n\Omega_0(-iz)^n \\ W_s(z) &= \frac{1}{(-iz)^s} + (-1)^s\sum_{n=0}^{\infty} {}^n\Omega_s(-iz)^n \end{aligned}\right\} \quad \ldots\ldots [38]$$

TABLE 5 THE COEFFICIENTS ω_k

k	$c = \frac{1}{2}$		$c = \frac{1}{4}$	
	ω_{2k}	ω_{2k+1}	ω_{2k}	ω_{2k+1}
1	1.439317	0.968946	2.088679	0.793482
2	1.023134	0.996158	1.182281	0.923140
3	1.001944	0.999555	1.052905	0.972085
4	1.000186	0.999950	1.017621	0.989929
5	1.000019	0.999994	1.006159	0.996373
6	1.000001	0.999999	1.002193	0.998694
7	1.000000	1.000000	1.000786	0.999530
8	1.000000	1.000000	1.000282	0.999831

TABLE 6 THE FUNCTION $S_{2s}(0, \pm 1 - c)$

2s	$c = \frac{1}{2}$		$c = \frac{1}{4}$	
	$S_{2s}(0,1-c)$	$S_{2s}(0,-1-c)$	$S_{2s}(0,1-c)$	$S_{2s}(0,-1-c)$
2	8.42423	1.44537	3.99698	1.78450
4	3.20195x10	4.50163x10^{-1}	6.34423	8.58376x10^{-1}
6	7.69718x10	1.39659x10^{-1}	6.82463	3.53634x10^{-1}
8	2.19929x10^{2}	4.66869x10^{-2}	8.67081	1.62109x10^{-1}
10	5.86965x10^{2}	1.52500x10^{-2}	1.03226x10	7.29861x10^{-2}

where

$$ {}^{n}\Omega_0 = \frac{\omega_n}{n(2-2c)^n}, \quad {}^{n}\Omega_s = \binom{n+s-1}{n}\frac{\omega_{n+s}}{(2-2c)^{n+s}} \cdots [39] $$

and in particular

$$ {}^{0}\Omega_0 = -\log\left(\frac{\pi}{4}\cos\frac{\pi c}{2}\right), \quad {}^{1}\Omega_0 = \frac{\pi}{4}\tan\frac{\pi c}{2} $$

in which, for $k \geq 1$

$$ \left.\begin{aligned} \omega_{2k} &= (1-c)^{2k}\left\{\sum_{n=-\infty}^{\infty}\frac{1}{(2n+1-c)^{2k}} + 2\sum_{n=1}^{\infty}\frac{1}{(2n)^{2k}}\right\} \\ \omega_{2k+1} &= (1-c)^{2k+1}\sum_{n=-\infty}^{\infty}\frac{1}{(2n+1-c)^{2k+1}} \end{aligned}\right\} \cdots [40] $$

Denote the real and imaginary parts of the functions by

$$ W_s(z) = S_s(x, y) + i\,T_s(x, y) \cdots [41] $$

The following expansions are obtained in terms of the polar coordinates (r, θ) defined previously in Equation [11]

$$ \left.\begin{aligned} S_0 &= -\log r + \sum_{n=0}^{\infty} {}^{n}\Omega_0 r^n \cos n\theta \\ T_0 &= \theta - \sum_{n=1}^{\infty} {}^{n}\Omega_0 r^n \sin n\theta \\ S_s &= \frac{\cos s\theta}{r^s} + (-1)^s \sum_{n=0}^{\infty} {}^{n}\Omega_s r^n \cos n\theta \\ T_s &= \frac{\sin s\theta}{r^s} - (-1)^s \sum_{n=1}^{\infty} {}^{n}\Omega_s r^n \sin n\theta \end{aligned}\right\} \cdots [42] $$

The Cauchy-Riemann equations give the following relations

$$ \left.\begin{aligned} \frac{\partial S_0}{\partial x} &= \frac{\partial T_0}{\partial y} = -T_1, \quad \frac{\partial T_0}{\partial x} = -\frac{\partial S_0}{\partial y} = S_1 \\ \frac{\partial S_s}{\partial x} &= \frac{\partial T_s}{\partial y} = -sT_{s+1}, \quad \frac{\partial T_s}{\partial x} = -\frac{\partial S_s}{\partial y} = sS_{s+1} \end{aligned}\right\} \cdots [43] $$

The functions S_s are even in x while T_s are odd in x. In addition, it can be shown that when x tends to infinity

$$ S_s = 0, (s \geq 1); \quad T_1 = \frac{\pi}{2}, \quad T_s = 0, \quad (s \geq 2); $$

when $x = 0$

$$ T_s = 0 \cdots [44] $$

and when $y = 4n \pm 1 - c$, n being an integer or zero

$$ S_{2s-1} = 0, \qquad T_{2s} = 0 $$

The following formula is useful in evaluating the initial coefficients of ω_k

$$ \sum_{n=-\infty}^{\infty}\frac{1}{(2n+1-c)^{k+1}} = \frac{\pi}{2(k!)}\frac{d^k}{dc^k}\tan\frac{\pi c}{2} \cdots [45] $$

Values of ω_k corresponding to $c = 1/2$ and $1/4$ are shown in Table 5.

The functions $S_{2s}(x, \pm 1 - c)$ can be evaluated from the following recurrence formula in terms of the initial function S_2. For $s \geq 2$

$$ \frac{1}{3}(2s-3)(2s-2)G_{2s} = G_2G_{2s-2} + G_4G_{2s-4} + \cdots + G_{2s-2}G_2 - \frac{\pi^2}{12}G_{2s-2} \cdots [46] $$

where

$$ G_{2s}(x) = (2s-1)S_{2s}(x, \pm 1 - c) \cdots [47] $$

When $x = 0$, the initial function G_2 is equal to

$$G_2(0) = S_2(0, \pm 1 - c) = \frac{\pi^2}{8}\csc^2\frac{\pi}{4}(1 \mp c) \quad [48]$$

Table 6 shows the values of $S_{2s}(0, \pm 1 - c)$ for $c = 1/2$ and $1/4$.

Appendix 2

Evaluation of Integrals

Consider the integrals in Equations [19]. By developing the integrand of the first integral into power series of c, we have

$$K_{2k} = J_{2k}^* = (1-c)^{2k+1}\sum_{n=0}^{\infty}\binom{2n+2k+1}{2k}(I_{2n+2k+1} + I_{2n+2k+1}^*)\,c^{2n+1} \quad [49]$$

where

$$\left.\begin{matrix} I_k \\ I_k^* \end{matrix}\right\} = \frac{2^k}{k!}\int_0^{\infty}\frac{m^k\,dm}{\sinh 2m \pm 2m} \quad [50]$$

The convergence of the series can be improved by using Kummer transformation (5). The series then becomes

$$K_{2k} = J_{2k}^* = 1 - \left(\frac{1-c}{1+c}\right)^{2k+1} + (1-c)^{2k+1}\sum_{n=0}^{\infty}\binom{2n+2k+1}{2k}(I_{2n+2k+1} + I_{2n+2k+1}^* - 2)c^{2n+1} \quad [51]$$

Similarly, the following series are obtained

$$\left.\begin{aligned} K_{2k+1} &= 1 + \left(\frac{1-c}{1+c}\right)^{2k+2} + 2(I_{2k+1} - 1)(1-c)^{2k+2} \\ &\quad + (1-c)^{2k+2}\sum_{n=1}^{\infty}\binom{2n+2k+1}{2k+1}(I_{2n+2k+1} + I_{2n+2k+1}^* - 2)c^{2n} \\ J_{2k+1}^* &= K_{2k+1} - 2(I_{2k+1} - I_{2k+1}^*)(1-c)^{2k+2} \\ K_{2k}^* &= 1 + \left(\frac{1-c}{1+c}\right)^{2k+1} + 2(IV_{2k} - 1)(1-c)^{2k+1} \\ &\quad + (1-c)^{2k+1}\sum_{n=1}^{\infty}\binom{2n+2k}{2k}(III_{2n+2k}^* + IV_{2n+2k} - 2)c^{2n} \\ J_{2k} &= 1 + \left(\frac{1-c}{1+c}\right)^{2k+1} + 2(IV_{2k}^* - 1)(1-c)^{2k+1} \\ &\quad + (1-c)^{2k+1}\sum_{n=1}^{\infty}\binom{2n+2k}{2k}(III_{2n+2k} + IV_{2n+2k}^* - 2)c^{2n} \end{aligned}\right\} \quad [52]$$

$$\left.\begin{aligned} K_{2k+1}^* &= 1 - \left(\frac{1-c}{1+c}\right)^{2k+2} + (1-c)^{2k+2}\sum_{n=1}^{\infty}\binom{2n+2k}{2k+1}(III_{2n+2k}^* + IV_{2n+2k} - 2)c^{2n-1} \\ J_{2k+1} &= 1 - \left(\frac{1-c}{1+c}\right)^{2k+2} + (1-c)^{2k+2}\sum_{n=1}^{\infty}\binom{2n+2k}{2k+1}(III_{2n+2k} + IV_{2n+2k}^* - 2)c^{2n-1} \end{aligned}\right\} \quad [52]\ (cont.)$$

where

$$\left.\begin{matrix} III_k \\ III_k^* \end{matrix}\right\} = \frac{2^k}{k!}\int_0^{\infty}\frac{m^k\tanh m\,dm}{\sinh 2m \pm 2m}$$

$$\left.\begin{matrix} IV_k \\ IV_k^* \end{matrix}\right\} = \frac{2^k}{k!}\int_0^{\infty}\frac{m^k\coth m\,dm}{\sinh 2m \pm 2m} \quad [53]$$

The integrals in Equation [50] were tabulated by Howland (1) and Stevenson (2) to five decimals and recently by Nelson and the writer (6) to six decimals. The integrals in Equations [53] also were tabulated recently by the writer (7) to six decimals. Values of the integrals in Equations [51] and [52] corresponding to $c = 1/2$ and $1/4$ are shown in Table 7.

Again, consider the integrals H_s, H_s^*, L_s, and L_s^* in Equation [28]. Their notations are as follows

$$\left.\begin{aligned} \left.\begin{matrix} H_{2s} \\ H_{2s}^* \end{matrix}\right\} &= \frac{(1 \mp c)^{2s+1}}{(2s)!}\int_0^{\infty}m^{2s}\left(\frac{\cosh m\coth m\cosh mc}{\sinh 2m + 2m} \pm \frac{\sinh m\tanh m\sinh mc}{\sinh 2m - 2m}\right)dm \\ \left.\begin{matrix} H_{2s+1} \\ H_{2s+1}^* \end{matrix}\right\} &= \frac{(1 \mp c)^{2s+2}}{(2s+1)!}\int_0^{\infty}m^{2s+1}\left(\frac{\cosh m\cosh mc}{\sinh 2m + 2m} \pm \frac{\sinh m\sinh mc}{\sinh 2m - 2m}\right)dm \\ \left.\begin{matrix} L_{2s} \\ L_{2s}^* \end{matrix}\right\} &= \frac{(1 \mp c)^{2s+1}}{(2s)!}\int_0^{\infty}m^{2s}\left(\frac{\sinh m\cosh mc}{\sinh 2m - 2m} \pm \frac{\cosh m\sinh mc}{\sinh 2m + 2m}\right)dm \\ \left.\begin{matrix} L_{2s+1} \\ L_{2s+1}^* \end{matrix}\right\} &= \frac{(1 \mp c)^{2s+2}}{(2s+1)!}\int_0^{\infty}m^{2s+1}\left(\frac{\cosh m\cosh mc}{\sinh 2m - 2m} \pm \frac{\sinh m\sinh mc}{\sinh 2m + 2m}\right)dm \end{aligned}\right\} \quad [54]$$

By the same procedure as used previously, we find

$$\left.\begin{aligned}
\begin{matrix} H_{2s} \\ H_{2s}^{*} \end{matrix} &= 1 + (1 \mp c)^{2s+1} \sum_{n=0}^{\infty} \left\{ \binom{2n+2s}{2s} (\mathrm{VIII}_{2n+2s} - 1) c^{2n} \pm \binom{2n+2s+1}{2s} (\mathrm{VII}_{2n+2s+1}^{*} - 1)\, c^{2n+1} \right\} \\
\begin{matrix} H_{2s+1} \\ H_{2s+1}^{*} \end{matrix} &= 1 + (1 \mp c)^{2s+2} \sum_{n=0}^{\infty} \left\{ \binom{2n+2s+1}{2s+1} (\mathrm{VI}_{2n+2s+1} - 1)\, c^{2n} \pm \binom{2n+2s+2}{2s+1} (\mathrm{V}_{2n+2s+2}^{*} - 1) c^{2n+1} \right\} \\
\begin{matrix} L_{2s} \\ L_{2s}^{*} \end{matrix} &= 1 + (1 \mp c)^{2s+1} \sum_{n=0}^{\infty} \left\{ \binom{2n+2s}{2s} (\mathrm{V}_{2n+2s}^{*} - 1)\, c^{2n} \pm \binom{2n+2s+1}{2s} (\mathrm{VI}_{2n+2s+1} - 1)\, c^{2n+1} \right\} \\
\begin{matrix} L_{2s+1} \\ L_{2s+1}^{*} \end{matrix} &= 1 + (1 \mp c)^{2s+2} \sum_{n=0}^{\infty} \left\{ \binom{2n+2s+1}{2s+1} (\mathrm{VI}_{2n+2s+1}^{*} - 1) c^{2n} \pm \binom{2n+2s+2}{2s+1} (\mathrm{V}_{2n+2s+2} - 1) c^{2n+1} \right\}
\end{aligned}\right\} \quad \ldots\ldots [55]$$

TABLE 7 THE INTEGRALS K_k, K_k^*, J_k, J_k^*

c	k	K_{2k} or J_{2k}^*	K_{2k+1}	K_{2k}^*	K_{2k+1}^*	J_{2k}	J_{2k+1}	J_{2k+1}^*
½	0	–	1.16463	–	–	–	–	–
	1	1.13933	1.00547	1.08843	1.00785	–	1.06464	1.15685
	2	1.00412	1.00029	1.00314	1.00007	1.05489	1.00168	1.00752
	3	1.00005	1.00003	1.00021	0.99994	1.00256	1.00002	1.00055
	4	0.99998	1.00001	1.00002	0.99999	1.00018	0.99999	1.00004
	5	1.00000	1.00000	1.00000	1.00000	1.00001	1.00000	1.00000
	6	1.00000	1.00000	1.00000	1.00000	1.00000	1.00000	1.00000
¼	0	–	1.19194	–	–	–	–	–
	1	1.06367	1.03739	1.31837	0.91427	–	1.04937	1.80372
	2	0.94827	1.02309	1.05246	0.95954	1.42459	0.96706	1.10545
	3	0.97513	1.01178	1.02019	0.98401	1.05772	0.98466	1.02510
	4	0.99029	1.00509	1.00835	0.99405	1.01414	0.99411	1.00733
	5	0.99641	1.00201	1.00329	0.99783	1.00424	0.99784	1.00238
	6	0.99869	1.00075	1.00125	0.99922	1.00140	0.99922	1.00082
	7	0.99953	1.00028	1.00046	0.99972	1.00048	0.99972	1.00029
	8	0.99983	1.00010	1.00017	0.99990	1.00017	0.99990	1.00010
	9	0.99994	1.00004	1.00006	0.99996	1.00006	0.99996	1.00004
	10	0.99998	1.00001	1.00002	0.99999	1.00002	0.99999	1.00001

TABLE 8 THE INTEGRALS H_k, H_k^*, L_k, L_k^*

c	k	H_{2k}	H_{2k}^*	H_{2k+1}	H_{2k+1}^*	L_{2k}	L_{2k}^*	L_{2k+1}	L_{2k+1}^*
½	0	–	–	1.07757	−0.22275	–	–	–	–
	1	1.01315	0.69534	1.00092	+0.25569	1.04884	2.81860	1.01159	2.58542
	2	1.00012	0.60664	1.00001	0.59485	1.00080	1.62132	1.00017	1.53368
	3	1.00000	0.76993	1.00000	0.80157	1.00002	1.29343	1.00000	1.23531
	4	1.00000	0.88512	1.00000	0.90944	1.00000	1.12835	1.00000	1.10296
	5	1.00000	0.94739	1.00000	0.96145	1.00000	1.05986	1.00000	1.04289
	6	1.00000	0.97853	1.00000	0.98652	1.00000	1.02377	1.00000	1.01490
	7	1.00000	0.99387	1.00000	0.99745	1.00000	1.00659	1.00000	1.00285
	8	1.00000	0.99935	1.00000	0.99991	1.00000	1.00067	1.00000	1.00010
¼	0	–	–	1.06529	0.53581	–	–	–	–
	1	1.02859	0.95888	0.99640	0.79746	1.16425	1.88783	1.05919	1.59033
	2	0.99928	0.92076	0.99942	0.93321	1.00648	1.15267	1.00213	1.09904
	3	0.99987	0.97168	0.99995	0.98082	1.00037	1.03911	1.00011	1.02390
	4	0.99999	0.99170	1.00000	0.99492	1.00002	1.01019	1.00001	1.00591
	5	1.00000	0.99778	1.00000	0.99872	1.00000	1.00258	1.00000	1.00144
	6	1.00000	0.99944	1.00000	0.99969	1.00000	1.00063	1.00000	1.00034
	7	1.00000	0.99987	1.00000	0.99994	1.00000	1.00014	1.00000	1.00007
	8	1.00000	0.99998	1.00000	1.00000	1.00000	1.00002	1.00000	1.00000

TABLE 9 THE INTEGRALS

k	I_k	II_k	III_k	IV_k	V_k	VI_k	VII_k	$VIII_k$
0	–	–	0.296620	–	0.526856	–	0.369801	–
1	0.768575	0.220120	0.474430	–	0.738844	0.917477	0.658935	–
2	0.767847	0.087927	0.630841	1.095967	0.869866	0.922590	0.834030	1.027978
3	0.827710	0.043348	0.753836	0.943138	0.940054	0.958311	0.925284	0.983124
4	0.883507	0.022583	0.842839	0.936323	0.974010	0.980498	0.968275	0.988102
5	0.925476	0.011923	0.903237	0.951644	0.989249	0.991545	0.987116	0.994054
6	0.954192	0.006288	0.942192	0.967515	0.995711	0.996515	0.994942	0.997361
7	0.972669	0.003295	0.966315	0.979538	0.998337	0.998615	0.998066	0.998902
8	0.984124	0.001713	0.980771	0.987635	0.999369	0.999464	0.999275	0.999561
9	0.990949	0.000884	0.989207	0.992746	0.999765	0.999797	0.999732	0.999830
10	0.994922	0.000453	0.994025	0.995839	0.999913	0.999924	0.999902	0.999935
11	0.997189	0.000231	0.996730	0.997654	0.999968	0.999972	0.999965	0.999976
12	0.998460	0.000117	0.998227	0.998695	0.999989	0.999990	0.999987	0.999991
13	0.999164	0.000059	0.999046	0.999283	0.999996	0.999996	0.999995	0.999997
14	0.999549	0.000030	0.999490	0.999609	0.999999	0.999999	0.999998	0.999999
15	0.999759	0.000015	0.999729	0.999789	0.999999	1.000000	0.999999	1.000000
16	0.999871	0.000008	0.999856	0.999886	1.000000	1.000000	1.000000	1.000000
17	0.999932	0.000004	0.999924	0.999939	1.000000	1.000000	1.000000	1.000000
18	0.999964	0.000002	0.999960	0.999968	1.000000	1.000000	1.000000	1.000000
19	0.999981	0.000001	0.999979	0.999983	1.000000	1.000000	1.000000	1.000000
20	0.999990	0.000000	0.999989	0.999991	1.000000	1.000000	1.000000	1.000000

TABLE 10 THE INTEGRALS

k	I_k^*	II_k^*	III_k^*	IV_k^*	V_k^*	VI_k^*	VII_k^*	$VIII_k^*$
1	–	–	–	–	–	–	1.511155	–
2	–	–	2.135618	–	1.408796	–	1.155464	–
3	2.038711	0.460714	1.415063	–	1.105226	1.204004	1.057387	–
4	1.353294	0.099316	1.195553	1.707569	1.034388	1.051213	1.022143	1.081719
5	1.156864	0.032413	1.100493	1.240001	1.012123	1.016248	1.008602	1.021461
6	1.076730	0.012617	1.053580	1.105385	1.004398	1.005564	1.003325	1.006864
7	1.039251	0.005391	1.029034	1.050822	1.001611	1.001965	1.001273	1.002339
8	1.020538	0.002433	1.015834	1.025608	1.000591	1.000703	1.000483	1.000817
9	1.010870	0.001136	1.008647	1.013199	1.000216	1.000252	1.000181	1.000289
10	1.005785	0.000542	1.004715	1.006886	1.000079	1.000091	1.000067	1.000102
11	1.003085	0.000263	1.002564	1.003615	1.000029	1.000032	1.000025	1.000036
12	1.001645	0.000128	1.001390	1.001903	1.000010	1.000012	1.000009	1.000013
13	1.000876	0.000063	1.000750	1.001003	1.000004	1.000004	1.000003	1.000005
14	1.000466	0.000031	1.000403	1.000529	1.000001	1.000001	1.000001	1.000002
15	1.000247	0.000016	1.000216	1.000278	1.000000	1.000001	1.000000	1.000001
16	1.000131	0.000008	1.000115	1.000146	1.000000	1.000000	1.000000	1.000000
17	1.000069	0.000004	1.000061	1.000077	1.000000	1.000000	1.000000	1.000000
18	1.000036	0.000002	1.000033	1.000040	1.000000	1.000000	1.000000	1.000000
19	1.000019	0.000001	1.000017	1.000021	1.000000	1.000000	1.000000	1.000000
20	1.000010	0.000000	1.000009	1.000011	1.000000	1.000000	1.000000	1.000000

where

$$\left.\begin{aligned} V_s &= \frac{1}{s!}\int_0^\infty \frac{m^s \sinh m\, dm}{\sinh 2m \pm 2m} \\ V_s^* &= \frac{1}{s!}\int_0^\infty \frac{m^s \cosh m\, dm}{\sinh 2m \pm 2m} \\ VII_s^* &= \frac{1}{s!}\int_0^\infty \frac{m^s \tanh m \sinh m\, dm}{\sinh 2m - 2m} \\ VIII_s &= \frac{1}{s!}\int_0^\infty \frac{m^s \coth m \cosh m\, dm}{\sinh 2m + 2m} \end{aligned}\right\} \quad \ldots\ldots [56]$$

The integrals in Equations [56] also were tabulated by the writer in one of the papers mentioned (7). Values of the integrals in Equations [55] corresponding to $c = 1/2$ and $1/4$ are shown in Table 8.

For convenience of reference, values of the integrals in Equations [50], [53], and [56] are reproduced in Tables 9 and 10. Values of the following four integrals, though not used presently, also are tabulated therein

$$\left.\begin{aligned} II_k &= \frac{2^k}{k!}\int_0^\infty \frac{m^k e^{-2m}\, dm}{\sinh 2m \pm 2m} \\ II_k^* &= \frac{1}{k!}\int_0^\infty \frac{m^k \tanh m \sinh m\, dm}{\sinh 2m + 2m} \\ VII_k &= \frac{1}{k!}\int_0^\infty \frac{m^k \coth m \cosh m\, dm}{\sinh 2m - 2m} \end{aligned}\right\} \quad \ldots\ldots [57]$$

Axisymmetric Thermal Stresses in a Spherical Shell of Arbitrary Thickness[1]

By E. L. McDOWELL[2] AND E. STERNBERG,[3] CHICAGO, ILL.

This paper contains an explicit series solution, exact within the classical theory of elasticity, for the steady-state thermal stresses and displacements induced in a spherical shell by an arbitrary axisymmetric distribution of surface temperatures. The corresponding solutions for a solid sphere and for a spherical cavity in an infinite medium are obtained as limiting cases. The convergence of the series solutions obtained is discussed. Numerical results are presented appropriate to a solid sphere if two hemispherical caps of its boundary are maintained at distinct uniform temperatures.

Basic Thermoelastic Equations—Thermoelastic Potential

THE steady-state thermoelastic problem has been the object of numerous investigations.[4] In what follows, we deal with the particular problem which arises when the region under consideration is bounded by two concentric spheres, on the assumption that the prescribed distribution of surface temperatures possesses rotational symmetry. The corresponding problems for the spherical cavity in an infinite medium and for the solid sphere, are treated as limiting cases. In this connection we cite a classical paper by Borchardt (4) who obtained a formal solution in integral representation for the sphere subjected to an arbitrary (not necessarily axisymmetric) temperature distribution. Further investigations of thermal stresses in a sphere are cited in (1), art. 136. To these we add two recent papers by Melan (5, 6) on transient thermal stresses and an (inexplicit) series solution by Muki (7) of the axisymmetric steady-state problem for a spheroid.

Before turning to our main objective, we recall briefly the relevant governing equations.[5] Thus consider a medium occupying a region of space D with the boundary B. Let $T = F(Q)$ be the given surface distribution of temperature, Q being a point on B. The corresponding temperature field $T(Q)$, Q in D, is characterized by the steady-state heat-flow equation and is the solution of the Dirichlet problem

$$\nabla^2 T = 0 \text{ in } D, \qquad T = F(Q) \text{ on } B \ldots\ldots [1]$$

The stresses, strains, and displacements produced by the temperature field $T(Q)$, within the classical theory of elasticity and in the absence of body forces, are characterized by the homogeneous stress equations of equilibrium, the linear isotropic stress-strain relations (including the temperature terms), and the linearized strain-displacement relations. In indicial notation, and with reference to rectangular Cartesian co-ordinates x_i, we have throughout D

$$\tau_{ij,j} = 0 \ldots\ldots [2]$$

$$\tau_{ij} = 2\mu\left[e_{ij} + \left(\frac{\nu}{1-2\nu}e_{kk} - \frac{1+\nu}{1-2\nu}\alpha T\right)\delta_{ij}\right] \ldots\ldots [3]$$

$$2e_{ij} = u_{i,j} + u_{j,i} \ldots\ldots [4]$$

Here τ_{ij}, e_{ij}, and u_i are the Cartesian components of stress, strain, and displacement, respectively, and the usual conventions for summation and space differentiation have been employed; δ_{ij} stands for the Kronecker delta, while μ, ν, and α designate the shear modulus, Poisson's ratio, and the coefficient of thermal expansion. To Equations [2], [3], [4], we must adjoin the boundary conditions which, in the absence of surface tractions, take the form

$$\tau_{ij}n_j = 0 \text{ on } B \ldots\ldots [5]$$

where n_j denotes the scalar components of the outer unit normal of B.

A particular solution of the Field Equations [2], [3], [4] is obtained by setting

$$u_i = \phi_{,i} \ldots\ldots [6]$$

with

$$\nabla^2\phi = \frac{\alpha(1+\nu)T}{1-\nu} \ldots\ldots [7]$$

where ∇^2 is the Laplacian operator, provided the strains and stresses associated with the Displacements [6] are computed consistent with Equations [3], [4]. The function $\phi(Q)$ is the well-known thermoelastic potential, which was apparently first introduced by Borchardt (4) and was applied systematically by Goodier (8) to problems concerning the entire space, and by Mindlin and Cheng (9) to the thermoelastic problem for the half-space. Evidently, $\phi(Q)$ is biharmonic if $T(Q)$ satisfies Equations [1].

The complete solution[6] [S] to the thermoelastic equilibrium problem governed by Equations [1] to [5] may be represented in the form

$$[S] = [S^\circ] + [S^*] \ldots\ldots [8]$$

where $[S^\circ]$ is a particular solution of the field equations generated by ϕ, and $[S^*]$ is the solution of a "residual problem," the characterization of which is implicit in Equation [8]. Thus, $[S^*]$ in D

---

[1] The results presented in this paper were obtained in the course of an investigation conducted under Contract N7onr-32906 with the Office of Naval Research, Department of the Navy, Washington, D. C.

[2] Senior Research Engineer, Armour Research Foundation. Assoc. Mem. ASME.

[3] Professor of Applied Mechanics, Brown University, Providence, R. I.; formerly Professor of Mechanics, Illinois Institute of Technology. Assoc. Mem. ASME.

[4] A bibliography of this general subject is beyond the scope of the present paper. For relevant references, see (1), (2), (3). Numbers in parentheses refer to the Bibliography at the end of the paper.

[5] See, for example, (1) and (2) for general discussions of the thermoelastic problem.

Presented at the Applied Mechanics Division Summer Conference, Berkeley, Calif., June 13–15, 1957, of The American Society of Mechanical Engineers.

Discussion of this paper should be addressed to the Secretary, ASME, 29 West 39th Street, New York, N. Y., and will be accepted until October 10, 1957, for publication at a later date. Discussion received after the closing date will be returned.

Note: Statements and opinions advanced in papers are to be understood as individual expressions of their authors and not those of the Society. Manuscript received by ASME Applied Mechanics Division, May 31, 1956. Paper No. 57—APM-14.

[6] Throughout this paper, capital letters in brackets denote the displacement-vector field and the stress-tensor field of a solution to the field equations; equality, addition, and multiplication by a scalar are to be interpreted accordingly.

must satisfy Equations [2], [3], [4] with $T = 0$ and must annul the surface tractions to which [8°] gives rise on B.

Spherical Shell of Arbitrary Thickness

We turn next to the particular problem at hand and to this end introduce spherical co-ordinates (r, θ, γ) by means of the mapping

$$\left.\begin{aligned} x = r\sin\theta\cos\gamma, \quad y = r\sin\theta\sin\gamma, \quad z = r\cos\theta \\ 0 \le r < \infty, \quad 0 \le \theta \le \pi, \quad 0 \le \gamma < 2\pi \end{aligned}\right\} \ldots [9]$$

where the Cartesian co-ordinates are now designed[7] by (x, y, z). For future convenience we introduce the auxiliary position parameters

$$p = \cos\theta, \qquad \hat{p} = \sin\theta \ldots [10]$$

Let D be the region

$$0 < r_1 < r < r_2 < \infty \ldots [11]$$

r_1 and r_2 being the inner and outer radii of the spherical shell under consideration.

If the given distribution of surface temperatures has rotational symmetry about the z-axis, the formulation of the steady-state temperature problem given in Equations [1] becomes

$$\left.\begin{aligned} \nabla^2 T = 0 \text{ in } D \\ T(r_k, p) = F_k(p), \quad (k = 1, 2), \quad (-1 \le p \le 1) \end{aligned}\right\} \ldots [12]$$

We assume that the functions $F_k(p)$ are piecewise continuously differentiable whence they admit Fourier-Legendre expansions[8] of the form

$$\left.\begin{aligned} F_k(p) = \sum_{n=0}^{\infty} \lambda_n^{(k)} P_n(p) \\ \lambda_n^{(k)} = \frac{2n+1}{2}\int_{-1}^{1} F_k(p)\, P_n(p)\, dp \\ (k = 1, 2;\ n = 0, 1, 2, \ldots) \end{aligned}\right\} \ldots [13]$$

where $P_n(p)$ is the Legendre polynomial of degree n.

The solution of the elementary Dirichlet problem characterized by Equations [12], may be written as

$$T(r, p) = \sum_{n=-\infty}^{\infty} s_n H_n(r, p) \ldots [14]$$

Here

$$H_n(r, p) = \left(\frac{r}{r_2}\right)^n P_n(p) \ldots [15]$$

are interior and exterior spherical harmonics according as $n \ge 0$ and $n < 0$. We recall that

$$P_{-n-1}(p) = P_n(p) \ldots [16]$$

The coefficients s_n are given by

$$s_n = \frac{\lambda_n^{(2)} - \rho^{n+1}\lambda_n^{(1)}}{1 - \rho^{2n+1}} \qquad (n = 0, \pm 1, \pm 2, \ldots) \ldots [17]$$

with

$$\lambda_{-n-1}^{(k)} = \lambda_n^{(k)} \qquad (n = 0, 1, 2, \ldots) \ldots [18]$$

and

$$\rho = \frac{r_1}{r_2} \qquad 0 < \rho < 1 \ldots [19]$$

The defining requirements on the desired solution [8] to the axisymmetric steady-state thermal-stress problem for the spherical shell may now be summarized as follows: [8] in D must meet the Field Equations [2], [3], [4] for the Temperature Field [14] and must conform to the boundary conditions

$$\left.\begin{aligned} \tau_{rr}(r_k, p) = \tau_{r\theta}(r_k, p) = 0 \\ (k = 1, 2), \qquad (-1 \le p \le 1) \end{aligned}\right\} \ldots [20]$$

in which τ_{rr} and $\tau_{r\theta}$ are spherical components of normal and shearing stress.

Guided by the structure of Equation [14], we assume [8] in the form

$$[8] = \sum_{n=-\infty}^{\infty} s_n\, [8_n] \ldots [21]$$

where $[8_n]$ is the complete solution of the thermoelastic problem characterized by the temperature field

$$T = T_n(r, p) = H_n(r, p) \ldots [22]$$

and the Boundary Conditions [20]. Moreover, in accordance with the decomposition underlying Equation [8], we set

$$[8_n] = [8_n^{\circ}] + [8_n^{*}] \qquad (n = 0, \pm 1, \pm 2, \ldots) \ldots [23]$$

where $[8_n^{\circ}]$ is the particular solution generated by the thermoelastic potential

$$\phi = \phi_n(r, p) = \frac{\alpha(1+\nu)}{2(1-\nu)(2n+3)} r^2 H_n(r, p) \ldots [24]$$

It is readily confirmed, with the aid of the identity

$$r\frac{\partial H_n}{\partial r} = nH_n \ldots [25]$$

that ϕ_n of Equation [24] conforms to Equation [7] provided T is replaced by T_n of Equation [22]. The spherical components of displacement and stress appropriate to $[8_n^{\circ}]$ follow from Equation [24] by means of Equations [3], [4], [6] referred to spherical co-ordinates. A trivial computation yields for $[8_n^{\circ}]$

$$\left.\begin{aligned} 2\mu u_r &= \frac{\omega(n+2)}{2n+3} rH_n \\ 2\mu u_\theta &= -\frac{\omega}{2n+3} r\hat{p}H_n' \\ \tau_{rr} &= \frac{\omega(n^2 - n - 4)}{2n+3} H_n \\ \tau_{\theta\theta} &= \frac{-\omega}{2n+3}\left[(n+2)^2 H_n - pH_n'\right] \\ \tau_{\gamma\gamma} &= \frac{-\omega}{2n+3}\left[(3n+4)H_n + pH_n'\right] \\ \tau_{r\theta} &= \frac{-\omega(n+1)}{2n+3}\hat{p}H_n' \end{aligned}\right\} \ldots [26]^9$$

[7] It is expedient henceforth to depart from indicial notation.

[8] See reference (10), Chapter VII.

[9] The displacement u_γ and the stresses $\tau_{\gamma r}$, $\tau_{\gamma\theta}$ vanish identically and are omitted from this, as well as from subsequent, axisymmetric solutions of the field equations.

where

$$\omega = \frac{\mu\alpha(1+\nu)}{1-\nu} \quad \ldots\ldots [27]$$

$H_n(r, p)$ is given by Equation [15], and the primes denote differentiation with respect to p.

By virtue of Equations [23], [26], the solution $[S_n^*]$ to the residual problem obeys the boundary conditions

$$\left.\begin{aligned} \tau_{rr}(r_k, p) &= \xi_n H_n(r_k, p) \\ \tau_{r\theta}(r_k, p) &= \eta_n \hat{p} H_n'(r_k, p) \\ (k = 1, 2), \qquad & (n = 0, \pm 1, \pm 2, \ldots) \end{aligned}\right\} \quad \ldots\ldots [28]$$

provided

$$\xi_n = -\omega\frac{n^2 - n - 4}{2n+3}, \qquad \eta_n = \omega\frac{n+1}{2n+3} \quad \ldots\ldots [29]$$

In addition, $[S_n^*]$ must satisfy the Field Equations [2], [3], [4] for $T = 0$. $[S_n^*]$ may be reached through a linear combination of particular solutions which were established elsewhere (11). Thus, we set

$$\left.\begin{aligned} [S_n^*] &= a_n[A_n] + b_n[B_n] + c_n[C_n] + d_n[D_n] \\ [C_n] &= [A_{-n-1}], \quad [D_n] = [B_{-n-1}], \quad (n = 0, \pm 1, \\ & \qquad \pm 2, \ldots) \end{aligned}\right\} \quad \ldots [30]$$

where the spherical components of displacement and stress belonging to $[A_n]$, $[B_n]$ will now be cited.[10]

For $[A_n]$

$$\left.\begin{aligned} 2\mu u_r &= \frac{nr_2^2}{r} H_n \\ 2\mu u_\theta &= -\frac{\hat{p} r_2^2}{r} H_n' \\ \tau_{rr} &= n(n-1)\left(\frac{r_2}{r}\right)^2 H_n \\ \tau_{\theta\theta} &= -\left(\frac{r_2}{r}\right)^2 [n^2 H_n - pH_n'] \\ \tau_{\gamma\gamma} &= \left(\frac{r_2}{r}\right)^2 [nH_n - pH_n'] \\ \tau_{r\theta} &= -(n-1)\left(\frac{r_2}{r}\right)^2 \hat{p} H_n' \end{aligned}\right\} \quad \ldots\ldots [31]$$

For $[B_n]$

$$\left.\begin{aligned} 2\mu u_r &= -(n+1)(n-2+4\nu) r H_n \\ 2\mu u_\theta &= (n+5-4\nu) r \hat{p} H_n' \\ \tau_{rr} &= -(n+1)[(n+1)(n-2) - 2\nu] H_n \\ \tau_{\theta\theta} &= (n+1)(n^2+4n+2+2\nu) H_n \\ &\qquad - (n+5-4\nu) p H_n' \\ \tau_{\gamma\gamma} &= -(n+1)[n-2-2(2n+1)\nu] H_n \\ &\qquad + (n+5-4\nu)\, p H_n' \\ \tau_{r\theta} &= (n^2+2n-1+2\nu)\hat{p} H_n' \end{aligned}\right\} \quad \ldots [32]$$

Next, we apply the Boundary Conditions [28], [29] to $[S_n^*]$ and, with the aid of Equations [30] to [32], are led to a system of linear algebraic equations for the unknown coefficients of superposition a_n, b_n, c_n, d_n. The solution of this system is given by

$$\left.\begin{aligned} \Delta_n a_n &= \frac{(1-\rho^{2n+1})(1-\rho^{2n+3})}{n-1}[(n+1)\alpha_{-n-1} \\ &\qquad -n\beta_{-n-1}][\alpha_n\xi_n + (n+1)\beta_n\eta_n], \qquad (n \neq 0, 1) \\ \Delta_n b_n &= (1-\rho^{2n-1})(1-\rho^{2n+3})[(n+1)\alpha_{-n-1} \\ &\qquad - n\beta_{-n-1}](\xi_n + n\eta_n) - \rho^{2n-1}(1-\rho^2)^2 n(\alpha_{-n-1} \\ &\qquad + \beta_{-n-1})[\xi_n - (n+1)\eta_n] \quad (n \neq -1) \\ \Delta_n c_n &= -\rho^{2n+1}(1-\rho^2)(1-\rho^{2n+1})\frac{n}{n+2}(\alpha_{-n-1} \\ &\qquad + \beta_{-n-1})[\alpha_n\xi_n + (n+1)\beta_n\eta_n], \quad (n \neq -1, -2) \\ \Delta_n d_n &= \rho^{2n-1}(1-\rho^2)(1-\rho^{2n+3})(2n+1)[\alpha_n\xi_n \\ &\qquad + (n+1)\beta_n\eta_n], \qquad (n \neq 0) \end{aligned}\right\} \quad \ldots [33]$$

where

$$\left.\begin{aligned} \Delta_n &= (1-\rho^{2n-1})(1-\rho^{2n+3})[(n+1)\alpha_{-n-1} \\ &\qquad - n\beta_{-n-1}][n\alpha_n - (n+1)\beta_n] + \rho^{2n-1}(1 \\ &\qquad - \rho^2)^2 n(n+1)(\alpha_n + \beta_n)(\alpha_{-n-1} + \beta_{-n-1}) \\ \alpha_n &= n^2 + 2n - 1 + 2\nu, \qquad \beta_n = n^2 - n - 2 - 2\nu \end{aligned}\right\} \quad \ldots [34]$$

As is evident by inspection of Equations [31], [32], the solutions $[A_0]$, $[A_1]$, $[B_{-1}]$, and hence $[C_{-1}]$, $[C_{-2}]$, $[D_0]$, have identically vanishing stress fields and thus represent rigid-body displacements[11]; for this reason the corresponding coefficients of superposition a_0, a_1, b_{-1}, c_{-1}, c_{-2}, and d_0 remain indeterminate. The stress fields appropriate to $[S_0]$ and $[S_1]$ in Equations [23] are also found to vanish identically. This result is in agreement with general theory since, according to Equations [22], the corresponding temperature fields T_0, T_1 are linear in (x, y, z) and hence do not induce any thermal stresses.[12]

The Series Representation [21] of the solution [S] to the thermoelastic problem under consideration is now complete. The convergence of this infinite series will be examined in the Appendix.

Solid Sphere and Spherical Cavity as Limiting Cases

We now consider a solid sphere of radius R. Let the prescribed surface temperature be represented by

$$\left.\begin{aligned} T(R, p) &= F(p) = \sum_{n=0}^{\infty} \lambda_n P_n(p) \\ \lambda_n &= \frac{2n+1}{2}\int_{-1}^{1} F(p) P_n(p)\, dp \\ & \qquad (n = 0, 1, 2, \ldots) \end{aligned}\right\} \quad \ldots [35]$$

The corresponding solution for the steady-state temperature, displacement, and stress distribution, is obtained from the preceding solution for the spherical shell by letting r_1 tend to zero, and replacing $\lambda_n^{(2)}$, r_2 with λ_n, R, respectively. An elementary computation yields

$$T(r, p) = \sum_{n=0}^{\infty} \lambda_n \left(\frac{r}{R}\right)^n P_n(p) \quad \ldots\ldots [36]$$

[10] It should be noted that the particular solutions here designated by $[A_n]$ and $[B_n]$ correspond to $r_2^{-n+2}[A_{-n-1}]$ and $r_2^{-n}[B_{-n-1}]$ in the notation of the previous paper (11).

[11] These solutions have been included in the Aggregate [30] for the sake of convenience only.

[12] See reference (2), p. 9.

$$[S] = \sum_{n=0}^{\infty} \lambda_n [S_n] \quad \ldots [37]$$

with the following components of displacement and stress for $[S_n]$

$$\left.\begin{aligned}
2\mu u_r &= \delta_n r\left[n + 2 + n\frac{R^2}{r^2}\right]\frac{r^n}{R^n}P_n \\
2\mu u_\theta &= \delta_n r\left[3 - \frac{R^2}{r^2}\right]\frac{r^n}{R^n}\beta P_n' \\
\tau_{rr} &= -\delta_n n(n-1)\left[1 - \frac{R^2}{r^2}\right]\frac{r^n}{R^n}P_n \\
\tau_{\theta\theta} &= \delta_n\left\{n\left[n + 2 - n\frac{R^2}{r^2}\right]P_n \right. \\
&\qquad \left. - \left[3 - \frac{R^2}{r^2}\right]pP_n'\right\}\frac{r^n}{R^n} \\
\tau_{\gamma\gamma} &= -\delta_n\left\{n\left[2n + 1 - \frac{R^2}{r^2}\right]P_n \right. \\
&\qquad \left. - \left[3 - \frac{R^2}{r^2}\right]pP_n'\right\}\frac{r^n}{R^n} \\
\tau_{r\theta} &= \delta_n(n-1)\left[1 - \frac{R^2}{r^2}\right]\frac{r^n}{R^n}\beta P_n'
\end{aligned}\right\} \quad \ldots [38]$$

where

$$\delta_n = \frac{\omega(1-\nu)}{n^2 + n + 1 + (2n+1)\nu} \quad \ldots [39]$$

and the primes denote differentiation of P_n with respect to its argument p.

Finally, consider an infinite medium with a spherical cavity of radius R. Let the surface distribution of the temperature again be given by Equations [35] and assume that T as well as all components of stress tend to zero as $r \to \infty$. An analogous limit process yields for the solution to the present problem

$$T(r, p) = \sum_{n=0}^{\infty} \lambda_n \left(\frac{R}{r}\right)^{n+1} P_n(p) \quad \ldots [40]$$

$$[S] = \sum_{n=-1}^{-\infty} s_n [S_n] \quad \ldots [41]$$

where

$$s_{-2n-1} = \lambda_n \qquad (n = 0, 1, 2, \ldots) \quad \ldots [42]$$

and $[S_n]$ is once more given by Equations [38], [39].

Applications, Numerical Results, Discussion

As a first illustration we apply the general solution of the shell problem, given in Equation [21], to the trivial case in which the two spherical boundaries are maintained at distinct uniform temperatures. Thus let

$$F_1(p) = 1, \qquad F_2(p) = 0 \quad \ldots [43]$$

in Equations [12]. Equations [13], [17], [18] here imply

$$s_{-1} = \frac{-\rho}{\rho - 1}, \qquad s_0 = \frac{-\rho}{1 - \rho}, \qquad s_n = 0 \text{ for } n \neq -1, 0 \ldots [44]$$

and hence, from Equations [14], [21]

$$T = \frac{-\rho}{\rho - 1}\left(\frac{r_2}{r} - 1\right), \qquad [S] = \frac{-\rho}{\rho - 1}\{[S_{-1}] - [S_0]\} \quad \ldots [45]$$

Equations [23], [26], and [29] to [34] yield for the stress field belonging to [S]

$$\left.\begin{aligned}
\tau_{rr} &= \frac{2\omega\rho}{1 - \rho^3}\left[1 + \rho - (1 + \rho + \rho^2)\frac{r_2}{r} + \rho^3\frac{r_2^3}{r^3}\right] \\
\tau_{\theta\theta} = \tau_{\gamma\gamma} &= \frac{2\omega\rho}{1 - \rho^3}\left[1 + \rho - (1 + \rho + \rho^3)\frac{r_2}{2r} \right. \\
&\qquad \left. - \rho^3\frac{r_2^3}{2r^3}\right] \\
\tau_{r\theta} &= 0
\end{aligned}\right\} \quad \ldots [46]$$

This re-establishes the known closed solution to the problem.[13]

As a nontrivial application, we consider a solid sphere and assume that a spherical cap and its complement are held at uniform distinct temperatures. Specifically, let $F(p)$ in Equations [35] be defined by

$$\left.\begin{aligned}
F(p) &= 1 \text{ for } 0 \leq p_0 < p \leq 1 \\
F(p) &= 0 \text{ for } -1 \leq p < p_0
\end{aligned}\right\} \quad \ldots [47]$$

in which

$$2\theta_0 = \cos^{-1} p_0 \; (0 < \theta_0 \leq \pi/2)$$

is the opening angle of the circular cone which has its vertex at the origin and contains the common boundary of the two spherical caps in question. The second of Equations [35] here leads to

$$\lambda_0 = \frac{1}{2}(1 - p_0), \qquad \lambda_n = \frac{2n+1}{2n(n+1)}\beta_0^2 P_n'(p_0), \qquad (n = 1, 2, \ldots) \quad \ldots [48]$$

and the complete solution of the steady-state thermoelastic problem under consideration is given by Equations [36] to [39] and [48].

For the special case of hemispherical caps, $p_0 = 0$ and the coefficients of superposition in Equations [48] take the form

$$\left.\begin{aligned}
\lambda_0 &= \frac{1}{2}, \qquad \lambda_{2n} = 0, \qquad (n = 1, 2, \ldots) \\
\lambda_{2n+1} &= \frac{(-1)^n(4n+3)(2n)!}{2^{2n+2}(n+1)(n!)^2}, \qquad (n = 0, 1, 2, \ldots)
\end{aligned}\right\} \quad \ldots [49]$$

Figs. 1 and 2 show the variation of the radial displacement and of the normal stresses $\tau_{\theta\theta}$, $\tau_{\gamma\gamma}$ on the surface of the sphere, for the case $p_0 = 0$ and $\nu = 0.3$; the distribution of the principal stresses along the z-axis is given in Fig. 3. With reference to Fig. 2 we note that $\tau_{\gamma\gamma}$ exhibits a finite jump discontinuity at the equator, where the surface temperature is similarly discontinuous. The connection between these two discontinuities is found to be

$$\tau_{\gamma\gamma}(R, 0+) - \tau_{\gamma\gamma}(R, 0-) = -\alpha E[T(R, 0+) - T(R, 0-)] \quad \ldots [50]$$

if E designates Young's modulus. This result was to be anticipated on the basis of the plane-strain theory of steady-state thermal stresses.[14] The analogous relationship was encountered in the steady-state thermoelastic problem for a half-space (12), at finite surface discontinuities of the temperature field. It appears, therefore, that this connection between a jump discon-

[13] See, for example, reference (1), p. 420.
[14] See reference (1), Equation [d] on p. 428.

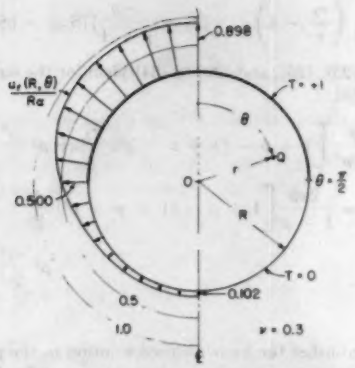

FIG. 1 SURFACE VALUES OF RADIAL DISPLACEMENT u_r

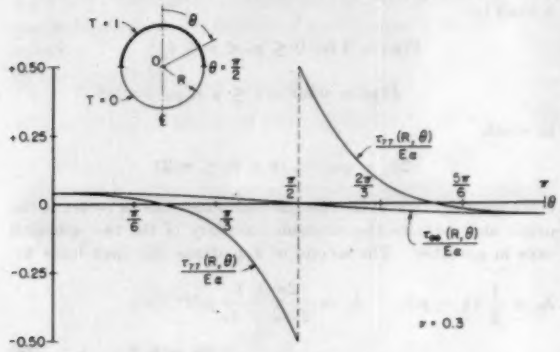

FIG. 2 SURFACE VALUES OF STRESSES $\tau_{\theta\theta}$, $\tau_{\gamma\gamma}$

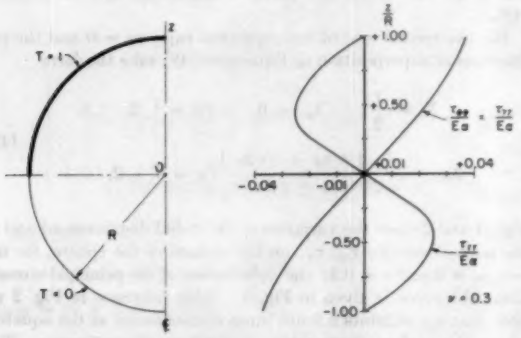

FIG. 3 PRINCIPAL STRESSES ALONG AXIS OF SYMMETRY

tinuity in the surface temperature and the corresponding discontinuity in the surface values of the normal stress on planes perpendicular to the line of temperature discontinuity, is generally characteristic of traction-free boundaries and is not affected by the curvature of the boundary.

BIBLIOGRAPHY

1 "Theory of Elasticity," by S. Timoshenko and J. N. Goodier, McGraw-Hill Book Company, Inc., New York, N. Y., second edition, 1951.

2 "Wärmespannungen," by Ernst Melan and Heinz Parkus, Julius Springer, Vienna, Austria, 1953.

3 "Temperature Stresses in the Theory of Elasticity" (in Russian), by N. N. Lebedev, ONTI, Moscow, Russia, 1937.

4 "Untersuchungen über die Elasticität fester isotroper Körper unter Berücksichtigung der Wärme," by C. W. Borchardt, *Monatsber. Akad. Wiss.*, Berlin, Germany, vol. 9, 1873.

5 "Mitteilung, Sitzungsbericht der math.-naturwiss.," by Ernst Melan, Klasse, Oesterr. Akad. Wiss., October 13, 1955.

6 "Wärmespannungen bei der Abkühlung einer Kugel," by Ernst Melan, *Acta Physica Austriaca*, vol. 10, nos. 1–2, 1956, p. 81.

7 "Thermal Stresses in a Spheroid with Steady Axisymmetric Distribution of Temperature," by R. Muki, Proceedings of the Faculty of Engineering, Keio University, vol. 6, no. 20, 1953, p. 10.

8 "On the Integration of the Thermo-Elastic Equations," by J. N. Goodier, *Philosophical Magazine*, vol. 23, 1937, p. 1017.

9 "Thermoelastic Stress in the Semi-Infinite Solid," by R. D. Mindlin and D. H. Cheng, *Journal of Applied Physics*, vol. 21, 1950, p. 931.

10 "The Theory of Spherical and Ellipsoidal Harmonics," by E. W. Hobson, University Press, Cambridge, England, 1931.

11 "On the Axisymmetric Problem of Elasticity Theory for a Region Bounded by Two Concentric Spheres," by E. Sternberg, R. A. Eubanks, and M. A. Sadowsky, Proceedings of the First U. S. National Congress of Applied Mechanics, ASME, New York, N. Y., 1952.

12 "On the Steady-State Thermoelastic Problem for the Half-Space," by E. Sternberg and E. L. McDowell, *Quarterly of Applied Mathematics*, vol. 14, January, 1957, p. 381.

Appendix

REMARKS ON CONVERGENCE OF SERIES SOLUTIONS

We show here that the infinite series for the displacements and stresses of solution [S], given by Equation [21], as well as their space derivatives of all finite orders, converge uniformly and absolutely in the interior of the region occupied by the medium; i.e., for

$$\left.\begin{aligned} r_1 + \epsilon < r < r_2 - \epsilon, \qquad 0 \le p \le 1 \\ \left[0 < \epsilon < \frac{r_2 - r_1}{2}\right] \end{aligned}\right\} \quad \ldots\ldots [51]$$

To this end, in view of the form of Equations [21], [23], [26], [29], [30], and [31] to [34], it suffices to establish the uniform and absolute convergence of the series

$$\sum_{n=-\infty}^{\infty} G(n) t^n P_n(p) \quad (-1 \le p \le 1) \ldots\ldots [52]$$

on the assumption that

$$\left.\begin{aligned} |t| < 1 - \epsilon \qquad (\epsilon > 0) \text{ for } n \ge 0 \\ |t| > 1 + \epsilon \qquad (\epsilon > 0) \text{ for } n < 0 \end{aligned}\right\} \quad \ldots\ldots [53]$$

and that $G(n)$ is a rational function. This convergence, however, follows at once by observing that

$$|P_n(p)| \le 1, \qquad \lim_{n \to \infty} \frac{|G_{n+1}|}{|G_n|} = 1 \ldots\ldots [54]$$

As far as the behavior on the boundaries $r = r_1$, $r = r_2$ is concerned, we need examine merely the series for u_r, u_θ, $\tau_{\gamma\gamma}$, and $\tau_{\theta\theta}$, since the stresses τ_{rr}, $\tau_{r\theta}$ of the component solutions $[S_n]$ in Equation [21] vanish on the boundaries. It is not difficult to show that the several infinite series in question are convergent on the boundaries if the same is true of the corresponding series appropriate to the limit solutions for the solid sphere and the spherical cavity, given by Equations [37] to [39] and [41], [42]. The convergence of these series for $r = R$, on the other hand, may be deduced from the known convergence of the surface-temperature Expansion [35].

Saint Venant's Principle: A Biharmonic Eigenvalue Problem

By G. HORVAY,[1] SCHENECTADY, N. Y.

Saint Venant's principle is formulated as a biharmonic eigenvalue problem for the symmetrical truncated wedge $x \geq 0$, $|y| \leq y_b$ ($y_b = 1 + x \tan \omega$) which is stress-free along the lateral edges, and is loaded by self-equilibrating shear and normal tractions $\tau_k^\circ(y)$, $\sigma_k^\circ(y)$ along edge $x = 0$. It is found that for the wedge angle $2\omega = 0$ the law of decay is of the type $e^{-\alpha_k r}$; for $2\omega \neq 0$ the law of decay is of type $r^{-\mu_k}$; μ_k is minimum for $2\omega = \pi$. The indexes k attached to τ°, σ° indicate that we deal with systems of characteristic tractions which produce characteristic decay rates. Practical implications of the results, as they apply to structural design, are discussed in a separate paper, "Some Aspects of Saint Venant's Principle."

Introduction

SAINT VENANT announced his celebrated principle (as related to the torsion problem) in 1855(1).[2] "According to this principle the strains that are produced in a body by the application, to a small part of its surface, of a system of forces statically equivalent to zero force and zero couple are of negligible magnitude at distances which are large compared with the linear dimensions of the (loaded) part."[3] The principle soon acquired, in structural analysis, a most prominent role and indiscriminate use, as it provided justification for ignoring major difficulties in a large number of problems.

The dangers of such indiscriminate use are pointed up in Fig. 1(*c*). The figure illustrates a doubly connected body, loaded by self-equilibrating tractions which are spread over a small arc length $2h$; the stresses reach, with increasing distance from the load region, arbitrarily large values. (It is easy to see that net tension and bending moment are transmitted across any radial section of the ring; hence by prescribing a suitable variation of the cross-section—as suggested in Fig. 1(*c*)—arbitrary large stresses may be achieved.) Further examples and counter-examples may be found in papers by Goodier (1937, 1942) as summarized in (3), Hoff (4), von Mises (5), Reissner (6), Horvay [Fig. 7 of (7)], Sternberg (8), and others; these publications contain many additional literature references. They show that some classes of structures are notoriously reluctant to abide by the principle.

The modern formulation and establishment of the principle have been taking place in three stages. In the first stage—beginning with Saint Venant and Boussinesq, and culminating in the work of Goodier—one arrived at a demonstration that the strain energy per unit area (we restrict ourselves to plane figures)

$$U = \frac{1}{2E} \int_{\text{unit area}} [\sigma_x^2 + \sigma_y^2 + 2\tau^2 + 2\nu(\tau^2 - \sigma_x\sigma_y)]dA$$

becomes as small as one pleases when the distance r of the unit area from the loaded arc $2h$ is sufficiently increased (3).[4] However, Fig. 1(*c*) is a forceful reminder that the smallness of the integral U does not necessarily insure the smallness of the stresses: a strain energy integral evaluation is, in itself, insufficient to establish Saint Venant's principle for arbitrary bodies.

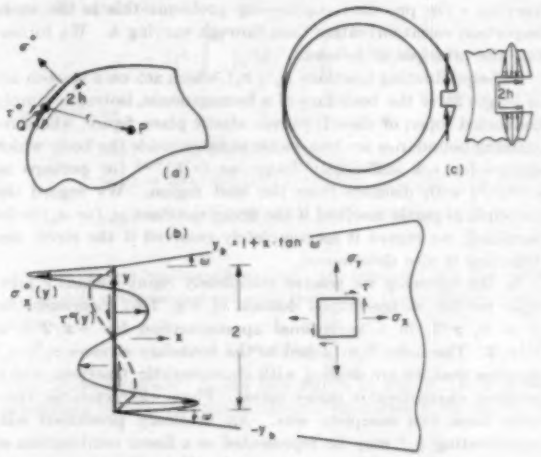

Fig. 1

The papers of von Mises and Sternberg constitute the second phase of the development. Their principal results may be stated, for our purposes, as follows. Let distributed tractions be applied to the portion $2h$ of the boundary of a (sufficiently regular) plane elastic figure such as Fig. 1(*a*) (which has but a finite number of abrupt changes in the slope of the bounding curve), and let Q be a (non-corner, but otherwise arbitrary) point of the arc $2h$. Denote the stresses at a *fixed* internal point P of the figure, at distance r from Q, by σ_{ij}. Then as $2h$ is gradually shrunk down onto Q, and the traction distribution is likewise contracted—without, however, changing the original magnitudes of the boundary stresses—the variation of the σ_{ij} with h may be written in the form

$$\sigma_{ij} = S_{ij}(r/h)^{-\alpha} \quad \text{[I]}$$

when the tractions are self-equilibrating, and in the form

$$\sigma_{ij} = S_{ij}(r/h)^{-\beta} \quad \text{[II]}$$

when the tractions are in "astatic" equilibrium, where *the stress coefficients S_{ij} tend to constant values as r/h becomes large.*

[1] Research Associate, Metallurgy and Ceramics Research Department, General Electric Research Laboratory. Mem. ASME.

[2] Numbers in parentheses refer to the Bibliography at the end of the paper.

[3] From Love (2).

Presented at the Applied Mechanics Division Summer Conference, Berkeley, Calif., June 13–15, 1957, of The American Society of Mechanical Engineers.

Discussion of this paper should be addressed to the Secretary, ASME, 29 West 39th Street, New York, N. Y., and will be accepted until October 10, 1957, for publication at a later date. Discussion received after the closing date will be returned.

Note: Statements and opinions advanced in papers are to be understood as individual expressions of their authors and not those of the Society. Manuscript received by ASME Applied Mechanics Division, June 29, 1956. Paper No. 57—APM-21.

[4] For another illuminating presentation of the strain energy approach, see (26).

(Astatic equilibrium means: self-equilibration persists as the loads are rotated at an arbitrary angle about their points of application. Thus in Fig. 1(b) the normal tractions $\sigma_x^\circ(y)$ are in astatic equilibrium, the shear tractions $\tau^\circ(y)$ are not.[5])

The important results of von Mises-Sternberg are unsuitable for engineering estimates, mainly because for "small" distances r the "constants" S_{ij} are exceedingly sensitive (and undetermined) functions of the body geometry, the location of the points Q and P, the traction distribution, and the load spread over distance ratio, $2h/r$. In connection with Fig. 1(c) one observes, for instance, that the increase of S_{ij} with r may overshadow the r^{-2} decay when the load application arc $2h$ is longer than the width of the narrowest cross section of the ring. The generality of the regions considered, the need for properly accounting for irregular cases like Fig. 1(c), renders the von Mises-Sternberg results necessarily vague.

For this reason both von Mises and Sternberg suggested the existence of much stronger forms of the principle for special classes of bodies and proposed that research be undertaken in this direction. The present investigation ushers in this third phase of the development. It reverts to varying the r/h ratio through varying r (in practical engineering problems this is the more important variation) rather than through varying h. We formulate the principle as follows.

Self-equilibrating tractions σ_k°, τ_k° which act on a smooth arc of length $2h$ of the boundary of a homogeneous, isotropic, simply connected (open or closed) convex elastic plane figure, whose remaining boundaries are free, cause stresses inside the body which decay—for r/h sufficiently large—as $(r/h)^{-\mu_k}$ (or perhaps as $e^{-\alpha_k r/h}$) with distance from the load region. We regard the principle as partly resolved if the decay constant μ_k (or α_k) is determined; we regard it as completely resolved if the stress distribution is also determined.

In the following we resolve completely Saint Venant's principle for the wedge-shaped domain of Fig. 1(b), rigorously for $\omega = 0, \pi/2$, in a variational approximation for $-\pi/2 < \omega < \pi/2$. The index k attached to the boundary stresses σ_k°, τ_k° signifies that we are dealing with characteristic tractions which produce characteristic decay rates. These characteristic tractions form two complete sets: An arbitrary prescribed self-equilibrating σ_x° may be represented as a linear combination of the σ_k°, and an arbitrary prescribed self-equilibrating τ° may be represented as a linear combination of the τ_k°.

Mathematically, the problem of Saint Venant's principle consists of (a) finding the two complete sets of characteristic self-equilibrating boundary tractions $\sigma_k^\circ(y)$, $\tau_k^\circ(y)$;[6] (b) determining the corresponding eigensolutions $G_k(x, y)$, $H_k(x, y)$ of the biharmonic equation; (c) determining the rates of decay of the second derivatives of G_k, H_k. In the rigorous solution the three steps are started simultaneously (but usually only step (c) is completed). In the variational approximation the steps are carried out consecutively, step (c) preceding step (b). In either method the characteristic decay rates μ_k (or α_k) are obtained as the real parts of roots of appropriate eigenvalue equations.

Rigorous Solution of the End Problem for $\omega = 0$

We only outline here the solution; the details are given elsewhere (9). The objective is to establish functions $H_n(x, y)$, $G_n(x, y)$, even in y for even n, odd in y for odd n (the evenness or oddness of the function insures that the values at $y = +1$ also specify the values at $y = -1$; * denotes values at $y = +1$, $^\circ$ denotes values at $x = 0$, subscript after comma means differentiation; for simplicity of notation we use h as distance unit, the modulus of elasticity as stress unit) such that

$$\left.\begin{aligned} &(a)\ \nabla^4 H_n = \nabla^4 G_n = 0 \\ &(b)\ H_{n,xx}{}^* = H_{n,xy}{}^* = G_{n,xx}{}^* = G_{n,xy}{}^* = 0 \\ &(c)\ H_{n,yy}{}^\circ = G_{n,xy}{}^\circ = 0 \\ &(d)\ -H_{n,xy}{}^\circ \equiv t_n(y),\quad G_{n,yy}{}^\circ \equiv s_n(y) \end{aligned}\right\} \quad \ldots [1]$$

where $t_n(y)$, $s_n(y)$ constitute complete orthonormal sets of self-equilibrating shear and normal boundary tractions into which prescribed self-equilibrating tractions τ°, σ_x°, i.e., tractions satisfying

$$\int_{-1}^{1} \tau^\circ dy = \int_{-1}^{1} \sigma_x^\circ dy = \int_{-1}^{1} \sigma_x^\circ y dy = 0 \quad \ldots [2]$$

may be expanded[7]

$$\tau^\circ(y) = \Sigma B_n t_n(y), \qquad \sigma_x^\circ(y) = \Sigma A_n s_n(y) \quad \ldots [3a]$$

For then

$$H(x, y) = \Sigma B_n H_n(x, y), \qquad G(x, y) = \Sigma A_n G_n(x, y) \quad \ldots [3b]$$

are the stress functions of the H and G problems, and the stresses throughout the body are obtained in the usual fashion

$$\tau = -H_{,xy}, \qquad \sigma_x = H_{,yy}, \qquad \sigma_y = H_{,xx} \quad \ldots [4]$$

To arrive at functions H_n and G_n we first solve the two "mixed" problems of determining functions $K_k(x, y)$ and $J_k(x, y)$, $k = 2, 3, \ldots$ which comply with Equations [1a, b] and with the modified conditions

$$\left.\begin{aligned} &(c')\ \ \sigma^\circ = K_{k,yy}{}^\circ = 0, \quad -\int_{-1}^{y} \tau^\circ dy = I_{k,xx}{}^\circ = 0 \\ &(d')\ \ dv^\circ/dy = K_{k,xx}{}^\circ = 1 - y^2, y - y^4, \\ &\qquad\qquad 1 - 8y^3 + 7y^4, \ldots \\ &u^\circ = I_{k,yy}{}^\circ = \frac{1}{2}(-1 + 3y^2), \frac{1}{2}(-3y + 5y^3), \\ &\qquad\qquad \frac{1}{8}(3 - 30y^2 + 35y^4), \ldots \end{aligned}\right\} \quad \ldots [5]$$

where u and v are the x and y displacements, and $I_{k,x} \equiv J_k$. The polynomials $K_{k,xx}{}^\circ$ are the (unnormalized) Horvay-Spiess polynomials $Q_2(y), Q_3(y), \ldots$ (denoted formerly (10),[8] except for normalization factors, by $f_2(y), f_3(y), \ldots$) with leading coefficient chosen as 1, which constitute a complete orthogonal set with respect to the boundary condition

$$Q_k(+1) = 0 \quad \ldots [6a]$$

while the $I_{k,yy}{}^\circ$ are the Legendre polynomials $P_2(y), P_3(y), \ldots$ which form a complete orthogonal set with respect to

$$P_k(+1) = 1 \quad \ldots [6b]$$

[5] These are not all the results obtained by von Mises (who stated the theorems and exhibited them for two examples) and Sternberg (who established them in general). They evaluated, in addition, the effects of concentrated and nonequilibrated loads and found that when the force resultant of the tractions is zero, the moment resultant is not, the stresses still decay as $(r/h)^{-2}$; they found that for 3-dimensional space the variations are $(r/h)^{-3}$ and $(r/h)^{-4}$ respectively; and showed (Sternberg) that limitation of the bodies to simple connectivity is not required. Needless to say, the above rates of decay are lower limits. For special bodies—or for special tractions—the rates of decay may become much faster. In the present paper the von Mises-Sternberg Formulas [I], [II] are shown to be by-products of the more specific Results [25], [26]. (As $h \to 0$, the arc $2h$ and the adjacent boundary may be regarded as the edge of a half-plane.)

[6] These will be denoted by s_k, t_k in the next section.

[7] We assume for simplicity that the wedge is of unit thickness.

[8] See Equation [12] of reference.

(We disregard the trivial polynomials $P_0 = 1, P_1 = y$ which represent rigid body motions.)

From the solutions K_k, J_k we can calculate the corresponding boundary values

$$-\tau_k^\circ(y) \equiv K_{k,xy}{}^\circ, \qquad \sigma_k^\circ(y) \equiv J_{k,yy}{}^\circ \ldots\ldots\ldots [7]$$

of shear and normal stresses, reorthogonalize these by proper choice of coefficients b_{nk}, a_{nk} into functions

$$\left.\begin{aligned} t_2(y) &= b_{22}\tau_2^\circ \\ t_4(y) &= b_{44}\tau_4^\circ + b_{42}\tau_2^\circ \\ t_6(y) &= b_{66}\tau_6^\circ + b_{64}\tau_4^\circ + b_{62}\tau_2^\circ \\ &\cdots\cdots \\ \int_{-1}^{1} t_n(y)t_m(y)dy &= \delta_{nm} \\ t_1, t_3, \ldots; \; s_2, s_4, \ldots; \; s_1, s_3, \ldots &= \text{similar} \end{aligned}\right\} \ldots\ldots [8]$$

and define

$$\left.\begin{aligned} H_n(x, y) &= \sum_{k=2}^{n} b_{nk}K_k(x, y) \\ G_n(x, y) &= \sum_{k=2}^{n} a_{nk}J_k(x, y) \end{aligned}\right\} \ldots\ldots\ldots [9]$$

The rigorous solution of the end problem is then given by Equations [3a, b].

One way of arriving at the functions K_k, I_k is to extend the semi-infinite strip to $x = -\infty$,[3] and determine the tractions $\sigma_y{}^*$, τ^* which must act at the horizontal edges, for $x < 0$ (still retaining the requirement $\sigma_y{}^* = \tau^* = 0$ for $x > 0$), so that they give rise to the prescribed dv°/dy, u°. One finds that when $K_{k,xx}{}^\circ$, $K_{k,xy}{}^\circ$ are prescribed, $\sigma_y{}^*$, τ^* are (for $x < 0$) k-degree and $k-1$ degree polynomials in x, respectively, when k is even, $k-1$ degree and k-degree polynomials when k is odd; and when $I_{k,xx}{}^\circ$, $I_{k,xy}{}^\circ$ are prescribed, $\sigma_y{}^*$, τ^* are $k-1$ and $k-2$ degree polynomials in x when k is even, and $k-2$ and $k-1$ degree polynomials when k is odd. In this fashion one finds, for instance, that for

$$\tau^\circ = 0, \qquad u^\circ = P_3(y) = (-1 + 3y^2)/2 \ldots\ldots [10a]$$

one must apply

$$\tau^\circ = 0 \qquad \sigma_y{}^* = 6|x| \qquad (x < 0) \ldots\ldots\ldots [10b]$$

and there results by the usual techniques for the infinite strip $(-\infty \leq x \leq \infty)$

$$\left.\begin{aligned} J_2(x, y) &= 3S_3(x) + \frac{12}{\pi}\int_0^\infty \left[\frac{\text{sh } \lambda + \lambda \text{ ch } \lambda}{\text{sh } 2\lambda + 2\lambda} \text{ ch } \lambda y \right. \\ &\quad \left. - \frac{\lambda \text{ sh } \lambda}{\text{sh } 2\lambda + 2\lambda} y \text{ sh } \lambda y - \frac{1}{2}\right] \frac{\cos \lambda x}{\lambda^4}\, d\lambda \\ S_3(x) &\equiv -\frac{x^3}{3!} + \frac{2}{\pi}\int_0^\infty \left(\cos \lambda x - 1 + \frac{\lambda^2 x^2}{2!}\right) \frac{d\lambda}{\lambda^4} \\ &= \begin{cases} 2|x|^3/3! & \text{for } x < 0 \\ 0 & \text{for } x > 0 \end{cases} \end{aligned}\right\} \ldots [11]$$

On applying the residue theorem one may convert Integral [11], for $x \geq 0$, into a "biharmonic eigenfunction expansion" ($\Re \equiv$ real part)

$$J_2(x, y) = 6\Re \sum_j \frac{\sin^2 z_j}{z_j \cos^2 z_j} \Phi_j(x, y) \ldots\ldots [12a]$$

$(j = 2, 4, 6, \ldots)$ where

$$\Phi_j(x, y) = z_j^{-2} e^{-z_j x}(\cos z_j y - y \cot z_j \sin z_j y) \ldots [12b]$$

are the "even" Fadle-Papkovich functions, obeying $\Phi^* = \Phi_{,y}{}^* = 0$, and $z_2, z_4, z_6, \ldots$ are the roots

$$z_k = \alpha_k + i\beta_k \ldots\ldots\ldots\ldots [12c]$$

of the eigenvalue equation

$$\sin 2z + 2z = 0 \ldots\ldots\ldots\ldots [12d]$$

which have positive real and imaginary parts. The stress and displacement distributions produced by $J_2/6$ are plotted in (12). The problems of J_k and K_k with indices 3, 5, 7, ... are associated with the eigenvalue equation $\sin 2z - 2z = 0$, and are treated similarly (13).

The decay constants α_k are indicated by small circles in Fig. 2; the squares refer to the variational approximation, as obtained from the equation

$$z^4 - 2z^2 \int_{-1}^{1} f_k'^2 dy + \int_{-1}^{1} f_k''^2 dy = 0 \ldots\ldots [13]$$

The functions

$$\left.\begin{aligned} f_2(y) &= (3\sqrt{35}/16)(1 - y^2)^2 \\ f_3(y) &= (3\sqrt{385}/16)(1 - y^2)^2 y \\ f_4(y) &= (3\sqrt{91}/32)(1 - y^2)(-1 + 11y^2) \\ &\cdots\cdots \end{aligned}\right\} \ldots [14]$$

are the author's "self-equilibrating" polynomials (14); they form a complete orthonormal set with respect to the boundary conditions

$$f_k(\pm 1) = f_k'(\pm 1) = 0 \ldots\ldots\ldots [15]$$

The "wave numbers" β_k are also shown in Fig. 2. It is rather interesting to note that the variational estimates of α_2, α_3, α_4, α_5

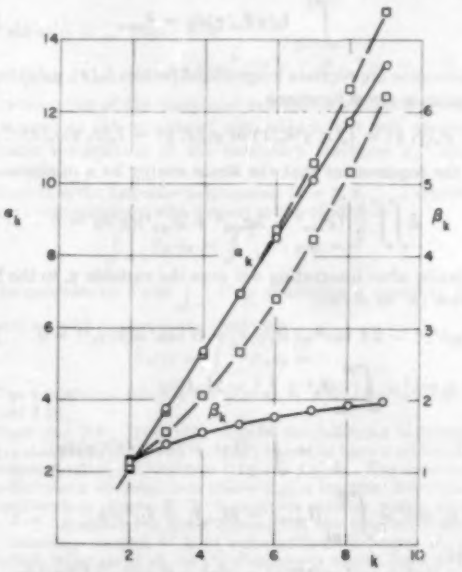

FIG. 2

[3] An alternate procedure, based on elegant results by R. C. T. Smith (11), which by-passes the extension of the strip to minus infinity is also given in (9).

are below the exact values, and so is the modulus of z_1; on the other hand, all variational β_k are higher than the exact β_k.

Formula [12a] reveals a disturbing fact. *The eigenfunctions J_k, K_k, G_k, H_k are not monochromatic; all eigenvalues are contained in them.* Only for exceptional—and from an engineer's (and possibly also a mathematician's) point of view, useless—combinations of the applied tractions, which completely suppress Φ_2, Φ_4, . . . (but completely mix up the boundary shears and boundary normal stresses) will there exist a decay faster than α_2, at the rates α_3, α_4, . . . Nevertheless, a quasimonochromatic notion may still be salvaged. One finds that the J_2 (and K_2, G_2, H_2), J_3 (and K_3, G_3, H_3), . . . stress functions have the Φ_2, Φ_3, . . . functions as their dominant terms. Thus it is permissible to say, in first approximation, that the traction distributions τ_k°, σ_k° are "characterized" by the decay rates α_k. This statement, which is approximate for the rigorous solution, is found to be rigorous for the approximate, variational, solution.

Variational Solution for Arbitrary $\omega(\omega \neq 0, \pi/2)$

The wedge of Fig. 1(*b*) is free at the lateral edges, and is loaded by self-equilibrating tractions σ_x° or τ° at $x = 0$. We introduce the "self-equilibrating polynomials"

$$\left.\begin{aligned} \mathfrak{f}_2(x, y) &= 2^{-4}(3\cdot 7\cdot 11\cdot 13/2)^{1/2}(1 - \eta^2)^2 \\ \mathfrak{f}_3(x, y) &= 2^{-4}(5\cdot 7\cdot 9\cdot 11\cdot 13/2)^{1/2}(1 - \eta^2)^2\eta \\ \mathfrak{f}_4(x, y) &= 2^{-4}(3\cdot 11\cdot 13\cdot 17/2)^{1/2}(1 - \eta^2)^2(-1 + 15\eta^2) \\ &\cdots\cdots \end{aligned}\right\} \quad [16a]$$

where $\eta \equiv y/y_b$, $\quad y_b \equiv 1 + x\tan\omega$

$$\mathfrak{f}' \equiv d\mathfrak{f}/d\eta, \qquad \mathfrak{f}_x \equiv \partial\mathfrak{f}/\partial x, \qquad \mathfrak{f}_y \equiv \partial\mathfrak{f}/\partial y \quad [16b]$$

The Polynomials [16a] constitute a complete orthogonal set for the boundary conditions of stress-free lateral edges at $(x, \pm y_b)$:

$$\mathfrak{f} = \mathfrak{f}_y = \mathfrak{f}_x = 0 \quad [17a]$$

$$\mathfrak{f}_{yy} = \mathfrak{f}_{xy} = \mathfrak{f}_{xx} = 0 \quad [17b]$$

and for $x = 0$ they also constitute a normalized set

$$\int_{-1}^{1} \mathfrak{f}_n(\eta)\mathfrak{f}_m(\eta)d\eta = \delta_{nm} \quad [16c]$$

We determine appropriate longitudinal factors $h_n(x)$, $g_n(x)$ for the approximate stress functions

$$\varphi_n(x, y) = \mathfrak{f}_n(x, y)h_n(x) \text{ or } \varphi_n(x, y) = \mathfrak{f}_n(x, y)g_n(x) \quad [18]$$

from the requirement that the strain energy be a minimum

$$\delta\iint \frac{1}{2}\,(\varphi_{,xx}^2 + 2\varphi_{,xy}^2 + \varphi_{,yy}^2)dx\,dy = 0 \quad [19]$$

This leads, after integrating out over the variable y, to the Euler equation ($h' \equiv dh/dx$)

$$(y_b h'')'' - 2A\tan^2\omega(h'/y_b)' + B\tan^4\omega(h/y_b^3) = 0 \quad [20a]$$

$$A \equiv y_b\cot^2\omega\int_{-y_b}^{y_b}[\mathfrak{f}_x^2 + \mathfrak{f}_y^2 - 2\mathfrak{f}_{xx}\mathfrak{f}]dy$$

$$= \int_{-1}^{1}[3\eta^2 + \cot^2\omega]\mathfrak{f}'^2(\eta)d\eta \quad [20b]$$

$$B \equiv y_b^3\cot^4\omega\int_{-y_b}^{y_b}[\mathfrak{f}_{xxxx}\mathfrak{f} - 2\mathfrak{f}_{xxy}\mathfrak{f}_y + \mathfrak{f}_{yy}^2]dy$$

$$= \int_{-1}^{1}[(\eta^2 + \cot^2\omega)^2\mathfrak{f}''^2(\eta) - (6\eta^2 + 2\cot^2\omega)\,\mathfrak{f}'^2(\eta)]d\eta \quad [20c]$$

which is solved, in accordance with

$$h_n(0) = g_n'(0) = 0, \qquad h_n'(0) = g_n(0) = 1 \quad [21]$$

by

$$\left.\begin{aligned} \omega < 0:\quad h_n(x) &= \frac{\cot\omega}{\nu_n}\,y_b^{\mu_n}\sin(\nu_n \ln y_b), \quad g_n(x) \\ &= y_b^{\mu_n}\left[\cos(\nu_n \ln y_b) - \frac{\mu_n}{\nu_n}\sin(\nu_n \ln y_b)\right] \\ \omega > 0:\quad h_n(x) &= \frac{\cot\omega}{\nu_n}\,y_b^{2-\mu_n}\sin(\nu_n \ln y_b), \quad g_n(x) \\ &= y_b^{2-\mu_n}\left[\cos(\nu_n \ln y_b) - \frac{2 - \mu_n}{\nu_n}\sin(\nu_n \ln y_b)\right] \end{aligned}\right\} \quad [22a]$$

where

$\lambda_n \equiv \mu_n + i\nu_n$ = root, with positive real and imaginary parts, of

$$\lambda(\lambda - 2)(\lambda - 1)^2 - 2A_n\lambda(\lambda - 2) + B_n = 0 \quad [23]$$

(λ_{conj} and $2 - \lambda$, $2 - \lambda_{conj}$ are also roots.) In the cases where Equation [23] has real roots we denote the positive roots by $\lambda_n = \mu_n$, $\mu_n'(\mu_n > \mu_n')$; the negative roots are $2 - \mu_n$, $2 - \mu_n'$), and the solutions for $\omega < 0$ are

$$\left.\begin{aligned} h_n(x) &= \frac{\cot\omega}{\mu_n - \mu_n'}\,(y_b^{\mu_n} - y_b^{\mu_n'}) \\ g_n(x) &= \frac{1}{\mu_n' - \mu_n}\,(\mu_n' y_b^{\mu_n} - \mu_n y_b^{\mu_n'}) \end{aligned}\right\} \quad [22b]$$

For $\omega > 0$ the solutions are similar, with $2 - \mu$ replacing μ.

The parameters μ_n, μ_n', and ν_n are plotted versus ω in Figs. 3(*a*) and 3(*b*), respectively, for $n = 2, 3, 4$. The full lines refer to the present calculations, based on values of A_n, B_n derived from the Functions [16a]; the dashed lines—to be considered in more detail in section "Note"—are based on the Functions [14]. For values of ω near $\pi/2$ the variational results are undoubtedly quite unreliable; nevertheless they may be regarded as correctly portraying the qualitative features of the true state of affairs.

Since the $f_n(\eta)$ functions constitute a complete set of edge polynomials, the prescribed tractions τ°, σ_x° may be expanded in terms of them (13)

$$\tau^\circ(y) = -\Sigma b_n\mathfrak{f}_{n,y}(0, y) \qquad \sigma_x^\circ(y) = \Sigma a_n\mathfrak{f}_{n,yy}(0, y) \quad [24a,b]$$

and thus

$$\varphi(x, y) = \Sigma b_n\mathfrak{f}_n(x, y)h_n(x) \quad [24a']$$

$$\varphi(x, y) = \Sigma a_n\mathfrak{f}_n(x, y)g_n(x) + \Sigma B_n\mathfrak{f}_n(x, y)h_n(x) \quad [24b']$$

$$(\Sigma B_n\mathfrak{f}_{n,y}(0, y) = \Sigma a_n\mathfrak{f}_{n,xy}(0, y))$$

constitute the appropriate approximate stress functions. (Note that $\Sigma a_n\mathfrak{f}_n g_n$ creates boundary shears $-\Sigma a_n\mathfrak{f}_{n,xy}(0, y)$; these must be compensated by a type [24*a*] expansion (23), thence the appearance of the second summand in Equation [24*b*'].) This completes resolution of Saint Venant's principle, in the variational approximation, for the wedge domain of Fig. 1(*b*).

Rigorous Solution for $\omega = \pi/2$

For the special cases $\omega = 0, \pi/2$ some changes in the development are necessary. The variational solution for $\omega = 0$ was given in the first paper written on the present subject (14), it utilizes the Polynomials [14]. In the case of $\omega = \pi/2$ the rigorous solution—based on Muskhelishvili's formulas (25)—is so simple that there is no need to develop an approximation method. We merely state the result (17). When tractions

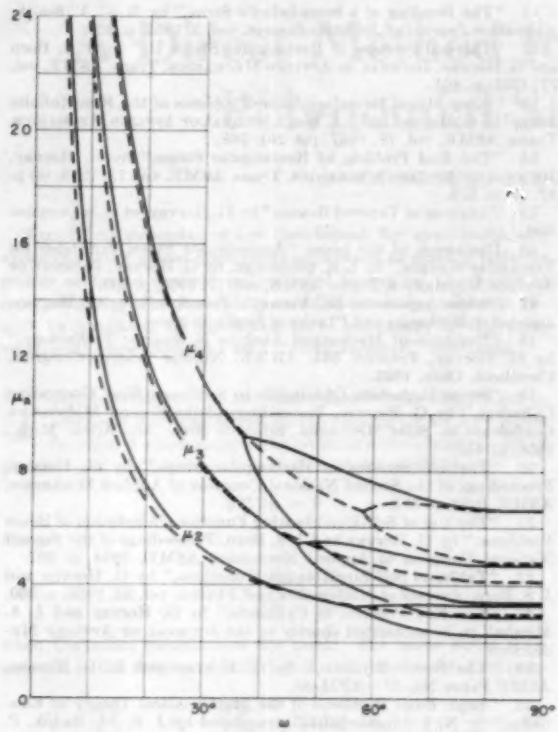

FIG. 3(a)

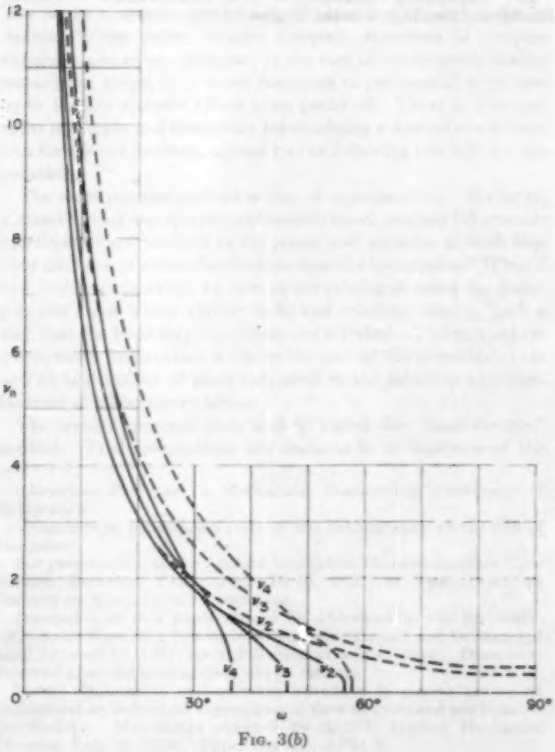

FIG. 3(b)

$$\tau^\circ = \int_{-1}^{y} P_3 dy, \quad \int_{-1}^{y} P_3 dy, \quad \int_{-1}^{y} P_4 dy, \ldots\ldots [25a]$$

$$\sigma_x^\circ = P_2(y), P_3(y), P_4(y), \ldots\ldots [26a]$$

act on the interval $-1 \leq y \leq 1$ of the edge of the semi-infinite plane [$P_k(y)$ are the Legendre polynomials],[10] then the stresses decay as

$$r^{-\mu_k} = \begin{cases} r^{-k} \ldots\ldots [25b] \\ (k = 2, 3, \ldots) \\ r^{-k-1} \ldots\ldots [26b] \end{cases}$$

respectively.[11] This result is an immediate consequence of Formulas [24] in (17) (replace $(t - Z)^{-1}$ in the integrand by $-\Sigma y^j / Z^{j+1}$) and the property of the Legendre polynomials that

$$\int_{-1}^{1} P_k(y) y^j dy = (2^j j!)^{-1} \int_{-1}^{1} [d^k (y^2 - 1)^k / dy^k] y^j dy = 0 \ldots [27]$$

when the positive integer j is less than k.[12]

A Paradox

Fig. 3(*a*) reveals a paradox. One would believe, offhand, that a flared wedge, like Fig. 1(*b*), enhances—through diffusion into a greater area—the attenuation of applied self-equilibrating end loads. The converse is true. Attenuation is fastest when the edges of the strip are parallel, $\omega = 0$, for there occurs more interference between the stresses, as they are reflected from the free edges, than in any other case. More extensive discussion of some practical aspects of the present results may be found in (16–19); further uses of the method of self-equilibrating functions in solving the biharmonic eigenvalue problem for various boundary conditions are presented in (20–24).

Note

The Conditions [17*a*, *b*] require that both σ_x° and τ° vanish at $y = \pm 1$. This is an appropriate prescription when one considers the action of arbitrary σ° or of arbitrary τ°. However, for *joint* action of σ_x° and τ° the stringent Conditions [17] may be relaxed to

$$\varphi_{,yy}^\circ \sin \omega - \varphi_{,xy}^\circ \cos \omega = 0,$$

$$\varphi_{,xx}^\circ \cos \omega - \varphi_{,xy}^\circ \sin \omega = 0 \ldots [28]$$

This weakening of the boundary conditions will lower (presumably) somewhat the *variational* eigenvalues, but will produce inextricable intermixing of the boundary tractions σ_x° and τ°.

---

[10] Note that the Legendre polynomials ($k = 2, 3, \ldots$) constitute a complete orthogonal set with respect to the conditions

$$\int_{-1}^{1} P_k \, dy = \int_{-1}^{1} P_k y dy = 0$$

and the polynomials $\bar{P}_k \equiv \int_{-1}^{y} P_k dy$ constitute a complete nonorthogonal set with respect to the conditions

$$\bar{P}_k(1) = \int_{-1}^{1} \bar{P}_k dy = 0$$

[11] The variational solution for μ_2 at $\omega = \pi/2$ gives [see Fig. 3(*a*)] 2.17 and 3.24.

[12] Formulas [25], [26], [27] suggest the following definition: A traction distribution $\mathbf{T}^\circ = X^\circ \mathbf{i} + Y^\circ \mathbf{j}$ is said to have a self-equilibration degree K when $\int \mathbf{T}^\circ x^i y^j ds = 0$ for $i + j \leq K$. The extended von Mises-Sternberg theorem then states that a traction distribution of self-equilibration degree $K \geq 0$ produces stresses which decay as $(r/h)^{-K-2}$. Similarly, in three dimensions, the theorem states that if the boundary traction $\mathbf{T}^\circ$ is of self-equilibration degree K, i.e., if the surface integrals of all its $x^i y^j z^k$ moments vanish for $i + j + k \leq K$, then, as the extent $2h$ of the loaded region is shrunk to zero, the stresses decay as $(r/h)^{-K-3}$.

The ensuing, mathematically more difficult, problem, where the functions $f_n(x, y)$, $g_n(x)$, $h_n(x)$ can no longer be considered successively but must be treated simultaneously, will be considered in (15). If one overweakens the Boundary Conditions [17] by omitting [17*b*] altogether, the polynomials $f_k(\eta)$, Equation [14], appropriate to the rectangular strip may be used also for the wedge (however Equations [28] are now violated), and one obtains the dashed lines of Figs. 3(*a*) and (*b*).

Acknowledgment

The author is indebted to Mrs. J. S. Born for checking his derivations, and to R. Haberman and Miss M. A. Havill for programming the numerical calculations.

BIBLIOGRAPHY

1 "Mémoire sur la torsion des prismes," by B. de Saint Venant, Mém. Savants Etrangers, Paris, France, 1855.

2 "A Treatise on the Mathematical Theory of Elasticity," by A. E. Love, Cambridge University Press, New York, N. Y., 1927.

3 "Theory of Elasticity," by S. Timoshenko and J. N. Goodier, McGraw-Hill Book Company, Inc., New York, N. Y., 1950.

4 "The Applicability of Saint Venant's Principle to Airplane Structures," by N. J. Hoff, *Journal of the Aeronautical Sciences*, vol. 12, 1945, p. 455.

5 "On Saint Venant's Principle," by R. von Mises, *Bulletin of the American Mathematical Society*, vol. 51, 1945, p. 555.

6 "Analysis of Shear Lag in Box Beams," by E. Reissner, *Quarterly of Applied Mathematics*, vol. 4, 1946, p. 268.

7 "The Plane Stress Problem of Perforated Plates," by G. Horvay, Journal of Applied Mechanics, Trans. ASME, vol. 74, 1952, p. 355.

8 "On St. Venant's Principle," by E. Sternberg, *Quarterly of Applied Mathematics*, vol. 11, 1954, p. 393.

9 "Biharmonic Eigenvalue Problem of the Semi-Infinite Strip," by G. Horvay, *Quarterly of Applied Mathematics*, in press.

10 "Orthogonal Edge Polynomials in the Solution of Boundary Value Problems," by G. Horvay and F. N. Spiess, *Quarterly of Applied Mathematics*, vol. 12, 1954, p. 57.

11 "The Bending of a Semi-Infinite Strip," by R. C. T. Smith, *Australian Journal of Scientific Research*, vol. 5, 1952, p. 227.

12 "Thermal Stresses in Rectangular Strips II," by J. S. Born and G. Horvay, Journal of Applied Mechanics, Trans. ASME, vol. 77, 1955, p. 401.

13 "Some Mixed Boundary-Value Problems of the Semi-Infinite Strip," by G. Horvay and J. S. Born, Journal of Applied Mechanics, Trans. ASME, vol. 78, 1957, pp. 261–268.

14 "The End Problem of Rectangular Strips," by G. Horvay, Journal of Applied Mechanics, Trans. ASME, vol. 75, 1953, (*a*) p. 87, (*b*) p. 576.

15 "Analysis of Tapered Beams," by G. Horvay, et al, in preparation.

16 Discussion of the paper "Approximate Stress Functions for Triangular Wedges," by I. K. Silverman, by G. Horvay, Journal of Applied Mechanics, Trans. ASME, vol. 77, 1955, p. 600.

17 "Some Aspects of St. Venant's Principle," by G. Horvay, *Journal of Mechanics and Physics of Solids*, in press.

18 "Problems of Mechanical Analysis in Reactor Technology," by G. Horvay, Preprint 355, AIChE, Nuclear Science Congress, Cleveland, Ohio, 1955.

19 "Stress Reduction Obtainable in Sectioned Heat Generating Cylinders," by G. Horvay, Proceedings of the Second Midwestern Conference on Solid Mechanics, Edwards Bros., Ann Arbor, Mich., 1956, p. 45.

20 "Thermal Stresses in Rectangular Strips," by G. Horvay, Proceedings of the Second National Congress of Applied Mechanics, ASME, 1954, p. 313.

21 "The Use of Self-Equilibrating Functions in Solution of Beam Problems," by G. Horvay and J. S. Born, Proceedings of the Second National Congress of Applied Mechanics, ASME, 1954, p. 267.

22 "Tables of Self-Equilibrating Functions," by G. Horvay and J. S. Born, *Journal of Mathematics and Physics*, vol. 33, 1955, p. 360.

23 "The End Problem of Cylinders," by G. Horvay and J. A. Mirabal, to be submitted shortly to the Journal of Applied Mechanics.

24 "The Sector Problem," by G. Horvay and K. L. Hanson, ASME Paper No. 57—APM-30.

25 "Some Basic Problems of the Mathematical Theory of Elasticity," by N. I. Muskhelishvili, translated by J. R. M. Radok, P. Noordhoff, Ltd., Groningen, 1953.

26 "Engineering Dynamics," by C. B. Biezeno and R. Grammel, Blackie and Son, Ltd., London, England, 1954.

A Direct Method for Determining Airy Polynomial Stress Functions

By CHING-YUAN NEOU,[1] BRIDGEPORT, CONN.

Simplified procedures are developed for systematically reducing Airy stress functions expressed as doubly infinite power series to desired polynomial forms on the bases of compatibility and boundary conditions only, without resort to patching or guessing, as is necessary in the conventional superposition and "semi-inverse" methods.

THE determination of two-dimensional stress distribution in an elastic body can be reduced to looking for an Airy stress function ϕ which satisfies the boundary conditions of a given problem and the biharmonic equation of compatibility

$$\nabla^2\nabla^2\phi = 0 \quad \ldots\ldots [1]$$

where

$$\nabla^2 = \frac{\partial^2}{\partial x^2} + \frac{\partial^2}{\partial y^2}$$

when Cartesian co-ordinates are used. The three stress components, in the absence of body forces, can then be obtained from

$$\sigma_x = \frac{\partial^2\phi}{\partial y^2}, \quad \sigma_y = \frac{\partial^2\phi}{\partial x^2}, \quad \text{and} \quad \tau_{xy} = -\frac{\partial^2\phi}{\partial x \partial y} \quad \ldots [2]$$

The stress function may be expressed in complicated forms of double Fourier series, Fourier integrals, functions of complex variables, and so on; however, in the case of continuously loaded rectangular strips, Airy stress functions of polynomial type used by G. B. Airy himself (1)[2] are often preferred. There is, however, so far no simple and direct way for obtaining a desired stress function for a given problem, except by the following two indirect approaches:

The most popular method is that of superposition. We write, without having any specific problems in mind, as many biharmonic functions in polynomials as we please and examine in each case their patterns of stress distribution over the boundaries. When a new problem comes up, we turn to our catalog of stress functions, pick out those which appear to fit and combine them in such a way that the boundary conditions are satisfied. The method requires much preparatory work on the part of the investigator, as well as the exercise of good judgment in the selection and combination of all necessary terms.

The second approach may well be called the "semi-inverse" method. Trial assumptions are made as to at least one of the states of stress distribution for the problem; thereupon ϕ can be deduced by successive integration of the stress components in Equation [2]. The resulting integration functions and constants are then determined from the boundary and compatibility conditions. Obviously the success of this method hinges, above all, on the correctness of the starting assumptions.

The present method expresses the stress function in the form of a doubly infinite power series

$$\phi = \sum_{m=0}^{\infty}\sum_{n=0}^{\infty} C_{mn}x^m y^n \quad \ldots\ldots [3]$$

where m and n are positive integers and C_{mn} are undetermined coefficients which may be arranged in the following matrix

$$\begin{Vmatrix} C_{00} & C_{01} & C_{02} & C_{03} & C_{04} & C_{05} & C_{06} & \ldots \\ C_{10} & C_{11} & C_{12} & C_{13} & C_{14} & C_{15} & C_{16} & \ldots \\ C_{20} & C_{21} & C_{22} & C_{23} & C_{24} & C_{25} & C_{26} & \ldots \\ C_{30} & C_{31} & C_{32} & C_{33} & C_{34} & C_{35} & C_{36} & \ldots \\ C_{40} & C_{41} & C_{42} & C_{43} & C_{44} & C_{45} & C_{46} & \ldots \\ C_{50} & C_{51} & C_{52} & C_{53} & C_{54} & C_{55} & C_{56} & \ldots \\ C_{60} & C_{61} & C_{62} & C_{63} & C_{64} & C_{65} & C_{66} & \ldots \\ \ldots & \ldots & \ldots & \ldots & \ldots & \ldots & \ldots & \ldots \end{Vmatrix} \quad \ldots\ldots [4]$$

On substituting from Equation [3], the three stress components become

$$\sigma_x = \sum_{m=0}^{\infty}\sum_{n=2}^{\infty} n(n-1)C_{mn}x^m y^{n-2} \quad \ldots\ldots [5]$$

$$\sigma_y = \sum_{m=2}^{\infty}\sum_{n=0}^{\infty} m(m-1)C_{mn}x^{m-2} y^n \quad \ldots\ldots [6]$$

$$\tau_{xy} = -\sum_{m=1}^{\infty}\sum_{n=1}^{\infty} mnC_{mn}x^{m-1}y^{n-1} \quad \ldots\ldots [7]$$

Evidently, C_{00}, C_{01}, and C_{10} can be omitted from Matrix [4], for they do not appear in the expressions for stresses. The equation of compatibility, after substituting from Equation [3] and regrouping, takes the following form

$$\sum_{m=2}^{\infty}\sum_{n=2}^{\infty}\{(m+2)(m+1)m(m-1)C_{m+2,n-2} + 2m(m-1)n(n-1)C_{mn} + (n+2)(n+1)n(n-1)C_{m-2,n+2}\}x^{m-2}y^{n-2} = 0$$

As the condition of compatibility is independent of x and y, the coefficient for $x^{m-2}y^{n-2}$ must be zero. Thus

$$(m+2)(m+1)m(m-1)C_{m+2,n-2} + 2m(m-1)n(n-1)C_{mn} + (n+2)(n+1)n(n-1)C_{m-2,n+2} = 0 \quad \ldots\ldots [8]$$

This expression establishes the interrelationships among any three alternate coefficients in the diagonals running from the lower left to the upper right diagonals in Matrix [4], starting with

---

[1] Associate Professor of Mechanical Engineering, University of Bridgeport.

[2] Numbers in parentheses refer to the Bibliography at the end of the paper.

For presentation at the Applied Mechanics Division Summer Conference, Berkeley, Calif., June 13–15, 1957, of THE AMERICAN SOCIETY OF MECHANICAL ENGINEERS.

Discussion of this paper should be addressed to the Secretary, ASME, 29 West 39th Street, New York, N. Y., and will be accepted until October 10, 1957, for publication at a later date. Discussion received after the closing date will be returned.

NOTE: Statements and opinions advanced in papers are to be understood as individual expressions of their authors and not those of the Society. Manuscript received by ASME Applied Mechanics Division, July 31, 1956. Paper No. 57—APM-2.

the $\{C_{40}, C_{22}, C_{04}\}$ group. For instance, C_{40}, C_{42}, and C_{24} are related by

$$(6\cdot5\cdot4\cdot3)C_{40} + 2(4\cdot3)(2\cdot1)C_{42} + (4\cdot3\cdot2\cdot1)C_{24} = 0$$

Other groups in the same diagonal are

$$\{C_{41}, C_{23}, C_{05}\} \text{ and } \{C_{31}, C_{13}, C_{15}\}$$

The whole problem is then reduced to the determination of C_{mn} in Equation [3] from the prescribed forces on the boundaries and the interdependence among C_{mn} governed by Equation [8]. The processes of eliminating unwanted terms and determining the values for C_{mn} of the remaining terms in Equation [3] can best be illustrated by way of the following two examples.

As a first example, the stress function is to be sought for a cantilever having a rectangular cross section of unit width, subjected to a force P at the free end and a uniformly distributed load w on the upper boundary as shown in Fig. 1.

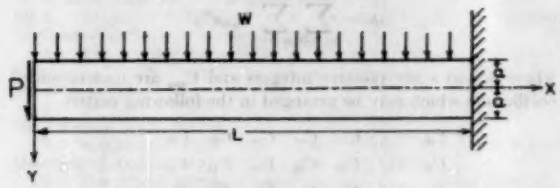

FIG. 1 CANTILEVER BEAM LOADED BY A CONCENTRATED FORCE AT THE FREE END AND A UNIFORM LOAD OVER THE UPPER SURFACE

Since $\tau_{xy} = 0$ at $y = \pm a$ for $0 < x < L$, i.e., being independent of x, the coefficients of powers of x in Equation [7] must all be zero

$$\sum_{n=1}^{\infty} nC_{mn}a^{n-1} = 0 \quad \text{for } m \geqslant 1 \ldots\ldots\ldots\ldots [9]$$

$$\sum_{n=1}^{\infty} nC_{mn}(-a)^{n-1} = 0 \quad \text{for } m \geqslant 1 \ldots\ldots\ldots [10]$$

Addition and subtraction of Equations [9] and [10], multiplied by a, yield

$$\sum_{n=2,4,6}^{\infty} nC_{mn}a^n = 0 \quad \text{for } m \geqslant 1 \ldots\ldots\ldots [11]$$

$$\sum_{n=1,3,5}^{\infty} nC_{mn}a^n = 0 \quad \text{for } m \geqslant 1 \ldots\ldots\ldots [12]$$

Similarly the boundary condition that $\sigma_y = 0$ at $y = a$ for $0 < x < L$ requires

$$\sum_{n=0}^{\infty} C_{mn}a^n = 0 \quad \text{for } m \geqslant 2 \ldots\ldots\ldots\ldots [13]$$

But $\sigma_y = -w$ at $y = -a$, for $0 < x < L$, Equation [6] becomes

$$-w = \sum_{m=2}^{\infty} \left\{ \sum_{n=0}^{\infty} C_{mn}(-a)^n \right\} m(m-1)x^{m-2}$$

hence

$$\sum_{n=0}^{\infty} C_{mn}(-a)^n = 0 \quad \text{for } m \geqslant 3 \ldots\ldots\ldots [14]$$

$$2\sum_{n=0}^{\infty} C_{2n}(-a)^n = -w \ldots\ldots\ldots\ldots [15]$$

Addition and subtraction of Equations [13] for $m \geqslant 3$ and [14] results in

$$\sum_{n=0,2,4}^{\infty} C_{mn}a^n = 0 \quad \text{for } m \geqslant 3 \ldots\ldots\ldots [16]$$

$$\sum_{n=1,3,5}^{\infty} C_{mn}a^n = 0 \quad \text{for } m \geqslant 3 \ldots\ldots\ldots [17]$$

Equations [17] for $m \geqslant 3$ and [16] can simultaneously be satisfied by

$$C_{mn} = 0 \text{ for } m \geqslant 3,\ n = 0, 2, 4 \ldots$$

Similarly, Equations [12] for $m \geqslant 3$ and [17] yield

$$C_{mn} = 0 \text{ for } m \geqslant 3,\quad n = 1, 3, 5 \ldots$$

These C_{mn} can now be dropped from Matrix [4] (shown by / in Matrix [18]). A check on the Compatibility Relation [8] shows that $C_{14} = 0$ because $C_{40} = C_{32} = 0$. Similarly, we can put to zero all the C_{mn} below the diagonal running from C_{32} to C_{05} (shown by $\times$ in Matrix [18]).

$$\left\| \begin{matrix} — & — & C_{02} & C_{03} & C_{04} & C_{05} & C_{06} & \times \\ — & C_{11} & C_{12} & C_{13} & C_{14} & C_{15} & C_{16} & \times \\ C_{20} & C_{21} & C_{22} & C_{23} & C_{24} & C_{25} & C_{26} & \times \\ C_{30} & C_{31} & C_{32} & C_{33} & C_{34} & C_{35} & C_{36} & \times \\ C_{40} & C_{41} & C_{42} & C_{43} & C_{44} & C_{45} & C_{46} & \times \\ C_{50} & C_{51} & C_{52} & C_{53} & C_{54} & C_{55} & C_{56} & \times \\ C_{60} & C_{61} & C_{62} & C_{63} & C_{64} & C_{65} & C_{66} & \times \\ \times & \times & \times & \times & \times & \times & \times & \times \end{matrix} \right\} \ldots\ldots [18]$$

Now Matrix [18] seems simple enough that we may write out Equations [11], [12], [13], and [15] for $m = 2$ in detail

$$2C_{22}a^2 = 0$$
$$C_{21}a + 3C_{23}a^3 = 0$$
$$C_{20} + C_{21}a + C_{22}a^2 + C_{23}a^3 = 0$$
$$C_{20} - C_{21}a + C_{22}a^2 - C_{23}a^3 = -\frac{w}{2}$$

from which we obtain

$$C_{22} = 0, \quad C_{20} = -\frac{w}{4}, \quad C_{21} = \frac{3w}{8a}, \quad C_{23} = -\frac{w}{8a^3}$$

and again the compatibility relation of Equation [8] shows

$$C_{04} = 0, \quad C_{05} = -\frac{1}{5}C_{23} = \frac{w}{40a^3}$$

Similarly, Equations [11] and [12] for $m = 1$ yield

$$C_{12} = 0, \quad C_{11} = -3C_{13}a^2$$

($C_{32} = C_{34} = C_{36} = 0$ are shown by \ in Matrix [18])

The stress function ϕ of Equation [3] now reduces to

$$\phi = C_{32}y^2 + C_{33}y^3 + \frac{w}{40a^2}y^5 - 3C_{13}a^2xy + C_{13}xy^3 - \frac{w}{4}x^2 + \frac{3w}{8a}x^2y - \frac{w}{8a^3}x^2y^3 \quad [19]$$

The three unknown coefficients C_{32}, C_{33}, and C_{13} in Equation [19] can readily be determined from the boundary conditions that for a self-equilibrating system, the resultant force and moment at its free end are zero and its resultant shearing force at the same end is equal to P; i.e.

$$\int_{-a}^{a}\left(\frac{\partial^2\phi}{\partial y^2}\right)_{x=0}dy = 0 \quad [20]$$

$$\int_{-a}^{a}\left(\frac{\partial^2\phi}{\partial y^2}\right)_{x=0}y\,dy = 0 \quad [21]$$

$$\int_{-a}^{a}\left(-\frac{\partial^2\phi}{\partial x\partial y}\right)_{x=0}dy = -P \quad [22]$$

Substituting Equation [19] in the foregoing three equations yields $C_{32} = 0$ (shown by | in Matrix [18]), $C_{33} = -w/20a$ and $C_{13} = -P/4a^3$.

The final form of the stress function for the problem is therefore

$$\phi = \frac{w}{40}\left[y^2\left(-2\frac{y}{a} + \frac{y^3}{a^3}\right) - 5x^2\left(2 - 3\frac{y}{a} + \frac{y^3}{a^3}\right)\right] + \frac{Px}{4}\left(3\frac{y}{a} - \frac{y^3}{a^3}\right) \quad [23]$$

from which we obtain the three stress components

$$\sigma_x = \frac{wy}{20a}\left(10\frac{y^2}{a^2} - 6 - 15\frac{x^2}{a^2}\right) - \frac{3}{2}\frac{P}{a^3}xy \quad [24]$$

$$\sigma_y = -\frac{w}{4}\left(2 + \frac{y}{a}\right)\left(1 - \frac{y}{a}\right)^2 \quad [25]$$

$$\tau_{xy} = -\frac{3}{4a}(wx + P)\left(1 - \frac{y^2}{a^2}\right) \quad [26]$$

The foregoing solution for the case $w = 0$ checks with that obtained by the superposition method (2b), while the results for $P = 0$ can be shown to be essentially the same as those obtained by Southwell who used a "semi-inverse" approach and wrongly admitted that his starting assumption was incorrect (3).

When the elastic body possesses certain geometrical and loading symmetry and asymmetry, advantage may be taken of such characteristics to simplify the problem. As a second example, we seek to determine the stress function for a simply supported rectangular beam under a triangular load as shown in Fig. 2.

Obviously, the symmetry of loading with respect to the y-axis reveals that the stress function of Equation [3] should contain no terms odd in x, except for $m = 1$ and 3, because of the dependence of σ_y at the top surface on the first degree of x. Also, the asymmetry of loadings at $y = \pm a$ leads to the dropping of terms even in y. These C_{ms} can now be dropped from Matrix [4] at an early stage (shown by / in Matrix [27]).

$$\left\|\begin{matrix} — & — & C_{02} & C_{03} & C_{04} & C_{05} & C_{06} & \times \\ — & C_{11} & C_{12} & C_{13} & C_{14} & C_{15} & C_{16} & \times \\ C_{20} & C_{21} & C_{22} & C_{23} & C_{24} & C_{25} & C_{26} & \times \\ C_{30} & C_{31} & C_{32} & C_{33} & C_{34} & C_{35} & C_{36} & \times \\ C_{40} & C_{41} & C_{42} & C_{43} & C_{44} & C_{45} & C_{46} & \diagdown \\ C_{50} & C_{51} & C_{52} & C_{53} & C_{54} & C_{55} & C_{56} & / \\ C_{60} & C_{61} & C_{62} & C_{63} & C_{64} & C_{65} & C_{66} & \diagdown \\ / & / & / & / & / & / & / & / \end{matrix}\right\| \quad [27]$$

Henceforth, we need only consider the right half of the beam. As in preceding example, the boundary conditions at $y = \pm a$ yield

$$C_{ms} = 0 \text{ for } m \geq 4 \text{ (shown by \ in Matrix [27])}$$

The compatibility relation further demands that $C_{32} = C_{33} = 0$ and also all C_{ms} for $s > 6$ be zero (shown by $\times$ in Matrix [27]). For $m \leq 3$, Equations [11] and [12] for $\tau_{xy} = 0$ at $y = \pm a$ yield

$$C_{11}a + 3C_{13}a^3 + 5C_{15}a^5 = 0 \quad [28]$$

$$C_{21}a + 3C_{23}a^3 = 0 \quad [29]$$

$$C_{31}a + 3C_{33}a^3 = 0 \quad [30]$$

and Equation [13] for $\sigma_y = 0$ at $y = a$ shows

$$C_{20} + C_{21}a + C_{22}a^2 = 0 \quad [31]$$

$$C_{30} + C_{31}a + C_{32}a^2 = 0 \quad [32]$$

while $\sigma_y = -w(1 - x/L)$ at $y = a$ results in

$$-w = 2(C_{20} - C_{21}a - C_{22}a^2) \quad [33]$$

$$\frac{w}{L} = 6(C_{30} - C_{31}a - C_{32}a^2) \quad [34]$$

From Equations [29], [31], and [33], we find

$$C_{20} = -\frac{w}{4}, \quad C_{21} = \frac{3w}{8a}, \quad C_{22} = -\frac{w}{8a^2}$$

and from Equations [30], [32] and [34], we obtain

$$C_{30} = \frac{w}{12L}, \quad C_{31} = -\frac{w}{8aL}, \quad C_{32} = \frac{w}{24a^2L}$$

The compatibility Equation [8] further shows

$$C_{50} = -\frac{1}{5}C_{32} = \frac{w}{40a^2}, \quad C_{15} = -\frac{3}{5}C_{33} = -\frac{w}{40a^3L}$$

thereby, from Equation [28] we obtain

$$C_{11} = \frac{w}{8L} - 3C_{13}a^2 \quad [35]$$

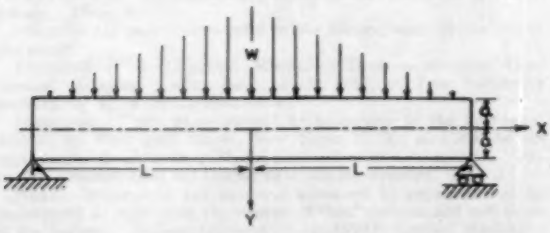

FIG. 2 SIMPLY SUPPORTED BEAM UNDER TRIANGULAR LOADING

Substituting the above values into Equation [3] and applying the boundary conditions that at $x = L$

$$\int_{-a}^{a} \tau_{xy} dy = \int_{-a}^{a} \left(- \frac{\partial^2 \phi}{\partial x \partial y} \right)_{x=L} dy = - \frac{wL}{2} \quad \ldots [36]$$

and

$$\sigma_x = \left(\frac{\partial^2 \phi}{\partial y^2} \right)_{x=L} = 0 \quad \text{for} - a < y < a \quad \ldots [37]$$

we find

$$C_{12} = \frac{w}{20aL}, \quad C_{32} = \frac{w}{60a} \left(5 \frac{L^2}{a^2} - 3 \right)$$

and thus from Equation [35]

$$C_{11} = - \frac{wa}{40L}$$

Finally, the stress function for the problem becomes

$$\phi = \frac{w}{60a} \left(5 \frac{L^2}{a^2} - 3 \right) y^3 + \frac{w}{40a^2} y^3 - \frac{wa}{40L} xy + \frac{w}{20aL} xy^3 - \frac{w}{40a^2 L} xy^3 - \frac{w}{4} x^2 + \frac{3w}{8a} x^2 y - \frac{w}{8a^2} x^2 y^2 + \frac{w}{12L} x^3 - \frac{w}{8aL} x^3 y + \frac{w}{24a^2 L} x^3 y^3 \quad \ldots [38]$$

and the three stress components are

$$\sigma_x = \frac{w}{20} \left(\frac{y}{a} \right) \left\{ -6 + 10 \frac{y^2}{a^2} + 10 \frac{L^2}{a^2} + \frac{x}{L} \left(6 - 10 \frac{y^2}{a^2} + 5 \frac{x^2}{a^2} - 15 \frac{Lx}{a^2} \right) \right\} \quad \ldots [39]$$

$$\sigma_y = - \frac{w}{4} \left(1 - \frac{x}{L} \right) \left(1 - \frac{y}{a} \right)^2 \left(2 + \frac{y}{a} \right) \quad \ldots [40]$$

$$\tau_{xy} = \frac{w}{40} \left(1 - \frac{y^2}{a^2} \right) \left\{ \frac{a}{L} \left(1 - 5 \frac{y^2}{a^2} \right) + 15 \frac{x}{a} \left(\frac{x}{L} - 2 \right) \right\} \quad \ldots [41]$$

Equations [24], [25], [26], and also [39] and [40] represent the exact solutions to their respective problems only when the boundary stresses or loadings are distributed according to these expressions. It is noted that in Example 1

$$\sigma_x = \frac{wy}{10a} \left(5 \frac{y^2}{a^2} - 3 \right)$$

over the free end, instead of $\sigma_x = 0$, as in Example 2. The latter condition, which physically sounds more logical than the boundary conditions expressed by Equations [20] and [21], is unfortunately not realizable, for it leads only to a trivial solution of $w = 0$ in $\sigma_x = 0$ after substitution from Equation [19]. The presence of extraneous end tractions, not uncommon in many other stress problems, has long been an interesting and challenging subject of investigation in the theory of elasticity (2*b*, 4, 5, 6). Some authors even proposed that we satisfy the boundary conditions exactly, but the compatibility conditions only approximately (7). Historically, Airy himself did not consider the matter of the compatibility of deformation either, and was criticized for such neglect (8). However, as the present paper aims at demonstrating a systematic and rational approach in arriving at a desired stress function for a given problem, we may conclude that, while rigorous fulfillment of boundary conditions is desirable but not always realizable, the solution resulting from substituting a statically equipollent self-equilibrating force system for exact boundary conditions along the short sides of a rectangular body arising from loadings along its long sides, represents, by virtue of Saint Venant's principle, a fairly good approximation to the exact state of stress distribution in the body, except near the ends where departures from true boundary conditions exist. Also, by Saint Venant's principle Equations [39], [40], and [41] in the second example hold for the most part of a long narrow beam, except near the end and in the neighborhood of the middle of the beam where load distribution is not smoothly continuous.

As is evidenced by the preceding examples, the formulation of a polynomial stress function now makes use of only the compatibility condition of Equation [8] and the prescribed boundary conditions, sometimes aided, merely as a shortcut, by the properties of symmetry and asymmetry in the geometry and loading of the beam. The method is therefore direct, rational, and straightforward. It not only enables us to write down the desired Airy stress functions of polynomial type for many problems formerly regarded as difficult, but also places the search for them on a logical basis.

BIBLIOGRAPHY

1 British Association Adv. Sci. Dept., 1862, and Philosophical Transactions of the Royal Society of London, vol. 153, 1863, p. 49.

2 "Theory of Elasticity," by S. Timoshenko and J. N. Goodier, McGraw-Hill Book Company, Inc., New York, N. Y., second edition, 1951, (*a*) p. 35, (*b*) p. 41.

3 "An Introduction to the Theory of Elasticity," by R. V. Southwell, Oxford University Press, Oxford, England, 1936, p. 377.

4 "Flachentragwerke," by K. Girkmann, Julius Springer, Berlin, Germany, 1948, p. 77.

5 "The End Problem of Rectangular Strip," by G. Horvay, JOURNAL OF APPLIED MECHANICS, Trans. ASME, vol. 75, 1953, p. 87.

6 "Bending of Rectangular Beam," by L. H. Donnell, JOURNAL OF APPLIED MECHANICS, Trans. ASME, vol. 74, 1952, p. 123.

7 "The Use of Self-Equilibrating Functions in Solution of Beam Problems," by G. Horvay and J. S. Born, Proceedings of the Second U. S. Congress of Applied Mechanics, ASME, 1954, p. 267.

8 "History of Strength of Materials," by S. Timoshenko, McGraw-Hill Book Company, Inc., New York, N. Y., 1953, p. 225.

Finite Twisting and Bending of Thin Rectangular Elastic Plates[1]

By ERIC REISSNER,[2] CAMBRIDGE, MASS

An exact solution is obtained of the nonlinear equations for finite deflections of thin elastic plates, for a rectangular plate acted upon by twisting moments T and bending moments M simultaneously applied to two opposite edges of the plate. The principal results of the paper are relations between the moments T and M, on the one hand, and the angle of twist per unit of length θ, and the curvature k of the plate, on the other hand. These relations which are of the form $T = T(\theta, k)$ and $M = M(\theta, k)$ generalize previously known relations for the special cases for which either $k = 0$ or $\theta = 0$. A numerical evaluation of the functions $T(\theta, k)$ and $M(\theta, k)$ reveals the existence of a characteristic jump phenomenon.

Introduction

IN THE following we desire an exact solution, within the framework of the nonlinear theory of finite deflections of thin elastic plates, for a rectangular plate acted upon by twisting moments and bending moments simultaneously applied to two opposite edges of the plate. Solutions for the special cases of this problem when either bending moments or twisting moments are absent are known (1, 2, 3).[3] Our reason for desiring a solution for the more general problem is an interest in the nature of the modification of the superposition principle, which is caused by the finiteness of the deflections of the plate.

Formulation of the Problem

We consider a thin plate of length $2a$ in the direction of an axis x, and of width $2b$ in the direction of an axis y. The origin of the co-ordinate system is taken at the mid-point of the plate. We limit ourselves to considering plates of constant thickness h and of isotropic homogeneous materials with Young's modulus E and Poisson's ratio ν. The differential equations for finite deflections of such plates are, in the absence of surface loads

$$D\nabla^2\nabla^2 w = F_{,xx}w_{,yy} + F_{,yy}w_{,xx} - 2F_{,xy}w_{,xy} \quad [1]$$

$$\nabla^2\nabla^2 F = C[w^2_{,xy} - w_{,xx}w_{,yy}] \quad [2]$$

In these equations w represents the transverse deflection of the plate, F is Airy's function representing stress resultants in the plane of the plate, $\nabla^2 = (\ )_{,xx} + (\ )_{,yy}$, $D = Eh^3/12(1 - \nu^2)$, $C = Eh$, and commas indicate differentiation.

Expressions for stress resultants and couples are known to be as follows

$$N_{xx} = F_{,yy},\ N_{yy} = F_{,xx},\ N_{xy} = -F_{,xy} \quad [3]$$

$$\left.\begin{aligned} M_{xx} &= -D(w_{,xx} + \nu w_{,yy}) \\ M_{yy} &= -D(w_{,yy} + \nu w_{,xx}) \\ M_{xy} &= -(1 - \nu)Dw_{,xy} \end{aligned}\right\} \quad [4]$$

$$Q_x = -D(\nabla^2 w)_{,x},\ Q_y = -D(\nabla^2 w)_{,y} \quad [5]$$

$$\left.\begin{aligned} R_x &= Q_x + M_{xy,y} + N_{xx}w_{,x} + N_{xy}w_{,y} \\ R_y &= Q_y + M_{xy,x} + N_{xy}w_{,x} + N_{yy}w_{,y} \end{aligned}\right\} \quad [6]$$

In addition to stress resultants as defined by Equations [3] and [6] it is necessary to consider concentrated forces at the corners of the rectangular plate, of magnitude $\pm 2M_{xy}$.

The problem to be solved is given by the Differential Equations [1] and [2] and by the following system of boundary conditions

$$y = \pm b\text{:}\ N_{yy} = N_{xy} = R_y = M_{yy} = 0 \quad [7]$$

$$x = \pm a \left\{ \begin{array}{l} \displaystyle\int_{-b}^{b} N_{xx}dy = 0, \quad \int_{-b}^{b} N_{xy}dy = 0 \\ \displaystyle\int_{-b}^{b} R_x dy - 2[M_{xy}]_{-b}^{b} = 0 \\ \displaystyle\int_{-b}^{b} N_{xx}y dy = 0 \end{array} \right\} \quad [8]$$

$$x = \pm a \left\{ \begin{array}{l} \displaystyle\int_{-b}^{b} (M_{xx} + wN_{xx})dy = M \\ \displaystyle\int_{-b}^{b} R_x y dy - 2[yM_{xy}]_{-b}^{b} = T \end{array} \right\} \quad [9]$$

We note that, while the boundary conditions along the free boundaries $y = \pm b$ are to be satisfied exactly, the boundary conditions at the loaded edges $x = \pm a$ are to be satisfied in an overall sense only. In view of Saint Venant's principle the results obtained in this manner will be meaningful provided the length $2a$ of the plate is sufficiently large compared to the width $2b$ of the plate.

Let θ be the angle of twist per unit length of the plate and k its curvature, due to the action of the twisting couple T and the bending couple M. We know that as long as the linear theory applies, the relations between θ and T, on the one hand, and between k and M, on the other hand, are as follows

$$T = 4(1 - \nu)Db\theta, \qquad M = 2(1 - \nu^2)Dbk \quad [10]$$

These formulas are a consequence of a deflection formula

$$w = \theta xy - \frac{1}{2}k(x^2 - \nu y^2) \quad [11]$$

which satisfies Equations [1], [2], [7], [8], and [9] provided all nonlinear terms in these relations are omitted.

[1] The present paper is a report on work done under the sponsorship of the Office of Naval Research under a contract with the Massachusetts Institute of Technology. The author is indebted to Prof. K. Washizu and to Mr. M. W. Johnson for effective help in the preparation of this paper.

[2] Professor of Mathematics, Massachusetts Institute of Technology. Mem. ASME.

[3] Numbers in parentheses refer to the Bibliography at the end of the paper.

Presented at the Applied Mechanics Division Summer Conference, Berkeley, Calif., June 13–15, 1957, of The American Society of Mechanical Engineers.

Discussion of this paper should be addressed to the Secretary, ASME, 29 West 39th Street, New York, N. Y., and will be accepted until October 10, 1957, for publication at a later date. Discussion received after the closing date will be returned.

Note: Statements and opinions advanced in papers are to be understood as individual expressions of their authors and not those of the Society. Manuscript received by ASME Applied Mechanics Division, October 2, 1956. Paper No. 57—APM-23.

We also know the generalizations $T = T(\theta)$ and $M = M(k)$ of Equation [10] which apply in the nonlinear range, provided $T = 0$ or $M = 0$ (1, 2). Our present object is to obtain relations

$$T = T(\theta,k), \qquad M = M(\theta,k) \ldots\ldots\ldots [12]$$

which apply without either one of these restrictions.

Solution of Boundary-Value Problem

The simplest manner in which nonlinearity can modify the deflection Formula [11] is by a modification of the anticlastic curvature term νy^2. Accordingly, we attempt a solution of Equations [1], [2], [7], [8], and [9] in the form

$$w(x,y) = \theta xy - \frac{1}{2}kx^2 + W(y) \ldots\ldots\ldots [13]$$

Furthermore, since we expect that tangential stress resultants N_{xx}, N_{yy}, and N_{xy} will be independent of the axial co-ordinate x we assume the stress function F independent of x

$$F(x,y) = F(y) \ldots\ldots\ldots [14]$$

Introduction of Equations [13] and [14] into Equations [1] and [2] leads to the following two ordinary differential equations

$$DW^{IV} = -kF'' \ldots\ldots\ldots [15]$$

$$F^{IV} = C[\theta^2 + kW''] \ldots\ldots\ldots [16]$$

where primes indicate differentiation with respect to y.

Equation [16] is integrated to

$$F'' = C\left[\frac{1}{2}\theta^2y^2 + kW\right] + A_0 + A_1y \ldots\ldots [17]$$

where A_0 and A_1 are two constants of integration. Introduction of Equation [17] into [15] gives as differential equation for W

$$DW^{IV} + Ck^2W = -\frac{1}{2}C\theta^2ky^2 - k(A_0 + A_1y) \ldots [18]$$

which has the solution

$$W = c_1 \cosh \alpha y \cos \alpha y + c_2 \sinh \alpha y \sin \alpha y + c_3 \cosh \alpha y \sin \alpha y + c_4 \sinh \alpha y \cos \alpha y - \frac{1}{2}\frac{\theta^2}{k}y^2 - \frac{1}{Ck}(A_0 + A_1y) \ldots\ldots [19]$$

with α given by

$$\alpha = \sqrt[4]{\left(\frac{Ck^2}{4D}\right)} = \sqrt[4]{[3(1-\nu^2)]}\sqrt{\left(\frac{k}{h}\right)} \ldots\ldots [20]$$

We omit the rigid-body displacement terms A_0 and A_1, and observe that the boundary conditions require W to be an even function of y, so that

$$c_3 = 0, c_4 = 0 \ldots\ldots\ldots [21]$$

With these reductions we have the following expressions for deflection w and for stress resultants and couples

$$w = \theta xy - \frac{1}{2}kx^2 - \frac{1}{2}\frac{\theta^2}{k}y^2 + c_1 \cosh \alpha y \cos \alpha y + c_2 \sinh \alpha y \sin \alpha y \ldots [22]$$

$$\left.\begin{aligned} N_{yy} &= 0, N_{xy} = 0 \\ N_{xx} &= Ck[c_1 \cosh \alpha y \cos \alpha y + c_2 \sinh \alpha y \sin \alpha y] \end{aligned}\right\} \ldots [23]$$

$$\left.\begin{aligned} M_{xx} &= D\left[k + \nu\frac{\theta^2}{k} + 2\nu\alpha^2(c_1 \sinh \alpha y \sin \alpha y - c_2 \cosh \alpha y \cos \alpha y)\right] \\ M_{yy} &= D\left[\frac{\theta^2}{k} + \nu k + 2\alpha^2(c_1 \sinh \alpha y \sin \alpha y - c_2 \cosh \alpha y \cos \alpha y)\right] \\ M_{xy} &= -(1-\nu)D\theta \end{aligned}\right\} \ldots [24]$$

$$\left.\begin{aligned} R_x &= (\theta y - kx)N_{xx} \\ R_y &= 2D\alpha^3[c_1(\cosh \alpha y \sin \alpha y + \sinh \alpha y \cos \alpha y) + c_2(\cosh \alpha y \sin \alpha y - \sinh \alpha y \cos \alpha y)] \end{aligned}\right\} \ldots [25]$$

If Equations [22] to [25] are to be the solution of the given problem, it must be possible to choose the four undetermined parameters θ, k, c_1, c_2 in such a manner that all ten Boundary Conditions [7] to [9] are satisfied.

We note that two of the four Conditions [7] for $y = \pm b$ are satisfied identically. The remaining two conditions for R_y and M_{yy} become two simultaneous equations for the constants c_1 and c_2, in terms of θ and k, and in terms of a quantity μ defined by

$$\mu = \alpha b = \sqrt[4]{[3(1-\nu^2)]}\sqrt{\left(\frac{kb^2}{h}\right)} \ldots\ldots [26]$$

as follows

$$\left.\begin{aligned} &c_1(\cosh \mu \sin \mu + \sinh \mu \cos \mu) + c_2(\cosh \mu \sin \mu - \sinh \mu \cos \mu) = 0 \\ &c_1 \sinh \mu \sin \mu - c_2 \cosh \mu \cos \mu = -\frac{1}{2\alpha^2}\left(\frac{\theta^2}{k} + \nu k\right) \end{aligned}\right\} \ldots [27]$$

Of the remaining Boundary Conditions [8] and [9], those in [8] may be seen to be satisfied automatically.[4] There remain the two Conditions [9] and these assume the following form

$$D\int_{-b}^{b}\left[k + \nu\frac{\theta^2}{k} + 2\nu\alpha^2(c_1 \sinh \alpha y \sin \alpha y - c_2 \cosh \alpha y \cos \alpha y)\right]dy - \frac{1}{2}C\theta^2\int_{-b}^{b}y^2(c_1 \cosh \alpha y \cos \alpha y + c_2 \sinh \alpha y \sin \alpha y)dy + Ck\int_{-b}^{b}(c_1 \cosh \alpha y \cos \alpha y + c_2 \sinh \alpha y \sin \alpha y)^2dy = M \ldots [28]$$

and

$$C\theta k\int_{-b}^{b}y^2(c_1 \cosh \alpha y \cos \alpha y + c_2 \sinh \alpha y \sin \alpha y)dy + 4b(1-\nu)D\theta = T \ldots\ldots [29]$$

Equations [27] may be solved for c_1 and c_2 as follows

$$\left.\begin{aligned} c_1 &= \frac{1}{\alpha^2}\left(\frac{\theta^2}{k} + \nu k\right)\frac{\sinh \mu \cos \mu - \cosh \mu \sin \mu}{\sinh 2\mu + \sin 2\mu} \\ c_2 &= \frac{1}{\alpha^2}\left(\frac{\theta^2}{k} + \nu k\right)\frac{\sinh \mu \cos \mu + \cosh \mu \sin \mu}{\sinh 2\mu + \sin 2\mu} \end{aligned}\right\} \ldots [30]$$

[4] To see this, observe that

$$\int_{-b}^{b}N_{xx}dy = \int_{-b}^{b}F''dy = -(D/k)\int_{-b}^{b}W^{IV}dy = -(D/k)[W''']_{-b}^{b} = (1/k)[R_y]_{-b}^{b} = 0.$$

Introduction of Equations [30] into [28] and [29] leads, after considerable manipulations, to the desired formulas giving M and T as functions of θ and k. We find, in generalization of Equations [10]

$$T = 4(1-\nu)bD\theta\left[1+\frac{\nu}{1-\nu}F_1(\mu)+\frac{4/45}{1-\nu}\lambda^4F_2(\mu)\right] \quad [31]$$

$$M = 2(1-\nu^2)bDk\left[1+\frac{\nu^2}{1-\nu^2}G_1(\mu)+\frac{8/45}{1-\nu^2}\lambda^4G_2(\mu)-\frac{32/45\cdot63}{1-\nu^2}\lambda^8G_3(\mu)\right] \quad [32]$$

The parameter μ is defined by Equation [26]. We may rewrite μ in terms of the radius of curvature $R = 1/k$ as follows

$$\mu = \sqrt[4]{[3(1-\nu^2)]}\,\frac{b}{\sqrt{(Rh)}} \quad [33]$$

The parameter λ bears the same relation to the angle of twist θ per unit length as μ bears to curvature k, namely

$$\lambda = \sqrt[4]{[3(1-\nu^2)]}\,b\sqrt{(\theta/h)} \quad [34]$$

The functions F_n and G_n are defined as follows

$$F_1(\mu) = 1-\frac{1}{\mu}\,\frac{\cosh 2\mu-\cos 2\mu}{\sinh 2\mu+\sin 2\mu},\quad F_2(\mu)=\frac{45}{4}\,\frac{F_1(\mu)}{\mu^4} \quad [35]$$

$$\left.\begin{aligned} G_1(\mu) &= F_1(\mu)+\frac{1}{4}\,\mu\,F_1'(\mu),\ G_2(\mu)=\frac{45}{16}\,\frac{F_1'(\mu)}{\mu^3}\\ G_3(\mu) &= \frac{45\cdot63}{32}\,\frac{1}{\mu^8}\,[F_1(\mu)-\frac{1}{4}\,\mu\,F_1'(\mu)]\end{aligned}\right\} \quad [36]$$

Numerical values of the functions F_n and G_n are given in Table 1 and illustrated in Fig. 1. For values of μ small and large compared to unity we have the following behavior

$$F_1 = \begin{cases} \frac{4}{45}\mu^4-\frac{32}{45\cdot63}\mu^8+\cdots \\ 1-\frac{1}{\mu}+\cdots \end{cases} \quad [37a]$$

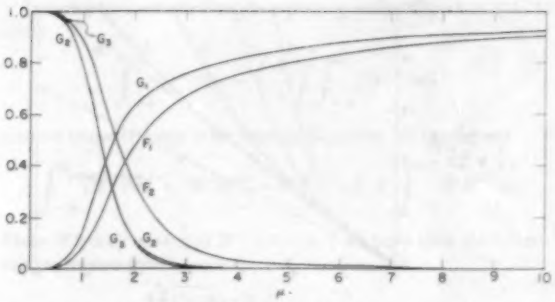

FIG. 1 GRAPHS OF FUNCTIONS F AND G OCCURRING IN EXPRESSIONS FOR TORQUE AND BENDING MOMENT

$$F_2 = \begin{cases} 1-\frac{8}{63}\mu^4+\cdots \\ \frac{45}{4}\frac{1}{\mu^4}-\frac{45}{4}\frac{1}{\mu^5}+\cdots \end{cases} \quad [37b]$$

$$G_1 = \begin{cases} \frac{8}{45}\mu^4-\frac{32}{45\cdot21}\mu^8+\cdots \\ 1-\frac{3}{4\mu}+\cdots \end{cases} \quad [37c]$$

$$G_2 = \begin{cases} 1-\frac{16}{63}\mu^4+\cdots \\ \frac{45}{16}\frac{1}{\mu^5}+\cdots \end{cases} \quad [37d]$$

$$G_3 = \begin{cases} 1-\cdots \\ \frac{1}{\mu^5}-\frac{5}{4}\frac{1}{\mu^9}+\cdots \end{cases} \quad [37e]$$

We may note that the approximations for large μ, as listed, are accurate to within 1 per cent for values of μ greater than 5.

DISCUSSION OF EXPRESSIONS FOR TORQUE AND BENDING MOMENT

Of the two Relations [31] and [32] for torque T and bending moment M, that for T has a relatively simple behavior. Fig. 2 represents a dimensionless torque function in its dependence on

TABLE 1 NUMERICAL VALUES FOR FUNCTIONS F AND G OCCURRING IN EQUATIONS [31] AND [32] FOR TORQUE T AND BENDING MOMENT M

μ	$F_1(\mu)$	$F_2(\mu)$	$G_1(\mu)$	$G_2(\mu)$	$G_3(\mu)$
0	0	1	0	1	1
0.35	0.0013	0.9982	0.00266	0.996	0.992
0.5	0.0055	0.9922	0.0110	0.984	0.991
0.75	0.0270	0.9614	0.0530	0.924	0.924
1.0	0.0789	0.8874	0.149	0.787	0.788
1.25	0.166	0.7636	0.292	0.584	0.581
1.50	0.274	0.6097	0.442	0.373	0.369
1.75	0.382	0.4583	0.559	0.212	0.207
2.0	0.473	0.3326	0.634	0.113	0.108
2.5	0.596	0.1717	0.710	0.0329	0.0280
3.0	0.668	0.0927	0.752	0.0117	0.0079
3.5	0.715	0.0536	0.785	0.00525	0.0025
4.0	0.750	0.0330	0.812	0.00271	0.00093
4.5	0.778	0.0213	0.833	0.00152	0.00038
5.0	0.800	0.0144	0.850	0.00090	0.00017
6.0	0.833	0.00723	0.875	0.00036	0.000042
∞	1	0	1	0	0

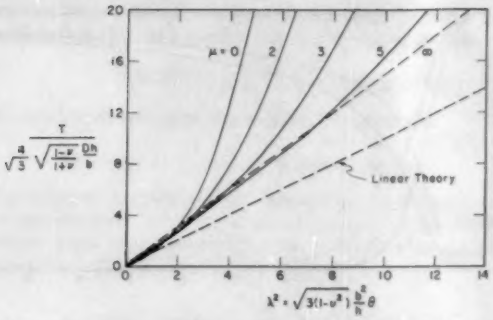

FIG. 2 DIMENSIONLESS TORQUE AS FUNCTION OF TWIST FOR VARIOUS VALUES OF $\mu^2 = \sqrt{[3(1-\nu^2)]}b^2k/h$ AND FOR $\nu = 1/3$

the twisting-angle function $b^2\theta/h$ for a specific value of Poisson's ratio ν. The curves labeled linear theory and $\mu = 0$ correspond to the previously known results. As known for the case $\mu = 0$ the plate becomes stiffer in torsion with increasing values of $b^2\theta/h$. Beyond this we see that a simultaneous bending moment M, or rather a simultaneous curvature k produced by some moment M, has an effect which differs qualitatively in different value regions of $b^2\theta/h$. For values of $b^2\theta/h$ up to about unity we have that torsional stiffness increases with bending curvature k, which enters in the dimensionless form b^2k/h. For values of $b^2\theta/h$ beyond about unity we have that torsional stiffness decreases with k.

Fig. 3 represents a dimensionless bending-moment function in its dependence on the curvature function b^2k/h, for various values of the twisting-angle function $b^2\theta/h$ and for $\nu = 1/3$. For moderate values of $\lambda^2 = \sqrt{[3(1-\nu^2)]}b^2\theta/h$ the behavior of M versus k is very nearly linear and about as expected. When $\lambda = 0$ we have the known slight variation of bending stiffness with μ, from its value for $\mu = 0$ according to linear theory to $1/(1-\nu^2)$ times this value for $\mu = \infty$. As λ^2 increases we approach a condition where in the range of moderate values of k the M versus k-relation is the opposite of what might be expected. As a consequence of this behavior, our mathematical solution provides three different possible values of k for a given value of M and associated with this, the occurrence of jump phenomena in the loading and unloading process.

We may determine the smallest value λ_c of λ for which this occurs by means of the condition that the M versus μ^2-curve has a horizontal tangent for $\mu = 0$. According to Equation [32] this will be the case when

$$1 + \frac{\nu^2}{1-\nu^2}G_1(0) + \frac{8/45}{1-\nu^2}\lambda_c^4 G_2(0) - \frac{32/45\cdot 63}{1-\nu^2}\lambda_c^8 G_3(0) = 0$$

or, in view of Equation [37], when

$$\lambda_c^2 = \sqrt{\left\{\frac{63}{8}\nu + \sqrt{\left[\frac{45\cdot 63}{32}\left(1 - \frac{3}{10}\nu^2\right)\right]}\right\}} \quad \ldots\ldots [38]$$

Values of λ_c^2 as a function of ν in the range $0 \leq \nu \leq \frac{1}{2}$ are given in Fig. 4.[5]

[5] It is instructive to consider the magnitudes of θ and T associated with $\mu = 0$ and $\lambda = \lambda_c$. According to Fig. 4 we have $\lambda_c^2 \simeq 3/\sqrt{(1-\nu^2)}$ and therewith

$$\theta_c \simeq \frac{\sqrt{3}}{1-\nu^2}\frac{h}{b^2}$$

According to Fig. 2 we have in this region a torque T which is about twice as large as predicted by linear theory. We have, according to Equation [31]

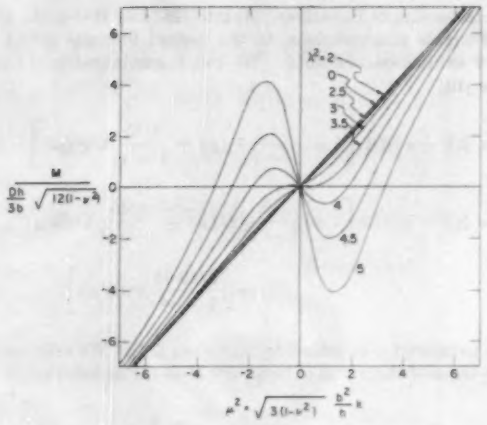

FIG. 3 DIMENSIONLESS MOMENT AS FUNCTION OF CURVATURE FOR VARIOUS VALUES OF $\lambda^2 = \sqrt{[3(1-\nu^2)]}b^2\theta/h$ AND FOR $\nu = 1/3$

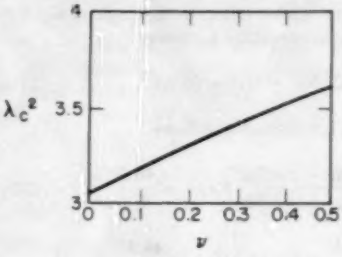

FIG. 4

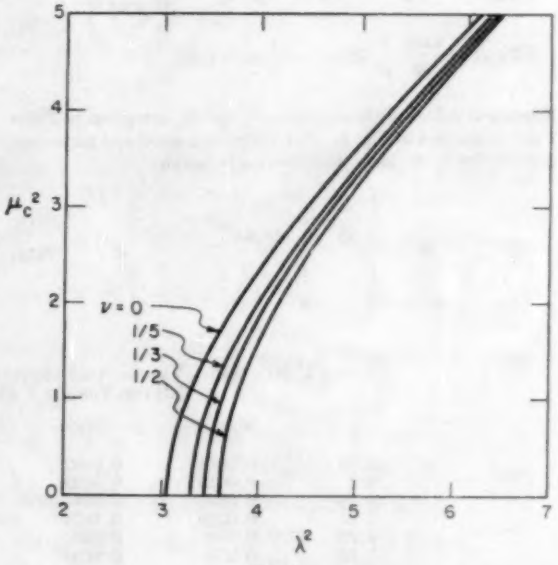

FIG. 5

$T_c \simeq 4(1-\nu)bD\theta_c\left[1 + \frac{4}{5(1-\nu)(1-\nu^2)}\right] \simeq \frac{7}{12}bEh^3\theta_c \simeq E\frac{h^4}{b}$.

Let T_c be produced by equal and opposite corner forces P_c such that $T_c = 2bP_c$. Then $P_c \simeq 2E(h^4/b^3)$. The foregoing value of T_c is smaller than that obtained by A. E. Green (4) for a different class of instabilities of a twisted strip. On the other hand, it is larger than a value which would follow from recent calculations of Pflüger (5) for the same type of instability phenomenon as Green's.

Also of interest are the nonzero values μ_c of μ which are associated with a zero value of M. According to Fig. 3 these values μ_c are, for given ν, functions of the parameter λ, determined by the relation

$$1 + \frac{\nu^2}{1-\nu^2} G_1(\mu_c) + \frac{8/45}{1-\nu^2} \lambda^2 G_2(\mu_c) - \frac{32/45 \cdot 63}{1-\nu^2} G_3(\mu_c) = 0 \quad \ldots\ldots [39]$$

Values of μ_c in their dependence on λ and ν are given in Fig. 5.

Strain-Energy Expressions

Considering the fact that, upon satisfaction of all boundary conditions other than the conditions of prescribed torque and bending moment, the solution functions W and F depend on twisting angle θ and curvature k alone, it follows that the specific strain energy U of the deformed plate, that is, the strain energy per unit of plate length, will be a function of the deformation variables k and θ only. The change δU of specific strain energy will be equal to the work of the torque T and of the moment M during generalized displacements $\delta\theta$ and δk, as follows

$$\delta U = T\delta\theta + M\delta k \quad \ldots\ldots [40]$$

In view of Equation [40] it must be possible to write the stress-strain Relations [31] and [32] as partial derivatives of U in the form

$$T = \frac{\partial U}{\partial \theta}, \qquad M = \frac{\partial U}{\partial k} \quad \ldots\ldots [41]$$

The use of Equation [41] affords an independent, and in fact somewhat simpler derivation of Equations [31] and [32] than the derivation based on the Boundary Conditions [9].

The specific strain energy U for the finitely bent plate under the assumption of isotropy and Hooke's law is given by the following expression

$$U = \int_{-b}^{b} \left\{ \frac{1}{2} D[(\nabla^2 w)^2 + 2(1-\nu)(w^2_{,xy} - w_{,xx}w_{,yy})] + \frac{1}{2}\frac{C}{1-\nu^2}\left[(\epsilon_x + \epsilon_y)^2 + 2(1-\nu)\left(\frac{1}{4}\gamma^2 - \epsilon_x\epsilon_y\right)\right] \right\} dy \quad [42]$$

For the present problem we have, in view of the fact that $N_{yy} = N_{xy} = 0$

$$\gamma = 0, \ \epsilon_y = -\nu\epsilon_x, \ C\epsilon_x = N_{xx} = F_{,yy} \quad \ldots\ldots [43]$$

Furthermore, from Equation [13]

$$w_{,xx} = -k, \ w_{,yy} = W', \ w_{,xy} = \theta \quad \ldots\ldots [44]$$

and therewith

$$U = \int_{-b}^{b} \left\{ \frac{1}{2} D[(W' - k)^2 + 2(1-\nu)(\theta^2 + kW')] + \frac{1}{2} C\left(\frac{F''}{C}\right)^2 \right\} dy$$

$$= \int_{-b}^{b} \left\{ \frac{1}{2} D[(W')^2 - 2\nu k W' + k^2 + 2(1-\nu)\theta^2] + \frac{1}{2}\frac{(F'')^2}{C} \right\} dy \quad \ldots\ldots [45]$$

In order to evaluate Equation [45] we utilize Equation [15] to write

$$\int_{-b}^{b} (F'')^2 dy = \left(\frac{D}{k}\right)^2 \int_{-b}^{b} (W^{IV})^2 dy$$

and we transform one other term in Equation [45] as follows

$$\int_{-b}^{b} (W'')^2 dy = [W'W'' - WW''']_{-b}^{b} + \int_{-b}^{b} WW^{IV} dy$$

Since $W''(\pm b) = \nu k$ and $W'''(\pm b) = 0$ we have then the following expression for U

$$U = [k^2 + 2(1-\nu)k^2]Db - \frac{1}{2}\nu k D W' \Big|_{-b}^{b} + \frac{1}{2} D \int_{-b}^{b} \left(W + \frac{D}{k^2 C} W^{IV}\right) W^{IV} dy \quad \ldots\ldots [46]$$

Furthermore, in view of Equation [18]

$$U = [k^2 + 2(1-\nu)\theta^2]Db - \frac{1}{2}\nu k D W' \Big|_{-b}^{b} - \frac{1}{2} D \frac{\theta^2}{2k} \int_{-b}^{b} y^2 W^{IV} dy$$

$$= [k^2 + 2(1-\nu)\theta^2]Db - \frac{1}{2}\nu k D W' \Big|_{-b}^{b} - \frac{D\theta^2}{4k}[y^2 W''' - 2yW'' + 2W']_{-b}^{b}$$

$$= [k^2 + 2(1-\nu)\theta^2]Db + \nu\theta^2 Db - \left[\nu k + \frac{\theta^2}{k}\right] D W'(b) \quad \ldots [47]$$

We introduce $W'(b)$ from Equations [19], [21], and [30] in the form

$$W'(b) = \frac{1}{\alpha}\left(\frac{\theta^2}{k} + \nu k\right)\frac{\cosh 2\mu - \cos 2\mu}{\sinh 2\mu + \sin 2\mu} - \frac{\theta^2}{k} b = b\left\{\nu k[1 - F_1(\mu)] - \frac{\theta^2}{k} F_1(\mu)\right\} \quad \ldots\ldots [48]$$

and obtain

$$U = Db\left\{[1 - \nu^2(1-F_1)]k^2 + 2[1 - \nu(1-F_1)]\theta^2 + \frac{1}{k^2} F_1\theta^4\right\}$$

$$= \frac{Db\lambda^2}{3(1-\nu^2)b^4}\left\{[1 - \nu^2(1-F_1)]\mu^4 + 2[1 - \nu(1-F_1)]\lambda^4 + \lambda^8 \frac{F_1}{\mu^4}\right\}$$

$$= \frac{Dh^2}{3b^2}\left\{\left(1 + \frac{\nu^2}{1-\nu^2} F_1\right)\mu^4 + \frac{2}{1+\nu}\left(1 + \frac{\nu}{1-\nu} F_1\right)\lambda^4 + \frac{F_1}{\mu^4}\frac{\lambda^8}{1-\nu^2}\right\} \quad \ldots\ldots [49]$$

It may be verified that

$$\frac{\partial U}{\partial \theta} = \frac{\partial U}{\partial \lambda}\frac{\partial \lambda}{\partial \theta} = \frac{\partial U}{\partial \lambda}\frac{\sqrt[4]{[3(1-\nu^2)]}b}{2\sqrt{(\theta h)}}$$

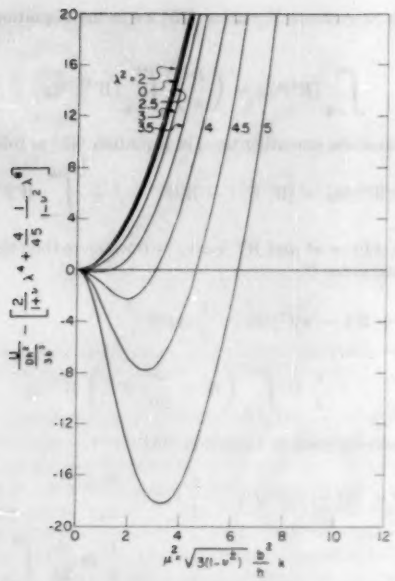

FIG. 6 VARIATION OF SPECIFIC STRAIN ENERGY U WITH CURVATURE k, FOR VARIOUS VALUES OF λ AND FOR $\nu = 1/3$

and

$$\frac{\partial U}{\partial k} = \frac{\partial U}{\partial \mu}\frac{\partial \mu}{\partial k} = \frac{\partial U}{\partial \mu}\frac{\sqrt[4]{[3(1-\nu^2)]}b}{2\sqrt{(kh)}}$$

reduce as they should to the functions T and M determined by Equations [21] and [22].

Fig. 6 contains curves showing the variation of specific strain energy U as a function of μ for various values of λ. It is noted that the specific strain-energy curves show a similar behavior as a function of λ, as we have previously encountered for the M versus μ-curves in Fig. 3. This fact will be of importance in the discussion of the stability of the various solutions in the range of parameter values where several different values of μ correspond to one and the same value of M.

BIBLIOGRAPHY

1 "Bifilar Property of Twisted Strips," by J. C. Buckley, *Philosophical Magazine*, vol. 28, 1914, pp. 778–787.

2 "Anti-Clastic Curvature of Rectangular Beams and Plates," by D. G. Ashwell, *Journal of the Royal Aeronautical Society*, vol. 54, 1950, pp. 708–715.

3 "The Anticlastic Curvature of a Strip With Lateral Thickness Variation," by Y. C. Fung and W. H. Wittrick, JOURNAL OF APPLIED MECHANICS, Trans. ASME, vol. 76, 1954, pp. 351–358.

4 "The Elastic Stability of a Thin Twisted Strip—II," by A. E. Green, Proceedings of the Royal Society of London, series A, vol. 161, 1937, pp. 197–220.

5 "Nicht-lineare Beulprobleme," by A. Pflüger, *Zeitschrift für angewandte Mathematik und Mechanik*, vol. 35, 1955, pp. 353–355.

Deformation of Elastic Paraboloidal Shells of Revolution[1]

By C. NEVIN DE SILVA,[2] ANN ARBOR, MICH.

The present paper, using the contributions to the theory of shells of revolution given recently by Naghdi (1),[3] is concerned with the axisymmetric problem of thin elastic paraboloidal shells of revolution which includes the effect of transverse-shear deformation. Following the general scheme given in (1), an asymptotic solution is obtained for paraboloidal shells of uniform thickness and is valid at the apex of the shell. In the limit, these results reduce to the predictions of the classical theory of H. Reissner-Meissner. Solutions are given by both theories for a specific example, namely, a second-degree paraboloidal shell loaded uniformly over a small region about the apex when the open edge is clamped.

Nomenclature

The following nomenclature is used in the paper:

r, θ, z = cylindrical co-ordinates
ξ, θ = co-ordinates of middle surface
ϕ = inclination of tangent to meridian of middle surface
β = change in ϕ due to deformation
R_ξ, R_θ = principal radii of curvature of middle surface
$\lambda = R_\xi^{-1} - R_\theta^{-1}$ = difference of principal curvatures of middle surface
u_r, w_z = displacements of a point on middle surface
q_h, q_v = "horizontal" and "vertical" components of load intensity
N_ξ, N_θ, V_ξ = stress resultants
M_ξ, M_θ = stress couples
P_h, P_v = "horizontal" and "vertical" stress resultants
ψ = "horizontal" stress-resultant function
$\sigma_{\xi b}, \sigma_{\theta b}$ = maximum bending stresses
$\sigma_{\xi m}, \sigma_{\theta m}$ = membrane stresses
τ = shearing stress
h = thickness of shell
E = Young's modulus
G = shear modulus
ν = Poisson's ratio

$k^{1/2} = h/[12(1 - \nu^2)]^{1/2}$
$X_1 = \beta + \nu k^{1/2}\lambda\psi$
$X_2 = \psi - \nu k^{1/2}\lambda\beta$

Introduction

The classical theory of axisymmetrically loaded thin shells of revolution advanced by H. Reissner (2) and Meissner (3, 4) has been the subject of numerous investigations. Not the least important of these has been the developent of asymptotic solutions of the differential equations of this theory (5, 6, 7). These solutions, however, failed to yield results valid at singular points of the differential equations of the shell when the loaded region included these points. Later E. Reissner (8) formulated a theory for the finite deformation of thin elastic shells of revolution from which the linear theory is derived as a special case. In this linear theory the form of the resulting differential equations differs only slightly from that of H. Reissner-Meissner. Hildebrand (9) indicated how these equations can be solved by asymptotic integration; the solution, however, fails to be valid at points where the differential equations contain singularities. Subsequently, the E. Reissner equations were combined by Naghdi and De Silva (10) into a single complex differential equation, and a solution for the general shell (including variable thickness) which would be valid at the singularities of the differential equation was indicated by applying the method of asymptotic integration developed by Langer (11, 12).

The improvement of the classical theory of bending of plates, by including the effects of transverse normal stress and shear deformation due to E. Reissner (13), has been demonstrated previously [see for example (13, 14)]. In the extension of this improvement to shells, notable contributions have been made by Hildebrand, E. Reissner, and Thomas (15), Green and Zerna (16), E. Reissner (17), and Naghdi (18). References (15), (16), (17), and (18) are concerned chiefly with the formulation of appropriate stress-strain relations for thin elastic shells when the effects of transverse normal stress and shear deformation are not neglected. In (1), a theory for general shells of revolution of variable thickness has been given which, while neglecting the transverse normal stress, incorporates the effect of transverse-shear deformation. This theory yields equations which reduce to those of H. Reissner-Meissner as one limiting case, to those of a flat plate (13) in another. Reference (1) is rendered complete by indicating a solution of these general differential equations by asymptotic integration.

In the present paper, Naghdi's theory is applied to the deformation of thin elastic paraboloidal shells of revolution with uniform thickness. The solution, following the scheme given in (1), is obtained by asymptotic integration and requires the proof of the uniform convergence of an infinite series.[4] The results appropriate for the classical theory are given as a special case of this solution. To illustrate the predictions of the two theories, a second-degree paraboloidal shell, loaded uniformly over a small region about the apex and clamped about the edge, is solved in detail for various values of both the span-thickness ratio and the radius of the loaded region.

[1] The results presented in this paper were obtained in the course of research sponsored by the Office of Naval Research under Contract Nonr-1224(01), Project NR-064-408, with the University of Michigan.

[2] Research Associate, Department of Engineering Mechanics, University of Michigan.

[3] Numbers in parentheses refer to the Bibliography at the end of the paper.

Presented at the Applied Mechanics Division Summer Conference, Berkeley, Calif., June 13–15, 1957, of The American Society of Mechanical Engineers.

Discussion of this paper should be addressed to the Secretary, ASME, 29 West 39th Street, New York, N. Y., and will be accepted until October 10, 1957, for publication at a later date. Discussion received after the closing date will be returned.

Note: Statements and opinions advanced in papers are to be understood as individual expressions of their authors and not those of the Society. Manuscript received by ASME Applied Mechanics Division, October 10, 1956. Paper No. 57—APM-5.

[4] This proof is given in the Appendix.

The Basic Equations

The axisymmetric theory of thin shells of revolution to be described is restricted to the small deformation of elastic isotropic materials and is due to Naghdi (1). With the use of cylindrical co-ordinates r, θ, z, the parametric equations of the middle surface of the shell, Fig. 1, may be written as

$$r = r(\xi), \quad z = z(\xi) \qquad [1]$$

where ξ together with the polar angle θ in the x-y plane constitute the co-ordinates of the middle surface. Denoting by ϕ the inclination of the tangent to the meridian of the shell, then

$$\tan \phi = \frac{dz}{dr}, \quad r' = \alpha \cos \phi, \quad z' = \alpha \sin \phi \qquad [2]$$

where

$$\alpha = [(r')^2 + (z')^2]^{1/2} \qquad [3]$$

and prime denotes differentiation with respect to ξ.

To make the paper self-contained, we record here the relevant equations of the small-deflection theory of elastic shells of revolution which includes the effect of transverse shear deformation as given in (1)

$$\left.\begin{aligned}
rP_v &= -\int r\alpha q_r d\xi \\
\alpha N_\xi &= r'P_h + z'P_v \\
\alpha V_\xi &= -z'P_h + r'P_v \\
\alpha N_\theta &= (rP_h)' + r\alpha q_h \\
\alpha M_\xi &= D\left[\left(\beta' + \nu\frac{r'}{r}\beta\right) - \alpha\lambda\left(\frac{u_r' + z'\omega}{r'}\right)\right] \\
\alpha M_\theta &= D\left[\left(\frac{r'}{r}\beta + \nu\beta'\right) + \alpha\lambda\frac{u_r}{r}\right] \\
u_r &= \frac{r}{C}(N_\theta - \nu N_\xi) - k\lambda\frac{r}{\alpha}\left(\frac{r'}{r}\beta + \nu\beta'\right) \\
w_z &= \int\left\{\frac{z'}{C}(N_\xi - \nu N_\theta) + k\lambda\frac{z'}{\alpha}\left(\beta' + \nu\frac{r'}{r}\beta\right)\right. \\
&\qquad \left. - r'\beta + \frac{6}{5Gh}\frac{r'}{\alpha}(-z'P_h + r'P_v)\right\} d\xi
\end{aligned}\right\} \quad [4]$$

In the foregoing equations, N_θ, N_ξ, V_ξ, are the stress resultants, M_ξ, M_θ, the stress couples; P_h and P_v are the "horizontal" and "vertical" stress resultants related to V_ξ and N_ξ; u_r and w_z are the displacements in the radial and axial directions, respectively; β is the negative change in ϕ due to deformation, q_h and q_v are the components of the load intensity in the r and z-directions, h is the thickness of the shell, and

$$\left.\begin{aligned}
C &= Eh, \quad D = \frac{Eh^3}{m^2}, \quad m^2 = 12(1 - \nu^2) \\
\omega &= w_z'\frac{\cos\phi}{\alpha} - u_r'\frac{\sin\phi}{\alpha} \\
k &= \frac{h^2}{m^2}, \quad \lambda = \frac{1}{R_\xi} - \frac{1}{R_\theta} = \frac{\phi'}{\alpha} - \frac{\sin\phi}{r}
\end{aligned}\right\} \quad [5]$$

where R_ξ and R_θ are the principal radii of curvature of the middle surface. The maximum stresses due to the stress couples (bending) and due to the stress resultants $N\xi$, $N\theta$ (membrane) as well as the shearing stress τ are defined by expressions of the type

$$\left.\begin{aligned}
\sigma_{\xi b} &= \frac{6}{h^2}M_\xi = \frac{6}{m}\left[\frac{Eh}{m\alpha}\left(\beta' + \nu\frac{r'}{r}\beta\right)\right. \\
&\qquad \left.(1 - k\lambda^2) - k^{1/2}\lambda(\sigma_{\xi m} - \nu\sigma_{\theta m})\right] \\
\sigma_{\xi m} &= \frac{N_\xi}{h} = \frac{Eh}{m\alpha}\left(\frac{\alpha}{R_\theta}\cot\phi\right)\psi + \frac{(rP_v)}{R_\theta h} \\
\tau &= \frac{3}{2}\frac{V_\xi}{h} = -\frac{3}{2}\left[\frac{Eh}{m\alpha}\frac{\alpha}{R_\theta}\psi - \frac{(rP_v)}{R_\theta h}\cot\phi\right]
\end{aligned}\right\} \quad [6]$$

where

$$\psi = \frac{m}{Eh^2}(rP_h)$$

The differential equations governing the deformation of shells of revolution as given in (1) for the case of uniform thickness reduce to

$$\gamma'' + [i^2\mu^2\Psi^2 + (\Lambda_0 + \Lambda_s)]\gamma = \Theta[F_1 + i\bar{\delta}F_2 + \Phi X_3'] \qquad [7]$$

where μ^2 and $\bar{\delta}$ are constants; F_1 and F_2 are functions of the load intensity

$$\gamma = \Theta(X_1 + i\bar{\delta}X_2) \qquad [8]$$

$$X_1 = \beta + \nu k^{1/2}\lambda\psi; \quad X_2 = \psi - \nu k^{1/2}\lambda\beta \qquad [9]$$

$$\Theta = \left(\frac{r}{\alpha}\right)^{1/2}\exp\left\{i\bar{\delta}\frac{\nu}{2}k^{1/2}\lambda - i\bar{\delta}\int k^{1/2}\lambda\frac{r'}{r}d\xi\right\} \qquad [10]$$

$$\Psi^2 = (1 + i\nu k^{1/2}\lambda)f(\xi) \qquad [11]$$

$$\Lambda_0 = -\left(\frac{r'}{r}\right)^2 - \frac{1}{2}\frac{(r/\alpha)''}{(r/\alpha)} + \frac{1}{4}\left[\frac{(r/\alpha)'}{(r/\alpha)}\right]^2 - \frac{6(1+\nu)}{5}\left(\frac{z'}{r}\right)^2 \qquad [12a]$$

$$\Lambda_s = -\frac{1}{2}i\bar{\delta}\nu k^{1/2}\left\{\lambda'' + \lambda'\left[\left(1 - \frac{2}{\nu}\right)\frac{r'}{r} - \frac{\alpha'}{\alpha}\right] - \frac{2}{\nu}\lambda\left[\left(\frac{r'}{r}\right)^2 - \frac{r'}{r}\frac{\alpha'}{\alpha} + \left(\frac{r'}{r}\right)'\right]\right\} \qquad [12b]$$

$$\Phi = \nu k^{1/2}\lambda\left[\frac{2}{\nu}\left(\frac{r'}{r}\right)(1 + \bar{\delta}^2) + \frac{\lambda'}{\lambda}(1 - \bar{\delta}^2)\right] \qquad [13]$$

$$\bar{\delta} = 1 - i\frac{1}{\mu^2 f}\left[\nu\frac{(r'/\alpha)'}{(r/\alpha)} + \frac{6(1+\nu)}{5}\left(\frac{z'}{r}\right)^2\right] \qquad [14]$$

$$\mu^2 f = \frac{\alpha^2 m}{R_\theta h_0} \qquad [15]$$

and it should be noted that Equations [7] to [15] were deduced under the restrictions that (i) $k^{1/2}\lambda \ll 1$ and (ii) $\mu^{-2} = O(k^{1/2}\lambda)$.

Paraboloidal Shells of Uniform Thickness

Consider the middle surface of a paraboloidal shell of revolution whose trace on the $y - z$ plane (see Fig. 1 for the trace when $b = 1/2$), for example, is given by

$$y = a_0 z^b, \quad 0 < b < 1 \qquad [16]$$

The equation of the middle surface is

$$r^2 = a_0^2 z^{2b} \qquad [17]$$

and hence the co-ordinates of any point on the middle surface are specified by

$$x = r\cos\theta, \quad y = r\sin\theta, \quad z = \left(\frac{r}{a_0}\right)^{1/b} \qquad [18]$$

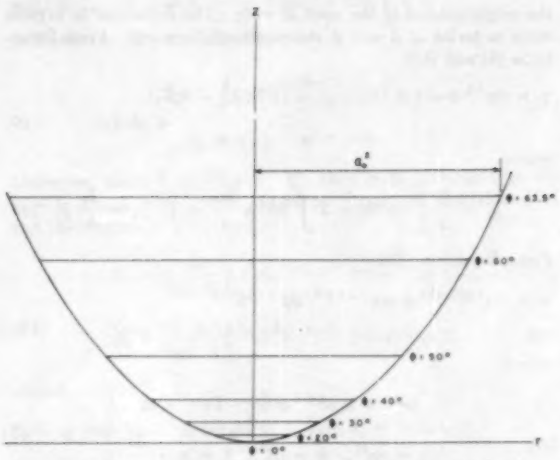

FIG. 1 TRACE IN r-z PLANE OF MIDDLE SURFACE OF PARABOLOIDAL SHELL $r = a_0 z^{1/2}$

We now choose ξ as ϕ and the principal radii of curvature of the middle surface are then given by

$$\left.\begin{aligned} R_\phi &= \alpha = b\delta a_0^2 \sec^3\phi \left[\frac{a_0 b \sin\phi}{\cos\phi}\right]^{\bar\delta - 1} \\ R_\theta &= \frac{r}{\sin\phi} = a_0 \sin^{\bar\delta - 1}\phi \left[\frac{a_0 b}{\cos\phi}\right]^{\bar\delta} \end{aligned}\right\} \quad \ldots\ldots [19]$$

so that

$$\frac{R_\phi}{R_\theta} = \delta \sec^2\phi, \quad \delta = \frac{b}{1-b} \quad \ldots\ldots [20]$$

Associated with the geometry of the middle surface will be the definitions of μ^2 and f given in Equation [15]

$$\left.\begin{aligned} u^2 &= \delta^3 b^{\bar\delta} a_0^{1+\bar\delta} \frac{m}{h_0} \\ f &= \sec^{4+\bar\delta}\phi \sin^{\bar\delta - 1}\phi \end{aligned}\right\} \quad \ldots\ldots [21]$$

Also the following relations, which follow from Equations [5] and [19] are relevant in the subsequent analysis

$$\lambda = \frac{1}{a_0}\left(\frac{a_0 b}{\cos\phi}\right)^{-\bar\delta} \sin^{1-\bar\delta}\phi \,[(1/b - 2)\cos^2\phi - \sin^2\phi]. \quad [22]$$

$$\lambda' = \frac{1}{a_0}\left(\frac{a_0 b}{\cos\phi}\right)^{-\bar\delta} \sin^{-\bar\delta}\phi \,\{(1-\delta)(1/b-2)\cos^3\phi + 2(\delta - 1/b)\sin^2\phi\cos\phi + \delta\sin^4\phi\sec\phi\} \quad \ldots\ldots [23]$$

$$\lambda'' = \frac{1}{a_0}\left(\frac{a_0 b}{\cos\phi}\right)^{-\bar\delta} \sin^{-1-\bar\delta}\phi \,\{-\delta(1-\delta)(1/b-2)\cos^2\phi + \sin^2\phi[-2\delta(\delta - 1/b) + \cos^2\phi\,\langle 4(\delta - 1/b) - 3(1-\delta)(1/b - 2)\rangle] + \sin^4\phi[2(\delta + 1/b) - \delta\sec^2\phi] + \delta\sin^6\phi\sec^2\phi\} \quad \ldots\ldots [24]$$

SOLUTION BY ASYMPTOTIC INTEGRATION OF THE DIFFERENTIAL EQUATION

Since an approximate particular solution of Equation [7] can be obtained by using the membrane theory of shells, we shall confine ourselves to the solution of the homogeneous Equation [7], i.e., $F_1 = F_2 = 0$, but $\Phi \neq 0$.

It may be mentioned that, as explained in (1), a necessary condition for the validity of this differential equation is that $\bar\delta$ must be constant. Since the principal radii of curvature of the middle surface are not constant, $\bar\delta$ can only be constant if h varies in a prescribed manner (1). However, guided by existing solutions (19), we shall approximate $\bar\delta$ by some complex constant, say, $\delta_1 + i\delta_2$ and thereby assume the validity of Equation [7].[5] We now proceed to examine the coefficient functions of γ in Equation [7]. From Equations [11], [21], and [22]

$$\Psi^2 = \sin^{\bar\delta - 1}\phi\,\bar\Psi^2 \quad \ldots\ldots [25]$$

$$\bar\Psi^2 = \sec^{4+\bar\delta}\phi \left\{1 + i\nu \frac{k^{1/2}}{a_0}(a_0 b \sec\phi)^{-\bar\delta} [(1/b - 2)\cos^2\phi - \sin^2\phi]\right\} \quad \ldots\ldots [26]$$

$$\Lambda_0 = \frac{A_1}{\sin^2\phi} + \Lambda_2 \quad \ldots\ldots [27]$$

$$\Lambda_2 = \frac{A_1}{\cos_2\phi} - \frac{9}{4}\tan^2\phi + \left(\frac{5}{2} - \frac{\delta}{2}\right)\sec^2\phi - \frac{6(1+\nu)}{5}\delta^2\sec^4\phi \quad \ldots\ldots [28]$$

$$A_1 = -\frac{1}{4}(4\delta^2 - 1) \quad \ldots\ldots [29]$$

It should be noted that Λ_0 has a pole of order two at $\phi = 0$ and that Λ_2 is analytic and bounded with respect to μ in the interval

$$I_\phi: \quad 0 \leqslant \phi \leqslant \frac{\pi}{2} - \epsilon \quad \ldots\ldots [30]$$

In order to determine the character of Λ, we record the following from Equations [19], [22], and [23]

$$-\frac{2}{\nu}\lambda\left[\left(\frac{r'}{r}\right)^2 - \frac{r'}{r}\frac{\alpha'}{\alpha} + \left(\frac{r'}{r}\right)'\right] = -\frac{2}{\nu}\frac{\delta}{a_0}(a_0 b\sec\phi)^{-\bar\delta}\sin^{-1-\bar\delta}\phi \{\sin^2\phi[\sec^2\phi - (1/b - 1)]\} \quad \ldots\ldots [31]$$

$$\left.\begin{aligned} &\lambda'\left[\left(1 - \frac{2}{\nu}\right)\frac{r'}{r} - \frac{\alpha'}{\alpha}\right] \\ &= \frac{1}{a_0}(a_0 b\sec\phi)^{-\bar\delta}\sin^{-1-\bar\delta}\phi \\ &\left\{(1-\delta)(1/b-2)\left(1 - \frac{2}{\nu}\delta\right)\cos^2\phi\right. \\ &+ \sin^2\phi\left[-3(1-\delta)(1/b-2)\cos^2\phi\right. \\ &\left. + 2(\delta - 1/b)\left(1 - \frac{2}{\nu}\delta\right)\right] \\ &+ \sin^4\phi\left[\delta\left(1 - \frac{2}{\nu}\delta\right)\sec^2\phi\right. \\ &\left.\left. - 6(\delta - 1/b)\right] + 3\delta\sec^2\phi\sin^6\phi\right\} \end{aligned}\right\} \quad \ldots [32]$$

Since δ from Equation [20] is always positive, we further restrict b such that

$$\left.\begin{aligned} 0 < b &\leqslant 1/2 \\ 0 < \delta &\leqslant 1 \end{aligned}\right\} \quad \ldots\ldots [33]$$

and hence from Equations [24], [31], [32], and [33] we conclude that

$$\Lambda_0 = B\sin^{-1-\bar\delta}\phi + \Lambda_{1_0} \quad \ldots\ldots [34]$$

[5] This approximation is analogous to that discussed in references (10, 19).

where

$$B = -\frac{1}{2}\,i\delta\nu\,\frac{k^{1/3}}{a_0}\,\frac{1-\delta}{(a_0 b)^{\bar{b}}}\,(1/b-2)\left[1-\left(1+\frac{2}{\nu}\right)\delta\right]\cos^{2+\bar{b}}\phi \quad \ldots\ldots [35]$$

and Λ_{1_0} is continuous and bounded with respect to μ in I_ϕ. It follows then that

$$\Lambda_0 + \Lambda_{s_0} = \frac{A}{\sin^2\phi} + \bar{\Lambda}_{s_0} \quad \ldots\ldots [36]$$

where

$$A = A_1 - B\sin^{1-\bar{b}}\phi \quad \ldots\ldots [37]$$

and $\bar{\Lambda}_{s_0}$ is continuous and bounded with respect to μ in I_ϕ. Finally we note that

$$\left.\begin{aligned}\lim_{\phi=0} A &= A_1\\ \lim_{b=1/2} A &= A_1\end{aligned}\right\} \quad \ldots\ldots [38]$$

and that, from Equations [26] and [33], $\bar{\Psi}^2$ is continuous and non-vanishing in I_ϕ, $\bar{\Psi}^2(0) = 1$. Hence the homogeneous differential Equation [7] may now be written in the equivalent form

$$\gamma'' + \left[i^3\mu^2\sin^{-1+\bar{b}}\phi\,\bar{\Psi}^2 + \frac{A_1}{\sin^2\phi} + \bar{\Lambda}_{s_0}\right]\gamma = \Theta\Phi X_2' \quad \ldots [39]$$

Following reference (1), the solution of Equation [39] may be written as

$$\gamma_j(\phi) = y_j(\phi) + \sum_{n=1}^{\infty} y_j^{(n)}(\phi); \quad j = 1, 2 \quad \ldots\ldots [40]$$

where

$$y_j^{(n+1)}(\phi) = \int_0^\phi K(\phi, \phi_1)(x_2)_j'^{(n)}(\phi_1)d\phi_1$$

$$(x_2)_j'^{(0)} = (x_2)_j' \quad \ldots\ldots [41]$$

$$K(\phi, \phi_1) = \frac{y_1(\phi)y_2(\phi_1) - y_2(\phi)y_1(\phi_1)}{\mathcal{W}(y_1, y_2)}\,\Theta(\phi_1)\Phi(\phi_1) \quad \ldots [42]$$

and $\mathcal{W}(y_1, y_2)$ is the Wronskian of y_1 and y_2, which are two independent solutions of Equation [39] with the right-hand side set equal to zero. Equation [40] is a valid solution if the series

$$\sum_{n=1}^{\infty} y_j^{(n)}(\phi)$$

is uniformly convergent in I_ϕ. The proof of the uniform convergence of this series is given in the Appendix where it is also shown that the solution is asymptotic to the dominant term of y_j. Hence a solution of Equation [39] which is asymptotic with respect to μ^2 to the true solution is given by

$$\gamma = \sin^{1/4(1-\bar{b})}\phi\,\bar{\Psi}^{-1/2}\Delta^{1/2}\,[A_0 J_{2\bar{b}}(\eta) + B_0 Y_{2\bar{b}}(\eta)] \quad \ldots [43]$$

where

$$\left.\begin{aligned}\Delta &= \int_0^\phi \sin^{-1/2(1-\bar{b})}\phi\,\bar{\Psi}\,d\phi\\ \eta &= i^{3/2}s, \quad s = \mu\Delta\end{aligned}\right\} \quad \ldots\ldots [44]$$

$J_\alpha(\eta)$, $Y_\alpha(\eta)$ are Bessel functions of the first and second kinds, respectively, and A_0, B_0 are complex constants. Solution [43] is valid in I_ϕ for the limiting case $b = 1/2$ and valid for $0 < b \leq 1/2$ in the neighborhood of the apex $\phi = 0$. The reduction to expressions in terms of β and ψ is now straightforward. From Equations [8] and [10]

$$\gamma = \sin^{1/2}\phi\,\cos\phi\,\exp(-g_2 + ig_1)[(X_1 - \delta_2 X_2) + i\delta_1 X_2] \quad \ldots\ldots [45]$$

where

$$g_1 = \frac{\delta_1}{2}\left[\nu k^{1/3}\lambda - 2\int k^{1/3}\lambda\,\frac{r'}{r}\,d\phi\right], \quad g_2 = \frac{\delta_2}{\delta_1}\,g_1 \quad \ldots [46]$$

From Equation [43]

$$\gamma = \sin^{1/4(1-\bar{b})}\phi\,\cos^{1/4(4+\bar{b})}\phi\rho^{-1/4}\Gamma^{1/2}\,[A_0 J_{2\bar{b}}(\eta) + B_0 Y_{2\bar{b}}(\eta)] \quad \ldots\ldots [43a]$$

where

$$\left.\begin{aligned}\rho e^{i\Omega} &= \cos^{4+\bar{b}}\phi\,\bar{\Psi}^2; \quad \Gamma e^{i\chi} = \Delta\\ \eta &= \bar{\eta}e^{i\bar{\chi}}; \quad \bar{\eta} = \mu\Gamma; \quad \bar{\chi} = \chi + \frac{3\pi}{4}\end{aligned}\right\} \quad \ldots\ldots [47]$$

Equating the real and imaginary parts of Equations [43a] and [45], and applying Equation [9] we have

$$\beta = \sin^{-1/4(1+\bar{b})}\phi\,\cos^{1/4\bar{b}}\phi\rho^{-1/4}\Gamma^{1/2}\exp(g_2)\left\{S\left[\cos\alpha_1 + \frac{1}{\delta_1}(\delta_2 - \nu k^{1/3}\lambda)\sin\alpha_1\right] - T\left[\sin\alpha_1 - \frac{1}{\delta_1}(\delta_2 - \nu k^{1/3}\lambda)\cos\alpha_1\right]\right\} \quad \ldots\ldots [48]$$

$$\psi = \sin^{-1/4(1+\bar{b})}\phi\,\cos^{1/4\bar{b}}\phi\rho^{-1/4}\Gamma^{1/2}\exp(g_2)\left\{T\left[\frac{1}{\delta_1}\cos\alpha_1 - \nu k^{1/3}\lambda\left(\sin\alpha_1 - \frac{\delta_2}{\delta_1}\cos\alpha_1\right)\right] + S\left[\frac{1}{\delta_1}\sin\alpha_1 + \nu k^{1/3}\lambda\left(\cos\alpha_1 + \frac{\delta_2}{\delta_1}\sin\alpha_1\right)\right]\right\} \quad \ldots\ldots [49]$$

In Equations [48] and [49], α_1, S, and T are defined as follows

$$\left.\begin{aligned}\alpha_1 &= \frac{1}{2}\left(\chi - \frac{\Omega}{2} - 2g_1\right)\\ S &= a_1 P_{2\bar{b}}(\bar{\eta}, \bar{\chi}) - a_2 Q_{2\bar{b}}(\bar{\eta}, \bar{\chi}) + b_1 U_{2\bar{b}}(\bar{\eta}, \bar{\chi}) - b_2 V_{2\bar{b}}(\bar{\eta}, \bar{\chi})\\ T &= a_1 Q_{2\bar{b}}(\bar{\eta}, \bar{\chi}) + a_2 P_{2\bar{b}}(\bar{\eta}, \bar{\chi}) + b_1 V_{2\bar{b}}(\bar{\eta}, \bar{\chi}) + b_2 U_{2\bar{b}}(\bar{\eta}, \bar{\chi})\\ J_\alpha(\eta) &= J_\alpha(\bar{\eta}e^{i\bar{\chi}}) = P_\alpha(\bar{\eta}, \bar{\chi}) + iQ_\alpha(\bar{\eta}, \bar{\chi})\\ Y_\alpha(\eta) &= Y_\alpha(\bar{\eta}e^{i\bar{\chi}}) = U_\alpha(\bar{\eta}, \bar{\chi}) + iV_\alpha(\bar{\eta}, \bar{\chi})\end{aligned}\right\} \quad \ldots [50]$$

and the a_i, b_i are real constants.

Reduction to Solution of Classical Theory

The solution of the classical theory stems directly from Equation [43] by setting $\lambda = 0$ in the expression for $\bar{\Psi}^2$ [26]; i.e.

$$\bar{\Psi}^2(\lambda = 0) = \bar{\Psi}_0^2 = \sec^{4+\bar{b}}\phi \quad \ldots\ldots [51]$$

with the corresponding change in the definition of Δ and η. Moreover the restriction Equation [33] on b is no longer necessary for $\bar{\Psi}_0^2$ and Λ_{s_0} which vanishes identically when $\lambda = 0$. Hence for the classical theory

$$\gamma(\lambda = 0) = \gamma_0 = \sin^{1/4(1-\bar{b})}\phi\,\cos^{1+1/4\bar{b}}\phi\Delta_0^{1/2}\,[A_0 J_{2\bar{b}}(\eta_0) + B_0 Y_{2\bar{b}}(\eta_0)] \quad \ldots\ldots [52]$$

valid in I_ϕ: $0 \leq \phi \leq \frac{\pi}{2} - \epsilon$ and for $0 < b < 1$.

In Equation [52], the following hold

$$\left.\begin{aligned} \Delta_0 &= \int_0^\phi \sin^{1/2(\bar{b}-1)} \zeta \overline{\Psi}_0 \, d\zeta \\ \eta_0 &= i^{\bar{b}/2} s_0, \quad s_0 = \mu \Delta_0 \end{aligned}\right\} \quad \ldots\ldots [53]$$

Moreover, since $1/\mu^2 = O(k^{1/2}\lambda)$, then it is consistent to set $\bar{\delta}_1 = 1$; i.e., $\delta_1 = 1$, $\delta_2 = 0$. It will be found that Equations [48] and [49] reduce to

$$\beta_0 = \left(\frac{\Delta_0}{\sin\phi}\right)^{1/2} \sin^{1/4(1-\bar{b})}\phi \cos^{1/4\bar{b}}\phi \, S_0 \ldots\ldots [54]$$

$$\psi_0 = \left(\frac{\Delta_0}{\sin\phi}\right)^{1/2} \sin^{1/4(1-\bar{b})}\phi \cos^{1/4\bar{b}}\phi \, T_0 \ldots\ldots [55]$$

where[6]

$$\left.\begin{aligned} S_0 &= a_1 \operatorname{ber}_{\bar{b}} s_0 - a_2 \operatorname{bei}_{\bar{b}} s_0 + b_1 \operatorname{ker}_{\bar{b}} s_0 - b_2 \operatorname{kei}_{\bar{b}} s_0 \\ T_0 &= a_1 \operatorname{bei}_{\bar{b}} s_0 + a_2 \operatorname{ber}_{\bar{b}} s_0 + b_1 \operatorname{kei}_{\bar{b}} s_0 + b_2 \operatorname{ker}_{\bar{b}} s_0 \end{aligned}\right\} \quad .. [56]$$

The question is raised why b can range over a greater interval of the real numbers in the classical theory than in the improved theory

classical theory $\quad 0 < b < 1$

improved theory $\quad 0 < b \leq \frac{1}{2}$

To answer this, it must be pointed out that the quasi-normal form Equation [7] of reference (1) was deduced under the assumption that $k^{1/2}\lambda = O(1/\mu^2)$. From Equations [5], [21], and [22]

$$k^{1/2}\lambda = \frac{1}{\mu^2} \bar{b}^2 \cos^b\phi \sin^{1-\bar{b}}\phi [(1/b - 2)\cos^2\phi - \sin^2\phi]$$

Because of the factor $\sin^{1-\bar{b}}\phi$, this expression is of $O(1/\mu^2)$ in the neighborhood of $\phi = 0$ only if $\bar{b} \leq 1$; i.e., $0 < b \leq \frac{1}{2}$. In the classical theory, $\lambda \equiv 0$ and no such restriction on b is necessary.

Example of Deformation of a Paraboloidal Shell

The example to be treated is that of a paraboloidal shell of second degree, clamped around the edge $\phi = \overline{\phi} < \pi/2$, subjected to a uniform normal load q distributed symmetrically in the region $0 \leq \phi \leq \bar{\phi}$, $\bar{\phi}$ being small. The value of the parameter b is taken as equal to $1/2$. As a result, we take $\bar{\delta}_1 = 1$, $\delta_2 = 0$, and therefore $g_2 = 0$, $\exp(g_2) = 1$. In view of the presence of a distributed load, it becomes necessary to obtain a particular solution of Equation [7]. By the first of Equation [4]

$$rP_z = \left\{\begin{aligned} &-\frac{1}{2} q r^2(\phi), \quad 0 \leq \phi \leq \bar{\phi} \\ &-\frac{1}{2} q r^2(\bar{\phi}), \quad \bar{\phi} \leq \phi \leq \overline{\phi} \end{aligned}\right\} \ldots\ldots [57]$$

As in (9), a suitable particular solution may be approximated by the membrane theory of shells as follows

$$\beta_P = 0 \quad 0 \leq \phi \leq \overline{\phi} \ldots\ldots [58]$$

$$\psi_P = 0 \quad \bar{\phi} \leq \phi \leq \overline{\phi} \ldots\ldots [59a]$$

[6] It is readily seen that, in view of the form of η_0 in Equation [53], the components of the Bessel functions in Equation [50] reduce to the Kelvin functions.

$$\psi_P = -\frac{m}{E}\left(\frac{a_0^2/2}{h_0}\right)^2 \frac{1}{2} q \tan\phi, \quad 0 \leq \phi \leq \bar{\phi} \ldots [59b]$$

The requirement that the stresses and displacements remain finite at $\phi = 0$ demands that $b_1 = b_2 = 0$. Let the subscript I refer to the loaded region $0 \leq \phi \leq \bar{\phi}$ then by Equation [48] with $b_1 = b_2 = 0$, $\beta_1 = (\beta_H)_1$. Similarly, using Equation [49] with $b_1 = b_2 = 0$ and Equation [59b], $\psi_1 = (\psi_H)_1 + (\psi_P)_1$. Denoting the unloaded region, i.e., $\bar{\phi} \leq \phi \leq \overline{\phi}$ by the subscript II, we have $\beta_{II} = (\beta_H)_{II}$ where $(\beta_H)_{II}$ is given by Equation [48] with a_i replaced by c_i, and b_i by d_i. Likewise, $\psi_{II} = (\psi_H)_{II}$ is given by Equation [49] with a_i replaced by c_i, b_i by d_i in the same order as for $(\beta_H)_{II}$. The problem then reduces to finding the six constants of integration a_i, c_i, d_i, $i = 1, 2$. These will be determined by

(i) Continuity conditions at $\phi = \bar{\phi}$

$$\phi = \bar{\phi}: \quad \left.\begin{aligned} \beta_I &= \beta_{II}; \quad (\psi_H)_I + (\psi_P)_I = \psi_{II} \\ \beta'_I &= \beta'_{II}; \quad (\psi_H)_I' + (\psi_P)_I' = \psi_{II}' \end{aligned}\right\} \quad .. [60]$$

(ii) Boundary conditions at the clamped edge

$$\phi = \overline{\phi}: \quad \beta_{II} = 0, \quad u_r = 0$$

or equivalently

$$\left.\begin{aligned} &\beta_{II} = 0 \\ &\psi_{II}' - \nu\left(\frac{\alpha}{R_\phi}\cot\phi\right)\psi_{II} - k^{1/2}\lambda \\ &\qquad \left(\frac{\alpha}{R_\phi}\cot\phi\beta_{II} + \nu\beta_{II}'\right) = \frac{m}{Eh_0^2}\frac{\alpha}{R_\phi}\nu(rP_z) \end{aligned}\right\} \quad .. [61]$$

Carrying out the conditions imposed by Equations [60] and [61], we obtain the following system of simultaneous equations

(a) For the improved theory

$$\left.\begin{aligned} a_1\alpha_{11} - a_2\alpha_{12} - c_1\alpha_{11} + c_2\alpha_{12} - d_1\alpha_{15} + d_2\alpha_{16} &= 0 \\ a_1\alpha_{12} + a_2\alpha_{11} - c_1\alpha_{12} - c_2\alpha_{11} - d_1\alpha_{16} - d_2\alpha_{15} &= \xi_2 \\ a_1\alpha_{21} - a_2\alpha_{22} - c_1\alpha_{21} + c_2\alpha_{22} - d_1\alpha_{25} + d_2\alpha_{26} &= \xi_3 \\ a_1\alpha_{22} + a_2\alpha_{21} - c_1\alpha_{22} - c_2\alpha_{21} - d_1\alpha_{26} - d_2\alpha_{25} &= \xi_4 \\ c_1\alpha_{32} - c_2\alpha_{34} + d_1\alpha_{35} - d_2\alpha_{36} &= 0 \\ c_1\alpha_{41} + c_2\alpha_{44} + d_1\alpha_{45} + d_2\alpha_{46} &= \xi_5 \end{aligned}\right\} \quad .. [62]$$

With the following definitions

$$\left.\begin{aligned} e_1 &= \cos\alpha_1 - \nu k^{1/2}\lambda \sin\alpha_1; \qquad \delta_1 = \cos\alpha_2 + \nu k^{1/2}\lambda \sin\alpha_2 \\ e_2 &= \sin\alpha_1 + \nu k^{1/2}\lambda \cos\alpha_1; \qquad \delta_2 = \sin\alpha_2 - \nu k^{1/2}\lambda \cos\alpha_2 \\ q_1 &= \mathfrak{L} - \frac{2\nu}{\sin 2\phi} - \nu k^{1/2}\lambda\mathfrak{R} \\ q_2 &= \mathfrak{R} - \nu k^{1/2}\lambda\left(\frac{\lambda'}{\lambda} - \mathfrak{L} - \frac{2}{\nu\sin 2\phi}\right) \end{aligned}\right\} \quad .. [63]$$

where

$$\left.\begin{aligned} \alpha_1 &= \frac{1}{2}\left(\chi - \frac{\Omega}{2} - 2g_1\right); \qquad \alpha_2 = \frac{1}{2}\left(\chi - \frac{\Omega}{2} + 2g_1\right) \end{aligned}\right|$$

$$
\left.
\begin{aligned}
\mathfrak{L} &= -\frac{1}{2}\cot\phi - \frac{1}{4}\tan\phi + g_2' \\
&\quad - \frac{1}{4}\frac{H}{p}\cos(\mathfrak{M}-\Omega) \\
&\quad + \frac{1}{2}\sec^{5/3}\phi\,\frac{\rho^{1/2}}{\Gamma}\cos\left(\chi-\frac{\Omega}{2}\right) \\
\mathfrak{N} &= g_1' + \frac{1}{4}\frac{H}{\rho}\sin(\mathfrak{M}-\Omega) \\
&\quad + \frac{1}{2}\sec^{1/3}\phi\,\frac{\rho^{1/2}}{\Gamma}\sin\left(\chi-\frac{\Omega}{2}\right) \\
\rho e^{i\Omega} &= 1 - i\frac{\nu}{\mu^2}\cos\phi\sin^2\phi \\
He^{i\mathfrak{M}} &= -i\frac{\nu}{\mu^2}\sin\phi(2\cos^2\phi-\sin^2\phi) \\
\eta &= i^{3/2}\mu\Delta = \bar{\eta}e^{i\bar{\chi}} \\
\bar{\eta} &= \mu\Gamma, \quad \bar{\chi} = \chi + \frac{3\pi}{4} \\
\Gamma e^{i\chi} &= \bar{\Delta} = \int_0^{\phi}\sec^{5/3}\zeta\left[1-\frac{i\nu}{\mu^2}\cos\zeta\sin^2\zeta\right]^{1/3}d\zeta
\end{aligned}
\right\} \quad \ldots [64]
$$

and S and T are defined in Equation [50] with $2b = 1$, we have

$$
\left.
\begin{aligned}
\alpha_{11} &= [e_1P_1(\bar{\eta},\bar{\chi}) - e_2Q_1(\bar{\eta},\bar{\chi})](\bar{\phi}) \\
\alpha_{12} &= [e_1Q_1(\bar{\eta},\bar{\chi}) + e_2P_1(\bar{\eta},\bar{\chi})](\bar{\phi}) \\
\alpha_{13} &= \left[\bar{e}_1\frac{\partial}{\partial\bar{\eta}}P_1(\bar{\eta},\bar{\chi}) + \bar{e}_2\frac{\partial}{\partial\bar{\eta}}Q_1(\bar{\eta},\bar{\chi})\right](\bar{\phi}) \\
\alpha_{14} &= \left[\bar{e}_1\frac{\partial}{\partial\bar{\eta}}Q_1(\bar{\eta},\bar{\chi}) - \bar{e}_2\frac{\partial}{\partial\bar{\eta}}P_1(\bar{\eta},\bar{\chi})\right](\bar{\phi}) \\
\alpha_{21} &= [e_1P_1(\bar{\eta},\bar{\chi}) - e_2Q_1(\bar{\eta},\bar{\chi})](\overline{\phi}) \\
\alpha_{22} &= [e_1Q_1(\bar{\eta},\bar{\chi}) + e_2P_1(\bar{\eta},\bar{\chi})](\overline{\phi}) \\
\alpha_{23} &= \Big\{Q_1(\bar{\eta},\bar{\chi})(e_1g_1+e_2g_2) + P_1(\bar{\eta},\bar{\chi})(e_2g_1-e_1g_2) \\
&\quad + \mu\sec^{5/3}\phi\rho^{1/2}\left[\frac{\partial}{\partial\bar{\eta}}Q_1(\bar{\eta},\bar{\chi})(\bar{e}_1-\nu k^{1/3}\lambda\bar{e}_2)\right. \\
&\quad \left.\left. - \frac{\partial}{\partial\bar{\eta}}P_1(\bar{\eta},\bar{\chi})(\bar{e}_2+\nu k^{1/3}\lambda\bar{e}_1)\right]\right\}(\overline{\phi}) \\
\alpha_{24} &= \Big\{P_1(\bar{\eta},\bar{\chi})(e_1g_1+e_2g_2) - Q_1(\bar{\eta},\bar{\chi})(e_2g_1-e_1g_2) \\
&\quad + \mu\sec^{5/3}\phi\rho^{1/2}\left[\frac{\partial}{\partial\bar{\eta}}P_1(\bar{\eta},\bar{\chi})(\bar{e}_1-\nu k^{1/3}\lambda\bar{e}_2)\right. \\
&\quad \left.\left. + \frac{\partial}{\partial\bar{\eta}}Q_1(\bar{\eta},\bar{\chi})(\bar{e}_2+\nu k^{1/3}\lambda\bar{e}_1)\right]\right\}(\phi)
\end{aligned}
\right\} \quad \ldots [65]
$$

$\alpha_{ik} = \alpha_{im}$ with P_1 replaced by U_1, Q_1 by V_1 where $k = 5, 6$ and $m = k-4$ for $i = 1, 3$, $m = k-2$ for $i = 5, 6$

$$
\left.
\begin{aligned}
\xi_3 &= 1/2\,[\Gamma(\bar{\phi})\operatorname{cosec}\bar{\phi}]^{-1/3}\sec^{1/4}\bar{\phi}\rho^{1/4}(\bar{\phi})\tan\bar{\phi}\bar{Q} \\
\xi_5 &= -\frac{1}{2\mu}[\Gamma(\bar{\phi})\operatorname{cosec}\bar{\phi}]^{-1/3}\cos^{3/4}\bar{\phi}\rho^{-1/4}(\bar{\phi}) \\
&\qquad \tan\bar{\phi}(\mathfrak{M}-\nu k^{1/3}\lambda')(\bar{\phi})\bar{Q}
\end{aligned}
\right\}
$$

$$
\left.
\begin{aligned}
\xi_4 &= \frac{1}{2\mu}[\Gamma(\bar{\phi})\operatorname{cosec}\bar{\phi}]^{-1/3}\cos^{3/4}\bar{\phi}\rho^{-1/4}(\bar{\phi}) \\
&\qquad [\sec^2\bar{\phi} - \mathfrak{L}(\bar{\phi})\tan\bar{\phi}]\bar{Q} \\
\xi_6 &= -[\nu/2\tan^2\bar{\phi}][\Gamma(\overline{\phi})\operatorname{cosec}\overline{\phi}]^{-1/3} \\
&\qquad \sec^{5/4}\overline{\phi}\rho^{-1/4}(\overline{\phi})\bar{Q} \\
\bar{Q} &= \frac{m}{E}\left(\frac{a_0^{2}/2}{h_0}\right)^2 q
\end{aligned}
\right\} \quad \ldots [66]
$$

(*b*) *Classical Theory.* Following the same procedure as in (*a*) and noting that the Boundary Conditions, Equation [61], are modified by setting $\lambda = 0$, the system of simultaneous equations is again given by Equations [62], but with the expressions for the α_{ij} considerably simplified. For example

$$
\alpha_{11} = \operatorname{ber}_1\bar{s}_0, \quad \alpha_{12} = \left(\mathfrak{L}_0(\overline{\phi}) - \frac{2\nu}{\sin 2\overline{\phi}}\right)\operatorname{bei}_1\bar{s}_0 + \mu\sec^{5/3}\overline{\phi}\,\operatorname{bei}_1'\bar{s}_0
$$

where $\qquad J_0 = s_0(\bar{\phi}) \quad \bar{s}_0 = s_0(\overline{\phi})$

and primes denote differentiation with respect to s_0.

In order to obtain the stress distribution, the system of Equations [62] must be solved for the two theories by using the appropriate α_{ij}.

To demonstrate clearly the predictions of the two theories, the constants are obtained for several cases varying both the span-thickness ratio and the loaded region while keeping the clamped edge $\phi = \bar{\phi}$ constant at $\overline{\phi} = 63^1/_2°$. Then the ratio of the maximum stresses (which occur at the apex) predicted by the two theories for each case is plotted against the value of

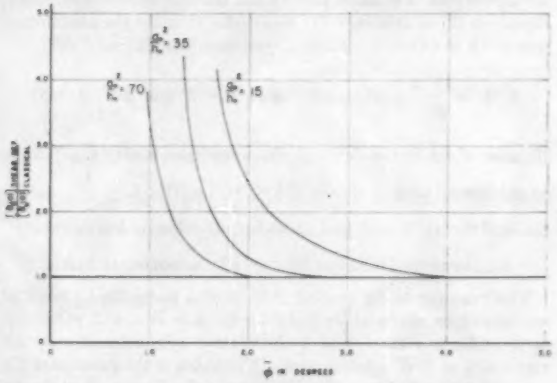

FIG. 2 RATIO OF MAXIMUM BENDING STRESS AT APEX PREDICTED BY IMPROVED THEORY AND BY CLASSICAL THEORY VERSUS $\bar{\phi}$ (LOADED REGION PARAMETER) FOR VARIOUS VALUES OF SPAN-THICKNESS RATIOS

the loading-region parameter as shown in Fig. 2. The error in the classical theory is of no little consequence as the loading area becomes small and depends on the span-thickness ratio, i.e., the "thinness" of the shell, the thicker the shell the greater the error.

ACKNOWLEDGMENT

The author wishes to thank Prof. P. M. Naghdi for his capable direction of this study and for his many enlightening and discerning criticisms.

BIBLIOGRAPHY

1 "The Effect of Transverse Shear Deformation on the Bending of Elastic Shells of Revolution," by P. M. Naghdi, *Quarterly of Applied Mathematics*, vol. 15, 1957, pp. 41–52.

2 "Spannungen in Kugelschalen (Kuppeln)," by H. Reissner, Festschrift Müller-Breslau, 1912, pp. 181–193.

3 "Das Elastizitätsproblem dünner Schalen von Ringflächen-Kugel—oder Kegelform," by E. Meissner, *Physikalische Zeitschrift*, vol. 14, 1913, pp. 343–349.

4 "Über Elastizität und Festigkeit dünner Schalen," by E. Meissner, *Vierteljahrschrift der Naturforschenden Gesellschaft in Zürich*, vol. 60, 1915, pp. 23–47.

5 "Über asymptotische Integration von Differentialgleichungen mit Anwendung auf die Berechnung von Spannungen in Kugelschalen," by O. Blumenthal, Proceedings of the Fifth International Congress of Mathematics, vol. 2, 1912, pp. 319–327.

6 "Some Considerations of the Calculation of Elastic Shells," by E. Steuermann, Proceedings of The Third International Congress for Applied Mechanics, Stockholm, Sweden, vol. 2, 1930, pp. 60–65.

7 "Über die Festigkeit achsensymmetrischer Schalen," by J. Geckeler, *Forschungsarbeiten auf dem Gebiete des Ingenieurwesens*, Heft 276, 1926.

8 "On the Theory of Thin Elastic Shells," by E. Reissner, H. Reissner Anniversary Volume, 1949, pp. 231–247.

9 "On Asymptotic Integration in Shell Theory," by F. Hildebrand, Proceedings of the Third Symposium in Applied Mathematics, vol. 3, 1950, pp. 53–66.

10 "On the Deformation of Elastic Shells of Revolution," by P. M. Naghdi and C. N. De Silva, *Quarterly of Applied Mathematics*, vol. 12, 1955, pp. 369–374.

11 "On the Asymptotic Solution of Ordinary Differential Equations," by R. E. Langer, Transactions of the American Mathematical Society, vol. 33, 1931, pp. 23–64.

12 "On the Asymptotic Solution of Ordinary Differential Equations with Reference to the Stokes' Phenomenon about a Singular Point," by R. E. Langer, Transactions of the American Mathematical Society, vol. 37, 1935, pp. 397–416.

13 "The Effect of Transverse Shear Deformation on the Bending of Elastic Plates," by E. Reissner, Trans. ASME, vol. 67, 1945, p. A-69.

14 "The Effect of Elliptic Holes on the Bending of Thick Plates," by P. M. Naghdi, JOURNAL OF APPLIED MECHANICS, Trans. ASME, vol. 77, 1955, pp. 89–94.

15 "Notes on the Foundations of the Theory of Small Displacements of Orthotropic Shells," by F. Hildebrand, E. Reissner, and G. Thomas, NACA TN 1833, 1949.

16 "Equilibrium of Thin Elastic Shells," by A. E. Green and W. Zerna, *Quarterly Journal of Mechanics and Applied Mathematics*, vol. 3, 1950, pp. 9–22.

17 "Stress-Strain Relations in the Theory of Thin Elastic Shells," by E. Reissner, *Journal of Mathematics and Physics*, vol. 31, 1952, pp. 109–119.

18 "On the Theory of Thin Elastic Shells," by P. M. Naghdi, *Quarterly of Applied Mathematics*, vol. 14, 1957, pp. 369–380.

19 "Deformation of Elastic Ellipsoidal Shells of Revolution," by P. M. Naghdi and C. N. De Silva, Proceedings of the Second U. S. National Congress of Applied Mechanics, ASME, 1955, pp. 333–343.

Appendix

It has been shown by Naghdi (1) that the theory of shells of revolution leading to the differential Equation [39] for paraboloidal shells has Equation [40] as a valid solution if the series

$$\sum_{n=1}^{\infty} y_i^{(n)}(\phi)$$

(in [40]) is uniformly convergent in I_ϕ. Moreover, Equation [40] has [43] as its asymptotic solution if $y_i(\phi)$ given by[7]

$$\left.\begin{aligned} y_1 &= Z(\phi)\eta^{1+b}\left[\eta^{-2b}J_{2b}(\eta) + \left(\frac{\eta}{\mu}\right)^{4(1-b)} O(1)\right] \\ y_2 &= Z(\phi)\eta^{1-3b}\left[\eta^{2b}Y_{2b}(\eta) + \frac{1}{\mu^2}\,O(1)\right] \end{aligned}\right\} \quad \ldots [67]$$

are dominant in [40]. In Equation [67], $O(1)$ denotes a bounded function, η and Δ are as in [44],

$$\mu^2 = \begin{cases} \mu^2/\log \mu^2 & \text{if } b = 1/2 \\ \mu^2 & \text{if } b < 1/2 \end{cases} \quad \ldots [68]$$

and $Z(\phi)$ which is continuous and bounded with respect to μ in I_ϕ is given by

$$Z(\phi) = \sin^{-1/4(\bar{b}-1)}\phi\,\bar{\Psi}^{-1/2}\Delta^{b-1/2} \quad \ldots [69]$$

To establish the convergence of

$$\sum_{n=1}^{\infty} y_i^{(n)}(\phi)$$

in Equation [40], it is desirable to integrate in I_ϕ. For this purpose we recall that in Equation [41] it was assumed, consistent with Equation [8], that

$$\left.\begin{aligned} y_i^{(n)} &= \Theta(x_1 + i\delta x_2)_i^{(n)} \\ y_i^{(0)} &= y_i = \Theta(x_1 + i\delta x_2)_i \end{aligned}\right\} \quad \ldots [70]$$

Hence

$$y_i^{(n+1)} = \int_0^{\eta} K(\eta, \eta_1)\frac{d}{d\eta_1}(x_2)_i^{(n)}(\eta_1)d\eta_1 \quad \ldots [71]$$

and since from Equations [69] and [44]

$$\frac{d\eta}{d\phi} = \eta' = \frac{\mu^{2(1-b)}}{Z^2}\,\eta^{2b-1} \quad \ldots [72]$$

$$\mathbb{W}(y_1, y_2) = \mu^{2(1-b)}\left[1 + \frac{O(1)}{\mu^2}\right]\left[1 + \frac{\eta^{4(1-b)}}{\mu^{4(1-b)}}\,O(1)\right] \quad [73]$$

then by Equations [10], [13], [31], [32], and [68], near the origin

$$\Theta = \left(\frac{\eta}{\mu}\right)^{1-b} O(1) \quad \ldots [74]$$

$$\Phi = \begin{cases} \dfrac{1}{\mu^2}\left(\dfrac{\eta}{\mu}\right)^{-2b} O(1), & 0 < b < 1/2 \\ \dfrac{1}{\mu^2}\left(\dfrac{\eta}{\mu}\right) O(1), & b = 1/2 \end{cases} \quad \ldots [75]$$

$$y_1(\phi) = y_1^{(0)}(\phi) = \eta^{1+b}O(1) \quad \ldots [76]$$

$$y_2(\phi) = y_2^{(0)}(\phi) = \eta^{1-3b}O(1) \quad \ldots [77]$$

and hence for $0 < b < 1/2$

$$K(\eta, \eta_1) = \frac{1}{\mu^{5(1-b)}}\left[\eta_1^{2(1-3b)}\eta^{1+b} - \eta_1^{2(1-b)}\eta^{1-3b}\right]O(1) \quad [78]$$

The uniform convergence of the series

$$\sum_{n=1}^{\infty} y_i^{(n)}(\phi)$$

is now evident. Consider, for example, when $j = 1, 2, 0 < b < 1/2$ the following relation

$$y_i^{(n)}(\phi) = \frac{\eta^{2n(1-2b)+1+(5-4j)b}}{\mu^{4n(1-b)}}\,O(1) \quad \ldots [79]$$

which by virtue of Equations [76] and [77] is valid when $n = 0$. Assuming then that Equation [79] is valid, it follows from Equations [72] and [74] that

[7] As mentioned earlier, Equations [67] are solutions of Equation [39] with the right-hand side set equal to zero. See, in this connection, references (12, 1).

$$\frac{d}{d\eta}(x_2)_j^{(n)} = [2n(1-2b) + 2(3-2j)b] \frac{\eta^{2n(1-2b)-1+2(3-2j)b}}{\mu^{(4n-1)(1-b)}} O(1) \quad [80]$$

Substitution of Equations [78] and [80] in [71] yields

$$y_j^{(n+1)} = \frac{\eta^{2(n+1)(1-2b)+1+(5-4j)b}}{\mu^{4(n+1)(1-b)}} O(1) \quad [81]$$

and this establishes the validity of Equation [79] when n is replaced by $(n+1)$. Hence the series in Equation [40] is uniformly convergent in I_ϕ, $0 < b < \frac{1}{2}$, and Equation [40] may now be written as

$$\gamma_j = y_j + \frac{\eta^{3-(4j-1)b}}{\mu^{4(1-b)}} O(1) \quad [82]$$

Finally, by using Equations [67] and [68], we have

$$\left.\begin{aligned} \gamma_1 &= Z\eta^{1+b}\left[\eta^{-2b}J_{2b}(\eta) + \frac{\eta^{4(1-b)}}{\mu^{4(1-b)}} O(1) + \frac{\eta^{2(1-2b)}}{\mu^{4(1-b)}} O(1)\right] \\ \gamma_2 &= Z\eta^{1-3b}\left[\eta^{2b}Y_{2b}(\eta) + \frac{O(1)}{\mu^2} + \frac{\eta^{2(1-2b)}}{\mu^{4(1-b)}} O(1)\right] \end{aligned}\right\} \quad [83]$$

Similarly for the limiting case of $b = 1/2$, it can be shown that the series in Equation [40] is uniformly convergent in I_ϕ and that γ_j is asymptotic with respect to μ^2 to the dominant term of y_j. Hence an asymptotic solution of Equation [39] with respect to μ^2 is given by

$$\gamma = \sin^{-1/4(\bar{b}-1)}\phi\bar{\Psi}^{-1/2}\Delta^{b-1/2}\eta^{1-b}[A_0 J_{2b}(\eta) + B_0 Y_{2b}(\eta)] \quad [84]$$

Buckling of Thin Cylindrical Shell Under Hoop Stresses Varying in Axial Direction[1]

By N. J. HOFF,[2] BROOKLYN, N. Y.

The buckling of a thin cylindrical shell simply supported along the perimeter of its end sections is analyzed under hoop compressive stresses varying in the axial direction. The thermal stresses arising from a uniform increase in the temperature of the cylinder are determined. It is found that such thermal stresses are not likely to cause elastic buckling. Simple approximate formulas are developed for buckling stress and thermal stress.

Introduction

NONUNIFORM hoop compression can arise in a thin circular cylindrical shell when it is so heated that its temperature varies in the axial direction, or if it is heated uniformly or compressed by a uniform external pressure while the deformations of some of its sections are prevented by geometric constraints. In this paper the cylinder is assumed to be simply supported along the circumference of its end sections; this support does not allow any radial or circumferential displacements but it does not restrict the end rotations nor the axial displacements. If compressive circumferential (hoop) stresses develop in such a cylinder with the intensity of the stress varying in the axial direction, the cylinder buckles if the stresses are high enough. The calculation of the buckling stress under these conditions is the purpose of this paper.

The buckling of thin cylindrical shells provided with equidistant circumferential reinforcements and subjected to uniform external pressure was analyzed earlier by von Sanden and Tölke (1)[3] on the basis of Love's (2) shell theory. A more explicit and complete treatment of the problem of buckling under variable hoop compression is given here with the aid of the equations proposed by Donnell (3). The accuracy of these equations has been discussed by Batdorf (4), Naghdi and Berry (5), Kempner (6), and the author (7) by comparing their solutions with those obtained for the more accurate Flügge (8) equations [see also paper by Moe, reference (9)].[4] They yield the buckling stress with satisfactory accuracy except when the unsupported length of the cylinder is much greater than the diameter; and even for indefinitely long cylinders subjected to uniform external pressure the error committed by using Donnell's equations is only 33 per cent.

The thermal stresses are calculated for the case when the cylinder is uniformly heated, and the critical temperature that causes the cylinder to buckle is determined. It is so high that plastic deformations must take place locally in the neighborhood of the supports where the compressive stresses are the highest before the critical condition is reached. The resulting readjustment in the stresses is likely to prevent elastic buckling.

The Buckling Problem

The buckling of the shell is analyzed on the basis of Donnell's equations written in the nondimensional form used by the author (11) in an earlier paper

$$\nabla^8 w + 4K^4(\partial^4 w/\partial x^4) + 4K^4\nabla^4[(\sigma_\varphi/E)(\partial^2 w/\partial\varphi^2)] = 0 \quad [1]$$

$$\nabla^4 u = \nu(\partial^3 w/\partial x^3) - (\partial^3 w/\partial x \partial\varphi^2) \quad [2]$$

$$\nabla^4 v = (2+\nu)(\partial^3 w/d^2 x\partial\varphi) + (\partial^3 w/\partial\varphi^3) \quad [3]$$

where

$$4K^4 = 12(1-\nu^2)(a/h)^2 \quad [4]$$

with σ_φ the hoop compression, ν Poisson's ratio, a the mean radius, and h the shell thickness. Moreover, ∇^2 is Laplace's operator

$$\nabla^2 = (\partial^2/\partial x^2) + (\partial^2/\partial\varphi^2) \quad [5]$$

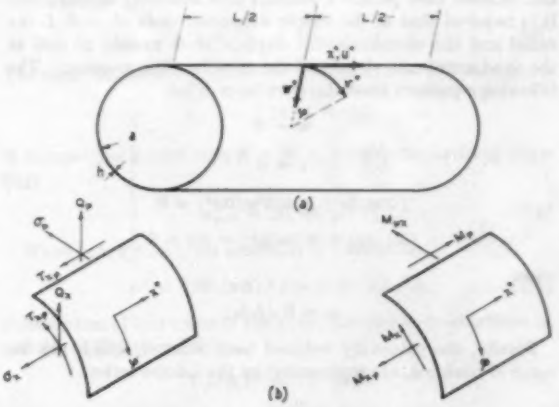

Fig. 1 Sign Convention for Co-Ordinates, Displacements, Stresses, and Stress Resultants

[1] The work, the results of which are presented herein, was carried out under a consulting contract with the Special Defense Projects Department of the General Electric Company, Philadelphia, Pa.

[2] Head, Department of Aeronautical Engineering and Applied Mechanics, Polytechnic Institute of Brooklyn. Now, Head, Division of Aeronautical Engineering, Stanford University, Stanford, Calif. Mem. ASME.

[3] Numbers in parentheses refer to the Bibliography at the end of the paper.

[4] A paper by Naghdi and Cooper (10), published after completion of this manuscript, may be of interest in this connection.

Presented at the Applied Mechanics Division Summer Conference, Berkeley, Calif., June 13–15, 1957, of The American Society of Mechanical Engineers.

Discussion of this paper should be addressed to the Secretary, ASME, 29 West 39th Street, New York, N. Y., and will be accepted until October 10, 1957, for publication at a later date. Discussion received after the closing date will be returned.

Note: Statements and opinions advanced in papers are to be understood as individual expressions of their authors and not those of the Society. Manuscript received by ASME Applied Mechanics Division, August 8, 1956. Paper No. 57—APM-20.

the nondimensional distances and displacements are defined by the equations

$$x = x^*/a \quad u = u^*/a \quad v = v^*/a \quad w = w^*/a \ldots\ldots [6]$$

and the co-ordinate x^* and the displacements, u^*, v^*, w^* are shown in Fig. 1.

In the system employed the components ϵ, γ of the middle-surface strain and the curvatures κ are defined as

$$\left.\begin{aligned} \epsilon_x &= \partial u/\partial x \\ \epsilon_\varphi &= (\partial v/\partial\varphi) - w \\ \gamma_{x\varphi} &= (\partial u/\partial\varphi) + (\partial v/\partial x) \end{aligned}\right\} \ldots\ldots [7]$$

$$\left.\begin{aligned} \kappa_x &= (1/a)(\partial^2 w/\partial x^2) \\ \kappa_\varphi &= (1/a)(\partial^2 w/\partial\varphi^2) \\ \kappa_{x\varphi} &= (1/a)(\partial^2 w/\partial x\partial\varphi) \end{aligned}\right\} \ldots\ldots [8]$$

The membrane stresses developing in consequence of the deformations are

$$\left.\begin{aligned} \sigma_x &= [E/(1-\nu^2)][(\partial u/\partial x) + \nu(\partial v/\partial\varphi) - \nu w] \\ \sigma_\varphi &= [E/(1-\nu^2)][\nu(du/\partial x) + (\partial v/\partial\varphi) - w] \\ \tau_{x\varphi} &= [E/2(1+\nu)][(\partial u/\partial\varphi) + (\partial v/\partial x)] \end{aligned}\right\} \ldots [9]$$

where E is Young's modulus. The mor[illegible]ultants, shown in Fig. 1 in accordance with the right-han[illegible] can be given as

$$\left.\begin{aligned} M_x &= -(D/a)[(\partial^2 w/\partial x^2) + \nu(\partial^2 w/\partial\varphi^2)] \\ M_\varphi &= -(D/a)[(\partial^2 w/\partial\varphi^2) + \nu(\partial^2 w/\partial x^2)] \\ M_{x\varphi} &= [(1-\nu)D/a](\partial^2 w/\partial x\,\partial\varphi) \end{aligned}\right\} \ldots [10]$$

where

$$D = Eh^3/[12(1-\nu^2)] \ldots\ldots [11]$$

The effective shear resultants in the sense of Kirchhoff are

$$\left.\begin{aligned} Q_{x.\mathrm{eff}} &= -(D/a^2)[(\partial^3 w/\partial x^3) + (2-\nu)(\partial^3 w/\partial x\,\partial\varphi^2)] \\ Q_{\varphi.\mathrm{eff}} &= -(D/a^2)[(\partial^3 w/\partial\varphi^3) + (2-\nu)[\partial^3 w/\partial x^2\,\partial\varphi)] \end{aligned}\right\} \ldots [12]$$

The boundary conditions of the problem will be stated in the conventional manner, because they represent a reasonable approximation to conditions that may actua[illegible]y exist in the structure, and because they permit a solution in a relatively simple form. It is required that at the simply supported ends $x^* = 0$, L the radial and the circumferential displacements vanish, as well as the axial membrane stress and the axial bending moment. The following equations must therefore be satisfied

$$\left.\begin{aligned} w &= 0 \\ v &= 0 \\ (\partial^2 w/\partial x^2) + \nu(\partial^2 w/\partial\varphi^2) &= 0 \\ (\partial u/\partial x) + \nu(\partial v/\partial\varphi) - \nu w &= 0 \end{aligned}\right\} \ldots\ldots [13]$$

when

$$x = 0, (L/a)$$

Finally, the externally induced hoop stresses, which are the cause of buckling, are represented by the infinite series

$$\sigma_\varphi = RE \sum_{m=0}^{\infty} s_m \cos(m\pi x/\lambda) \ldots\ldots [14]$$

where

$$\lambda = L/a \ldots\ldots [15]$$

R is a multiplying factor (a number), and a positive stress σ_φ is a compressive hoop stress.

Solution. It is easy to check that the boundary condtions are identically satisfied if the solution is assumed in the form

$$\left.\begin{aligned} w &= \cos n\varphi \sum_{m=1}^{\infty} a_m \sin(m\pi x/\lambda) \\ u &= \cos n\varphi \sum_{m=1}^{\infty} b_m \cos(m\pi x/\lambda) \\ v &= \sin n\varphi \sum_{m=1}^{\infty} c_m \sin(m\pi x/\lambda) \end{aligned}\right\} \ldots\ldots [16]$$

Here a_m, b_m, c_m are coefficients to be determined in such a manner as to satisfy the differential equations. Substitution in Equation [2] yields the requirement

$$b_m = (m\pi/\lambda)\,\frac{n^2 - \nu(m\pi/\lambda)^2}{[(m\pi/\lambda)^2 + n^2]^2}\,a_m \ldots\ldots [17]$$

This relationship explains why the term multiplied by b_0 was omitted from Equations [16]; it would have had to vanish as a_0 is zero.

Substitution in Equation [3] leads to the condition

$$c_m = n\,\frac{n^2 + (2+\nu)(m\pi/\lambda)^2}{[(m\pi/\lambda)^2 + n^2]^2}\,a_m \ldots\ldots [18]$$

In the process of satisfying Equation [1] one has to calculate

$$(\partial^2 w/\partial\varphi^2) = -n^2 \cos n\varphi \sum_{m=1}^{\infty} a_m \sin(m\pi x/\lambda) \ldots [19]$$

Hence

$$2(\sigma_\varphi/RE)(\partial^2 w/\partial\varphi^2) =$$

$$-2n^2 \cos n\varphi \left[\sum_{q=1}^{\infty} a_q \sin(q\pi x/\lambda)\right]\left[\sum_{m=0}^{\infty} s_m \cos(m\pi x/\lambda)\right]$$

$$= -n^2 \cos n\varphi \sum_{q=1}^{\infty}\sum_{m=0}^{\infty} a_q s_m \left\{\sin\frac{(q+m)\pi x}{\lambda} + \sin\frac{(q-m)\pi x}{\lambda}\right\} \ldots [20]$$

The double infinite series in the last member of this equation has the typical term A_p

$$A_p = -n^2 \cos n\varphi \sin(p\pi x/\lambda) \times \left\{\sum_{q=1}^{p} a_p s_{p-q} + \sum_{q=p}^{\infty} a_q s_{q-p} - \sum_{q=1}^{\infty} a_q s_{q+p}\right\} \ldots [21]$$

Consequently

$$4K^4\nabla^4[(\sigma_\varphi/E)(\partial^2 w/\partial\varphi^2)]$$

$$= -2K^4 R n^2 \cos n\varphi \sum_{p=1}^{\infty} \left\{[(p\pi/\lambda)^2 + n^2]^2 \left[\sum_{q=1}^{p} a_q s_{p-q} + \sum_{q=p}^{\infty} a_q s_{q-p} - \sum_{q=1}^{\infty} a_q s_{p+q}\right] \sin(p\pi x/\lambda)\right\} \ldots [22]$$

Also

$$\nabla^8 w = \cos n\varphi \sum_{m=1}^{\infty} [(m\pi/\lambda)^2 + n^2]^4 a_m \sin (m\pi x/\lambda) \quad [23]$$

$$4K^4(\partial^4 w/\partial x^4) = 4K^4 \cos n\varphi \sum_{m=1}^{\infty} (m\pi/\lambda)^4 a_m \sin (m\pi x/\lambda) \quad [24]$$

Equation [1] is satisfied if the sum of the right-hand members of Equations [22], [23], and [24] vanishes identically. This means that the sums of the multipliers of like trigonometric terms must vanish. If the notation

$$U_m = \frac{[(m\pi/\lambda)^2 + n^2]^4 - 4K^4(m\pi/\lambda)^4}{2K^4 n^2[(m\pi/\lambda)^2 + n^2]^2} \quad [25]$$

$$r = (1/R) \quad [26]$$

is introduced, the conditions of equilibrium can be written in the form

$$\sum_{q=1}^{m-1} a_q(s_{m-q} - s_{m+q}) - a_m(rU_m - 2s_0 + s_{2m}) + \sum_{q=m+1}^{\infty} a_q(s_{q-m} - s_{q+m}) = 0 \quad [27]$$

This equation must be satisfied for every value of m. The matrix of the multipliers of a_p is

$$M = \begin{pmatrix} rU_1 - 2s_0 + s_2 & -s_1 + s_3 & -s_2 + s_4 & -s_3 + s_5 & \dots \\ -s_1 + s_3 & rU_2 - 2s_0 + s_4 & -s_1 + s_5 & -s_2 + s_6 & \dots \\ -s_2 + s_4 & -s_1 + s_5 & rU_3 - 2s_0 + s_6 & -s_1 + s_7 & \dots \\ -s_3 + s_5 & -s_2 + s_6 & -s_1 + s_7 & rU_4 - 2s_0 + s_8 & \dots \\ \cdot & \cdot & \cdot & \cdot & \\ \cdot & \cdot & \cdot & \cdot & \\ \cdot & \cdot & \cdot & \cdot & \end{pmatrix} \quad [28]$$

As the set of linear equations whose matrix is given in Equation [28] is homogeneous, a nontrivial solution exists only if the determinant of the matrix vanishes. This condition will now be discussed in some detail for a few particular cases.

Single Hoop-Stress Term s_0. The matrix of the homogeneous set of linear equations given in Equation [28] naturally simplifies if the hoop stress can be represented by a few terms of the infinite series of Equation [14]. For instance, when the hoop compression is uniform over the length of the cylinder

$$\left.\begin{aligned} s_0 &= 1 \\ s_m &= 0 \quad \text{when} \quad m \neq 0 \end{aligned}\right\} \quad [29]$$

the matrix reduces to

$$M_0 = \begin{pmatrix} rU_1 - 2 & 0 & 0 & \dots \\ 0 & rU_2 - 2 & 0 & \dots \\ 0 & 0 & rU_3 - 2 & \dots \\ \cdot & \cdot & \cdot & \\ \cdot & \cdot & \cdot & \\ \cdot & \cdot & \cdot & \end{pmatrix} \quad [30]$$

For buckling, the determinant formed of the coefficients of the linear equations must vanish. But the value of this determinant is simply the product of all the principal diagonal elements since all the other elements are zero. This product vanishes if any of its factors vanishes. Thus the coefficients R corresponding to the various distinct modes are

$$\left.\begin{aligned} R_1 &= (1/r_1) = (U_1/2) \\ R_2 &= (1/r_2) = (U_2/2) \\ R_3 &= (1/r_3) = (U_3/2) \\ &\cdot \quad \cdot \quad \cdot \\ &\cdot \quad \cdot \quad \cdot \\ &\cdot \quad \cdot \quad \cdot \end{aligned}\right\} \quad [31]$$

Because of Equation [25] we have

$$R_m = \frac{[(m\pi/\lambda)^2 + n^2]^4 + 4K^4(m\pi/\lambda)^4}{4K^4 n^2[(m\pi/\lambda)^2 + n^2]^2} \quad [32]$$

Naturally of greatest practical interest is the lowest buckling load, and thus the lowest value of R_m. For a fixed value of n, R_m has its least value when $m = 1$. Hence under uniform compression the shell buckles into a single half wave in the axial direction at the value

$$R_1 = \frac{[(\pi/\lambda)^2 + n^2]^4 + 4K^4(\pi/\lambda)^4}{4K^4 n^2[(\pi/\lambda)^2 + n^2]^2} \quad [33]$$

This result agrees, except for its form, with Equation [B6] of Batdorf's paper (4).

The value of n that makes R_1 a minimum is certainly greater than π/λ. If n is considered a continuous variable, a formal minimization with respect to n yields the condition

$$\frac{[n^4 - (\pi/\lambda)^4][n^2 + (\pi/\lambda)^2]^2}{(\pi/\lambda)^4[3n^2 + (\pi/\lambda)^2]} = 4K^4 \quad [34]$$

As this condition is an algebraic equation of the fifth degree in n^2, in general it is more convenient to compute R from Equation [33] for a number of values of n and to determine the minimum numerically rather than to solve Equation [34] analytically.

A numerical example has been worked out for the following values of the parameters

$$a = 10 \text{ in.} \quad L = 3.14 \text{ in.} \quad h = 0.0331 \text{ in.} \quad \nu = 0.3 \quad [35]$$

This implies

$$\pi/\lambda = 10 \qquad 4K^4 = 10^6 \quad [36]$$

The minimum buckling stress corresponds to $n = 19$; its value is

$$\sigma_{\varphi,cr} = 7.18 \times 10^{-4} E \quad [37]$$

If the material is steel with $E = 29 \times 10^6$ psi, the buckling stress is

$$\sigma_{\varphi,cr} = 20{,}800 \text{ psi} \quad [38]$$

When $(n\lambda/\pi)^2 \gg 1$, the condition of a minimum is

$$n^2 = 1.86\,(\pi K/\lambda) = 5.85\,(Ka/L) \quad [39]$$

Substitution of this value in the inequality yields the condition of validity of Equation [39] as

$$0.763(L^2/a\lambda)^{1/2} \gg 1 \quad [40]$$

This condition is satisfied by most thin-walled cylinders. Substitution of the value of n^2 in Equation [33] gives

$$R_{\cdot} = 0.92(h^2/aL^2)^{1/3} \quad [41]$$

With this value the critical stress becomes

$$\sigma_{0.cr} = 0.92E(h^2/aL^2)^{1/3} \quad [42]$$

These simplified formulas yield $n = 20.4$ and $\sigma_{0.cr} = 16{,}000$ psi for the numerical example; the latter represents an error of 23 per cent as compared to the value given in Equation [38]. However, the cylinder is very short and the left-hand member of inequality 40 is only 4.17.

Equation [42] can be derived from the approximate formulas in Batdorf's paper[4] by simple substitutions.

Single Hoop-Stress Term s_1. When the hoop stress is represented by

$$\left.\begin{aligned} s_1 &= 1 \\ s_m &= 0 \quad \text{when} \quad m \neq 1 \end{aligned}\right\} \quad [43]$$

all the modes are present simultaneously in the deflected shape. The matrix given in Equation [28] reduces to

$$M_1 = \begin{pmatrix} rU_1 & -1 & 0 & 0 & \cdots \\ -1 & rU_2 & -1 & 0 & \cdots \\ 0 & -1 & rU_3 & -1 & \cdots \\ 0 & 0 & -1 & rU_4 & \cdots \\ \cdot & \cdot & \cdot & \cdot & \\ \cdot & \cdot & \cdot & \cdot & \end{pmatrix} \quad [44]$$

The part of the matrix shown can be transformed into a triangular one by dividing the last row by rU_4 and adding the resulting new row to the one but last row. This operation replaces the -1 in the last column by zero. Next the new row is divided by $rU_3 - (1/rU_4)$ and the resulting new row is added to the third row from the bottom in the matrix of Equation [44]. This replaces the -1 in the second row and the third column by zero. If the operations are continued until the -1 term in the first row is cancelled, the principal diagonal element in the first row and the first column is replaced by the continuous fraction

$$\left.\begin{aligned} P_1 = rU_1 - \cfrac{1}{rU_2 - \cfrac{1}{rU_3 - \cfrac{1}{rU_4 - \cdots}}} \end{aligned}\right\} \quad [45]$$

If the entire infinite set of equations is transformed in this manner, P_1 is an infinite continuous fraction. The second element P_2 on the principal diagonal is a similar infinite fraction, but it begins with rU_2 and not with rU_1; the third term is an infinite fraction beginning with rU_3, and so on.

As the matrix is now a triangular one, the condition of buckling is that the product of the principal diagonal elements vanish. This condition will now be used in a step-by-step approximation procedure.

If only the first of the equations of the set represented by the matrix of Equation [44] is taken into account, the buckling condition is

$$rU_1 = 0 \quad [46]$$

This corresponds to

$$r = 0 \quad R^{(1)} = \infty \quad [47]$$

which is a rather useless upper limit on the buckling load. When two equations are taken into account, buckling takes place when

$$\begin{vmatrix} rU_1 - \dfrac{1}{rU_2} & 0 \\ -1 & rU_2 \end{vmatrix} = 0 \quad [48]$$

The determinental equation is therefore

$$r^2U_1U_2 - 1 = 0 \quad [49]$$

whose solution is

$$R^{(2)} = (1/r) = \pm(U_1U_2)^{1/2} = \pm U_1(U_2/U_1)^{1/2} \quad [50]$$

As U_2 is always larger than U_1, the amplitude of the critical stress is larger than U_1E. It should be remembered that the critical stress was found to be $(U_1/2)E$ in the uniform hoop stress case.

If three equations are taken into account simultaneously, similar manipulations lead to

$$R^{(3)} = \pm(U_1U_2)^{1/2}/[1 + (U_1/U_3)]^{1/2} \quad [51]$$

Hence in a third approximation the factor R in the buckling-stress formula is smaller than the geometric mean of U_1 and U_2. It is of interest to note that the sign of the hoop stress can be reversed without changing the absolute value of the maximum stress corresponding to the critical condition. This result could have been anticipated on physical grounds; it does not matter whether the compression zone is near the edge at $x = 0$ or at $x = \lambda$.

With the values of the numerical example one obtains from Equation [51] the smallest buckling stress when $n = 22$. Its value is

$$\left.\begin{aligned} \sigma_{\varphi.cr} &= 2.29 \times 10^{-3}E \cos(\pi x/\lambda) \\ &= 66{,}400 \cos(\pi x/\lambda) \text{ psi} \end{aligned}\right\} \quad [52]$$

It is worth noting that the third approximation to the buckling-stress amplitude differs only 7.4 per cent from the second approximation.

Single Hoop-Stress Term s_2. When the hoop stress is represented by

$$s_2 = 1 \quad s_m = 0 \quad \text{when} \quad m \neq 2 \quad [53]$$

Equation [28] becomes

$$M_2 = \begin{pmatrix} rU_1 + 1 & 0 & -1 & 0 & 0 & \cdots \\ 0 & rU_2 & 0 & -1 & 0 & \cdots \\ -1 & 0 & rU_3 & 0 & -1 & \cdots \\ 0 & -1 & 0 & rU_4 & 0 & \cdots \\ 0 & 0 & -1 & 0 & rU_5 & \cdots \\ \cdot & \cdot & \cdot & \cdot & \cdot & \\ \cdot & \cdot & \cdot & \cdot & \cdot & \\ \cdot & \cdot & \cdot & \cdot & \cdot & \end{pmatrix} \quad [54]$$

Buckling can take place according to a symmetric or to an antisymmetric pattern. The condition of the latter is in a two-equation approximation

$$R = \pm(U_2U_4)^{1/2} \quad [55]$$

The buckling condition of symmetric buckling is, if a single equation is taken into account

$$R^{(1)} = -U_1 \quad [56]$$

With two equations the buckling condition becomes

$$U_1U_2r^2 + U_2r - 1 = 0 \quad [57]$$

The solution is

$$r = -(1/2U_1)\{1 \pm [1 + 4(U_1/U_2)]^{1/2}\}$$

[4] Reference (4), p. 288.

If the absolute value of $4(U_1/U_2)$ is equal to or less than unity, the expression under the root sign can be expanded according to the binomial theorem. As the larger one of the two values of r corresponds to the smaller buckling stress, only the expression with the positive sign before the root expression will be taken into account. One obtains

$$R^{(2)} = -U_1/[1 + (U_1/U_2) - (U_1/U_2)^2 + 2(U_1/U_2)^3 - 5(U_1/U_2)^4 + \ldots] \quad [58]$$

This smaller coefficient R, as well as the only one obtained from the single-equation solution, is negative. This means that the middle of the cylinder is compressed while the regions near the supported edges are in tension. The situation is reversed when the minus sign holds before the root expression; then the buckling stress is much higher.

If the numerical example is continued, the lowest buckling stress corresponds to $n = 19$; its value is from Equation [58]

$$\left.\begin{aligned} \sigma_{\varphi,cr} &= -12.92 \times 10^{-4} E \cos(2\pi x/\lambda) \\ &= -37{,}400 \cos(2\pi x/\lambda) \text{ psi} \end{aligned}\right\} \quad [59]$$

Equation [55] yields a value 11 per cent higher than this value.

Combination of Hoop-Stress Terms s_0 and s_2. When a second harmonic of amplitude p is superimposed upon a constant hoop compression of intensity 1, one has

$$\left.\begin{aligned} s_0 &= 1 \qquad s_2 = p \\ s_m &= 0 \quad \text{when} \quad m \neq 0,2 \end{aligned}\right\} \quad [60]$$

In this case the matrix reduces to

$$M_{0,2} = \begin{pmatrix} rU_1 - 2 + p & 0 & -p & 0 & 0 & \ldots \\ 0 & rU_2 - 2 & 0 & -p & 0 & \ldots \\ -p & 0 & rU_3 - 2 & 0 & -p & \ldots \\ 0 & -p & 0 & rU_4 - 2 & 0 & \ldots \\ 0 & 0 & -p & 0 & rU_5 - 2 & \ldots \\ \cdot & \cdot & \cdot & \cdot & \cdot & \\ \cdot & \cdot & \cdot & \cdot & \cdot & \\ \cdot & \cdot & \cdot & \cdot & \cdot & \end{pmatrix} \quad [61]$$

Again, the buckling pattern is either symmetric or antisymmetric. The condition of symmetric buckling is

$$\begin{vmatrix} rU_1 - 2 + p & -p & 0 & 0 & \ldots \\ -p & rU_2 - 2 & -p & 0 & \ldots \\ 0 & -p & rU_3 - 2 & -p & \ldots \\ 0 & 0 & 0 & rU_4 - 2 & \ldots \\ \cdot & \cdot & \cdot & \cdot & \\ \cdot & \cdot & \cdot & \cdot & \\ \cdot & \cdot & \cdot & \cdot & \end{vmatrix} = 0 \quad [62]$$

A linear transformation reduces the matrix to the triangular form with the leading principal diagonal element given by the infinite continuous fraction

$$\left.\begin{aligned} P_1 &= rU_1 - 2 + p \\ &\quad - \cfrac{p^2}{rU_2 - 2 - \cfrac{p^2}{rU_3 - 2 - \cfrac{p^2}{rU_4 - 2 \ldots}}} \end{aligned}\right\} \quad [63]$$

When one mode alone is taken into account, the buckling condition is

$$rU_1 - 2 + p = 0 \quad [64]$$

with the solution

$$R^{(1)} = U_1/(2 - p) \quad [65]$$

Some of the consequences of this formula are shown in Fig. 2 in which three critical-stress patterns are plotted to the same scale.

With the first two symmetric modes the condition becomes

$$(rU_1 - 2 + p)(rU_2 - 2) - p^2 = 0 \quad [66]$$

The solution of this quadratic in r is

$$\frac{1}{R^{(2)}} = r^{(2)} = \left[\frac{1}{U_2} + \frac{2 - p}{2}\frac{1}{U_1}\right][1 \pm (1 - S)^{1/2}] \quad [67]$$

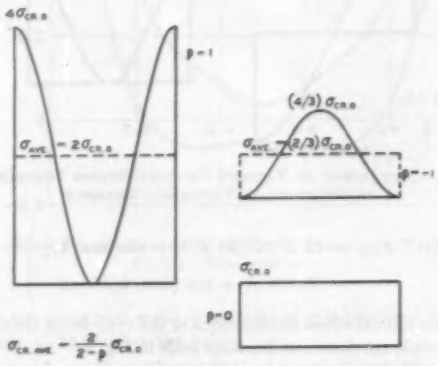

FIG. 2 ILLUSTRATION OF SIMPLE BUCKLING FORMULA

with

$$S = \frac{2(2 - p) - p^2}{\left[(U_1/U_2)^{1/2} + \frac{2 - p}{2}(U_2/U_1)^{1/2}\right]^2} \quad [68]$$

When $S \leq 1$, the square-root expression can be expanded and the smaller one of the two values of $R^{(2)}$ becomes

$$\frac{1}{R^{(2)}} = r^{(2)} = \frac{2 - p}{U_1}\left[1 + \frac{2}{2 - p}\frac{U_1}{U_2}\right] \times [1 - (1/4)S - (1/16)S^2 - (1/32)S^3 - \ldots] \quad [69]$$

The numerical example is now continued with the assumption

$$p = 1 \quad [70]$$

Values computed from Equations [65] and [69] are as follows

n =	19	20	21	23	25
$10^4 R^{(1)}$ =	14.36	14.50	14.85	15.92	17.44
$10^4 R^{(2)}$ =	13.23	12.45	12.72	13.23	14.06

Again the differences between the first and the second approximations are reasonably small. The minimal stress now occurs at $n = 20$ rather than at $n = 19$. Its value is

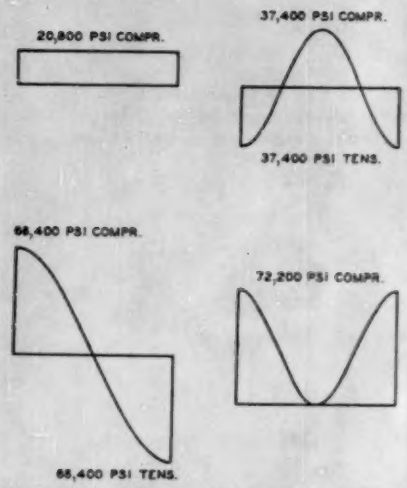

FIG. 3 COMPARISON OF VARIOUS CRITICAL STRESS DISTRIBUTIONS IN CYLINDER OF NUMERICAL EXAMPLE

$$\left.\begin{aligned}\sigma_{\varphi,cr} &= 12.45 \times 10^{-4}E[1 + \cos(2\pi x/\lambda)] \\ &= 36{,}100\ [1 + \cos\ (2\pi x/4/\lambda)\ \text{psi}\end{aligned}\right\} \quad \ldots [71]$$

The four critical-stress distributions of the cylinder of the numerical example are drawn to the same scale in Fig. 3.

Proof That the Buckling Load Obtained Is an Upper Limit. From Equation [62] the conditions of stability in the first and in the successively improved approximations can be written as

$$(1)\quad P_1 > 0 \quad \ldots [72]$$

$$(2)\quad P_1(rU_3 - 2) - p^2 > 0 \quad \ldots [73]$$

$$(3)\quad D_3(rU_4 - 2) - p^2P_1 > 0 \quad \ldots [74]$$

$$(4)\quad D_4(rU_7 - 2) - p^2D_2 > 0 \quad \ldots [75]$$

. . . . .

where . . . . .

$$P_1 = rU_1 - 2 + p \quad \ldots [76]$$

is the leading principal diagonal element of the matrix and D_2, D_3, . . . are the determinants formed of the first two, three, . . . rows and columns of the matrix.

Let us assume that p has a fixed finite value. As U_m is a positive quantity, Equation [72] is always satisfied if r is chosen large enough. That value of r at which Equation [72] ceases to be satisfied as r is gradually decreased is denoted $r^{(1)}$. There are certainly values of r greater that $r^{(1)}$ for which Equation [73] is not true because p^2 is a positive quantity. If r is gradually decreased from some large value until Equation [73] ceases to be satisfied, the value of r at which this happens is designated as $r^{(2)}$. It follows from the reasoning given that

$$r^{(2)} > r^{(1)} \quad \ldots [77]$$

A similar argument would show that the value $r^{(3)}$ at which Equation [74] ceases to be satisfied is greater than $r^{(2)}$. One arrives therefore at the result that

$$r^{(q)} > r^{(q-1)} > r^{(q-2)} > \ldots > r^{(2)} > r^{(1)} \quad \ldots [78]$$

which shows that any value obtained for r in the manner described from a finite number of the rows and columns of the determinant of Equation [62] is smaller than the value defined by the entire infinite set. Hence all the approximate values of r calculated from Equation [62] are lower bounds and the corresponding values of R are upper bounds. Fortunately the numerical example shows that the approximate values converge rapidly toward the exact value.

These conclusions are not unexpected. As the method used to derive the buckling load is essentially the Galerkin method, and since all the deflection functions used in the calculation (Equations [16]) satisfy both the geometric and the equilibrium boundary conditions, each approximate solution corresponds to a similar one obtainable through the Rayleigh-Ritz method. The Rayleigh-Ritz solutions are known to represent upper bounds and they usually converge rapidly to the exact solution.

The conclusions just given also hold true for the buckling loads derivable from the matrices of Equations [44] and [53].

THERMAL STRESSES

When the temperature of the cylinder rises uniformly, and this rise is designated by T, it is convenient to take advantage of the conditions of symmetry and to place the origin of the system of co-ordinates in the middle of the cylinder. Under these conditions the problem can be formulated mathematically in the following manner

$$\left.\begin{aligned}&(d^4w/dx^4) + 4K^4w + 4K^4\alpha T = 0 \\ &w = d^2w/dx^2 = 0 \quad \text{when} \quad x = \pm(\lambda/2)\end{aligned}\right\} \quad \ldots [79]$$

with α the coefficient of thermal expansion. When T is a constant, a suitable particular solution of the differential equation is

$$w_p = -\alpha T \quad \ldots [80]$$

The complementary solution can be given as

$$w_c = A_1 \cosh Kx \cos Kx + A_2 \sinh kx \sin Kx \quad \ldots [81]$$

The boundary conditions are satisfied if

$$\left.\begin{aligned}A_1 &= \frac{\cosh\beta\cos\beta}{\sinh^2\beta + \cos^2\beta}\,\alpha T = C_1\alpha T \\ A_2 &= \frac{\sinh\beta\sin\beta}{\sinh^2\beta + \cos^2\beta}\,\alpha T = C_2\alpha T\end{aligned}\right\} \quad \ldots [82]$$

with

$$\beta = K\lambda/2 \quad \ldots [83]$$

If the basic parameters of the cylinder are introduced, β is expressed as

$$\beta = (1/2)[3(1 - \nu^2)]^{1/4}(L/ah)^{1/2} \quad \ldots [84]$$

With $\nu = 0.3$ this becomes

$$\beta = 0.643(L^2/ah)^{1/2} \quad \ldots [85]$$

In the numerical example discussed earlier the value of β is 3.51.

The hoop stress is

$$\sigma_\varphi = E(w + \alpha T) = Ew_c \quad \ldots [86]$$

with the positive sign again indicating compression. Substitutions yield

$$\sigma_\varphi = E\alpha T(C_1 \cosh Kx \cos Kx + C_2 \sinh Kx \sin Kx) \quad \ldots [87]$$

At the supported ends this reduces to

$$\sigma_{\varphi,\text{end}} = E\alpha T \quad \ldots [88]$$

and at the middle of the cylinder to

$$\sigma_{\varphi,\text{middle}} = C_1E\alpha T \quad \ldots [89]$$

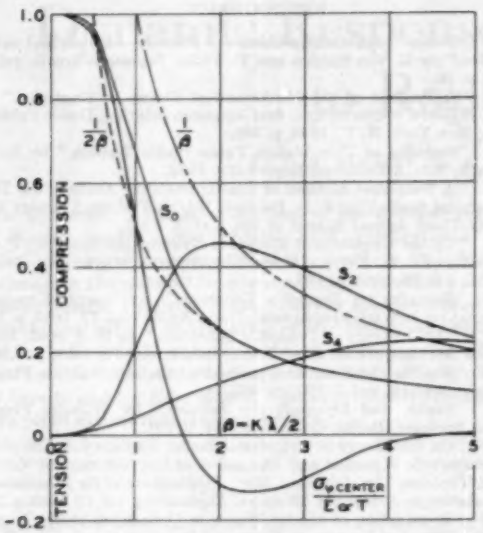

FIG. 4 THERMAL STRESSES IN CYLINDER

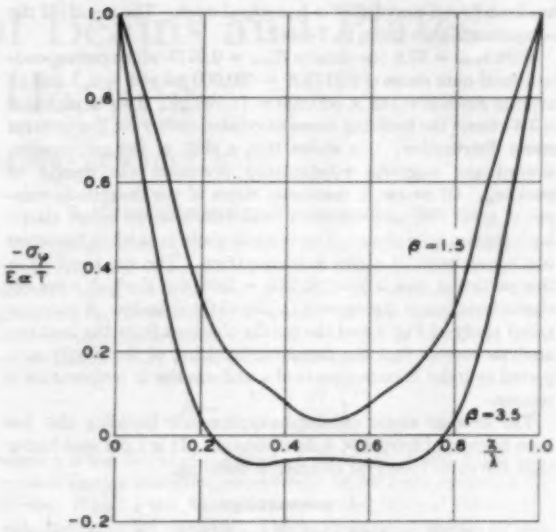

FIG. 5 HOOP STRESS VARIATION IN AXIAL DIRECTION WITH $\beta = K\lambda/2$ AS PARAMETER

Values of C_1 are plotted against β in Fig. 4. When $\beta > 3$, the functions $\cosh \beta$ and $\sinh \beta$ are almost equal. For this reason the absolute value of C_1 can be given as

$$|C_1| \leq 1/\cosh \beta \qquad \beta > 3 \ldots\ldots\ldots\ldots [90]$$

The average hoop stress over the length of the cylinder is

$$\sigma_{\varphi,\text{avg}} = s_0 E\alpha T \ldots\ldots\ldots\ldots [91]$$

with

$$s_0 = \frac{1}{2\beta} \frac{\sin 2\beta + \sinh 2\beta}{\cos 2\beta + \cosh 2\beta} \ldots\ldots\ldots\ldots [92]$$

When β is large, say greater than 4, the equation reduces to

$$\sigma_{\varphi,\text{avg}} \simeq (1/2\beta) E\alpha T \qquad \beta > 4 \ldots\ldots\ldots\ldots [93]$$

If the thermal stress is represented by a Fourier cosine series, with the two ends of the cylinder at $x = 0, \lambda$

$$\sigma_\varphi = E\alpha T \sum_{m=0,2,4}^{\infty} s_m \cos (m\pi x/\lambda) \ldots\ldots\ldots [94]$$

the expression for s_m is

$$s_m = 2(2/m\pi)^2 \beta \, (\sinh^2 \beta + \cos^2 \beta)^{-1} [4(2/m\pi)^4 \beta^4 + 1]^{-1} \times \{ [2(2/m\pi)^2 \beta^2 - 1] \cos \beta \sin \beta + [2(2/m\pi)^2 \beta^2 + 1] \times \cosh \beta \sinh \beta \} \ldots\ldots [95]$$

When β is large, this expression simplifies to

$$s_m \simeq 2(2/m\pi)^2 \beta [2(2/m\pi)^2 \beta^2 + 1]/[4(2/m\pi)^4 \beta^4 + 1] \ldots [96]$$

When the value of $\beta = K\lambda/2$ is fixed and m is increased beyond all bounds, s_m approaches the value

$$s_m \simeq (8/\pi^2)(\beta/m^2) \ldots\ldots\ldots\ldots [97]$$

Hence the cosine series converges. When m is fixed and β increases without limits, the Fourier coefficient approaches the value

$$s_m \simeq (1/\beta) \ldots\ldots\ldots\ldots [98]$$

Values of s_0, s_2, and s_4 are plotted against β in Fig. 4.

The cylinder of the numerical example is assumed to be heated uniformly. The values of the first eight even-numbered Fourier coefficients are listed as

m =	0	2	4	6	8	10	12	14
s_m =	0.143	0.346	0.208	0.093	0.050	0.031	0.021	0.015

The first eight terms of the Fourier series represent the stress distribution rather accurately except at $x = 0, \lambda$ where the series gives 0.907 instead of 1. The exact stress distribution is shown in Fig. 5. If the values of the coefficients are substituted in the stability determinant derivable from the first five odd-numbered rows and columns of the matrix of Equation [28], the value of r corresponding to symmetric buckling can be calculated from a fifth-degree algebraic equation. As r depends upon the number n of waves in the circumferential direction, the equation must be written and solved for several choices of n before the maximum of r corresponding to the minimum of R_1, that is to the smallest buckling load, can be determined. A procedure in which 2×2, 3×3, 4×4, and 5×5 determinants are evaluated successively

TABLE 1

Order of determinant	n=27	28	29	30	31	32	33	34	35	36
2	40.8	40.8	41	41	41	40.7				
3				55	55.3	55.6	55.3	55.2	54.7	
4				56.8		57.6		57.6		57
5						57.9				

has been found convenient in numerical work. The results of the computations are given in Table 1.

With $r_{max} = 57.9$ one obtains $R_{min} = 0.0173$ which corresponds to a maximum stress of $0.0173\ E = 500{,}000$ psi at $x = 0, \lambda$ and an average stress of $0.143 \times 500{,}000 = 71{,}500$ psi. This latter value is 3.44 times the buckling stress calculated earlier for the uniform stress distribution; this shows that a shift of the compression toward the supports substantially decreases the danger of buckling. Of course, a maximum stress of the magnitude computed gives rise to permanent local deformations before elastic buckling can take place. This is particularly true when the stress is a consequence of a rise in temperature. The rise required in this particular case is $500{,}000/210 = 2380$ deg F which rules out elastic buckling as the cause of failure of the cylinder. A more detailed study of Fig. 4 and the results obtained from the buckling analysis reveals that the danger of buckling of the simply supported cylinder in consequence of a uniform rise in temperature is remote.

The average stress causing antisymmetric buckling also has been calculated from 4×4 determinants. It is 1 per cent higher than the value found for symmetric buckling.

Acknowledgment

The author is grateful to the Special Defense Projects Department of the General Electric Company for permission to publish this paper, and to Profs. S. V. Nardo and Frederick V. Pohle for the computation of the buckling stress corresponding to a uniform temperature rise in the cylinder.

BIBLIOGRAPHY

1 "Ueber Stabilitätsprobleme dünner, kreiszylindrischer Schalen," by K. von Sanden and F. Tölke, *Ingenieur-Archiv*, vol. 3, 1932, p. 24.

2 "A Treatise on the Mathematical Theory of Elasticity," by A. E. H. Love, fourth edition, first American printing, Dover Publications, New York, N. Y., 1944, p. 568.

3 "Stability of Thin-Walled Tubes Under Torsion," by L. H. Donnell, NACA Technical Report 479, 1933.

4 "A Simplified Method of Elastic Stability Analysis for Thin Cylindrical Shells," by S. B. Batdorf, NACA Technical Report 874, Thirty-Third Annual Report of the NACA, 1947.

5 "On the Equations of Motion of Cylindrical Shells," by P. M. Naghdi and J. G. Berry, JOURNAL OF APPLIED MECHANICS, Trans. ASME, vol. 76, 1954, p. 160.

6 "Remarks on Donnell's Equations," by Joseph Kempner, JOURNAL OF APPLIED MECHANICS, Trans. ASME, vol. 77, 1955, p. 117.

7 "The Accuracy of Donnell's Equations," by N. J. Hoff, JOURNAL OF APPLIED MECHANICS, Trans. ASME, vol. 77, 1955, p. 329.

8 "Die Stabilität der Kreiszylinderschale," by Wilhelm Flügge, *Ingenieur-Archiv*, vol. 3, 1932, p. 463.

"Statik und Dynamik der Schalen," by Wilhelm Flügge, Julius Springer, Berlin, Germany, 1934, p. 191.

9 "On the Theory of Cylindrical Shells; Explicit Solution of the Characteristic Equation and Discussion of the Accuracy of Various Shell Theories," by Johannes Moe, *Publications of the International Association for Bridge and Structural Engineering*, vol. 13, 1953, p. 283.

10 "Propagation of Elastic Waves in Cylindrical Shells, Including the Effects of Transverse Shear and Rotatory Inertia," by P. M. Naghdi and R. M. Cooper, *Journal of the Acoustical Society of America*, vol. 28, 1956, p. 56.

11 "Boundary-Value Problems of the Thin-Walled Circular Cylinder," by N. J. Hoff, JOURNAL OF APPLIED MECHANICS, Trans. ASME, vol. 76, 1954, p. 343.

Dynamic Response of Beams and Plates to Rapid Heating[1]

By B. A. BOLEY[2] and A. D. BARBER,[3] NEW YORK, N. Y.

The thermally induced vibrations of rectangular plates and beams under some typical heat applications are studied. The basic parameter of the problem, B, is found to depend on the natural frequency of the structure and on a characteristic thermal time. Curves are presented of the variation with B of the ratio of the deflections calculated including and neglecting the effect of inertia. The role of inertia is found to be important for rapidly applied heat inputs and for thin plates. An approximate formula for its rapid estimation is also presented.

1 Introduction

The analysis of the behavior of various types of structural elements subjected to elevated temperatures is often of paramount importance in the design of high-speed aircraft or projectiles. In order to perform a practical analysis of this kind, it is of course always necessary to make a number of simplifying assumptions; it is the purpose of the present paper to examine the importance of one of these, namely, that concerned with the role of inertia.

It is customary in the analysis of thermal stresses to neglect the effect of inertia altogether. The stresses and deformations are calculated from a predetermined temperature distribution which is, in general, time dependent; time, however, is involved in such an analysis merely as a parameter, so that the structure is in effect considered to assume a succession of steady states. A solution obtained in this manner will be referred to in this paper as a "static" solution.

The assumption that inertia may be disregarded does not seem reasonable for structural elements exposed to rapid heating, as may be encountered, for example, in high-speed propulsion units or in problems of thermal shock. A thermoelastic analysis in which the inertia terms are retained will be referred to in this paper as a "dynamic" solution. Comparisons between static and dynamic solutions for a number of practical problems involving basic structural elements, i.e., beams and plates, are carried out in this paper. The results obtained are presented and discussed in section 2; some details of their derivation appear in sections 3, 4, and 5. Additional information may be found in reference (1).[4]

[1] The work described herein was carried out as part of Contract AF 33(616)-2071, sponsored by the Wright Air Development Center of the U. S. Air Force.

[2] Associate Professor of Civil Engineering, Institute of Flight Structures, Columbia University.

[3] Research Assistant, Institute of Flight Structures, Columbia University.

[4] Numbers in parentheses refer to the Bibliography at the end of the paper.

Presented at the Applied Mechanics Division Summer Conference, Berkeley, Calif., June 13–15, 1957, of The American Society of Mechanical Engineers.

Discussion of this paper should be addressed to the Secretary, ASME, 29 West 39th Street, New York, N. Y., and will be accepted until October 10, 1957, for publication at a later date. Dicusssion received after the closing date will be returned.

Note: Statements and opinions advanced in papers are to be understood as individual expressions of their authors and not those of the Society. Manuscript received by ASME Applied Mechanics Division, August 16, 1956. Paper No. 57—APM-17.

2 Presentation and Discussion of Results

A dynamic solution for a uniform simply supported rectangular beam, subjected to a suddenly applied heat input uniformly distributed along its span, was presented in reference (2). The governing nondimensional parameter of this problem is the ratio of the characteristic thermal time (h^2/κ) to the natural period of vibration; it can therefore be taken as

$$B = \frac{h}{L\sqrt{\kappa}}\left(\frac{EI}{\rho A}\right)^{1/4} \quad \ldots\ldots\ldots\ldots\ldots [1]$$

where h is the height of the beam, L its length, I and A the moment of inertia and area, respectively, of its cross section, ρ its density, E and κ the Young's modulus and thermal diffusivity, respectively, of its material. The importance of inertia in this problem may be seen from Fig. 1, which is a plot of the variation with B of the ratio of the maximum deflection v_{max} of the dynamic solution, to the maximum deflection $v_{st\ max}$ of the static solution. Fig. 1 also shows that the exact results are closely approximated by the relations

$$\frac{v_{max}}{v_{st\ max}} = \begin{cases} 1 + 2e^{-B} & \text{for} \quad B \geq \log_e 2 \approx 0.6931 \\ 2 & \text{for} \quad B \leq \log_e 2 \approx 0.6931 \end{cases} \quad \ldots [2]$$

For purposes of comparison, a second abscissa scale is provided in this figure, giving for each value of B the corresponding thickness of an aluminum beam 10 in. long. An examination of Fig. 1 clearly shows that the dynamic deflection greatly differs from the corresponding static one in the case of thin beams—thinner, for example, than about $^1/_8$ in. Such dimensions are characteristic of plates rather than beams, and it therefore is logical to analyze the corresponding plate problem in detail. This was done for a rectangular plate, as outlined in section 3; the principal results are shown in Fig. 2 in a form similar to that of Fig. 1. Note that the governing parameter is now

$$B_1 = \frac{h}{a\sqrt{\kappa}}\left(\frac{D}{\rho h}\right)^{1/4} \quad \ldots\ldots\ldots\ldots\ldots [3]$$

where a is taken to be the short side of the plate, and where the bending rigidity per unit of width, in terms of Poisson's ratio ν, is

$$D = Eh^3/[12(1 - \nu^2)] \quad \ldots\ldots\ldots\ldots\ldots [3a]$$

An additional parameter is the aspect ratio (a/b) of the plate. The quantity h of the second abscissa scale of Fig. 2 is the thickness of an aluminum plate with $a = 10$ in.

The full-line curve of Fig. 1, and that labeled $a/b = 0$ in Fig. 2, are identical; the other curves of Fig. 2 are similar to it in appearance, the greatest deviation occurring for a square plate ($a/b = 1$). The same general estimate of the importance of inertia therefore holds for plates of all aspect ratios, as well as for beams. For this reason, in the subsequent studies of some more complicated types of heat application, it was considered permissible to restrict the analyses to the case of beams; a correction accounting for different aspect ratios, if necessary, could be estimated with the aid of Fig. 2.

A suddenly applied heat input represents a more severe heating

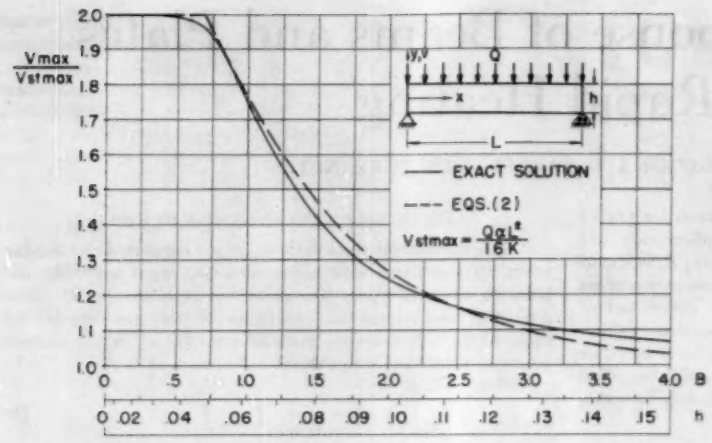

FIG. 1 VARIATION OF RATIO OF DYNAMIC MAXIMUM DEFLECTION TO STATIC MAXIMUM DEFLECTION WITH PARAMETER B, AND WITH THICKNESS OF A RECTANGULAR ALUMINUM BEAM WITH $L = 10$ IN., AT $x = (L/2)$, UNDER SUDDEN HEATING

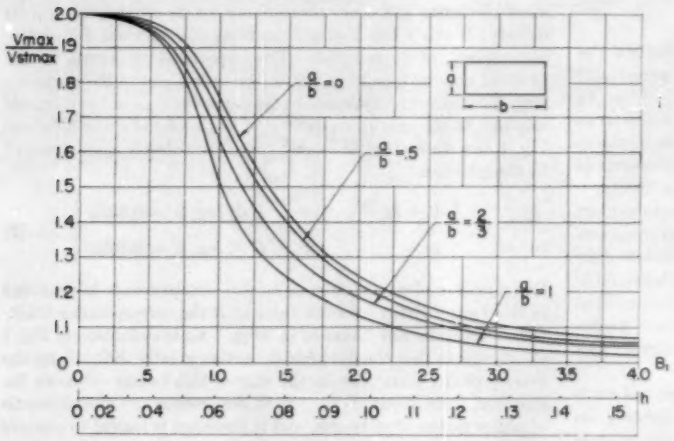

FIG. 2 VARIATION OF RATIO OF DYNAMIC MAXIMUM DEFLECTION TO STATIC MAXIMUM DEFLECTION WITH PARAMETER B_1 AND WITH THICKNESS OF A RECTANGULAR ALUMINUM PLATE WITH $a = 10$ AT CENTER OF PLATE

condition than is encountered in practice; a more realistic problem may be formulated by considering the heat input $Q(t)$ to be applied gradually, for example, as

$$\left.\begin{aligned} Q(t) &= Q_0(t/t_0) \quad 0 < t \leq t_0 \\ Q(t) &= Q_0 \qquad\qquad t \geq t_0 \end{aligned}\right\} \quad \ldots\ldots\ldots [4]$$

In cases of aerodynamic heating, the structure may be taken to be exposed to a high ambient temperature T_0 through a boundary conductance H; the appropriate thermal boundary condition is then

$$\frac{\partial T}{\partial(y/h)} = N(T - T_0) \quad \ldots\ldots\ldots\ldots\ldots [5]$$

where T is the surface temperature of the exposed member, and

$$N = hH/K \quad \ldots\ldots\ldots\ldots\ldots [5a]$$

The thermal conductivity is denoted by K. The results corresponding to Equations [4] and [5] are presented in Figs. 3 and 4, respectively.

Fig. 3 shows the variation with τ_0 ($= t_0K/h^2$) of the ratio of maximum dynamic to static deflections, for a simply supported beam with $B = 1$. The ordinate for $\tau_0 = 0$ is of course the same as that of the curve of Fig. 1 for $B = 1$; as the heat is more gradually applied, the maximum deflection rapidly decreases.

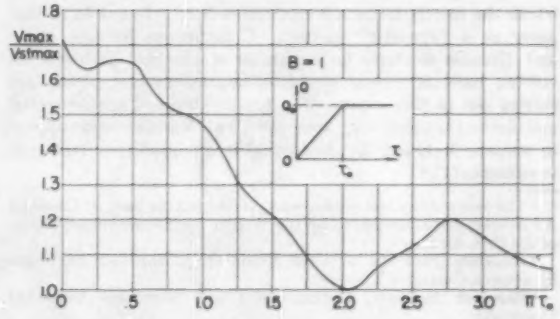

FIG. 3 VARIATION OF RATIO OF DYNAMIC MAXIMUM DEFLECTION TO STATIC MAXIMUM DEFLECTION WITH PARAMETER τ_0 FOR A RECTANGULAR BEAM UNDER GRADUAL HEAT APPLICATION

Fig. 4 is a plot, similar to that of Fig. 1, showing the effect of the parameter N. The curve labeled $N = 0$ is identical with that of Fig. 1, and the other curves are very close to it for values of $B > 0.8$ approximately. This range for the parameter B includes most of the plate thicknesses which are usually employed in practice. (The variation of the maximum static deflection with the parameter N is shown in Fig. 5.)

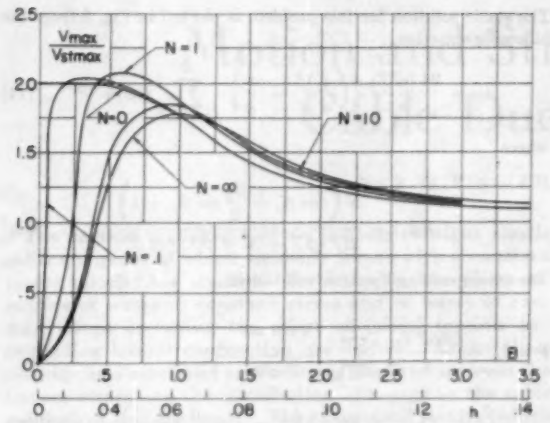

FIG. 4 VARIATION OF RATIO OF DYNAMIC MAXIMUM DEFLECTION TO STATIC MAXIMUM DEFLECTION WITH PARAMETERS B AND N, AND WITH THICKNESS OF A RECTANGULAR ALUMINUM BEAM WITH L = 10 IN., AT $x = (L/2)$

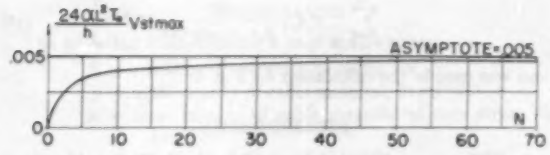

FIG. 5 VARIATION OF MAXIMUM STATIC DEFLECTION WITH PARAMETER N

In conclusion, one may note that use of Fig. 1 or of Equation [2] yields in all cases a reasonably accurate result, and may therefore be adopted for purposes of rapid estimates of the importance of inertia.

3 ANALYSIS OF PLATES

Consider a simply-supported rectangular plate occupying the space $0 \leq x \leq a, 0 \leq z \leq b, (-h/2) \leq y \leq (h/2)$, under a uniform heat input suddenly applied over the face $y = h/2$. The corresponding temperature distribution is (3)

$$T = \frac{hQ}{K}\left[\tau + \frac{1}{2}\left(\frac{y}{h} + \frac{1}{2}\right)^2 - \frac{1}{6} - \frac{2}{\pi^2}\sum_{j=1}^{\infty}(-1)^j e^{-j^2\pi^2\tau}\cos j\pi\left(\frac{y}{h} + \frac{1}{2}\right)\right] \quad \ldots\ldots [6]$$

where $\tau = \kappa t/h^2$. The differential equation for the transverse deflection $v(x, z, t)$ is (4, 5, 6)

$$D\nabla^4 v + \rho h\frac{\partial^2 v}{\partial t^2} = -\frac{1}{1-\nu}\nabla^2 M_T \quad \ldots\ldots [7]$$

where

$$\nabla^2 = \frac{\partial^2}{\partial x^2} + \frac{\partial^2}{\partial z^2}; \quad M_T = \frac{2\alpha E}{1-\nu^2}\int_{-h/2}^{h/2} Ty\,dy \quad \ldots [7a]$$

and α is the coefficient of thermal expansion. For the present problem the boundary and initial conditions are

$$v(0, z, t) = v(a, z, t) = v(x, 0, t) = v(x, b, t) = 0$$

$$\frac{\partial^2 v(0, z, t)}{\partial x^2} = \frac{\partial^2 v(a, z, t)}{\partial x^2} = \frac{\partial^2 v(x, 0, t)}{\partial z^2} = \frac{\partial^2 v(x, b, t)}{\partial z^2} = M_T \quad [8a]$$

$$u(x, z, 0) = \frac{\partial v(x, z, 0)}{\partial t} = 0$$

and

$$M_T(\tau) = \frac{96Q\,D\,\alpha}{\pi^4 K}\left[\frac{\pi^4}{96} - \sum_{j=1,3,5}^{\infty}\frac{e^{-j^2\pi^2\tau}}{j^4}\right] \quad \ldots\ldots [8b]$$

The static solution is obtained from the foregoing formulation by disregarding the term $\rho h(\partial^2 v/\partial t^2)$ in Equation [7] and the initial conditions; it is

$$v_{st} = -\frac{96Q\alpha a^2}{\pi^4 K}\sum_{j=1,3,5}^{\infty}\sum_{n=1,3,5}^{\infty}\sum_{m=1,3,5}^{\infty}\left(\frac{\pi^4}{96} - \frac{e^{-j^2\pi^2\tau}}{j^4}\right)\frac{16}{\pi^4 mn\left(n^2 + \frac{a^2m^2}{b^2}\right)} \quad \ldots\ldots [9]$$

The dynamic solution obtained by the method of references (7) and (2) is

$$v = v_{st} + \frac{1536Q\alpha^2}{\pi^4 K}\sum_{n=1,3,5}^{\infty}\sum_{m=1,3,5}^{\infty}\sin n\pi\left(\frac{x}{a}\right)\sin m\pi\left(\frac{y}{b}\right)\left[\frac{\pi^2}{8\left(n^2 + \frac{a^2}{b^2}m^2\right)}\sin B_1 t\pi^2\left(n^2 + \frac{a^2}{b^2}m^2\right)\tau - \sum_{j=1,3,5}^{\infty}\frac{e^{-j^2\pi^2\tau} + \frac{j^2\sin B_1 t\pi^2\left(n^2 + \frac{a^2}{b^2}m^2\right)\tau}{B_1 t(n^2 + a^2/b^2m^2)}}{j^4 + B_1{}^4\left(n^2 + \frac{a^2}{b^2}m^2\right)^2} + \frac{\cos B_1 t\pi^2\left(n^2 + \frac{a^2}{b^2}m^2\right)\tau}{j^4 + B_1{}^4\left(n^2 + \frac{a^2}{b^2}m^2\right)^2}\right] \quad \ldots\ldots [10]$$

Calculations from these formulas resulted in the plot shown in Fig. 2; the summations were simplified for purposes of calculation as described in reference (2).

4 ANALYSIS OF GRADUALLY HEATED BEAMS

The deflection $v(x, t)$ of a uniform simply supported rectangular beam (see inset in Fig. 1) under any temperature distribution independent of the spanwise co-ordinate x, must satisfy the following differential equation

$$B^4\frac{\partial^4 v}{\partial(x/L)^4} + \frac{\partial^2 v}{\partial\tau^2} = 0 \quad \ldots\ldots [11]$$

and the following boundary and initial conditions

$$\left.\begin{aligned} v(0, t) = v(L, t) = v(x, 0) = \frac{\partial v(x, 0)}{\partial t} = 0 \\ \frac{\partial^2 v(0, t)}{\partial(x/L)^2} = \frac{\partial^2 v(L, t)}{\partial(x/L)^2} = \frac{L^2}{EI}\iint \alpha\,ET(y, t)y\,dA \end{aligned}\right\} \quad [11a]$$

The solution of the foregoing boundary value problem for the special case of a suddenly applied heat input was obtained in reference (2); and will be denoted here by $v_0(x, t)$. The solution $v(x, t)$ for a gradually applied heat input $Q(t)$ may then be obtained from v_0 by the use of Duhamel's theorem, i.e.

$$v(x, t) = \int_0^t v_0(x, t_1)\frac{\partial Q(t - t_1)}{\partial t}\,dt_1 \quad \ldots\ldots [12]$$

In the special case of Equation [4] the result is

$$v_{st} = \frac{192Q\alpha l^2}{\pi^4 K}\left\{\left(\frac{x}{a}\right)^2 - \left(\frac{x}{a}\right)\right\}\frac{1}{8\tau_0} \times \left[\frac{\pi^4}{96}\left\{\tau - (\tau-\tau_0)u(\tau-\tau_0)\right\} - \frac{1}{j^2\pi^2}\left\{1 - e^{-j^2\pi^2\tau} - \left[1 - e^{-j^2\pi^2(\tau-\tau_0)}\right]u(\tau-\tau_0)\right\}\right] \quad [12a]$$

and

$$v(x,t) = v_{st} + \frac{192Q\alpha l^2}{\pi^4 K}\sum_{n=1,3,5}^{\infty}\frac{\sin n\pi\left(\frac{x}{a}\right)}{n^2\pi^2\tau_0}\left[\sum_{j=1,3,5}^{\infty}\frac{1}{j^2\pi^2} \times \frac{e^{-j^2\pi^2(\tau-\tau_0)}u(\tau-\tau_0)}{j^4+n^4B^4} + \sum_{j=1,3,5}^{\infty}\frac{1}{\pi^2n^2B^2(j^4+n^4B^4)}\left\{\sin n^2\pi^2B^2\tau - \sin n^2\pi^2B^2(\tau-\tau_0)u(\tau-\tau_0)\right\} - \sum_{j=1,3,5}^{\infty}\frac{1}{j^2\pi^2(j^4+n^4B^4)}\left\{\cos n^2\pi^2B^2\tau - \cos n^2\pi^2B^2(\tau-\tau_0)u(\tau-\tau_0)\right\}\right] \quad [12b]$$

where

$$u(\tau-\tau_0) = \begin{matrix} 0 & \text{for} & \tau < \tau_0 \\ 1 & \text{for} & \tau \geq \tau_0 \end{matrix}$$

Use of Equations [12a] and [12b] was made in the calculations pertaining to Fig. 3.

5 Beam Heated Through a Boundary Conductance

The solution in this case again must satisfy the boundary-value problem formulated in the previous section, with the appropriate temperature distribution in Equations [11a]. Reference (3) gives for the case of Equation [5] the following solution

$$T = T_0\left\{1 - \sum_{j=1}^{\infty}\frac{2N\cos\beta_j\left(\frac{y}{h}+\frac{1}{2}\right)e^{-\beta_j^2\tau}}{(\beta_j^2+N+N^2)\cos\beta_j}\right\} \quad [13]$$

where β_j are the roots of the equation

$$\beta\tan\beta = N \quad [13a]$$

The static solution for this problem is plotted in Fig. 5 from the following equation

$$v_{st} = \frac{24\,\alpha l^2 T_0}{h}\left\{\left(\frac{x}{a}\right)^2 - \frac{x}{a}\right\}\sum_{j=1,2,3}^{\infty} f(\beta_j)e^{-\beta_j^2\tau} \quad [14]$$

where

$$f(\beta_j) = \frac{N\left(\cos\beta_j + \frac{\beta_j}{2}\sin\beta_j - 1\right)}{\beta_j^2(\beta_j^2+N+N^2)\cos\beta_j} \quad [14a]$$

The corresponding dynamic solution is

$$v = v_{st} + \frac{24\alpha l^2 T_0}{h}\sum_{n=1,3,5}^{\infty}\frac{4\sin n\pi\frac{x}{a}}{n^2\pi^2}\left[\frac{1}{n^2\pi^2B^2}\sum_{j=1,2,3}^{\infty}B_j^2 f(\beta_j)\left(1 - \frac{\beta_j^4}{\beta_j^4+n^4\pi^4B^4}\right)\sin n^2\pi^2B^2\tau + \sum_{j=1,2,3}^{\infty}f(\beta_j)\frac{\beta_j^4}{\beta_j^4+n^4\pi^4B^4}\cos n^2\pi^2B^2\tau - \sum_{j=1,2,3}^{\infty}f(\beta_j)\frac{\beta_j^4}{\beta_j^4+n^4\pi^4B^4}e^{-\beta_j^2\tau}\right] \quad [15]$$

and was used in the calculation for Fig. 4.

BIBLIOGRAPHY

1 "Vibrations of Heated Beams," by A. D. Barber, MS thesis, Department of Civil Engineering, Columbia University, New York, N. Y., 1955.

2 "Thermally Induced Vibrations of Beams," by B. A. Boley, *Journal of the Aeronautical Sciences*, vol. 23, February, 1956, pp. 179–181.

3 "Conduction of Heat in Solids," by H. S. Carslaw and J. C. Jaeger, Clarendon Press, Oxford, England, 1947.

4 "Thermal Stress Analysis for Aircraft Structures," by B. A. Boley and J. H. Weiner, WADC TR 56-102, 1956.

5 "Similarity Laws for Stressing Heated Wings," by H. S. Tsien, *Journal of the Aeronautical Sciences*, vol. 20, January, 1953, pp. 1–11.

6 "The Determination of Temperature, Stresses, and Deflections in Two-Dimensional Thermoelastic Problems," by B. A. Boley, *Journal of the Aeronautical Sciences*, vol. 23, January, 1956, pp. 67–75.

7 "Beam Vibrations with Time-Dependent Boundary Conditions," by R. D. Mindlin and L. E. Goodman, Journal of Applied Mechanics, Trans. ASME, vol. 72, 1950, p. 377.

Motion and Stress of an Elastic Cable Due to Impact[1]

By F. O. RINGLEB,[2] PHILADELPHIA, PA.

The motion and stress of an initially straight elastic cable one point of which suddenly moves with a constant vector velocity are studied. Formulas for the phase velocities of waves of constant stress and of waves of constant slope including the effect of initial tension and neglecting lateral contraction are derived. Under these assumptions exact and approximate relations between the impact stress and the distribution of energy in the cable are derived and discussed. The theoretical results (which had been classified for a considerable time) are compared with results from tests on aircraft arresting gears carried out at the Naval Air Engineering Facility (Ship Installations), Philadelphia, Pa.

Nomenclature

The following nomenclature is used in the paper:

E = modulus of elasticity of cable, psf
ρ = mass density of cable material, lb sec^2/ft^4
ρ_0 = mass density of cable material at zero stress, lb sec^2/ft^4
q = cross-section area of cable, sq ft
l, l_0 = cable lengths, ft
T = tension, lb
$\sigma = \frac{T}{q}$ = stress, psf
T_0 = initial tension, lb
σ_0 = initial stress, psf
δ, δ_0 = elongation, ft
x, y = rectangular co-ordinates in plane of cable motion, ft
s = abscissa of a cable point in initial position along x-axis at time $t = 0$, ft
t = time, sec
θ = angle between cable element and x-axis
c = longitudinal wave velocity, fps
c_0 = longitudinal wave velocity at zero stress, fps
$\bar{c}$ = transverse wave velocity, fps
v_0 = impact velocity, fps
u = particle velocity, fps
ω = kink velocity, fps
β = impact angle
$H_1, H_0, \ldots$ = energies, ft/lb
$\eta, \eta_1, \ldots$ = dimensionless energy coefficients

[1] Statements and opinions advanced in this paper are to be understood as individual expressions of the author and not necessarily those of the Navy Department.

[2] Staff Physicist, Naval Air Engineering Facility (Ship Installations), Naval Air Material Center.

Presented at the Applied Mechanics Division Summer Conference, Berkeley, Calif., June 13–15, 1957, of The American Society of Mechanical Engineers.

Discussion of this paper should be addressed to the Secretary, ASME, 29 West 39th Street, New York, N. Y., and will be accepted until October 10, 1957, for publication at a later date. Discussion received after the closing date will be returned.

Note: Statements and opinions advanced in papers are to be understood as individual expressions of their authors and not those of the Society. Manuscript received by ASME Applied Mechanics Division, February 20, 1956. Paper No. 57—APM-10.

Introduction

In 1868 B. de Saint Venant (1)[3] derived the formula

$$\sigma = v_0 (E\rho)^{1/2}$$

for the longitudinal impact stress of an elastic string or bar where v_0 is the impact velocity with which the end of the string or bar suddenly moves, E is the elasticity modulus, and ρ is the mass density of the material. The initial stress is assumed to be zero. In the case of an elastic bar, the stress can be produced by tension or compression. In the case of a string, the tensile stress only has a practical meaning.

It seems that the corresponding transverse-impact problem had not been studied until in 1948 the author of the present paper (2) derived, among other impact relations, for the stress in an elastic string or cable due to perpendicular impact with the velocity v_0 the approximate formula

$$\frac{\sigma}{E} = \left(\frac{1}{2}\right)^{2/3} \left(\frac{v_0}{c}\right)^{4/3}$$

In this expression $c = (E/\rho)^{1/2}$ is the longitudinal wave velocity. This formula has been used subsequently for the computation of the impact stress in the deck pendant of an aircraft arresting gear in this country as well as abroad. It had been classified as restricted information together with many other impact investigations, until publications by other authors made such classification superfluous.

The purpose of the present paper is to publish and to discuss some of the more general results of the author's investigations, especially the exact solutions as well as approximate solutions of the problems of determining the stress at oblique impact with a constant impact velocity and the relations for the energy distribution within the moving cable. A formula is called exact if it has been derived from the basic assumptions without further approximations, though the basic assumptions may represent approximations themselves. We will assume as fact that Hooke's law of elasticity is valid, and that there is no lateral contraction or expansion of the cable due to change of stress.

The main result derived in this paper consists in the formula

$$\left(\frac{v_0}{c_0}\right)^2 + 2\,\frac{v_0}{c_0}\left[\left(\frac{\sigma}{E}\right)^{1/2}\left(1+\frac{\sigma}{E}\right)^{1/2} - \frac{\sigma-\sigma_0}{E}\right]\cos\beta = 2\,\frac{\sigma-\sigma_0}{E}\left(\frac{\sigma}{E}\right)^{1/2}\left(1+\frac{\sigma}{E}\right)^{1/2} - \left(\frac{\sigma-\sigma_0}{E}\right)^2$$

which determines the oblique impact stress σ for a given impact velocity v_0 and a given impact angle β (see Fig. 2). σ_0 is the initial stress of the cable, E its elasticity modulus, and $c_0 = (E/\rho_0)^{1/2}$ is the longitudinal wave velocity, ρ_0 being the mass density of the cable at zero stress. A graph, Fig. 5, permits the evaluation of this formula for any given data without further computational work if σ/E and σ_0/E are negligibly small compared with unity, as is the case for all steel-wire cables, with or without hemp core. Measured values agree very well with the theoretical results, as shown in Fig. 7 for different cable sizes, in the case of perpendicular impact.

[3] Numbers in parentheses refer to the Bibliography at the end of the paper.

The formula for the oblique impact stress is not limited in its application to the special case of such impact. It can be applied directly to many general problems of cable motion. If, for instance, the end of a cable moves along a given path with a given variable velocity, this motion can be replaced, with any desired degree of accuracy, by a motion along a polygon with stepwise constant velocities. This latter motion may then be computed as that resulting from a series of oblique impacts.

Hooke's Law

If l_0 is the length of a straight string with invariable constant cross section and if the initial stress is zero, then Hooke's law states that to an elongation δ_0 there corresponds a stress σ_0 which is proportional to that elongation. Therefore

$$\frac{\sigma_0}{E} = \frac{\delta_0}{l_0}$$

where the factor of proportionality is E/l_0. This factor defines the elasticity modulus E. If l is the length of the same string with the initial stress σ_0 then

$$l = l_0 + \delta_0$$

If now δ is an elongation of this string with the initial stress σ_0 we have

$$\frac{\sigma}{E} = \frac{\delta + \delta_0}{l_0}$$

for the corresponding stress σ. Eliminating l_0 and δ_0 from these equations we obtain

$$\frac{\dfrac{\sigma - \sigma_0}{E}}{1 + \dfrac{\sigma_0}{E}} = \frac{\delta}{l} \qquad [1]$$

This is an expression for Hooke's law if the string has initially the length l and if the initial stress is σ_0.

The ratio σ_0/E is usually a very small number. For a steel cable with hemp core, for instance, a value of σ/E as low as 0.019 corresponds about to the ultimate strength of the cable. Thus, if σ_0/E is small compared with unity, Equation [1] can be simplified to

$$\frac{\sigma - \sigma_0}{E} = \frac{\delta}{l} \qquad [2]$$

There exist very extensible materials for which the stress can be considerably higher than the elasticity modulus without breaking the string. In such cases, Equation [2] is not applicable. However, the assumption of an invariable cross section of the string implies that σ/E has to be small compared with unity because there exist no real materials with the Poisson's ratio $\nu = 0$ which must be true for an invariable cross section. In spite of this, we will use Equation [1] generally without approximation and will obtain results which are exact for all stresses in hypothetical materials with $\nu = 0$. We note that Equation [1] can be written also in the form

$$\frac{1 + \dfrac{\sigma}{E}}{1 + \dfrac{\sigma_0}{E}} = \frac{\delta}{l} + 1 \qquad [3]$$

A steel cable with hemp core is not a homogeneous string. But we replace it by an equivalent homogeneous string. Since its elastic properties will be determined mainly by the steel wires in it, we define as cross-section area the metallic area q and add the mass of the hemp to the steel mass. Thus the density of the material of the equivalent string becomes somewhat higher than that of steel. This procedure proves to be practically satisfactory.

General Equations for Two-Dimensional Motion and Stress of a Cable

We assume that the initial position of a cable at the time $t = 0$ is the straight position along the x-axis of a rectangular x, y-co-ordinate system and that its initial stress is $\sigma_0 = \text{const}$. The x-co-ordinate of a cable point in the initial position will be denoted in the following by s, Fig. 1. The motion of the cable is described generally by two functions

$$x = f(s, t), \quad y = g(s, t) \qquad [4]$$

satisfying the initial conditions

$$x = f(s, 0) = s, \quad y = g(s, 0) = 0 \qquad [5]$$

for $t = 0$. If s is a constant value denoting a special cable point, the curve [4] with the variable parameter t is the path of this special cable point during the motion of the cable. For a constant time value t the curve [4] with the variable parameter s defines the shape of the cable at that time.

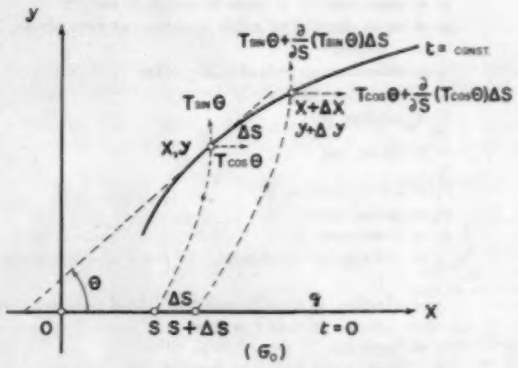

Fig. 1 Derivation of Equations for Motion and Stress of a Cable

We denote by θ the angle between a cable element ΔS at the time t, corresponding to an initial element Δs at $t = 0$ and the x-axis. ΔS is defined as positive in direction of increasing s. Then θ is the angle about which the positive x-direction has to be turned in order to coincide with the positive ΔS direction, θ being counted positive in counterclockwise direction. We denote further by σ the stress in any cable point s at any time t. We assume that there is no lateral contraction or expansion due to a change of stress or that such is neglected. This implies that the cross-section area q is a constant and equal to the initial cross-section area. We denote finally the mass density of the cable material in its initial position at the initial stress σ_0 by ρ. Owing to the assumed constancy of q the mass density of a cable element ΔS during the motion is equal to the mass $\rho q \Delta s$ of the corresponding initial element. The tension in the cable point s at the time t is $T = q\sigma$.

We assume now that a cable element ΔS corresponding to Δs adjacent to s moves under the influence of the tension only. The components of the tension acting in the end points of ΔS in the x-direction are

$$T\cos\theta, \quad T\cos\theta + \frac{\partial}{\partial s}(T\cos\theta)\,\Delta s$$

and in the y-direction

$$T\sin\theta, \quad T\sin\theta + \frac{\partial}{\partial s}(T\sin\theta)\,\Delta s$$

The components of the net force on the moving element are therefore

$$\frac{\partial(T\cos\theta)}{\partial s}\Delta s, \quad \frac{\partial(T\sin\theta)}{\partial s}\Delta s$$

The mass of the element ΔS is equal to the mass of the element Δs which is $\rho q \Delta s$, since we denote the mass density of the cable in its initial position under constant stress σ_0 by ρ. From Newton's law the following is obtained (3)

$$\rho q\,\Delta s\,\frac{\partial^2 x}{\partial t^2} = \frac{\partial(T\cos\theta)}{\partial s}\Delta s$$

$$\rho q\,\Delta s\,\frac{\partial^2 y}{\partial t^2} = \frac{\partial(T\sin\theta)}{\partial s}\Delta s$$

or, replacing T by σ/q, we can write

$$\frac{\partial^2 x}{\partial t^2} = \frac{E}{\rho}\frac{\partial}{\partial s}\left(\frac{\sigma}{E}\cos\theta\right) \quad [6]$$

$$\frac{\partial^2 y}{\partial t^2} = \frac{E}{\rho}\frac{\partial}{\partial s}\left(\frac{\sigma}{E}\sin\theta\right) \quad [7]$$

where E is the elasticity modulus.

It is now shown that Hooke's law, Equation [1], yields two other equations between the unknown functions x, y, σ, and θ of s and the time t. The elongation of the original cable element Δs after the time t is $\delta = \Delta S - \Delta s$. Now

$$\frac{dS}{ds} = \left[\left(\frac{\partial x}{\partial s}\right)^2 + \left(\frac{\partial y}{\partial s}\right)^2\right]^{1/2} \quad [8]$$

Thus Hooke's law applied to this element yields

$$\frac{\dfrac{\sigma-\sigma_0}{E}}{1+\dfrac{\sigma_0}{E}} = \left(\frac{\Delta S - \Delta s}{\Delta s}\right)_{\Delta s \to 0} = \left[\left(\frac{\partial x}{\partial s}\right)^2 + \left(\frac{\partial y}{\partial s}\right)^2\right]^{1/2} - 1$$

or

$$\frac{1+\dfrac{\sigma}{E}}{1+\dfrac{\sigma_0}{E}} = \left[\left(\frac{\partial x}{\partial s}\right)^2 + \left(\frac{\partial y}{\partial s}\right)^2\right]^{1/2} \quad [9]$$

Because of

$$\frac{\partial x}{\partial s} = \frac{dS}{ds}\cos\theta, \quad \frac{\partial y}{\partial s} = \frac{dS}{ds}\sin\theta$$

we find

$$\frac{\partial x}{\partial s} = \frac{1+\dfrac{\sigma}{E}}{1+\dfrac{\sigma_0}{E}}\cos\theta \quad [10]$$

$$\frac{\partial y}{\partial s} = \frac{1+\dfrac{\sigma}{E}}{1+\dfrac{\sigma_0}{E}}\sin\theta \quad [11]$$

Equations [6], [7], [10], and [11] are the basic conditions for the unknown functions x, y, σ, and θ describing the motion and stress of the cable [compare also reference (4)].

For values of σ/E and σ_0/E which are small compared with 1, we have approximately

$$\frac{1+\dfrac{\sigma}{E}}{1+\dfrac{\sigma_0}{E}} = 1 + \frac{\sigma-\sigma_0}{E}$$

and the last two equations take the form

$$\frac{\partial x}{\partial s} = \left(1+\frac{\sigma-\sigma_0}{E}\right)\cos\theta \quad [12]$$

$$\frac{\partial y}{\partial s} = \left(1+\frac{\sigma-\sigma_0}{E}\right)\sin\theta \quad [13]$$

Elimination of x and y from the general Equations [6], [7], [10], and [11] yields for σ and θ the conditions

$$\frac{\partial^2}{\partial t^2}\left(\frac{1+\dfrac{\sigma}{E}}{1+\dfrac{\sigma_0}{E}}\cos\theta\right) = \frac{E}{\rho}\frac{\partial^2}{\partial s^2}\left(\frac{\sigma}{E}\cos\theta\right) \quad [14]$$

$$\frac{\partial^2}{\partial t^2}\left(\frac{1+\dfrac{\sigma}{E}}{1+\dfrac{\sigma_0}{E}}\sin\theta\right) = \frac{E}{\rho}\frac{\partial^2}{\partial s^2}\left(\frac{\sigma}{E}\sin\theta\right) \quad [15]$$

Wave Velocities

If a cable element moves parallel to itself so that θ is constant during the motion, both Equations [14] and [15] yield for the stress σ the same condition

$$\frac{\partial^2\sigma}{\partial t^2} = \left(1+\frac{\sigma_0}{E}\right)\frac{E}{\rho}\frac{\partial^2\sigma}{\partial s^2}$$

which is the classical wave equation for the function $\sigma(s, t)$. Therefore, the stress value σ propagates with respect to s with the velocity

$$c = \left[\left(1+\frac{\sigma_0}{E}\right)\frac{E}{\rho}\right]^{1/2} \quad [16]$$

representing the longitudinal wave velocity. If the initial stress $\sigma_0 = 0$, this velocity is the same as in the classical theory of the vibrating string.

If we consider further a cable element which has during its motion a constant stress σ then the Equations [14] and [15] yield

$$\frac{\partial^2}{\partial t^2}[\cos(\theta-\theta_0)] = \frac{1+\dfrac{\sigma_0}{E}}{1+\dfrac{\sigma}{E}}\frac{\sigma}{\rho}\frac{\partial^2}{\partial s^2}[\cos(\theta-\theta_0)] \quad [17]$$

which is again the classical wave equation now for the quantity $\cos(\theta - \theta_0)$ as function of s and t. Here θ_0 is an arbitrary constant. This means that a θ-value propagates with the velocity

$$c = \left(\frac{1 + \frac{\sigma_0}{E}}{1 + \frac{\sigma}{E}} \frac{\sigma}{\rho} \right)^{1/2} \quad \ldots\ldots\ldots\ldots [18]$$

with respect to ε. This velocity represents the transverse wave velocity which coincides with the value obtained in the classical theory of the vibrating string only if σ_0/E and σ/E are negligibly small compared with unity.

If σ_0/E and σ/E are small but not negligibly small compared with unity, this formula yields approximately

$$c = \left(\frac{\frac{\sigma}{\rho}}{1 + \frac{\sigma - \sigma_0}{E}} \right)^{1/2} \quad \ldots\ldots\ldots\ldots [19]$$

From the Formulas [16] and [18] the following general relation is obtained

$$\frac{c}{c} = \left(\frac{\frac{\sigma}{E}}{1 + \frac{\sigma}{E}} \right)^{1/2} \quad \ldots\ldots\ldots\ldots [20]$$

We mentioned that most steel cables with hemp core have a value σ_{max}/E approximately constant equal to 0.019, where σ_{max} denotes the ultimate stress of the cable. For a hemp rope the same value is about 0.16. Thus in the case of a steel cable σ/E can be considered as negligibly small compared with unity, and in the case of a hemp rope as small enough to neglect second powers of σ/E compared with 1. In the case of nylon or rubber cables, the influence of lateral contraction and hysteresis require extensions of the results presented here.

Longitudinal Impact

If the end point of a long straight cable with the initial stress σ_0 suddenly moves longitudinally with a constant velocity v_0, a stress σ is produced which propagates along the cable. It can be proved mathematically from the general equations, but is physically clear without computation, that this stress is constant. Ideally the end cross section of the cable with infinitely small mass is accelerated infinitely by a finite force to the velocity v_0. Assuming that the end cross section is connected by massless springs with the next layer of infinitely small mass, the same force acts now on this second layer in the same way, and so on. Owing to the assumed homogeneity of the material and constancy of the cross section, the produced stress must be constant as far as the stress has propagated. Every particle which has been reached by the stress front suddenly moves with the velocity v_0.

According to the preceding section, the velocity of propagation is

$$c = \left[\left(1 + \frac{\sigma_0}{E} \right) \frac{E}{\rho} \right]^{1/2}$$

At the time t the influenced length is equal to ct and the elongation of the cable equal to $v_0 t$. According to Hooke's law (Equation [1]) the stress is determined by

$$\frac{\frac{\sigma - \sigma_0}{E}}{1 + \frac{\sigma_0}{E}} = \frac{v_0}{c} \quad \ldots\ldots\ldots\ldots [21]$$

In the special case $\sigma_0 = 0$ this yields the result

$$\frac{\sigma}{E} = \frac{v_0}{c}$$

where now

$$c = \left(\frac{E}{\rho} \right)^{1/2}$$

which is the formula that B. de Saint Venant obtained in 1868.

The total work done at the cable end during the time t is

$$H = \sigma q v_0 t \quad \ldots\ldots\ldots\ldots [22]$$

if q is the cable cross section. The kinetic energy which the moving cable part has at this time

$$H_k = \rho q c t \frac{v_0^2}{2} \quad \ldots\ldots\ldots\ldots [23]$$

and the elastic energy stored in this cable part is given by

$$H_\sigma = \frac{\sigma + \sigma_0}{2} q v_0 t \quad \ldots\ldots\ldots\ldots [24]$$

From Formula [21] it is evident that

$$H = H_k + H_\sigma \quad \ldots\ldots\ldots\ldots [25]$$

If especially $\sigma_0 = 0$, Equations [24] and [21] yield

$$H_\sigma = \frac{1}{2} \rho c v_0^2 q t = H_k \quad \ldots\ldots\ldots\ldots [26]$$

Thus if the initial stress is zero, the energy added to the cable end is equally split into kinetic and strain energy.

Oblique Impact

If the end point O of a straight long cable with the initial stress σ_0 suddenly moves with a constant velocity v_0 in a given direction $\beta > 0$, Fig. 2, the cable moves at any time in two straight parts, the part PQ in the direction β with the velocity v_0 and the part RQ in the direction from R to Q while the part beyond R is at this moment at rest. The points between Q and R move toward the left with constant velocities. This again can be proved mathematically from the general equations but follows also from elementary physical considerations similar to those of the preceding section in the case of the longitudinal impact. The moving force now produces longitudinal and transverse displacements of the cable particles with the possibility that the longitudinal displacements propagate with a different velocity along the cable from that of the transverse displacements as is actually the case. At the same time a particle at Q obtains a transverse displacement in the direction β while a particle at R obtains a longitudinal displacement in the direction toward Q. After these displacements no force acts on the two particles any more. They are moving with constant speeds. From the homogeneity of the material and the constancy of the cross section it follows that the momentum magnitudes at points Q and R must be at any time the same. Thus the stresses along PQ and QR must be constant. Moreover these two constant stresses must be equal because of the results of the section "Wave Velocities." For any constant θ the longitudinal wave velocity c, Equation [16], is a constant. If there would be any stress difference in two elements in a neighborhood of Q, separated by Q, the corresponding transverse wave velocities $\bar{c}$, Equation [20], would be different, in disagreement with the continuous motion of Q.

From this knowledge we now can derive the formula for the

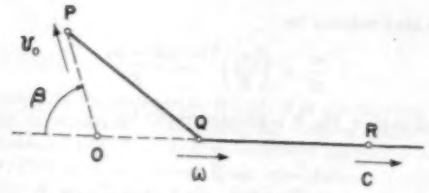

FIG. 2 CONFIGURATION OF OBLIQUE IMPACT

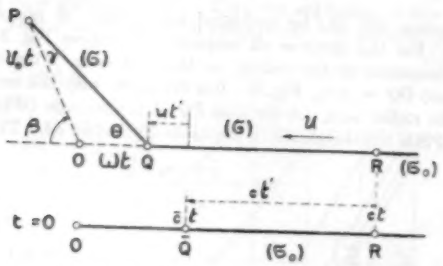

FIG. 3 DYNAMICS OF OBLIQUE IMPACT

stress due to oblique impact. For this purpose Fig. 3 shows the cable in its straight initial shape and above it its shape at any time $t > 0$. The end point O of the cable moves during the time t in the direction OP with the velocity v_0 from O to P. Thus $OP = v_0 t$. If $\bar{Q}$ is the point which corresponds to Q at the time $t = 0$, then $O\bar{Q} = \bar{\varepsilon}t$. The point $\bar{Q}$ moves toward Q and coincides with Q at the time t. But $\bar{Q}$ starts its motion toward Q only after the longitudinal wave arrived at $\bar{Q}$, which is the time $(\bar{\varepsilon}/c)t$. If t' is the time which $\bar{Q}$ needs to travel up to Q, then the longitudinal wave propagates in the same time t' from $\bar{Q}$ to R in the distance ct from 0. Thus

$$t' = \left(1 - \frac{\bar{\varepsilon}}{c}\right) t$$

In the part QR the cable has a stress σ which is produced by the oblique impact. But here the cable is insensitive to whether the stress has been produced by an oblique or a longitudinal impact with a certain velocity u. Therefore the cable must move between Q and R with a velocity u which is determined by the longitudinal impact Equation [21] so that

$$\frac{\dfrac{\sigma - \sigma_0}{E}}{1 + \dfrac{\sigma_0}{E}} = \frac{u}{c} \qquad \ldots\ldots [27]$$

Now $Q\bar{Q} = ut'$ and therefore

$$\omega t = \bar{\varepsilon}t - ut' = \bar{\varepsilon}t - u\left(1 - \frac{\bar{\varepsilon}}{c}\right) t$$

or

$$\frac{\omega}{c} = \frac{\bar{\varepsilon}}{c} - \frac{u}{c}\left(1 - \frac{\bar{\varepsilon}}{c}\right) \qquad \ldots\ldots [28]$$

This relation determines the velocity ω of the kink Q if the stress is known.

The initial cable length which is influenced by the motion at the time t is $l = OR = ct$. The elongation at this time is $\delta = PQ - OQ$. From the triangle OPQ the following is obtained

$$PQ = [(v_0^2 t^2 + \omega^2 t^2 + 2\omega v_0 t^2 \cos\beta)]^{1/2}$$

Thus

$$\frac{\delta}{l} = \frac{\delta}{ct} = \left[\left(\frac{v_0}{c}\right)^2 + \left(\frac{\omega}{c}\right)^2 + 2\,\frac{v_0}{c}\,\frac{\omega}{c}\cos\beta\right]^{1/2} - \frac{\omega}{c}$$

According to Hooke's law, Equation [1], we obtain

$$\frac{\dfrac{\sigma - \sigma_0}{E}}{1 + \dfrac{\sigma_0}{E}} = \frac{u}{c} = \left[\left(\frac{v_0}{c}\right)^2 + \left(\frac{\omega}{c}\right)^2 + 2\,\frac{v_0}{c}\,\frac{\omega}{c}\cos\beta\right]^{1/2} - \frac{\omega}{c} \qquad \ldots\ldots [29]$$

Here u/c and ω/c are functions of σ according to Equations [27], [28], and [20]. If we introduce σ and $c_0 = (E/\rho_0)^{1/2}$ instead of c we find as the solution of the oblique impact problem the following result:

The impact velocity v_0 and the impact stress σ are connected by the relation

$$\left(\frac{v_0}{c_0}\right)^2 + 2\,\frac{v_0}{c_0}\left[\left(\frac{\sigma}{E}\right)^{1/2}\left(1 + \frac{\sigma}{E}\right)^{1/2} - \frac{\sigma - \sigma_0}{E}\right]\cos\beta = 2\,\frac{\sigma - \sigma_0}{E}\left(\frac{\sigma}{E}\right)^{1/2}\left(1 + \frac{\sigma}{E}\right)^{1/2} - \left(\frac{\sigma - \sigma_0}{E}\right)^2 \qquad \ldots [30]$$

where β is the impact angle, σ_0 the initial stress, E the elasticity modulus, $c_0 = (E/\rho_0)^{1/2}$, the longitudinal wave velocity, and ρ_0 the mass density at zero stress.[4]

This general result includes, of course, as a special case Equation [21] for the longitudinal impact ($\beta = 0$ deg). For the perpendicular impact ($\beta = 90$ deg) we obtain the formula

$$\frac{v_0}{c_0} = \left[2\,\frac{\sigma - \sigma_0}{E}\left(\frac{\sigma}{E}\right)^{1/2}\left(1 + \frac{\sigma}{E}\right)^{1/2} - \left(\frac{\sigma - \sigma_0}{E}\right)^2\right]^{1/2}$$

Of further interest is the case $\beta = 180$ deg in which the end point O of the cable suddenly moves along the cable with the velocity v_0. Equation [29] yields in this case (reverse impact)

$$\frac{v_0}{c} = 2\,\frac{\omega}{c} + \frac{u}{c}$$

[4] If the same derivation is performed starting from the approximation

$$\bar{\varepsilon} = \left(\frac{\dfrac{\sigma}{\rho}}{1 + \dfrac{\sigma - \sigma_0}{E}}\right)^{1/2}$$

(see Equation [19]) one obtains

$$\left(\frac{v_0}{c_0}\right)^2 + 2\,\frac{v_0}{c_0}\left[\left(\frac{\sigma}{E}\right)^{1/2}\left(1 + \frac{\sigma - \sigma_0}{E}\right)^{1/2} - \frac{\sigma - \sigma_0}{E}\right]\cos\beta = 2\,\frac{\sigma - \sigma_0}{E}\left(\frac{\sigma}{E}\right)^{1/2}\left(1 + \frac{\sigma - \sigma_0}{E}\right)^{1/2} - \left(\frac{\sigma - \sigma_0}{E}\right)^2$$

This yields for $\beta = 90$ deg (perpendicular impact)

$$\frac{v_0}{c_0} = \left[2\,\frac{\sigma - \sigma_0}{E}\left(\frac{\sigma}{E}\right)^{1/2}\left(1 + \frac{\sigma - \sigma_0}{E}\right)^{1/2} - \left(\frac{\sigma - \sigma_0}{E}\right)^2\right]^{1/2}$$

It can be proved that the latter formula is identical with the result contained in the rather complicated Equation [31] of a paper by J. D. Cole, C. B. Dougherty, and J. H. Huth (5). The method applied in the present paper, based on elementary mathematical procedures which reflect more closely the physics of the impact process, is considerably simpler and results immediately in this simpler formula.

or

$$\frac{\omega}{c} = \frac{1}{2}\left(\frac{v_0}{c} - \frac{u}{c}\right)$$

This result shows that the 180-deg kink moves with a velocity ω which is smaller than $(1/2)v_0$. This must be so because mass is picked up continuously during the motion, resulting in stress which runs ahead of the kink along the cable. Only in the case of a massless cable the kink would move with the velocity $v_0/2$.

Approximations and Evaluations

If σ/E and σ_0/E are negligibly small compared with unity Equation [30] can be simplified to

$$\left(\frac{v_0}{c_0}\right)^2 + 2\,\frac{v_0}{c_0}\left[\left(\frac{\sigma}{E}\right)^{1/2} - \frac{\sigma - \sigma_0}{E}\right]\cos\beta = 2\,\frac{\sigma - \sigma_0}{E}\left(\frac{\sigma}{E}\right)^{1/2} - \left(\frac{\sigma - \sigma_0}{E}\right)^2 \quad [31]$$

This and the following formulas up to Equation [35] are sufficiently correct for conventional steel cables and steel cables with hemp cores. Equation [31] yields

$$\frac{v_0}{c_0} = -\left[\left(\frac{\sigma}{E}\right)^{1/2} - \frac{\sigma - \sigma_0}{E}\right]\cos\beta + \left[\frac{\sigma}{E} - \left(\left(\frac{\sigma}{E}\right)^{1/2} - \frac{\sigma - \sigma_0}{E}\right)^2 \sin^2\beta\right]^{1/2} \quad [32]$$

The corresponding approximations for the longitudinal and transverse wave velocities are

$$c = c_0 = \left(\frac{E}{\rho_0}\right)^{1/2}, \quad \bar{c} = \left(\frac{\sigma}{\rho_0}\right)^{1/2}, \quad \rho = \rho_0 \quad [33]$$

The particle velocity is now determined by

$$\frac{u}{c_0} = \frac{\sigma - \sigma_0}{E} \quad [34]$$

and the kink velocity by

$$\frac{\omega}{c_0} = \left(\frac{\sigma}{E}\right)^{1/2} - \frac{\sigma - \sigma_0}{E} \quad [35]$$

The kink angle θ, Fig. 3, is given correctly by

$$\operatorname{ctg}\theta = \frac{\dfrac{\omega}{v_0} + \cos\beta}{\sin\beta}, \quad \sin\theta = \frac{\dfrac{v_0}{c}}{\dfrac{\bar{c}}{c}}\sin\beta \quad [36]$$

Equation [32] can be evaluated for all data by one simple graph. For this purpose all lengths of the upper Fig. 3 have to be measured by the unit $c_0 t$, so that $OR = 1$. Then $OP = v_0/c_0$ and $OQ = \omega/c_0$, Fig. 4. Let the circle with the center Q and the radius ω/c_0 cut the side PQ of the triangle OPQ in S. Then PS is the elongation of the cable divided by $c_0 t$. Thus

$$PS = \frac{\sigma - \sigma_0}{E}$$

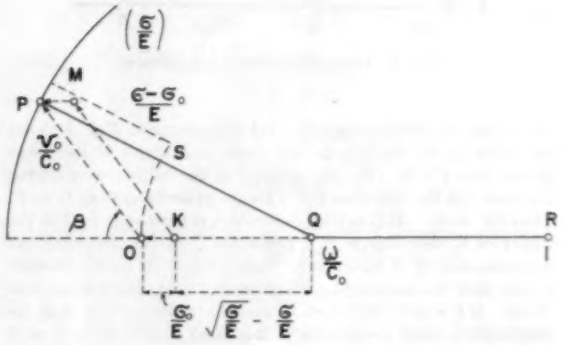

Fig. 4 Geometry of Oblique Impact

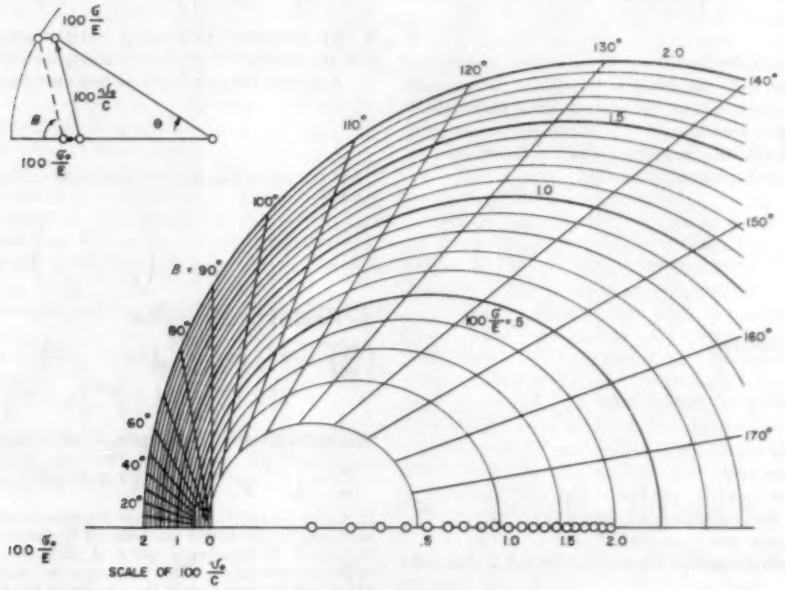

Fig. 5 Oblique Impact Stress

Now

$$PQ = \left(\frac{\sigma}{E}\right)^{1/2}$$

We choose K in the distance σ_0/E from O as a fixed point for the following construction: Computing for various values of σ/E the expression $(\sigma/E)^{1/2} - \sigma/E$ we construct the circles with the radii $(\sigma/E)^{1/2} - \sigma/E$ and the centers Q in the distance $(\sigma/E)^{1/2} - \sigma/E$ from K and denote these circles by their corresponding value (σ/E). We construct from K the vector with the length v_0/c_0 having the angle β with KO up to point M and from M the vector σ_0/E parallel to KO. Then the end point of this vector is the point P situated on the circle (σ/E). A sufficiently dense set of circles yields a graph from which the oblique impact tensions can be determined for any given data. Fig. 5 shows this graph.

In the case of perpendicular impact ($\beta = 90$ deg) Equation [31] yields

$$\left(\frac{v_0}{c_0}\right)^2 = 2\,\frac{\sigma - \sigma_0}{E}\left(\frac{\sigma}{E}\right)^{1/2} - \left(\frac{\sigma - \sigma_0}{E}\right)^2 \quad \ldots\ldots [37]$$

Fig. 6 represents this relation between σ/E and v_0/c_0 for various values of σ_0/E in order to show the influence of the initial stress on the resulting impact stress.

If $(\sigma - \sigma_0)/E$ is negligibly small compared with $(\sigma/E)^{1/2}$ then Equation [31] yields a further approximation, which is

$$\left(\frac{v_0}{c_0}\right)^2 + 2\,\frac{v_0}{c_0}\left(\frac{\sigma}{E}\right)^{1/2}\cos\beta = 2\,\frac{\sigma - \sigma_0}{E}\left(\frac{\sigma}{E}\right)^{1/2} \quad \ldots [38]$$

In the special case of perpendicular impact ($\beta = 90$ deg) and a σ_0 which is zero or negligibly small compared with σ this equation yields

$$\frac{\sigma - \sigma_0}{E} = \left(\frac{1}{2}\right)^{2/3}\left(\frac{v_0}{c_0}\right)^{4/3} \quad \ldots\ldots [39]$$

This formula was derived first by the author of the present paper in 1948 (2) together with other impact formulas using direct approximations. The curve, Fig. 7, represents this relation and shows measured values obtained from different cables, initial tensions, and impact velocities (compare also reference 6).

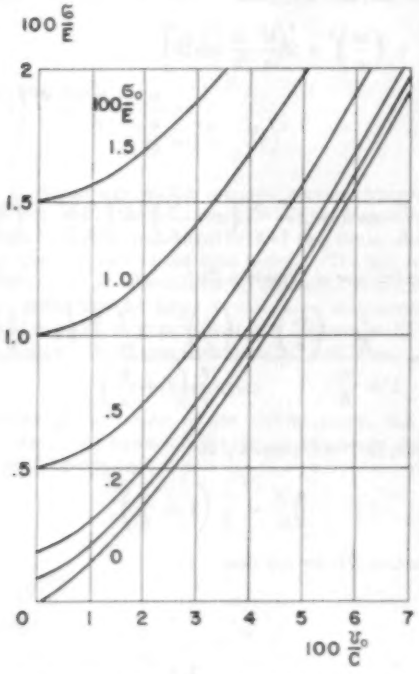

Fig. 6 Transverse Impact Stress for Various Initial Stress Values

Energy Relations

As in the case of longitudinal impact, it is of interest to study the distribution of the input energy on the moving-cable parts in the general case of oblique impact and especially in the case of perpendicular impact.

There have to be considered now three parts into which the work done at the cable end point O will be split: the kinetic energy of the cable segment PQ, Fig. 3, the kinetic energy of the segment QR, and the potential energy stored in both segments in form of stress. The mass m_1 of PQ at the time t is the same as the mass of $O\bar{Q}$ at the time zero, which is $m_1 = \rho q \bar{c} t$. The segment PQ moves with the velocity v_0. Thus its kinetic energy

$$H_1 = \rho q \bar{c} t\,\frac{v_0^2}{2} \quad \ldots\ldots [40]$$

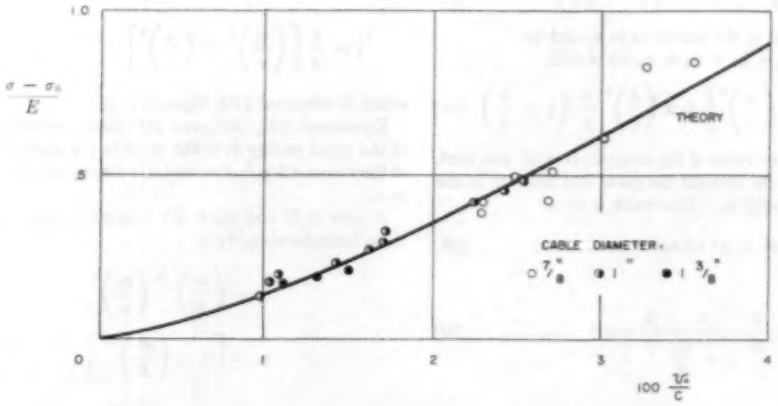

Fig. 7 Comparison of Measured and Theoretical Transverse Impact-Stress Values

The cable segment QR has at the time t the same mass as $\bar{Q}R$ at the time zero, which is $m_2 = \rho q(c - \bar{c})t$. Its velocity is the particle velocity u. Therefore its kinetic energy

$$H_2 = \rho q(c - \bar{c})t \frac{u^2}{2} \quad \ldots\ldots [41]$$

The work required to elongate the cable statically from the stress σ_0 to the stress σ

$$H_\sigma = \frac{\sigma + \sigma_0}{2} q\delta$$

where δ is the elongation. Now $\delta/(ct) = u/c$. Thus

$$H_\sigma = \frac{\sigma + \sigma_0}{2} qct \frac{u}{c} \quad \ldots\ldots [42]$$

We use dimensionless energy coefficients dividing the energies by the arbitrarily chosen energy

$$H_0 = \rho qct \frac{c^2}{2} \quad \ldots\ldots [43]$$

and obtain

$$\eta_1 = \frac{H_1}{H_0} = \frac{\bar{c}}{c}\left(\frac{v_0}{c}\right)^2 \quad \ldots\ldots [44]$$

$$\eta_2 = \frac{H_2}{H_0} = \left(1 - \frac{\bar{c}}{c}\right)\left(\frac{u}{c}\right)^2 \quad \ldots\ldots [45]$$

$$\eta_\sigma = \frac{H_\sigma}{H_0} = \frac{\sigma + \sigma_0}{E} \frac{1}{1 + \frac{\sigma_0}{E}} \frac{u}{c} \quad \ldots\ldots [46]$$

Using Equations [20] and [27] we can express σ/E and σ_0/E by u/c and $\bar{c}/c$. We get

$$\frac{\sigma}{E} = \frac{\left(\frac{\bar{c}}{c}\right)^2}{1 - \left(\frac{\bar{c}}{c}\right)^2}, \quad \frac{\sigma_0}{E} = \frac{\frac{\left(\frac{\bar{c}}{c}\right)^2}{1 - \left(\frac{\bar{c}}{c}\right)^2} - \frac{u}{c}}{1 + \frac{u}{c}}$$

Then η_σ takes the form

$$\eta_\sigma = 2\left(\frac{\bar{c}}{c}\right)^2 \frac{u}{c}\left(1 + \frac{u}{c}\right) - \left(\frac{u}{c}\right)^2 \quad \ldots\ldots [47]$$

a form which corresponds in the variables to η_1 and η_2.

For the total energy $\eta = \eta_1 + \eta_2 + \eta_\sigma$ we obtain

$$\eta = \frac{\bar{c}}{c}\left[\left(\frac{v_0}{c}\right)^2 - \left(\frac{u}{c}\right)^2\right] + 2\left(\frac{\bar{c}}{c}\right)^2 \frac{u}{c}\left(1 + \frac{u}{c}\right). \quad [48]$$

We must find the same value η by computation of the work done against the tension by moving the cable end point O in the direction β with the velocity v_0. This work is equal

$$H = q\sigma v_0 t \cos\gamma \quad \ldots\ldots [49]$$

or in dimensionless form

$$\eta = 2\frac{\sigma}{E} \frac{1}{1 + \frac{\sigma_0}{E}} \frac{v_0}{c} \cos\gamma \quad \ldots\ldots [50]$$

From

$$\cos\gamma = \cos(\beta - \theta) = \cos\beta\cos\theta + \sin\beta\sin\theta$$

and Equation [36]

$$\operatorname{ctg}\theta = \frac{\frac{\omega}{v_0} + \cos\beta}{\sin\beta}$$

follows

$$\cos\gamma = \frac{\frac{v_0}{c} + \frac{\omega}{c}\cos\beta}{\left[\left(\frac{v_0}{c}\right)^2 + \left(\frac{\omega}{c}\right)^2 + 2\frac{v_0}{c}\frac{\omega}{c}\cos\beta\right]^{1/2}} \quad \ldots [51]$$

Equations [29] and [28] yield

$$\left[\left(\frac{v_0}{c}\right)^2 + \left(\frac{\omega}{c}\right)^2 + 2\frac{v_0}{c}\frac{\omega}{c}\cos\beta\right]^{1/2} = \frac{\omega}{c} + \frac{u}{c} = \frac{\bar{c}}{c}\left(1 + \frac{u}{c}\right)$$

and

$$2\frac{v_0}{c}\frac{\omega}{c}\cos\beta = 2\frac{\bar{c}}{c}\frac{u}{c}\left(1 + \frac{u}{c}\right) - \left(\frac{v_0}{c}\right)^2 - \left(\frac{u}{c}\right)^2$$

Therefore because of Equation [50]

$$\eta = \frac{\frac{\sigma}{E}}{1 + \frac{\sigma_0}{E}} \frac{\left(\frac{v_0}{c}\right)^2 - \left(\frac{u}{c}\right)^2 + 2\frac{\bar{c}}{c}\frac{u}{c}\left(1 + \frac{u}{c}\right)}{\frac{\bar{c}}{c}\left(1 + \frac{u}{c}\right)}. \quad [52]$$

Equation [20] for $\bar{c}/c$ shows that

$$\frac{\sigma/E}{\bar{c}/c} = \frac{\bar{c}}{c}\left(1 + \frac{\sigma}{E}\right)$$

and Equation [27] for u/c that

$$1 + \frac{u}{c} = \frac{1 + \frac{\sigma}{E}}{1 + \frac{\sigma_0}{E}}$$

Therefore Expression [52] for η becomes

$$\eta = \frac{\bar{c}}{c}\left[\left(\frac{v_0}{c}\right)^2 - \left(\frac{u}{c}\right)^2\right] + 2\left(\frac{\bar{c}}{c}\right)^2 \frac{u}{c}\left(1 + \frac{u}{c}\right). \quad [53]$$

which is identical with Equation [48].

Equations [44], [45], and [47] show correctly the distribution of the input energy over the cable in the general case as functions of the stress σ if v_0/c, $\bar{c}/c$, and u/c are replaced by their expressions in σ.

If now σ/E and σ_0/E are negligibly small compared with 1, these formulas simplify to

$$\left.\begin{aligned} \eta_1 &= \left(\frac{\sigma}{E}\right)^{1/2}\left(\frac{v_0}{c}\right)^2 \\ \eta_2 &= \left[1 - \left(\frac{\sigma}{E}\right)^{1/2}\right]\left(\frac{\sigma - \sigma_0}{E}\right)^2 \\ \eta_\sigma &= 2\frac{\sigma}{E}\frac{\sigma - \sigma_0}{E} - \left(\frac{\sigma - \sigma_0}{E}\right)^2 \end{aligned}\right\} \quad \ldots\ldots [54]$$

Thus

$$\frac{\eta_2}{\eta_\sigma} = \left[1 - \left(\frac{\sigma}{E}\right)^{1/2}\right] \frac{\sigma - \sigma_0}{\sigma + \sigma_0} \quad \ldots\ldots\ldots [55]$$

If, moreover, σ_0 is zero or small compared with σ the last formula shows that the strain energy is always approximately equal to the kinetic energy of the longitudinally moving cable segment.

In the case of perpendicular impact we have, because of Equation [38], the following approximate expression

$$\left(\frac{v_0}{c}\right)^2 = 2\,\frac{\sigma - \sigma_0}{E}\left(\frac{\sigma}{E}\right)^{1/2}$$

and therefore, approximately

$$\eta_1 = 2\left(\frac{\sigma - \sigma_0}{E}\right)^2$$

while approximately

$$\eta_\sigma = \left(\frac{\sigma - \sigma_0}{E}\right)^2$$

So the kinetic energy of the segment moving transversely is about 50 per cent of the total energy while the kinetic energy of the segment moving longitudinally and the strain energy are about 25 per cent each of the total energy. The last result has been found by J. Thomlinson (England). Equation [55], however, shows that for larger stresses these statements can be considered as crude approximations only because $(\sigma/E)^{1/2}$ is not always negligibly small compared with 1 if σ/E is so.

Conclusion

Summarizing the results of the present paper, the relation between the impact stress and the impact velocity in the general case of an oblique impact at a cable has been determined, Equation [30], including as special cases de Saint Venant's formula for the longitudinal and the author's earlier formula for the perpendicular impact stress. Using a slight approximation, the general formula has been represented by a graph, Fig. 5, from which the impact stress can be determined for a given impact velocity, a given impact angle, and any practical values of the cable material constants and its initial stress. It has been verified that the impact energy and the kinetic and strain energy of the cable are balanced correctly because of the oblique impact relation. Measured impact stresses are compared with the theory in the case of perpendicular impact for three different cable diameters, Fig. 7.

Acknowledgment

The author is indebted to the U. S. Navy for the permission to use cable impact measurements in this paper, to Mr. Walter J. Kaufman for many inspiring discussions, and to Mr. James S. Hughes, Jr., for valuable contributions and assistance in the computational work.

BIBLIOGRAPHY

1 "Choc longitudinal de deux barres élastiques," by B. de Saint Venant, *Comptes Rendus de l'Académie des Sciences*, Paris, France, vol. 66, 1868, pp. 650–653.

2 "Dynamics of a Moving Cable," by F. O. Ringleb, Naval Air Material Center, Philadelphia, Pa., Report No. M-4812, 1948.

3 "On the Non-Linear Vibration Problem of the Elastic String," by G. F. Carrier, *Quarterly of Applied Mathematics*, vol. 3, 1945, pp. 157–165.

4 "The Motion of a Finite Elastic Cable," by F. E. Marble, Report of North American Instruments, Inc., Altadena, Calif., 1954.

5 "Constant-Strain Waves in Strings," by J. D. Cole, C. B. Dougherty, and J. H. Huth, Journal of Applied Mechanics, Trans. ASME, vol. 75, 1953, pp. 519–522.

6 "High Velocity Engagement of Arresting Wires," by C. Tuman, Report of U. S. Naval Air Missile Test Center, Point Mugu, Calif., 1954.

The Specific Damping Energy of Fixed-Fixed Beam Specimens

By W. C. HAGEL[1] AND J. W. CLARK,[2] SCHENECTADY, N. Y.

The internal-damping effects of varying composition, heat-treatment, cold work, magnetic-field strength, stress history, and static tension stress have been studied at room temperature using fixed-fixed beam specimens supported in a new bending vibration-decay apparatus. Experimental logarithmic decrements are converted to specific damping energies by a straightforward numerical method; such information is needed to extend a fundamental understanding of the physical nature of damping and to provide useful engineering-design data. Changing hardness from 225 to 388 Bhn was found to cause a wider variation in AISI 403 specimen damping than the application of a static tension stress or d-c magnetic field. Even at relatively low vibration stresses, considerable energy dissipation originates from microscopic plastic flow in soft materials.

Nomenclature

The following nomenclature is used in the paper:

- σ = normal vibration stress at any point in member, psi
- σ_m = maximum normal stress at outside fibers of member, psi
- σ_T = static tension stress, psi
- δ = logarithmic decrement per cycle associated with σ_m
- D_0 = total energy dissipated by member per cycle, in-lb per cycle
- W_0 = total elastic energy in member at σ_m, in-lb
- V_0 = total effective volume of member contributing to dissipation of energy D_0, cu in.
- V = member volume at stress less than σ, cu in.
- $f(\sigma/\sigma_m)$ = volume-stress function, defined as the fraction of member volume possessing a stress ratio less than a given σ/σ_m
- D = specific damping energy of a material associated with σ, in-lb per cu in. per cycle
- ν = first-mode resonant frequency of fixed-fixed beam specimen, cps
- d = beam thickness, in.
- b = beam width, in.
- l = effective beam length, in.
- E = Young's modulus of material, psi
- g = acceleration due to gravity, in. per sq sec
- ρ = weight per unit volume, lb per cu in.
- A_n = amplitude of nth cycle of vibration, in.
- Δdb = incremental change in decibel level for a corresponding change, Δl, in decay time
- φ'' = second derivative of characteristic function for a fixed-fixed beam
- x = distance from one end of beam specimen, in.
- δ_0 = logarithmic decrement per cycle associated with σ

Introduction

When machine members such as propeller, compressor, and turbine blades operate near resonance, high-amplitude vibrations can cause faulty operation and failure unless sufficient internal and external damping sources are available to decrease induced stresses. Several investigators (1, 2, 3)[3] have emphasized the importance of internal damping in calculations of resonance response using a stress function $f(\sigma/\sigma_m)$ of a member and the specific damping energy D of the material. Since the origins of internal damping (at higher vibration stresses and frequencies than those normally considered for physical internal-friction measurements) are plastic flow and magnetomechanical effects in ferromagnetic alloys (4), variables known to affect D are composition, heat-treatment, cold work, magnetic-field strength, stress history, static tension stress σ_T, and temperature. The bending-vibration apparatus employed here is ideal for obtaining information of a fundamental nature. It can be adapted to provide satisfactory variation in the afore-mentioned variables; the effect of σ_T can be determined under conditions in which the principal stress planes are the same for both static tension and normal vibration stresses; the fixed-fixed beam specimens are of relatively simple shape and have a volume-stress function similar to a turbine blade; the measurements show evidence of high sensitivity and reproducibility.

The purpose of this investigation was to conduct bending vibration-decay tests on AISI 403 and A-nickel specimens of known heat-treatment and mechanical properties at σ_T equal to 0, 5600, 11,000 and 19,000 psi and within d-c magnetic fields of 0 to 500 oersteds. If the volume-stress functions of complicated machine members are determinable, the specific damping energies calculated here can be used to derive their internal damping and ability to withstand failure under near-resonant operating conditions.

Testing Procedure

Although a brief description of procedure is necessary to establish experimental validity, a more detailed explanation of the theory and instrumentation required will be reported elsewhere (5). As depicted in Fig. 1, each specimen is machined in the form of a 20.0 × 0.300 × 0.125-in. beam, connected with 0.500-in. fillets, to the center of 1.94 × 4.00 × 0.125-in. end grips. It is firmly fixed to two large steel blocks that are suspended by steel straps to minimize the loss of vibrational energy to the supporting frame; a static tension stress can be applied by lowering one block in an arc below the other and adding weights. On obtaining its energy from a power amplifier and audio oscillator, an electromagnetic drive coil positioned near a zero-stress point causes bending vibration normal to the 0.125-surface. In effect, the specimen closely approximates a turbine blade, whose root and

[1] Research Engineer, Large Steam Turbine-Generator Department, General Electric Company.

[2] Research Engineer, Advanced Science Program, General Electric Company.

Presented at the Applied Mechanics Division Summer Conference, Berkeley, Calif., June 13–15, 1957, of The American Society of Mechanical Engineers.

Discussion of this paper should be addressed to the Secretary, ASME, 29 West 39th Street, New York, N. Y., and will be accepted until October 10, 1957, for publication at a later date. Discussion received after the closing date will be returned.

Note: Statements and opinions advanced in papers are to be understood as individual expressions of their authors and not those of the Society. Manuscript received by ASME Applied Mechanics Division, September 24, 1956. Paper No. 57—APM-18.

[3] Numbers in parentheses refer to the Bibliography at the end of the paper.

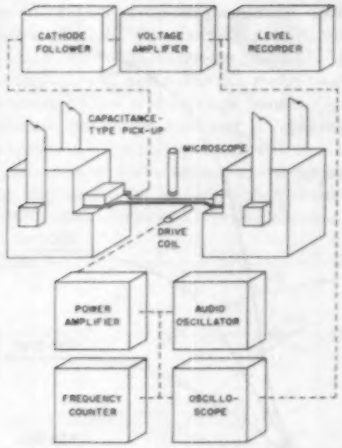

FIG. 1 BLOCK DIAGRAM OF TEST INSTRUMENTATION

tip are respectively fixed to the rotor and shrouding, tangentially vibrating in its first mode under a centrifugal stress. Vibration amplitudes can be observed through a calibrated optical microscope focused on fiducial particles located at beam center. The first-mode resonant frequency ν is measured with a frequency counter on driving the specimen at a constant vibration amplitude and frequency such that a suitable Lissajous pattern appears on an oscilloscope. If one could determine the effective length l of these beams, the expression

$$\nu = 1.03 \frac{d}{l^2}\sqrt{\frac{Eg}{\rho}} \quad \ldots\ldots [1]$$

would permit accurate determination of dynamic E. Within the range of stresses (0–40,000 psi) and frequencies (150–250 cycles per sec) used, dynamic E shows no significant change from static E.

When the specimen is vibrating at resonance and at a steady-state amplitude, equivalent to σ_m not exceeding 75 per cent of the 2×10^7 cycle fatigue strengths of these materials, the drive force is disconnected, and a capacitance-type pickup located near a fixed specimen end converts mechanical vibration to sinusoidal voltage which is amplified and fed to a level recorder. Using a decibel-time scale, the decay curve is scribed in wax on a high-speed recorder chart. To accommodate sudden changes in amplitude when high-damping materials are tested, frequency response of the recording amplifier is at least 40 times greater than the test frequencies. Since logarithmic decrement δ is defined as

$$\delta = \ln\left(\frac{A_n}{A_{n+1}}\right) \quad \ldots\ldots [2]$$

and the amplitude ratio is plotted on a scale where the change in decibel level between two successive amplitudes

$$(db)_1 = 20 \log\left(\frac{A_n}{A_{n+1}}\right) = \frac{1}{\nu}\frac{\Delta db}{\Delta t} \quad \ldots\ldots [3]$$

$$\delta = 0.115 \frac{1}{\nu}\frac{\Delta db}{\Delta t} \quad \ldots\ldots [4]$$

Determining the slope ($\Delta db/\Delta t$) involves the use of tangents at decibel levels logarithmically proportional to σ_m, but no error greater than ±4.3 per cent between 5000 and 30,000 psi was detected among those observers who analyzed the same decay curves. At σ_m greater than 30,000 psi, decay has just started; at σ_m less than 5000 psi, a small amount of noise pickup occurs. Aside from experimental mistakes in allowing specimen prestressing or looseness at the fixed ends, the maximum probable error of each δ and σ_m measurement between the foregoing limits is respectively ±4.6 and ±1.3 per cent. Air damping and loss of energy to the large steel blocks are negligible.

Listed in Table 1 are the heat-treatments and mechanical properties of specimens tested. The AISI 403 material used contained 12.05 Cr, 0.54 Mn, 0.38 Ni, 0.26 Si, 0.12 C, balance Fe; the A-nickel specimen contained 0.18 Mn, 0.14 Fe, 0.11 Cr, 0.10 C, balance Ni. After removing a portion of heat-treated stock for tensile testing, the rough beams were machined to 0.003 in. oversize, polished to size, and stress-relieved in an inert atmosphere. Brinell hardness numbers, converted from Rockwell C and A scales, were taken on each damping specimen at the conclusion of the investigation. The relation that tensile strength in pounds per square inch equals 485 times the Brinell hardness has been found to hold for AISI 403 (6); the same general agreement appears here to show that subsequent machining, polishing, and stress-relieving caused no further change in mechanical properties. In order to prevent accidental prestressing, the long, thin beam specimens were stored and transported in felt-lined containers.

TABLE 1 HEAT-TREATMENT AND MECHANICAL PROPERTIES

Specimen No.	Heat-treatment	Bhn	Tensile strength × 10^3, psi	0.02 per cent yield strength × 10^3, psi
403-1	1850 F—3 hr—WQ 900 F—2 hr—AC	388	190	122
403-2	1850 F—3 hr—WQ 1000 F—2 hr—AC	335	160	112
403-3	1850 F—3 hr—WQ 1100 F—2 hr—AC	293	140	110
403-4	1850 F—3 hr—WQ 1200 F—2 hr—AC	280	133	99
403-5	1850 F—3 hr—WQ 1300 F—2 hr—AC	250	115	85
403-6	1850 F—3 hr—AC 1300 F—8 hr—AC	225	110	83
403-7	1850 F—3 hr—AC 1200 F—2 hr—AC	248	123	94
403-8	Same as 403-7	243	120	93
403-9	Same as 403-7 Shot-peened to −50,000 psi	252 261 SP	125	93
403-10	Same as 403-7 Shot-peened to −70,000 psi	249 280 SP	122	92
403-11	Same as 403-3	291	138	106
Ni-12	1400 F—4 hr—AC	103	67	26

Two specimens were shot-peened to surface compressive stresses of 50,000 ± 5000 psi and 70,000 ± 5000 psi; x-ray stress analyses showed that these values parabolically decreased to zero at a depth of 0.002 in. Magnetically, the domain crystal structure of AISI 403 changes from cubic to tetragonal in the direction of magnetization or strain (positive magnetostriction), whereas that in A-nickel changes from cubic to tetragonal normal to the direction of magnetization or strain (negative magnetostriction). Since the high damping of ferromagnetic materials is caused by domain motion under stress, known d-c magnetic fields were applied for various degrees of domain alignment; on achieving magnetic saturation, no damping originated from magnetomechanical effects.

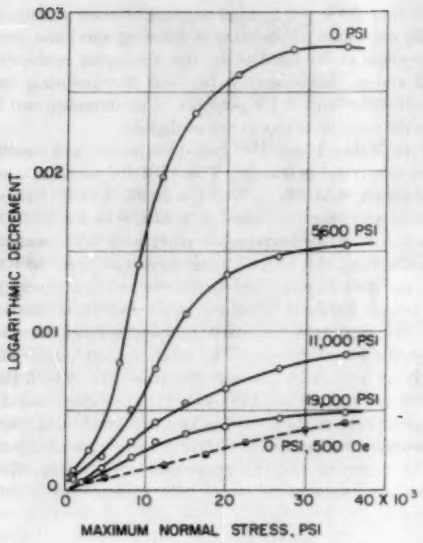

FIG. 2 EFFECT OF STATIC TENSION STRESS AND MAGNETIC SATURATION ON DAMPING OF SPECIMEN 403-6

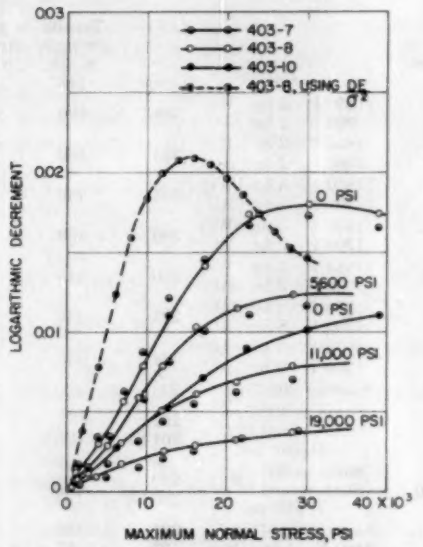

FIG. 3 EFFECT OF STATIC TENSION STRESS AND SHOT-PEENING ON DAMPING OF SPECIMENS 403-7, 8, 10

(Dotted curve shows a superposition of δ_0 versus σ for specimen 403-8.)

EXPERIMENTAL RESULTS

Fig. 2 shows the typical decrease in damping caused by increasing σ_T to 19,000 psi. Although there is a small initial damping increase at low oersted values, a similar decrease in damping occurs when the specimen is placed within a solenoid and subjected to an increasing magnetic field; at magnetic saturation and $\sigma_T = 0$ psi, the damping curve is displaced slightly lower than the 19,000-psi curve. As evidence of the sensitivity and reproducibility of this method of measurement, experimental points are shown in Fig. 3 for two specimens (403-7, 8) of the same heat-treatment and nearly the same Brinell hardness (248 and 243).

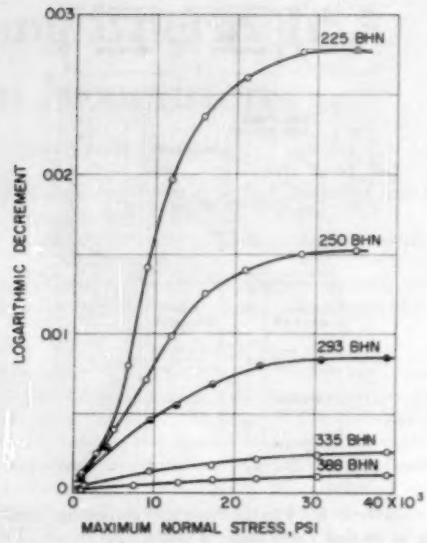

FIG. 4 EFFECT OF HARDNESS ON DAMPING OF SPECIMENS 403-1 2, 3, 5, 6, UNDER ZERO STATIC TENSION STRESS

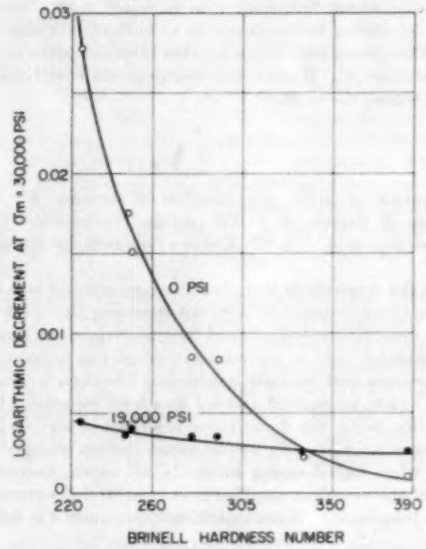

FIG. 5 LOGARITHMIC DECREMENT AT σ_m = 30,000 PSI VERSUS SPECIMEN BRINELL HARDNESS AT σ_T EQUAL TO 0 AND 19,000 PSI

At σ_T equal to 0, 5600 and 11,000 psi, the data for the softer specimen fall slightly above those of the harder. Since the maximum probable error of each hardness measurement is about $\pm$ 3 per cent, it could have been possible for no real difference to exist in the hardness of these two specimens. However, the damping data do present confirmatory evidence of such a small difference. Specimen 403-10 was given a similar heat-treatment and shot-peened to a surface compressive stress of $-70{,}000$ psi, causing a damping decrease of 45 per cent at $\sigma_T = 0$ psi; the results for shot-peened specimen 403-9 ($-50{,}000$ psi) fell intermediate between the two extremes plotted in Fig. 3.

For brevity, all of the experimental data obtained cannot be shown, but the general effect of specimen hardness on logarithmic

decrement as a function of maximum normal stress at $\sigma_T = 0$ psi is plotted in Fig. 4. By choosing a particular maximum normal stress level, $\sigma_m = 30{,}000$ psi, the graph of Fig. 5 shows the relation of damping, with and without a static tension stress, to specimen hardness. Most of the damping for the lower curve results from microscopic plastic flow and is relatively insensitive to specimen hardness. No matter what heat-treatment is given AISI 403, application of static tension stress equivalent to that present in rotating turbine blades longer than about 7 in. will decrease the logarithmic-decrement values to less than 0.005.

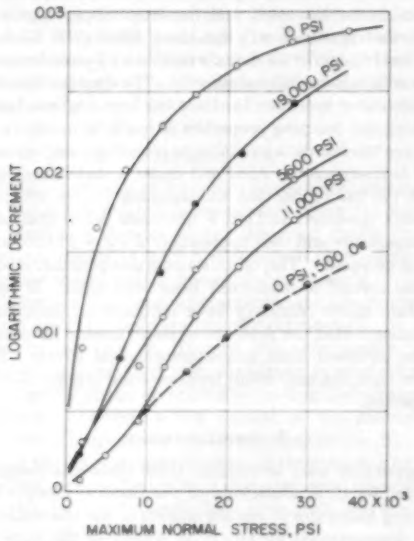

FIG. 6 EFFECT OF STATIC TENSION STRESS AND MAGNETIC SATURATION ON DAMPING OF SPECIMEN NI-12

In the case of A-nickel, Fig. 6, one can see that static tension stress first causes a decrease in damping as the domains become strain aligned; at $\sigma_T = 19{,}000$ psi, damping increases owing to the microscopic plastic flow within this relatively soft material. The maximum damping possible from magnetomechanical effects is the difference between the curves at zero static tension stress with and without a saturating magnetic field.

Specific Damping-Energy Calculations. Provided D_0 is small, as it is with these examples of internal damping, the logarithmic decrement defined in Equation [2] may also be expressed as

$$\delta = \frac{D_0}{2W_0} \quad [5]$$

Using the second derivative of the characteristic function ϕ'' for a fixed-fixed beam, $\phi'' = 2$ at $x = 0$ (7), one can calculate that

$$W_0 = \frac{bdl}{6E(\phi'')^2}\sigma_m^2 = \frac{V_0\sigma_m^2}{24E} \quad [6]$$

for the first-mode vibration of these specimens. Since specimen stress distribution is nonuniform

$$D_0 = \int_0^{V_0} D dV \quad [7]$$

or

$$D_0 = D(\sigma_m)V_0 - V_0\int_0^{\sigma_m} D'(\sigma) f\left(\frac{\sigma}{\sigma_m}\right) d\sigma \quad [8]$$

on substituting

$$dV = f'\left(\frac{\sigma}{\sigma_m}\right) d\left(\frac{\sigma}{\sigma_m}\right) V_0$$

and integrating by parts. If the quantities D_0, $D(\sigma_m)$, and $D(\sigma)$ are expressed as polynomials of the type

$$D_0 = k_1\sigma_m + k_2\sigma_m^2 + \ldots\ldots k_n\sigma_m^n \ldots\ldots [9]$$

$$D(\sigma_m) = K_1\sigma_m + K_2\sigma_m^2 + \ldots\ldots K_n\sigma_m^n \ldots\ldots [10]$$

$$D(\sigma) = K_1\sigma + K_2\sigma^2 + \ldots\ldots K_n\sigma^n \ldots\ldots [11]$$

then the integral in Equation [8]

$$\int_0^{\sigma_m} D'(\sigma) f\left(\frac{\sigma}{\sigma_m}\right) d\sigma = K_1\int_0^{\sigma_m} f\left(\frac{\sigma}{\sigma_m}\right) d\sigma + 2K_2\int_0^{\sigma_m} f\left(\frac{\sigma}{\sigma_m}\right)\sigma d\sigma + \ldots nK_n\int_0^{\sigma_m} f\left(\frac{\sigma}{\sigma_m}\right)\sigma^{n-1} d\sigma \ldots [12]$$

For any one logarithmic-decrement curve at $\sigma_T = 0$ psi, the con-

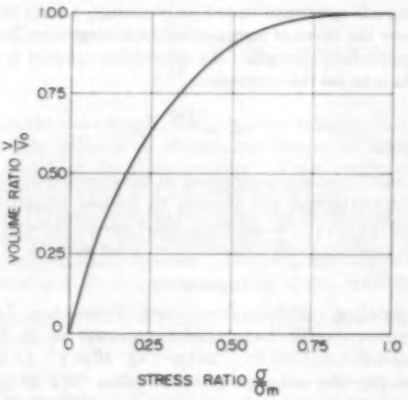

FIG. 7 VOLUME-STRESS FUNCTION FOR FIRST-MODE VIBRATION OF FIXED-FIXED BEAM

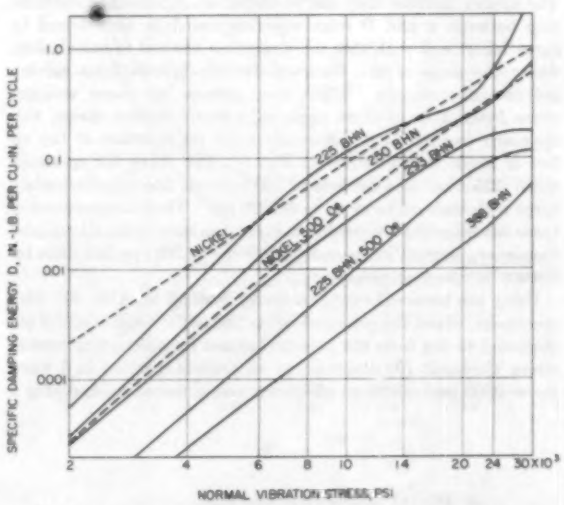

FIG. 8 SPECIFIC DAMPING ENERGY CURVES SHOWING EFFECT OF MATERIAL COMPOSITION, HEAT-TREATMENT (HARDNESS), AND MAGNETIC-FIELD STRENGTH

stants of Equation [9] can be found by using $n = 5$ and Equations [5] and [6] in the form

$$\delta = \frac{12E}{V_0}(k_1\sigma_m^{-1} + k_2 + \ldots k_n\sigma_m^{n-2}) \ldots\ldots\ldots [13]$$

The volume-stress function plotted in Fig. 7 was derived from the tabulations of Young and Felgar (7); the integrals in Equation [12] were solved numerically on applying Simpson's one-third rule with 10 subdivisions. Therefore, the constants needed for Equation [11] are determinable, and specific damping-energy curves can be plotted as shown in Fig. 8. The effect of root fillets in these specimens is negligible; the value of E used for both alloys was 30×10^6 psi. Since logarithmic-decrement curves were used to obtain the constants in Equation [13], the calculated curves of Fig. 8 show no data scatter; a reasonable estimation of the accuracy of these curves is ± 5 per cent, on carrying out the calculations with aid of a digital computer. Application of a static tension stress does not permit a rigorous solution of the aforementioned equations, and they do not apply when appreciable plastic flow occurs. Although specific damping energies were calculated for all specimens tested, only enough curves were plotted to show the effect of composition, heat-treatment (hardness), and magnetic-field strength. An alternative method of plotting these data is to use the expression

$$\delta_0 = \frac{DE}{\sigma^2} \ldots\ldots\ldots\ldots\ldots\ldots [14]$$

and one such curve is superimposed on the experimental curves of Fig. 3, on converting the abscissa to normal vibration stress. Note that the curve for specimen 403-8 passes through δ_0 equal to zero, indicating perfect elasticity at lower stresses.

Discussion

From rotating cantilever-beam tests, Person and Lazan (8) have reported specific damping-energy results on an AISI 403 beam heat-treated (1750 F—0.25 hr—OQ; 1050 F—1.5 hr—AC), approximately the same as specimen 403-3 (293 Bhn). Since they report no mechanical properties, it is difficult to make a direct comparison. However, their curve at zero static tension stress best coincides with that of specimen 403-5 (250 Bhn). The approximations they use to obtain an exponential relationship between σ and D from experimental data were found to agree fairly well with this more rigorous method of calculation, where the slope of the D-curves directly follows from solving polynomial constants. While they assume the same volume-stress function to hold on applying a static tension stress, this approach was not held sufficiently valid for insertion of the effect of static tension stress in Fig. 8. The curve for specimen 403-6 (225 Bhn) in a d-c field of 500 oersteds does approximately agree with their curve at $\sigma_T = 30{,}000$ psi. The fair agreement of these investigations provides indirect evidence that vibrational frequency, at least in the range of 6 cps to 200 cps, has little influence on damping properties.

Using the torsional vibration-decay method on AISI 403 wire specimens, where the principal stress planes for tension stress are displaced 45 deg from the principal planes for alternating torsion stress, Cochardt (9) observed an anomalous increase in δ when $\sigma_T = 9800$ psi. Such an effect was not observed on applying a static tension stress to any of the specimens tested in this investigation and is inconsistent with theory. Although Cochardt (4) states that D of a hollow AISI 403 specimen increases in proportion to the third power of stress up to the critical stress and remains essentially constant thereafter, the influence of microscopic plastic flow in specimen 403-6 (225 Bhn) causes an initial slope of 3.5 up to the critical stress (10,000 psi) and a slope of one until excessive plastic deformation begins to occur at 20,000 psi. Extreme increases in D by plastic flow offer good evidence for impending fatigue damage. As the specimens increase in hardness, permitting less microscopic plastic flow, initial slope decreases, the critical stress increases, and the latter slopes approach zero before further plastic flow. Specimen 403-1 (388 Bhn) is sufficiently hard to hinder all domain motion and provides no damping from magnetomechanical effects. The quantitative effect of heat-treatment or specimen hardness has been neglected generally in reporting the damping properties of machine members.

There are too few data available to permit generalization of the effect of temperature on AISI 403 under a static tension stress; Cochardt (9) has found that the damping ($\sigma_T = 910$ psi) of a wire torsion specimen at 1110 F decreases below that of one at room temperature and that application of $\sigma_T = 51{,}000$ psi causes additional decrease. This effect is undergoing further study using a furnace around a fixed-fixed beam specimen. If operating temperature exerts relatively little influence on damping, these results indicate that the presence of static tension stresses nullify any gains obtained from magnetomechanical effects. In practice, more damping may result from external origins than heretofore suspected.

Acknowledgment

The apparatus used to conduct these tests was designed and constructed by C. S. Duckwald of the General Electric General Engineering Laboratory; certain aspects of the theoretical analysis were demonstrated by Dr. P. R. Paslay of the same laboratory.

BIBLIOGRAPHY

1 "A New Fatigue Strength-Damping Criterion for Design of Resonant Members," by J. Marin and F. B. Stulen, Trans. ASME, vol. 69, 1947, pp. A-209–A-212.

2 "Effect of Damping Constants and Stress Distribution on the Resonance Response of Members," by B. J. Lazan, Journal of Applied Mechanics, Trans. ASME, vol. 75, 1953, pp. 201–209.

3 "A Method for Determining the Internal Damping of Machine Members," by A. W. Cochardt, Journal of Applied Mechanics, Trans. ASME, vol. 76, 1954, pp. 257–262.

4 "The Origin of Damping in High-Strength Ferromagnetic Alloys," by A. W. Cochardt, Journal of Applied Mechanics, Trans. ASME, vol. 75, 1953, pp. 196–200.

5 Private communication by C. S. Duckwald, July, 1956.

6 "Structural Stability of Modified 12-Chromium Alloys," by W. C. Hagel and E. F. Becht, Trans. ASME, vol. 78, 1956, pp. 1439–1446.

7 "Table of Characteristic Functions Representing Normal Modes of Vibration of a Beam," by D. Young and R. P. Felgar, Jr., Engineering Research Series, No. 44, University of Texas, Austin, Texas.

8 "The Effect of Static Mean Stress on the Damping Properties of Materials," by N. L. Person and B. J. Lazan, ASTM Preprint No. 5, presented at Annual Meeting of the Society, June, 1956.

9 "Effect of Static Stress on the Damping of Some Engineering Alloys," by A. W. Cochardt, Trans. ASM, vol. 47, 1955, pp. 440–450.

A Study of the Propagation of Flexural Waves in Elastic Beams

By E. A. RIPPERGER[1] and H. NORMAN ABRAMSON[2]

Experimental results for flexural wave propagation in elastic beams of circular cross sections resulting from very sharp impacts are presented. It is noted that a well-defined wave system precedes the main pulse. The experimental results are correlated with theoretical predictions from both the Pochhammer-Chree and Timoshenko theories.

Introduction

RECENT studies of transients in elastic beams have largely been concentrated independently along the lines of approximate theories (1–3),[3] the exact theory (4, 5), and experimental results (6–8). A comparison of experimental and approximate theory results was published recently (9, 10), while a comparison of the exact and approximate theories was made some time ago (11), and very recently extended (5).

It has been shown (9, 10) that the approximate theory of Timoshenko may be used with confidence in predicting the response of elastic beams to impulsive loadings for all except very short pulses; however, a few aspects of the phenomenon of flexural wave propagation remained obscure (5, 8). It is a purpose of the present paper to clear up these aspects by presenting experimental results for very sharp impacts, discussing these results with respect to predictions from both the approximate and exact theories.

Theoretical Considerations

A procedure for studying the propagation of a pulse of flexural waves in a solid circular cylinder, based on Kelvin's method of stationary phase, has been described by Davies (11). Briefly, the analysis is based upon the propagation of an infinitesimally thin pulse of infinitely large magnitude which is applied at some time $t' = 0$; the initial distribution of stress is expressed as a Fourier integral in such a way that it may be regarded as the superposition of sinusoidal stress waves covering the whole spectrum of wave lengths. All of the waves are of equal magnitude, agreeing in phase at the origin and canceling out everywhere else. The stress distribution at any subsequent time may then be investigated by means of group-velocity curves. Since the waves are of different phase they interfere in such a way that the main effect is produced by a small group of waves whose phase velocities, periods, and wave lengths are nearly equal, and which are in nearly the same phase at a point z along the beam at time t'.

Let the period of the dominant group of waves be denoted by T_p, and let T_a and $\frac{1}{2}T_0$ be the time required for a longitudinal wave traveling at the "bar velocity" to traverse the radius a and the distance z along the bar, respectively. These quantities may then be written as two nondimensional ratios

$$\frac{T_p}{T_a} = \frac{1}{\frac{(a)}{(\Lambda)}\frac{(C)}{(C_0)}} \quad \ldots\ldots [1]$$

$$\frac{t'}{\frac{1}{2}T_0} = \frac{1}{C_g/C_0} \quad \ldots\ldots [2]$$

where Λ is the wave length, C is the phase velocity, C_0 is the bar velocity (the velocity of longitudinal waves of infinite wave length), and C_g is the group velocity. These results are shown conveniently by a plot of T_p/T_a versus $t'/[(1/2)T_0]$.

Davies (11) compared, on this basis, the predictions of flexural wave propagation by the Pochhammer-Chree[4] (exact) and Timoshenko (approximate) theories. The comparison was made on the basis of a single transmission mode of the exact theory (4)

[4] This solution is exact only for an infinitely long bar; it is referred to as "exact" here for convenience.

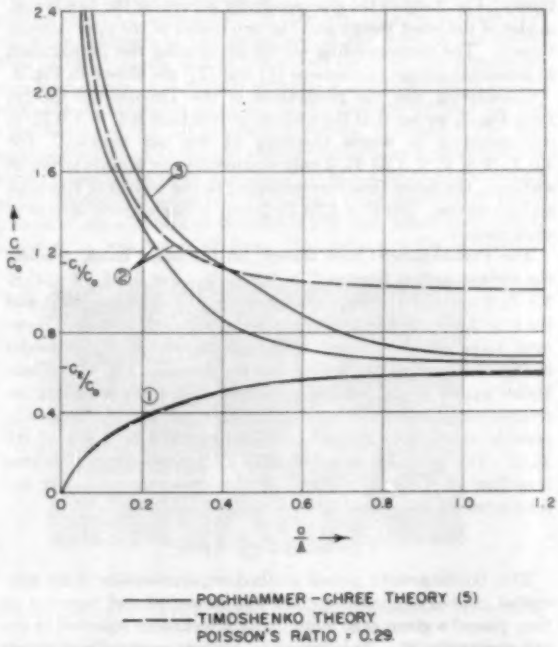

Fig. 1 Phase Velocity of Flexural Waves

[1] Associate Professor of Engineering Mechanics and Research Engineer, Defense Research Laboratory, The University of Texas, Austin, Texas. Mem. ASME.

[2] Manager, Engineering Analysis Section, Southwest Research Institute, San Antonio, Texas. Assoc. Mem. ASME.

[3] Numbers in parentheses refer to the Bibliography at the end of the paper.

Presented at the Applied Mechanics Division Summer Conference, Berkeley, Calif., June 13–15, 1957, of The American Society of Mechanical Engineers.

Discussion of this paper should be addressed to the Secretary, ASME, 29 West 39th Street, New York, N. Y., and will be accepted until October 10, 1957, for publication at a later date. Discussion received after the closing date will be returned.

Note: Statements and opinions advanced in papers are to be understood as individual expressions of their authors and not those of the Society. Manuscript received by ASME Applied Mechanics Division, October 4, 1956. Paper No. 57—APM-11.

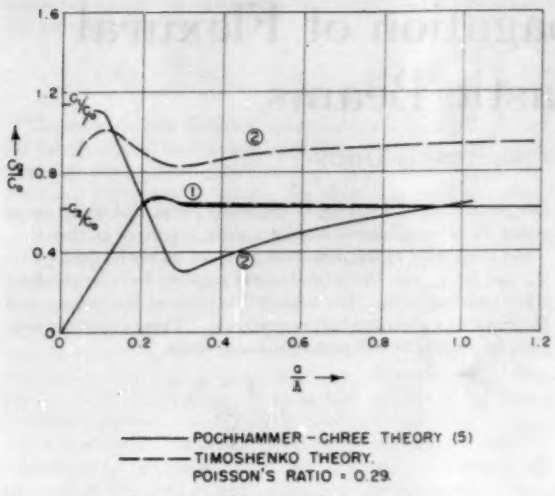

FIG. 2 GROUP VELOCITY OF FLEXURAL WAVES

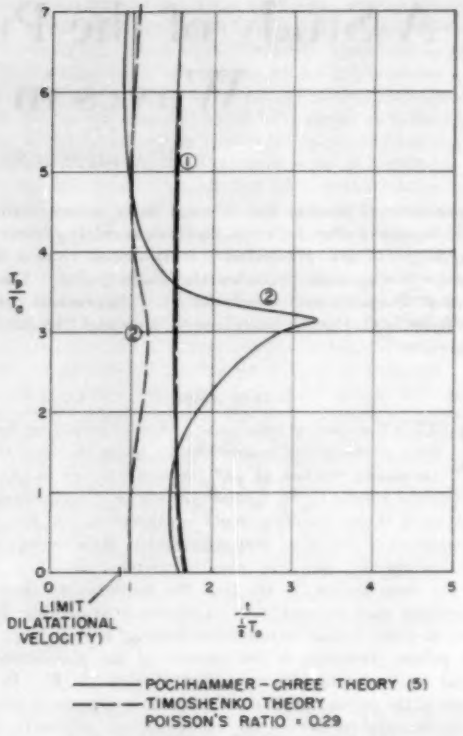

FIG. 3 PROPAGATION OF FLEXURAL WAVES

and the lower of the two transmission modes of the approximate theory. The comparison indicated that no disturbance would arrive at a section z along the beam until a time $t' = 1.56\ T_0/2$; for $1.56\ T_0/2 \leq t' \leq 1.73\ T_0/2$ two groups of different wave lengths and periods arrive simultaneously at each value of t'; for $t' > 1.73\ T_0/2$ only one group arrives at z at each instant.

The Pochhammer-Chree theory has recently been extended (5) so that knowledge of the higher transmission modes is now available and therefore may be used for a more extensive study and comparison with experimental results. Fig. 1 shows the phase-velocity curves for the three lowest transmission modes from the exact theory and the two modes from the approximate theory; Fig. 2 shows the group-velocity curves for the two lowest modes of the exact theory and the two modes of the approximate theory. The corresponding curves illustrating the propagation of dominant groups (Equations [1] and [2]) are shown in Fig. 3.

Considering now the predictions of the Timoshenko theory, from Fig. 3, we see that the earliest arrival time is $t' = 1.0\ T_0/2$, corresponding to waves traveling at the bar velocity. For $1.0\ T_0/2 \leq t' \leq 1.73\ T_0/2$ only scattered wave groups arrive at section z, the latter time corresponding to the arrival of Rayleigh surface waves. For $t' > 1.73\ T_0/2$ only a single group arrives at each instant.

The Pochhammer-Chree theory, on the other hand, predicts the earliest arrival time as $t' = 0.9\ T_0/2$. For $0.9\ T_0/2 < t' \leq 3.3\ T_0/2$ a number of wave groups arrive at z at each instant and for $t' > 3.3\ T_0/2$ only one group arrives at each instant. However, there are also present an infinite number of higher modes in this theory (only the lowest two are shown in Fig. 3). These higher modes would tend to provide additional wave-group arrivals during the entire range $t' \geq 0.9\ T_0/2$, and would additionally provide wave-group arrivals in the range $0.875\ T_0/2 \leq t' \leq 0.9\ T_0/2$. The arrival time $t' = 0.875\ T_0/2$ corresponds to waves traveling at the dilatational velocity, this velocity being the maximum group velocity attainable (5).

EXPERIMENTAL STUDIES

The bending-wave pulses studied experimentally were generated in a bar of circular section, and measured and recorded as they passed a given gage point, using a technique reported in detail previously (8). This technique consists essentially of shooting a small steel ball against the plane end of a steel bar so that it strikes eccentrically and thus applies a moment to the bar. The pulse passing a given gage point is detected by wire-resistance strain gages connected so as to eliminate the symmetrical strain components. The strain-gage signal is then recorded by means of an oscilloscope and camera. Previous studies (7) have shown that pulses generated in this way are essentially Hertzian in character and that their duration can be computed with acceptable precision according to the Hertz theory of impact between elastic spheres (12).

In order to generate an extremely sharp pulse of short duration, which would approximate the Kelvin condition upon which the theoretical analysis is based, a $^1/_{16}$-in-diam ball was fired against the hardened end of a $^1/_2$-in-diam cylindrical bar at a velocity of approximately 460 fps. Calculations indicate that the pulse generated by this impact should be about 2 microsec long. Such a pulse will not contain as complete a spectrum of wave lengths as the infinitesimally short pulse of infinitely large magnitude contains, but its wave-length content does cover a large portion of the spectrum.

In order to examine the form of the input-bending wave pulse and to determine its duration, a few preliminary measurements of longitudinal waves generated by centric impact were made. Two wire-resistance strain gages were affixed in diametrically opposed positions to a $^1/_4$-in-diam steel drill rod 2.5 in. from the impact end. The gages were SR-4, Type CD-7 which have a $^1/_4$-in. gage length. These gages were connected with external resistors in a bridge circuit so as to be sensitive only to symmetrical strains.

For the first measurements the $^1/_{16}$-in. ball was fired against the end of the bar at the relatively low velocity of 16.1 fps. The pulse generated and measured is shown in Fig. 4(*a*). From this

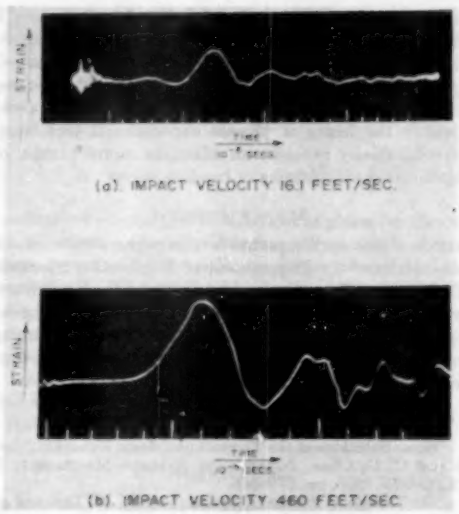

FIG. 4 PULSES GENERATED BY IMPACT OF 1/16-IN. BALL ON A 1/4-IN-DIAM STEEL BAR

(Wire-resistance strain gages with 1/4-in. gage length, connected to cancel nonsymmetrical strains. Gages 2.5 in. from impact end.)

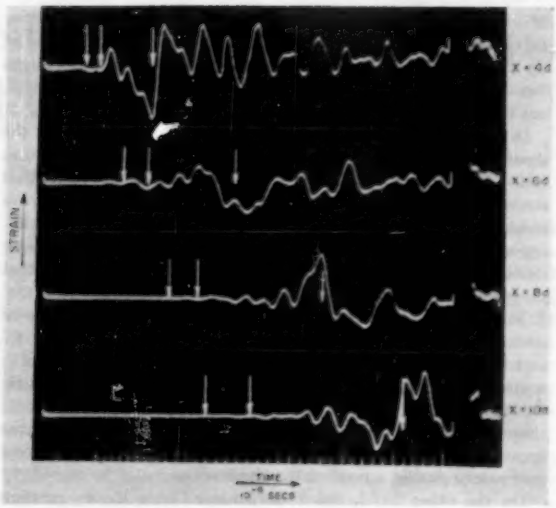

FIG. 5 BENDING-WAVE PULSES

(1/16-in. ball; impact velocity, 460 fps; bar diameter, 1/2 in.; X = distance from impact end.)

figure it may be seen that the pulse is about 4 microsec in duration and Hertzian in form. For the second set of measurements the ball was fired with a velocity of 460 fps against the end of the bar. The pulse which was recorded and shown in Fig. 4(*b*) appears to have a duration of about 3.5 microsec.

Previous investigations have shown that a pulse only 2 microsec long will be distorted seriously by dispersion as it propagates along a bar unless the bar is 1/16-in. diam or smaller (7). Nevertheless, mounting strain gages on such a small bar poses such a difficult problem it was decided to use a 1/4-in-diam bar and then attempt to deduce from the measurements the true characteristics of the pulse. That there has been some dispersion of the pulse is evidenced by the tail of lesser pulses which follows the main pulse. One of the effects of dispersion is a gradual broadening and flattening of the pulse as it travels along the bar (7). Therefore it may be concluded that the pulse generated by the impact is shorter than the 3.5 microsec indicated in the record, but how much shorter is uncertain. Furthermore, it should be noted that the gage length of 1/4 in. would cause the apparent pulse length to be about 1 microsec longer than the actual pulse duration. Limitations in the measuring equipment, such as amplifier band widths and shunting capacities in cables, also cause some distortion which generally takes the form of a decrease in slopes and a widening of the pulse. Thus it may be concluded that the pulse generated by the impact of a 1/16-in. ball at a velocity of 460 fps has a duration of about 2 microsec.[8] The rise time of such a pulse would be of the order of 1 microsec. This insures the wide frequency spectrum required for the measurements which were planned.

Bending waves generated by eccentric impacts of a 1/16-in. ball on the plane end of a 1/2-in. bar were measured at various points along the bar by means of diametrically opposed CD-7 gages (1/4-in. gage length). These gages were connected so as to cancel out the effects of any symmetrical strain components. Results of some of these bending-wave measurements are shown in Fig. 5. The arrival times indicated by the vertical arrows on these oscilloscope traces are of direct interest since they are predicted by the theory in the previous section. The first arrow shows the time at which a disturbance traveling at the dilatational velocity should arrive. The second arrow shows the time at which a disturbance traveling at the bar velocity arrives, and the third arrow shows the time at which a rotational or shear disturbance arrives. For the gages at 4 diam, each arrow falls at a point where a marked change in the strain takes place. These points evidently represent the three phases of the disturbance; that is, dilatational, bar velocity, and shear velocity. At 6 diam the arrows do not appear to coincide with significant changes in the character of the disturbance. However, if each of the arrows is shifted about 1.5 microsec toward the left, they do coincide with significant changes in the amplitude of the wave of the pulse. This probably means that in this record the trace, for some undetermined reason, was slightly delayed in starting. At 8 and 10 diam the disturbances traveling at the dilatational and the bar velocities have, for all practical purposes, vanished. The disturbance traveling at the bar velocity arriving at 8 diam can just barely be seen, but there is no evidence of a disturbance traveling at the dilatational velocity. That part of the disturbance which travels at the shear-wave velocity is still very much in evidence, however, at both 8 and 10 diam. The pulse arriving at 8 and at

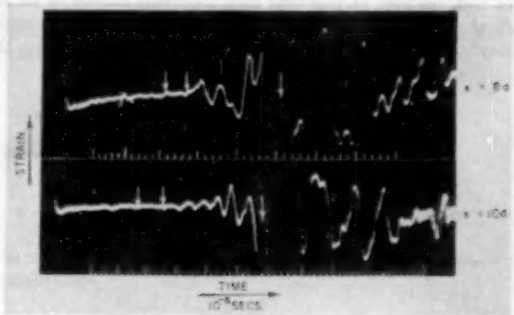

FIG. 6 BENDING-WAVE PULSES AT 8 AND 10 DIAMETERS WITH HIGH AMPLIFIER GAIN

(Main part of pulse has been driven off screen. 1/16-in. ball; impact velocity 460 fps; 1/2-in. bar.)

[8] The pulse durations reported by Goland, Wickersham, and Dengler (9) were about 10 times the duration of this pulse.

10 diam is repeated again in Fig. 6, but at a much higher amplifier gain. Here the pulse arriving at the bar velocity and the one at the shear-wave velocity are very evident. There is also a slight disturbance at the time corresponding to the dilatational arrival, but this may be nothing more than amplifier noise.

In general, damping, which is not considered in either of the theories of propagation under discussion, is not an important factor in the propagation problem. However, it seems that structural-type damping would increase in effectiveness as wave length decreases. Consequently, the first two parts of the bending-wave pulse might be expected to damp out in a relatively short distance from the impact point since it can be shown that they are composed of very short waves.

The Timoshenko theory predicts the earliest arrival time as corresponding to the bar velocity; between the earliest arrival and the time corresponding to the arrival of the shear wave, only scattered wave groups appear, and for a large portion of this interval only one wave group can appear. For example, at 8 diam there would be few arrivals between 24 and 31 microsec after the impact; this corresponds to the interval between 1 and 8 microsec just preceding the arrival of the shear wave.

On the other hand, the Pochhammer-Chree theory predicts the earliest arrival time as corresponding to the dilatational velocity; between the earliest arrival and the time corresponding to the arrival of the shear wave, very many more groups appear. The experimental records support these predictions.

Conclusions

The experimental results support the principal predictions of the Pochhammer-Chree theory concerning arrival times; namely (*a*) the initial disturbance arrives at a given point in the bar at a time corresponding to the arrival of dilatational waves; (*b*) the bending-wave pulse is propagated by a continuous series of arrivals.

The Timoshenko theory predicts arrival times quite accurately with the exception of the first arrival traveling at the dilatational velocity. This theory also indicates that the bulk of a bending disturbance is propagated at velocities in the range between the shear and Rayleigh velocities and the experimental data bear out this prediction.

At appreciable distances from the impact end the faster moving parts of the pulse have been attenuated practically out of existence.

Previous experimental investigations have not provided values for the velocity of propagation of bending waves, and consequently there has been some question as to the validity of existing analytical theory. It is believed that this question has now been resolved.

In fact, we may at this time give a definite answer to an important question of long standing: How good is the Timoshenko theory? The amplitude response is predicted very well by the Timoshenko theory for all but the very sharpest of impacts (9, 10) and, from the results of the present investigation, the same may now be said of propagational velocities. The Pochhammer-Chree theory may give somewhat better results in both of these respects for extremely sharp impacts, but for all practical purposes, and even within the limits of present experimental technique, the Timoshenko theory provides an adequate representation of the propagational characteristics of bending waves.

Acknowledgment

Portions of the work reported in this paper were conducted in the laboratories of the Department of Engineering Mechanics of The University of Texas under sponsorship of the Navy Bureau of Ordnance. Appreciation is expressed to the sponsoring agency for permission to publish this work and to Mr. James Cunningham for valuable assistance in the experimental phase of the investigation.

BIBLIOGRAPHY

1 "Some Solutions of the Timoshenko Beam Equation," by B. A. Boley and C. C. Chao, Journal of Applied Mechanics, Trans. ASME, vol. 77, 1955, pp. 579–586.

2 "On Traveling Waves in Beams," by R. W. Leonard and B. Budiansky, National Advisory Committee for Aeronautics Report 1173 (formerly Technical Note 2874), 1953.

3 "Transverse Impact of Long Beams, Including Rotatory Inertia and Shear Effects," by M. A. Dengler and M. Goland, Proceedings of the First U. S. National Congress of Applied Mechanics, The American Society of Mechanical Engineers, New York, N. Y., 1951, pp. 179–186.

4 "Stress Waves in Solids," by H. Kolsky, Oxford University Press, Oxford, England, first edition, 1953, Chapter 3.

5 "The Propagation of Flexural Elastic Waves in Solid Circular Cylinders," by H. N. Abramson, PhD dissertation, The University of Texas, Austin, Texas, 1956. See also *Journal of the Acoustical Society of America*, vol. 29, January, 1957, pp. 42–46.

6 "Propagation of Waves in Solids," by H. D. Conway, et al., Progress Report No. 2, Applied Physics Laboratory, The Johns Hopkins University, APL/JHU (P.O. No. 33031-2), 1952.

7 "An Experimental Investigation of Stress Wave Propagation," by E. A. Ripperger, Proceedings of the First Midwestern Conference on Solid Mechanics, University of Illinois, Urbana, Ill., 1953, pp. 29–39.

8 "Measurements of Short Bending Wave Pulses in Steel Bars," by E. A. Ripperger, The University of Texas, Defense Research Laboratory, Report CM-821, DRL-367, July, 1955.

9 "Propagation of Elastic Impact in Beams in Bending," by M. Goland, P. D. Wickersham, and M. A. Dengler, Journal of Applied Mechanics, Trans. ASME, vol. 77, 1955, pp. 1–7.

10 "Studies on Longitudinal and Bending Waves in Long Elastic Rods," by H. J. Plass, Jr. and C. C. Steyer, The University of Texas, Defense Research Laboratory, Report CM-860, DRL-376, May, 1956.

11 "A Critical Study of the Hopkinson Pressure Bar," by R. M. Davies, Philosophical Transactions of the Royal Society of London, England, series A, vol. 240, January, 1948, pp. 375–457.

12 "Ueber die Beruhrung fester elastischer Körper," by H. Hertz, *Zeitschrift für die reine u. angewandte Mathematik (Crelle's Journal)*, vol. 92, 1882, pp. 156–171.

Forced Vibration of Systems With Nonlinear, Nonsymmetrical Characteristics

By S. MAHALINGAM,[1] COLOMBO, CEYLON

A one-term approximate solution is given for the amplitudes of steady forced vibration of a single-degree-of-freedom system with a nonlinear (nonsymmetrical) spring characteristic. The method is similar to that of Martienssen (1),[2] but the construction uses a modified curve (or "frequency function") in place of the actual spring characteristic, the curve being so chosen that it gives the correct frequency for free vibrations. The method is extended to deal with a nonlinear vibration absorber fitted to a linear system.

Nomenclature

The following nomenclature is used in the paper:

m = mass of body subject to vibration
k = stiffness of linear spring
$f(x)$ = spring characteristic of nonlinear system
P = amplitude of impressed force
p = frequency of impressed force
x = displacement of mass
ω = natural circular frequency of linear system
ω_x = natural circular frequency of nonlinear mass-spring system corresponding to an amplitude of vibration x
$F(x)$ = frequency function
$= \omega_x^2 x$ for a nonlinear system
c = damping coefficient
t = time

In the section on dynamic vibration absorbers the suffixes 1 and 2 refer to the main mass and absorber system, respectively.

Introduction

Many approximate methods have been suggested for determining the forced vibration of single-degree-of-freedom systems with nonlinear elasticity and, while short methods are available for solving special problems, the most general methods involve a great deal of numerical computation. The comparative accuracies of the methods available appear to vary with the problems considered.

Little is known about the behavior of systems with two or more degrees of freedom. In recent years the performance of vibration absorbers with nonlinear characteristics has been investigated, but so far the study has been confined to a few special cases only.

The present paper gives a new approximate solution for forced vibrations. Here the problem of free vibration is first solved and the response to forced vibration is then found by using a modification of the Martienssen method, in which a modified curve or frequency function is used in place of the actual spring characteristic. The method is particularly powerful where the spring characteristic is made up of a number of straight lines. The effect of damping is easily incorporated into the procedure. Comparison with some published experimental evidence shows that in some cases the present method is not only shorter but also more accurate.

It is also shown that the method is of general application to problems of nonlinear vibration absorbers attached to linear systems.

The Undamped Nonlinear System

The general equation for the forced vibration of an undamped system with a nonlinear restoring force may be written in the form

$$m\ddot{x} + f(x) = P \cos pt \quad \ldots\ldots\ldots\ldots\ldots\ldots [1]$$

In the Martienssen method a one-term solution of the form $x = a_1 \cos pt$ is assumed. Consideration of the equilibrium at $pt = 0, \pi, \ldots$ gives the relation $f(a_1) = P + mp^2a_1$. This is solved graphically by considering the intersection of the spring characteristic $y = f(x)$ and the straight line $y = P + mp^2x$. A point to note here is that if $P = 0$, i.e., free vibrations, the solution will still be approximate.

In order to explain the proposed method, consider a linear system the equation of which is

$$m\ddot{x} + kx = P \cos pt \quad \ldots\ldots\ldots\ldots\ldots\ldots [2]$$

from which

$$\ddot{x} + \omega^2 x = \frac{P}{m} \cos pt \quad \ldots\ldots\ldots\ldots\ldots\ldots [3]$$

where

$$\omega^2 = \frac{k}{m}$$

Assuming a solution $x = a \cos pt$ and substituting in Equation [3], we get

$$\omega^2 a \cos pt = \frac{P}{m} \cos pt + p^2 a \cos pt$$

which gives

$$\omega^2 a = \frac{P}{m} + p^2 a \quad \ldots\ldots\ldots\ldots\ldots\ldots [4]$$

The solution of Equation [4] is given by the intersection of the straight lines

$$y = F(x) = \omega^2 x \quad \text{and} \quad y = \frac{P}{m} + p^2 x$$

Equation [4] considers the maxima of three quantities which

---

[1] Assistant Lecturer, University of Ceylon.

[2] Numbers in parentheses refer to the Bibliography at the end of the paper.

Presented at the Applied Mechanics Division Summer Conference, Berkeley, Calif., June 13–15, 1957, of The American Society of Mechanical Engineers.

Discussion of this paper should be addressed to the Secretary, ASME, 29 West 39th Street, New York, N. Y., and will be accepted until October 10, 1957, for publication at a later date. Discussion received after the closing date will be returned.

Note: Statements and opinions advanced in papers are to be understood as individual expressions of their authors and not those of the Society. Manuscript received by ASME Applied Mechanics Division, October 4, 1956. Paper No. 57—APM-3.

vary sinusoidally and are in phase. The solution is therefore exact.

One of the features of problems with nonlinear restoring forces is that, even for marked degrees of nonlinearity, the wave form of free vibrations is approximately sinusoidal. This has been verified experimentally by Ludeke (2). Now let us consider a nonlinear characteristic made up of a number of straight lines as shown in Fig. 1. If the mass is released from any arbitrary

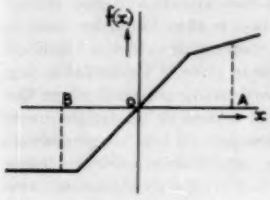

FIG. 1 NONLINEAR, NONSYMMETRICAL SPRING CHARACTERISTICS

point A, the end of swing B on the other side can be calculated easily from considerations of energy. The time of the swing, and hence the frequency of free vibrations, can also be calculated. Let

$$\tfrac{1}{2}AB = x = \text{amplitude of vibration}$$
$$\omega_x = \text{frequency of this vibration}$$

We can thus draw the frequency function

$$y = F(x) = \omega_x^2 x$$

Comparing with Equation [3] the problem can be written in the form

$$\ddot{x} + F(x) = \frac{P}{m}\cos pt \quad \ldots\ldots\ldots\ldots\ldots\ldots [5]$$

Assuming a one-term solution $x = a_1 \cos pt$, the amplitude is given by the intersection of

$$y = F(x) \quad \text{and} \quad y = \frac{P}{m} + p^2 x$$

The following points are of interest:

1 As seen from the foregoing, the basic equation for the method is

$$\omega_{a1}^2 a_1 = \frac{P}{m} + p^2 a_1$$

i.e.

$$m\omega_{a1}^2 a_1 = P + mp^2 a_1 \quad \ldots\ldots\ldots\ldots\ldots\ldots [6]$$

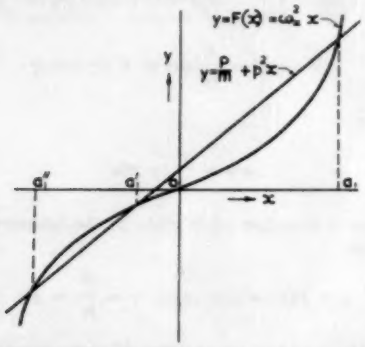

FIG. 2 CONSTRUCTION OF THE AMPLITUDE OF FORCED VIBRATION

Here maximum inertia force for a free vibration is equated to that due to a forced vibration of the same amplitude + exciting force. Since the free and forced vibrations are approximately sinusoidal with time, the method gives a high degree of accuracy.

2 If $P = 0$, i.e., free vibrations, the construction of Fig. 2 gives an exact solution (this is not the case with the Martienssen method).

3 The method is applicable to symmetrical and nonsymmetrical systems. The determination of the frequency of free vibrations has an integrating effect, which takes into account all the features of the restoring-force characteristic.

As an illustration of the method, a nonlinear spring with the characteristic $f(x) = \alpha x + \beta x^3$ is considered, α and β being constants. The solutions of the free and forced vibrations of this system have been given by many authors; for instance, McLachlan (3). Considering a numerical example where $m = 1$, $\alpha =$

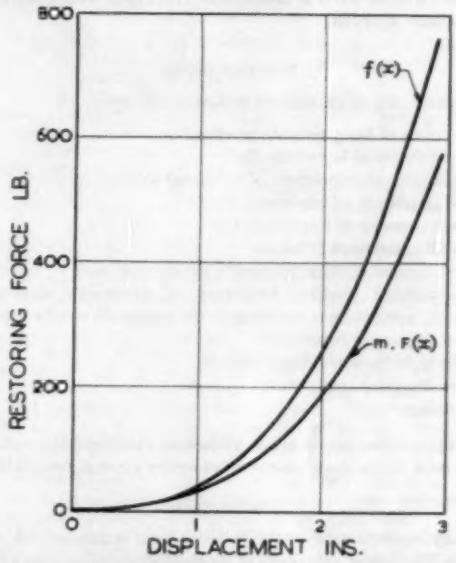

FIG. 3(a) COMPARISON OF RESTORING FORCE CHARACTERISTIC $f(x)$ AND FREQUENCY FUNCTION $F(x)$ FOR NUMERICAL EXAMPLE

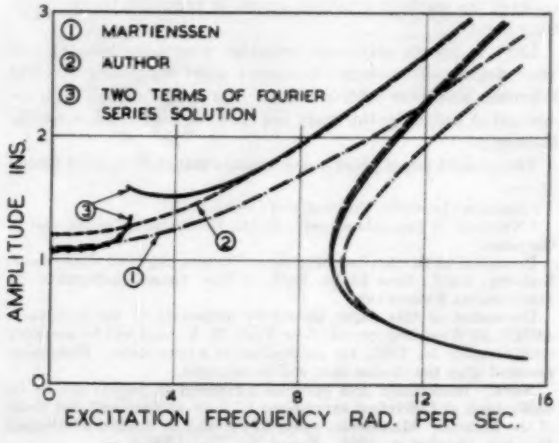

FIG. 3(b) AMPLITUDE-FREQUENCY CURVES

10, $\beta = 30$, $P = 50$, comparison of $f(x)$ and $m\,F(x)$ is made in Fig. 3(*a*). Owing to the high degree of nonlinearity the curves show considerable difference at large amplitudes. Fig. 3(*b*) shows the response curves given by (*a*) Martienssen, (*b*) the author's method, and (*c*) two terms of a Fourier-series solution. The author's method shows close agreement with the analytical solution for $p > 5$. At low excitation frequencies the two-term solution exhibits large amplitudes due to the resonance of the factor cos $3pt$. This phenomenon has been called "pseudo-resonance" and has been discussed by Wylie (4). It should be mentioned that in the region of pseudo-resonance, maximum amplitudes of the left-hand branch of the curve may occur at points other than $pt = 0, \pi$.

Another problem to be considered is that in which the support is subject to a harmonic displacement $z = b \cos pt$. As before, considering a linear system, we have the equation of motion

$$m\ddot{x} + k(x - z) = 0 \qquad [7]$$

from which

$$\ddot{x} + \omega^2(x - z) = 0 \qquad [8]$$

Assuming a solution $x = a \cos pt$, and substituting in Equation [8] we have

$$\omega^2(a - b) \cos pt = p^2 a \cos pt$$

which gives

$$\omega^2(a - b) = p^2 a \qquad [9]$$

The solution is given graphically by the intersection of the straight lines

$$y = F_1(x) = \omega^2(x - b) \text{ and } y = p^2 x$$

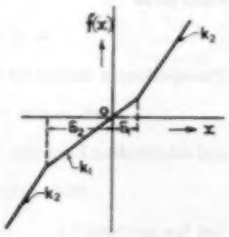

Fig. 4 Spring Characteristic Investigated by Jacobsen and Jespersen

For a nonlinear problem, the solution is given by the intersection of the modified frequency function

$$y = F_1(x) = \omega_x^2(x - b)$$

and the straight line $y = p^2 x$.

An experimental investigation of a system of this type has been made by Jacobsen and Jespersen (5). In their apparatus the restoring force was contributed by a nonlinear, nonsymmetric arrangement of a number of linear springs, Fig. 4. Vibrations were set up by giving the support a harmonic displacement.

Jacobsen and Jespersen also solved their problem theoretically, using a laborious method. Their theoretical and experimental results are given in Fig. 5. In the same figure the theoretical curve by the present method has been plotted. It shows that in this particular case the present method is not only shorter but also more accurate.

In practical problems the restoring-force characteristic is quite often a curve. In such problems Brock's iteration method (6) can be used to obtain the frequencies of free vibration.

Forced Vibration of a Nonlinear System With Viscous Damping

The general equation of the forced vibration of a linear system with viscous damping is

$$m\ddot{x} + c\dot{x} + kx = P \cos pt \qquad [10]$$

which gives

$$\ddot{x} + \frac{c}{m}\dot{x} + \omega^2 x = \frac{P}{m} \cos pt \qquad [11]$$

Assume a solution $x = a \cos(pt - \phi)$. Substituting in Equation [11] we get the equations

$$\left.\begin{aligned} \omega^2 a - p^2 a &= \frac{P}{m} \cos\phi \\ \frac{c}{m} pa &= \frac{P}{m} \sin\phi \end{aligned}\right\} \qquad [12]$$

For a nonlinear characteristic the equations will be

$$\left.\begin{aligned} F(a_1) - p^2 a_1 &= \frac{P}{m} \cos\phi \\ \frac{c}{m} pa_1 &= \frac{P}{m} \sin\phi \end{aligned}\right\} \qquad [13]$$

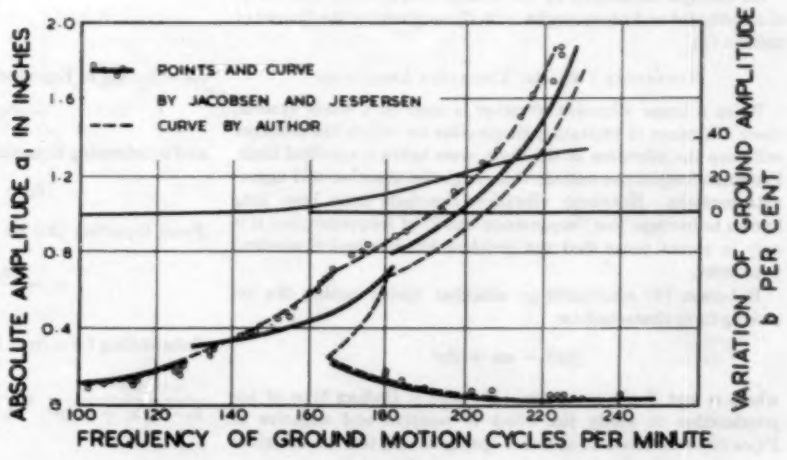

Fig. 5 Theoretical and Experimental Results of Jacobsen and Jespersen (5)
($m = 0.0664$ lb/386; $k_2 = 49.0$ lb/in.; $k_1 = 15.8$ lb/in.; $\delta_1 = 0.25$ in.; $\delta_2 = 0.75$ in.; $b = 0.060$ in.)

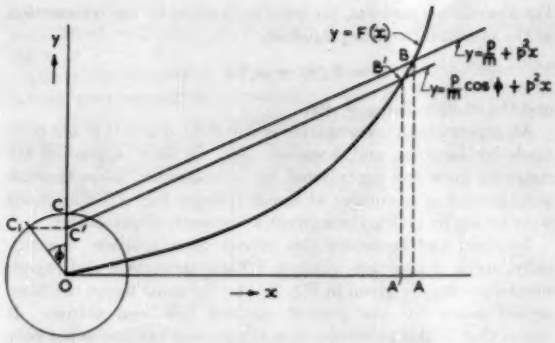

FIG. 6 CONSTRUCTION OF THE AMPLITUDE OF FORCED VIBRATION WITH LINEAR DAMPING

Since the damping coefficient is small, the change of amplitude due to damping is small except near resonance. The phase angle, however, is not small. The procedure in solving Equation [13] will then be as follows:

Plot the curve $y = F(x)$. As a first approximation, neglect damping and find the amplitude of steady forced vibration. In Fig. 6, $OC = P/m$ and the equation of CB is

$$y = \frac{P}{m} + p^2x$$

This gives OA as the first approximation. From the relation

$$\frac{c}{m}\, p(OA) = \frac{P}{m} \sin \phi$$

in Equation [13] calculate ϕ.

With center O and radius OC draw a circle. Mark off angle $COC_1 = \phi$ as in the figure. Project C_1 onto the y-axis and draw the line

$$y = \frac{P}{m} \cos \phi + p^2x$$

The intersection of this line with the curve $y = F(x)$ gives the second approximation OA'.

The procedure may be repeated for greater accuracy.

An example considered by the author showed close agreement of amplitudes and phase angles with those given by the Rauscher method (7).

NONLINEAR DYNAMIC VIBRATION ABSORBERS

When a linear vibration absorber is used on a linear system, there is a range of excitation frequencies for which the absorber will keep the vibration of the main mass below a specified limit. For some frequencies outside this range the absorber will aggravate matters. Nonlinear vibration absorbers have been long known to increase this "suppression band" of frequency, but it is only in recent years that the problem has received theoretical treatment.

Roberson (8) considered an absorber spring having the restoring-force characteristic

$$f(x) = \alpha x + \beta x^3$$

where α and β are constants. He used a Duffing type of approximation to study the effect of positive and negative β. Pipes (9) considered an absorber spring having the characteristic

$$f(x) = \frac{k_0}{a} \sinh (ax)$$

where k_0 and a are constants. In the limit when $a \to 0$ this reduces to a linear spring of stiffness k_0. He assumed a one-term solution $x = A \sin pt$ which on substitution gives

$$f(x) = \frac{k_0}{a} \sinh (aA \sin pt)$$

He expanded this expression in terms of modified Bessel functions and, using a Duffing type of approximation, obtained a pair of equations which were solved graphically.

The author's method outlined in the foregoing can be adapted easily for this problem and has the merit of being applicable to any form of characteristic. To start with, one requires a curve of the frequency function which can be obtained using the iteration method. In order to explain the remainder of the procedure let us consider a linear absorber.

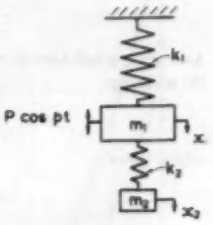

FIG. 7 UNDAMPED LINEAR DYNAMIC VIBRATION ABSORBER

The equation of motion for the absorber is

$$m_2\ddot{x}_2 + k_2(x_2 - x_1) = 0 \qquad [14]$$

which gives

$$\ddot{x}_2 + \omega_2^2(x_2 - x_1) = 0 \qquad [15]$$

The equation of motion for the main mass is

$$m_1\ddot{x}_1 + k_1x_1 - k_2(x_2 - x_1) = P \cos pt \qquad [16]$$

and substituting Equation [14] into [16]

$$m_1\ddot{x}_1 + k_1x_1 + m_2\ddot{x}_2 = P \cos pt \qquad [17]$$

Let the solutions be

$$\left.\begin{aligned} x_1 &= a_1 \cos pt \\ x_2 &= a_2 \cos pt \end{aligned}\right\} \qquad [18]$$

Substituting in Equation [15] we have

$$-p^2a_2 + \omega_2^2(a_2 - a_1) = 0 \qquad [19]$$

and substituting Equation [18] in [17] we get

$$(k_1 - m_1p^2)a_1 - m_2p^2a_2 = P \qquad [20]$$

From Equation [20] we have

$$a_2 = \frac{(a_2 - a_1)(k_1 - m_1p^2) + P}{k_1 - (m_1 + m_2)p^2}$$

Substituting for a_2 from Equation [19] gives

$$\frac{Pp^2}{k_1 - (m_1 + m_2)p^2} + \frac{p^2(k_1 - m_1p^2)}{k_1 - (m_1 + m_2)p^2}(a_2 - a_1) = \omega_2^2(a_2 - a_1) \qquad [21]$$

We can solve $(a_2 - a_1)$ in Equation [21] by considering the intersection of the straight lines $y = \omega_2^2 x$ and

$$y = \frac{Pp^2}{k_1 - (m_1 + m_2)p^2} + \frac{p^2(k_1 - m_1p^2)}{k_1 - (m_1 + m_2)p^2}x$$

In dealing with a nonlinear absorber, the two lines to be considered will be $y = \omega_{2x}^2 x = F_2(x)$ and

$$y = \frac{Pp^2}{k_1 - (m_1 + m_2)p^2} + \frac{p^2(k_1 - m_1p^2)}{k_1 - (m_1 + m_2)p^2}x$$

where ω_{2x} is the natural frequency of the absorber mass-spring system for an amplitude of vibration x.

Having thus determined $(a_2 - a_1)$, a_2 can be obtained from Equation [19].

As an example, the author considered an absorber spring having a hyperbolic sine characteristic and compared his results with those given by Pipes' method. Very close agreement was shown at all parts of the response curves. It is to be noted that the final method of solution of both methods is the same; i.e., graphical intersection of a curve and a straight line. In this particular example Pipes' method is shorter because the curve can be plotted easily using a table of Bessel functions. The drawback in his method is that it is applicable to a special characteristic only.

ACKNOWLEDGMENT

The author wishes to thank Dr. R. P. N. Jones of the University of Sheffield for many helpful criticisms and suggestions during the course of this investigation.

BIBLIOGRAPHY

1 "Über neue Resonanzerscheinungen in Wechselstromkreisen," by O. Martienssen, *Physikalische Zeitschrift*, vol. 11, 1910, pp. 448–460.

2 "An Experimental Investigation of Forced Vibrations in Mechanical Systems Having a Non-Linear Restoring Force," by C. A. Ludeke, *Journal of Applied Physics*, vol. 17, 1946, pp. 603–609.

3 "Ordinary Non-Linear Differential Equations in Engineering and Physical Sciences," by N. W. McLachlan, Oxford, England, 1950, pp. 24–27, 52–55.

4 "On the Forced Vibration of Non-Linear Springs," by C. R. Wylie, *Journal of the Franklin Institute*, vol. 236, 1943, pp. 273–284.

5 "Steady Forced Vibration of a Single Mass System With a Non-Linear Restoring Force," by L. S. Jacobsen and H. J. Jespersen, *Journal of the Franklin Institute*, vol. 220, 1935, pp. 467–496.

6 "Iterative Numerical Method for Nonlinear Vibrations," by J. E. Brock, JOURNAL OF APPLIED MECHANICS, Trans. ASME, vol. 73, 1951, pp. 1–11.

7 "Steady Oscillations of Systems With Nonlinear and Unsymmetrical Elasticity," by M. Rauscher, Trans. ASME, vol. 60, 1938, pp. A-16 to 9A-177.

8 "Synthesis of a Non-Linear Dynamic Vibration Absorber," by R. E. Roberson, *Journal of the Franklin Institute*, vol. 254, no. 3, 1952, pp. 205–220.

9 "Analysis of a Nonlinear Dynamic Vibration Absorber," by L. A. Pipes, JOURNAL OF APPLIED MECHANICS, Trans. ASME, vol. 75, 1953, pp. 515–518.

Stresses in Beams During Transverse Impact[1]

By K. E. BARNHART, JR.,[2] and WERNER GOLDSMITH,[3] BERKELEY, CALIF.

A theory is developed for the transverse impact of spheres on elastic beams which incorporates a dynamic plastic force-indentation law and linear elastic boundary conditions. A method is devised to account for the effect of an infinite number of bending modes. The influence of various force-indentation relations on the calculated stress history is discussed and a comparison with an experimental stress curve is provided.

Nomenclature

The following nomenclature is used in the paper:

A = cross-sectional area of beam, sq in.
A_i = abbreviation for $d_i X_i^2/\sqrt{c_i}$
$B_{i,n-j+1}$ = abbreviation for $[\cos\sqrt{c_i}(n-j)\Delta\tau - \cos\sqrt{c_i}(n-j+1)\Delta\tau]$
C = coefficients depending on boundary conditions
D = beam depth, in.
D_{n-j+1} = beam-deflection coefficient
E = modulus of elasticity, psi
E_{n-j+1} = beam-deflection coefficient
G_i = bending stress coefficient
H_{n-j+1} = bending stress coefficient
I = moment of inertia of beam cross section, in.[4]
K = dimensionless linear spring constant
M = dimensionless angular spring constant
P = contact force, lb
P_j = contact force during jth time increment, lb
T = kinetic energy, in-lb
W = weight of sphere, lb
X_i = normal mode function for Euler-Bernoulli beam $X_i = \cos\lambda_i x + \cosh\lambda_i x + C_i(\cos\lambda_i x - \cosh\lambda_i x) + C_2(\sin\lambda_i x + \sinh\lambda_i x) + C_4(\sin\lambda_i x - \sinh\lambda_i x)$
a = abbreviation for $\sqrt{(EIg/A\gamma)}$
c = value of co-ordinate x at point of impact, in.
c_i = square of mode frequency, rad^2/sec^2, $c_i \equiv a^2\lambda_i^4$
d = diameter of contact indentation, in.
d_i = abbreviation for $(a^2/EI)\int_0^l X_i^2\,dx$
g = acceleration of gravity, in./sec^2
i = subscript and index denoting mode number
j = subscript and index denoting time increments
k = linear elastic spring constant of supports, lb/in.
l = length of beam between supports, in.
m = index denoting mode number beyond which roots of frequency equation are assumed to be evenly spaced
n = subscript and index denoting time increment
p = proportionality constant in force-indentation relations
q = exponent in force-indentation relation during recovery
r = radius of sphere, in.
t = time, sec
v = velocity of sphere, in/sec
x = co-ordinate measured from one end of beam, in.
y = beam deflection, in.
Δ = increment
α = depth of penetration of sphere, in.
γ = weight density, lb/in.^{3}
η = exponent in force-indentation relation during indentation
$\lambda_i x$ = argument of eigenfunction
μ = angular spring constant of supports
σ = outer fiber bending stress, psi
τ = time, sec

Subscripts

f = final condition for sphere
l = condition at $x = l$
m = maximum condition
0 = initial condition for sphere, or condition at $x = 0$
r = condition at end of recovery process

Introduction

Transverse impact on elastic beams has been studied by numerous investigators. Timoshenko (1)[4] presented a basic approach to this problem by combining the Hertz contact-force law with the Bernoulli beam equation. Simplifications concerning the contact force have been introduced to reduce the labor of the numerical solution of the Timoshenko equation (2, 3) and various types of beam supports have been considered (4, 5, 6). On the other hand, correction terms for shear, rotatory inertia, and lateral contraction have been proposed in efforts to provide a more elegant one-dimensional theory. Numerous experimental investigations have been performed in this field, but the correlation of stresses with existing theories has received little attention (7). Other investigations have been concerned with the plastic bending of beams under impulsive loading.

The purpose of this paper is to present the theoretical relations necessary to describe the behavior of elastically mounted beams subjected to the transverse impact of a sphere. The present paper differs from previous investigations in the use of a contact force permitting the establishment of permanent indentation at the contact point, and in presenting a device which permits the convenient evaluation of the effect of an arbitrarily large number of beam bending modes. A numerical evaluation of the bending-stress time history at the center of the beam is compared with experimental data for the same impact parameters for the case of central impact.

---

[1] The results presented in this paper are based on a thesis submitted in partial fulfillment of the requirements for the degree of Doctor of Philosophy at the University of California, Berkeley, Calif.

[2] Assistant Professor of Engineering Design, University of California. Assoc. Mem. ASME.

[3] Associate Professor of Engineering Design, University of California. Assoc. Mem. ASME.

Presented at the Applied Mechanics Division Summer Conference, Berkeley, Calif., June 13–15, 1957, of The American Society of Mechanical Engineers.

Discussion of this paper should be addressed to the Secretary, ASME, 29 West 39th Street, New York, N. Y., and will be accepted until October 10, 1957, for publication at a later date. Discussion received after the closing date will be returned.

Note: Statements and opinions advanced in papers are to be understood as individual expressions of their authors and not those of the Society. Manuscript received by ASME Applied Mechanics Division, November 7, 1956. Paper No. 57—APM-27.

[4] Numbers in parentheses refer to the Bibliography at the end of the paper.

Method of Solution

The solution of the problem is carried out under the assumptions of a one-dimensional theory of transverse vibrations of the beam and neglects the effects of shear, rotatory inertia, lateral beam contraction, and internal damping. Under these restrictions, the problem is described by the integral equation

$$y(c, t) = v_0 t - \frac{g}{W}\int_0^t dt \int_0^t P dt - \alpha \ldots\ldots\ldots [1]$$

which was originally solved by Timoshenko (1) and subsequently by others (2, 4, 5, 6), using the elastic reversible Hertz contact-force equation, a limited number of modes, and boundary conditions involving combinations of clamped, simply supported, and free ends. Equation [1] is solved by a small-increment technique extending over a number of time increments n such that $t = n\Delta\tau$, where each time increment is sufficiently small so that a linear force-time relation may be employed during each increment.

If P_j represents the average force during the jth interval, Equation [1] is then expressed as

$$\sum_{j=1}^{n} E_{n-j+1} P_j = v_0 n \Delta\tau - \frac{g(\Delta\tau)^2}{W}\sum_{j=1}^{n} D_{n-j+1} P_j - \alpha \ldots [2]$$

where

$$E_{n-j+1} = \sum_{i=1}^{\infty} A_i B_{i,n-j+1} \quad A_i = \frac{d_i}{c_i}[X_i^2]_{x=c}$$

and $B_i = \cos\sqrt{(c_i)}(n-j)\Delta\tau - \cos\sqrt{(c_i)}(n-j+1)\Delta\tau$

and D_{n-j+1} is a numerical coefficient resulting from the double integral term. If the deformation α at the point of contact can be expressed in terms of a contact force $P = p\alpha^q$, Equation [2] may be written as

$$P_n[E_1 + D_1] + \left(\frac{P_n}{p}\right)^{\frac{1}{q}} = v_0 n\Delta\tau - \frac{g(\Delta\tau)^2}{W} \sum_{j=1}^{n-1} D_{n-j+1} P_j - \sum_{j=1}^{n-1} E_{n-j+1} P_j \ldots\ldots [3]$$

which can be solved numerically by an iterative procedure.

The special case selected for detailed examination in the present paper is that of symmetrical elastic springs at the end supports, so that the governing frequency equation is

$$2(1 - \cos\lambda_i l \cosh\lambda_i l) - \frac{4K}{(\lambda_i l)^3}(\sin\lambda_i l \cosh\lambda_i l - \cos\lambda_i l \sinh\lambda_i l) + \frac{4K^2}{(\lambda_i l)^6}(\sin\lambda_i l \sinh\lambda_i l) = 0 \ldots\ldots [4]$$

An Approximation for Estimating the Effect of an Infinite Number of Bending Modes

The series solution usually obtained from the Euler-Bernoulli beam equation for free vibrations implies the existence of an infinite number of bending modes. The physical significance of the higher modes may be questioned, in view of the failure of this elementary theory to account for vibrational modes other than bending and its neglect of internal damping. Since this theory obviously cannot predict a limit to the number of modes which are physically realistic, it appears reasonable, if one is committed to this theory as the basis of a solution, to ignore the contribution of the higher modes only if it can be shown that their numerical effect is negligible.

Since a term-by-term summation of an infinite series is clearly impossible, some device must be employed to estimate the effect of those modes beyond a pre-established limit. This section describes a device for the case of central impact, based on the assumption that the roots of the frequency Equation [4] are evenly spaced beyond this limit, which reduces significantly the labor involved in the computation of the deflection and stress coefficients, when large numbers of modes are considered.

For purposes of the present approximation, the deflection coefficient is expressed in terms of two partial sums as

$$E_{n-j+1} = \sum_{i=1,3,5\ldots}^{m} A_i B_{i,n-j+1} + \sum_{i=m+2}^{\infty} A_i B_{i,n-j+1} \ldots [5]$$

where m is the number of the mode beyond which the roots of the frequency equation are considered to be evenly spaced. Approximations for the present case of symmetrical modes are

$$\lambda_i l = \left(i - \frac{3}{2}\right)\pi, \quad \int_0^l X_i^2 dx = l, \quad |X_i| = \sqrt{2} \text{ at } x = \frac{l}{2} \ldots [6]$$

which have been verified numerically, so that

$$A_i = \frac{2l^3}{\left(i - \frac{3}{2}\right)^4 \pi^4 EI}$$

For example, for $i = 35$, $\lambda_i l = 105.24335$ for $K = 0$ while $\lambda_i l = 105.24336$ for $K = 5.308416$. For $i = 65$, both $K = 0$ and $K = 5.308416$ give $\lambda_i l = 199.49113$.

The second summation in Equation [5], which may be considered as a remainder term, then becomes

$$\sum_{i=m+2}^{\infty} A_i B_{i,n-j+1} = Q\left\{\sum_{i=m+2}^{\infty} \frac{\cos\left[b_{n-j}\left(i - \frac{3}{2}\right)^2\right]}{\left(i - \frac{3}{2}\right)^4} - \sum_{i=m+2}^{\infty} \frac{\cos\left[b_{n-j+1}\left(i - \frac{3}{2}\right)^2\right]}{\left(i - \frac{3}{2}\right)^4}\right\} \ldots\ldots [7]$$

with the notation

$$Q = \frac{2l^3}{\pi^4 EI}, \quad b_{n-j} = (n-j)\frac{\pi^2 a \Delta\tau}{l^2}$$

The even spacing of roots permits use of the Gregory central-difference formula (9) which represents an arbitrary function $f(\xi)$ by the series

$$\frac{1}{w}\int_h^{h+sw} f(\xi)d\xi = \left\{\frac{1}{2}f_0 + f_1 + f_2 + \ldots + f_{s-1} + \frac{1}{2}f_s\right\} - \frac{1}{12}\left\{\frac{\Delta f_s + \Delta f_{s-1}}{2} - \frac{\Delta f_0 + \Delta f_{-1}}{2}\right\} + \frac{11}{720}\left\{\frac{\Delta^3 f_{s-1} + \Delta^3 f_{s-2}}{2} - \frac{\Delta^3 f_{-1} + \Delta^3 f_{-2}}{2}\right\} - \frac{191}{60{,}480}\left\{\frac{\Delta^5 f_{s-2} + \Delta^5 f_{s-3}}{2} - \frac{\Delta^5 f_{-2} + \Delta^5 f_{-3}}{2}\right\} + \frac{2497}{3{,}627{,}800}\left\{\frac{\Delta^7 f_{s-3} + \Delta^7 f_{s-4}}{2} - \frac{\Delta^7 f_{-3} + \Delta^7 f_{-4}}{2}\right\} - \ldots\ldots\ldots [8]$$

Choosing

$$h = m + \frac{1}{2}, \quad z = \infty, \quad w = 2, \quad \xi = \left(i - \frac{3}{2}\right), \quad f(\xi) = \frac{\cos b_{n-j}\xi^2}{\xi^4}$$

noting that terms involving all orders of difference of $f_{n-1}, f_{n-2}, \ldots$ approach zero as $z \to \infty$, and expressing the integral on the left side in terms of Fresnel's integral leads to

$$\sum_{i=m+2}^{\infty} \frac{\cos b_{n-j}\left(i - \frac{3}{2}\right)^2}{\left(i - \frac{3}{2}\right)^4} = \frac{1}{2}\frac{\cos b_{n-j}\left(m + \frac{1}{2}\right)^2}{\left(m + \frac{1}{2}\right)^4} + \frac{1}{6}\frac{\cos b_{n-j}\left(m + \frac{1}{2}\right)^2}{\left(m + \frac{1}{2}\right)^2} + \frac{(b_{n-j})^{1/2}}{3}\left[\int_0^{b_{n-j}\left(m+\frac{1}{2}\right)^2} \frac{\cos u\, du}{\sqrt{u}} - \sqrt{\frac{\pi}{2}}\right] - \frac{b_{n-j}\sin b_{n-j}\left(m + \frac{1}{2}\right)^2}{3\left(m + \frac{1}{2}\right)} - \frac{1}{12}\left[\frac{\Delta^2 f_0 + \Delta^2 f_{-1}}{2}\right] + \frac{11}{720}\left[\frac{\Delta^2 f_{-1} + \Delta^2 f_{-2}}{2}\right] - \frac{191}{60{,}480}\left[\frac{\Delta^2 f_{-2} + \Delta^2 f_{-3}}{2}\right] + \frac{2497}{3{,}627{,}800}\left[\frac{\Delta^2 f_{-3} + \Delta^2 f_{-4}}{2}\right] - \ldots\ldots\ldots\ldots [9]$$

This expression permits replacement of the slowly convergent terms of Equation [7] by rapidly converging series.

The bending stress at the outer fiber for an elastic beam can be written

$$\sigma = -\frac{ED}{2}\frac{d^2y}{dx^2} = -\frac{ED}{2}\sum_{j=1}^{n} H_{n-j+1} P_j \ldots\ldots [10]$$

where

$$H_{n-j+1} = \sum_{i=1,3,5\ldots}^{\infty} G_i B_{i,n-j+1} \quad \text{and} \quad G_i = \frac{d_i}{c_i}\frac{d^2 X_i}{dx^2}[X_i]_{x=c}$$

In particular, for the stress at mid-span with central impact, the assumption of evenly spaced roots permits the approximation

$$G_i = \frac{-2l}{EI\pi^2\left(i - \frac{3}{2}\right)^2}$$

Proceeding in a manner identical to that employed for the deflection coefficients, except that now $f(\xi) = [\cos(b_{n-j}\xi^2)]/\xi^2$, the remainder term for the stress coefficients can be expressed in terms of

$$\sum_{i=m+2}^{\infty} \frac{\cos b_{n-j}\left(i - \frac{3}{2}\right)^2}{\left(i - \frac{3}{2}\right)^2} = \frac{1}{2}\frac{\cos b_{n-j}\left(m + \frac{1}{2}\right)^2}{m + \frac{1}{2}} + \frac{1}{2}\frac{\cos b_{n-j}\left(m + \frac{1}{2}\right)^2}{\left(m + \frac{1}{2}\right)^2} + \frac{(b_{n-j})^{1/2}}{2}\left[\int_0^{b_{n-j}\left(m+\frac{1}{2}\right)^2} \frac{\sin u\, du}{\sqrt{u}} - \sqrt{\frac{\pi}{2}}\right] - \frac{1}{12}\left[\frac{\Delta^2 f_0 + \Delta^2 f_{-1}}{2}\right] + \frac{11}{720}\left[\frac{\Delta^2 f_{-1} + \Delta^2 f_{-2}}{2}\right] - \frac{191}{60{,}480}\left[\frac{\Delta^2 f_{-2} + \Delta^2 f_{-3}}{2}\right] + \frac{2497}{3{,}627{,}800}\left[\frac{\Delta^2 f_{-3} + \Delta^2 f_{-4}}{2}\right] - \ldots\ldots\ldots [11]$$

This rapidly convergent expression permits a ready computation of the bending stress on the basis of an infinite number of bending modes. It should be pointed out, however, that the number of terms involving higher orders of the central differences must be increased as the size of the time increment is reduced to effect a specified degree of approximation. An increase in the number of time increments considered also requires additional central-difference terms, as does a decrease in the mode number beyond which the roots of the frequency equation are considered to be evenly spaced.

Plastic Contact Deformation

Previous solutions to the impact problem which required a force-deformation relation at the point of contact have relied on the elastic, reversible relation originally proposed by Hertz for static loading. However, Davies (10) has shown that a $^3/_8$-in-diam steel sphere dropped from a height of 0.15 in. is sufficient to produce a permanent crater in armor plate having a Brinell hardness of 321. The present paper is designed to cover those cases for which the impact velocity is high enough to produce permanent deformation in the immediate region of the contact point, but not so high that plastic flow extends through the entire beam cross section. Since no adequate theoretical relationship is available to replace the Herts law for cases of strain-hardening materials in the plastic range, an experiment was designed from which an empirical dynamic force-indentation relationship could be deduced.

Hardened 1-in-diam steel spheres were dropped onto mild steel blocks from heights of 1 to 13 ft. The initial and final kinetic energies of the ball were determined from the measured fall and rebound heights, while the depth and diameter of the permanent indentations in the block were obtained from profilometer traces.

The derivation of the relation between contact force and indentation is based on the following assumptions: (*a*) the initial kinetic energy is completely transformed into energy associated with the formation of the permanent indentation and into the kinetic energy of rebound; (*b*) the rebound energy of the ball is derived solely from the release of elastic strain energy stored equally in the ball and the block during compression; and (*c*) the force law has the form $P = p\alpha^q$ while the force is increasing (indentation process), and has the form

$$P = P_m[(\alpha - \alpha_r)/(\alpha_m - \alpha_r)]^q$$

while the force is decreasing (recovery process).

The first assumption requires that the ball deform only elastically, that no energy escape to the foundation, and that vibrations of the ball and block can be neglected. The elastic deformation of the ball was verified by experimental observation. Theoretical considerations (11) show that internal vibrations of the ball account but for a negligible fraction of the initial kinetic energy. A rigid foundation was employed to minimize the energy loss to the foundation. The second assumption is substantiated by the work of Tabor (12) for identical elastic properties of the ball and block. The force laws as expressed in the third assumption have been used previously (13, 14, 15) and possess the advantages of generality and convenience.

With these assumptions, the work-energy equations applied to the ball during indentation and recovery are, respectively:

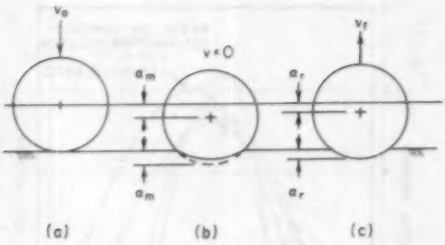

FIG. 1 GEOMETRY OF ASSUMED INDENTATION AND RECOVERY PROCESSES

Indentation

$$\int_0^{\alpha_m} P d\alpha = T_0 - \text{strain energy stored in ball}$$

$$= \frac{p}{\eta+1}\alpha_m^{\eta+1} = \frac{1}{2}\frac{W}{g}v_0^2 - \frac{1}{4}\frac{W}{g}v_f^2 \ldots\ldots [12]$$

Recovery

$$-\int_{\alpha_m}^{\alpha_r} P d\alpha = T_f - \text{strain energy stored in ball}$$

$$= \frac{1}{2}\frac{W}{g}v_f^2 - \frac{1}{4}\frac{W}{g}v_f^2 = \frac{1}{4}\frac{W}{g}v_f^2 \ldots\ldots [13]$$

where α_m is the maximum penetration relative to the center of gravity of the sphere, and α_r represents the depth of the indentation remaining after rebound relative to the initial point of contact. The terminology is illustrated in Fig. 1. Substitution of the force equation during recovery in Equation [13] yields for the recovery process

$$\frac{Wv_f^2}{4g} = \frac{P_m}{q+1}(\alpha_m - \alpha_r) \ldots\ldots [14]$$

Equations [12] and [13] in conjunction with experimental data were used to determine a force-indentation law for selected values of the exponent q. Values of $q = 3/2$, corresponding to an elastic recovery according to the Hertz theory, previously used by Crook (15), and $q = 1$ corresponding to a linear elastic spring, were considered.

The determination of the P-α curve requires a knowledge of the value of the maximum penetration α_m which cannot be measured directly. Consequently, an iterative procedure was employed using a logarithmic plot of Equation [12] with an assumed $\alpha_m = d^2/8r$ from which an equation of the form $P = p\alpha^\eta$ was determined. The computed maximum force at any point was then substituted in Equation [14] to determine $\Delta\alpha = \alpha_m - \alpha_r$ which yielded an improved value of α_m. This procedure was repeated until successive identical values of α_m were obtained for all points. By this method, curves of P versus α and α_m versus α_r were obtained.

Fig. 2 shows the final dynamic-plastic indentation relations. For purposes of comparison the Hertz law and a static-plastic relation have been included in this figure. The static-plastic force law is based on static tests utilizing a measured force and a maximum indentation computed on the basis of a measured recovered crater depth and an assumed Hertzian recovery. The dynamic force law determined from Equations [12] and [14] applies only during the indentation process. In the force law during recovery, the values of α_m and α_r are governed by the computed maximum value of the force during indentation, and the value of q corresponds to that selected for the determination of the force law during indentation.

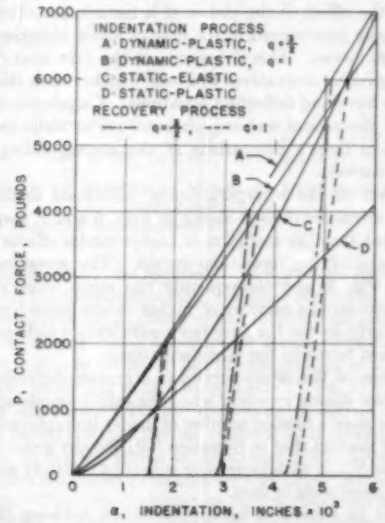

FIG. 2 ELASTIC AND PLASTIC INDENTATION LAWS FOR A 1-IN-DIAM STEEL SPHERE AND PLANE SURFACES OF COLD-ROLLED MILD STEEL

NUMERICAL SOLUTIONS

Force and stress histories at the center of the beam were computed for various force-indentation relations for the case of central impact using a time increment of 2 microsec. Coefficients E_{n-j+1} and H_{n-j+1} were computed from Equations [2] and [10] for 35 modes. Correction terms based on the approximation described earlier were used to incorporate the effect of all modes beyond the 35th. These coefficients are shown in Fig. 3 for various numbers of modes for the particular beam considered in the numerical example.

Equation [3] was solved for a particular force-indentation relation, shown in Fig. 2, up to the maximum value of P_m. The corresponding value of α_m then determined the α_r needed in the recovery relation, and the solution of Equation [3] was continued to a total time of 40 microsec.

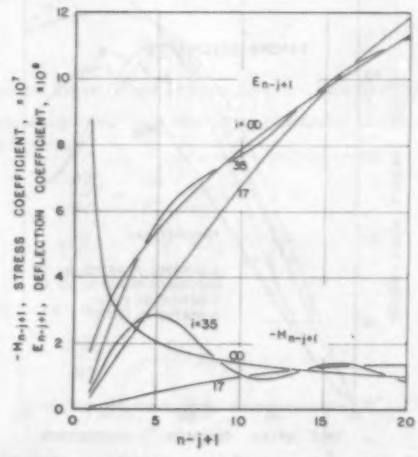

FIG. 3 DEFLECTION AND STRESS COEFFICIENTS FOR 17, 35, AND ∞ MODES

(Steel beam: 1/4 in. × 2 in. × 24 in. Supports: 30 lb/in. springs.)

Results and Discussion

An experimental and four theoretical stress-time curves are shown in Fig. 4 for a 1-in.-diam steel sphere having a velocity of 346 ips and striking a $^1/_4$-in. × 2-in. × 24-in. beam mounted at the ends on 30-lb-per-in. springs. The experimental curve was obtained from SR-4 strain-gage measurements using oscillographic equipment with a flat frequency response to 100 kilocycles. The apparatus and procedure used were substantially identical to those described in reference (16). The beam material was cold-rolled mild steel with a dynamic yield point of about 90,000 psi.

The theoretical stress-time histories based on the infinite-mode approximation are in fair agreement with the observed data up to the peak value. While the present calculations were not carried far beyond the time of contact, it is expected that theoretical predictions of bending stress become increasingly unreliable as times further from the contact period are considered. This condition, noted in references (8) and (17), can be ascribed to the previously noted limitations of the elementary theory and in particular to the lack of consideration of damping of the bending modes. However, the initial-peak transient stress is affected but little by damping and hence should be reasonably well predicted by this theory. Furthermore, this initial-peak stress is of primary concern since it frequently represents the maximum-stress condition during the entire beam response.

While the validity of theoretical analyses of problems in the field of impact can best be ascertained by comparison with experimental results, comparisons between alternative theoretical approaches are also desirable. Inspection of the curves shown in Fig. 4 reveals that, during the indentation process, any reasonable force-indentation relation will yield about the same stress history. While the magnitude and location of the peak stress are significantly altered by the choice of a reversible or nonreversible process, the choice of q in the latter process has little effect on the stress curve. Unlike the stress curves based on dynamic-plastic indentation relations, the Herts law yields a curve whose shape during the initial stress increase does not agree too well with experimental results. Contrary to observation,

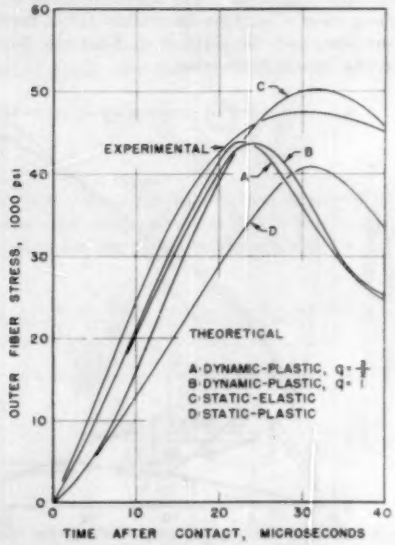

Fig. 4 Experimental and Theoretical Stress-Time Histories
(Ball: 1 in. diam. Impact velocity: 346 ips.
Beam: $^1/_4$ in. × 2 in. × 24 in. Supports: 30 lb./in. springs.
Theoretical curves based on infinite number of modes.)

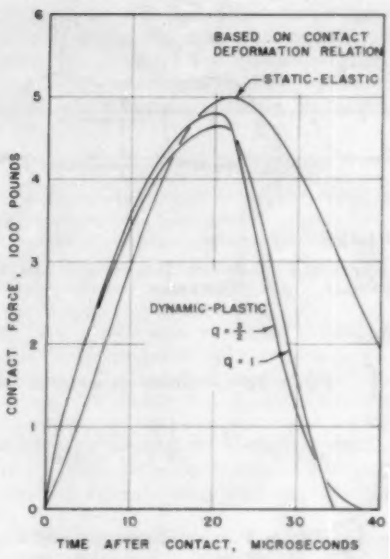

Fig. 5 Theoretical Force-Time Histories
(Ball: 1 in. diam. Impact velocity: 346 ips.
Beam: $^1/_4$ in. × 2 in. × 24 in. Supports: 30 lb/in. springs.
Curves based on an infinite number of modes.)

the Herts law allows no permanent indentation at the contact point; however, as has been noted by other investigators, the peak stress obtained with the use of the static-elastic law is in reasonable agreement with the experimental result. The stress based on a static-plastic relation is considerably less than that for the comparable dynamic cases, as would be expected in view of the difference between dynamic and static flow pressures for identical crater sizes (13).

Although recent attempts have been made to measure the impact force, no completely satisfactory technique is available for the experimental determination of the force at the point of contact. Theoretical force-time curves are presented in Fig. 5 for the corresponding stress histories shown in Fig. 4. It is significant that the effect of the choice of a force-indentation relation is much more pronounced in the case of stress histories than for the contact forces. This is because of the fact that the stress equation involves derivatives two orders higher than those occurring in the force and deflection equations. Consequently, a comparison of theoretical and experimental stress histories is much more critical than a comparison of the corresponding force or deflection curves.

The effect of the incorporation of additional modes on the force and stress histories is shown in Figs. 6 and 7, respectively. It is evident that the inclusion of higher modes effects but little improvement of the force-time curves. The stress coefficients shown in Fig. 3, and consequently the stress level, depend in great degree on the number of higher modes considered. This is particularly so for the first few coefficients which control the predominant terms in the stress equation.

The shape of the stress curve has a greater dependence upon the force law during recovery when the infinite-mode approximation rather than a limited number of modes is employed. This is because of the fact that in Equation [10], for any given time t, the coefficients H_{n-j+1} with increasing subscript multiply successively the forces decreasing in time.

In order to achieve a better correlation between the experimental and theoretical stress-time curves beyond the peak stress with the elementary theory, a better understanding of the re-

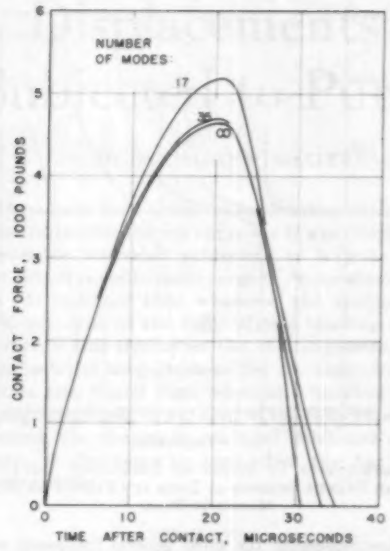

FIG. 6 EFFECT OF NUMBER OF MODES ON THEORETICAL FORCE-TIME HISTORY
(Based on dynamic-plastic relation with $q = 1$.)

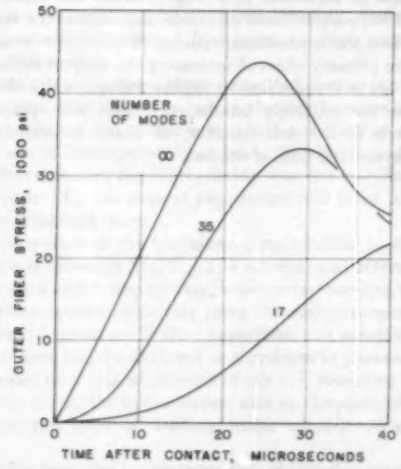

FIG. 7 EFFECT OF NUMBER OF MODES ON THEORETICAL STRESS-TIME HISTORY
(Based on dynamic-plastic relation with $q = 1$.

covery process would be required. The various assumptions pertaining to the force-indentation relations employed here represent reasonable interpretations of the recovery process. They are, however, only a few of the possible mechanisms that could be proposed. It is to be noted that the assumption of a Hertzian recovery law, which has been widely used (13, 14, 15), provides the poorest correlation with the experimental data. Although Crook (15) reported experimental evidence of increasing plastic deformation during the period of relaxation of the force, neither his mechanism nor those presented in this paper permit such a phenomenon. The force-indentation curves presented by Crook are in excellent qualitative agreement with those obtained in this investigation, in spite of the differences in materials, impact velocities, and geometry of the colliding members.

BIBLIOGRAPHY

1 "Zur Frage nach der Wirkung eines Stosses auf einen Balken," by S. Timoshenko, *Zeitschrift für Mathematik und Physik*, vol. 62, 1913, p. 198.

2 "The Impact of a Mass Striking a Beam," by E. H. Lee, Trans. ASME, vol. 62, 1940, p. A-129.

3 "A Method of Calculating Energy Losses During Impact," by C. Zener and H. Feshbach, Trans. ASME, vol. 61, 1939, p. A-67.

4 "Impact of a Mass on a Damped Elastically Supported Beam," by W. H. Hoppmann, 2nd, Trans. ASME, vol. 70, 1948, p. A-125.

5 "Impact on a Multispan Beam," by W. H. Hoppmann, JOURNAL OF APPLIED MECHANICS, Trans. ASME, vol. 72, 1950, p. 409.

6 "Transverse Impact on Beams and Plates," by A. C. Eringen, JOURNAL OF APPLIED MECHANICS, Trans. ASME, vol. 75, 1953, p. 461.

7 "Impulsive Loads on Beams," by W. H. Hoppmann, Proceedings of the Society for Experimental Stress Analysis, vol. 10, no. 2, 1952, p. 157.

8 "An Experimental Device for Obtaining Elastic Rotational Constraint on Boundary of a Plate," by W. H. Hoppmann and J. Greenspon, Proceedings of the Second U. S. National Congress of Applied Mechanics, ASME, 1954, p. 187.

9 "The Calculus of Observations," by E. T. Whittaker and G. Robinson, Blackie, London, 1944, pp. 146–147.

10 "The Determination of Static and Dynamic Yield Stresses Using a Hard Steel Ball," by R. M. Davies, Proceedings of the Royal Society of London, series A, vol. 197, 1949, p. 416.

11 "On the Production of Vibrations by Forces of Relatively Long Duration, With Applications to the Theory of Collisions," by J. W. S. Rayleigh, *The London, Edinburgh and Dublin Philosophical Magazine*, series 6, vol. 11, 1906, p. 283.

12 "Elastic Work Involved in Rolling a Sphere on Another Surface," by D. Tabor, *British Journal of Applied Physics*, vol. 6, 1955, p. 79.

13 "The Hardness of Metals," by D. Tabor, Oxford University Press, 1951.

14 "The Theory of Collisions of Spheres of Soft Metals," by J. P. Andrews, *The London, Edinburgh and Dublin Philosophical Magazine*, series 7, vol. 9, 1930, p. 593.

15 "A Study of Some Impacts Between Metal Bodies by a Piezo-Electric Method," by A. W. Crook, Proceedings of the Royal Society of London, series A, vol. 212, 1952, p. 377.

16 "An Experimental Investigation of the Oblique Impact of Spheres Upon Simply Supported Beams," by W. Goldsmith and D. M. Cunningham, Proceedings of the Society for Experimental Stress Analysis, vol. 14, no. 1, 1956, p. 179.

17 "Beanspruchungen eines Biegeträgers bei schlagartiger Querbelastung," by H. Emschermann and K. Rühl, *VDI Forschungsheft* 443, 1954.

Appendix

AN ELASTIC BEAM WITH LINEAR ELASTIC END CONSTRAINT

The boundary conditions expressing constraint at the ends of an elastic beam are

$$\left.\begin{aligned} \frac{d^2X_i}{dx^2} &= \frac{\mu_0}{EI}\frac{dX_i}{dx} \quad \text{at } x = 0 \\ \frac{d^2X_i}{dx^2} &= -\frac{\mu_l}{EI}\frac{dX_i}{dx} \quad \text{at } x = l \end{aligned}\right\} \qquad [15]$$

for elastic moments and

$$\left.\begin{aligned} \frac{d^2X_i}{dx^2} &= -\frac{k_0}{EI}X_i \quad \text{at } x = 0 \\ \frac{d^2X_i}{dx^2} &= \frac{k_l}{EI}X_i \quad \text{at } x = l \end{aligned}\right\} \qquad [16]$$

for elastic forces. Satisfaction of these relations by the mode

function X_i for the Euler beam then leads to the frequency equation

$$2(1 - \cos \lambda_i l \cosh \lambda_i l) - \frac{2(M_0 + M_1)}{(\lambda_i l)} (\sin \lambda_i l \cosh \lambda_i l + \cos \lambda_i l \sinh \lambda_i l) + \frac{4M_0M_1}{(\lambda_i l)^2} (\sin \lambda_i l \sinh \lambda_i l) - \frac{2(K_0 + K_1)}{(\lambda_i l)^3} (\sin \lambda_i l \cosh \lambda_i l - \cos \lambda_i l \sinh \lambda_i l) + \frac{2(K_0 + K_1)(M_0 + M_1)}{(\lambda_i l)^4} (1 + \cos \lambda_i l \cosh \lambda_i l) - \frac{2(K_0M_1 + K_1M_0)}{(\lambda_i l)^4} (1 - \cos \lambda_i l \cosh \lambda_i l) + \frac{2M_0M_1(K_0 + K_1)}{(\lambda_i l)^5} (\sin \lambda_i l \cosh \lambda_i l + \cos \lambda_i l \sinh \lambda_i l) + \frac{4K_0K_1}{(\lambda_i l)^6} (\sin \lambda_i l \sinh \lambda_i l) + \frac{2K_0K_1(M_0 + M_1)}{(\lambda_i l)^7} (\sin \lambda_i l \cosh \lambda_i l - \cos \lambda_i l \sinh \lambda_i l) + \frac{2K_0K_1M_0M_1}{(\lambda_i l)^8} (1 - \cos \lambda_i l \cosh \lambda_i l) = 0 \quad \ldots\ldots [17]$$

where the dimensionless coefficients expressing the constraint conditions are defined by

$$\left.\begin{aligned} M_0 &= \frac{\mu_0 l}{EI}, \quad M_1 = \frac{\mu_1 l}{EI} \\ K_0 &= \frac{k_0 l^3}{EI}, \quad K_1 = \frac{k_1 l^3}{EI} \end{aligned}\right\} \quad \ldots\ldots [18]$$

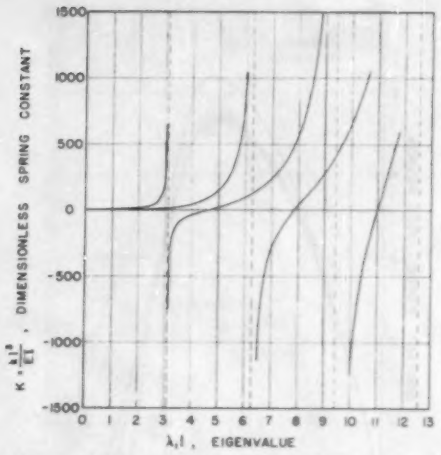

FIG. 8 DISTRIBUTION OF ROOTS OF FREQUENCY EQUATION FOR SYMMETRICAL ELASTIC SPRINGS AT ENDS FOR FIRST FIVE FLEXURAL MODES OF BEAM

This relation represents the most general frequency equation for an elastic beam with linear end constraints.

For the particular case of symmetrical elastic spring supports at the beam ends, i.e., $M_0 = M_1 = 0$, this general frequency equation reduces to Equation [4]. Fig. 8 shows the effect of both beam and support stiffness on mode distribution for the first 5 modes where the nonuniform spacing of the roots is most evident. The primary effect of increasing the support stiffness is to shift the lower frequencies to higher values, while the higher frequencies are relatively unaffected. This shift plays a significant role in the determination of beam deflections during periods beyond the time of contact.

Displacements in a Wide Curved Bar Subjected to Pure Elastic-Plastic Bending[1]

By BERNARD W. SHAFFER[2] and RAYMOND N. HOUSE, JR.,[3] NEW YORK, N. Y.

Equations have been obtained for the displacements and strains within a wide curved bar made of a perfectly plastic, incompressible material subjected to a pure bending moment which is sufficiently large to cause elastic-plastic stresses. It is found that whenever the applied load is within 95 per cent of the fully plastic bending moment, displacements and strains in the elastic-plastic problem are of the order of magnitude of the corresponding elastic case. It is also found that when the bending moment reaches approximately 65 per cent of the fully plastic bending moment, the change in material thickness reaches a maximum. It decreases to zero when the bar becomes completely plastic.

Introduction

THE elastic-plastic stress distribution within a wide curved bar made of a perfectly plastic material and subjected to pure bending was presented in a previous paper (1).[4] It is the authors' present objective to continue the analysis of this problem in order to evaluate the displacements and strains as the bending moment is increased from zero to that required for the fully plastic case.

In addition to the original supposition that the bar is made of a material which obeys Hooke's law in the elastic range and does not work-harden in the plastic range, it is now further assumed that the bar is incompressible in both the elastic and plastic ranges. Even though incompressibility was not specified in the previous paper (1), the present assumption will in no way alter the results presented there.

A typical section of the bar taken perpendicular to its longitudinal axis is shown in Fig. 1. The internal and external radii of the bar are a and b, respectively, whereas the bending moment per unit width applied uniformly along the surface perpendicular to the plane of curvature is M. Aside from end sections, therefore, the stresses may be analyzed as a problem in plane strain.

The stresses on a typical element of the bar, described in polar co-ordinates, are σ_r, the radial stress, and σ_θ the circumferential stress. For the type of loading under consideration, these stresses vary only in the radial and not in the circumferential direction. Furthermore, it may be seen from symmetry considerations that the shear stresses on the typical element are zero, and, therefore, the only equation of equilibrium which the nonzero stresses have to satisfy is

$$\frac{\partial \sigma_r}{\partial r} = \frac{\sigma_\theta - \sigma_r}{r} \quad \ldots\ldots [1]$$

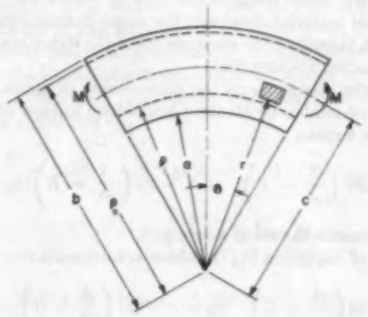

FIG. 1 GEOMETRY OF THE CURVED BAR

The partial derivative is used because the stresses vary with the radius r and the applied bending moment. The latter condition also may be expressed in terms of the position of the elastic-plastic boundary ρ.

Since the shear stress is zero and the material is incompressible, it can be shown (2) that the radial displacement u, the circumferential displacement v, the longitudinal displacement w, and the rotation $\partial w/\partial r$ may be written

$$u = -\left(\frac{A}{r} + Br\right) + K_1 \cos\theta; \quad v = 2Br\,\theta - K_1 \sin\theta \ldots [2a\text{–}b]$$

$$w = 0; \quad \frac{\partial w}{\partial r} = 2B\theta \quad \ldots\ldots [2c]$$

whereas the strain components in the radial, circumferential, and longitudinal directions, respectively, may be written

$$\epsilon_r = \frac{\partial u}{\partial r} = \frac{A}{r^2} - B;$$

$$\epsilon_\theta = \frac{u}{r} + \frac{1}{r}\frac{\partial v}{\partial \theta} = -\left(\frac{A}{r^2} - B\right); \quad \epsilon_z = 0 \ldots . [3]$$

where A, B, and K_1 are constants.

As the bending moment M increases and the bar is deformed, one point remains in a fixed position and does not rotate. If this point is taken at the centroid of the central section from which θ is measured, we may write the following boundary conditions

$$u = v = \frac{\partial w}{\partial r} = 0 \text{ at } \theta = 0 \text{ and } r = r_0 = \frac{a+b}{2} \ldots . [4]$$

---

[1] The results presented in this paper were obtained in the course of research sponsored by the Office of Ordnance Research, Department of the Army (Ordnance Corps), under Contract No. DA-30-069-ORD-1398, with New York University.

[2] Associate Professor of Mechanical Engineering, New York University. Assoc. Mem. ASME.

[3] Senior Engineer, Project Research Department, American Bosch Arma Corporation, Garden City; formerly, Instructor of Mechanical Engineering, New York University. Assoc. Mem. ASME.

[4] Numbers in parentheses refer to the Bibliography at the end of the paper.

Presented at the Applied Mechanics Division Summer Conference, Berkeley, Calif., June 13–15, 1957, of THE AMERICAN SOCIETY OF MECHANICAL ENGINEERS.

Discussion of this paper should be addressed to the Secretary, ASME, 29 West 39th Street, New York, N. Y., and will be accepted until October 10, 1957, for publication at a later date. Discussion received after the closing date will be returned.

NOTE: Statements and opinions advanced in papers are to be understood as individual expressions of their authors and not those of the Society. Manuscript received by ASME Applied Mechanics Division, July 24, 1956. Paper No. 57—APM-24.

In view of this, the constant K_1 can be expressed in terms of A and B, so that the displacement equations may be written

$$\left.\begin{aligned} u &= -A\left[\frac{1}{r} - \frac{2\cos\theta}{(a+b)}\right] - B\left[r - \frac{(a+b)}{2}\cos\theta\right] \\ v &= -\frac{2A}{(a+b)}\sin\theta - B\left[\frac{(a+b)}{2}\sin\theta - 2r\theta\right] \end{aligned}\right\} \quad \ldots [5]$$

The two remaining constants A and B will be evaluated separately for each of the three phases of the problem.

The Elastic Range

The stress components σ_r, σ_θ, and σ_z may be written as the sum of the mean normal stress s and the components of the stress deviation s_r, s_θ, and s_z, respectively (3, 4)

$$\sigma_r = s + s_r; \quad \sigma_\theta = s + s_\theta; \quad \sigma_z = s + s_z \ldots\ldots [6]$$

Similarly, the strain components may be separated. For an incompressible material, however, the mean normal strain is equal to zero and, therefore, the components of the strain tensor and the strain deviation are identical.

Within the elastic range the components of stress and strain deviation are related by Hooke's law, which in view of Equations [3] may be written

$$s_r = 2G\left(\frac{A}{r^2} - B\right); \quad s_\theta = -2G\left(\frac{A}{r^2} - B\right); \quad s_z = 0 \ldots [7]$$

where G denotes the shear modulus.

In view of Equation [6] the stress components may be written

$$\sigma_r = s + 2G\left(\frac{A}{r^2} - B\right); \quad \sigma_\theta = s - 2G\left(\frac{A}{r^2} - B\right);$$

$$\sigma_z = s \ldots\ldots [8a\text{–}c]$$

When they are introduced into the equilibrium condition, Equation [1], and the resulting expression is integrated, the mean normal stress s is found to be

$$s = 4GB\log_e r + f(\rho) \ldots\ldots [9]$$

where $f(\rho)$ is an arbitrary function of integration.

For the problem under consideration the concave and convex boundaries of the curved bar are stress-free, whereas the circumferential stresses at the ends give rise to the applied bending moment M; i.e.

$$\sigma_r = 0 \text{ for } r = a \text{ and } r = b; \qquad \int_a^b \sigma_\theta r\, dr = -M \ldots [10]$$

As a consequence, the constants appearing in this range of the problem are found to be

$$A = -\frac{2M}{GN}a^2b^2\log_e\frac{b}{a}; \quad B = -\frac{M}{GN}(b^2 - a^2) \ldots [11a\text{–}b]$$

$$f(\rho) = -\frac{2M}{N}[b^2 - a^2 - 2(b^2\log_e b - a^2\log_e a)] \ldots [11c]$$

where

$$N = (b^2 - a^2)^2 - 4a^2b^2\left(\log_e\frac{b}{a}\right)^2 \ldots\ldots [11d]$$

When these constants are introduced into Equations [3] and [5] the resulting expressions are the nonvanishing strain and displacement components for the completely elastic solution of the pure bending problem of a wide curved bar made of an incompressible material loaded under plane-strain conditions.

The Yield Condition

The strain components within the elastic and plastic regions are given as Equations [3]. Since the strain deviation e is identical with the strain tensor ϵ, we may write the proportionality

$$e_r : e_\theta : e_z = \dot{e}_r : \dot{e}_\theta : \dot{e}_z = 1 : -1 : 0 \ldots\ldots [12]$$

at every point in the bar. The dot indicates the derivative with respect to any parameter which increases monotonically with time, such as the bending moment M.

According to Hooke's law, the stress-deviation components at any point in the elastic domain satisfy the proportionality

$$s_r : s_\theta : s_z = e_r : e_\theta : e_z = 1 : -1 : 0 \ldots\ldots [13]$$

Continuity requires the same proportionality to hold at the instant the element enters the plastic zone. Within the plastic domain, the rate of change of the stress deviation, according to the Prandtl-Reuss stress-strain law (3, 4) satisfies the relationship

$$\dot{s}_r : \dot{s}_\theta : \dot{s}_z = 2G\left(\dot{e}_r - \frac{\dot{W}}{2k^2}s_r\right) : 2G\left(\dot{e}_\theta - \frac{\dot{W}}{2k^2}s_\theta\right) : 2G\left(\dot{e}_z - \frac{\dot{W}}{2k^2}s_z\right) \ldots\ldots [14]$$

where $\dot{W}$ may be interpreted as the rate at which the stresses do work in connection with the change of shape and k is the maximum shear stress of the material.

In view of Equations [12] and [13], at an instant an element enters the plastic domain the right-hand side of the continued proportion in Equation [14] is equal to $1 : -1 : 0$. From this fact and Equation [12] it follows then that

$$\dot{s}_r : \dot{s}_\theta : \dot{s}_z = \dot{e}_r : \dot{e}_\theta : \dot{e}_z = 1 : -1 : 0 \ldots\ldots [15]$$

must hold throughout the plastic domain.

With $s_z = 0$ and, furthermore, since the sum of the components of the stress deviation is equal to zero, the Mises yield condition may be written

$$s_\theta - s_r = 2k \qquad a \leq r \leq c \ldots\ldots [16a]$$

or

$$s_r - s_\theta = 2k \qquad c \leq r \leq b \ldots\ldots [16b]$$

In view of Equations [6], the Mises yield condition is mathematically identical with the Tresca yield condition. Furthermore, since $\sigma_\theta > \sigma_r$ for the region $a \leq r \leq c$, where $r = c$ is the neutral axis, Equation [16a] applies only within the range indicated. The reverse is true for $c \leq r \leq b$ and consequently Equation [16b] applies.

The Elastic-Plastic Solution—Stage 1

When the bending moment M becomes large enough, the components of the stress deviation, described in Equations [7] and [11], satisfy the yield condition, Equation [16a], at the surface $r = a$, and the bar enters what is called the first stage of the elastic-plastic solution. With an increase in bending moment, a plastic zone forms around the concave surface of the bar and increases in size as the bending moment increases. In view of the symmetry of the problem, the elastic-plastic boundary is a circular arc of radius $r = \rho_i$. Its position depends on the applied bending moment M. (See Equation [17] of reference 1.)

As a consequence of the proportionality expressed in Equation [15] and the yield condition shown in Equation [16a], the stress components within the plastic zone, $a \leq r \leq \rho_i$, are according to Equations [6]

$$\sigma_r = s - k; \quad \sigma_\theta = s + k; \quad \sigma_z = s \ldots\ldots [17a\text{–}c]$$

Since these stress components satisfy the condition of equilibrium, Equation [1], the mean normal stress can be evaluated, and it is found that

$$s = D(\rho) + 2k \log_e r \quad [18]$$

where $D(\rho)$ is an arbitrary function of integration.

Within the elastic zone, $\rho_i \leq r \leq b$, the stresses are given by Equations [8] and [9], and the components of the stress deviation are given by Equations [7]. At the convex surface of the elastic zone, $r = b$, and the concave surface of the plastic zone, $r = a$, the radial stresses are equal to zero. At the boundary between the elastic and plastic regions, the radial stresses are continuous and the stress deviation components must satisfy the yield condition. Consequently in view of Equations [7], [8a], [9], [16a], [17a], and [18] the constants for the first stage are

$$A = \frac{k\rho_i^2 b^2}{GN_1} \log_e \frac{b}{a} \quad [19a]$$

$$B = \frac{k}{2GN_1}\left(b^2 - \rho_i^2 + 2b^2 \log_e \frac{\rho_i}{a}\right) \quad [19b]$$

$$D(\rho) = k(1 - 2\log_e a) \quad [19c]$$

$$f(\rho) = \frac{k}{N_1}\left[b^2(1 - 2\log_e b)\left(1 + 2\log_e \frac{\rho_i}{a}\right) - \rho_i^2(1 - 2\log_e a)\right] \quad [19d]$$

where

$$N_1 = b^2 - \rho_i^2 - 2b^2 \log_e \frac{b}{\rho_i} \quad [19e]$$

These expressions apply throughout the elastic and plastic regions of the bar.

From Equations [17], [18], and [19] the stress components within the plastic region $a \leq r \leq \rho_i$ are

$$\sigma_r = 2k \log_e \frac{r}{a}; \quad \sigma_\theta = 2k\left(1 + \log_e \frac{r}{a}\right);$$

$$\sigma_z = k\left(1 + 2\log_e \frac{r}{a}\right) \quad [20a\text{–}c]$$

The stress components within the elastic region may be computed similarly, but because they are not required in the present analysis, their expressions will not be presented in this paper.

As the bending moment increases, the radius to the inner elastic-plastic boundary ρ_i also increases until the bending moment becomes so large that yielding begins at the outer surface of the curved bar. We then enter what is called the second stage of the elastic-plastic solution. (See Equations [17] and [18] of reference 1 for the bending moment at which this occurs.)

The Elastic-Plastic Solution—Stage 2

During the second stage of the elastic-plastic solution a plastic zone forms around the convex surface of the bar. Consequently three separate zones exist; the lower plastic zone $a \leq r \leq \rho_i$, the elastic zone $\rho_i \leq r \leq \rho_o$, and the upper plastic zone $\rho_o \leq r \leq b$.

The stresses within the lower plastic zone are prescribed in Equations [20]. Within the upper plastic zone, however, stress components are, in view of Equations [6], [15], and [16b]

$$\sigma_r = s + k; \quad \sigma_\theta = s - k; \quad \sigma_z = s \quad [21]$$

These stress components satisfy the condition of equilibrium, Equation [1]. Substituting Equations [21] into Equation [1] and integrating, the mean normal stress s is found to be

$$s = D_1(\rho) - 2k \log_e r \quad [22]$$

where $D_1(\rho)$ may be determined from the boundary conditions. The stress components defined in Equations [21] may, therefore, be written

$$\sigma_r = D_1(\rho) + k(1 - 2\log_e r) \quad [23a]$$

$$\sigma_\theta = D_1(\rho) - k(1 + 2\log_e r) \quad [23b]$$

$$\sigma_z = s = D_1(\rho) - 2k \log_e r \quad [23c]$$

within the upper plastic region, $\rho_o \leq r \leq b$.

The radial, circumferential, and longitudinal stresses within the elastic region are still given by Equations [8] and [9], and the components of the stress deviation are given by Equations [7].

The radial stresses are continuous across the elastic-plastic boundaries, $r = \rho_i$ and $r = \rho_o$, and they vanish at the upper surface of the plastic zone, $r = b$. Furthermore, the components of the stress deviation must satisfy the appropriate yield conditions at the elastic-plastic boundaries. Hence in view of Equations [7], [8a], [9], [16], [20a], and [23a] one may write the following equalities

$$2G\frac{A}{\rho_i^2} - 2GB(1 - 2\log_e \rho_i) + f(\rho) = 2k \log_e \frac{\rho_i}{a} \quad [24a]$$

$$-2G\left(\frac{A}{\rho_i^2} - B\right) = k \quad [24b]$$

$$2G\frac{A}{\rho_o^2} - 2GB(1 - 2\log_e \rho_o) + f(\rho) = D_1(\rho) + k(1 - 2\log_e \rho_o) \quad [24c]$$

$$D_1(\rho) + k(1 - 2\log_e b) = 0 \quad [24d]$$

$$2G\left(\frac{A}{\rho_o^2} - B\right) = k \quad [24e]$$

From the first four of these equations one finds

$$A = \frac{k\rho_i^2\rho_o^2}{GN_2} \log_e \frac{\rho_o^2}{ab} \quad [25a]$$

$$B = \frac{k}{2GN_2}\left(\rho_o^2 - \rho_i^2 - 2\rho_o^2 \log_e \frac{ab}{\rho_i\rho_o}\right) \quad [25b]$$

$$D_1 = -k(1 - 2\log_e b) \quad [25c]$$

$$f(\rho) = \frac{k\rho_o^2}{N_2}\left[(1 - 2\log_e \rho_o)\left(1 + 2\log_e \frac{\rho_i}{a}\right) + 4\log_e \rho_i \log_e \frac{b}{\rho_o} - \left(\frac{\rho_i}{\rho_o}\right)^2(1 - 2\log_e a)\right] \quad [25d]$$

where

$$N_2 = \rho_o^2 - \rho_i^2 - 2\rho_o^2 \log_e \frac{\rho_o}{\rho_i} \quad [25e]$$

The fifth equation gives a relationship between the positions of the elastic-plastic boundaries

$$\rho_o^2\left(1 - \log_e \frac{ab}{\rho_o^2}\right) = \rho_i^2\left(1 + \log_e \frac{\rho_o^2}{ab}\right) \quad [26]$$

obtained by introducing the constants A and B described in Equations [25] into Equation [24e].

Thus the constants A and B are defined in terms of ρ_i, the

radius of the inner elastic-plastic boundary, and ρ_o, the radius of the outer elastic-plastic boundary. They are related to each other by Equation [26] and are uniquely prescribed for a given bending moment. (See Equation [28] of reference 1.)

The Completely Plastic Solution

When the bending moment is large enough, the boundary of the upper plastic zone $r = \rho_o$, and the boundary of the lower plastic zone $r = \rho_i$ meet at the surface which represents the limit of the degenerating elastic zone $r = c$. Although we may regard the fully plastic state as a limiting case of the elastic-plastic state to obtain the stress distributions for a corresponding bending moment, such a procedure assigns infinitely large values to the displacements at each point. This may be immediately verified in the following manner: If the value of N_2 described in Equation [25e] is substituted into Equations [2] and [25], and the expression for $\rho_o^2 - \rho_i^2$, obtained from Equation [26], is introduced into the resulting expression, then the displacements u and v may be written

$$\frac{2G}{k}u = -\frac{2\rho_i^2\rho_o^2}{(\rho_i^2-\rho_o^2)}\left[\frac{1}{r}-\frac{2\cos\theta}{(a+b)}\right] - \frac{(\rho_i^2+\rho_o^2)}{(\rho_i^2-\rho_o^2)}\left[r-\frac{(a+b)}{2}\cos\theta\right] \quad [27a]$$

$$\frac{2G}{k}v = -\frac{4\rho_i^2\rho_o^2}{(\rho_i^2-\rho_o^2)}\frac{\sin\theta}{(a+b)} - \frac{(\rho_i^2+\rho_o^2)}{(\rho_i^2-\rho_o^2)}\left[\frac{(a+b)}{2}\sin\theta - 2r\theta\right] \quad [27b]$$

In the limit, $\rho_i = \rho_o = c$, and the displacements u and v assume infinitely large values at each point. This result is compatible with the idea of flow within a perfectly plastic material where we expect the displacements to increase under a constant state of stress [4].

In view of this, the expressions for displacements may give good results up to bending moments within approximately 95 per cent of the bending moment that would cause complete plastic flow. This idea is in agreement with the Prandtl-Reuss stress-strain law which is postulated only for small strains and contained plastic deformation.

Dimensional Changes

As the bending moment increases in the direction which tends to straighten the initially curved bar, the internal and external radii of the bar increase and the total angle subtended by the end sections decreases. According to Equations [2], each radial cross section translates $-K_1 \sin\theta$ and rotates through the angle

$$\Delta\theta = \frac{\partial v}{\partial r} = 2B\theta \quad [28]$$

where θ is measured from the Y-axis, which is a plane of symmetry (Fig. 2). The constant B in Equation [28] is given by Equation [11b] for the completely elastic case and by Equations [19b] and [25b] for the first and second stages of the elastic-plastic solution, respectively.

The change of radii may be evaluated by studying the geometric relationships shown in Fig. 2. It can be seen that as the bending moment is applied and the bar tends to "open up," the center of curvature moves from the point O to the point O'.

Let a and b denote the internal and external radii of the bar and let $r_o = (a+b)/2$ be the radius to the centroid of the cross section for the initial unstrained state. The total angle of the bar subtended by the end sections is equal to $2\theta_1$. After deformation let the internal and external radii be denoted by a' and b', respectively, and let $r_o' = (a'+b')/2$ denote the radius to the centroid of the cross section. In the deformed state the total angle of the bar subtended by the end sections is $2\theta_1'$.

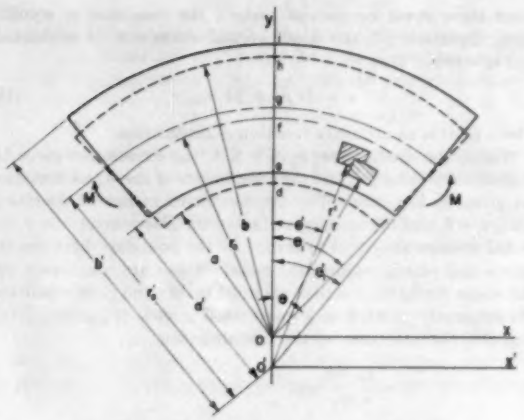

Fig. 2 Change of Radii During Bending

Constant-volume considerations require that the volume before deformation be equal to the volume after deformation

$$2\theta_1 r_o(b-a) = 2\theta_1' r_o'(b'-a') \quad [29]$$

thereby providing a relationship between prime and unprimed dimensions.

In view of Equation [28] the angle θ_1 has been decreased during deformation by an amount equal to $2B\theta_1$. Therefore Equation [29] may be rewritten to provide an expression for the radius r_o' to the centroid of the cross section in the deformed state

$$r_o' = \frac{r_o(b-a)}{(1+2B)(b'-a')} \quad [30]$$

The thickness after deformation $b'-a'$ is yet to be evaluated. It will be found with the aid of an expression for the change in material thickness during bending.

The change in thickness Δt is equal to $u_b - u_a$, where u_a is the radial displacement at $r = a$, and u_b is the radial displacement at $r = b$. For $\theta = 0$, these displacements are, in view of Equation [2a]

$$u_a = -\left(\frac{A}{a}+Ba\right) + K_1 \quad [31a]$$

$$u_b = -\left(\frac{A}{b}+Bb\right) + K_1 \quad [31b]$$

and therefore the change in thickness

$$\Delta t = (b-a)\left(\frac{A}{ab}-B\right) \quad [32]$$

where the constants A and B have been evaluated in Equations [11] for the elastic phase and in Equations [19] and [25] for the first and second stages of the elastic-plastic solution, respectively.

In order to find an expression for the change of thickness in the completely plastic case, the ratio of the constants A/B when $\rho_i = \rho_o = c$ must be examined. During the second stage of the elastic-plastic solution, one may write, in view of Equations [25a], [25b], and [26]

$$\frac{A}{B} = \frac{2\rho_i^2\rho_o^2}{\rho_i^2+\rho_o^2} \quad [33]$$

In the limit when the bar is completely plastic, $\rho_i = \rho_o = c$, and the ratio A/B is equal to c^2. It has been shown (1, 5, 6), however, that $c^2 = ab$ for the fully plastic case, so that in the limit the change in thickness is equal to zero. This result is in agreement with the previous work of Hill (5).

The thickness after deformation $(b' - a')$ is equal to the thickness before deformation $(b - a)$ plus the change in thickness. In view of Equations [30] and [32], the radius r_o' after deformation is

$$r_o' = \frac{r_o}{(1 + 2B)\left(1 + \frac{A}{ab} - B\right)} \quad \ldots\ldots [34]$$

where $r_o = (a + b)/2$ and the constants A and B have been defined previously for each phase of the problem.

It will be convenient in evaluating the change of internal and external radii to find an expression for the distance fg on the Y-axis in Fig. 2. It can be seen from the geometry of the problem that

$$fg = r_o' - r_o - O'O \quad \ldots\ldots [35]$$

The radii r_o' and r_o may in turn be written $(a' + b')/2$ and $(a + b)/2$, respectively. Since u_a is the distance de and u_b is the distance hi, a' is equal to $O'O + a + u_a$ and b' is equal to $O'O + b + u_b$. Therefore in view of Equations [31], Equation [35] may be rewritten

$$fg = -\frac{(a + b)}{2}\left(\frac{A}{ab} + B\right) + K_1 \quad \ldots\ldots [36]$$

The change of internal radius $(a' - a)$ is equal to $O'O + de$, where $O'O$ is given in Equation [35] and de is the displacement u_a. In view of Equations [35], [31a], [34], and [36], one may write

$$\Delta a = a' - a$$

$$= \frac{2B^2(a + b) - (1 + 2B)\left[\frac{A}{a} + Ba + \frac{(b - a)}{2}\left(\frac{A}{ab} - B\right)^2\right]}{(1 + 2B)\left(1 + \frac{A}{ab} - B\right)} \quad \ldots\ldots [37]$$

It may be noted that the constant K_1 did not enter the expression for change in thickness, Equation [32], or change in radius, Equation [37]. These expressions are, therefore, independent of the location of the fixed point used in the analysis.

Discussion of Results

The nonvanishing components of displacements and strains within a wide curved bar subjected to pure bending were expressed in terms of two constants A and B. These constants were subsequently defined either in terms of the applied bending moment or the position of the elastic-plastic boundaries. Since there already exist relationships between the applied bending moment and the corresponding position of the elastic-plastic boundary (1), the constants A and B always can be evaluated for a prescribed bending moment.

Rotation of end sections, change in material thickness, as well as change in internal radius were found by direct application of the displacement equations. In order to study the relationships between these effects and the applied bending moment, it is convenient to perform some numerical computations. For this purpose, four different wide curved bars having b/a ratios of 1.5, 2.0, 2.5, and 3.0, respectively, were considered. Whenever the ratio of maximum shear stress to shear modulus k/G was required, a numerical value of 0.002 was used as representative of an incompressible material. The results of these computations in dimensionless form are shown in Figs. 3–5. In each case it was found convenient to use the ratio M/M_p for one of the co-ordinates, where M is the applied bending moment per unit width and M_p is the bending moment per unit width for the completely plastic case.

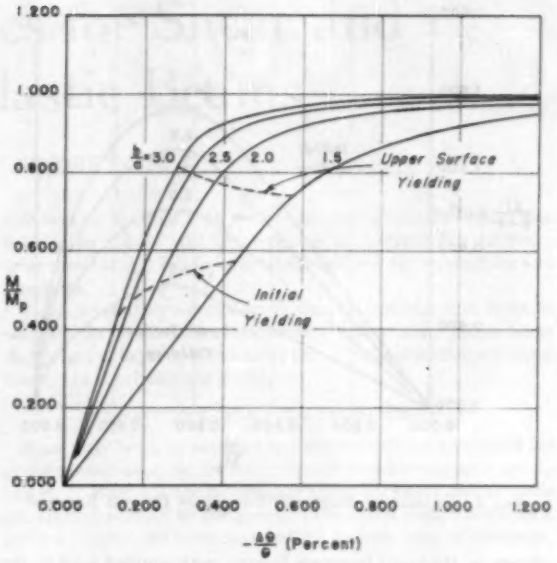

Fig. 3 Decrease of Angle During Bending

Fig. 3 describes the rotation $\Delta\theta$ of any radial cross section as the bending moment M tends to straighten the initially curved wide bar by presenting the relationship between $-\Delta\theta/\theta$, plotted as a percentage, and the bending moment ratio M/M_p. The negative sign was introduced in the abscissa because the angle θ decreases for the assumed direction of bending. The solid lines shown in Fig. 3 were calculated from Equation [28] where B is given in Equations [11b], [19b], and [25b], respectively, for the different phases of the elastic-plastic problem. The dashed lines, which indicate the relationship between the bending-moment ratio and the instant initial and upper surface yielding begins, were computed with the aid of the equations which were obtained in the previous paper (1).

It can be seen by examining the figure that, as the bending moment M increases, the angle θ decreases linearly within the elastic range, almost linearly within the first stage of the elastic-plastic range, but then decreases very rapidly within the second stage of the elastic-plastic range. When the bending moment reaches about 95 per cent of the fully plastic bending moment, rapid changes in angle occur for very small increases in the applied moment. It is in the small interval between M/M_p equal to 0.95 and 1.000, as the bar approaches the fully plastic state, that the change of angle becomes infinitely large. Before reaching this range, the change in angle is still very small, equal approximately to 1.2 per cent for a b/a ratio of 1.5 and even smaller values for the larger b/a ratios. Since these figures are as small as they are, the deformations resulting within this range of loading may still be said to be of the order of magnitude encountered within small strain theory.

The change in material thickness during bending is shown in Fig. 4 as a set of curves relating the ratio of the change in thickness to the original thickness $\Delta t/(b - a)$ versus the bending moment ratio M/M_p. It can be seen that, for a given bar, the

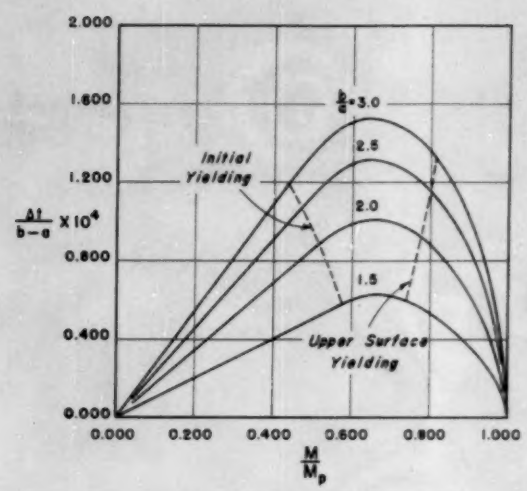

FIG. 4 CHANGE IN MATERIAL THICKNESS DURING BENDING

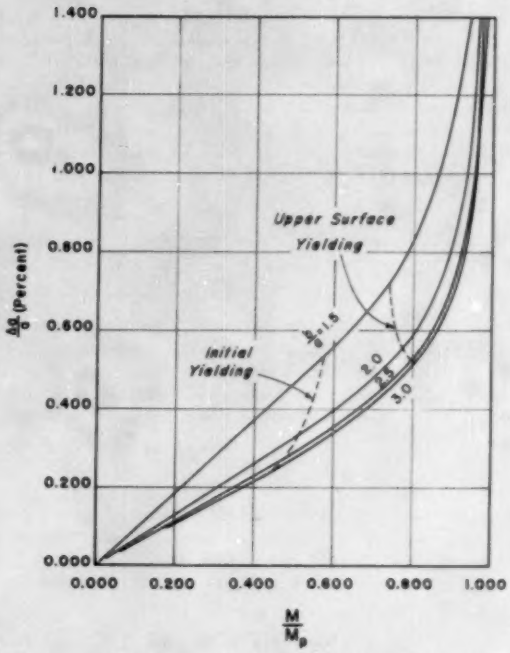

FIG. 5 CHANGE OF INTERNAL RADIUS DURING BENDING

change in thickness increases linearly with applied load in the elastic range, reaches a maximum during the first stage of the elastic-plastic phase, and decreases rapidly to zero soon after the upper surface begins yielding. When the bar is completely plastic, there is no change in material thickness. This result was previously reported by Hill (5). On the whole, it can be said that the change in material thickness is very small for all values of b/a throughout the entire loading range, being only 0.0152 per cent at the maximum point of the curve, $b/a = 3.0$.

The increase in the internal radius of the bar may be studied by examining Fig. 5 where the ratio $\Delta a/a$ is plotted against the ratio M/M_p. The change in radii, for a given wide curved bar, increases linearly within the elastic range, almost linearly within the first stage of the elastic-plastic solution, and then increases more rapidly once yielding begins at the upper surface. The change in radii is very pronounced once M/M_p reaches 0.95. Below this value, however, the change in dimensions is less than 1.5 per cent.

We see, therefore, that as originally postulated, the physical dimensions of the bar do not change significantly during the loading process if we concern ourselves with the problem of contained plastic deformation corresponding to values of M/M_p less than 95 per cent. The present analysis therefore gives good results within this loading range.

BIBLIOGRAPHY

1 "The Elastic-Plastic Stress Distribution Within a Wide Curved Bar Subjected to Pure Bending," by B. W. Shaffer and R. N. House, Jr., JOURNAL OF APPLIED MECHANICS, Trans. ASME, vol. 77, 1955, pp. 305–310.

2 "The Significance of Zero Shear Stress in the Pure Bending of a Wide Curved Bar," by B. W. Shaffer and R. N. House, Jr., *Journal of the Aeronautical Sciences*, vol. 24, April, 1957, pp. 307–308.

3 "Theory of Perfectly Plastic Solids," by W. Prager and P. G. Hodge, Jr., John Wiley & Sons, Inc., New York, N. Y., 1951, pp. 12–32.

4 "An Introduction to the Mathematical Theory of Perfectly Plastic Solids," by P. G. Hodge, Jr., Office of Naval Research, Contract N7 onr-358, T.O.I. NR-041-032, Graduate Division of Applied Mathematics, Brown University, Providence, R. I., A11-82/396, February, 1950, pp. 135–138, 156–157.

5 "The Mathematical Theory of Plasticity," by R. Hill, Oxford University Press, London, England, 1950, pp. 238, 287–292.

6 "Bending of an Ideal Plastic Metal," by J. D. Lubahn and G. Sachs, Trans. ASME, vol. 72, 1950, pp. 201–208.

Interaction Curves for Shear and Bending of Plastic Beams[1]

By P. G. HODGE, JR.,[2] BROOKLYN, N. Y.

Interaction curves are presented for plastic beams subject to combined shear and bending. A general formula is obtained and specific curves are drawn for rectangular and I-sections. A simply supported beam with a concentrated load is considered as an example. The results are compared with those of simple beam theory and with available plane-stress solutions. It is concluded that the elementary theory is adequate for height-to-length ratios of less than 0.1, while the present theory is useful in the range from 0.1 to 1.0.

Introduction

IN A RECENT paper Drucker (1)[3] has shown that there cannot be a true interaction curve between bending moment and shear force in a plastic beam since the relation depends upon the entire span of the beam. He arrived at his results by considering plane-stress fields within the beam and by using the upper and lower bound theorems of limit analysis. While such an approach is more accurate than a directly formulated beam theory, it also leads to more difficult problems to solve. On the other hand, the simple bending theory of plastic beams takes no account of shear, and hence has an unknown amount of inaccuracy when applied to short beam spans.

A compromise between two approaches is to consider both bending moment and shear as generalized stress variables. The stress problem is then fully defined in terms of the resultant bending moment M and resultant shear V. According to Prager (2), the corresponding strain variables must be proportional to the curvature rate κ and the resultant shear-strain rate γ of the section. All of these quantities are defined at each section so that it is possible to obtain a unique interaction curve between M and V and a flow rule relating κ and γ. To be sure, it may not be possible to associate stress and strain-rate fields with these quantities which will satisfy the plane-stress equilibrium and compatibility equations. However, the resulting theory will certainly be an improvement on the simple bending theory which completely neglects shear.

The next two sections will be concerned with the derivation of the interaction curve. This will first be approached from the viewpoint of statically admissible stress fields. The maximum safe domain will be obtained by use of the variational calculus. Next, it will be shown that the same interaction curve can be obtained by starting with a kinematically admissible strain-rate field. The results will be presented as integrals for arbitrary cross sections and will be evaluated explicitly for rectangular and I-sections.

Some elementary examples will then be considered in order to compare the predictions of the present theory with simple beam theory and with plane-stress analysis. The final section will summarize the conclusions of the paper.

Interaction Curve From Stress Viewpoint

Since only bending moment and shear are to be accounted for in the present analysis, the only relevant stress components are σ_x and τ_{xy}. Here x is the co-ordinate along the beam and all loads are applied parallel to the y-axis. The stress components for a perfectly plastic material must satisfy an inequality of the form

$$f(\sigma_x, \tau_{xy}) \leq Y^2$$

where Y is the tensile yield stress of the material. States of stress which satisfy the strict inequality above correspond to elastic material, while states of stress which satisfy the equality are plastic. In particular, the equation for plastic states of stress according to the theory of maximum shear stress is

$$f(\sigma_x, \tau_{xy}) = \sigma_x^2 + 4\tau_{xy}^2 = Y^2 \quad \ldots\ldots [1]$$

while according to the Mises theory of maximum octahedral stress it is

$$f(\sigma_x, \tau_{xy}) = \sigma_x^2 + 3\tau_{xy}^2 = Y^2 \quad \ldots\ldots [2]$$

For definiteness it will be assumed in the following that the material satisfies the maximum shear-stress condition, Equation [1]. Obviously the same techniques also can be used to analyze Equation [2].

According to Equation [1], then, the resultant moment and shear at a fully plastic section are given by

$$\left.\begin{aligned} M &= \int_A y\sigma_x dA \\ V &= \int_A \tau_{xy} dA = (1/2)\int_A \sqrt{(Y^2 - \sigma_x^2)}\, dA \end{aligned}\right\} \quad \ldots [3]$$

The problem of finding the interaction curve may now be stated as follows: given a value M, determine a function σ_x so as to maximize V. Obviously it is necessary to consider σ_x only as a function of y, and it is necessary to consider only the first quadrant of the V, M-plane.

This problem is a particularly simple application of the variational calculus since both integrands involved contain only σ_x and none of its derivatives. Therefore the Euler equation will be finite rather than differential. With Euler's multiplier denoted by λ, this equation is[4]

$$\frac{\partial}{\partial \sigma_x}\frac{\sqrt{(Y^2 - \sigma_x^2)}}{2} + \lambda \frac{\partial}{\partial \sigma_x}(y\sigma_x) = 0$$

or

$$-(\sigma_x/2)(Y^2 - \sigma_x^2)^{-1/2} + \lambda y = 0 \quad \ldots\ldots [4]$$

[4] See reference (3), p. 520.

[1] This investigation was supported by the Office of Naval Research.

[2] Professor of Applied Mechanics, Polytechnic Institute of Brooklyn. Now at Illinois Institute of Technology, Chicago, Ill. Mem. ASME.

[3] Numbers in parentheses refer to Bibliography at end of paper.

Presented at the Applied Mechanics Division Summer Conference, Berkeley, Calif., June 13–15, 1957, of The American Society of Mechanical Engineers.

Discussion of this paper should be addressed to the Secretary, ASME, 29 West 39th Street, New York, N. Y., and will be accepted until October 10, 1957, for publication at a later date. Discussion received after the closing date will be returned.

Note: Statements and opinions advanced in papers are to be understood as individual expressions of their authors and not those of the Society. Manuscript received by ASME Applied Mechanics Division, August 2, 1956. Paper No. 57—APM-19.

Solution of Equation [4] for σ_z and substitution into Equations [3] then lead to

$$\left.\begin{aligned} M &= 2\lambda Y \int_A y^2(1 + 4\lambda^2 y^2)^{-1/2} dA \\ V &= (Y/2) \int_A (1 + 4\lambda^2 y^2)^{-1/2} dA \end{aligned}\right\} \quad \ldots\ldots [5]$$

For any given cross section, Equations [5] are representations of the interaction curve in terms of the positive parameter λ.

As an example, Equations [5] have been evaluated for the I-section in Figure 1

$$\left.\begin{aligned} V &= (Y/\lambda)\{w \sinh^{-1} 2\lambda(h - d) \\ &\quad + b[\sinh^{-1} 2\lambda h - \sinh^{-1} 2\lambda(h - d)]\} \\ M &= (Y/2\lambda^2)\{(w - b)[[2\lambda(h - d) \\ &\quad \sqrt{[1 + 4\lambda^2(h - d)^2]} - \sinh^{-1} 2\lambda(h - d)]] \\ &\quad + b[2\lambda h \sqrt{(1 + 4\lambda^2 h^2)} - \sinh^{-1} 2\lambda h]\} \end{aligned}\right\} \ldots [6]$$

Equations [6] may be simplified if the thickness of web and flange are small compared with their widths. To this end, let

$$\eta = 2\lambda h, \quad \delta = d/h, \quad \omega = w/b \ldots\ldots [7]$$

and expand Equations [6], keeping only first-order terms in δ and ω. After some computation the results

$$\left.\begin{aligned} V &= 2Ybh[(\omega/\eta) \sinh^{-1} \eta + \delta(1 + \eta^2)^{-1/2}] \\ M &= 2Ybh^2\{(\omega/\eta^2)[\eta \sqrt{(1 + \eta^2)} - \sinh^{-1} \eta] \\ &\quad + 2\delta\eta(1 + \eta^2)^{-1/2}\} \end{aligned}\right\} \ldots [8]$$

are obtained. Now, to within first-order terms in ω and δ, the limiting moment without shear and shear without moment are easily seen to be

$$\left.\begin{aligned} M_0 &= 2Yh^2b(\omega + 2\delta) \\ V_0 &= 2Yhb(\omega + \delta) \end{aligned}\right\} \ldots\ldots [9]$$

Therefore if a further section parameter is defined by

$$\nu = \omega/\delta = wh/bd \ldots\ldots [10a]$$

the curve parameter η replaced by

$$\vartheta = \sinh^{-1} \eta \ldots\ldots [10b]$$

and dimensionless resultants defined by

$$m = M/M_0, \quad v = V/V_0 \ldots\ldots [10c]$$

then Equation [8] for the interaction curve may finally be written in the form

$$\left.\begin{aligned} v &= (\operatorname{sech} \vartheta + \nu\vartheta \operatorname{csch} \vartheta)/(1 + \nu) \\ m &= [2 \tanh \vartheta + \nu(\coth \vartheta - \vartheta \operatorname{csch}^2 \vartheta)]/(2 + \nu) \end{aligned}\right\} \ldots [11]$$

If $\delta = d/h$ remains constant while $\omega = w/b$ tends to zero, the case of an ideal I-beam with vanishing web is obtained. The substitution of $\nu = 0$ in Equations [11] leads to the particularly simple interaction curve.

$$m^2 + v^2 = 1 \ldots\ldots [12]$$

Alternatively, if $\delta = d/h$ tends to zero while $\omega = w/b$ is held constant, a rectangular section is obtained. This corresponds to $\nu = \infty$, hence Equations [11] become

$$v = \vartheta/\sinh \vartheta, \quad m = \coth \vartheta - \vartheta/\sinh^2 \vartheta \ldots\ldots [13]$$

Equation [13] also may be obtained by direct consideration of a rectangle without any restriction on the magnitude of w/b.

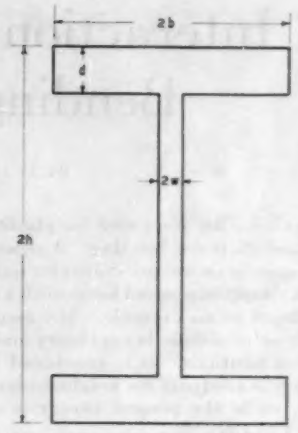

FIG. 1 CROSS SECTION OF I-BEAM

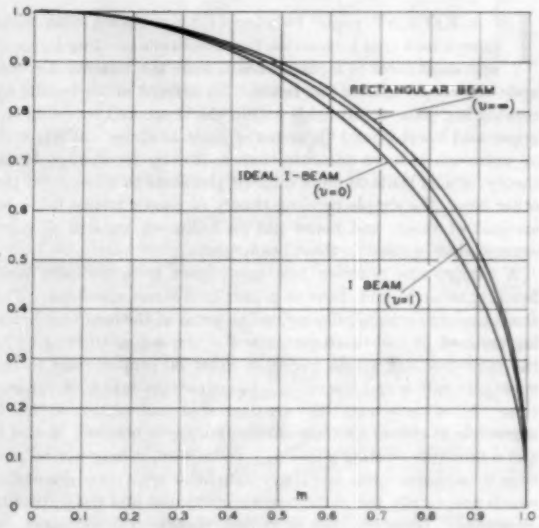

FIG. 2 SHEAR-MOMENT INTERACTION CURVE

The interaction curves corresponding to Equations [12] and [13] are shown in Fig. 2. Those for any intermediate value of ν must lie between these two, hence the interaction curve differs little between rectangular and I-sections. As an example, the case $\nu = 1$ is also shown.

INTERACTION CURVE FROM STRAIN-RATE VIEWPOINT

According to Prager (2), once generalized stresses have been chosen, the generalized strain rates must be such that the rate of dissipation of energy is proportional to the scalar product of stress and strain rate. At any cross section of the beam this dissipation is

$$D = \int_A (\sigma_z \dot{e}_z + \tau_{xy}\dot{\gamma}_{xy}) dA \ldots\ldots [14]$$

and it is necessary to evaluate this in terms of M, V, and appropriate generalized strain-rate variables. To this end, it is assumed that the deformation is the composite of a pure bending

and a uniform shear. Then if κ is the rate of curvature and γ the rate of shear

$$\epsilon_x = y\kappa, \quad \gamma_{xy} = \gamma \ldots\ldots\ldots\ldots\ldots [15]$$

where κ and γ are independent of y or z. Substitution of Equations [15] into [14] then leads to

$$\left.\begin{aligned} D &= \kappa \int_A \sigma_x y dA + \gamma \int_A \tau_{xy} dA \\ &= \kappa M + \gamma V \end{aligned}\right\} \ldots\ldots\ldots [16]$$

Therefore κ and γ are the appropriate strain-rate variables to be associated with the generalized stresses M and V.

In order to derive an upper bound on the interaction curve, arbitrary values of κ and γ are assumed and substituted into Equation [15]. Next, it is observed that according to Equation [1] and the plastic potential-flow rule, the stresses and strain rates are related by

$$\epsilon_x = \mu \partial f/\partial \sigma_x = 2\mu\sigma_x, \; \gamma_{xy} = \mu \partial f/\partial \tau_{xy} = 8\mu\tau_{xy} \ldots\ldots [17]$$

where μ is an arbitrary positive scalar. Combination of Equations [15] and [17] then furnishes

$$\sigma_x = y\kappa/2\mu, \quad \tau_{xy} = \gamma/8\mu \ldots\ldots\ldots\ldots [18]$$

If μ is evaluated from Equation [1], Equations [18] become

$$\sigma_x = \frac{y\kappa Y}{\sqrt{[(\gamma/2)^2 + (y\kappa)^2]}}, \quad \tau_{xy} = \frac{(\gamma/4)Y}{\sqrt{[(\gamma/2)^2 + (y\kappa)^2]}} \ldots [19]$$

Finally, substitution of Equations [19] into Equations [3] leads to[4]

$$\left.\begin{aligned} M &= 2(\kappa/\gamma)Y \int_A y^2 [1 + 4(\kappa/\gamma)^2 y^2]^{-1/2} dy \\ V &= (Y/2) \int_A [1 + 4(\kappa/\gamma)^2 y^2]^{-1/2} dy \end{aligned}\right\} \ldots [20]$$

A comparison with Equations [5] shows that it is merely necessary to associate the arbitrary strain rate ratio κ/γ with the parameter λ in order to regain the interaction curve of the previous section. Therefore since this curve is both an upper and lower bound of the true interaction curve, it must, in fact, be this curve to within the limits of the proposed theory.

[4] Equations [20] were first obtained by Drucker (1).

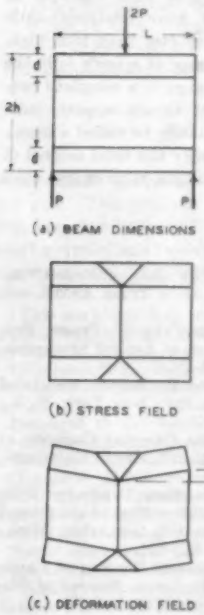

FIG. 3 IMPLY SUPPORTED BEAM

SIMPLY SUPPORTED BEAM

In order to compare the results obtainable from the interaction curve here presented with those of other investigators, a simply supported beam with a concentrated load P applied at its midpoint will be considered, Fig. 3(*a*). Evidently the beam will collapse when the central section under the load becomes fully plastic. From statical considerations the load, moment, and shear at this point are related by

$$M = PL, \quad V = P \ldots\ldots\ldots\ldots\ldots [21]$$

According to simple beam theory which completely neglects shear, the limit load of the beam will occur when the moment at the center is equal to M_0, hence

$$\rho = PL/M_0 = 1 \ldots\ldots\ldots\ldots\ldots [22]$$

independently of the beam length.

If shear is considered, then it follows from Equations [9], [10], and [21] that

$$\left.\begin{aligned} m &= M/M_0 = PL/M_0 = \rho \\ v &= V/V_0 = (PL/M_0)/(V_0 L/M_0) \\ &= \rho t(\nu + 2)/(\nu + 1) \end{aligned}\right\} \ldots [23]$$

where

$$t = h/L \ldots\ldots\ldots\ldots\ldots [24]$$

is the thickness ratio. Equations [11] and [23] then define the limit load ρ for each value of t. The solid curves in Figs. 4 and 5 show the limit load as a function of t, according to the present theory, for the case of a rectangular and an I-section respectively.

A plane-stress theory for I-beams has been presented by Leth (4). A kinematically admissible velocity field for a short section can be constructed as shown in Figs. 3(*b*, *c*). Here the two flanges are in states of pure tension or compressions, while the web carries only shear. If the internal and external work are equated, the result

$$P\Delta = (Y/2)(2w)\,2(h - d)\,L(\Delta/L) + Y(2b)d^2(\Delta/L) \ldots [25]$$

is obtained. By using notations previously introduced and keeping only first order terms in ω and δ, the foregoing equation can

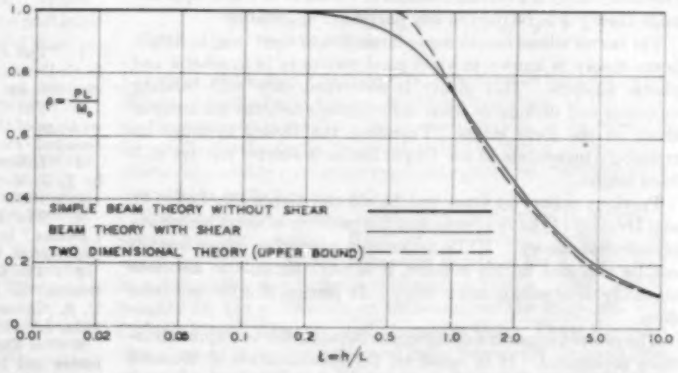

FIG. 4 MAXIMUM LOAD CARRIED BY SIMPLY SUPPORTED RECTANGULAR BEAM

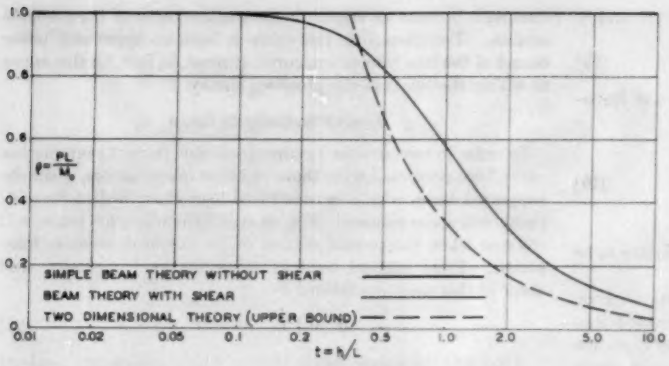

FIG. 5 MAXIMUM LOAD CARRIED BY SIMPLY SUPPORTED I-BEAM ($\nu = wh/bd = 1$)

be transformed to

$$\rho = t\nu/(\nu + 2) \quad [26]$$

The dashed curve in Fig. 5 shows the yield load as a function of the thickness ratio. Since the theory was based only upon a kinematically admissible stress field, the result is an upper bound only.

Kinematically admissible plane-stress fields for rectangular beams have been presented by Onat and Shield (5) and Green (6). However, Drucker (1) has shown that a better result for short beams is obtained by a modification of Leth's I-beam solution. Thus Fig. 3 is still to be used, but w must be replaced by b in Equation [25], leading to

$$\rho = PL/M_0 = \delta^2 + (1 - \delta)/t \quad [27]$$

Since there is no longer any physical restriction on δ, it may be chosen so as to minimize ρ and hence obtain the best upper bound. Thus

$$\delta = 1/2t$$

and

$$\rho = (1/t)(1 - 1/4t) \quad [28]$$

This upper bound is shown as the dashed curve in Fig. 4.

CONCLUSIONS

From a precise physical viewpoint, all continuum problems are three-dimensional and the concepts of beam theory, plate theory, and so on, are meaningless. However, since problems in three-dimensional elasticity can rarely, if ever, be solved, it is usually desirable to resort to simpler inexact theories as approximations. Obviously there is a certain freedom of choice as to which approximate theory is to be used in any particular application.

For beams whose height is small relative to their length, simple beam theory is known to yield good results in both elastic and plastic analysis. This theory is concerned only with bending moments and disregards shear deformations and the influence of shear on the yield stress. Therefore the theory becomes increasingly inaccurate as the length becomes shorter relative to a fixed height.

Previous papers by Onat and Shield (5), Green (6), Leth (4), and Drucker (1) have approached the problem of short beams via plane-stress theory. While reasonable appearing upper bounds can be obtained in this manner, it is more difficult to associate statically determinate stress fields. In general this has not been done.

The present paper is a compromise between the two approximations mentioned. It is based on the consideration of moment and shear as generalized stress variables which can be defined at each section of the beam. The interaction curve relating these two resultants has been derived and some simple examples have been solved.

If, as seems reasonable, conclusions as to the effect of shear can be drawn from the example of a simply supported beam, the various theories can be discussed in terms of Figs. 4 and 5. When the length of the beam is more than 10 times the beam height ($t = h/L < 0.1$) the effect of shear is negligible and hence shear can reasonably be neglected. For lengths down to the beam height for rectangular sections (about three times the height for the I-beam considered) the approximate theory predicts a more conservative value for the limit load than does the best two-dimensional upper bound obtained to date. For still shorter beams the approximate theory still yields fairly close results, but they are no longer conservative. Thus it would appear reasonable to use simple beam theory for $h/L < 0.1$ and to use the present theory for

$$0.1 < h/L < 1.0$$

Finally, for $h > L$ a two-dimensional theory appears to be necessary, particularly for the I-section.

However, it should be pointed out that such concepts as simply supported, clamped, and so on, have relatively little meaning applied to a "beam" which is shorter than it is high. For such problems it would appear necessary to specify fully the tractions on all edges of the beam and engage in a complete two-dimensional analysis. Thus the present theory appears adequate for any structure which can legitimately be called a beam. Further, the present analysis helps to justify the total neglect of shear in all beams where the height-to-length ratio is less than about 10 per cent.

BIBLIOGRAPHY

1 "The Effect of Shear on the Plastic Bending of Beams," by D. C. Drucker, JOURNAL OF APPLIED MECHANICS, Trans. ASME, vol. 78, 1956, pp. 509–514.

2 "The General Theory of Limit Design," by W. Prager, Proceedings of the Eighth International Congress of Applied Mechanics, Istanbul, Turkey, 1952, vol. 2, 1956, pp. 65–72.

3 "Differential and Integral Calculus," by R. Courant, translated by E. J. McShane, Interscience Publishers, Inc., New York, N. Y., vol. 2, 1936.

4 "The Effect of Shear Stresses on the Carrying Capacity of I-Beams," by C. F. Leth, DAM Report A11-107, Brown University, Providence, R. I., 1954.

5 "The Influence of Shear Forces on the Plastic Bending of Wide Beams," by E. T. Onat and R. T. Shield, Proceedings of the Second U. S. National Congress of Applied Mechanics, Ann Arbor, Mich., 1954, ASME, New York, N. Y., 1955, pp. 535–537.

6 "A Theory of the Plastic Yielding Due to Bending of Cantilevers and Fixed-Ended Beams," by A. P. Green, *Journal of Mechanics and Physics of Solids*, vol. 3, 1954, pp. 1–15, 143–155.

On the Plane Plastic Flow of an Inset Block[1]

By E. W. ROSS, JR.,[2] WATERTOWN, MASS.

The yield-point pressure is found for the plane-flow problem of a rectangular metal block, set into a rough entrenchment and squashed from above by a flat, smooth die. The pressure is a function of both the block width and depth, and for large ratios of width/depth approaches the linear pressure variation associated with the Prandtl (cycloidal) stress distribution.

Introduction

IN THIS paper, we deal with the plane-strain problem shown in Fig. 1. A block of ductile material is set into a rigid support and loaded from above by a flat, smooth die. The support is imagined as rough enough so that there is no relative motion between the support and the block material at the contact surfaces. The block is assumed to be made of nonhardening,

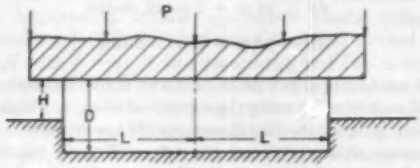

FIG. 1 BLOCK SET INTO ROUGH ENTRENCHMENT AND SQUASHED BY FLAT, SMOOTH DIE

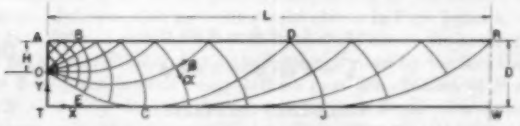

FIG. 2 CO-ORDINATES AND NOMENCLATURE FOR BLOCK, AND GENERAL APPEARANCE OF SLIP-LINE FIELD

elastic-plastic material obeying the Mises yield condition and flow rule. This problem is an extension of the one discussed by Hill, Lee, and Tupper (1),[3] who treated the case $D = H$. It also may be viewed as a two-dimensional specialization of the problem where a smooth die of finite width indents an inset block of ductile material. An upper bound on the indentation pressure for this problem was found (in certain ranges of the parameters) by Ross (2).

The average yield pressure on the upper surface of the block is found as a function of $\lambda = L/H$ and $\delta = D/H$ by using Christianovich's approach (3) for numerical integration of the plane-strain equations [see Hill (4)]. The average yield pressure is found to increase or remain unchanged with increasing λ and to either decrease or remain unchanged as δ increases. The effect of the boundary conditions at the edge of the block ($x = 0$ in Fig. 2) is observed to die away at a distance in from the edge that is roughly proportional to the block depth.

Summary of Limit-Analysis Theory for Plane-Flow Problems

In a body undergoing plane, plastic deformation the Cartesian stress components (σ_x, σ_y, τ_{xy}) must at all interior points satisfy the equilibrium relations (body forces are presumed absent)

$$\left.\begin{aligned}\frac{\partial \sigma_x}{\partial x} + \frac{\partial \tau_{xy}}{\partial y} &= 0\\ \frac{\partial \sigma_y}{\partial y} + \frac{\partial \tau_{xy}}{\partial x} &= 0\end{aligned}\right\} \quad \ldots\ldots\ldots\ldots [1]$$

and a yield inequality, usually that of Mises (which coalesces with the Tresca inequality)

$$\left(\frac{1}{4}\right)(\sigma_x - \sigma_y)^2 + \tau_{xy}^2 \leq k^2 \quad \ldots\ldots\ldots\ldots [2]$$

Here k is the yield stress in shear of the body material, and the equality sign holds in the region of plastic deformation. Where the flow is uncontained the Cartesian velocity components (V_x, V_y) satisfy the condition of incompressibilty

$$\frac{\partial V_x}{\partial x} + \frac{\partial V_y}{\partial y} = 0 \quad \ldots\ldots\ldots\ldots [3]$$

and the flow rule (or compatibility relation) associated with Yield Condition [2]

$$\frac{\partial V_x}{\partial x} : \frac{\partial V_y}{\partial y} : \frac{1}{2}\left(\frac{\partial V_x}{\partial y} + \frac{\partial V_y}{\partial x}\right) = \sigma_x : \sigma_y : \tau_{xy} \quad \ldots\ldots [4]$$

The stress and velocity components are subject to boundary conditions of loading and motion at the body surface, to the usual elastic stress-strain relations in the elastic region, to the relations for small, elastic-plastic deformation in the region of contained plastic flow, and to continuity conditions at the interfaces between the various regions.

The solution of a plane, plastic flow problem is in general a formidable proposition. However, yield-load problems, in which the chief piece of information sought is the applied load at which uncontained plastic deformation begins, usually can be handled by the yield-point or limit-analysis theorems [see Hill (5) and Prager, Drucker, and Greenberg (6)]. These theorems give a means of finding upper and lower bounds for the yield load when the boundary conditions on a body are of stress-type;

---

[1] This work was done at Watertown Arsenal, Watertown, Mass., and originally appeared as Watertown Arsenal Laboratory Report No. 880/52.

[2] Mathematician, Watertown Arsenal Laboratory.

[3] Numbers in parentheses refer to the Bibliography at the end of the paper.

Presented at the Applied Mechanics Division Summer Conference, Berkeley, Calif., June 13–15, 1957, of THE AMERICAN SOCIETY OF MECHANICAL ENGINEERS.

Discussion of this paper should be addressed to the Secretary, ASME, 29 West 39th Street, New York, N. Y., and will be accepted until October 10, 1957, for publication at a later date. Discussion received after the closing date will be returned.

NOTE: Statements and opinions advanced in papers are to be understood as individual expressions of their authors and not those of the Society. Manuscript received by ASME Applied Mechanics Division, September 6, 1956. Paper No. 57—APM-33.

i.e., the stresses are prescribed except where the corresponding velocity components are prescribed to vanish. The theorems may be stated as follows:

Theorem (*a*). Suppose a purely plastic deformation pattern is chosen which satisfies the incompressibility condition everywhere in the body and all velocity boundary conditions. Such a pattern is called a kinematically admissible velocity state. Then the value of the applied load, found by equating the internal plastic dissipation and work of the external loads in the assumed velocity state, equals or exceeds the yield value of the applied load.

Theorem (*b*). Suppose a stress state is chosen which satisfies the equilibrium equations and the yield inequality everywhere in the body and all stress boundary conditions. Such a stress distribution is called a statically admissible stress state. Then the value of the applied load in equilibrium with this stress state never exceeds the yield value of the applied load.

In choosing the velocity and stress states to be used in finding these bounds on the yield load, we are aided by the well-known theory of the slip-line field [see Hill (4) and Prager and Hodge (7)], originally developed for a plastic-rigid medium. In this theory, it is shown that the system of plane-flow plasticity equations in the region of uncontained deformation, i.e., the set of Equations [1], [2] with the equality sign holding, [3] and [4], is hyperbolic with respect to both the stress and velocity components, and the same two families of lines are characteristics for both the stresses and velocities. These two orthogonal characteristic or slip-line families are commonly denoted as the α and β-families with the convention that if the α and β-lines are viewed as a right-handed co-ordinate system, the algebraically largest principal stress acts in the first and third quadrants. If ϕ is the angle between the x-axis and the α-line, and p is the mean compressive stress at a point, then we may write the stresses as

$$\left.\begin{aligned} \sigma_x &= -p - k \sin 2\phi \\ \sigma_y &= -p + k \sin 2\phi \\ \tau_{xy} &= k \cos 2\phi \end{aligned}\right\} \quad \ldots\ldots\ldots\ldots [5]$$

and the equilibrium equations in the slip-line co-ordinates become

$$\left.\begin{aligned} dp + 2k\, d\phi &= 0 \text{ on an } \alpha\text{-line} \\ dp - 2k\, d\phi &= 0 \text{ on a } \beta\text{-line} \end{aligned}\right\} \quad \ldots\ldots\ldots [6]$$

Similarly, if V_α, V_β are the velocity components in the α,β-directions, respectively, then in the slip-line co-ordinates

$$\left.\begin{aligned} dV_\alpha - V_\beta d\phi &= 0 \text{ on an } \alpha\text{-line} \\ dV_\beta + V_\alpha d\phi &= 0 \text{ along a } \beta\text{-line} \end{aligned}\right\} \quad \ldots\ldots\ldots [7]$$

Once a slip-line field has been found satisfying all the conditions in the zone of uncontained flow (this will be discussed later), the stress and velocity components there can be found from Equations [5], [6], [7], and the boundary conditions. In the region of uncontained deformation this process gives a distribution of velocities satisfying Equation [3] and all the velocity-boundary conditions, and a distribution of stresses satisfying Equations [1], [2] with the equality sign holding, and the stress boundary conditions. Furthermore, the stresses and velocities are related by Equation [4]. The applied load corresponding to this slip-line distribution of stress and velocity is clearly an upper bound on the yield load; for, since the material is rigid outside the region of uncontained deformation, the velocity distribution satisfies all the conditions of theorem (*a*), and the energy calculation of theorem (a) will lead to the same load as is in equilibrium with the stresses computed from the velocities through Equation [4]. However, we cannot state that this slip-line load is also a lower bound, because the stress distribution satisfies the conditions of theorem (*b*) only in the region of uncontained deformation; an additional investigation must be made to show that the slip-line stress distribution may be extended to the region of small deformation and satisfy there Equations [1], [2], and the stress boundary conditions. If this extension can be carried out, then we may assert that the load given by the slip-line distribution is also a lower bound and, consequently, is the exact yield load within the framework of the physical assumptions made.

It still remains to summarize the method of finding the slip-line field satisfying all the conditions in the zone of uncontained flow. This is usually done by an inverse method involving numerical integration. The method most often used is due to Hill, Lee, and Tupper (1) [see also Hill (4)]; an alternative but similar procedure, developed by Christianovich (3), was used in the present investigation and will be described.

A pair of auxiliary variables (ξ, η) is first introduced. These are defined in terms of the co-ordinates (x, y) and the angle ϕ at a point by

$$\left.\begin{aligned} \xi &= x \cos\phi + y \sin\phi \\ \eta &= -x \sin\phi + y \cos\phi \end{aligned}\right\} \quad \ldots\ldots\ldots [8]$$

It turns out that (ξ, η) satisfy the equations

$$\left.\begin{aligned} d\eta + \xi d\phi &= 0 \text{ on an } \alpha\text{-line} \\ d\xi - \eta d\phi &= 0 \text{ on a } \beta\text{-line} \end{aligned}\right\} \quad \ldots\ldots\ldots [9]$$

ξ and η are found as functions of α and β by integrating Equations [9] numerically, using the stress boundary conditions to get the initial data; in practice Equations [9] are replaced by linear-difference equations involving the values of ξ and η at the nodal points of a mesh, the points being chosen so that the change in ϕ between adjacent points is constant. The values of x and y at the nodal points are found by the relations inverse to Equations [8]

$$\left.\begin{aligned} x &= \xi \cos\phi - \eta \sin\phi \\ y &= \xi \sin\phi + \eta \cos\phi \end{aligned}\right\} \quad \ldots\ldots\ldots [10]$$

Yield-Load Calculation

The limit-analysis theorems are applied to the assemblage consisting of the block and the die. The die is imagined as rigid and stressed by uniaxial compression of magnitude $\bar{p}$. The boundary conditions on the block are: (i) $V_y = V_0$, $\tau_{xy} = 0$ on the upper surface, (ii) $\sigma_x = \tau_{xy} = 0$ on the open side, AO in Fig. 2, (iii) $\tau_{xy} = V_x = 0$ on the line of symmetry RW, and (iv) $V_x = V_y = 0$ on the surfaces of contact between the block and support, OT and TW. The last condition does not preclude the occurrence of a discontinuity of tangential velocity in the block material immediately adjacent to the bottom or side.

A typical slip-line field [similar to that given for extrusion by Hill (4)] for the present problem is shown in Fig. 2. OAB is a region of constant state, OBE is a circular fan region, and $BECD$ is a portion of the known field generated by a circular arc and a line of symmetry. Beyond CD, the field was continued using Christianovich's approximate scheme, up to the β-slip line JR. Increments of 5 deg were used in the construction of the equiangular slip-line mesh. The boundary conditions implied that slip lines of the α-family intersect the upper surface AR, at an angle of -45 deg and the lower surface (where they meet it) at an angle of -90 deg. The slip-line calculation was carried out as described in the preceding section.

The plastic-deformation pattern consistent with this slip-line

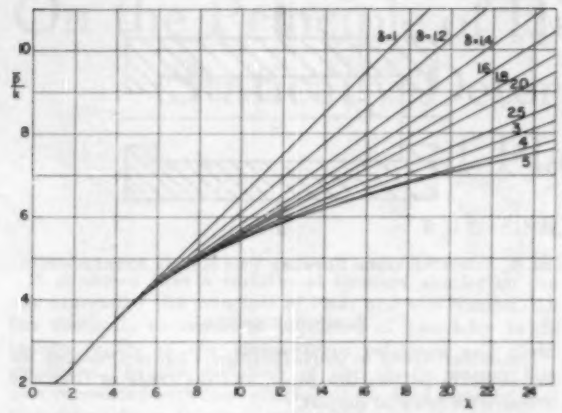

FIG. 3 VARIATION OF AVERAGE DIE PRESSURE WITH BLOCK WIDTH, $\bar{p}/k$ VERSUS λ, WITH δ AS PARAMETER. $\lambda = L/H$, $\delta = D/H$, AND k IS YIELD STRESS IN SHEAR OF BLOCK MATERIAL

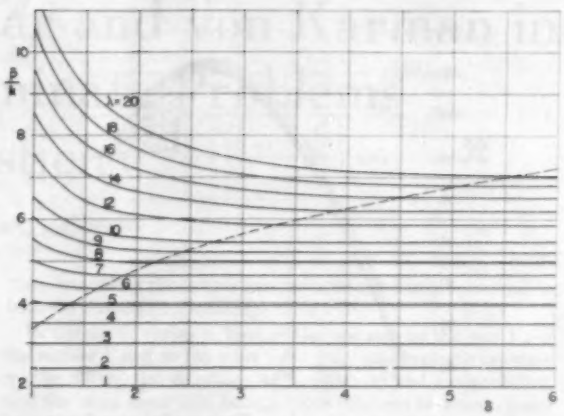

FIG. 4 VARIATION OF AVERAGE DIE PRESSURE WITH BLOCK DEPTH, $\bar{p}/k$ VERSUS δ, WITH λ AS PARAMETER. $\delta = D/H$, $\lambda = L/H$, AND k IS YIELD STRESS IN SHEAR OF BLOCK MATERIAL

field and the velocity boundary conditions was assumed to occur within the region *OARJCEO;* elsewhere the material was motionless, the slip-line *RJCEO* being a locus of discontinuity in tangential velocity. The average die pressure $\bar{p}$, found from the slip-line field is thus known to be an upper bound on the die pressure required to initiate appreciable plastic indentation. Fig. 3 shows $\bar{p}/k$ (k is the yield stress in shear) plotted against $\lambda = L/H$ with $\delta = D/H$ as a paremeter, and Fig. 4 shows the cross curves $\bar{p}/k$ plotted versus δ with λ as a parameter. These curves were obtained by carrying out computations up to the slip line *JR* for five different geometries, defined by the angles made with the x-axis by the slip-line *OE* in each case. These angles were 0, −15, −30, −45, and −60 deg, and corresponded to $\delta = 1$, 1.472, 2.222, 3.414, and 5.336. The die pressures for various λ-values were found by integrating numerically the σ_y values from *A* up to the point corresponding to the desired λ-value. Interpolation gave the results shown in Figs. 3 and 4.

It is difficult to make rigorous statements about the accuracy of the numerical work, but an indication is given by the fact that for $\delta = 1$ the present computations gave the abscissa of *R* as $x/H = 6.709$. In (1), the value 6.722 was found as a consequence only of incompressibility. This difference (the error is less than 0.2 per cent) indicates that the errors in the present computations are small enough for practical purposes.

Before one can claim that $\bar{p}$ is indeed the average pressure required to initiate appreciable plastic indentation, we must show that the stress field, hitherto defined only in the region of uncontained deformation, can be extended to the rigid zones. It is sufficient to show that the (fully plastic) slip-line field may be continued into the rigid region so as to satisfy the given boundary conditions on stresses. This may be done easily because the only boundary condition on stresses in the rigid region is $\tau_{xy} = 0$ on the block center line *RW*.

In particular (see Fig. 2) for combinations of λ and δ such that the boundary of the zone of uncontained deformation has no points in common with the bottom surface *TW*, an immediate continuation is given by the slip-line field defined in the rigid region by the β-slip line *OECJR* (i.e., the plastic-rigid boundary) and the line of symmetry *RW*. This may fail to fill up the entire rigid region (a small zone near the corner *T* may be left unfilled), but trivial further extensions can be constructed to fill the remainder.

When the boundary of the zone of uncontained deformation touches the bottom surface of the block, the rigid region is split into two zones like *JRW* and *OTCE* in Fig. 2. The slip-line field can be extended into *JRW* as before, and the continuation into *OTCE* is trivial as no stress boundary conditions are imposed there.

Thus we are justified in concluding that, within the framework of the basic physical assumptions, $\bar{p}$ is the average die pressure required to cause uncontained plastic deformation of the block.

DISCUSSION

Prandtl (8) has shown that the slip-line field becomes two orthogonal families of cycloids whenever the slope of the slip lines is independent of x. It may be expected that this situation will be realized near the center of the block in our case when λ/δ becomes sufficiently large. This may be observed in Fig. 3; for, as λ increases, the curves of $\bar{p}$ versus λ (for any δ) approach the straight lines that are characteristic of the Prandtl distribution, with slopes as given by Prandtl's theory. The Prandtl results may then be used to extend the results to all larger λ-values than those shown. Thus these results permit us to find the yield pressure for a block of any width with depths in the present range.

It should be noted that as $\lambda \to 0$ this structure degenerates into a slender column. Large deformations will become possible due to elastic or plastic instability at lower loads than those needed to enforce direct plastic deformation. Therefore little importance should be attached to the $\bar{p}$-values in this range.

The main trends are clearly observable in Figs. 3 and 4. Increasing λ tends to increase the yield pressure (except for $\lambda \leqslant 1$), while increasing δ either decreases the yield pressure or leaves it unaffected.

The present calculations shed some light on the question, at what distance in from the edge of such a block does the slip-line field approach Prandtl's field of cycloids, which is valid for $\lambda/\delta \gg 1$. Hill, Lee, and Tupper (1) have suggested that a sensitive criterion of approximation to the cycloidal field is the ratio $(\Delta x)/(\Delta x_p)$, where Δx is the length of the projection on the x-axis of a β-slip line (like $\overline{CD}$ in Fig. 2), and Δx_p is the length of the projection of the corresponding cycloids. Δx_p is a constant for any particular block depth but changes as the depth changes. The application of this criterion is shown in Fig. 5, where $(\Delta x)/(\Delta x_p)$ is plotted against S/D for each computed δ-value, D being the block depth and S the abscissa of the upper terminus of the slip line whose projected length is Δx.

The oscillatory nature of the approach of $(\Delta x)/(\Delta x_p)$ to unity,

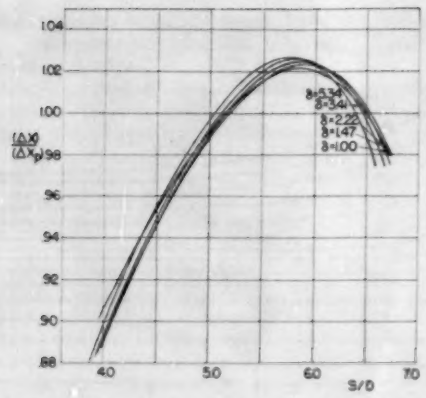

FIG. 5 APPROACH OF SLIP-LINE FIELD TO PRANDTL FIELD
([Δx]/[Δx_p] is ratio of x-projected lengths of β-slip lines to those for Prandtl field; S = abscissa of upper terminus of slip line, D = block depth.)

noted in (1) as being characteristic of hyperbolic equations, is observable in Fig. 5. If we adopt the convention that as S/D increases, the cycloidal field becomes well enough approximated when $(\Delta x)/(\Delta x_p)$ first becomes equal to some arbitrary critical value near unity, then it is apparent from Fig. 5 that the value of S/D at which this occurs is nearly independent of δ; that is to say, the distance in from the edge of the block at which the effect of the edge conditions dies away is roughly proportional to the block depth. This conclusion is not affected by the particular choice of critical value in the convention. It should, of course, be noted that the convention adopted is not as well suited to the treatment of hyperbolic differential equations as to elliptic equations, where the approach to limiting values is apt to be monotonic.

The present calculations also give the yield-point pressures for the problem where a rectangular block, recessed into two rough rigid dies, is compressed between the dies, Fig. 6. This problem is obtained from the present one by reflecting the whole geometry in the line of symmetry AR, Fig. 2.

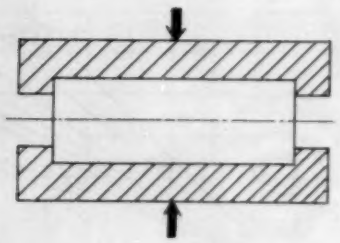

FIG. 6 BLOCK SQUEEZED BETWEEN TWO SIMILAR ENTRENCHMENTS

ACKNOWLEDGMENT

The author wishes to thank the Office, Chief of Ordnance, for permission to publish this paper, and the Office of Ordnance Research for financial support.

BIBLIOGRAPHY

1 "A Method of Numerical Analysis of Plastic Flow in Plane Strain and Its Application to the Compression of a Ductile Material Between Rough Plates," by R. Hill, E. H. Lee, and S. J. Tupper, JOURNAL OF APPLIED MECHANICS, Trans. ASME, vol. 73, 1951, pp. 46–52.

2 "On the Ideally Plastic Indentation of Inset Rectangular Bands," by E. W. Ross, Jr., JOURNAL OF APPLIED MECHANICS, Trans. ASME, vol. 78, 1956, pp. 244–246.

3 "The Plane Problem of the Mathematical Theory of Plasticity in the Case Where the Surface Tractions Are Given Along a Closed Contour," by S. Christianovich (Russian with French summary), *Matematishki Sbornik*, vol. 1, 1936, pp. 511–543.

4 "The Mathematical Theory of Plasticity," by R. Hill, Clarendon Press, Oxford, England, 1950.

5 "On the State of Stress in a Plastic-Rigid Body at the Yield Point," by R. Hill, *Philosophical Magazine*, vol. 42, 1951, pp. 868–875.

6 "Extended Limit Design Theorems for Continuous Media," by D. C. Drucker, W. Prager, and H. J. Greenberg, *Quarterly of Applied Mathematics*, vol. 9, 1951, pp. 381–390.

7 "Theory of Perfectly Plastic Solids," by W. Prager and P. C. Hodge, Jr., John Wiley & Sons, Inc., New York, N. Y., 1951.

8 "Anwendungsbeispiele zu einem Henckyschen Satz ueber das plastische Gleichgewicht," by L. Prandtl, *Zeitschrift für angewandte Mathematik und Mechanik*, vol. 3, 1923, pp. 401–406.

On the Principle of Haar and von Karman in Statically Determinate Problems of Plasticity

By LEO FINZI,[1] MILAN, ITALY

It is shown that a variational formula similar to the one expressing the principle of Haar and von Karman in the statically determinate problems of plasticity holds independently of the stress-strain relations and yield condition. In the variation of the elastic energy the part connected with the variation of the field must be distinguished from the part connected with the variation of the energy density. These points are illustrated by an example.

Introduction

In 1909 Haar and von Karman stipulated a variational principle as the basis of the theory of plasticity. This principle[2] is an extension of the principle of least work to elastic-plastic bodies; it involves not only the strain energy of the elastic part of the body, but also an elastic strain energy attributed to the plastic part.

The latter strain energy is defined as the energy that would be recovered on removing the loads and relieving all internal bonds connecting the particles of the body. Accordingly, the principle of Haar and von Karman is not suitable for a generic elastic-plastic body but only for the bodies with special stress-strain relations; for instance, the relation of Hencky.

This paper is concerned with problems of contained plastic deformation, particularly the completely statically determinate problems of plasticity. It is shown that, for these problems, a variational formula, similar to the one expressing the principle of Haar and von Karman, holds independently of the plastic stress-strain relations and the yield condition. The fact is emphasized that in these problems the essential element in the variational formulation is the elastic region surrounding the plastic one, so that the latter appears only inasmuch as its presence allows the elastic-region variations of field besides variations of energy density. These ideas are explained by way of a simple example.

The Completely Statically Determinate Problems of Plasticity

Let us consider a homogeneous and isotropic body that is subjected to specified surface tractions on part of its surface Γ, while the displacements are required to vanish on the remainder of Γ. Let us suppose that these boundary conditions induce a state of contained plastic deformation, the elastic and plastic regions of which will be denoted by α and β, respectively, these regions being separated by the elastic-plastic interface γ. Under these conditions the strains may be considered as infinitesimal in both the elastic and plastic regions.

In the elastic region α, bounded on one side by the part Γ_α of the surface Γ and on the other side by the elastic-plastic interface γ, the differential equations of equilibrium and compatibility, and the usual linear and homogeneous relations between stresses and strains are satisfied. In the plastic region β, bounded on one side by the part Γ_β of Γ and on the other side by the elastic-plastic interface γ, the differential equations of equilibrium and compatibility, stress-strain relations that are holonomic or not holonomic (according to the adopted theory[3]), and the yield condition are satisfied. The boundary conditions on the surfaces Γ_α and Γ_β, and the continuity conditions on the elastic-plastic interface γ will be specified later.

The problem of determining the state of stress and the state of strain satisfying the foregoing equations is the general problem, in which the unknown quantities are the components of stress and those of strain. There is, however, a large class of problems for which the equations of equilibrium and the yield condition, which contain only the components of stress, and the stress-boundary conditions on the surface Γ_β, suffice for the determination of the stresses in the plastic region β. The remaining equations can then be used to determine the state of strain. For these problems all boundary conditions must be in terms of stress. Problems of this type will be called completely statically determinate.

The conditions just enumerated, while necessary for complete statical determinacy, are not sufficient as will be shown by the following examples: The plastic region may not be adjacent to the surface Γ; the plastic region may extend beyond the domain of influence of that portion of the boundary which it adoins; the basic equations for some yield conditions may be elliptic, in which case the boundary conditions over any incomplete portion of the boundary would be insufficient. These cases will be excluded in the following, as will be the possibility of discontinuous displacement fields.

In the class of completely statically determinate problems are included some problems on torsion, plane strain, and plane stress.

A Variational Principle for the Completely Statically Determinate Problems

Let us consider a generic quantity

---

[1] Associate Professor of Strength of Materials, Polytechnic of Milan.

[2] "Theorie der Spannungszustaende in plastischen und sandartigen Medien," by A. Haar and Th. von Kármán, *Goettinger Nachrichten Math. Phys. Kl.*, 1909, pp. 204–218.

[3] "Formulazioni variazionali della congruenza nei corpi elasto-plastici," by L. Finzi, *Rendiconti Seminario Matematico e Fisico di Milano*, vol. 26, 1955.

Presented at the Applied Mechanics Division Summer Conference, Berkeley, Calif., June 13–15, 1957, of The American Society of Mechanical Engineers.

Discussion of this paper should be addressed to the Secretary, ASME, 29 West 39th Street, New York, N. Y., and will be accepted until October 10, 1957, for publication at a later date. Discussion received after the closing date will be returned.

Note: Statements and opinions advanced in papers are to be understood as individual expressions of their authors and not those of the Society. Manuscript received by ASME Applied Mechanics Division, September 7, 1956. Paper No. 57—APM-6.

$$F = \int_\tau f(p_{ik})\, d\tau \quad \ldots\ldots [1]$$

dependent on the stresses p_{ik} and the region τ in which they are considered. The variation δF of this quantity, subjected to certain conditions (g) for the stresses, may be expressed as follows

$$\delta F = \delta_p F + \delta_\tau F \quad \ldots\ldots [2]$$

where $\delta_p F$ is the variation of the quantity F when the region τ is not varied and the stresses p_{ik} are altered subject to conditions (g), while $\delta_\tau F$ is the variation of the quantity F when the stresses p_{ik} are not altered and the region τ is varied by means of the simple addition (or subtraction) of the area $\delta\tau$.

In particular, in the plastic region β, according to the complete statical determinacy and the definition given for $\delta_p F$

$$\delta F = \delta_\beta F \quad \ldots\ldots [3]$$

Consider now the elastic region α. Here the conditions (g) are the equations of equilibrium and the boundary conditions

$$\delta p_{ik}\, n^k = \delta f_i \quad \text{on } \Gamma_\alpha \quad \ldots\ldots [4]$$

Let the surface tractions f_i on Γ_α be prescribed so that $\delta f_i = 0$. On account of the complete statical determinacy in the β region, δf_i vanishes also on the original elastic-plastic interface γ. Thus $\delta f_i = 0$ on all the boundaries of the region α; i.e.

$$\delta p_{ik} n^k = 0 \quad \text{on } \Gamma_\alpha + \gamma \quad \ldots\ldots [5]$$

The differential equations of equilibrium together with the Boundary Conditions [5] are not sufficient to determine uniquely δp_{ik}, and so δp_{ik} does not necessarily vanish. We have therefore in the elastic region

$$\delta F = \delta_p F + \delta_\alpha F \quad \ldots\ldots [6]$$

and $\delta_p F$ does not vanish as a rule.

In the foregoing discussion γ is considered as fixed. In general, a third term should be added in Equation [6] to express the variation of the stresses in $\delta\tau$ due to the variation of the boundary, but for $\delta\tau$ sufficiently small this can be neglected.

If the quantity F is assumed to be the elastic strain energy V in the considered body (region $\tau = \alpha + \beta$)

$$V = V_\alpha + V_\beta \quad \ldots\ldots [7]$$

with obvious meaning of the symbols.

According to equations [3] and [6]

$$\delta V = \delta_p V_\alpha + \delta_\alpha V_\alpha + \delta_\beta V_\beta \quad \ldots\ldots [8]$$

On account of the principle of least work, V_α is such that, in the real state of stress, which satisfies not only the equations of equilibrium in α but also those of compatibility, one has

$$\delta_p V_\alpha = 0 \quad \ldots\ldots [9]$$

In fact, the partial variation $\delta_p V_\alpha$ refers to an elastic body with fixed surfaces γ and Γ_α, which is subjected to fixed surface tractions on account of Equation [5].

From Equation [8] it follows then that

$$\delta V = \delta_\alpha V_\alpha + \delta_\beta V_\beta \quad \ldots\ldots [10]$$

Observe now that the partial variations $\delta_\alpha V_\alpha$ and $\delta_\beta V_\beta$, respectively, concern only the variation of the areas α and β by means of the simple addition (or subtraction) of an infinitesimal portion of the field in which, for $\delta\tau$ sufficiently small, the specific elastic strain energy can be considered as a constant.

Moreover

$$\delta(\alpha + \beta) = \delta\alpha + \delta\beta = 0 \quad \ldots\ldots [11]$$

and thus

$$\delta_\alpha V_\alpha = -\delta_\beta V_\beta \quad \ldots\ldots [12]$$

Equation [10] therefore becomes

$$\delta V = 0 \quad \ldots\ldots [13]$$

In this equation the symbol δ (as distinct from the symbols of partial variation δ_p and δ_τ) indicates total variation, which involves simultaneous variations of field, of stress, and consequently also of stresses transmitted across the elastic-plastic interface.

Equation [13] has been deduced using Equations [9] and [11]. The first expresses the compatibility of strains in every element of the region α, the second expresses the continuity at the elastic-plastic interface. Among all equilibrium fields of stress that satisfy the yield condition in the plastic region, the Variational Principle [13] therefore characterizes the real state of stress as the one that also satisfies the compatibility conditions.[4]

Equation [13] states the stationary character of the elastic strain energy V of the elastic-plastic body.[5] The principle expressed by Equation [13] is therefore analogous to the one postulated by Haar and von Karman.

Recently Greenberg[6] showed that the function V has an absolute minimum in the case of the elastic-plastic bodies of Hencky.

In the present paper the following has been proved instead: The variational principle expressed by Equation [13] is valid for the completely statically determinate problems, regardless of the stress-strain relation and the yield condition.

It should be noted that in the Equation [13] appears the elastic strain energy in α and in β, but the last one is introduced only through the analytic artifice specified by Equation [12]. The physical quantity that must be considered is only the elastic strain energy in α. One might say that the elastic energy in the plastic zone β plays no essential role, because Equation [13] does not vary if any portion of the region β is suppressed except a thin layer near the elastic-plastic interface.

Examples

The simplest examples illustrating the application of the Variational Formula [13] in completely statically determinate problems of plasticity are those concerning elastic-plastic trusses. In fact, in these structures the differential equations of equilibrium state only that the axial forces in the bars are constant, and the yield relation gives explicitly the value of these forces in the plastic bars. These structures will not be considered because they have been treated in an earlier paper.[7]

As an example, consider a thick tube of infinite length, subjected to internal pressure (plain strain). Referring to Fig. 1, let r denote the generic radius of the tube, a the internal and b the external one, ρ the radius of the plastic boundary, p the internal pressure, σ_r the radial stress, σ_θ the circumferential stress, ϵ_r the radial strain, ϵ_θ the circumferential strain, E the elastic modulus, and ν Poisson's ratio, and assume that the material is isotropic and incompressible in both the elastic and the plastic domains ($\nu = 0.5$).

The state of stress and strain in the elastic region α may be calculated by means of the equations of equilibrium and com-

[4] As was stated in the second section, the conditions given for the complete statical determinacy are necessary but not sufficient. Of course, it must be verified that the solution given by Equation [13] satisfies the other conditions mentioned.

[5] The case of unloading processes is always excluded by these considerations.

[6] See the Report A 11, S 4, by H. J. Greenberg, Brown University, Applied Mathematics Division, 1949.

[7] "Proprietà delle strutture elastoplastiche nello spazio delle iperstatiche," by L. Finzi, *Acta Pontificiae Academiae Scientiarum*, vol. 15, 1953, pp. 121–136.

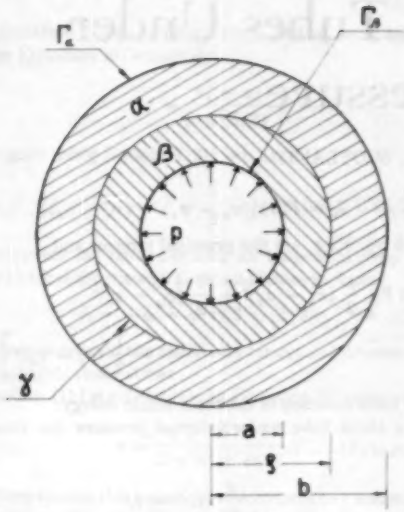

FIG. 1

patibility, and the stress-strain relations. It is characterized by the following relations[5]

$$\left.\begin{aligned}\sigma_r &= p_\rho \frac{\rho^2}{b^2-\rho^2}\left(1-\frac{b^2}{r^2}\right)\\ \sigma_\theta &= p_\rho \frac{\rho^2}{b^2-\rho^2}\left(1+\frac{b^2}{r^2}\right)\\ \sigma_z &= p_\rho \frac{\rho^2}{b^2-\rho^2}\end{aligned}\right\} \quad \ldots\ldots [14]$$

$$\left.\begin{aligned}\epsilon_r &= -\frac{3}{2E} p_\rho \frac{\rho^2}{b^2-\rho^2}\frac{b^2}{r^2}\\ \epsilon_\theta &= \frac{3}{2E} p_\rho \frac{\rho^2}{b^2-\rho^2}\frac{b^2}{r^2}\\ \epsilon_z &= 0\end{aligned}\right\} \quad \ldots\ldots [15]$$

In Equations [14] and [15] p_ρ is the pressure across the cylindrical elastic-plastic interface γ (with radius $r = \rho$). The state of stress in the plastic region can be calculated uniquely by means of the differential equations of equilibrium, the yield condition, and the boundary conditions on the surface Γ_β.

The yield relation in this problem of plane strain is

$$\sigma_\theta - \sigma_r = 2k \quad \ldots\ldots [16]$$

where k is the yield stress in simple shear, and the boundary condition on the surface Γ_β is

$$\sigma_r = -p \quad \ldots\ldots [17]$$

The state of stress is thus given by the following relations

$$\left.\begin{aligned}\sigma_r &= 2k \lg \frac{r}{a} - p\\ \sigma_\theta &= 2k\left(\lg \frac{r}{a} + 1\right) - p\\ \sigma_z &= 2k\left(\lg \frac{r}{a} + \frac{1}{2}\right) - p\end{aligned}\right\} \quad \ldots\ldots [18]$$

According to Equations [14] and [15] the elastic strain energy in α is

$$V_\alpha = \frac{3\pi}{2E} p_\rho^2 \frac{b^2\rho^2}{b^2-\rho^2} \quad \ldots\ldots [19]$$

According to Equation [16] the elastic strain energy in β is

$$V_\beta = \frac{3\pi}{2E} k^2(\rho^2 - a^2) \quad \ldots\ldots [20]$$

The total elastic strain energy thus is

$$V = V_\alpha + V_\beta = \frac{3\pi}{2E}\left[p_\rho^2 \frac{b^2\rho^2}{b^2-\rho^2} + k^2(\rho^2 - a^2)\right] \quad \ldots\ldots [21]$$

If p_ρ is varied, the interface radius ρ also must be varied since the two parameters are connected by the condition that $\sigma_r = -p_\rho$ for $r = \rho$. From the first of the Relations [18] it follows that

$$p_\rho = -2k \lg \frac{\rho}{a} + p \quad \ldots\ldots [22]$$

Apply now the Variational Principle [13]. The stationary character of the elastic strain energy is expressed by the relation

$$\frac{dV}{dp_\rho} = \frac{dV}{d\rho}\frac{d\rho}{dp_\rho} = 0 \quad \ldots\ldots [23]$$

On account of Equation [21], this can be written as follows

$$\frac{dV}{d\rho} = \frac{3\pi}{2E}\left[2p_\rho \frac{dp_\rho}{d\rho}\frac{\rho^2 b^2}{b^2-\rho^2} + p^2 \frac{2b^2\rho(b^2-\rho^2) + 2b^2\rho^2}{(b^2-\rho^2)^2} + 2k^2\rho\right] = 0 \quad \ldots\ldots [24]$$

Observe now that

$$\frac{dp_\rho}{d\rho} = -\frac{2k}{\rho} \quad \ldots\ldots [25]$$

in view of Equation [22]. With the use of Equation [24] this yields

$$p - 2k \lg \frac{\rho}{a} - k\frac{b^2-\rho^2}{b^2} = 0 \quad \ldots\ldots [26]$$

Equation [26] gives the radius of the elastic-plastic interface, and Equation [22] then furnishes the pressure p_ρ across this interface. Thus the state of stress in the regions α and β is completely specified.[6]

[5] See, for instance, "Theory of Perfectly Plastic Solids," by W. Prager and P. G. Hodge, John Wiley & Sons, Inc., New York, N. Y., 1951.

[6] It must be noted that Equation [26] could be obtained more readily by using, at the interface γ, not only the continuity of the radial stress σ_r, but also that of the circumferential stress σ_θ. This continuity condition simply provides that the yield condition is satisfied on the elastic side of the interface γ.

The Creep of Thick Tubes Under Internal Pressure

By C. D. WEIR,[1] GLASGOW, SCOTLAND

Using the usually accepted assumption that the strain rate of a material undergoing creep is given by the product of the stress deviator and a function of the shear-strain energy, and assuming constant density, equations are derived for the creep stresses in a thick-walled tube under internal pressure for a generalized form of the shear strain-energy function. It is shown that these reduce to previously published equations on the substitution of a power law stress-strain rate equation. The nonisothermal case is considered also and creep-stress equations are obtained in a similarly generalized form.

Introduction

RELATIONSHIPS for the creep-stress distribution in closed thick-walled isotropic cylinders under internal pressure have been developed by Bailey (1, 2),[2] Nadai (3), and Johnson (4). Each of these treatments is characterized by the four following assumptions:

(*a*) The creep rate in the direction of a principal stress in a complex stress system is equal to the product of a function of the shear-strain energy and the stress deviator for that direction.[3]

(*b*) The function of the shear-strain energy involved is a simple power function.

(*c*) The density of the material remains constant.

(*d*) The axial creep rate is zero.

Assumptions (*c*) and (*d*) have been substantiated experimentally. Assumption (*a*), which is in accordance with the Saint Venant-von Mises criterion for plastic flow, appears to be fulfilled within the limits of the available experimental results. As regards assumption (*b*), however, it is known from the results of the creep tests in simple tension that the simple power law is not always obeyed with precision. In the present paper it is shown that, for the stress distribution under consideration, it is possible to obtain relationships in both the isothermal case and for radial heat flow in which the form of the shear-strain-energy function is quite general.

Isothermal Case

General Equations. In accordance with assumption (*a*) we take the creep strain rate $\dot{\epsilon}_x$ in the direction x of a principal stress in a complex stress system to be given by

$$\dot{\epsilon}_x = F(\sigma)\{(\sigma_x - \sigma_y) - (\sigma_z - \sigma_x)\} \quad [1]$$

in which σ_x, σ_y, σ_z are the principal stresses and

$$F(\sigma) \equiv F\left[\frac{1}{2}(\sigma_x - \sigma_y)^2 + \frac{1}{2}(\sigma_y - \sigma_z)^2 + \frac{1}{2}(\sigma_z - \sigma_x)^2\right] \quad [2]$$

that is, some function of the shear-strain energy.

For a thick tube under internal pressure the compatibility equation is (3)

$$\frac{d}{dr}(\dot{\epsilon}_t r) = \dot{\epsilon}_r \quad [3]$$

where r is the radius and $\dot{\epsilon}_t$, $\dot{\epsilon}_r$ are, respectively, the instantaneous tangential and radial-strain rates.

Assumptions (*c*) and (*d*) give, respectively

$$\dot{\epsilon}_r + \dot{\epsilon}_t + \dot{\epsilon}_z = 0$$

and

$$\dot{\epsilon}_z = 0$$

from which

$$\dot{\epsilon}_t = -\dot{\epsilon}_r \quad [4]$$

On substituting this in Equation [3] and integrating, we obtain the known result

$$\dot{\epsilon}_t = \frac{B}{r^2} \quad [5]$$

Consideration of the equilibrium of the stresses on an element in the tube wall gives the well-known equation

$$r\frac{d\sigma_r}{dr} = \sigma_t - \sigma_r \quad [6]$$

in which σ_t, σ_r are, respectively, the tangential and radial stresses.

Now consider the expression for the octahedral shear stress. This is, for any system of principal stresses σ_x, σ_y, σ_z

$$\tau = \frac{1}{3}\sqrt{[(\sigma_x - \sigma_y)^2 + (\sigma_y - \sigma_z)^2 + (\sigma_z - \sigma_x)^2]} \quad [7]$$

and we see, on referring to Equation [2], that in general we can put

$$F(\sigma) = \phi(\tau) \quad [8]$$

In a tube under internal pressure the principal stresses are σ_t, σ_r, σ_z and Equation [1] using Equation [8] becomes, for the axial creep-strain rate

$$\dot{\epsilon}_z = \phi(\tau)[(\sigma_z - \sigma_t) - (\sigma_r - \sigma_z)]$$

Since we assume $\dot{\epsilon}_z = 0$ and, by hypothesis, $\phi(\tau) \neq 0$ this equation gives

$$\sigma_z = \frac{\sigma_t + \sigma_r}{2} \quad [9]$$

---

[1] University of Glasgow, Mechanical Engineering Research Annex.

[2] Numbers in parentheses refer to the Bibliography at the end of the paper.

[3] In Bailey's original treatment (1) a slightly more complex expression was used.

Presented at the Applied Mechanics Division Summer Conference, Berkeley, Calif., June 13–15, 1957, of The American Society of Mechanical Engineers.

Discussion of this paper should be addressed to the Secretary, ASME, 29 West 39th Street, New York, N. Y., and will be accepted until October 10, 1957, for publication at a later date. Discussion received after the closing date will be returned.

Note: Statements and opinions advanced in papers are to be understood as individual expressions of their authors and not those of the Society. Manuscript received by ASME Applied Mechanics Division, October 3, 1956. Paper No. 57—APM-32.

If in Equation [7] we write $\sigma_x \equiv \sigma_t$ and $\sigma_y \equiv \sigma_r$ and substitute from Equation [9] we obtain

$$\tau = \frac{\sigma_t - \sigma_r}{2\sqrt{(3/2)}} \quad [10]$$

Also, again using Equation [9], we have

$$(\sigma_t - \sigma_z) - (\sigma_r - \sigma_t) = \frac{3}{2}(\sigma_t - \sigma_r) = 3\sqrt{(3/2)}\tau$$

This expresses the stress deviator for tangential creep in terms of the octahedral shear stress alone and hence we have

$$\dot{\epsilon}_t = -\dot{\epsilon}_r = \phi(\tau)\, 3\sqrt{(3/2)}\tau \quad [11]$$

It remains to express in the radial and tangential stresses in terms of the octahedral shear stress.

If Equation [11] is substituted in Equation [5] there results

$$\tau = \frac{\sqrt{2}}{3\sqrt{3}} \frac{B}{r^2} \frac{1}{\phi(\tau)} \quad [12]$$

On differentiating this equation with respect to r and substituting in Equation [6], using Equation [10] we obtain

$$\frac{d\sigma_r}{d\tau} = -\sqrt{(3/2)}\left[1 + \tau \frac{\phi'(\tau)}{\phi(\tau)}\right] \quad [13]$$

which on integration by parts gives

$$\sigma_r = \sqrt{(3/2)}\,\{\tau[1 + \ln \phi(\tau)] - \int \ln \phi(\tau) d\tau\} + C \quad [14]$$

and, using Equation [10]

$$\sigma_t = \sqrt{(3/2)}\,\{\tau[1 - \ln \phi(\tau)] + \int \ln \phi(\tau) d\tau\} - C \quad [15]$$

where C is an integration constant.

These equations express the radial and tangential stresses as functions of the octahedral shear stress and the integration may be performed if the form of $\phi(\tau)$ is known. Formally we may write Equation [12] as

$$\tau = \Psi(D, r)$$

in which D is a constant, and on substituting this equation in Equation [14] we obtain σ_r as a function of r. The constants C and D may then be evaluated from the boundary conditions in the usual way.[4] This completes the solution for the isothermal case.

It is to be noted that the foregoing analysis refers to the instantaneous form of $\phi(\tau)$ which is, in general, a function of the time. This does not invalidate the argument, but if the total strain at any instant is required then a further integration with respect to time is necessary. Generally a graphical or numerical approach will be required.

Applications. In the following the form of $\phi(\tau)$ is assumed independent of the time. As an example we consider very briefly the case where $\phi(\tau)$ has the form

$$\phi(\tau) = A\tau^n \quad [16]$$

in which A and n are constants. This is essentially the usual power-law relation assumed by previous authors as already noted.

On substituting Equation [16] in [14] and integrating we obtain

$$\sigma_r = -\sqrt{(3/2)}(n+1)\tau + C \quad [17]$$

while Equation [12] becomes

$$\tau^{n+1} = \frac{D}{r^2} \quad [18]$$

where $D = \sqrt{(2)}B/[3\sqrt{(3)}A]$. On substituting Equation [18] in [17] we have

$$\sigma_r = -\sqrt{(3/2)}(n+1)\left(\frac{D}{r^2}\right)^{\frac{1}{n+1}} + C \quad [19]$$

Using the boundary conditions $\sigma_r = -p$ when $r = r_i$ and $\sigma_r = 0$ when $r = r_0$, r_i and r_o being, respectively, the internal and external radii of the cylinder, we get after some reduction

$$\sigma_r = p\,\frac{\left[\left(\frac{r_i}{r}\right)^{\frac{2}{n+1}} - \left(\frac{r_i}{r_o}\right)^{\frac{2}{n+1}}\right]}{1 - \left(\frac{r_i}{r_o}\right)^{\frac{2}{n+1}}} \quad [20]$$

This is identical in form with the corresponding equation obtained directly, for example by Bailey and by Nadai, and constitutes a check of the analysis.

The case where $\phi(\tau)$ has the form

$$\phi(\tau) = \frac{A \sinh \beta\tau}{\tau} \quad [21]$$

is of some interest since in the case of pure tensile stress it reduces to the hyperbolic sine law advocated by McVetty (5) as providing the best fit to his experimental results.[5]

On substituting Equation [21] in [14] we obtain, after an integration by parts

$$\sigma_r = -\sqrt{(3/2)}\beta \int \tau \coth \beta\tau\, d\tau + C \quad [22]$$

From Equation [12] we get

$$\sinh \beta\tau = \frac{\sqrt{2}}{3\sqrt{3}} \frac{B}{r^2}$$

and putting $D = \sqrt{(2)}B/[3\sqrt{(3)}A]$ and writing $\beta\tau = \sinh^{-1}(D/r^2)$ we easily obtain

$$\sigma_r = \sqrt{(3/2)}(1/\beta) \int \frac{\sinh^{-1}\left(\frac{D}{r^2}\right)}{r^2/D}\, d(r^2/D) + C \quad [23]$$

This integral may be evaluated in series form (6) giving

$$\sigma_r = -\frac{1}{2}\ln\left(\frac{r^2}{2D}\right)^2 + \frac{1}{2^2}\left(\frac{r^2}{D}\right)^2 - \frac{1.3}{2.4^2}\left(\frac{r^2}{D}\right)^4 + - \ldots + C \quad (0 < r^2/D \leqslant 1) \quad [24a]$$

or

$$\sigma_r = -\frac{D}{r^2} + \frac{1}{2.3^2}\left(\frac{D}{r^2}\right)^3 - \frac{1.3}{2.4.5^2}\left(\frac{D}{r^2}\right)^5 + \ldots + C \quad (r^2/D \geqslant 1) \quad [24b]$$

In this case it is simplest to proceed by taking as boundary conditions $\sigma_r = 0$ at $r = r_o$ and a provisional fixed creep-strain rate at the bore. D is thus fixed and C may then be evaluated from Equation [24a] or [24b] as appropriate. If the design criterion is not a fixed value of the bore creep strain, then a range

[4] It may be useful in some cases to take a definite creep-strain rate at the bore as the inner boundary condition, leaving the pressure p to be determined from the final equations.

[5] This law was originally proposed on theoretical grounds by Prandtl.

of values of the bore creep-strain rate must be assumed until that corresponding to the given criterion is found.

Nonisothermal Case

General Equations. In the practically important case where there is a radially and axially uniform flow of heat through the tube wall, the tangential creep-strain rate is a function of both the octahedral shear stress and the temperature. Thus in place of Equation [11] we may write

$$\dot{\epsilon}_t = 3\sqrt{(3/2)}\zeta(\tau, T)\tau \quad [25]$$

where T is the temperature. It may be noted that both τ and T are functions of the radius.

Proceeding as before, we have, in virtue of Equation [5]

$$\tau = \frac{\sqrt{2}}{3\sqrt{3}}\frac{B}{r^3}\frac{1}{\zeta(\tau, T)} \quad [26]$$

Differentiating this equation with respect to r and collecting terms gives

$$r\frac{d\tau}{dr}\left[1 + \frac{\tau}{\zeta}\left(\frac{\partial\zeta}{\partial\tau} + \frac{\partial\zeta}{\partial T}\frac{dT}{d\tau}\right)\right] = -2\tau$$

and finally in Equation [6], using Equation [10]

$$\frac{d\sigma_r}{d\tau} = -\sqrt{(3/2)}\left[1 + \frac{\tau}{\zeta}\left(\frac{\partial\zeta}{\partial\tau} + \frac{\partial\zeta}{\partial T}\frac{dT}{d\tau}\right)\right] \quad [27]$$

In the case T = const this reduces to Equation [13].

If, as has been discussed briefly by Soderberg (7) and applied in a particular form by Bailey (1), we take ζ to have the form

$$\zeta(\tau, T) = \phi(\tau)\chi(T)$$

then Equation [27] assumes the form

$$\frac{d\sigma_r}{d\tau} = -\sqrt{(3/2)}\left[1 + \tau\left(\frac{\phi'}{\phi} + \frac{\chi'}{\chi}\frac{dT}{d\tau}\right)\right] \quad [28]$$

$$\frac{d\sigma_r}{d\tau} = -\sqrt{(3/2)}\left[1 + \tau\left(\frac{d\ln\phi}{d\tau} + \frac{d\ln\chi}{dT}\frac{dT}{d\tau}\right)\right] \quad [28a]$$

This completes the analysis.

It is easily shown that if it is assumed ζ is given by

$$\zeta(\tau, T) = \phi(\tau)\chi(T) = A\tau^n e^{\alpha T}$$

then Equation [28] (or [28*a*]) may be solved explicitly and gives (as it should) results identical with those obtained by Bailey on the direct assumption of a relation essentially of this form.

Acknowledgments

Acknowledgments are due to the University of Glasgow where facilities were provided for this work and to Prof. James Small for kindly encouragement. The content formed part of a program sponsored by Messrs. Mera and McLellan, Newcastle upon Tyne.

BIBLIOGRAPHY

1 "The Utilization of Creep Test Data in Engineering Design," by R. W. Bailey, The Institution of Mechanical Engineers, London, England, 1935, p. 246.

2 "Creep Relationships and Their Application to Pipes, Tubes and Cylindrical Parts under Internal Pressure," by R. W. Bailey, Proceedings of The Institution of Mechanical Engineers, vol. 164, no. 4, 1951, pp. 425–431.

3 "On the Creep of Solids at Elevated Temperature," by A. Nadai, *Journal of Applied Physics*, vol. 8, 1937, pp. 418–432. See also "Theory of Flow and Fracture of Solids," by A. Nadai, vol. 1, McGraw-Hill Book Company, Inc., New York, N. Y., 1950.

4 "Creep under Complex Stress Systems at Elevated Temperatures," by A. E. Johnson, Proceedings of The Institution of Mechanical Engineers, vol. 164, no. 4, 1951, pp. 432–446.

5 "Creep of Metals at Elevated Temperatures—The Hyperbolic-Sine Relation Between Stress and Creep Rate," by P. G. McVetty, Trans. ASME, vol. 65, 1943, p. 761.

6 "Integraltafeln," by W. Meyer zur Capellen, Julius Springer-Verlag, Berlin, Germany, 1950.

7 C. R. Soderberg discussion of paper by R. W. Bailey, Trans. ASME, vol. 58, 1936, p. A-150.

Design Data and Methods

It is important that the data contained in technical papers be made readily available to design engineers. In order to satisfy these needs of industry, this section of the Journal includes a concise presentation of data and information drawn chiefly from papers previously published by the Applied Mechanics Division of The American Society of Mechanical Engineers.

Thermal Stress and Deformation[1]

By J. N. GOODIER,[2] STANFORD, CALIF.

Nomenclature

The following nomenclature is used in the paper:

E = Young's modulus
ν = Poisson's ratio
α = linear coefficient of thermal expansion
T = temperature at any point
T_1, T_2 = surface temperatures
ΔT = difference of temperature between faces of plate or shell
σ_x, σ_y = normal stress components
τ_{xy} = shear-stress component
$2c$, t = thickness of plate or shell
σ_r = radial-stress component
σ_θ = circumferential-stress component
$\tau_{r\theta}$ = shear-stress component
u = radial displacement
M_x, M_y = bending moments per unit run
M_r = radial bending moment per unit run
M_θ = circumferential bending moment per unit run
w = plate deflection
h = heat-transfer coefficient
D = flexural rigidity of plate or shell, $2Ec^3/3(1 - \nu^2)$

Introduction

Thermal stress, alone or in combination with load stress, can be the cause of brittle fracture and fatigue failure (1, 2),[3] plastic deformation to shakedown or incremental collapse (3), reduction of torsional stiffness (4), reduction of flexural stiffness, buckling, and detrimental warping (5).

Formulas available for design purposes usually assume an isotropic homogeneous elastic material which obeys Hooke's law to the highest temperatures involved without serious alteration of the elastic moduli. The moduli vary with temperature in actual materials, but significant thermal stress can occur before they are more than slightly affected. The coefficient of linear thermal expansion α need not be supposed constant. It can be a function of the temperature T, since it is the product αT which governs, and the temperature distribution T is supposed to be given.[4]

The order of magnitude of thermal stress in general may be represented by the stress required to suppress the free thermal expansion completely. In a rod with fixed ends preventing linear axial expansion, this is a compressive stress with the value $E\alpha T$ when T is uniform. In other cases the greatest thermal stress is representable as $kE\alpha T$, where k is a number usually between 0.5 and 2.5, and T is the temperature rise or the greatest difference of temperature between one part of the body and another. In steels $E\alpha T$ reaches a value of about 200 T psi, T being here in degrees Fahrenheit. Therefore a yield stress of 40,000 psi may be reached when temperature differences of about 200 deg F exist within the material, or when expansion from temperature changes of this magnitude is restrained. For such temperatures (above atmospheric), changes of elastic moduli are usually disregarded.

Some of the formulas are quoted for heating, some for cooling. If the one is substituted for the other the effect is merely to change the sign of the stress, tension becoming compression. Each of the cases given in the following represents a stress distribution which could be locally intensified by holes, flaws, notches, inclusions, or other sources of stress concentration.

Elementary fundamental cases

1 A uniform bar is uniformly heated from T_1 to T_2 deg, and expansion is prevented at the ends. Compressive stress $E\alpha(T_2 - T_1)$ is developed. Buckling will have begun when this reaches the Euler critical stress for the bar, and the development of buckling deflection can be worked out on the assumption that the compressive stress then remains constant and the further thermal expansion of length is accommodated by bending.

2 A uniform flat plate (in the x-y-plane) of any shape is uniformly heated from T_1 to T_2 deg. Expansion in the plane is pre-

---

[1] This paper represents a revision and expansion of the article "Thermal Stress," which appeared in the JOURNAL OF APPLIED MECHANICS, Trans. ASME, vol. 59, March, 1937, and in the first edition of the Design Data Booklets.

[2] Professor of Engineering Mechanics, Stanford University. Mem. ASME.

[3] Numbers in parentheses refer to the Bibliography at the end of the paper.

Discussion of this paper should be addressed to the Secreary, ASME, 29 West 39th Street, New York, N. Y., and will be accepted until October 10, 1957, for publication at a later date. Discussion received after the closing date will be returned.

NOTE: Statements and opinions advanced in papers are to b understood as individual expressions of their authors and not those of the Society. Manuscript received by ASME Applied Mechanics Division, May 21, 1957.

[4] There is a thermodynamic relation requiring that α vary with stress (at constant temperature) when the elastic moduli vary with T (at constant stress) (6).

vented at the edges. Compressive stress components σ_x, σ_y are developed, each of magnitude $E\alpha(T_2 - T_1)/(1 - \nu)$.

3 A solid of any shape is uniformly heated from T_1 to T_2 deg. Expansion is completely prevented all over the boundary (including holes, if any). Compressive stress components σ_x, σ_y, σ_z are developed, each of magnitude $E\alpha(T_2 - T_1)/(1 - 2\nu)$.

4 A part or the whole of the surface of a free[4] solid at temperature T_2 is suddenly cooled to T_1. Initially, before the temperature change has penetrated below the surface, tensile stress (biaxial) $E\alpha(T_2 - T_1)/(1 - \nu)$ is developed in the surface layer only, wherever the cooling occurs.

5 A free solid of any shape has a nonuniform temperature distribution $T(x, y, z)$ expressible in the linear form $Ax + By + Cz + D$, where A, B, C, D are constants or functions of time. No thermal stress is induced. (The free thermal strain $\epsilon_x = \epsilon_y = \epsilon_z = \alpha T$, $\gamma_{xy} = \gamma_{yz} = \gamma_{zx} = 0$, is compatible). For any nonlinear temperature distribution the stress will not vanish.

Thin flat uniform plates. No variation of temperature through the thickness[4]

6 References (7, 8). A thin flat plate of any shape, in the x-y plane, has a steady-state temperature distribution $T(x, y)$, satisfying Laplace's equation as the equation of steady heat conduction

$$\frac{\partial^2 T}{\partial x^2} + \frac{\partial^2 T}{\partial y^2} = 0 \quad [1]$$

and the coefficient of expansion α is constant. The plate is free, and has no holes. There is no thermal stress.[7] If there is a hole, the stress may not vanish. It does not when there is a net heat flow out of the hole into the plate (for formulas, see Case 29).

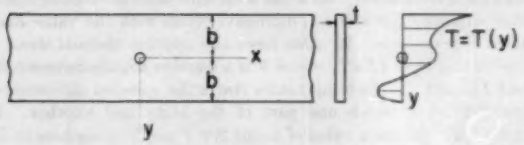

Fig. 1 Nonuniformly heated strip. Temperature varies in y-direction only. Case 7

7 Reference (8). A long strip, Fig. 1 (edges $y = \pm b$), in the x-y-plane, of small thickness t (in the z-direction), has a variation of temperature between one edge and the other (T a function of y only). There is only one nonzero stress component σ_x, given by

$$\sigma_x = -E\left(\alpha T - \frac{1}{2b}\int_{-b}^{b} \alpha T\, dy - \frac{3y}{2b^3}\int_{-b}^{b} \alpha T y\, dy\right) \quad [8]$$

This is the same at all cross sections x = const, including the ends, and on such sections has zero force and couple resultant. When the ends are free, the Formula [8] is not valid for points near the ends.

If E is a function of y (only), as when it is temperature-dependent, or when the strip is composite, consisting of two or more strips of different material bonded together along lines y = const, the formula becomes

$$\sigma_x = E(-\alpha T + \epsilon + \beta y) \quad [9]$$

where

$$\epsilon = \frac{\int_{-b}^{b} E\alpha T t\, dy}{\int_{-b}^{b} Et\, dy}, \quad \beta = \frac{\int_{-b}^{b} E\alpha T t y\, dy}{\int_{-b}^{b} Et y^2\, dy} \quad [10]$$

and t, the thickness, can vary moderately with y. In a composite strip thermal stress can occur when the temperature is changed from one uniform level to another, on account of the differences in α from one material to the other. Photoelastic measurements on a three-ply laminate are reported in (9). There is severe stress concentration near the ends where Formula [9] does not apply.

8 See, for instance, reference (8). A free thin circular disk of radius b has a temperature T which is a function of the radial coordinate r only, the origin being at the center. There are two nonzero components of stress, the radial component σ_r and the circumferential component σ_θ, which can be calculated from

$$\sigma_r = E\left(\frac{1}{b^2}\int_0^b \alpha T r\, dr - \frac{1}{r^2}\int_0^r \alpha T r\, dr\right) \quad [11]$$

$$\sigma_\theta = E\left(-\alpha T + \frac{1}{b^2}\int_0^b \alpha T r\, dr + \frac{1}{r^2}\int_0^r \alpha T r\, dr\right) \quad [12]$$

The radial displacement u is given by

$$u = (1 + \nu)\frac{1}{r}\int_0^r \alpha T r\, dr + (1 - \nu)\frac{r}{b^2}\int_0^b \alpha T r\, dr \quad [13]$$

Since the disk is free, $\sigma_r = 0$ when $r = b$. If the actual boundary is not free (for instance, when the radial displacement, Equation [13], is prevented), the effects of the boundary forces or imposed displacements may be calculated as an ordinary isothermal elastic problem. Special cases occur as Cases 9 and 14 which follow.

Corresponding formulas for a ring plate $a < r < b$ can be derived, analogous to Cases 28, 29, 30 (see reference 8, chapter 14).

9 A small circular spot in a plate is at uniform temperature T_1, the rest of the plate at uniform temperature T_0. The spot is not near the boundary (say 5 diameters away). This is calculable as a special case of Case 7, with the results[5]

$$\sigma_r = \sigma_\theta = -\frac{1}{2}E\alpha(T_1 - T_0) \text{ inside the hot spot} \quad [14]$$

$$\left.\begin{aligned} \sigma_r &= -\frac{1}{2}E\alpha(T_1 - T_0)\frac{a^2}{r^2} \quad [15] \\ \sigma_\theta &= \frac{1}{2}E\alpha(T_1 - T_0)\frac{a^2}{r^2} \quad [16] \end{aligned}\right\} \text{ outside the hot spot}$$

The maximum shear stress is $\frac{1}{2}E\alpha(T_1 - T_0)$ just outside the hot spot [from $\frac{1}{2}(\sigma_\theta - \sigma_r)$]. Any heating around the spot, as must in reality occur, tends to relieve this stress.

10 References (10, 8). If the hot spot is elliptical,[5] instead of circular as in Case 9, there is a "circumferential" tension (corresponding to σ_θ in the circular case) of magnitude $E\alpha(T_1 - T_0)/(1 + b/a)$ at the ends of the major axis, a and b being the major and minor semiaxes. The greatest value occurs when the ellipse is very much elongated, being $E\alpha(T_1 - T_0)$, or twice as great as for the circular hot spot in Case 9.

For a hot spot of any shape, the greatest stress depends on the shape but not on the size.

---

[4] There are no external forces, reactions, or constraints.

[4] Cases 6, 7, 8, 9, 10, 11, 12 can be extended as plane strain, appropriate when the thickness dimension becomes large instead of small. See (8), ch. 14, especially p. 408. Cases 27, 28, 29, 30 may be derived in this way from the corresponding thin-plate (plane stress) results, or, conversely, thin-plate results can be derived from them.

[7] This case does not violate the last statement in Case 5. In the thin plate the noncompatibility of strain components affecting the thickness direction has only trivial consequences which are neglected.

[5] If α varies with T, $\alpha(T_1 - T_0)$ is replaced by $(\alpha_1 T_1 - \alpha_0 T_0)$.

[5] For ellipsoidal *inclusions*, and references for related problems, see reference (35).

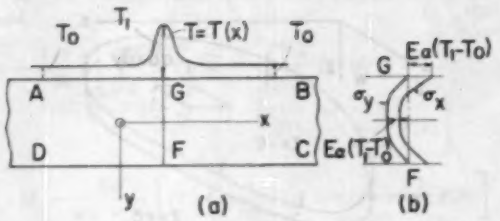

Fig. 2 Strip locally heated, temperature varying in x-direction only. Case 12

11 References (10, 8). If the hot spot is rectangular, instead of circular as in Case 9, the sharp corners cause very high local shear stress (theoretically infinite for a perfect rectangle) which depends on the local shape of the corner. The normal stress components (σ_x, σ_y) do not exceed $\frac{1}{2}E\alpha(T_1 - T_0)$.

12 References (11, 8). In Fig. 2, $ABCD$ represents a rectangular plate, or part of a strip. The plate is hot in the neighborhood of the line FG. On FG the temperature is T_1, and it falls rapidly to T_0 on either side of FG. There is no variation of temperature transversely (vertically in Fig. 2) or through the thickness. T, the temperature at any point, is a function only of x, the longitudinal co-ordinate.

A tensile stress $\sigma_x = E\alpha(T - T_0)$ is developed along the edges AB and CD. The maximum is $E\alpha(T_1 - T_0)$ occurring at F and G. A compressive stress σ_y of this magnitude occurs in the middle part of FG, falling to zero at F and G. This is shown in Fig. 2(b), together with the distribution of σ_x along FG.

For the cases of T discontinuous, or dT/dx discontinuous, in infinite and semi-infinite strips, see (12, 13).[10]

For the effect of cooling one face, inducing temperature variation through the thickness, see Case 23.

13 Reference (25). A thin flat (semi-infinite) plate ($y > 0$) with one straight edge ($y = 0$) is perfectly clamped on a finite length of its edge ($y = 0$, $-a < x < a$). It is otherwise free. The temperature of the plate is changed, uniformly, but no displacements are permitted on the clamped segment of the edge. As a result stress is induced. Curves are given in (25). At the ends of the clamped segment infinite stress occurs, indicating that in real cases there will be stress concentrations depending on local departures from the idealized conditions.

14 References (16, 10). A large (infinite) plate has a hole of radius a, far from the edge. The temperature at the hole $r = a$, is maintained at T_1 above atmospheric. The plate loses heat from its faces according to the Newtonian law, the rate of loss per unit area being hT, with T the temperature above atmospheric. T is given by the formula

$$T = T_1 \frac{K_0(mr)}{K_0(ma)} \quad \ldots\ldots\ldots\ldots\ldots\ldots [17]$$

where $K_0(\ )$ is the modified Bessel function of the second kind, zero order.[11] The thermal stress is (K_1 denoting the function of order one)

$$\sigma_r = -E\alpha T_1 \frac{1}{mr}\left[-\frac{K_1(mr)}{K_0(ma)} + \frac{a}{r}\frac{K_1(ma)}{K_0(ma)}\right] \ldots [18]$$

$$\sigma_\theta = -E\alpha T_1 \frac{1}{mr}\left[\frac{mrK_0(mr) + K_1(mr)}{K_0(ma)} - \frac{a}{r}\frac{K_1(ma)}{K_0(ma)}\right] \ldots [19]$$

[10] Reference (13) also contains results for a disk uniformly hot on one side of a diameter, uniformly cold on the other.

[11] The notation corresponds to that of G. N. Watson's "Bessel Functions," F. E. Relton's "Applied Bessel Functions," and W. Flügge's "Four-Place Tables of Transcendental Functions."

and the radial displacement is

$$u = -(1 + \nu)\alpha T_1 \frac{1}{m}\left[\frac{K_1(mr)}{K_0(ma)} - \frac{a}{r}\frac{K_1(ma)}{K_0(ma)}\right] \ldots [20]$$

where $m = (2h/\lambda t)^{1/2}$, t is the plate thickness, and λ is the coefficient of conductivity. For further solutions of this kind see (16).

Flat uniform plates. Variation of temperature through the thickness only

15 An originally flat uniform plate, of any shape, has one face at temperature T_1 (uniformly) and the other at T_2 (uniformly). The transition through the thickness t is linear (steady heat flow). There is no stress if the plate is free. This is an instance of Case 5. The plate becomes curved, its middle surface fitting a sphere of radius

$$\alpha(T_1 - T_2)/t$$

If the plate is circular, its edge line (bounding curve of middle surface) will lie in a plane, and therefore it may be treated as simply supported. If the plate is noncircular the edge line will not lie in a plane, and stress would be induced by any support which constrained it to do so.

16 The plate of Case 15, of any shape, is brought back to flatness by the application of bending couple uniformly distributed all around the edge, such that the extreme fiber tensile stress is

$$E\alpha(T_1 - T_2)/2(1 - \nu)$$

at the T_2 face, and the negative of this at the T_1 face. Throughout the plate the stress in the faces is then

$$\sigma_x = \sigma_y = \pm E\alpha(T_1 - T_2)/2(1 - \nu) \ldots\ldots [21]$$

the middle surface being the x-y-plane. This is the condition of the plate when slope is prevented round the edge, provided expansion in the plane is unrestrained.

17 Reference (15). If the plate of Case 15 is square, and the edges simply supported, there is bending stress near the edges approaching an extreme value $\frac{1}{2}E\alpha(T_1 - T_2)$. High shear stress occurs near the corners (where the support prevents curling). Analysis of triangular as well as square plates is found in (15).

18 Reference (8). The middle surface of the plate (any bounding curve) being the x-y-plane, the z-co-ordinate is in the thickness direction. The faces are $z = \pm c$. The temperature T is some function of z only. The only nonzero stress components are σ_x and σ_y. These are equal, each being given by the expression on the right of Equation [8] multiplied by $1/(1 - \nu)$. On the edges, this solution conforms to the condition of zero force and couple per unit run, but self-equilibrating forces remain. When the edges are absolutely free, corrections are required for the edge zone.

When E and ν are functions of z (only), Equation [9] gives σ_x provided E is replaced by $E/(1 - \nu)$, and t is replaced by unity. The value of σ_y is again the same as that of σ_x.

A slab containing a heat-emitting layer is considered in reference (16, p. 67). Stress from heat generated internally, or conducted inward from the surface, is examined in detail in (14).

Thin flat uniform plates. Arbitrary variation of temperature over the faces. Linear variation through the thickness

19 The temperature on the upper face $z = -c$ (Fig. 3) is $T_1(x, y)$, and the temperature on the lower face $z = c$ is $T_2(x, y)$. These will be written T_1 and T_2. On the assumption of linear variation through the thickness, the temperature $T(x, y, z)$ at any point of the plate is

$$T = \frac{1}{2}(T_1 + T_2) - \frac{1}{2}(T_1 - T_2)\frac{z}{c} \quad \ldots\ldots [22]$$

The effects of the term $^1/_2(T_1 + T_2)$, which is independent of z, come under a preceding section, "Thin Flat Plates. No Variation of Temperature Through the Thickness." Provided the corresponding (plane) thermal stress is small compared with that required for buckling, the effects of the term $-^1/_2(T_1 - T_2)(z/c)$ in Equation [22] can be evaluated independently as follows:

With the temperature distribution

$$T' = -\frac{1}{2}\Delta T\frac{z}{C}, \quad \Delta T = T_1 - T_2 \quad \ldots\ldots [23]$$

the plate can be held flat by applying upward distributed loading, Fig. 3, q' per unit area, where

$$q' = \frac{Ec^2}{3(1-\nu)}\left(\frac{\partial^2}{\partial x^2} + \frac{\partial^2}{\partial y^2}\right)(\alpha\Delta T) \quad \ldots\ldots [24]$$

It has bending moments[12] M_x, M_y, per unit run, given by

$$M_x = M_y = \frac{Ec^2}{3(1-\nu)}\alpha\Delta T \quad \ldots\ldots [25]$$

and these imply normal bending couple M_n per unit run round the edge, Fig. 4, of the same magnitude.

$$M_n = \frac{Ec^2}{3(1-\nu)}\alpha\Delta T \quad \ldots\ldots [26]$$

The distributed loading q', Equation [24], can be annulled by superposing the solution of an ordinary (isothermal) plate flexure problem corresponding to downward distributed load

$$q = \frac{Ec^2}{3(1-\nu)}\left(\frac{\partial^2}{\partial x^2} + \frac{\partial^2}{\partial y^2}\right)(\alpha\Delta T) \quad \ldots\ldots [27]$$

The boundary conditions of this problem are chosen so that, in conjunction with the edge moment M_n of Equation [26], the actual boundary conditions of the plate will be fulfilled.

The deflection w of this ordinary problem satisfies the equation

$$\left(\frac{\partial^2}{\partial x^2} + \frac{\partial^2}{\partial y^2}\right)^2 w = \frac{1+\nu}{2c}\left(\frac{\partial^2}{\partial x^2} + \frac{\partial^2}{\partial y^2}\right)(\alpha\Delta T) \quad \ldots [28]$$

This equation is always satisfied by a solution of the simpler equation

$$\left(\frac{\partial^2}{\partial x^2} + \frac{\partial^2}{\partial y^2}\right) w = \frac{1+\nu}{2c}\vartheta\Delta T \quad \ldots\ldots [29]$$

but such a solution will not necessarily satisfy the edge conditions. When it does not, the problem has nevertheless been reduced to an ordinary problem of edge loading only. Application to the symmetrical problem of the circular plate follows.

Axially symmetrical thermal flexure of the circular plate

20 A uniform circular ring plate $a < r < b$ has $\Delta T\ (= T_1 - T_2)$ a function of the radial co-ordinate r only. The edge conditions are consistent with a deflection w which is also a function of r only. Then

$$w = \frac{1+\nu}{2c}\left[\int_a^r \frac{1}{r}F(r)dr + C_1 + C_2\log r + C_3 r^2 + C_4 r^2\log r\right] \quad \ldots\ldots [30]$$

[12] These moments annul the free thermal curvature $\alpha\Delta T/2c$ of each plate element. The variation of the moments with x and y requires the loading q' for equilibrium of each element.

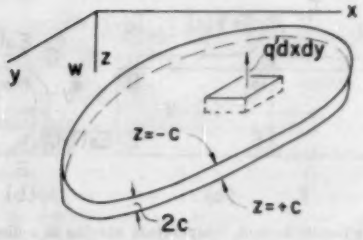

Fig. 3 Flat plate with middle surface in x-y-plane, surface loading q'. Case 19

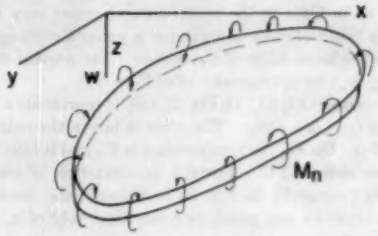

Fig. 4 Flat plate with middle surface in x-y-plane. Loading by normal moment M_n around the edge. Case 19

where

$$F(r) = \int_a^r \alpha\Delta T r\,dr$$

and C_1, C_2, C_3, C_4 are arbitrary constants to be determined by the conditions on $r = a$, $r = b$.

The bending moments per unit run M_r, M_θ are

$$\left.\begin{aligned} M_r &= \frac{Ec^2}{3(1-\nu)}\alpha\Delta T - D\left(\frac{d^2w}{dr^2} + \nu\frac{1}{r}\frac{dw}{dr}\right) \\ M_\theta &= \frac{Ec^2}{3(1-\nu)}\alpha\Delta T - D\left(\frac{1}{r}\frac{dw}{dr} + \nu\frac{d^2w}{dr^2}\right) \end{aligned}\right\} \quad \ldots [31]$$

where

$$D = \frac{2Ec^3}{3(1-\nu^2)} \quad \ldots\ldots [32]$$

21 For a *simply supported solid plate* ($r < b$) we have $M_r = 0$ at $r = b$. The terms in Equation [30] which contain C_3 and C_4 would give rise to singularities at $r = 0$ and must therefore be discarded. Then

$$w = \frac{1+\nu}{2c}\left[\int_0^r \frac{1}{r}F(r)dr + \frac{1-\nu}{1+\nu}\frac{F(b)}{2b^2}r^2 + C_1\right] \quad \ldots [33]$$

and the constant C_1 can be adjusted to make $w = 0$ at the edge $r = b$. Here

$$F(r) = \int_0^r \alpha\Delta T r\,dr \quad \ldots\ldots [34]$$

The bending moments, Equations [31], are now

$$\left.\begin{aligned} M_r &= \frac{1}{3}Ec^2\left[\frac{1}{r^2}F(r) - \frac{1}{b^2}F(b)\right] \\ M_\theta &= \frac{1}{3}Ec^2\left[\alpha\Delta T - \frac{1}{r^2}F(r) - \frac{1}{b^2}F(b)\right] \end{aligned}\right\} \quad \ldots [35]$$

The extreme fiber stresses are $3M_r/2c^2$, $3M_\theta/2c^2$, and are independent of the thickness $2c$, the temperature difference ΔT being regarded as independent of the thickness.

A numerical example is worked out in reference (17).

22 For a *clamped solid plate* ($r < b$), $w = dw/dr = 0$ at $r = b$, and

$$w = \frac{1+\nu}{2c}\left[\int_0^r \frac{1}{r}F(r)dr - \int_0^b \frac{1}{r}F(r)dr - \frac{1}{2}F(b)\frac{r^2}{b^2} + \frac{1}{2}F(b)\right] \quad [36]$$

$$M_r = \frac{Ec^2}{3(1-\nu)}\left[(1-\nu)\frac{1}{r^2}F(r) + (1+\nu)\frac{1}{b^2}F(b)\right] \quad [37]$$

$$M_\theta = \frac{Ec^2}{3(1-\nu)}\left[(1-\nu)\alpha\Delta T - (1-\nu)\frac{1}{r^2}F(r) + (1+\nu)\frac{1}{b^2}F(b)\right] \quad [38]$$

with $F(r)$ given by Equation [34].

A numerical example is worked out in reference (17).

The strip. Temperature varying lengthwise and through the thickness

23 Reference (11). The strip of Case 12 has the temperature T as described there, a function of x with a localized maximum T_1, but now this temperature applies to one face only. The other face has a similar temperature distribution with a different maximum T_2 lower than T_1, and the same datum temperature T_0 at a distance. The transition through the thickness is linear.

Bending now occurs, and the extreme tensile stress in the edges occurring at F and G, Fig. 2, is

$$\frac{1}{2}E\alpha\left[T_1 + T_2 - 2T_0 + \frac{1-\nu}{3+\nu}(T_1 - T_2)\right] \quad [39]$$

When one face is kept quite cold ($T_2 = T_0$), this becomes

$$2E\alpha(T_1 - T_0)/(3+\nu)$$

The cooling of the face has reduced the maximum tensile stress in the ratio $2/(3+\nu)$, or by about 40 per cent in steel.

Thin-walled tubes, straight

24 Reference (18). The inside temperature is T_1 (uniform) and the outside T_2 (uniform). The transition through the thickness is linear. Irrespective of the form of the cross section, there is uniform circumferential bending moment entailing linear stress with extreme values

$$\pm\tfrac{1}{2}E\alpha(T_1 - T_2)/(1-\nu)$$

the positive sign pertaining to the outside. If the ends are free, they cause local irregularity of stress, which can be evaluated for the circular section, reference (8, p. 415). The maximum tensile stress (circumferential) is 25 per cent greater than the value just given.

Away from the ends there is longitudinal stress varying from $-\tfrac{1}{2}E\alpha(T_1 - T_2)$ inside to $\tfrac{1}{2}E\alpha(T_1 - T_2)$ outside, whatever the form of the cross section.

For temperature variation along the axis (circular section) refer to (19, 20) and for variation also through the thickness, reference (20). When there is variation around the section and through the thickness, but not along the length (as, for instance, when a tube is heated all along from below, Fig. 5), the stress and deformation can be calculated, except for local irregularity at the free ends, whatever the form of the section (18).

25 *Circular Section* (18). The temperature varies around the section and through the thickness, but not along the length. Let θ be the angular co-ordinate from a fixed radius in any cross section, Fig. 5. Then the inside T_1 and outside T_2 temperatures are functions of θ only and can be developed in Fourier series

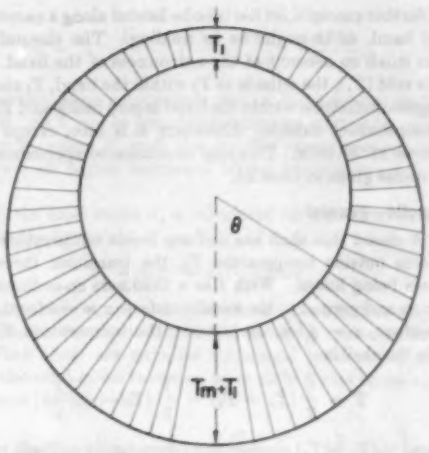

Fig. 5 Temperature variation around outside of a thin-walled cylinder in example of Case 25

$$T_1 = A_0 + A_1\cos\theta + \ldots + B_1\sin\theta + \ldots \quad [40]$$

$$T_2 = A_0' + A_1'\cos\theta + \ldots + B_1'\sin\theta \quad [41]$$

The thermal stress can be expressed fully by means of the coefficients written down, so that it is not necessary to carry the Fourier analysis further. The extreme circumferential (bending) stress is

$$\pm\frac{1}{2}\frac{E\alpha}{1-\nu}[A_0 - A_0' + (A_1 - A_1')\cos\theta + (B_1 - B_1')\sin\theta] \quad [42]$$

the positive sign pertaining to the inside. The maximum is thus one of the two quantities

$$\frac{1}{2}\frac{E\alpha}{1-\nu}\{A_0 - A_0' \pm [(A_1 - A_1')^2 + (B_1 - B_1')^2]^{1/2}\} \quad [43]$$

according as A_0 is greater or less than A_0'. The extreme longitudinal stress away from the free ends is given by

$$E\alpha\left[\frac{1}{2}(T_1 + T_2) \pm \frac{1}{2}(T_1 - T_2) + \frac{1}{2}(A_0 + A_0')\right] \quad [44]$$

the positive sign pertaining to the outside. A_0 and A_0' are the same as the mean inside and outside temperatures, respectively.

It will be observed that all the results given for thin-walled tubes are independent of the size and thickness, depending only on the material and the temperatures occurring within them.

As an example, we may take a tube heated from below, Fig. 5, with an outside temperature $T_2 = T_1 + \tfrac{1}{2}T_m(1 + \cos\theta)$, T_1 being the uniform inside temperature. T_m is then the maximum temperature difference.

The maximum circumferential stress is $\pm\tfrac{1}{2}E\alpha T_m/(1-\nu)$, at the hottest part, tensile inside, compressive outside. The extreme longitudinal stress away from the free ends is nearly $\tfrac{3}{4}E\alpha T_m$ (compression) on the inside, and nearly $\tfrac{1}{4}E\alpha T_m$ (tension) at the outside, at the hottest part.

As a further example, let the tube be heated along a narrow longitudinal band, as it might be in welding. The circumferential stress is small on account of the narrowness of the band. If the inside is cold (T_1), the outside at T_2 within the band, T_1 elsewhere, the longitudinal stress within the band is zero inside and $E\alpha(T_2 - T_1)$ (compressive) outside. Elsewhere it is zero, except for the local stress at the ends. This may be estimated approximately by the formulas given in Case 23.

Thin shells—general

26 A closed thin shell has uniform inside temperature T_1 and a uniform outside temperature T_2, the transition through the thickness being linear. With z as a thickness co-ordinate measured from and normal to the middle surface, $z = -c$ for the inside shell surface, $z = c$ for the outside, the temperature T at any point in the shell is

$$T = \frac{1}{2}(T_1 + T_2) - \frac{1}{2}(T_1 - T_2)\frac{z}{c} \quad \ldots\ldots [45]$$

The term $\frac{1}{2}(T_1 + T_2)$ represents a temperature uniform throughout the shell, and therefore gives rise to thermal expansion without stress. The contained volume expands as though it were of solid metal similarly heated.

The term $-\frac{1}{2}(T_1 - T_2)(z/c)$ gives rise to uniform bending moment (per unit run)

$$M = \frac{Ec^2}{3(1-\nu)}\alpha\Delta T, \quad \Delta T = T_1 - T_2 \quad \ldots\ldots [46]$$

on any normal section. This is the moment required to annul the free thermal curvature change (Case 15 may be taken over from the flat-plate element to the element of the curved shell), and the conditions of equilibrium and compatibility are obviously satisfied.

If the shell is open, moments given by Equation [46] are left over round the rim. The effect of removing these presents a problem of edge loading only.

27 The temperatures T_1 and T_2 vary (independently) over the inside and outside surfaces,[13] with linear transition through the thickness. The term $\frac{1}{2}(T_1 + T_2)$ in Equation [45] produces a free thermal expansion of an element of the shell, which can be annulled by normal stresses parallel to the middle surface and uniform through the thickness; but on account of the curvature, normal force is required for equilibrium. On account of the variation of $\frac{1}{2}(T_1 + T_2)$ over the middle surface, tangential forces also will be required. The elements fit and the conditions of compatibility are met. The effects of removing the normal and tangential forces present an ordinary problem of the loaded shell.

The term $-\frac{1}{2}(T_1 - T_2)(z/c)$ in Equation [45], with $(T_1 - T_2)$ a function of position on the middle surface, produces a free thermal curvature change which can be annulled by bending moments, after which the shell element fit together. The variation of these, on account of the variation of $T_1 - T_2$ over the surfaces, calls for transverse shear forces which in turn require normal surface loading. The removal of this loading presents an ordinary problem of the loaded shell. Case 19 is the special case of the flat plate.

A brief treatment of the axisymmetric problem is given in (16), with references. The problem for wings, without neglect of the buckling terms, is considered in (28).

Thick-walled tubes,[14] circular, straight

28 Reference (8). The concentric inside and outside surfaces are $r = a$, $r = b$. The temperature T, symmetrical about the axis, and the same at all cross sections, is a function of r only.[15]

(a) The plane ends of the tube are confined between smooth, absolutely rigid surfaces, so that axial expansion is completely prevented (plane strain with zero axial displacement). The average of αT is

$$(\alpha T)_{av} = \frac{2}{b^2 - a^2}\int_a^b \alpha T r\, dr \quad \ldots\ldots [47]$$

and the stress components are

$$\sigma_r = \frac{E}{1-\nu}\left[\left(1 - \frac{a^2}{r^2}\right)(\alpha T)_{av} - \frac{1}{r^2}\int_a^r \alpha T r\, dr\right] \quad \ldots [48]$$

$$\sigma_\theta = \frac{E}{1-\nu}\left[\left(1 + \frac{a^2}{r^2}\right)(\alpha T)_{av} + \frac{1}{r^2}\int_a^r \alpha T r\, dr\right] \quad \ldots [49]$$

$$\sigma_z = \nu(\sigma_r + \sigma_\theta) - E\alpha T \quad \ldots\ldots [50]$$

(b) The resultant axial force on the tube ends due to the axial stress σ_z of Equation [50] is now removed by application of uniform σ_z with resultant of opposite sign. The stress components σ_r, σ_θ of Equations [48] and [49] remain unchanged. The axial stress becomes

$$\sigma_z = \frac{E}{1-\nu}[(\alpha T)_{av} - \alpha T] \quad \ldots\ldots [51]$$

To make the ends absolutely free, this σ_z must be removed from the ends by applying the equal and opposite self-equilibrating distribution. This will introduce a local modification of the foregoing stress components at the ends.

Detailed tabular and graphical results are given in (22) for the following:

(a) A solid cylinder is initially at uniform temperature. The surface temperature is suddenly changed to, and maintained at, a different value.

(b) A solid cylinder initially at uniform temperature loses heat by Newtonian cooling from the surface.

The hollow cylinder and periodically fluctuating surface temperature also are considered. In (a) the surface stress immediately after the sudden temperature change ΔT is

$$\sigma_r = 0, \quad \sigma_\theta = \sigma_z = -\frac{\alpha E \Delta T}{1-\nu}$$

in accordance with Case 4. The subsequent stress magnitudes are smaller.

[13] For the change of contained volume in this case, see Case 33.

[14] Formulas for thick-walled hollow spheres are given in (8), p. 416.

[15] Axial variation, in particular that arising from heat transfer from a fluid flowing in the tube, is considered in (24).

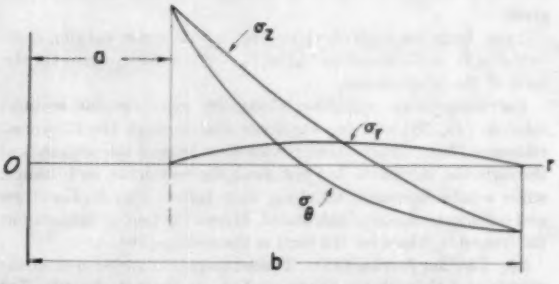

Fig. 6 Character of stress distribution in a thick-walled tube in steady heat conduction, temperature varying only radially. Case 29

29 Reference (8). The temperature T of Case 28 is particularized to that of steady heat flow

$$T = (T_1 - T_2)\frac{\log (b/r)}{\log (b/a)} \quad \ldots\ldots [52]$$

where T_1 is the inside ($r = a$), T_2 the outside temperature.

For uniform α the stresses are

$$\left.\begin{matrix}\sigma_r\\ \sigma_\theta\\ \sigma_z\end{matrix}\right] = \frac{E\alpha(T_1 - T_2)}{2(1-\nu)\log (b/a)} \left\{\begin{matrix}\left[-\log\frac{b}{r} - \frac{a^2}{b^2-a^2}\left(1-\frac{b^2}{r^2}\right)\log\frac{b}{a}\right] \ldots\ldots [53]\\ \left[1 - \log\frac{b}{r} - \frac{a^2}{b^2-a^2}\left(1+\frac{b^2}{r^2}\right)\log\frac{b}{a}\right] \ldots\ldots [54]\\ \left[\nu - 2\log\frac{b}{r} - \frac{2\nu a^2}{b^2-a^2}\log\frac{b}{a}\right] \ldots\ldots [55]\end{matrix}\right.$$

for zero axial displacement and

$$\left[1 - 2\log\frac{b}{r} - \frac{2a^2}{b^2-a^2}\log\frac{b}{a}\right] \ldots\ldots [56]$$

for zero axial force

Alignment charts for the rapid evaluation of these stresses are given in (23).

The character of the stress distribution may be seen from Fig. 6, drawn for $a/b = 0.3$. If $T_1 - T_2$ is positive, the stress is compressive at the inside, tensile at the outside.

For a very small bore

$$(a/b \to 0),\ \sigma_\theta = -E\alpha(T_1 - T_2)/(1-\nu)$$

at $r = a$, zero at $r = b$. The σ_z component of Equation [56] takes the same values. The maximum stress is twice as great as for the thin-walled tube, for the same temperatures.

30 Reference (8). The inside and outside temperatures, T_1 and T_2, are not uniform, but vary with the polar angle θ as in Case 25. They are represented as Fourier series in $\cos n\theta$, $\sin n\theta$, exactly as in Equations [40] and [41].

Two-dimensional steady heat flow being established, the stress components σ_r, σ_θ, $\tau_{r\theta}$ may be found by superposition of two parts. The first part is calculated for uniform inside and outside temperatures according to Equations [53] and [54], with T_1 replaced by A_0, T_2 replaced by A_0', from Equations [40] and [41]. A_0 and A_0' are in fact the mean inside and the mean outside temperatures. The second part of the stress consists of components σ_r, σ_θ, $\tau_{r\theta}$, calculated as follows:

Owing to the terms $A_1 \cos\theta$, $A_1' \cos\theta$ in Equations [40] and [41] there will be stress components

$$\sigma_r = \kappa\cos\theta\, r\left(1 - \frac{a^2}{r^2}\right)\left(\frac{b^2}{r^2} - 1\right) \ldots\ldots [57]$$

$$\sigma_\theta = \kappa\cos\theta\, r\left(\frac{a^2b^2}{r^4} + \frac{a^2+b^2}{r^2} - 3\right) \ldots\ldots [58]$$

$$\tau_{r\theta} = \kappa\sin\theta\, r\left(1 - \frac{a^2}{r^2}\right)\left(\frac{b^2}{r^2} - 1\right) \ldots\ldots [59]$$

where $$\kappa = -\frac{E\alpha}{2(1-\nu)}\left(\frac{A_1}{a} - \frac{A_1'}{b}\right)\frac{a^2b^2}{b^2-a^2} \ldots\ldots [60]$$

The corresponding components due to the temperature terms $B_1 \sin\theta$, $B_1' \sin\theta$, can be found from these by writing them $B_1 \cos\theta'$, $B_1' \cos\theta'$, where $\theta' = \theta - \pi/2$. The stress components σ_r, σ_θ, $\tau_{r\theta}$ from all higher harmonics of the temperature series are zero.

Finally, the axial stress σ_z is calculated for zero axial displacement from the formula

$$\sigma_z = \nu(\sigma_r + \sigma_\theta) - E\alpha T \ldots\ldots [61]$$

using the complete σ_r, σ_θ, and T, the actual temperature at (r, θ). This σ_z implies resultant forces and bending moments on the ends. When these are annulled by simple tension and simple bending, the axial stress becomes, when only cosine terms appear in Equations [40] and [41]

$$\sigma_z = -E\alpha(T - T_{av_z}) + \left[2\kappa\nu\left(\frac{a^2+b^2}{r^2} - 2\right) + \kappa'\right] r\cos\theta \quad \ldots\ldots [62]$$

where $$\kappa' = E\alpha\,\frac{A_1 a + A_1' b}{b^2 + a^2} \ldots\ldots [63]$$

Removal of the remaining self-equilibrating σ_z on the ends wil introduce a local disturbance at the ends.

Solid cylinders and prisms

31 References (7, 8). If the heat flow is steady and the same at all sections (two-dimensional heat flow) the stress components are zero except for the axial normal component σ_z. If axial expansion is prevented, $\sigma_z = -E\alpha T$. The axial forces and bending moments on the ends implied by this may be annulled by simple tension and simple bending.

For the circular rod with temperature a function of r only, not in steady heat conduction, the components σ_r, σ_θ are given by Equations [11] and [12] when the factor $1/(1-\nu)$ has been introduced on the right-hand side. When axial displacement is prevented at the ends, σ_z is given by Equation [61]. The resultant forces and bending moments on the ends may be annulled by simple tension and simple bending.

Over-all thermoelastic deformation—Changes of volume, length, angle—Arbitrary temperature distribution

32 References (26, 27). A free solid of any shape, with or without holes or cavities, is initially at uniform temperature, then acquires a nonuniform rise of temperature $T(x, y, z)$. The increase of volume ΔV of the solid material is simply

$$\Delta V = \int 3\alpha T\, dV \ldots\ldots [64]$$

where dV is the element of volume, and the volume integral extends throughout the solid material. This is the same as the sum of volume increases the elements would exhibit if they were cut free; that is, relieved entirely of the thermal stress. The elastic strain due to the thermal stress has, in the linearly elastic solid, zero total volume change.

33 Reference (27). A hollow sphere, bounded by concentric surfaces $r = a$, $r = b$, acquires a nonuniform rise of temperature $T(x, y, z)$. The volume of the contained cavity, $4/3\,\pi a^3$, increases by

$$\Delta V_a = \frac{a^3}{b^3 - a^3}\int_{r=a}^{r=b} 3\alpha T\, dV \ldots\ldots [65]$$

the volume integral extending throughout the solid material.

In combination with Case 32, this implies that the increase of the total volume, $^4/_3\pi b^3$, is

$$\Delta V_t = \frac{b^3}{b^3 - a^3} \int_{r=a}^{r=b} 3\alpha T \, dV \quad [66]$$

For other shapes, corresponding formulas can be found whenever the problems of internal and external uniform pressures are completely solved.

34 Reference (27). A cylinder or prism, of any cross section, acquires a nonuniform rise of temperature $T(x, y, z)$.

(a) An average increase of length ΔL can be defined as the extension of longitudinal fibers averaged over the cross-sectioned area A. It is given by

$$\Delta L = \frac{1}{A} \int \alpha T \, dV \quad [67]$$

the volume integral extending throughout the solid material.

(b) Rotation of one end relative to the other can be defined as that occurring when a rigid plate is attached to each end, the two rigid plates being otherwise unconstrained. The cylinder or prism is supposed long so that end effects introduced by such plates are unimportant in the over-all deformations. The rotation of the torsional type is zero. The rotation of the bending type may be taken as components about each of the two principal axes of section for which the centroidal moments of inertia of area are I_1 about an Ox axis, I_2 about an Oy axis. The rotations θ_x about Ox and θy about O_y are given by

$$\theta_x = \frac{1}{I_1} \int \alpha T y \, dV, \quad \theta_y = \frac{1}{I_2} \int \alpha T x \, dV \quad [68]$$

the volume integrals extending throughout the solid material.

(c) The "cantilever deflection" of one end relative to the other has components

$$\delta_x = -\frac{1}{I_2} \int \alpha T x(l - z) dV, \quad \delta_y = -\frac{1}{I_1} \int \alpha T y(l - z) dV \quad [69]$$

the volume integrals extending throughout the solid material. The axial co-ordinate z is measured from one end regarded as fixed, and l is the length.

Temperature-dependent elastic moduli—Plastic flow

35 A temperature-dependent coefficient of expansion presents no difficulty (see Introduction). For the circular cylinder or disk with temperature-dependent elastic modulli, see references (29) and (30). A calculation of rotational and thermal stress in a disk of arbitrary profile is given in (31), and in addition (32) deals with stress beyond the elastic limit.

A mathematical elastoplastic analysis of a slab with heat flowing in uniformly over one face (cf. Case 18) is given in (33). In (34) residual stresses in a butt-welded steel plate following welding are determined by measurement and by calculation from the temperature history, taking account of temperature dependence of coefficient of expansion, elastic modulus, and yield stress.

Bibliography

1 "A Study of the Effects of Cyclic Thermal Stresses on a Ductile Metal," by L. F. Coffin, Jr., Trans. ASME, vol. 76, 1954, p. 931.

2 "Behavior of Materials Under Conditions of Thermal Stress," by S. S. Manson, NACA Report No. 1170, 1954.

3 "Wings Under Repeated Thermal Stress," by E. W. Parkes, *Aircraft Engineering*, vol. 26, 1954, pp. 402–406.

4 "Influence of Aerodynamic Heating on the Effective Torsional Stiffness of Thin Wings," by B. Budiansky and J. Mayers, *Journal of the Aeronautical Sciences*, vol. 23, 1956, pp. 1081–1093, 1108.

5 "Temperature Gradients and Heat Stress in Brake Drums," by G. A. G. Fasekas, SAE Transactions, vol. 61, 1953, pp. 279–308.

6 "Effect of Stress on the Expansion Coefficient," by A. R. Rosenfield and B. L. Averbach, *Journal of Applied Physics*, vol. 27, 1956, pp. 154–156.

7 "Distributed Gravity and Temperature Loading in Two-Dimensional Elasticity Replaced by Boundary Pressures and Dislocations," by M. A. Biot, Trans. ASME, vol. 57, 1935, p. A-41.

8 "Theory of Elasticity," by S. Timoshenko and J. N. Goodier, McGraw-Hill Book Company, Inc., New York, N. Y., second edition, 1951, p. 406.

9 "Determination of Thermal Stresses in Three-Ply Laminates," by A. J. Durelli and C. H. Tsao, JOURNAL OF APPLIED MECHANICS, Trans. ASME, vol. 77, 1955, pp. 190–192.

10 "On the Integration of the Thermoelastic Equations," by J. N. Goodier, *Philosophical Magazine*, vol. 23, 1937, p. 1017.

11 "The Thermal Stress in a Strip Due to Variation of Temperature Along the Length and Through the Thickness," by J. N. Goodier, *Physics*, vol. 7, April, 1936, pp. 156–159.

12 "Thermal Stresses in Rectangular Strips—II," by J. S. Born and G. Horvay, JOURNAL OF APPLIED MECHANICS, Trans. ASME, vol. 77, 1955, p. 401.

13 "Mathematical Analysis of Thermal Stress in Thin Plates," by H. Wang, PhD dissertation, Cornell University (Library), 1940.

14 "Transient Thermal Stresses in Slabs and Circular Pressure Vessels," by M. P. Heisler, JOURNAL OF APPLIED MECHANICS, Trans. ASME, vol. 75, 1953, p. 261.

15 "Thermal Stresses in Plates," by J. L. Maulbetsch, Trans. ASME, vol. 57, 1935, pp. A-141 to A-146.

16 "Wärmespannungen," by E. Melan and H. Parkus, Springer, Vienna, Austria, 1953, p. 44.

17 "Axisymmetric Flexural Temperature Stresses in Circular Plates," by J. E. Goldberg, JOURNAL OF APPLIED MECHANICS, Trans. ASME, vol. 75, 1953, pp. 257–260.

18 "Thermal Stress in Long Cylindrical Shells Due to Temperature Variation Round the Circumference and Through the Wall," by J. N. Goodier, *Canadian Journal of Research*, vol. 15, 1937, p. 49.

19 "Theory of Plates and Shells," by S. Timoshenko, McGraw-Hill Book Company, Inc., New York, N. Y., 1940, p. 422.

20 "Temperature Stresses in Flat Rectangular Plates and in Thin Cylindrical Tubes," by J. P. den Hartog, *Journal of the Franklin Institute*, vol. 222, 1936, p. 149.

21 "Thermal Stresses in Thin-Walled Cylinders," by C. H. Kent, Trans. ASME, vol. 53, 1931, p. 167.

22 "On Thermal Stresses in Circular Cylinders," by J. C. Jaeger, *Philosophical Magazine*, vol. 36, 1945, pp. 414–428.

23 "The Calculation of Temperature Stresses in Tubes," by L. H. Barker, *Engineering*, vol. 124, 1927, pp. 443–444.

24 "Thermal Stress in Pipes," by H. Parkus, JOURNAL OF APPLIED MECHANICS, Trans. ASME, vol. 75, 1953, pp. 485–488.

25 "Thermal Stresses in a Partially Clamped Elastic Half-Plane," by J. H. Huth, *Journal of Applied Physics*, vol. 23, 1952, pp. 1234–1237.

26 "Eine indirekte Bestimmung der Airyschen Fläche bei unstetigen Wärmespannungen," by M. Hieke, *Zeitschrift für angewandte Mathematik und Mechanik*, Band 35, 1955, pp. 285–294.

27 Proofs of formulas under this reference are given in a forthcoming paper by the author.

28 "Similarity Laws for Stressing Heated Wings," by H. S. Tsien, *Journal of the Aeronautical Sciences*, vol. 20, 1953, pp. 1–11.

29 "Stresses in a Metal Tube Under Both High Radial Temperature Variation and Internal Pressure," by C. C. Chang and W. H. Chu, JOURNAL OF APPLIED MECHANICS, Trans. ASME, vol. 76, 1954, pp. 101–108.

30 "Thermal Stresses in Bodies Exhibiting Temperature-Dependent Elastic Properties," by H. H. Hilton, JOURNAL OF APPLIED MECHANICS, Trans. ASME, vol. 74, 1952, pp. 350–354.

31 "Centrifugal and Thermal Stresses in Rotating Disks," by W. R. Leopold, JOURNAL OF APPLIED MECHANICS, Trans. ASME, vol. 70, 1948, pp. 322–326.

32 "Stresses in Rotating Disks at High Temperatures," by A. S. Thomson, JOURNAL OF APPLIED MECHANICS, Trans. ASME, vol. 68, 1946, pp. A-45 to A-52.

33 "An Elasto-Plastic Thermal Stress Analysis of a Free Plate," by J. Weiner, JOURNAL OF APPLIED MECHANICS, Trans. ASME, vol. 78, 1956, pp. 395–402.

34 "The Determination of Internal Stresses From the Temperature History of a Butt-Welded Plate," by O. E. Rodgers and J. R. Fletcher, *Welding Journal*, vol. 17, November, 1938, Welding Research Supplement, pp. 4–7.

35 "Elastic Energy of an Ellipsoidal Inclusion in an Infinite Solid," by K. Robinson, *Journal of Applied Physics*, vol. 22, 1951, pp. 1045–1054.

Brief Notes*

On the recommendations of the Executive Committee of the ASME Applied Mechanics Division, it has been decided to initiate a section devoted to brief notes on technical matters in mechanics. These notes must not be longer than 750 words (about 2½ double-spaced typewritten pages, including figures) and will be subject to the usual review procedure prior to publication. After approval such notes will be published as soon as possible, normally in the next issue of the Journal. The notes should be submitted to the Technical Editors of the *Journal of Applied Mechanics*.

The Mobility of Levers Having Uniformly Distributed Mass

By M. D. CREECH,[1] STATE COLLEGE, NEW MEXICO

This paper shows how the mobility of a uniform rigid lever of mass *M* with *m* arbitrary mobilities connected along its length can be analyzed. The mass of the lever is divided into *n* equal mobilities connected to a rigid weightless lever together with the *m* other mobilities. It is shown that the infinite-series expansion representing this case is convergent to a finite value.

Nomenclature

The following nomenclature is used in the paper:

F = force
j = $\sqrt{-1}$
M = mass of the lever
v = velocity
$z = \frac{v}{F}$ = mobility
Z_A = mobility at point A
ω = angular frequency

Introduction

The mobility method[2] is a well-known method of great utility for the solution of problems of the steady-state harmonic vibrations of mechanical systems with lumped parameters. Weightless levers are used by Olson and Massa[3] in mechanical filter circuits. However, they were used in a very restricted sense in this reference. A later development[4] derived the mobility of a weightless lever having any finite number of mobilities distributed along its length.

It is the purpose here to extend this development to a lever having a uniformly distributed mass and having an arbitrary number of finite mobilities connected at arbitrary locations along its length.

Discussion

In the reference cited[4] the mobility of a weightless lever, looking into it at end A and having n-mobilities connected along its length, is given by

$$Z_A = \sum_{\substack{i=1 \\ j=1}}^{n} \frac{\dfrac{\alpha_i^2}{Z_i}}{\dfrac{(\alpha_i - \alpha_j)^2}{Z_i Z_j}} \qquad [1]$$

The uniform lever can be replaced by an equivalent rigid weightless lever having n-mobilities

$$z = \frac{n}{j\omega M}$$

connected to it at points

$$L/2n,\ 3L/2n,\ \ldots\ \frac{(2n-1)L}{2n}$$

in addition to any other mobilities $z_1, z_2, \ldots$ etc., the mobilities $z_1, z_2 \ldots$ being connected at $a_1, a_2 \ldots$ etc., Fig. 1.

The summation in the numerator and denominator of Equation [1] will now be written for this case. For the numerator the summation becomes

$$\sum_{i=1}^{n} \frac{\alpha_i^2}{z_i} = \frac{j\omega M}{n}\left[\left(\frac{L}{2n}\right)^2 + \left(\frac{3L}{2n}\right)^2 + \left(\frac{5L}{2n}\right)^2 + \ldots \frac{(2n-1)^2L^2}{(2n)^2}\right] + \sum_{i=1}^{m} \frac{a_i^2}{z_i}$$

$$= \frac{j\omega ML^2}{4n^3}\left[1 + 9 + 25 + 49 + \ldots (2n-1)^2\right] + \frac{a_1^2}{z_1} + \frac{a_2^2}{z_2} + \ldots \frac{a_m^2}{z_m}$$

Substituting the value of the summation given in Equation [2b] of Appendix 2

$$\sum_{i=1}^{n} \frac{\alpha_i^2}{z_i} = \frac{j\omega ML^2}{4n^3}\left[n + 4n(n-1) + \frac{8n(n-1)(n-2)}{6}\right] + \sum_{i=1}^{m} \frac{a_i^2}{z_i}$$

Letting $n \to \infty$ the numerator of Equation [1] becomes

$$\sum_{i=1}^{n} \frac{\alpha_i^2}{z_i} = \frac{j\omega ML^2}{3} + \sum_{i=1}^{m} \frac{a_i^2}{z_i} \qquad [2]$$

---

[1] Professor, Department of Mechanical Engineering, School of Engineering, New Mexico College of Agriculture and Mechanic Arts. Mem. ASME.

[2] "The Mobility Method of Computing the Vibrations of Linear Mechanical and Acoustical Systems: Mechanical-Electrical Analogies," by F. A. Firestone, *Journal of Applied Physics*, vol. 9, 1938, pp. 373–387.

[3] "Applied Acoustics," by H. F. Olson and F. Massa, P. Blakiston's Son & Company, Inc., Philadelphia, Pa., 1934. p. 42.

[4] "The Mobility Method Applied to Mechanical Wave Filters With Inductive Coupling," by A. Winsor, Trans. ASME, vol. 69, 1947, pp. A-143 to A-146.

* Discussion of papers in Brief Notes should be addressed to the Secretary, ASME, 29 West 39th Street, New York, N. Y., and will be accepted until July 10, 1957 for publication at a later date. Discussion received after the date will be returned.

Note: Statements and opinions advanced in papers are to be understood as individual expressions of their authors and not those of the Society. Manuscript received by Applied Mechanics Division, December 21, 1956

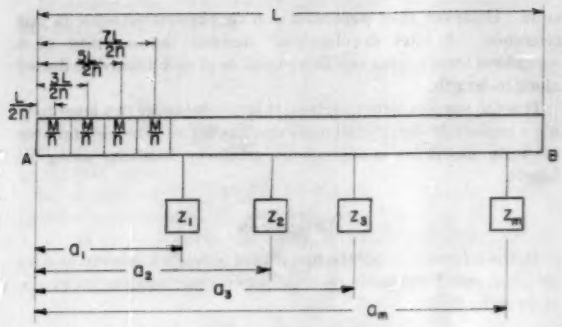

FIG. 1 LEVER HAVING UNIFORMLY DISTRIBUTED MASS CONNECTING ARBITRARY MOBILITIES

The series expansion of the summation in the denominator of Equation [1] is given in Appendix 3. Using the series listed in Appendix 2 the denominator of Equation [1] can be written

$$\sum_{i,j=1}^{n} \frac{(a_i - a_j)^2}{z_i z_j} = \frac{(j\omega ML)^2}{4n^4} \sum_{m=1}^{n} \sum_{k=1}^{m} (2k)^2 + \frac{j\omega ML^2}{4n^3} \left[\sum_{k=1}^{n} (2k-1)^2 \right] \sum_{i=1}^{m} \frac{1}{z_i} - \frac{j\omega ML}{n^2} \left[\sum_{k=1}^{n} (2k-1) \right] \sum_{i=1}^{m} \frac{a_i}{z_i} + \frac{j\omega M}{n} \left[n \sum_{i=1}^{m} \frac{a_i^2}{z_i} \right] + \sum_{i,j=1}^{m} \frac{(a_i - a_j)^2}{z_i z_j}$$

Letting $n \to \infty$ this becomes

$$\frac{(j\omega ML)^2}{12} + \frac{j\omega ML^2}{3} \sum_{i=1}^{m} \frac{1}{z_i} - j\omega ML \sum_{i=1}^{m} \frac{a_i}{z_i} + j\omega M \sum_{i=1}^{m} \frac{a_i^2}{z_i} + \sum_{i,j=1}^{m} \frac{(a_i - a_j)^2}{z_i z_j} \quad \ldots\ldots [3]$$

The mobility of the lever looking into it at A can be found by substituting the values of Equations [2] and [3] into Equation [1]

$$Z_A = \frac{\frac{j\omega ML^2}{3} + \sum_{i=1}^{m} \frac{a_i^2}{z_i}}{\frac{(j\omega ML)^2}{12} + \frac{j\omega ML^2}{3} \sum_{i=1}^{m} \frac{1}{z_i} - j\omega ML \sum_{i=1}^{m} \frac{a_i}{z_i} + j\omega M \sum_{i=1}^{m} \frac{a_i^2}{z_i} + \sum_{i,j=1}^{m} \frac{(a_i - a_j)^2}{z_i z_j}} \quad \ldots\ldots [4]$$

Appendix 1

Here, a method of finding the sum of the first n-terms of an infinite series by means of finite differences, will be reviewed briefly.

Suppose the first n-terms of the series

$$A_1 + A_2 + A_3 + \ldots\ldots A_n \ldots\ldots [5]$$

are to be summed.

A new series whose terms are the partial sums of the Series [5] is formed

$$0 + A_1 + (A_1 + A_2) + (A_1 + A_2 + A_3) + \ldots (A_1 + \ldots A_n) \ldots [6]$$

The first term of the various difference orders of Series [6] are

$$D_{11} = A_1$$
$$D_{21} = -A_1 + A_2$$
$$D_{31} = A_1 - 2A_2 + A_3$$
$$\ldots\ldots\ldots\ldots$$
$$D_{n1} = (n-1)D_{11} + \frac{(n-1)(n-2)}{2!} D_{21} + \frac{(n-1)(b-2)(n-3)}{3!} D_{31} + \ldots \text{etc} \ldots\ldots\ldots\ldots [7]$$

The $(n+1)$ term of the series of partial sums [2a] is equal to the sum of the first n-terms of the Series [5]

$$\sum_{i=n}^{n} A_i = nD_{11} + \frac{n(n-1)}{2!} D_{21} + \frac{n(n-1)(n-2)}{3!} D_{31} + \ldots\ldots \text{etc} \ldots\ldots\ldots\ldots [8]$$

Appendix 2

Here, using the method of Appendix 1, the sum of the first n-terms of the series used in the expansion of the numerator and denominator of Equation [1] will be given:

Series 1

$$1 + 3 + 5 + 7 + \ldots\ldots (2k-1)$$

$$\sum_{k=1}^{n} (2k-1) = n^2 \ldots\ldots\ldots\ldots [9]$$

Series 2

$$1 + 9 + 25 + 49 + \ldots\ldots (2k-1)^2$$

$$\sum_{k=1}^{n} (2k-1)^2 = n + 4n(n-1) + \frac{8n(n-1)(n-2)}{6} = \frac{n(4n^2-1)}{3} \ldots\ldots [10]$$

Series 3

$$4 + 16 + 36 + 64 + \ldots\ldots (2k)^2$$

$$\sum_{k=1}^{n} (2k)^2 = 4n + 6n(n-1) + \frac{4n(n-1)(n-2)}{3} = \frac{2n(2n^2+3n+1)}{3} \ldots\ldots [11]$$

Series 4

$$4 + 20 + 56 + 120 + \ldots\ldots \frac{2k(2k^2+3k+1)}{3}$$

$$\sum_{k=1}^{n} \frac{2k(2k^2+3k+1)}{3} = 4n + 8n(n-1)$$

$$+\frac{10n(n-1)(n-2)}{3}+\frac{n(n-1)(n-2)(n-3)}{3}$$

$$=\frac{(n^4+4n^3+5n^2+2n)}{3} \quad \ldots\ldots\ldots [12]$$

Appendix 3

Here, the summation in the denominator of Equation [1] will be written

$$\sum_{i,j=1}^{n}\frac{(\alpha_i-\alpha_j)^2}{z_iz_j}=\frac{(j\omega M)^2}{n^2}\left\{\left(\frac{L}{2n}-\frac{3L}{2n}\right)^2+\left(\frac{L}{2n}-\frac{5L}{2n}\right)^2+\left(\frac{L}{2n}-\frac{7L}{2n}\right)^2+\ldots\ldots\left(\frac{L}{2n}-\frac{(2n-1)L}{2n}\right)^2\right.$$

$$+\left(\frac{3L}{2n}-\frac{5L}{2n}\right)^2+\left(\frac{3L}{2n}-\frac{7L}{2n}\right)^2+\left(\frac{3L}{2n}-\frac{9L}{2n}\right)^2+\ldots\ldots$$

$$+\left(\frac{3L}{2n}-\frac{(2n-1)L}{2n}\right)^2+\left(\frac{5L}{2n}-\frac{7L}{2n}\right)^2+\left(\frac{5L}{2n}-\frac{9L}{2n}\right)^2$$

$$+\left(\frac{5L}{2n}-\frac{11L}{2n}\right)^2+\ldots\ldots\left(\frac{5L}{2n}-\frac{(2n-1)L}{2n}\right)^2+\ldots\ldots$$

$$\left.\left(\frac{(2n-1)L}{2n}-\frac{(2n+1)L}{2n}\right)^2\right\}+\frac{j\omega M}{n}\left[\left(\frac{L}{2n}\right)^2+\left(\frac{3L}{2n}\right)^2+\left(\frac{5L}{2n}\right)^2+\ldots\ldots\frac{(2n-1)^2L^2}{(2n)^2}\right]\sum_{k=1}^{m}\frac{1}{z_k}$$

$$-\frac{j\omega M}{n}\left[\frac{2L}{2n}+\frac{6L}{2n}+\frac{10L}{2n}+\ldots\frac{2(2n-1)}{2n}\right]\sum_{k=1}^{m}\frac{a_k}{z_k}$$

$$+\frac{j\omega M}{n}\left[n\sum_{k=1}^{m}\frac{a_k^2}{z_k}\right]+\sum_{i,j=1}^{m}\frac{(a_i-a_j)^2}{z_iz_j}$$

A Note on Torsion of Circular Shafts of Variable Diameter

By P. P. CHATTARJI,[1] CALCUTTA, INDIA

Certain stress functions which are in the form of polynomials have been obtained for various curves forming the generating surface of the shaft.

Introduction

ABBASSI[2] has considered the problem of circular shafts of variable diameter twisted by couples M_t applied at the ends. By using spherical polar co-ordinates, he has expressed the stress function in terms of the Legendre's associated functions of the second order and has obtained it for various curves forming the generating surface of the shaft. Most of Abbassi's work was anticipated by Fish.[3] The object of the present note is to obtain certain stress functions which are in the form of polynomials for various curves forming the generating surface of the shaft. In addition to Abbassi's results some new ones also are obtained.

Equations and boundary conditions

Using cylindrical polar co-ordinates (r, θ, z) where r and θ define the position of a point in the plane of a cross section of the body and the axis of the shaft is taken as the z-axis, the only non-vanishing stress components are $\tau_{r\theta}$ and $\tau_{\theta z}$, and these are given by

$$\tau_{r\theta}=-\frac{1}{r^2}\frac{\partial\psi}{\partial z},\quad \tau_{\theta z}=\frac{1}{r^2}\frac{\partial\psi}{\partial r} \quad \ldots\ldots\ldots [1]$$

where ψ is a stress function satisfying the equation[4]

$$\frac{\partial^2\psi}{\partial r^2}-\frac{3}{r}\frac{\partial\psi}{\partial r}+\frac{\partial^2\psi}{\partial z^2}=0 \quad \ldots\ldots\ldots [2]$$

The condition that the surface is free from traction is given by

$$\psi = \text{constant on entire surface} \quad \ldots\ldots\ldots [3]$$

The magnitude of the torque M_t at any cross section of radius a is given by

$$M_t=\int_0^{2\pi}\int_0^a \tau_{\theta z}r^2dr d\theta$$

$$=2\pi\int_0^a\frac{\partial\psi}{\partial r}dr=2\pi[\psi(a,z)-\psi(0,z)] \quad \ldots\ldots [4]$$

Solution of Equation [2]

(*a*) A solution independent of r is

$$\psi = z \quad \ldots\ldots\ldots [5]$$

and a solution independent of z is

$$\psi = r^4 \quad \ldots\ldots\ldots [6]$$

(*b*) Let us consider a solution of the form

$$\psi=\sum_{i=0}^{n}\psi_i(r)z^{2(n-i)} \quad \ldots\ldots\ldots [7]$$

Substituting Equation [7] in [2] we get

$$z^{2n}\left[\psi_0''-\frac{3}{r}\psi_0'\right]+\sum_{i=1}^{n}z^{2(n-i)}\left\{\psi_i''-\frac{3}{r}\psi_i'+[2(n-i)+2][2(n-i)+1]\psi_{i-1}\right\}=0 \quad \ldots\ldots [8]$$

where

$$\psi_i'=\frac{d\psi_i}{dr},\quad \psi_i''=\frac{d^2\psi_i}{dr^2};\quad i=0,1,2,\ldots n$$

Therefore

$$\psi_0''-\frac{3}{r}\psi_0'=0 \quad \ldots\ldots\ldots [9a]$$

$$\psi_i''-\frac{3}{r}\psi_i'+[2(n-i)+2][2(n-i)+1]\psi_{i-1}=0;\quad i=1,2,\ldots n \quad \ldots\ldots [9b]$$

---

[1] Junior Lecturer in Mathematics, Calcutta Technical School.

[2] "Torsion of Circular Shafts of Variable Diameter," by M. M. Abbassi, JOURNAL OF APPLIED MECHANICS, Trans. ASME, vol. 77, 1955, pp. 530–532.

Manuscript received by ASME Applied Mechanics Division, August 22, 1956.

[3] "A Particular Boundary Value Problem," by M. J. Fish, *Journal of Mathematics and Physics*, vol. 14, 1935, pp. 262–273.

[4] "Theory of Elasticity," by S. Timoshenko and J. N. Goodier, McGraw-Hill Book Company, Inc., New York, N. Y., second edition, 1951, p. 307.

whence $\psi_0 = r^4$ ..... [10a]

(The solution of Equation [9a] in the conventional way turns out to be $r^4/4$, but r^4 will do just as well; so the factor 1/4 is dropped.)

$$\psi_1 = -\frac{1}{12}\,2n\,(2n-1)r^6 \quad \text{..... [10b]}$$

$$\psi_2 = \frac{1}{384}\,2n(2n-1)(2n-2)(2n-3)r^8 \quad \text{..... [10c]}$$

and so on. One can, with little trouble, show that

$$\psi_i = (-1)^i \frac{[2(n-i)+1]}{2^{2i-1}(i+2)!i!} \frac{[2(n-i)+2]\,..\,2n}{} r^{2i+4}; \quad i = 1, 2, .. n \quad \text{..[11]}$$

Thus

$$\psi = z^{2n}r^4 + \sum_{i=1}^{n} (-1)^i \frac{[2(n-i)+1]}{2^{2i-1}(i+2)!i!} \frac{[2(n-i)+2]\,..\,2n}{} r^{2i+4}z^{2(n-i)} \quad \text{..[12]}$$

so that ψ is a polynomial of degree $2n$ in z and $2n + 4$ in r. This gives

$$\psi = r^4, \qquad \text{when} \quad n = 0 \quad \text{..... [13a]}$$

$$\psi = r^4z^2 - \frac{1}{6}r^6, \qquad \text{when} \quad n = 1 \quad \text{..... [13b]}$$

$$\psi = r^4z^4 - r^6z^2 + \frac{1}{16}r^8, \qquad \text{when} \quad n = 2 \quad \text{..... [13c]}$$

and so on.

(c) Next let us consider a solution of Equation [2] of the form

$$\psi = \sum_{i=0}^{n-1} \Psi_i(r) z^{2(n-i)-1} \quad \text{..... [14]}$$

As before, we get

$$\psi = z^{2n-1}r^4 + \sum_{i=1}^{n-1} (-1)^i \frac{[2(n-i)][2(n-i)+1]\,...\,[2n-1]}{2^{2i-1}(i+2)!i!} r^{2i+4}z^{2(n-i)-1} \quad \text{..... [15]}$$

so that ψ is a polynomial degree $2n - 1$ in z and $2n + 2$ in r. This gives

$$\psi = r^4z, \qquad \text{when} \quad n = 1 \quad \text{....[16a]}$$

$$\psi = r^4z^3 - \frac{1}{2}r^6z, \qquad \text{when} \quad n = 2 \quad \text{....[16b]}$$

$$\psi = r^4z^5 - \frac{5}{3}r^6z^3 + \frac{5}{16}r^8z, \qquad \text{when} \quad n = 3 \quad \text{....[16c]}$$

and so on.

Possible shapes of circular shafts of variable diameter

1 Consider the Solution [13b]

$$\psi = c\left(r^4z^2 - \frac{1}{6}r^6\right) = \frac{c}{6}r^4(6z^2 - r^2), \quad c = \text{const.} \quad \text{..[17]}$$

This already has been discussed by Abbassi.[2]

2 Consider the Solution [16a]

$$\psi = cr^4z, \quad c = \text{const.} \quad \text{..... [18]}$$

This also has been discussed by Abbassi.[2]

3 Consider the solution obtained by superposing Equations [5] and [6]

$$\psi = c(r^4 - az), \quad c, a = \text{const} \quad \text{..... [19]}$$

The shaft whose generating curve is given by $r^4 - az = k$, where k is a constant, has $\psi = c(r^4 - az)$ as a stress function. Equation [4] gives

$$c = \frac{M_t}{2\pi k} \quad \text{..... [20]}$$

4 Consider the solution obtained by superposing Equations [5], [6], and [16a]

$$\psi = c(ar^4 + br^4z + cz), \quad c, a, b, e = \text{const}$$
$$= c(ar^4 - r^4z - z), \quad \text{if} \quad b = e = -1 \quad \text{..... [21]}$$

The shaft whose generating curve is given by $ar^4 - r^4z - z = k$, where k is a constant, has

$$\psi = c(ar^4 - r^4z - z)$$

as a stress function. Equation [4] gives

$$c = \frac{M_t}{2\pi k} \quad \text{..... [22]}$$

Other forms of shaft may be obtained in a similar manner.

Acknowledgment

The author extends his heartiest thanks to Prof. B. Sen for his helpful guidance during the progress of the work. He also wishes to thank the reviewer for his kind suggestions and helpful criticisms for improving the paper.

Reduction of Three-Dimensional Stress Distributions to Two-Dimensional Analysis by Superposition

By G. A. ZIZICAS,[1] LOS ANGELES, CALF.

In a recent note[2] the author proposed a graphical procedure which supplements the classical three-dimensional Mohr-circle representation by specifying the direction of the total shear on any element of surface. The same results are reached here by superposition which simplifies and clarifies the analysis considerably. The associated analytical results are presented in a more useful form and are shown to lead readily to the classical Mohr representation. An application is made to the practically important stress components on the octahedral planes.

Superposition and graphical representation

LET the stress components be known for a certain orientation of an elementary parallelepiped. An element of arbitrary orientation can be located on a sphere with infinitesimal radius in the neighborhood under consideration by the angular spherical co-ordinates ϕ and θ, Fig. 1. The stress components

[1] Associate Professor of Engineering, University of California.

[2] "Representation of Three-Dimensional Stress Distributions by Mohr Circles," by G. A. Zizicas. JOURNAL OF APPLIED MECHANICS, Trans. ASME, vol. 77, 1955, pp. 273–275.

Manuscript received by ASME Applied Mechanics Division, March 18, 1957.

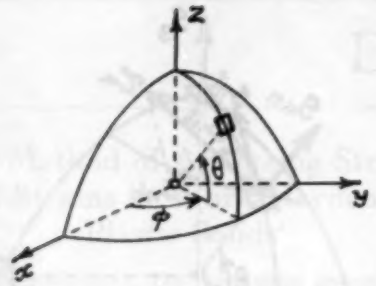

Fig. 1 Angular spherical co-ordinates ϕ and θ of an element of surface

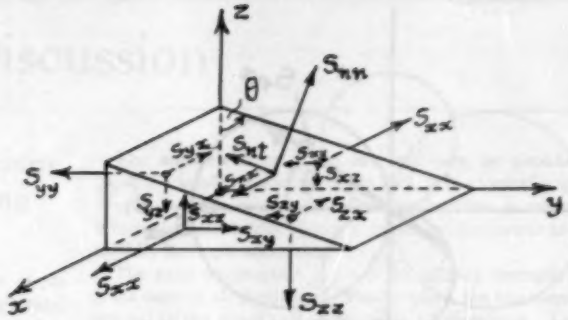

Fig. 2 Stress components on an infinitesimal prism

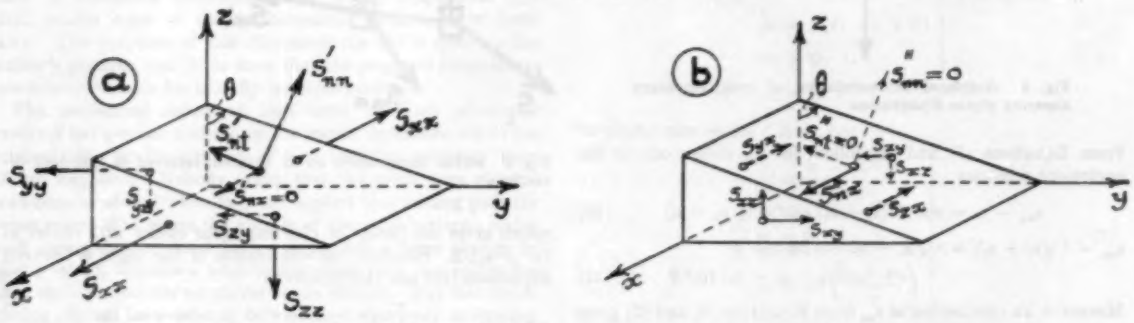

Fig. 3 Two-dimensional part and complementary shearing stress distribution of an infinitesimal prism

corresponding to elements with θ = const or ϕ = const can be analyzed by considering an infinitesimal prism whose inclined surface obtains all possible orientations parallel to the opposite edge. Such a prism with the stress components on its surfaces is indicated in Fig. 2.

The stress components on the elements of the prism perpendicular to the co-ordinate axes are divided into two groups shown separately in Figs. 3(a) and (b). The stress components s_{nn}' and s_{nn}'', s_{nt}'' correspondingly are evaluated by the equations of equilibrium or motion in the x-direction for the case of Fig. 3(a) and in the y and z-directions for the case of Fig. 3(b). It follows readily that

$$s_{nx}' = 0, \quad s_{nn}'' = 0, \quad s_{nt}'' = 0 \ldots\ldots\ldots\ldots [1]$$

Simple superposition, with Equations [1] taken into consideration, shows that the components s_{nn}, s_{nt}, s_{nx} of the original prism of Fig. 2 are

$$\left.\begin{aligned} s_{nn} &= s_{nn}' + s_{nn}'' = s_{nn}' \\ s_{nt} &= s_{nt}' + s_{nt}'' = s_{nt}' \\ s_{nx} &= s_{nx}' + s_{nx}'' = s_{nx}'' \end{aligned}\right\} \ldots\ldots\ldots\ldots [2]$$

It is pointed out carefully that the original prism of Fig. 2 and the two prisms of Figs. 3(a) and (b) are all assumed in the state of deformation corresponding to the stresses of the prism of Fig. 2. In this way the analysis and superposition become valid for both small and large strains. Since the derived relations are based on the equations of equilibrium alone, the only requirement is that the geometry of all three cases is identical. In this sense, the elementary prism can be considered as an ideally rigid (completely undeformable) body in the geometrical configuration corresponding to the state of deformation indicated in Fig. 2.

The first two of Equations [2] show that the components s_{nn} and s_{nt} can be found by means of the generalized two-dimensional stress distribution exhibited in Fig. 3(a). The presence of s_{zz} has no significant effect on the equilibrium or motion of the element, and the corresponding analytical relations are

$$\left.\begin{aligned} s_{nn}\cos\theta - s_{nt}\sin\theta &= s_{yy}\cos\theta + s_{xy}\sin\theta \\ s_{nn}\sin\theta + s_{nt}\cos\theta &= s_{xx}\sin\theta + s_{yx}\cos\theta \end{aligned}\right\} \ldots\ldots [3]$$

The graphical representation given in a previous note by the author[2] follows immediately. The stress configuration shown in Fig. 3(b) may be called the "complementary shearing stress distribution" with respect to the normal stress s_{xx}. The equations of equilibrium show that the only nonzero component on the inclined surface is

$$s_{nx} = s_{yx}\cos\theta + s_{zx}\sin\theta \ldots\ldots\ldots\ldots [4]$$

A graphical construction is indicated in Fig. 4.

Stress components

For a surface element whose orientation is defined by the polar angles ϕ and θ with respect to the principal stress directions, Fig. 5, one may write the standard two-dimensional relations

$$s_{aa} = {}^1/_2(s_1 + s_2) + {}^1/_2(s_1 - s_2)\cos 2\phi \ldots\ldots [5]$$

$$s_{ab} = {}^1/_2(s_2 - s_1)\sin 2\phi \ldots\ldots\ldots\ldots [6]$$

$$s_{nn} = {}^1/_2(s_{aa} + s_3) + {}^1/_2(s_{aa} - s_3)\cos 2\theta \ldots\ldots [7]$$

$$s_{nt} = {}^1/_2(s_3 - s_{aa})\sin 2\theta \ldots\ldots\ldots\ldots [8]$$

while Equation [4] combined with Equation [6] reduces to

$$s_{nb} = s_{ab}\cos\theta = {}^1/_2(s_2 - s_1)\cos\theta\sin 2\phi \ldots\ldots [9]$$

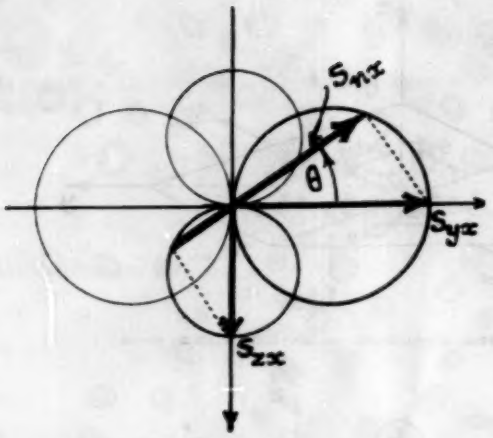

Fig. 4 Graphical representation of complementary shearing stress distribution

From Equations [7] and [5] follow for s_{nn} either one of the equivalent relations

$$s_{nn} - s_3 = \cos^2\theta[(s_1 - s_2)\cos^2\phi + s_2 - s_3] \quad \ldots\ldots [10]$$

$$s_{nn} - {}^1/_2(s_1 + s_2) = {}^1/_2(s_1 - s_2)\cos 2\phi \cos^2\theta + {}^1/_2(2s_3 - s_1 - s_2)\sin^2\theta \quad \ldots\ldots [11]$$

Moreover, an elimination of s_{aa} from Equations [8] and [7] gives

$$s_{nl} = (s_3 - s_{nn})\tan\theta \quad \ldots\ldots [12]$$

This relation is obvious in the graphical construction proposed by the author.[2] Now either Equation [10] or [11] gives the value of s_{nn} for specified ϕ and θ. With this value of s_{nn} the value of s_{nl} is readily calculated from Equation [12]. The third rectangular component s_{nb} is specified by Equation [9]. According to Equations [12] and [9] the value of the square of the total shear $\tau_n^2 = s_{nl}^2 + s_{nb}^2$ is

$$\tau_n^2 = (s_{nn} - s_3)^2\tan^2\theta + \frac{1}{4}(s_1 - s_2)^2\cos^2\theta\sin^2 2\phi \quad \ldots [13]$$

Finally for the angle ω_{nl} in Fig. 5, Equations [9] and [12] give

$$\cot\omega_{nl} = \frac{s_{nl}}{s_{nb}} = \frac{2(s_3 - s_{nn})\sin\theta}{(s_2 - s_1)\cos^2\theta\sin 2\phi} \quad \ldots\ldots [14]$$

Classical Mohr circles

The equation satisfied by s_{nn} and τ_n of all elements on a parallel circle is obtained by eliminating ϕ between Equations [11] and [13]. It suffices to keep on one side of Equation [11] the term containing $\cos 2\phi$, square both sides and add with Equation [13] which is first multiplied through by $\cos^2\theta$. The result is that either

$$\cos^2\theta = 0, \quad \text{giving} \quad s_{nn} = s_3 \quad \text{and} \quad s_{nl} = s_{nb} = \tau_n = 0$$

or

$$\left[s_{nn} - \frac{1}{2}(s_1 + s_2)\right]^2 + \tau_n^2 = \frac{1}{4}(s_1 - s_2)^2 + (s_1 - s_3)(s_2 - s_3)\sin^2\theta \quad \ldots\ldots [15]$$

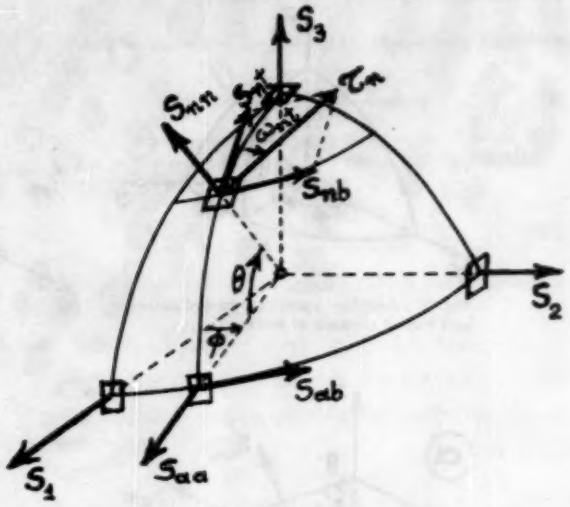

Fig. 5 Stress components on an element referred to principal directions

which gives the family of classical Mohr circles with center at $(s_1 + s_2)/2$. Similarly, an elimination of the angle ϕ between Equations [10] and [13] results in

$$\tau_n^2 = (s_{nn} - s_3)\left[\frac{s_1(s_1 - s_3)\cos^2\phi + s_2(s_2 - s_3)\sin^2\phi}{s_1\cos^2\phi + s_2\sin^2\phi - s_3} - s_{nn}\right] \quad \ldots\ldots [16]$$

which represents the other family of classical Mohr circles through the point s_3 and with center on the s_{nn}-axis. Their center is readily found to be the point with abscissa

$$s_1^2\cos^2\phi + s_2^2\sin^2\phi - s_3^2/2(s_1\cos^2\phi + s_2\sin^2\phi - s_3)$$

Application to octahedral planes

An interesting result is obtained by an application of the foregoing analysis to the octahedral planes, for which

$$s_{nn} = \frac{1}{3}(s_1 + s_2 + s_3)$$

and

$$\phi = 45°, \quad \sin\theta = \pm\frac{1}{3}\sqrt{3}, \quad \cos^2\theta = 2/3$$

With the middle stress point s_2 considered as a pole of the sphere, Equation [14] gives

$$\cot\omega_{nl}^{oct} = \pm\frac{2s_2 - s_1 - s_3}{s_1 - s_3}\frac{\sqrt{3}}{3} = \pm\nu_s\frac{\sqrt{3}}{3} \quad \ldots [17]$$

where ν_s is the index of stress deviation. Here it acquires new physical significance and indicates an easy way of finding the direction of the shear within the octahedral planes from Equation [17]. Since $-1 \leq \nu_s \leq +1$, it follows that the direction of the octahedral shear within the octahedral planes is always within a 30-deg angle from the direction parallel to the plane containing the maximum and minimum principal stresses.

Discussion

New Method of Analyzing Stresses and Strains in Work-Hardening Plastic Solids[1]

BERNARD BUDIANSKY.[2] The paper under discussion stems from the premise that (except for proportional loading) total stress-strain laws of plasticity for strain-hardening materials are "physically unsound." The author then presents what he calls "a reasonable stress-strain law" of the incremental type that retains some of the mathematical advantages of total laws. The purposes of this discussion are (*a*) to question the author's premise, and (*b*) to show that the proposed stress-strain law is unreasonable for initially isotropic materials.

The unqualified statement that total laws are physically unsound has become a cliché in the recent literature, while the original basis for the criticism of such laws has evidently been all but forgotten. Nobody denies that the predictions of total laws become absurd when they are applied to a loading path (in stress space) that skims the outside of the yield surface; under such circumstances, total laws can predict a large change in plastic strain, whereas a neighboring stress path just inside the yield surface produces no plastic strain change. But this shortcoming of total laws can only be construed rigorously as limiting their domain of validity, and can have no bearing whatsoever on the accuracy of total laws when the conditions that disqualify them from universal applicability are not encountered. A total law is certainly valid for proportional loading; must it then be impossible for a total law to be rigorously valid for all loading paths in some finite vicinity of proportional loading? Certainly not; indeed, the work of Sanders[3,4] displays incremental laws based on many plane loading surfaces that, for a variety of loading paths in the vicinity of proportional loading, give strains which coincide rigorously with the predictions of a total law. (The same type of limited path independence is a feature of the slip theory of plasticity.[5,6])

In his introduction to the paper under discussion the author decries the fact that solutions to specific problems are offered in the contemporary literature on the basis of total laws, and describes as a "paradoxical situation" the fact that promulgators of such solutions argue that their results may be approximately correct even though the conditions for proportional loading are not completely fulfilled. But, as Sanders' work confirms, the argument is a sensible one, and the paradox is nonexistent.

The author's stress-strain law will now be considered. In brief, the law is unreasonable (in fact, it is physically unsound!) simply because of the fact that it describes a material that is initially anisotropic, contrary to the evident intent to consider initially isotropic materials.

The axial stress-strain curve of an initially isotropic material is the same in all directions. Furthermore, the transverse strains normal to the stress axis are equal in all directions. Let us calculate the predictions of the author's law based on the moving Tresca "frame" (Fig. 6 of the paper) for the stress history

$$\left.\begin{aligned} \sigma_1 &= \lambda(t) \quad (\dot{\lambda} > 0) \\ \sigma_2 &= 0 \\ \sigma_3 &= 0 \end{aligned}\right\} \qquad [1]$$

The plastic strains, for $\lambda > \sigma_0$, are

$$\left.\begin{aligned} \epsilon_1 &= \frac{\lambda - \sigma_0}{c} \\ \epsilon_2 &= 0 \\ \epsilon_3 &= -\left(\frac{\lambda - \sigma_0}{c}\right) \end{aligned}\right\} \qquad [2]$$

where ϵ_3 is calculated on the basis of the usually made assumption that the material is plastically incompressible. It is seen immediately that the inequality of ϵ_2 and ϵ_3 is in violent disagreement with the requirement of isotropy. Let us consider further the stress history

$$\left.\begin{aligned} \sigma_1 &= -\lambda(t) \quad (\dot{\lambda} > 0) \\ \sigma_2 &= -\lambda(t) \\ \sigma_3 &= 0 \end{aligned}\right\} \qquad [3]$$

The resultant strains, according to the author's theory, are, for $\lambda > \sigma_0$

$$\left.\begin{aligned} \epsilon_1 &= -\frac{\lambda - \sigma_0}{c} \\ \epsilon_2 &= -\frac{(\lambda - \sigma_0)}{c} \\ \epsilon_3 &= \frac{2(\lambda - \sigma_0)}{c} \end{aligned}\right\} \qquad [4]$$

where, again, plastic incompressibility is assumed. But, if hydrostatic tension is to have no influence on plastic strain, the stress history [3] is equivalent to

$$\left.\begin{aligned} \sigma_1 &= 0 \\ \sigma_2 &= 0 \\ \sigma_3 &= \lambda(t) \quad (\dot{\lambda} > 0) \end{aligned}\right\} \qquad [5]$$

Thus a uniaxial stress-strain test in the direction of the 3-axis would produce the strains given by Equation [4]. The transverse strains ϵ_1 and ϵ_2 are now equal, as they should be for initially isotropic materials, but the slope of the uniaxial stress-strain curve in the 3-direction differs from that in the direction of the 1-axis by a factor of 2!

---

[1] By William Prager, published in the December, 1956, issue of the JOURNAL OF APPLIED MECHANICS, Trans. ASME, vol. 78, pp. 493–496.

[2] Associate Professor of Structural Mechanics, Division of Engineering and Applied Physics, Harvard University, Cambridge, Mass.

[3] "Plastic Stress-Strain Relations Based on Linear Loading Functions," by J. L. Sanders, Jr., Proceedings of the Second U. S. National Congress of Applied Mechanics, ASME, 1954, pp. 455–460

[4] "Plastic Stress-Strain Relations Based on Infinitely Many Plane Loading Surfaces," by J. L. Sanders, Jr., Brown University Report No. A11-106, 1952.

[5] "A Mathematical Theory of Plasticity Based on the Concept of Slip," by S. B. Batdorf and Bernard Budiansky, NACA TN 1871, 1949.

[6] "Polyaxial Stress-Strain Relations of a Strain-Hardening Metal," by S. B. Batdorf and Bernard Budiansky, JOURNAL OF APPLIED MECHANICS, Trans. ASME, vol. 76, 1954, pp. 323–326.

The initial anisotropy implicit in the author's stress-strain law is thus so great that it is difficult to accept the law as reasonable for materials that are supposed to be initially isotropic.

P. G. HODGE, JR.[7] The author has presented a most interesting and valuable contribution to the theory of plasticity. Previously, almost all of the solutions for a strain-hardening plastic solid have been based upon isotropic hardening, although experimental evidence[8] indicates rather less than perfect agreement with theory It is to be hoped that some attempt will be made to re-evaluate these experimental results in relation to the hardening law introduced by the author.

In this connection, it may be worth while to point out more explicitly the relation between the author's approach and isotropic

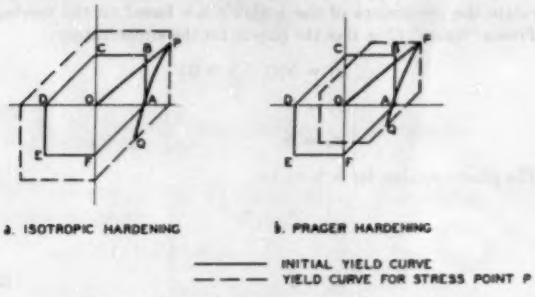

FIG. 1 YIELD FUNCTIONS AFTER HARDENING

hardening. This is done in Fig. 1, herewith. In each case the stress point first moves along a straight line from O to P, and plastic deformation takes place from the time the stress point touches the side AB. According to isotropic hardening, the stress point is always on the side AB, so that the strain component ϵ_2 is zero, while, according to the author, hardening the stress point goes into the corner B and produces both ϵ_1 and ϵ_2 strains. Further, if the stress point then is unloaded along PQ, the point Q at which plastic behavior recommences is different for the two theories.

Despite the differences between the two theories, their mathematical formulation is quite similar. In particular, both theories can be integrated so long as the stress point remains on a particular side, or corner. Indeed, the integrated form for a corner is also valid, if the stress point first touches a side and then moves into an adjacent corner. The author used this fact in his example although he did not mention it explicitly in his general discussion. Table 1 of this discussion shows the integrated laws for typical sides and corners according to both theories. It also may be worth pointing out that a somewhat more general law

[7] Professor of Applied Mechanics, Polytechnic Institute of Brooklyn, Brooklyn, N. Y.; now at Illinois Institute of Technology, Chicago, Ill. Mem. ASME.

[8] "Combined Stress Tests in Plasticity," by A. Phillips and L. Kaechle, JOURNAL OF APPLIED MECHANICS, Trans. ASME, vol. 78, 1956, pp. 43–48.

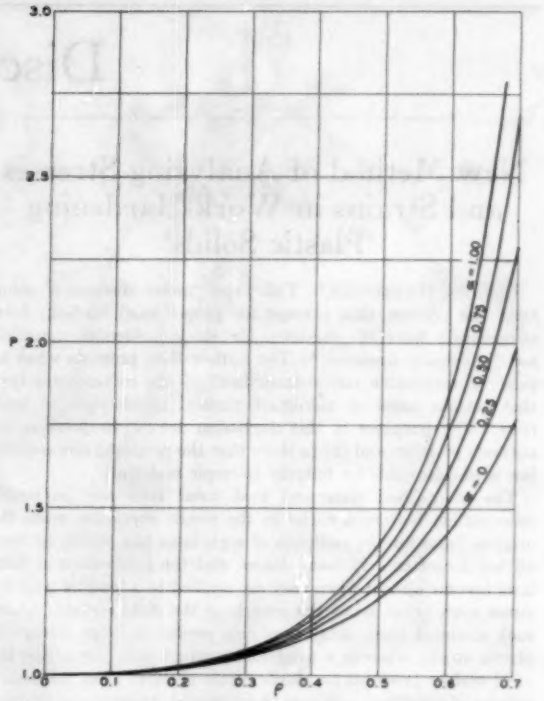

FIG. 2 RELATION BETWEEN P AND ρ FOR VARIOUS α

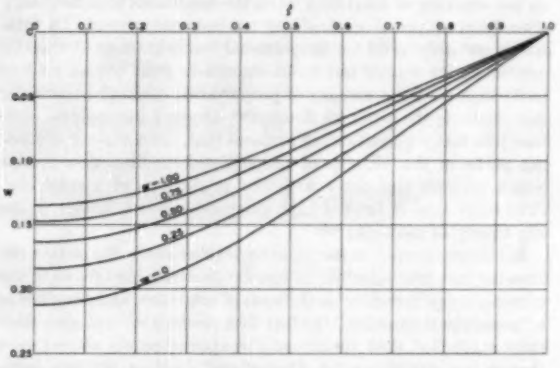

FIG. 3 DEFLECTED SHAPE OF PLATE FOR $1p = 1.5$ TIMES COLLAPSE LOAD

can be obtained by combining the two theories. To this end, let us visualize a physical element of the plate as being divided into a large number N of subelements of which αN harden iso-

TABLE 1 COMPARISON OF INTEGRATED STRESS—STRAIN LAWS

Regime	Prager hardening	Isotopic hardening	Combined hardening
A	$\sigma_1 - Y = c\epsilon_1$ $\sigma_2 - Y = c\epsilon_2$	$\sigma_1 - Y = c(\epsilon_1 + \epsilon_2)$ $\sigma_2 - Y = c(\epsilon_1 + \epsilon_2)$	$\sigma_1 - Y = c(\epsilon_1 + \alpha\epsilon_2)$ $\sigma_2 - Y = c(\alpha\epsilon_1 + \epsilon_2)$
AB	$\epsilon_1 = 0$ $\sigma_2 - Y = c\epsilon_2$	$\epsilon_1 = 0$ $\sigma_2 - Y = c\epsilon_2$	$\epsilon_1 = 0$ $\sigma_2 - Y = c\epsilon_2$
B	$\sigma_1 = c\epsilon_1$ $\sigma_2 - Y = c\epsilon_2$	$\sigma_1 = 0$ $\sigma_2 - Y = c\epsilon_2$	$\sigma_1 = c(1 - \alpha)\epsilon_1$ $\sigma_2 - Y = c\epsilon_2$
BC	$\sigma_1 - \sigma_2 + Y = 2c\epsilon_1$ $\epsilon_2 = -\epsilon_1$	$\sigma_1 - \sigma_2 + Y = c\epsilon_1$ $\epsilon_2 = -\epsilon_1$	$\sigma_1 - \sigma_2 + Y = c(2 - \alpha)\epsilon_1$ $\epsilon_2 = -\epsilon_1$

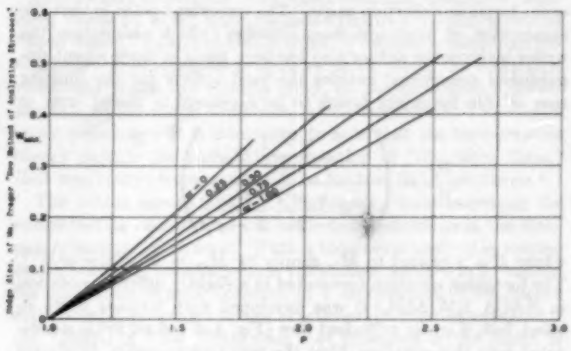

FIG. 4 MAXIMUM PLATE DISPLACEMENT AS A FUNCTION OF LOAD

tropically and $(1 - \alpha)N$ harden according to the author's theory. The resulting stress-strain law is easily obtained and is shown in the third column of Table 1. It is seen to be of the same mathematical form as the other two, and hence can be as easily used in the solution of problems. Further, the additional material constant may be chosen so as to obtain better experimental agreement.

The example of a simply supported circular plate can be solved for the general theory in exactly the same manner as in the paper, the solution being

$$0 \leq r \leq \rho$$

$$w = (p/64c)\,(8R\rho^2 - 3\rho^4 - 6\rho^2 r^2 + R^4)$$

$$M_r = M_0 + (3p/48)\,[3(\rho^2 - r^2) + \alpha(3\rho^2 - r^2)]$$

$$M_\varphi = M_0 + (3p/48)\,[3\alpha(\rho^2 - r^2) + (3\rho^2 - r^2)]$$

$$\rho \leq r \leq R$$

$$w = (p\rho^3/8c)\,(R - r)$$

$$M_r = M_0(1 - R/r) + (p\rho^3/8r)\ln(r/R) + (pR^2/6)\,[(R/r) - (r/R^2)]$$

$$M_\varphi = M_0 + p\rho^3/8r$$

where p and ρ are related by

$$p = (24M_0/R^2)\,[3(\rho/R)^3 \ln(\rho/R) + 4 - (4 + 3\alpha)\,(\rho/R)^2]^{-1}$$

Evidently if $\alpha = 0$ these results reduce to Equations [12], [13], [15], and [16] of the paper. Figs. 2 through 5 of the discussion show salient features of the solution for various values of α. It is seen that although the solutions are qualitatively similar there exist significant quantitative differences depending upon the value of the parameter α.

AUTHOR'S CLOSURE

Since Professor Budiansky admits that the predictions of the total stress-strain laws of plasticity may be far from the observed mechanical behavior, his objection to the author's use of the term "physically unsound" seems to be of a semantic nature. To the author's mind, a stress-strain law that describes the observed behavior only under very special conditions of loading is physically unsound, although it may be mathematically acceptable when these conditions prevail. In support of his agreement, Professor Budiansky mentions the slip theory of plasticity and the theory of Sanders, both of which exhibit a limited path independence of the final plastic strain. The author's model using a polygonal frame (Fig. 5) exhibits a similar limited path

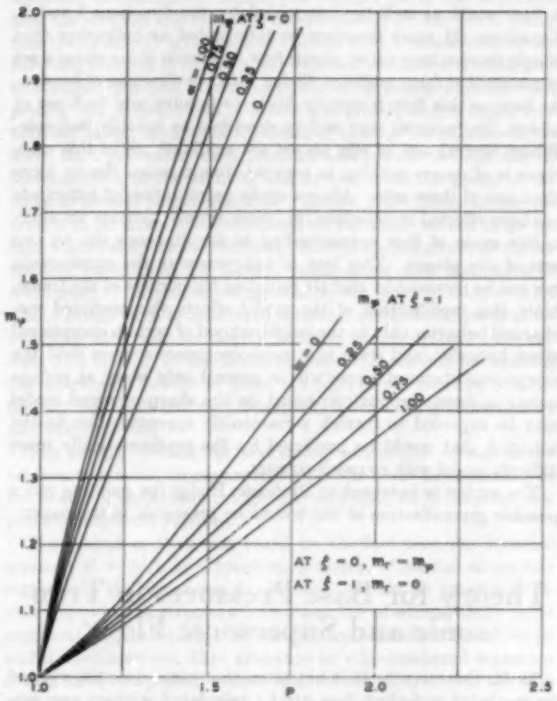

FIG. 5 BENDING MOMENTS AT CENTER AND EDGE AS A FUNCTION OF LOAD

independence, and it is precisely this effect which is responsible for the simplification of the mathematical analysis. The author would certainly not object to the use of total stress-strain laws when this could be justified by showing that the actual conditions of stressing a generic element are sufficiently close to proportional loading. Unfortunately, this justification would, in most cases, have to be obtained from the solution based on incremental laws. Once, however, this solution is available, the solution based on the problematic total laws is no longer of interest.

The second part of the discussion, which is concerned with questions of isotropy, could be treated summarily by the remark that Professor Budiansky first attributes to the author "the evident intent to consider initially isotropic materials" and then proceeds to take the author to task for not sticking to this alleged program.

Since, however, Professor Budiansky's argument serves to bring out instructive points, detailed comment seems preferable, even though this means following Professor Budiansky in using the pin-frame model based on the Tresca hexagon (Fig. 6) for plane stress, when it was only used for flexure of plates in the paper under consideration.

For the bent plate considered in the paper, the pin-frame model completely represents the generalized stresses (principal bending moments) and generalized strains (principal curvatures), and the questions of isotropy discussed by Professor Budiansky do not arise. If, however, the model is to be used for plane stress, it must be kept in mind that the model does not represent all principal stresses and strains. Caution is therefore required when the considered state of stress can be interpreted in more than one way as a state of plane stress. Equations [1] of the discussion represent such an exceptional state of stress; whereas the plane of stress would normally be determined by the directions 1 and 2,

it here could as well be determined by the directions 1 and 3. Equations [2] must therefore be interpreted as indicating that simple tension may cause plastic flow by simple shear along a set of planes that form angles of 45 deg with the direction of tension. As long as this flow is equally likely to involve any such set of planes, the material may well be described as initially isotropic. Where several sets of slip planes are available, as in this case, there is of course nothing to prevent simultaneous slip on more than one of these sets. After a cyclic permutation of subscripts has been effected in Equation [4], these simply indicate an alternative mode of flow corresponding to simultaneous slip on two sets of slip planes. This lack of uniqueness in the stress-strain law can be removed by slightly rounding the corners of the frame. Since this modification of the model affects the predicted mechanical behavior only in the neighborhood of certain exceptional stress histories, and since in a nonhomogeneous stress field the exceptional states of stress will in general only occur at certain points or lines, the analysis based on the sharp-cornered model may be expected to furnish a reasonable approximation to the behavior that would be predicted by the mathematically more difficult model with rounded corners.

The author is indebted to Professor Hodge for pointing out a possible generalization of the technique presented in the paper.

Theory for Base Pressures in Transonic and Supersonic Flow[1]

D. R. Chapman.[2] It is not often that some quantity related to separated turbulent flow can be calculated without any empirical constants and still agree with experiments. The author's theory of base pressure for the limiting case of thin turbulent boundary layers falls within this category; it appears to be an original and first-class contribution.

As the author points out, the flow model postulated is similar qualitatively to one with which the writer has worked on a semiempirical basis. He has improved and simultaneously put this model on a quantitative basis for entirely turbulent flows. In discussing his theory, it is pertinent to note that at the Ames Aeronautical Laboratory we recently have put essentially the same model on a quantitative basis although for entirely laminar flow. The two independent researches are complementary in that they involve different flows yet they involve the same essential idea, namely, the base pressure is determined by equating the total pressure of the "discriminating" streamline (called "dividing" streamline in our research) to the static pressure just downstream of the recompression zone (see Equation [22]). Consequently, it may be of interest here to compare the main features of these two researches, as each has a bearing on the other.

There is one small difference between the two analyses. We used the isentropic equations when relating P_3, the pressure just upstream of the recompression zone, to P_4, the pressure just downstream. The author uses the oblique shock-wave equations. For pure laminar recompression, experiments show the outer edge of the laminar wake to curve smoothly, and not to involve a shock wave along this edge. For turbulent recompression, however, the outer edge bends almost discontinuously, thereby enabling the oblique shock wave to originate essentially within the wake. The two types of recompression are the same up to second-order terms in deflection angle. The important point is that the assumption of isentropic recompression (which assumption the writer believes the author also has been using in more recent unpublished researches) enables the final answer for the limiting case of thin boundary layers to be expressed in closed form as

$$\frac{P_2}{P_1} = \left(\frac{1 + \frac{\gamma - 1}{2} M_{1e}^2}{1 + \frac{\gamma - 1}{2} \frac{M_{1e}^2}{1 - \varphi_i^2}} \right)^{\gamma/\gamma - 1}$$

where M_{1e} is related to M_{2e} simply by $M_{1e} = M_{2e}(1 - \varphi_i^2)^{1/2}$. The foregoing equation (presented in a slightly different notation in NACA RM A55L14) was developed with laminar flows in mind, but, if φ_i for turbulent flow (Fig. 4 of the paper) is substituted into this equation, then the resulting values of P_2/P_1 are found to be very close to his values (curve in Fig. 5) at Mach numbers below about 3 and only slightly higher at Mach numbers above about 3. The two analyses, therefore, are essentially the same.

For completely laminar flow the solution of the differential equations of viscous motion yield $\varphi_i = 0.59$ independent of Mach number, and the foregoing equation has been found to be in excellent agreement with experiments involving pure laminar separations of the base-pressure type at both subsonic and supersonic speeds (see NACA RM A55L14). Inasmuch as the ideas of the two theories are essentially the same, neither involving any empirical information, it follows that the agreement of theory with the completely laminar flow base measurements may be taken as confirmation of the essential ideas behind the author's theory for turbulent flow.

We have viewed the excellent agreement we obtained in the laminar case as meaning that there probably is a pair of phenomena which have been disregarded but which tend to compensate each other. Strictly speaking, it would seem that the total pressure along the discriminating streamline should be equated to the static pressure at the reattachment point P_R, rather than to the static pressure P_4 a short distance downstream. The few available observations of the reattachment point in turbulent separations indicate that the difference between P_R and P_4 can amount to the order of 30 per cent of the over-all pressure rise $P_4 - P_2$ through the recompression zone. On the other hand, the recompression along the discriminating streamline within the wake would not be completely isentropic (as is assumed in both analyses) and the disregard of the "losses" which could exist along the dividing streamline during recompression might tend to compensate for the disregard of the pressure rise downstream of the reattachment point. It is possible though that such compensation might not persist to cases where the boundary layer is not thin but is a sizable fraction of the base height. In such cases the pressure rise downstream of the reattachment point may be a much larger fraction of the over-all pressure rise. It will be of interest to hear the author's news on this point.

Author's Closure

The author wishes to thank Dr. Chapman for his discussion in which he points out the close relationship between our researches carried out with differences in emphasis as to laminar and turbulent mixing components. While the author restricted his problem formulation in the paper to transonic and supersonic flows, Fig. 6 showing the curve representing his base-pressure theory extended into the subsonic range confirms the alternate use of the isentropic recompression concept for the adjacent free stream, as was suggested by Dr. Chapman.

The equation for the base-pressure ratio in the form just given

[1] By H. H. Korst, published in the December, 1956, issue of the Journal of Applied Mechanics, Trans. ASME, vol. 78, pp. 593–600.

[2] Aeronautical Research Scientist, National Advisory Committee for Aeronautics, Moffett Field, Calif.

by Dr. Chapman applies directly to the "closed wake" case, where "jet-boundary streamline" and "discriminating streamline" coincide; hence $\varphi_d = \varphi_f$, while for base-pressure problems involving "open wakes," φ_d and φ_f are different. Problems arising from jet-slipstream interaction on propulsive units, where the stagnation conditions of the two streams differ, do not show such a recompression at the end of the wake, which restores the free-stream static pressure.[2] It is interesting to note that the base-pressure theory permits the correct interpretation of "simulated flight" (but stationary) tests of jet engines for free flight conditions.[4]

The author agrees with Dr. Chapman's views concerning the compensating character of two neglected phenomena in the dissipative recompression zone. While a theoretical analysis involving small, but finite, boundary-layer thicknesses resulted in a reasonable correlation of data obtained in a simultaneously conducted experimental program,[5] severe shortcomings must be expected if the "Model of Flow Mechanism," as presented in the paper, is applied to cases where the thickness of the dissipative region is not small compared to any significant length in the wake. This was indeed the reason for the restricting remarks (under iii) of this section of the paper.

Some Effects of Vortex Formation in the Wake of a Suspended Cylindrical Cable[1]

E. A. Richardson.[2] The writer finds that the data of the paper may have value in the study of aeolian vibrations of suspended cables, and should have value in the work of discovering means for minimizing or preventing such oscillations. Unfortunately, this paper is deficient in the data furnished. What is the configuration of the cable used? How was it strung? How were the stress changes during oscillation measured? Were the five groups of men noted workers on this project, or were their data separately obtained, and so on? This sets the experiment in the qualitative rather than the quantitative class and greatly reduces the value of the whole, rather lengthy, investigations.

The writer discovered two methods for limiting or preventing the oscillations of suspension bridges, both of which have proved of merit. Hence the author of this paper should have carried on his work with due regard to the basic principles governing, yet there is no reference to any such work. Within one week after the collapse of the Tacoma Narrows bridge, the Bethlehem Steel Company engineers were given a discussion of the probable process of failure. Later, the writer devised a method for preventing torsional oscillations of suspension bridges (it is not important that the method was invented independently by Dr. D. B. Steinman[3]) and shortly afterward he utilized what is now known as the Strouhal number to devise a more general method of avoiding oscillations. The first invention amounted to taking a system comprising two separate sets of cables and girders supporting a floor between them, capable of torsional or vertical oscillations of the floor, then prevented such torsional oscillations through the interconnection of the cable of one system with the girder of the other at several points spanwise. Hence, if the girder on one side tended to go down while the cable on the other tended to go up, load was at once transferred from the descending girder to the ascending cable, and no torsion could occur (see discussion of Steinman).[4] It had been suggested by the late Dr. Bleich that if a thin bridge floor is kept from torsional oscillations, vertical oscillations also will be largely reduced or prevented.[5] In any case, at a later date, Dr. Steinman used this method in repairing the suspension bridge at Deer Island, Maine, securing a satisfactory repair at a cost very materially lower than that possible by any other method.

The second method for preventing oscillations of suspension bridges was noted in connection with the first[6] as applicable to the center of suspension bridges not well adapted to diagonal suspenders across the roadway.

The second method was based on the fact that the Strouhal number, $S = fd/v$, is a function, possibly, of section shape and certainly of the dimension d. Hence it should be possible to divide any wirelike structure into a number of substantially equal segments longitudinally, then insure, by a combination of shape and d modifications, that alternate or odd-numbered segments should have one period, even-numbered another, so that the rate of vortex emission between adjacent segments would tend to nullify a tendency to set up vibrations. It was merely suggested that the bridge center[6] should differ in width from the ends, as it did not seem practicable to use this method alone on a bridge (see also footnote 8).

This method has been used successfully in the prevention of oscillations in pipeline suspension bridges. In fact, the Fluor Corporation has secured a patent upon the very special arrangement used by them.[7] The writer of the paper describing the work gives Steinman as reference.[5,4]

To return to the paper under discussion: It becomes of importance to see whether a strung wire or cable can be adapted to our second solution of the aeolian-vibration problem. Hence the wire would be divided into a relatively large number of segments to meet the highest number of nodes to be expected. It becomes essential to know (and this paper does not help us as given) whether a rough cable in the odd-numbered segments can be neutralized, oscillationwise, by a smooth cylindrical wrapping in the even-numbered segments. The adjacent sections should differ in frequency over the whole range of Reynolds numbers to be expected. It might be necessary to use a light, rather thick wrapping to enhance d by 10 to 20 per cent, or perhaps even more, supposing that the rough cable and the smooth cylinder had substantially the same Strouhal number. This would be particularly

---

[2] Korst, H. H., and Wilson Tripp, "The Pressure on a Blunt Trailing Edge Separating Two Supersonic Two-Dimensional Air Streams of Different Mach Numbers and Stagnation Pressures, but Identical Stagnation Temperatures," presented at the Midwest Conference on Solid and Fluid Mechanics, University of Michigan, Ann Arbor, Mich., April 1–2, 1957.

[4] "Some Aerodynamic Considerations of Nozzle-Afterbody Combinations," Cortright, E. M., Jr., presented at the 42nd Annual Meeting of the Institute of the Aeronautical Sciences, Jan. 23–26, 1956, Preprint No. 614.

[5] "The Influence of Finite Bleed Velocities on the Effectiveness of Base Bleed in the Two-Dimensional Supersonic Base Pressure Problem," by C. Y. Wu, and H. H. Korst, presented at the Midwest Conference on Solid and Fluid Mechanics, University of Michigan, Ann Arbor, Mich., April 1–2, 1957.

[1] By R. F. Steidel, Jr., published in the December, 1956, issue of the Journal of Applied Mechanics, Trans. ASME, vol. 78, pp. 649–650.

[2] Technical Engineer, Bethlehem Steel Company, Bethlehem, Pa.; also, Partner, Firm of Edward (Nellie) & George Richardson, Bethlehem, Pa. Mem. ASME.

[3] "Rigidity and Aerodynamic Stability of Suspension Bridges," by D. B. Steinman, Paper No. 2243, reprinted from Trans. ASCE, vol. 110, 1945, pages 439 and so on, particularly p. 471.

[4] Ibid., p. 484, discussion of Steinman.

[5] "Dynamic Instability of Truss-Stiffened Suspension Bridges Under Wind Action," by Dr. Friedrich Bleich, Report No. 12, to American Institute of Steel Construction, Inc., New York, N. Y., December, 1946, p. 46.

[6] See footnote 3, p. 485.

[7] "Wind-Induced Vibrations of a Pipeline Suspension Bridge and Its Cure," by R. C. Baird, Trans. ASME, vol. 77, 1955, p. 797.

necessary if, in the Reynolds working range, the two sections should acquire substantially the same number. Unfortunately, the paper under discussion does not give information in a form useful for our purpose, or for that of the authors.

It is not impossible that three wires of a transmission line might be interconnected by straight, transverse, insulated rods at a number of points spanwise so as to secure a measure of the Richardson-Steinman method of preventing or reducing oscillations, utilizing the bending stiffness of the rods to limit movement. In such a case, at least one of such a group of possibly three wires should differ in diameter from the others so as to secure some of the benefits of the second Richardson method.

Although the writer's primary publication reference is to work in 1945,[4,5] publication in part occurred earlier and should have been available to all suspension-bridge engineers.[6]

In passing, the alternate sections should have different icing tendencies, if practicable, to avoid changes in form which would destroy the utility of the methods proposed. The covered sections could be "treated" during the stringing operation. It is not impossible to prepare the wire at the factory provided the wrapped sections are able to re-expand on stringing. Obviously, if oscillations are kept minor, there will be no serious vibrational stresses or strains.

Author's Closure

Mr. Richardson's criticism of the paper's brevity is certainly warranted. As originally presented, the article was more complete but was cut to be accommodated in the Brief Notes section of the *Journal*. For the sake of clarification, a selected bibliography is included giving the references cited in Fig. 1.

Mr. Richardson's remarks on suspension bridges are welcome and interesting. It must be understood that the oscillation of suspension bridges and the vibration of transmission-line cables are different phenomena. The oscillation of suspension bridges is an example of aerodynamic instability and is a self-excited vibration. The vibration of transmission-line cables induced by the regular shedding of von Karman vortexes in the wake of the cable is a forced vibration. The two phenomena are only vaguely related.

The paper presents a qualitative account of a somewhat exhaustive study of the aeolian vibration of a transmission-line cable. The cable used was aluminum cable, steel reinforced, 1.108 in. in diam. The cable was strung in a manner conventional to transmission-line practice. The strain measurements were made with type A-7 SR-4 resistance wire strain gages mounted directly on individual aluminum strands. Recording of strain variations was accomplished with a Sanborn recording oscillograph. The presentation of the data in terms of the dimensionless combination of frequency, wind velocity, and cable diameter is quite ordinary. This combination has been known as the Strouhal number for three quarters of a century.

It is interesting to note that, while the interconnection of adjoining electrical phases by insulated rods to secure a measure of the Richardson-Steinman method of preventing or reducing oscillations is not practical, in the current design of "double conductor" transmission lines the "spacers" being used between the two cables of any one electrical phase may offer the same result.

BIBLIOGRAPHY

"Über eine besondere Art der Tonerregung," by V. Strouhal, *Annalen der Physik und Chemie*, vol. 5, 1878, pp. 216–251.

"The Singing of Circular and Streamline Wires," by E. F. Relf and E. Ower, Aeronautical Research Committee Reports and Memoranda No. 825, March, 1921.

"The Frequency of Eddies Generated by the Motion of Circulars Through a Fluid," by E. F. Relf and L. F. G. Simmons, Aeronautical Research Committee Reports and Memoranda No. 917, June, 1924.

"Vortex Formation Behind Obstacles of Various Sections," by E. Tyler, *Philosophical Magazine*, vol. 11, 1931, pp. 849–890.

"The Strength and Position of the Eddies Behind a Circular Cylinder," by A. Thom, Aeronautical Research Committee Reports and Memoranda No. 1373, December, 1930.

"Hot-Wire Investigation of the Wake Behind Cylinders at Low Reynolds Numbers," by L. S. G. Kovasznay, Proceedings of the Royal Society of London, vol. 198 A.

[6] "Suspension Bridge Oscillations and Failure," by E. A. Richardson, a report to Advisory Board on Suspension Bridges, Bureau of Public Roads, Federal Works Agency, November 13, 1943 (although originally prepared and dated July 28, 1943), pp. 28 and 31.

Minimum Weight Design of Cylindrical Shells[1]

P. G. Hodge, Jr.[2] The author has presented a most interesting technique for the design of a circular cylindrical shell under arbitrary loading. However, it is not entirely evident that this technique will result in a shell of minimum weight. Indeed, if the same technique is applied to a simpler design problem, namely, that of a simply supported cylindrical shell under uniform pressure and without end load, it can be demonstrated that the resulting design is definitely not one for minimum weight.

For the example in question, the axial resultant N_x is equal to zero, so that only the resultants M_x and N_φ need be considered. The resulting yield curve was first obtained by Drucker[3] and is shown as the solid curve in Fig. 1 of this discussion. Evidently the only "corners" permitting multiple-flow mechanisms are the points A and D. Therefore, if the pressure is external, it follows from the author's criterion that the entire shell must be in regime A. Substituting the values

$$N_\varphi = N_0 = \sigma_0 h, \quad M_x = 0$$

into the equilibrium equation

$$M_x + N_\varphi/R + p = 0 \qquad [1]$$

we obtain the constant thickness

$$h = h_m = pR/2\sigma_0 \qquad [2]$$

or the shell. This result is a special case of that previously obtained by Onat and Prager (author's reference 4).

However, we may obtain a constant-thickness shell of less weight which will support the same load p. To this end, we observe first that if a shell is designed according to any yield curve lying wholly within the actual yield curve, it will support the applied load. This follows from the first theorem of limit analysis (author's reference 5). Therefore we shall first solve the analysis problem based upon the inscribed hexagon shown as the dotted curve in Fig. 1. Using the methods introduced by Drucker[3] and the writer,[4] we can easily find the complete solution to this problem in the form

[1] By Walter Freiberger, published in the December, 1956, issue of the Journal of Applied Mechanics, Trans. ASME, vol. 78, pp. 576–580.

[2] Professor of Applied Mechanics, Polytechnic Institute of Brooklyn, Brooklyn, N. Y.; now at Illinois Institute of Technology, Chicago, Ill. Mem. ASME.

[3] "Limit Analysis of Cylindrical Shells Under Axially Symmetric Loading," by D. C. Drucker, Proceedings of the First Midwest Conference on Solid Mechanics, Urbana, Ill., 1952, Engineering Equipment Station, University of Illinois, Urbana, Ill., 1953, pp. 158–163.

[4] "The Rigid Plastic Analysis of Symmetrically Loaded Cylindrical Shells," by P. G. Hodge, Jr., Journal of Applied Mechanics, Trans. ASME, vol. 76, 1954, pp. 336–342.

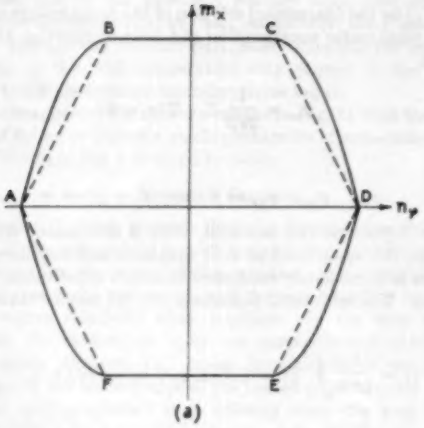

———Actual
- - - Approximate

FIG. 1 TWO-DIMENSIONAL YIELD CURVES

$$M_x = \frac{\sigma_0 h^2}{4} \cdot \frac{\cos(cx/L) - \cos c}{1 - \cos c}$$

$$N_\varphi = (2M_x/h) - \sigma_0 h \quad w = w_0 \sin c(1 - x/L) \quad \ldots\ldots [3]$$

when the load p is given by

$$\frac{p}{2\sigma_0}\left(\frac{R}{L}\right)^2 = \frac{1}{c^2}\left[1 + \frac{\cos c}{2(1 - \cos c)}\right] \quad \ldots\ldots [4]$$

and c is a parameter of the shell given by

$$c^2 = L^2/ah \quad \ldots\ldots [5]$$

This solution is valid for all $0 \leq c \leq \pi/2$. For $c > \pi/2$ it can be shown that the result given by Equation [2] is again obtained.

To use these results for the design problem, it is merely necessary to regard p as given and use Equation [4] to determine h. Fig. 2, herewith, shows the resulting shell thickness as a function of load according to Equation [4]. Also shown is the design prescribed by Equation [2]. Evidently, if $p > \sigma_0(L/R)^2$, the suggested procedure leads to a smaller thickness. Further, the total weight of the uniform shell is proportional to its thickness so that Fig. 2 also gives the weights according to the two theories.

The foregoing analysis was based upon a conservative approximation rather than upon the true yield curve. Also, only shells of uniform thickness were considered. For these reasons it is unlikely that Equation [4] is the true solution of the minimum-weight problem. However, we have shown that, in this particular example, the rather plausible reasoning used by the author in establishing a criterion for minimum weight is invalid. This being so, the more complex examples considered by the author also must be viewed with suspicion.

AUTHOR'S CLOSURE

It should be observed that the curve of Fig. 2 of the discussion is plotted in a most misleading manner. Professor Hodge's solution differs from that based on the heuristic criterion of the paper only for shells for which

$$\frac{L^2}{a^2} < 2.47\,\frac{h}{a}$$

that is, for such short and thick shells as to be practically without

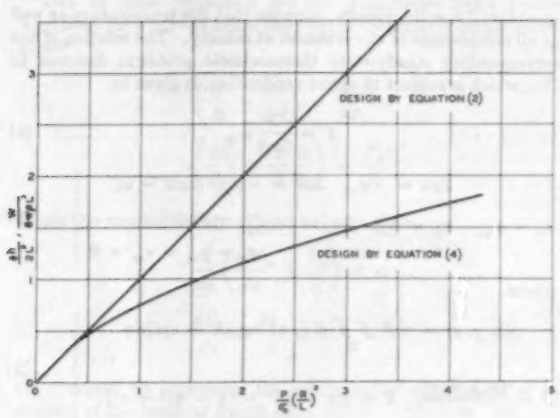

FIG. 2 MINIMUM-WEIGHT DESIGN OF UNIFORM SHELLS

importance for any plastic-rigid shell theory. In spite of this fact, those portions of the curves which show disagreement between the results are plotted to occupy over 80 per cent of the range, and the vast area of agreement is made to appear minute by being confined to a small neighborhood of the origin. It has yet to be shown that, especially for more complicated problems, with end load, where a simple analysis such as given in the discussion is not readily possible, the method of the paper does not lead to useful results; the above discussion demonstrates its practical usefulness even in such simple problems as that given by Professor Hodge. Since he uses a yield-curve different from the more accurate one of the paper, precise deductions as to the nature of the disagreement regarding extremely short and thick shells are impossible.

Thermal Stresses in Infinite Elastic Disks[1]

W. T. KOITER[2] AND E. STERNBERG.[3] This paper, hereinafter referred to as (A), is chiefly concerned with the axisymmetric steady-state thermoelastic problem appropriate to a region bounded by two parallel planes, for which a formal solution in terms of Fourier-Bessel integrals is established. In this connection it may be of interest to cite certain results from a related paper,[4] hereinafter referred to as (B), which deals by different means with the general (not necessarily axisymmetric) limiting case of the half-space.

In (B) the problem is approached on the basis of the method of Green's functions. Let $z \geq 0$ be the region occupied by the medium, let the body forces and surface tractions be absent, and let $f(x, y)$ be the given distribution of surface temperature, where $f(x, y) = 0$ outside a subregion Σ (region of exposure) of the

[1] By Brahmadev Sharma, published in the December, 1956, issue of the JOURNAL OF APPLIED MECHANICS, Trans. ASME, vol. 78, pp. 527–531.

[2] Professor of Applied Mechanics, Technische Hogeschool, Delft.

[3] Professor of Mechanics, Division of Applied Mathematics, Brown University; currently Visiting Professor, Technische Hogeschool, Delft. Assoc. Mem. ASME.

[4] "On the Steady-tSate Thermoplastic Problem for the Half-Space," by E. Sternberg and E. L. McDowell, *Quarterly of Applied Mathematics*, vol. 14, 1957, p. 381.

boundary,[5] $z = 0$. Finally, suppose that the temperature as well as all components of stress vanish at infinity. The solution of the corresponding steady-state thermoelastic problem, deduced in (B), which is subject to direct verification, is given by

$$T = \frac{1}{2\pi\beta}\varphi_{zz} \quad \ldots [1]$$

$$\left.\begin{aligned} 2\mu u = -\varphi_{xz}, \quad 2\mu v = -\varphi_{yz}, \quad 2\mu w = \varphi_{z} \\ \sigma_x = \varphi_{yy}, \quad \sigma_y = \varphi_{xx}, \quad \tau_{xy} = -\varphi_{xy}, \\ \sigma_z = \tau_{xz} = \tau_{yz} = 0 \end{aligned}\right\} \quad \ldots [2]$$

where

$$\left.\begin{aligned} \varphi(x, y, z) = -\beta \int\int_{\Sigma} f(\xi, \eta) \log (R + z) d\xi d\eta \\ \beta = \frac{\alpha\mu(1 + \nu)}{\pi}, \quad R = [(x - \xi)^2 + (y - \eta)^2 + z^2]^{1/2} \end{aligned}\right\} \quad \ldots [3]$$

Here subscripts attached to φ denote partial differentiation and the notation is otherwise the same as in (A). The function φ is Boussinesq's three-dimensional logarithmic potential for a disk coincident with Σ, the mass density of which is proportional to the prescribed surface temperature $f(x, y)$.

Closed explicit representations for φ are available corresponding to several physically significant choices of $f(x, y)$. Thus (B) contains closed solutions in terms of elementary functions for a uniform distribution of temperature over a rectangular region of exposure and a hemispheroidal (Hertzian) distribution of temperature over a circular region of exposure; it also contains a closed solution, in terms of elliptic integrals of the first and second kind, for a circular region of exposure at constant temperature. This last solution is represented in (A) by means of infinite series of hypergeometric functions.

Equations [1], [2], [3] of this discussion at once permit certain general conclusions which may go unnoticed in the analytically less transparent representations given in (A), or might erroneously be attributed to the presence of rotational symmetry:

1 The stress distribution induced by an arbitrary distribution of surface temperatures, in the steady state, is plane and parallel to the boundary (though dependent on z). Indeed, φ is evidently the Airy function belonging to the resulting two-dimensional field of thermal stress. Equation [36] of (A) is, therefore, not accidental. This severe degeneracy inherent in the solution to a three-dimensional problem has its two-dimensional counterpart in the trivial plain-strain solution for the analogous problem of the half-plane which is characterized by a uniaxial, i.e., one-dimensional, field of thermal stress.

2 All components of displacement and stress in Equations [2] are harmonic for $z > 0$. In view of a general theorem[6] we may, in turn, conclude that the maximum resultant displacement, the largest tensile stress, the largest compressive stress, as well as the absolute maxima of the total strain-energy density and of the energy densities of volume change and of distortion, all occur on the boundary.

It is not difficult to show that the foregoing two conclusions remain valid in the analogous steady-state problem for a body bounded by two parallel planes ($z = \pm t$), provided the body forces and surface tractions, together with the temperature and stresses at infinity, are again required to vanish. Indeed, let $T(x, y, z)$ be the (harmonic) solution of the temperature problem for the plate under consideration and define a function $\varphi(x, y, z)$ through

$$\varphi_{zz} = \frac{1}{2\pi\beta} T, \quad \nabla^2\varphi = 0 \quad \ldots [4]$$

with

$$\varphi_{zz}, \quad \varphi_{xz}, \quad \varphi_{yz} \to 0 \quad \text{as} \quad x^2 + y^2 \to \infty \quad \ldots [5]$$

Then Equations [2], herewith, with φ determined by Equations [4], [5], again meet all field equations and boundary conditions, as is immediately confirmed by direct substitution and inspection. The solution of Equations [4], [5] may be taken in the form

$$\varphi(x, y, z) = \frac{1}{2\pi\beta}\int_0^z (z - \zeta) T(x, y, \zeta) d\zeta + z\varphi_1(x, y) + \varphi_0(x, y) \quad \ldots [6]$$

where φ_0 and φ_1 satisfy

$$\nabla^2\varphi_0 = -\frac{1}{2\pi\beta} T(x, y, 0), \quad \nabla^2\varphi_1 = -\frac{1}{2\pi\beta} T_z(x, y, 0) \quad \ldots [7]$$

and must conform to Condition [5].

[5] If Σ is not bounded, assume that $f(x, y) = O(\rho^{-\epsilon})$ as $\rho^2 = x^2 + y^2 \to \infty$.

[6] "Liegt die Stelle der grössten Beanspruchung an der Oberfläche?" by G. Pólya, *Zeitschrift für angewandte Mathematik und Mechanik*, vol. 10, no. 4, 1930, p. 353.

Velocity, Temperature, and Heat-Transfer Measurements in a Turbulent Boundary Layer Downstream of a Stepwise Discontinuity in Wall Temperature[1]

J. P. HARTNETT.[2] The author indicates that the hydrodynamic boundary layer was essentially unaffected by the small amount of heating used in the test section. If this is the case, the significant length parameter should be the distance measured from the initiation of the hydrodynamic boundary layer, say from the boundary-layer tripper location. This would change Equation [22] and shift the scale in Figs. 4 and 9 of the paper.

[1] By D. S. Johnson, published in the March, 1957, issue of the JOURNAL OF APPLIED MECHANICS, Trans. ASME, vol. 79, pp. 2–8.

[2] Associate Professor, Department of Mechanical Engineering, Institute of Technology, University of Minnesota, Minneapolis, Minn. Mem. ASME.

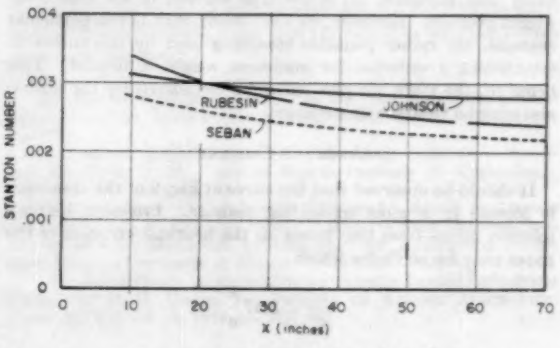

FIG. 1 STANTON NUMBER ALONG PLATE

In the case of the thermal boundary layer, two significant length parameters should be used; essentially, the x used by the author and another distance parameter indicating the location of the step in the wall temperature with respect to the position where the hydrodynamic boundary layer began.

A comparison of the author's results in Fig. 11 with the predictions of Seban or Rubesin would perhaps be of some interest, and this is shown in Fig. 1 of this discussion.

Author's Closure

Professor Hartnett suggests that the distance from the virtual origin of the momentum boundary layer is a significant length parameter for the configuration studied. This would be especially true if the momentum and thermal boundary layers had their origins relatively close together. In the case studied, however, the momentum layer was purposely originated a relatively great distance, i.e., many boundary-layer thicknesses, upstream of the leading edge of the heated plate in order to have a thick, well-established state existing when the step in wall temperature occurred. The virtual origin of the momentum layer will, of course, be somewhat upstream of the tripper.

As noted in the paper, Equation [22] is a simple power-law fitting of the experimental data for points along the heated plate only. An extrapolation of this relation upstream to the vicinity of the origin of the boundary layer would hardly be justifiable because it would extend over a distance more than twice the length of the plate itself. The abscissas of Figs. 4 and 9, being dimensional, would be unaffected by any translation of the origin for the z-co-ordinate used.

The Mathematical Analysis of Bow Girders of Any Shape[1]

Enrico Volterra.[2] The analysis of symmetrical arc-bow girders of any shape rigidly fixed at both ends carrying a uniformly distributed load w per unit length, considered by the author, admits a general solution in the cases in which the central line of the curved beam is a cycloid, a catenary, or a parabola. In fact, in these cases the results for the deflections, angles of twist, bending and twisting moments can be expressed in closed form. This is shown in a recent paper[3] of mine, where also curves of the deflections, angles of twist, bending and twisting moments are presented for certain cases, and are compared with the corresponding values for the simpler case of the bow girder of circular shape.

A more general method of approach than the one described by the author must then be applied. In fact, four differential equations connecting the bending moment M_z, the torque T_z, the deflection v, the twisting angle β, the initial curvature R of the central line of the beam, its inertia EI_x, and torsional characteristics K, and the external uniformly distributed load w have to be used.

Two of these equations are the well-known Saint Venant equations for a curved beam bent out of its plane of initial curvature[4,5]

$$\left.\begin{aligned}\left(\frac{\beta}{R}-\frac{d^2v}{ds^2}\right)&=\frac{M_z}{EI_x}\\ \left(\frac{d\beta}{ds}+\frac{1}{R}\frac{dv}{ds}\right)&=\frac{T_z}{K}\end{aligned}\right\}\quad\ldots\ldots\ldots\ldots[1]$$

While the two subsidiary differential equations

$$\left.\begin{aligned}\frac{d}{ds}\left(\frac{dM_z}{ds}+\frac{T_z}{R}\right)&=w\\ \frac{dT_z}{ds}-\frac{M_z}{R}&=0\end{aligned}\right\}\quad\ldots\ldots\ldots\ldots[2]$$

are obtained by expressing the conditions of equilibrium of an element of the beam of length ds.

The conditions of fixity of both extremities of the beam imply the following boundary conditions

$$\beta(\pm l)=v(\pm l)=\frac{dv(\pm l)}{ds}=0\quad\ldots\ldots\ldots\ldots[3]$$

$2l$ representing the total length of the bar.

In the particular cases in which the central line of the bow girder is a cycloid, a catenary, or a parabola, the relationships between radius of curvature R at a generic point of the central line, whose normal makes the angle φ with the axis of symmetry of the beam, and the curvature R_0 at the central point are expressed by the following simple formulas

$$\left.\begin{aligned}&\text{for the cycloid}\quad R=R_0\cos\varphi\\ &\text{for the catenary}\quad R=\frac{R_0}{\cos^2\varphi}\\ &\text{for the parabola}\quad R=\frac{R_0}{\cos^3\varphi}\end{aligned}\right\}\quad\ldots\ldots\ldots[4]$$

By substituting Equations [4] into Equations [1] and [2], the differential equations can be integrated and the functions M_z, T_z, v, and β, expressed in closed form.

By using the same method it should also be possible to give the general solution for the cases of arc-bow girders whose central axes are cycloids, catenaries, or parabolas submitted to a concentrated load. This was already done in the particular case of the arc-bow girder of circular shape under the action of a concentrated load.[6]

---

[1] By M. M. Abbassi, published in the December, 1956, issue of the Journal of Applied Mechanics, Trans. ASME, vol. 78, pp. 522–526.

[2] Professor of Mechanics, Rensselaer Polytechnic Institute, Troy, New York.

[3] "On the Deflections of Bow Girders of Non-Circular Shapes" by E. Volterra. Paper 870, Journal of the Engineering Mechanics Division, Proceedings of the American Society of Civil Engineers, vol. 82, January, 1956, pp. 1–24.

[4] "Mémoire sur le calcul de la résistance et de la flexion des pièces solides à simple ou à double courbure, en prenant simultanément en considération les divers efforts auxquels elles peuvent être soumises dans tous les sens," by Barré de Saint-Venant, *Comptes-Rendus de l'Académie des Sciences de Paris*, vol. 17, 1843, pp. 942–954, 1020–1031.

[5] "Strength of Materials—Advanced Theory and Problems—Part II," by S. Timoshenko, Macmillan and Co., New York, N. Y., 1936, pp. 467–473.

[6] "Deflections of a Circular Beam out of its Initial Plane," by E. Volterra, Paper No. 2727, Transactions of the American Society of Civil Engineers, vol. 120, 1955, pp. 65–91.

Book Reviews

Stresses in Aircraft Structures

STRESSES IN AIRCRAFT AND SHELL STRUCTURES. By Paul Kuhn. McGraw-Hill Publications in Aeronautical Sciences, McGraw-Hill Book Company, Inc., New York, N. Y., 1956. $14.

REVIEWED BY N. J. HOFF[1]

UNTIL about thirty years ago airplane structures consisted mainly of simple and continuous beams and of frameworks. In their analysis the well-established methods of structural engineering based essentially on equilibrium considerations and on the elementary concept of the continuous deformations of beams and frameworks could be used in a satisfactory manner. In the late 1920's reinforced thin-walled monocoque structures were introduced, and in the early 1930's they were generally adopted in airplane structural design. These structures are thin shells heavily reinforced both in the longitudinal and the circumferential directions.

Experiments carried out with the relatively flexible thin-walled monocoques showed that the stress distribution in them could not be predicted by the established methods of structural analysis. At the same time the complexity of the structural arrangement precluded the use of the rigorous methods of the theory of elasticity. For this reason a procedure intermediate between elementary engineering stress analysis and the rigorous theory of elasticity had to be developed. This development took place simultaneously in all the major airplane-building countries and was based heavily on experimental evidence produced in government research laboratories. Significant contributions to the development were made in the Langley Memorial Aeronautical Laboratory of the National Advisory Committee for Aeronautics at Langley Field, Va.; and Paul Kuhn, the author of the book, made many personal contributions to this work during his thirty years of service in the Laboratory. His book summarizes a great deal of the information that became available in this field through a judicious use of empiricism and theoretical considerations. Much of this information has been published only in the technical notes and reports of the NACA.

The fundamental assumption underlying most of the methods presented in the book is that normal stresses are carried only by the reinforcing elements of the shell, while the thin wall of the shell is capable of transmitting only shear stresses. A consequence of this assumption is that the shear stress must be constant in every panel bordered by two adjacent stringers and two adjacent rings. This assumption simplifies the analysis to a great extent. It is discussed in the first 44 pages of the book, together with the elementary theories of bending based on the Bernoulli-Navier assumptions and the Bredt-Batho theory of torsion. The next 50 pages are taken up with a lucid presentation of the theory of diagonal tension. This theory was originally proposed by Herbert Wagner in 1927. It is based on the assumption that a thin sheet subjected to shearing stresses buckles and develops deep bulges long before the structure fails under the loads. The existence of a uniaxial field of tension in the sheet again permits a significant simplification of the stress problem of the structure.

The following 200 pages deal with shear lag and load diffusion problems in continuous structures into which concentrated loads are introduced and in structures with large cutouts where the simple pattern of stress distribution is disturbed by the discontinuities in the structural elements. The method of attack consists of the establishment of a simple engineering stress distribution in a first approximation, and the calculation of perturbation stresses that are superimposed upon this stress distribution in consequence of the shear deformations of the elements in the neighborhood of concentrated loads and through the disturbance of the stress pattern in the neighborhood of the cutouts.

An unusual feature of the book is the description of experimental methods and the publication of detailed experimental data on the last 100 pages. The author presents an experimental verification of all the theories that are based on more or less arbitrary assumptions. Throughout the book the analytical methods used are relatively simple. Equilibrium considerations are augmented by straightforward geometric considerations of the continuity of deformations. From these, either simple differential equations are derived or use is made of the minimal principles of the theory of elasticity.

The presentation is oriented toward the practical engineer working in industry and not toward the research scientist exploring unknown stress problems at his desk or in the laboratory. The methods presented have been tried out, as a rule, both at Langley Field and by the stress analysis groups of the airplane industry. Both the methods of analysis presented and the empirical data will be of great value to all analysts of the conventional thin-walled monocoque-type structures of aircraft. They will also be useful to civil engineers who are interested in saving weight and in replacing some of their heavy conventional structures by the lighter aeronautical type of construction.

[1] Head, Division of Aeronautical Engineering, Stanford University, Stanford, Calif. Mem ASME.

Fundamentals of Vibration Analysis

FUNDAMENTALS OF VIBRATION ANALYSIS. By N. O. Myklestad. McGraw-Hill Book Company, Inc., New York, N. Y., 1956. Cloth, 9¼ × 6¼ in., viii and 260 pp., illus. $6.50.

REVIEWED BY LAWRENCE E. GOODMAN[2]

IT IS a pleasure to welcome an elementary treatment of mechanical vibrations from the hand of an authority in the field. The present volume is intended as a text for undergraduates at technical schools in the United States. It presumes on the part of the student an understanding of the elements of rigid and deformable-body mechanics, calculus, and ordinary differential equations. Throughout the text the mathematical techniques employed are the simplest consistent with a complete physical statement of the problem at hand. No reference is made to the application of the Laplace transform, the phase-plane diagram, or complex number representation of vibrations.

In the first three chapters the free and forced vibrations of single-degree-of-freedom systems are developed systematically, and the effect of viscous damping is then considered. This material occupies half of the book. Each topic is introduced by means of a simple physical situation. After the basic analysis has been carried out, special cases of technical interest are covered by means of examples. The lucid treatment of the critical speeds of shafts and the sections on vibration measuring instru-

[2] Professor of Mechanics, University of Minnesota, Minneapolis, Minn.

ments and on vibration isolation are especially noteworthy. Here the author's engineering experience makes itself felt. On the other hand, his claim to have treated transient vibrations in considerable detail seems to the reviewer to be misleading. True enough, one can count some seventeen pages dealing with this subject, but the material does not appear to have been organized so as to leave the student with a coherent picture of the response of simple structures to forces of short duration.

After a brief bow to nonviscous damping, the second half of the text treats the vibration of systems having more than one degree of freedom, with and without viscous damping. Many will be glad to learn that generalized co-ordinates and Lagrange's equations are developed at this point. The student is thereby introduced to a powerful tool of analytical mechanics which makes possible a unified treatment of the subject. Rayleigh's method, in the reviewer's opinion, might better have been taken up at this point than in the introductory material of Chapter II. The book closes with a clear presentation of the Holzer and Myklestad methods for finding natural frequencies of torsional and lateral modes of vibration of bars.

This is not intended to be a reference book. It contains the material, and essentially only that material, necessary for a first course in mechanical vibrations, presented in a straightforward literary style. The text is commendably free of error. An excellent collection of problems accompanies each section. After working about one quarter of these, the reviewer has found only one error, no. 21-4, in the answers given.

Any text at the level of a first course requires selection of illustrative material. It is perhaps a matter of personal preference which of several alternative peripheral topics are to have their claims recognized. In place of the detailed treatment of the balancing of rotors, this reviewer would have preferred an elementary introduction to stability analysis, some mention of the phase-plane diagram, and a treatment of the commonly used complex number notation. These are matters which tomorrow's engineer should encounter during his training.

Combustion Gases

PROPERTIES OF COMBUSTION GASES—SYSTEM C_nH_{2n}—AIR. VOLUME I. THERMODYNAMIC PROPERTIES. VOLUME II, CHEMICAL COMPOSITION OF EQUILIBRIUM MIXTURES, Aircraft Gas Turbine Development Department, General Electric Company, Cincinnati, Ohio, New York, McGraw-Hill Book Company, Inc. Copyright, 1955. Two volumes (not sold separately). Vol. I, 432 pp.; Vol. II, 676 pp., 10⅞ × 8½ in. $75.

REVIEWED BY JOSEPH KAYE[1]

IN THE brief span of the past two decades, the engineering profession has witnessed the development and rapid growth of a host of new power plants based on the use of high-temperature combustion gases. These power producers include the gas turbine and its variations, jet engines such as the turbojet, ramjet, pulsejet, etc., many kinds of rocket engines, and various combinations of these. For effective design and development of these power plants the engineer has been forced to pay more and more attention to the thermodynamic problems inherent in the dissociation processes which occur in the working fluids at high temperatures and low pressures. However, as the engineer attacks the thermodynamic problems of dissociating gases, he is confronted with a vast computing problem which is greater by at least two orders of magnitude than the corresponding problem of computation of processes for gases where dissociation can be safely ignored. The availability of high-speed computers has provided a solution to this situation. It is interesting to recall that Hershey, Eberhardt, and Hottel published in 1936 the first set of useful charts in this country which allowed for the effects of dissociation of the working fluid at high temperatures.

Since 1936, other charts have been published in this country and abroad, but none of these present properties of combustion gases in such great detail as found in the tables of the two volumes of "Properties of Combustion Gases—System C_nH_{2n}—Air." These tables are limited to the system of C_nH_{2n} and air, but the tabulated properties and composition of the equilibrium mixtures are based on the presence of the following fifteen individual constituents: A, C (graphite), CO, CO_2, H_2, H_2O, O_2, N_2, H, OH, O, N, NO, CH_4, and NH_3. For this multicomponent system the equilibrium composition was computed from equilibrium constants for reactions of the above species, except for A, by means of an IBM 701 Computer. Having found the equilibrium composition for a given temperature, pressure, and fuel-air ratio, the properties of the mixture were computed from tables of properties of the individual species, assuming that "taken separately, each of these fifteen constituents obeys the ideal gas law, excepting of course graphite." A second assumption, not specifically mentioned by the authors, was that the mixture is a Gibbs-Dalton mixture. The properties of the mixture do not take into account the departures of either the individual gases or of the mixture from ideal-gas behavior for any fixed composition as a function of pressure; i.e., an equation of state comparable to the Beattie-Bridgman equation was not used to evaluate properties of constituents or of the mixture.

The results of these extensive computations are tabulated in terms of the three independent variables: fuel-air ratio, temperature, and pressure. The dependent quantities include the equilibrium composition, enthalpy, entropy, molecular weight, density, equilibrium sonic velocity, frozen sonic velocity, specific heat at constant pressure, isobaric derivative of molecular weight with temperature, and isothermal derivative of molecular weight with pressure.

Volume I tabulates the above thermodynamic properties for fuel-air equivalence ratios (actual fuel-air ratio divided by stoichiometric fuel-air ratio) of 0.25, 0.50, 0.7, 0.8, 0.9, 1.0, 1.1, 1.2, 1.5, 1.75, 2.0, 2.5, 3.0, 3.5, and 4.0, for temperatures from 600 to 5000 R in 100 intervals, for pressures of 0.01, 0.1, 1.0, and 10.0 atm in the range of 600 to 2500 R and of 0.01, 0.015, 0.02, 0.03, 0.05, 0.075, 0.10, 0.15, 0.20, 0.30, 0.50, 0.75, 1.0, 1.5, 2.0, 3.0, 5.0, 7.5, 10, 15, 20, and 30 atm in the range of 2,500 to 5000 R. These tables require 377 pages. Volume I also contains some fifty pages of descriptive material, comprising discussions of sources of data and accuracy, symbols and definitions, notes on interpolation with respect to temperature, pressure, and fuel-air equivalence ratio, and several detailed applications illustrating the use of the tables. Special attention is given to the details of one, two, and three-way interpolations when an actual problem requires that one enter these tables at values of the independent variables different from those listed.

Volume II contains the chemical compositions for equilibrium mixtures of the fifteen species listed previously for the same values of the fuel-air equivalence ratios and pressures given in Volume I. However, these compositions are given only for the temperature range of 2500 to 5000 R instead of from 600 to 5000 R, in order to conserve space. These tables of chemical compositions require 660 pages of Volume II. The first 17 pages of Volume II present the enthalpy function $H_i°/RT$, free-energy function $G_i°/RT$, entropy function $S_i°/RT$, and heat-capacity function $C_{pi}°/RT$, for each of the 15 species over range of temperature from 600 to 5000 R, at intervals of 100 deg.

These tables of properties of combustion gases for the system C_nH_{2n} and air constitute a significant contribution to the engineering field. They represent a product, resulting from the use

[1] Professor of Mechanical Engineering, Massachusetts Institute of Technology, Cambridge, Mass. Mem. ASME.

of high-speed computing machines, which has been made available to the engineering profession in general. They emphasize the complexity and tedious nature of design calculations when one wishes to employ multicomponent systems at high temperatures. If one has available a high-speed computing machine of large storage capacity, then these tables form a valuable adjunct to the designer for many new power plants using working fluids based on this particular multicomponent system.

It seems fairly obvious that these tables were not intended for use by students in engineering schools. One can also note that the total of 1054 pages of tables in Volumes I and II could have been reduced to about 300 pages of tables, containing the same number of entries, if the entries had been set in type of the size used in the "Thermodynamic Properties of Steam" or in "Gas Tables." Such a reduction in size would considerably enhance the use of these tables by the engineering profession since it would result in a single volume of these tables at significantly less cost.

Several questions arise on careful examination of these two volumes. One wonders why the effects of pressure on the departure of the individual species from ideal-gas behavior were not included, especially in view of the fact that a high-speed computer was available to handle the detailed calculations, and that sufficient data and estimates are available to include this effect. The reader also questions the applicability of these tables to other carbon-hydrogen ratios—how much variation from C_2H_2 will result in serious design errors? A discussion of this variation would appear necessary for other applications. One also wonders about the effects of ionization of the many species present, especially at the higher temperatures of 5000 R, and for extrapolations to even higher temperatures. If the tables of Volume II are examined, it will be noted that only minute amounts of some of the fifteen species are present at temperatures near 5000 R; ionization of some of these fifteen species will likewise introduce small amounts of ionized species at temperatures near 5000 R or above, and one wonders how significant are the contributions of these ionized species to the tabulated values of enthalpy, entropy, etc.

Creep and Fracture of Metals at High Temperature

PROCEEDINGS of a Symposium Held at the National Physical Laboratory, 31st May–2nd June, 1954. Her Majesty's Stationery Office, London, 1956. Cardboard, $10^3/_4 \times 8^1/_2$ in., iv and 419 pp. 1£.-10s.0d. net.

REVIEWED BY M. J. MANJOINE[4]

Section I. Deformation Processes in Simple Materials

N. F. MOTT, A Discussion of Some Models of the Rate-Determining Process in Creep; R. D. Johnson, A. P. Young and A. D. Schwope, Plastic Deformation of Aluminum Single Crystals at Elevated Temperatures; F. N. Rhines, Mechanism of Grain Boundary Displacement and Its Relation to the Creep Process as a Whole; W. A. Wood, Creep Processes; D. McLean, Interaction Between Crystal Slip and Grain Boundary Sliding During Creep; J. E. Dorn, Some Fundamental Experiments on High-Temperature Creep.

Review of high points of papers: The rate-determining process in creep is slip, and the barriers of greatest importance are jogs in screw dislocations. This model or one involving dislocation climb leads to stress-dependent activation energy for creep which approaches that for self-diffusion.

Undeformed crystals of aluminum contain a fine substructure. Study of slip by electron and light microscopy revealed several slip systems.

Extension during creep can be divided into two components: (*a*) boundary flow, and (*b*) grain elongation. A linear interaction exists between these components.

Section II. Creep Resistance of Complex Materials

A. H. Cottrell, Creep and Ageing Effects in Solid Solutions; J. W. Freeman and C. L. Corey, Microstructure and Creep; L. Rotherman and C. R. Tottle, The Effect of Alloying on the Creep of Metals; A. Constant and C. Delbart, Basic Principles of a Creep Resisting Alloy; I. I. Kornilov, Creep of Solid Solutions and Compounds in Metallic Systems; Y. N. Rabotnov, The Effect of Changing Loads During Creep.

Creep resistance is increased by strain aging and reduced by recovery. Precipitation during creep is more effective than that before creep. More often the submicroscopic features of structure are more important than the microscopic ones. Introduction of the correct solute element in appropriate quantity and dispersion may lead to secondary effects in structure of complex alloys, rather than depend on them. Compounds of stoichiometric composition formed in the solid state (ordered structures) have higher creep resistance than solid solutions of same components. This is a result of the stability and absence of diffusion.

Section III. Theory of Fracture

R. Eborall, An Approach to the Problem of Intercrystalline Fracture; C. Crussard and J. Friedel, Theory of Accelerated Creep and Rupture; A. Kochendorfer, A Theory of Brittle and Ductile Fracture, with Application to Creep Fracture, Based on the Dynamic Behaviour of Dislocations and Condensation of Vacancies.

Section IV. Work on Tertiary Creep and Fracture

C. H. M. Jenkins, Observations on Third-Stage Creep and Fracture; W. Betteridge, Tertiary Creep of Nimonic 80A; N. J. Grant, Grain Boundary Participation in Creep Deformation and Fracture; W. Siegfried, Investigation Into the Development of Intercrystalline Fractures in Various Steels under Tri-Axial Stress; A. E. Johnson and N. E. Frost, Note on the Fracture under Complex Stress Creep Conditions of an 0.5%-Molybdenum Steel at 550° C and a Commercially Pure Copper at 250° C; R. W. Ridley and H. J. Tapsell, The Effect of a "V" Notch on the Tensile Creep Behaviour of Molybdenum-Vanadium Steel.

Large improvements in the fracture characteristics may be brought about by small alloying additions of high melting point elements of "unfavorable" size factor. Rupture is opposed by such factors as boundary migration and recrystallization and is promoted by factors such as boundary glide and intergranular oxidation.

Rupture may be initiated by the intergranular microcracks formed from clustering of excess vacancies which are produced by climb of dislocations or the crossing of dislocations of different glide systems. If dislocations are accelerated by the external shear stress to about 90 per cent of the velocity of sound, a crack of atomic dimensions can be produced by a pile of single dislocations. This crack may grow and lead to brittle failure. Tertiary creep is a result of the development of cavities and cracks or a change in the mode of deformation.

Under combined stress the creep relations can be expressed as a linear function between the log of the octahedral stress and the log of the minimum creep rate. The criterion of fracture, however, may be the maximum principal tensile stress.

The relationships between rupture time or creep rate and temperature can only be used for extrapolation to long time or low creep rates at lower temperatures if the same thermal action and modes of flow or failure are obtained.

[4] Mechanics Department, Westinghouse Research Laboratories, Beulah Road, Churchill Boro, Pittsburgh 35, Pa. Mem. ASME.

Information for Authors

• Manuscripts should be submitted in final form to the Technical Editors. Each manuscript must be accompanied by a statement that it has not been published elsewhere nor has it been submitted for publication elsewhere. A paper which would occupy more than five pages of the Journal may be returned to the author for abridgment.

• The author should state his business connection, the title of his position, and his mailing address. A short abstract (50 to 100 words) should be included on the first page immediately preceding the introductory paragraph of the paper.

• Three copies of the manuscript are required. One of these must be a carefully prepared printer's copy, typed in double spacing, on one side of the page only, with wide margins, on 8½ by 11-in. opaque white paper. Mimeographed manuscripts, if prepared with exceptional care, can be accepted provided they are completely edited.

• All mathematical expressions should be written by hand in ink or set out by typewriter in a way which would define each symbol unambiguously. Care should be taken to distinguish between capital and lower-case letters, between (0) and the letter (*O*), between the numeral (1) and the letter (*l*), etc. A list of symbols carefully marked, if it has not been included in the body of the paper, should accompany the manuscript on a separate page.

• Before preparing a manuscript the author should study printed articles in the Journal, with special attention to the form and style of mathematical expressions, tables, footnotes, references, and abstracts. Care should be taken to arrange all tables and mathematical expressions in such a way that they will fit into a single column when set in type. Equations that might extend beyond the width of one column (fractions that should not be broken or long expressions enclosed in parentheses) should be rephrased to go on two or more lines within column width. Fractional powers are preferred to root signs and should always be used in more elaborate formulas.

• A normal paper should not exceed five pages in the Journal. It is about 6500 words or twenty to twenty-five double-spaced typewritten pages inclusive of drawings. A Brief Note should not exceed 750 words or about one column in the Journal inclusive of drawings.

• Originals and two copies of figures must accompany the manuscript. Line drawings should not be larger than 8½ × 11 inches, and should be planned for reduction to column width. Lettering should be large enough to be clearly legible when the illustration is reduced. The originals of line drawings must be in India ink on white or pale blue tracing paper or tracing cloth. Photographs of equipment or test specimens must be glossy prints and should be used sparingly. Captions for figures should be typed double-spaced and included as the last page of the manuscript. The figure number and author's name should be written in the margin or on the back of each illustration.

• Titles of papers should be brief. If an adequate description of the subject requires a title which, along with the authors' names, would occupy more than one line on the cover of the Journal, a separate shorter title should be submitted.

• Authors can obtain copies of the ASME Manual MS-4, "An ASME Paper," from the Technical Editors and are urged to do so before drafting their papers in final form.

• Papers published in the Journal of Applied Mechanics must first be presented at a Meeting, either in person or by title. Scheduling of papers is in the hands of the Secretary of the Applied Mechanics Division. Authors should indicate their preference in this respect to the Technical Editors when submitting a paper.

• An author is entitled to 25 preprints free of charge (in the case of two authors, 15 each; three or more authors, 10 each). Larger quantities of preprints or reprints can be ordered from Editorial Department, The American Society of Mechanical Engineers, 29 West 39th Street, New York 18, N. Y. Quotations will be sent on request.

D. C. Drucker and J. Kestin, *Technical Editors*

Please address all communications to: Technical Editors
Journal of Applied Mechanics, ASME
Division of Engineering
Brown University
Providence 12, R. I.

Third U. S. National Congress of Applied Mechanics

at Brown University, Providence, Rhode Island
June 11–14, 1958

Complete papers must be submitted to Professor R. M. Haythornthwaite, Chairman of the Editorial Committee, Brown University, before January 1, 1958.

No paper, including text, equations, tables, and figures, should exceed the equivalent of 5000 words. Manuscripts should be submitted in *duplicate*, but it is requested that the first page of each manuscript containing only the title of the paper, the name and affiliation of the author, and an abstract of not more than 100 words be submitted in *triplicate*, because it is planned to publish abstracts of accepted papers in the June, 1958, issue of the *Journal of Applied Mechanics*.

One copy should be in original typewriting (for very clear mimeographing) on only one side of white paper, and be double spaced with margins at least one inch wide. Figures should be submitted in reproducible India ink drawings on separate sheets of drawing paper or cloth. The width of the lines of these drawings and the lettering should allow for the necessary reduction. Photographs should be glossy prints and not larger than 8 by 10 inches.

References should be grouped together in a bibliography at the end of the manuscript, listing title, author, publication or publisher, volume, year, and page numbers, in that order. Text references to the bibliography should be made by numbers in brackets, references to equations by numbers in parentheses.

Authors are advised to retain carbon copies of their manuscripts as the original manuscripts will not be returned with the proofs.

Inquiries regarding the Congress should be addressed to the Secretary of the Congress, Brown University, Box D, Providence 12, R. I.

Industrial groups, governmental agencies, and colleges and universities are requested to provide financial support for the Congress.

All industrial groups contributing $300 or more, and all universities or colleges contributing $150 or more, will be listed in the program of the Congress and in the printed Proceedings.